frontiers | Research Topics

Climate change and soil microbial control of carbon sequestration

Edited by
Yang Yang, Anna Gunina, Peng Shi and Yan Xing Dou

Published in
Frontiers in Microbiology
Frontiers in Environmental Science

ISSN 1664-8714
ISBN 978-2-8325-6424-0
DOI 10.3389/978-2-8325-6424-0

About Frontiers

Frontiers is more than just an open access publisher of scholarly articles: it is a pioneering approach to the world of academia, radically improving the way scholarly research is managed. The grand vision of Frontiers is a world where all people have an equal opportunity to seek, share and generate knowledge. Frontiers provides immediate and permanent online open access to all its publications, but this alone is not enough to realize our grand goals.

Frontiers journal series

The Frontiers journal series is a multi-tier and interdisciplinary set of open-access, online journals, promising a paradigm shift from the current review, selection and dissemination processes in academic publishing. All Frontiers journals are driven by researchers for researchers; therefore, they constitute a service to the scholarly community. At the same time, the *Frontiers journal series* operates on a revolutionary invention, the tiered publishing system, initially addressing specific communities of scholars, and gradually climbing up to broader public understanding, thus serving the interests of the lay society, too.

Dedication to quality

Each Frontiers article is a landmark of the highest quality, thanks to genuinely collaborative interactions between authors and review editors, who include some of the world's best academicians. Research must be certified by peers before entering a stream of knowledge that may eventually reach the public - and shape society; therefore, Frontiers only applies the most rigorous and unbiased reviews. Frontiers revolutionizes research publishing by freely delivering the most outstanding research, evaluated with no bias from both the academic and social point of view. By applying the most advanced information technologies, Frontiers is catapulting scholarly publishing into a new generation.

What are Frontiers Research Topics?

Frontiers Research Topics are very popular trademarks of the *Frontiers journals series*: they are collections of at least ten articles, all centered on a particular subject. With their unique mix of varied contributions from Original Research to Review Articles, Frontiers Research Topics unify the most influential researchers, the latest key findings and historical advances in a hot research area.

Find out more on how to host your own Frontiers Research Topic or contribute to one as an author by contacting the Frontiers editorial office: frontiersin.org/about/contact

Climate change and soil microbial control of carbon sequestration

Topic editors

Yang Yang — Institute of Earth Environment, Chinese Academy of Sciences (CAS), China

Anna Gunina — University of Kassel, Germany

Peng Shi — Xi'an University of Technology, China

Yan Xing Dou — Northwest A and F University, China

Citation

Yang, Y., Gunina, A., Shi, P., Dou, Y. X., eds. (2025). *Climate change and soil microbial control of carbon sequestration*. Lausanne: Frontiers Media SA.

doi: 10.3389/978-2-8325-6424-0

Table of contents

frontiers | Frontiers in Environmental Science

TYPE Editorial
PUBLISHED 21 May 2025
DOI 10.3389/fenvs.2025.1619408

OPEN ACCESS

EDITED AND REVIEWED BY
Yuncong Li,
University of Florida, United States

*CORRESPONDENCE
Yang Yang,
yangyang@ieecas.cn

RECEIVED 28 April 2025
ACCEPTED 09 May 2025
PUBLISHED 21 May 2025

CITATION
Dou Y and Yang Y (2025) Editorial: Climate change and soil microbial control of carbon sequestration.
Front. Environ. Sci. 13:1619408.
doi: 10.3389/fenvs.2025.1619408

Editorial: Climate change and soil microbial control of carbon sequestration

Yanxing Dou[1] and Yang Yang[2]*

[1]College of Forestry, Northwest A&F University, Yangling, Shaanxi, China, [2]Institute of Earth Environment, Chinese Academy of Sciences (CAS), Xi'an, China

KEYWORDS

soil organic carbon, soil microbes, microbial community and function, climate change, soil organic carbon sequestration

Editorial on the Research Topic
Climate change and soil microbial control of carbon sequestration

Soil microorganisms, as a major regulator in the dynamics of soil organic carbon (SOC) and nutrient availability, partake in a variety of biochemical reactions. Because of the large soil carbon pool, even small changes in the balance between inputs and outputs from the soil carbon pool can exert a significant impact on atmospheric CO_2 levels. Over the past few decades, the influence of climate change on soil carbon cycling has been intensively analyzed. The focus on investigating the global carbon cycle due to its connection with climate change has led to an increasing number of studies on microbial control of SOC. It has been extensively recognized that the extent of SOC reservoir is determined by microbial involvement since soil carbon dynamics ultimately stem from microbial activity and growth. However, the mechanisms by which these microbe-regulated processes cause soil carbon stabilization under climate change is still unclear. Therefore, the Research Topic "*Climate Change and Soil Microbial Control of Carbon Sequestration*" were organized.

The interest for this Research Topic were mainly included 1) novel insights into the interplay in soil microbial community function; 2) recent advancements in soil carbon dynamics under the influence of global climate change; 3) biogeochemical mechanisms connecting soil microbes and SOC; 4) the role of soil microbes in the SOC conversion process; 5) the new high-throughput sequencing for soil microbes, including metagenome, transcriptomics, metabonomics methods, etc.; 6) Response of soil microbes to climate change and their impacts on SOC transformation and fixation; 7) Addressing uncertainty in estimating SOC pool at the local, regional, and global scales. Twelve articles were published in this Research Topic, highlighting key progress in the field:

Smallwood et al. demonstrated that volatile organic compounds (VOCs) can potentially serve as bioindicators of subsurface biogeochemical processes, providing high-resolution data and broad-scale measurements that can be used to characterize biological roles in the thermokarst–permafrost continuum. This study also establishes methods and approaches for effectively capturing VOCs during winter seasons that could allow for more accurate measurements of subsurface microbial rates of carbon conversion.

Zheng et al. discovered that high-affinity CH_4 oxidation induced by high CH_4 concentrations is widespread in paddy soils. In acid-neutral paddy soils capable of oxidizing atmospheric CH_4, type II methanotrophs exhibited higher 16S rRNA: rDNA ratios and, higher potential activity than type I methanotrophs. CH_4 oxidation enhanced

biotic interactions between methanotrophs and other prokaryotic taxa. Soil pH and nutrient availability can significantly affect the methanotrophic community and high-affinity CH_4 oxidation activity.

Liu et al. revealed that soil respiration (Rs) decreased with increasing stand age in poplar plantations throughout the growth cycle. The microbial *r*-strategies were the key biotic factors that influenced Rs in different-age poplar plantations. Other abiotic factors such as pH, SOC and NO_3–N, and litter C: N were also important drivers of Rs. Soil properties such as pH and bulk density also significantly affected soil microbial community diversity and composition, and altered the ecological strategies of microbial communities, which in turn altered Rs.

Qiao et al. found that grazer exclosure is effective in increasing soil microbial diversity without affecting the stability of their networks. These benefits may be affected by climate warming, which reduces bacterial diversity and network complexity by increasing nitrate nitrogen contents. The recovery of soil microbial communities in degraded grasslands through grazing exclosure may be slow under future warming scenarios. Land managers need to consider the environmental as well as social and economic implications of degraded grassland restoration measures.

Wu et al. basing on 701 sampling points of topsoil, geostatistics and geodetectors revealed that the average value of effective phosphorus content in the topsoil of the study area was 14.28 mg/kg. Among all theoretical models, the exponential model has the best fitting effect. Elevation is the main controlling factor for the spatial variation of available phosphorus in the topsoil, followed by soil types, planting systems, annual precipitation, and organic matter. The diversity and complexity of spatial heterogeneity could affect available phosphorus content in cultivated soil.

Wang et al. found that higher soil organic matter levels were associated with greater species diversity, and both diversity and soil organic matter decreased with increasing soil depth. The Annelida greatly improved soil quality, fertility, and nutrient availability in karst basins. The major species influencing the soil organic matter distribution were *Agrotis segetum*. Earthworms thrived at relatively high soil humidity and thickness but are negatively impacted by rock outcrops. The spatial distribution of soil animals is positively influenced by interactions between soil thickness, humidity, structure, and bulk density and is negatively influenced by rock outcrops and soil types. Beneficial land use increases soil animal diversity and abundance, promoting SOM accumulation. Microtopography greatly impacts soil organic matter in karst basins by altering its spatial distribution.

Li et al. demonstrated that continuous 6-year conservation tillage (CT) significantly increased maize yields, aggregate stability, and POC (0–30 cm) and MAOC (0–20 cm) contents. Tillage practice and soil depth both influence bacterial, fungal and protistan communities. The connectivity of module 1 was significantly related to POC and MAOC contents CT increased the richness of specific fungal (*Cephalotrichum*) and protistan (*Cercozoa*) species and promoted SOC fraction accumulation through straw degradation, macroaggregate formation and predation effects. Stimulating the function of keystone taxa can drive the function of the module 1 community in SOC accumulation under CT practices, which is beneficial for maintaining soil fertility and productivity in eolian sandy soils on the Northeast China Plain.

Xuemei et al. illustrated that both climate warming and nitrogen deposition significantly increased soil organic carbon component and altered soil bacterial, leading to a positive impact on soil enzyme activity, and enzyme stoichiometry, as well as C: P and N: P ratios. Soil bacterial diversity also showed significant increments. Climate warming led to a decrease in the soil enzyme C: N ratio and C: P ratio, while increasing the soil enzyme N: P ratio. Nitrogen deposition resulted in a significant increase in the soil enzyme C: N ratio and a decrease in the soil enzyme N: P ratio. Soil organic carbon components were directly influenced by the negative impact of climate warming and the positive impact of nitrogen deposition.

Liu et al. found that the heavy metal pollution in the downwind direction of the automobile Parts Co., Ltd. is mainly As, CD, and Zn mixed heavy metal pollution, as well as the distribution is uneven. The coefficient of variation of As was the largest, and the regional variation amplitude was large. The accumulative index of AS and CD was 6, which reached a very serious pollution level. The content of As was 1994.7 mg/kg, exceeding the standard by more than 44 times, and the distribution of As in soil was uneven. The pollution level of Zn belonged to the moderate level. The pollution degree of heavy metals in the soil decreases as the distance from the downwind outlet of plant increases.

Li et al. indicated that arbuscular mycorrhizal fungi (AMF) communities varied through the increase or decrease of dominant *genera* and effectively buffered the impact of the ecosystem on environmental changes, finally improving the overall resilience of the dry environment. No tillage and subsoiling with mulch significantly changed the composition of AMF community at growth stages. Conventional tillage could promote proportions of the *genus Claroideoglomus*, whereas no tillage was good to proportion of *genera Glomus* and *Septoglomus*. No tillage and subsoiling with mulch influenced the composition of key *genera* by changing plant biomass and soil characteristics, result in the AMF community composition changing.

Luo et al. found that photovoltaic shading improved soil microbial biomass with the increasing of 20%–30%. Compared to light intensity, the soil depth had more important impacts on the diversity and relative abundance of soil bacterial communities. The dominant phyla were *Actinobacteria*, *Proteobacteria*, *Acidobacteria*, *Chlorobacteria*, and *Dimonobacteria*. The ecological network was more stable and better adapted to light stress under the photovoltaic. *Euryops pectinatus* is more conducive to maintaining the stability and health of subsurface ecosystems in vulnerable areas. Soil nutrients are the key driving factor in the dominant soil community changes.

Huang et al. investigated seasonal and biogeographic dynamics of soil ciliates community in the Yarlung Zangbo River and found that soil ciliates communities and environmental factors exhibited significant seasonal and geographic variations. The soil ciliate community was more complex in wet season than in dry season, and the stability of soil ciliate community in wet season was higher than that in dry season. The stability of soil ciliate community in wetland was higher than that in forestland, shrubland and grassland, and the anti-interference ability was stronger. Soil temperature, total nitrogen, soil organic matter and soil water content are the important factors affecting the structure of soil ciliate community.

The goal of this Research Topic is to explore how soil microorganisms exert two primary, contradictory impacts on controlling soil carbon dynamics by focusing on climate change and its impact on soil microbial control carbon sequestration. All results above in this Research Topic will provide good insights in understanding microbe-regulated processes cause soil carbon stabilization under climate change. In the future, we should continue to focus on soil carbon sequestration mediated by soil microorganism with the scenarios of climate change.

Author contributions

YD: Writing – original draft, Writing – review and editing. YY: Writing – original draft, Writing – review and editing.

Funding

The author(s) declare that no financial support was received for the research and/or publication of this article.

Conflict of interest

The authors declare that the research was conducted in the absence of any commercial or financial relationships that could be construed as a potential conflict of interest.

Generative AI statement

The author(s) declare that no Generative AI was used in the creation of this manuscript.

Publisher's note

frontiers | Frontiers in Environmental Science

TYPE Original Research
PUBLISHED 06 March 2024
DOI 10.3389/fenvs.2024.1360015

OPEN ACCESS

EDITED BY
Yan Xing Dou,
Chinese Academy of Sciences (CAS), China

REVIEWED BY
Baofeng Chai,
Shanxi University, China
Pan Wan,
Northwest A&F University, China
Yang Hu,
Xinjiang Agricultural University, China

*CORRESPONDENCE
Bu Pu,
purbu@utibet.edu.cn

RECEIVED 22 December 2023
ACCEPTED 27 February 2024
PUBLISHED 06 March 2024

CITATION
Huang Q, Li M, Li T, Zhu S, Wang Z and Pu B (2024), Spatiotemporal distribution patterns of soil ciliate communities in the middle reaches of the Yarlung Zangbo River.
Front. Environ. Sci. 12:1360015.
doi: 10.3389/fenvs.2024.1360015

Spatiotemporal distribution patterns of soil ciliate communities in the middle reaches of the Yarlung Zangbo River

Qian Huang, Mingyan Li, Tianshun Li, Shiying Zhu, Zhuangzhuang Wang and Bu Pu*

School of Ecology and Environment, Tibet University, Lhasa, China

Introduction: Soil ciliates, as protozoa, play a crucial role in biogeochemical cycling and the soil food web, yet they are highly sensitive to environmental fluctuations in soil conditions. The diversity and biogeographic characteristics of soil ciliates in the Tibetan Plateau remain poorly understood. As part of a regional survey focused on soil ciliate diversity, we investigated the composition and spatiotemporal variations of soil ciliate communities along the Yarlung Zangbo River, a representative soil habitat in the Tibetan Plateau.

Methods: A total of 290 soil samples were collected from four habitat types of grassland, shrubland, forestland and wetland in the middle reaches of the Yarlung Zangbo River during the wet and dry seasons, and 138 species of ciliates were identified.

Results: Soil ciliate diversity exhibited greater variation across habitat types than seasons. Moreover, soil ciliate diversity was higher during the wet season compared to the dry season, with the wetland habitat showing the highest diversity and the grassland habitat displaying the lowest. We observed spatiotemporal heterogeneity in the composition of soil ciliate communities across different seasons and habitat types. Notably, Litostomatea, Karyorelictea, and Prostomatea predominated in ciliate communities during the wet season and in grassland habitat. Phyllopharyngers dominated during dry seasons and in forested regions, while Spirotrichea species were prevalent in wetland and forested areas. The co-occurrence network analysis showed that soil ciliate community was more complex in wet season than in dry season, and the stability of soil ciliate community in wet season was higher than that in dry season. The stability of soil ciliate community in wetland was higher than that in forestland, shrubland and grassland, and the anti-interference ability was stronger. Soil temperature (ST), Total nitrogen (TN), Soil organic matter (SOM) and Soil water content (SWC) are important factors affecting the structure of soil ciliate community. By influencing the metabolic rate and nutrient acquisition of soil ciliates, the distribution pattern of soil ciliate community diversity in the middle reaches of Yarlung Zangbo River is shaped.

Discussion: In summary, this study revealed the distribution pattern of soil ciliate community diversity in the Yarlung Zangbo River Basin, and the key factors

affecting the spatial and temporal differences and stability of the community, enhancing our understanding of how ciliates adapt to environmental conditions in soil habitats across the Tibetan Plateau.

KEYWORDS

protozoa, soil ciliates, community diversity, soil ecology, Yarlung Zangbo River

1 Introduction

Protozoa is one of the main groups of soil microorganisms (Acosta-Mercado and Lynn, 2004; Abraham et al., 2019; 2019). Protozoa, as an important trophic level in microfood web, plays an important role in maintaining ecological balance, energy transport hub and biogeochemical cycle, and is an indispensable part of soil ecosystem (Bonkowski, 2004; Geisen et al., 2018; Xu et al., 2022). As the main group of soil protozoa community, soil ciliates have the characteristics of rich species, short life cycle and rapid community succession (Foissner, 1999), which has an important influence on the assembly, succession and maintenance of the community, and the change of their abundance can drive the direction of community succession (Domonell et al., 2013; Geisen et al., 2018). Soil ciliates are highly sensitive to environmental changes due to the constant interaction between their cell membranes and the external environment (Zheng et al., 2018; Liu et al., 2021). External disturbances promote rapid changes in their community structure and diversity, outpacing the responsiveness of large animals residing in the soil matrix (Bamforth et al., 2005; Foissner, 2005). This rapid response makes soil ciliates sentinel organisms of environmental changes, coupled with ease of culture and observation, can be used as dynamic indicators to assess soil environmental health (Heger et al., 2012; Debastiani et al., 2016). In addition, soil ciliates can decompose organic matter in the soil and maintain the stability of the soil environment (Xiong et al., 2018), a key role that can affect the ecological balance and overall health of the soil (Azam et al., 1983; Geisen et al., 2015). The Qinghai-Tibet Plateau is the region most sensitive to climate change in the world (Tian et al., 2020). The unique properties of soil ciliates make them valuable research objects in the context of ecological resilience of the Qinghai-Tibet Plateau, and have practical application value in assessing soil conditions of different ecosystems or different landscapes on the Qinghai-Tibet Plateau.

The Yarlung Zangbo River Basin is located in the southern part of the Qinghai-Tibet Plateau. With its high average altitude, long sunshine time and low temperature, this region has become a hotspot for studying biodiversity pattern due to its diverse and complex climatic and geographical characteristics (Liu et al., 2018; Shi et al., 2018). In recent years, under the influence of global warming and local human activities, the biodiversity and ecosystem stability of the Brahmaputra River Basin are changing, and the regional ecological risks are increasing (Liu et al., 2018). At present, there are relatively few research reports on protozoa in this region. Researchers Zhang et al. revealed the distribution pattern of protozoa diversity in the upper reaches of the Yarlung Zangbo River (Zhang et al., 2022), and researchers Yang et al. clarified the diversity and composition distribution pattern of eukaryotic microorganisms along the altitude gradient in the middle reaches of the Yarlung Zangbo River (Yang Q. et al., 2023). However, the diversity of soil ciliates in the Yarlung Zangbo River Basin has not been reported, and the soil ecological health status of different ecosystems or different landscapes in the basin is still unclear. The spatial and temporal distribution pattern, community stability, ecological networks among species and main driving factors of soil ciliates in the basin remain to be revealed. In this context, we studied the community composition, spatial and temporal distribution and diversity pattern of soil ciliates in the middle reaches of the Yarlung Zangbo River, analyzed the species association and community stability of soil ciliates in different seasons and different ecosystem types, and discussed the adaptability of soil ciliates in different habitats and the main environmental driving factors.

The purpose of this study was to reveal: (1) the spatial and temporal distribution pattern of soil ciliate communities in the middle reaches of Yarlung Zangbo River; (2) Species association and community stability of soil ciliates in different seasons and different ecosystem types; (3) Adaptability of soil ciliates in different habitats and its main environmental driving factors. This study provided valuable insights for the environmental adaptation of soil ciliates, and provided scientific basis for ecological environmental protection, biogeochemical cycle research and soil ecological risk assessment on the Qinghai-Tibet Plateau.

2 Materials and methods

2.1 Study area overview and sample collection

The Yarlung Zangbo River Basin (82°00′—97°07′E, 28°00′—31°16′N) is located between the Gangdis-Nianqing Tanggula Mountain range and the Himalayas (Zhang et al., 2014). It originates from Jemayang Zongqu in Zhongba County, Shigatze City, Tibet Autonomous Region, China. It runs through southern Tibet from east to west, with a high terrain in the west and low in the east. The drainage area is 240,000 km^2 (You et al., 2007). The river is divided according to the terrain characteristics and climate types of the basin. The middle reaches of the river are about 1,293 km long and the basin area is 165,000 km^2 (Li et al., 1999). The river banks are dominated by floodplains and terraces, and the average annual precipitation is between 300 mm and 600 mm in plateau temperate semi-arid climate (Wu et al., 2021). The complex habitats and vegetation types transition from alpine meadow to alpine scrub and then to forest. The study area covers the middle reaches of the Yarlung Zangbo River. A total of 29 sampling sites were set up in this area (Figure 1), and the sampling sites were divided according to habitat characteristics, including four types of grassland (GL),

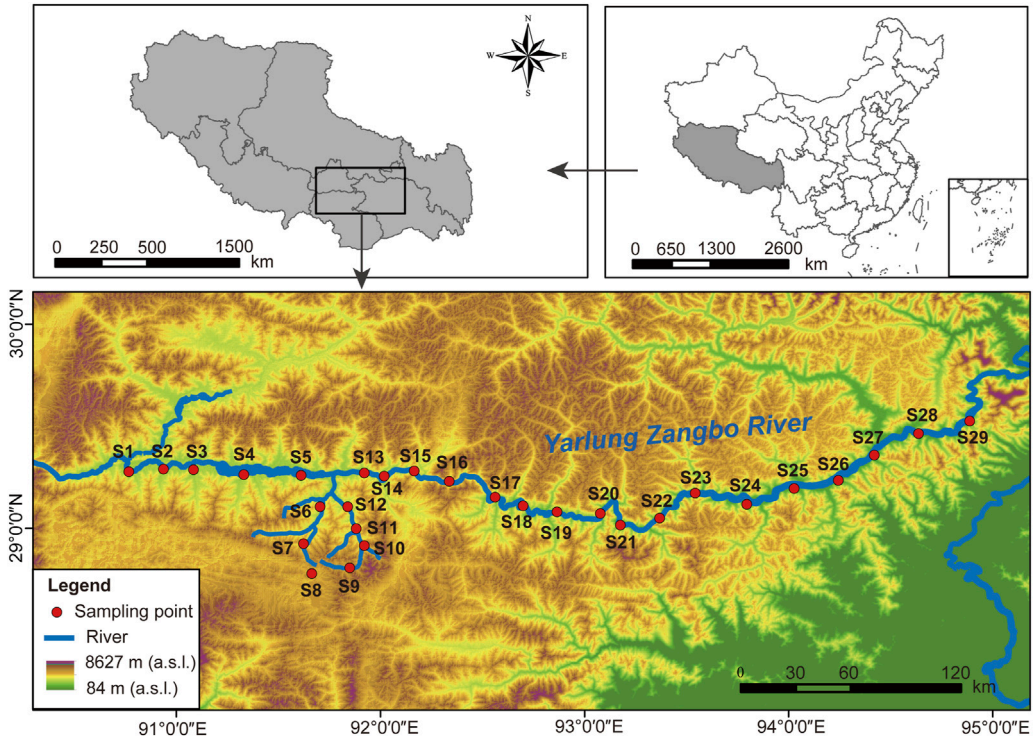

FIGURE 1
Distribution of the 29 sampling sites on the Yarlung Zangbo River.

shrubland (SL), forestland (FL) and wetland (WL) (Table 1). Soil biological sample collection and soil physicochemical index determination will be carried out in August (wet season) and November (dry season) in 2021.

Five sampling sites were set up within an area of about 100 m^2 in each sample plot, and the area of each sampling site was 25 m^2 (5 m × 5 m). Fresh litter on the soil surface was picked off before sample collection, and relevant data such as soil quality, soil temperature, altitude, geographical coordinates and vegetation status were recorded. Soil sampler (LEICI, JC-802B, China) was used to collect 0–5 cm surface soil samples according to the "five-point pattern of blossom" sampling method (Liu et al., 2022). One soil sample was collected from each sampling point, and a total of five soil samples were collected from each sample plot. The samples were mixed, sealed in bags, and marked. At the same time, the soil ring knife sampler (LEICI, JC-TRCY01A, China) with a volume of 100 cm^3 was used to cut the *in-situ* soil, fill the soil sample with it, seal it and bring it back to the laboratory for the determination of water content. A total of 290 soil samples were collected from 29 sites in two seasons (29 sites × 2 seasons × 5 replicates), and the number of samples was consistent among different habitat types. The soil samples were separately treated after being brought back to the laboratory. The fresh soil samples were used to determine the soil physical and chemical indexes, and the remaining soil samples were naturally air-dried in the laboratory for qualitative observation and quantitative culture of soil ciliates.

2.2 Sample handling and species identification

The "Non-Flooded Petri Dish Method" was employed for qualitative research (Foissner, 1992). Fifty grams of air-dried soil samples were added to Petri dishes with a diameter of 15 cm. Soil leachate was then added until the soil was thoroughly moistened but not submerged. The dishes were placed in a 25°C incubator and continuously cultured for 20 days. Species identification was performed by OLYMPUS CKX53 inverted fluorescence microscope every day after culture, and observations were recorded continuously. Quantitative research was conducted using the direct counting method in cultivation (Ning et al., 2018). Thirty grams of air-dried soil samples were weighed and placed in culture dishes with a diameter of 10 cm, with a water-to-soil ratio of 1:1. These dishes were maintained at a constant liquid level in a 25°C incubator until the maximum counting day (day 9, 10, or 11). On that day, the culture dishes were tilted at a 45° angle and allowed to stand for 5–7 min. The supernatant was then completely drawn off and measured. A drop of the supernatant was taken onto a glass slide, fixed under a microscope for counting, and records were maintained. This process was repeated five times for each soil sample. The obtained counts were converted into ciliate density per 1 mL of water (approximately equal to 22 drops). Using the ciliate density per 1 mL of water, the number of soil ciliates in 30 g of soil samples was calculated.

TABLE 1 Sites information of the middle reaches of the Yarlung Zangbo River.

Site	Longitude (E)	Latitude (N)	Altitude (m)	Habitat types	Soil types
S1	90.768292	29.275992	3555.94	SL	sandy soil
S2	90.937386	29.288484	3534.45	WL	clay soil
S3	91.085251	29.286345	3530.30	WL	clay soil
S4	91.331067	29.262169	3533.80	FL	sandy soil
S5	91.612019	29.258597	3521.10	FL	sandy soil
S6	91.705393	29.104931	3625.28	GL	sandy soil
S7	91.624075	28.923538	4038.18	GL	sandy soil
S8	91.664332	28.776647	4581.46	WL	clay soil
S9	91.850085	28.805475	4614.14	WL	clay soil
S10	91.921878	28.913834	4040.73	GL	sandy soil
S11	91.882193	28.997407	3806.51	GL	sandy soil
S12	91.840264	29.104441	3641.66	GL	sandy soil
S13	91.921600	29.269853	3517.73	WL	clay soil
S14	92.018830	29.254577	3512.68	SL	clay soil
S15	92.166001	29.279894	3520.90	FL	loam soil
S16	92.337692	29.229733	3499.66	SL	sandy soil
S17	92.562916	29.151465	3242.31	FL	loam soil
S18	92.699804	29.109214	3121.61	GL	sandy soil
S19	92.865627	29.079116	3097.78	GL	sandy soil
S20	93.078333	29.071086	3089.37	SL	sandy soil
S21	93.176376	29.014414	3036.19	SL	clay soil
S22	93.368569	29.048844	3008.72	SL	clay soil
S23	93.543089	29.171325	2997.20	FL	loam soil
S24	93.795871	29.116889	2942.66	FL	loam soil
S25	94.027581	29.194081	2934.20	WL	clay soil
S26	94.244026	29.233782	2938.01	FL	loam soil
S27	94.420024	29.357805	2900.10	WL	clay soil
S28	94.637056	29.462648	2887.72	FL	loam soil
S29	94.887494	29.524680	2883.01	FL	loam soil

SL, shrubland; GL, grassland; FL, forestland; WL, wetland.

2.3 Measurement of environmental parameters

Soil temperature (ST) was measured *in situ* (-10–60°C) with a curved pipe geotherm (NENGH, NHSQ2803,China). Soil pH value (soil: water = 1:2.5) was measured by soil acidity meter (LEICI, TSS-851,China) (Thunjai et al., 2001). The soil moisture content (SWC) was measured by drying method (Davidson et al., 1998). The content of soil available phosphorus (AP) was determined by ultraviolet spectrophotometer (INESA, 752N, China) according to sodium bicarbonate extraction and molybdenum-antimony resistance colorimetric method (Xue et al., 2004). Available potassium (RAK) was determined by ammonium acetate extraction and flame photometer (Chen et al., 2020). The content of total nitrogen (TN) was determined by elemental analyzer (VELP, CN802, Italy) (Bremner, 1960). The content of total potassium (TK) was determined by flame spectrophotometry (Zhang et al., 2013). Soil organic matter (SOM) was determined by potassium dichromate volumetric method using elemental analyzer (VELP, CN802, Italy) (Nóbrega et al., 2015). The content of total phosphorus (TP) was determined by ultraviolet spectrophotometer (INESA, 752N, China) according to sodium hydroxide alkali-molybdenum-antimony reactance colorimetry (Xue et al., 2004).

2.4 Statistical analysis

Alpha diversity indices (including richness index, Shannon-Wiener diversity index, Pielou evenness index, and Simpson dominance index) were calculated using "vegan" package in R (version 4.2.1). One-way analysis of variance was used to determine the significance of associations of alpha diversity indices with seasons or habitat types. Principal coordinate analysis (PCoA) and PERMANOVA analysis were performed based on the Bray–Curtis distance using the "Micoeco" package in R. Mantel tests were used to determine correlations between environmental variables and selected characteristics of ciliates composition. Ciliates co-occurrence patterns were constructed based on Spearman's rank correlation coefficients. Co-occurrence events were identified as statistically robust correlations ($|R| > 0.6$, $p < 0.05$) and the co-occurrence network was visualized in Gephi (version 0.9.7). Sampling sites were mapped in ArcMap 10.6.1.

3 Results

3.1 Environmental factors and ciliates diversity varied

The environmental factors of season and habitat type are presented in Supplementary Figure S1, The average concentrations of SWC and TP in wet season were 36.65% and 0.7 g/kg, respectively, as compared to the 10.31% and 0.54 g/kg in dry season. The Environmental factors SWC and TP contents in wet season were significantly higher than dry season ($p < 0.05$). In addition, Other environmental factors of average wet than dry season (Supplementary Figure S1A), including TN (1.49 g/kg and 1.35 g/kg, respectively), SOM (29.53 g/kg, 27.77 g/kg), RAK (96.65 mg/kg, 79.59 mg/kg), AP (18.42 mg/kg, 15.29 mg/kg)、pH (7.76, 7.40), TK (20.43 g/kg, 19.99 g/kg), ST (24.20°C, 20.83°C)and VC (71.65%, 67.90%). However, the majority of these environmental factors showed no significant difference between wet and dry season ($p > 0.05$). In addition, some environmental factors were significantly different among the different habitat types ($p < 0.05$), such as pH, TK and VC (Supplementary Figure S1B). The pH values of forestland, wetland and grassland were significantly higher than those of shrubland. TK and VC values were higher in forestland and grassland than in shrubland and wetland. The value of TN, SOM and TP in grassland were higher than in shrubland than in wetland than in forestland. The values of RAK, AP, and ST were higher in grassland than in shrubland, forestland, and wetland. The SWC value was higher in wetland than in forestland, shrubland, and grassland. However, there was no significant ($p < 0.05$) difference in these factors among the different habitat types.

In this study, 58 samples were obtained, of which 29 were wet samples and 29 were dry samples (Supplementary Table S1). In total, we obtained 138 species of ciliates from all samples. These ciliates were belonged to 20 orders, 37 families, 57 genera of wet season, and 20 orders, 37 families, 55 genera of dry season (Supplementary Table S2). The alpha diversity of ciliates varied among different seasons and habitat types for the different indices (Supplementary Table S3). For different seasons, the mean value of richness indices, Shannon indices and Simpson indices in wet was higher than in dry season, but these was no significant ($p > 0.05$) difference (Figure 2A). Of different habitat types, the mean value of richness and Simpson indices in wetland were higher than in forestland, shrubland and grassland, with significant difference ($p < 0.05$). The mean value of Shannon indices in wetland were higher than in shrubland and grassland, with significant difference. The mean value of Pielou indices in wetland were higher than in shrubland and grassland, with no significant difference. In general, alpha diversity of ciliates varied in a spatiotemporal manner. In addition, the alpha diversity indices suggested significant differences in ciliates diversity among environment types: wetland samples had the greatest diversity, forestland samples had the lowest Pielou index, and grassland had the lowest diversity (Figure 2B).

3.2 Community structure of soil ciliates in the middle reaches of Yarlung Zangbo River

The application of principal coordinate analysis (PCoA) and PERMANOVA analysis unveiled noteworthy dissimilarities in the composition of soil ciliates communities across various seasons and environmental habitat types. The findings indicated that PcoA1 and PcoA2 accounted for 9.0% and 8.2%, respectively, of the overall variation in ciliates communities among different seasons and habitat types (Figures 3A, B). The PERMANOVA analysis provided evidence that the composition of ciliates communities across different habitat types (R^2: 0.88, $p = 0.001$) displayed statistically significant disparities ($p < 0.05$), whereas variations in different seasons (R^2: 0.02, $p = 0.22$) were not statistically significant. Analysis of the seasonal richness of species revealed that 58.7% ($n = 81$) of species were present in samples from all two seasons (Figure 3C), 17.4% ($n = 24$) unique species in the dry season, 23.9% ($n = 33$) unique species in the wet season. Furthermore, we analyzed the ciliates community composition in different seasons and habitat types based on species abundance information (Figure 3E). In the wet season, the top three ciliate taxa at class levels with their mean relative abundance are as follows: Colpodea (28.2%), Spirotrichea (24.52%) and Oligohymenophorea (14.7%). In the dry season, the top three ciliate taxa at class levels with their mean relative abundance are as follows: Spirotrichea (31.42%), Colpodea (23.75%) and Oligohymenophorea (18.64%) (Supplementary Table S4). In the wet season, the top three ciliates taxa at genus levels with their mean relative abundance are as follows (Supplementary Table S5): *Colpoda* (21.83%), *Plagiocampa* (6.31%) and *Cyrtolophosis* (6.3%). In the dry season, the top three ciliates taxa at genus levels with their mean relative abundance are as follows: *Colpoda* (14.33%), *Cyrtolophosis* (9.42%) and *Halteria* (8.09%).

Analysis of samples from the four different habitats types showed that species from soil samples clustered separately, and the differences were statistically significant (Figure 3B): 18.1% ($n = 25$) were shared by the four different types (Figure 3D), 2.9% ($n = 4$) were shared wetland and grassland, 8% ($n = 11$) were shared by forestland and wetland, 5.1% ($n = 7$) were shared by wetland and shrubland, 2.2% ($n = 3$) were shared by forestland and grassland. Furthermore, we conducted an analysis of ciliate community composition in different habitat types based on species

10.3389/fenvs.2024.1360015

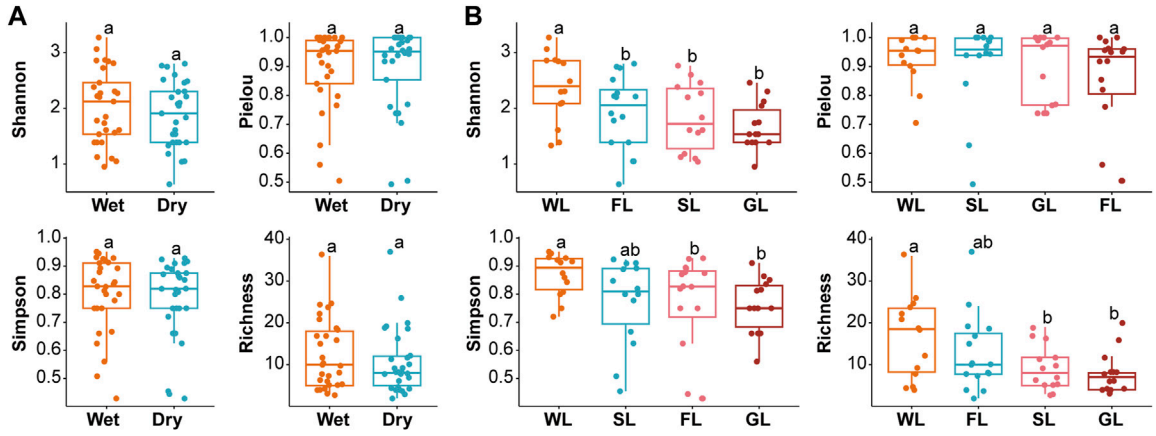

FIGURE 2
Alpha diversity of soil ciliate communities. Seasonal comparisons of alpha diversity estimators for soil ciliate communities **(A)**. Comparisons of alpha diversity estimators for soil ciliate communities in different habitat types **(B)**. Notes: SL: Shrubland; GL: Grassland; FL: Forestland; WL: Wetland.

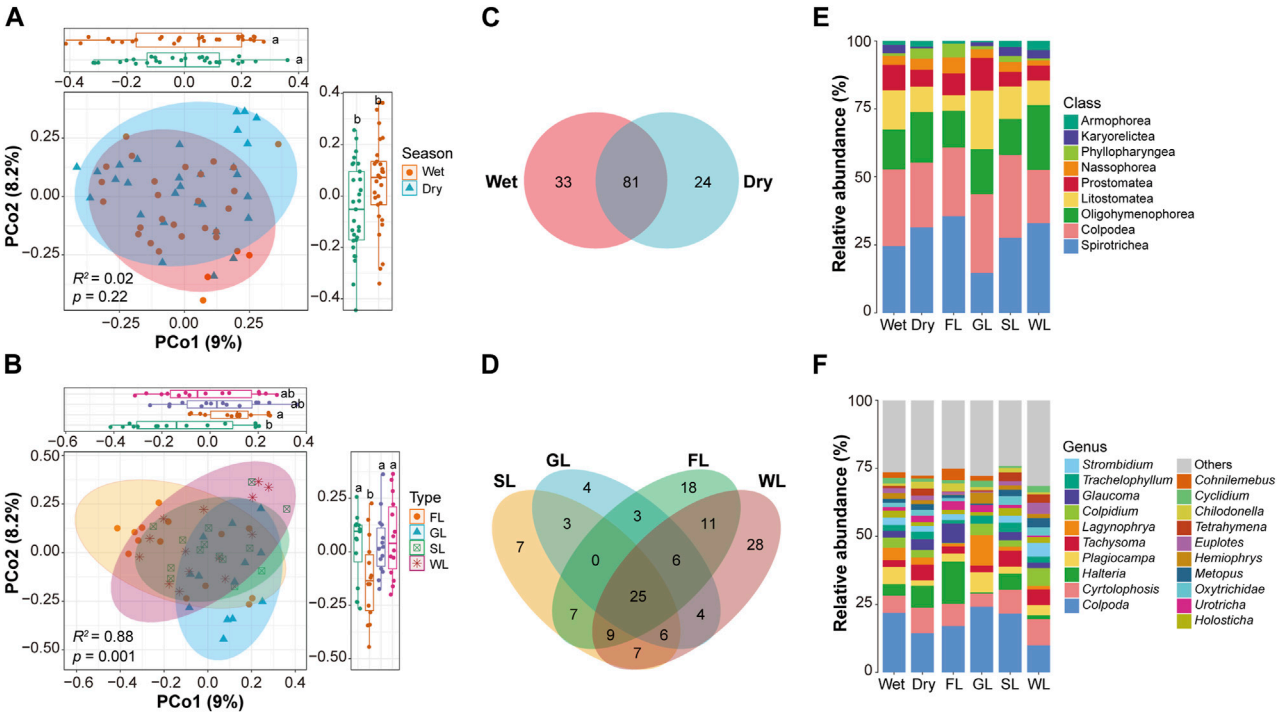

FIGURE 3
Species composition and abundance of soil ciliate communities. Principal coordinate analysis (PcoA) and PERMANOVA analysis of ciliate communities in the two seasons **(A)** and four habitat types **(B)**. Venn diagram showing the number of shared and specific species of soil ciliates for each season **(C)** and habitat types **(D)**. Relative abundance of the main phyla of soil ciliates in the two seasons and four habitat types **(E)**. Relative abundance of the main general of soil ciliates in the two seasons and four habitat types **(F)**. Notes: SL: Shrubland; GL: Grassland; FL: Forestland; WL: Wetland.

abundance information at the class level (Figure 3E). The results revealed the top three ciliate taxa at the class level for each habitat: In grassland: Colpodea (28.96%), Litostomatea (21.64%), and Oligohymenophorea (16.46%). In shrubland: Colpodea (30.37%), Spirotrichea (27.61%), and Oligohymenophorea (13.3%). In forestland: Spirotrichea (35.55%), Colpodea (25.14%), and Oligohymenophorea (13.54%). In wetland: Spirotrichea (32.97%), Oligohymenophorea (23.81%), and Colpodea (19.53%) (Supplementary Table S6). At the genus level, the top three ciliate taxa with their mean relative abundance are as follows: In grassland: *Colpoda* (24.11%), *Lagynophrya* (11.14%), and *Plagiocampa* (7.47%). In shrubland: *Colpoda* (21.58%), *Cyrtolophosis* (8.79%), and *Halteria* (5.89%). In forestland: *Colpoda* (17.01%), *Halteria* (15.6%), and *Cyrtolophosis* (8.14%). In wetland: *Colpoda* (9.92%), *Cyrtolophosis* (9.62%), and *Colpidium* (6.53%) (Figure 3F, Supplementary Table S7).

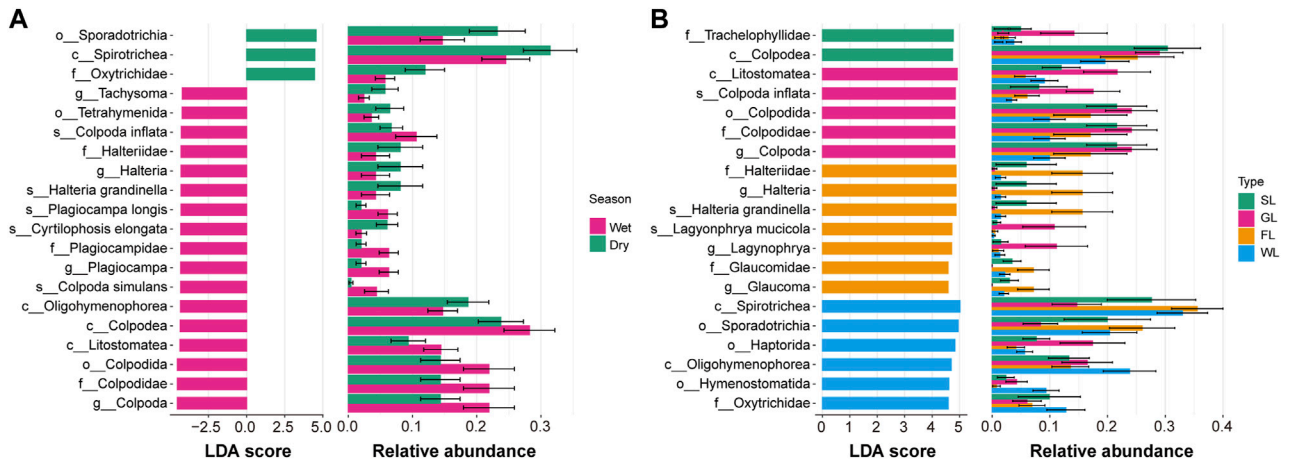

FIGURE 4
Indicator ciliate with LDA scores and relative abundance in soil ciliate communities associated with rhizosphere of different seasons **(A)** and habitat types **(B)**. Notes: SL: Shrubland; GL: Grassland; FL: Forestland; WL: Wetland.

To unveil the associations driving these spatiotemporal patterns, we focused on characterizing the composition of soil ciliate communities. Specifically, we identified distinct ciliate communities associated with different seasons and environmental habitat types. Subsequently, we employed the LEfSe tool to identify biomarkers ranging from the phylum level down to the species level Figure 4. In the dry season, the ciliate biomarkers included Sporadotrichia, Oxytrichidae, and Spirotrichea. In the wet season, the biomarkers consisted of Loxodidae, Loxodes, *Plagiocampa*, Plagiocampidae, Operculariidae, Plagiocampa longis, Karyorelictea, and Protostomztida. Regarding habitat types, in shrubland, the ciliate biomarkers were Trachelophyllidaec and Colpodeac. In grassland, they included Litostomateas, *Colpoda*, Colpodida, Colpodidae, and Colpoda. In forestland, the biomarkers were Halteriidae, *Halteria*, Grandinellas, Lagyonphrya mucicola, *Lagynophrya*, Glaucomidae, and *Glaucoma*. In wetland, they consisted of Spirotrichea, Sporadotrichia, Haptorida, Oligohymenophorea, Hymenostomatida, and Oxytrichidae.

3.3 Linkages between environmental factors and ciliate composition and diversity

We analyzed the relationship between the alpha diversity of ciliate communities and environmental factors. The Shannon index showed a significant positive correlation with VC and exhibited an initial increase followed by a decrease in relation to SWC. The Pielou index displayed a positive correlation with TN and SWC. The Simpson index was positively correlated with VC and displayed an initial increase followed by a decrease in relation to SWC. These results suggest a restricted alpha diversity of ciliate communities in conditions of extremely high SWC levels. The Richness index showed a positive correlation with VC, TN, and SOM. These findings indicate that alpha diversity was significantly influenced by TN, SOM, VC, and SWC. Particularly, VC and SWC were identified as the most important factors affecting alpha diversity (Figure 5A). To explore the associations underlying these spatiotemporal patterns, we employed the Mantel test to determine which environmental parameters significantly correlated with the abundance of ciliate communities. Ciliate communities exhibited significant correlations with TK values in the wet season, and with SOM and SWC values in the dry season (Figure 5B). The analysis of different habitat types revealed significant correlations between ciliate communities and SOM in forestland and SWC in wetland. In summary, SWC, TK, and SOM were identified as the major factors influencing the turnover in the seasonal and environmental type composition of ciliate communities (Figure 5C).

3.4 Co-occurrence network analysis of ciliate communities

Co-occurrence network analysis was performed to explore potential relationships between ciliate communities (Figure 6A). The co-occurrence network of ciliate communities followed different patterns on the basis of six network topological parameters (Figure 6B). Modularity coefficients for all co-occurrence networks were >0.4, indicating clear modularity. Different network metrics were found for all two seasons and four habitat types (Supplementary Table S3); particular differences were seen in node and edge numbers, indicating dynamic changes within soil ciliate communities. Analysis of the seasons showed that the co-occurrence network for wet season had the higher total number of edge and total number of nodes. This season also had the lower average path length, network diameter, and modularity than dry season. These results indicate that interactions within the ciliate communities are more complex in wet than in dry. Analysis of the four habitat types (Figure 6B) showed that the co-occurrence network for wetland and forestland types had the highest total number of nodes, edge, and average degree. This environmental type also had the lowest mean clustering coefficient. These results indicate that interactions within the ciliate

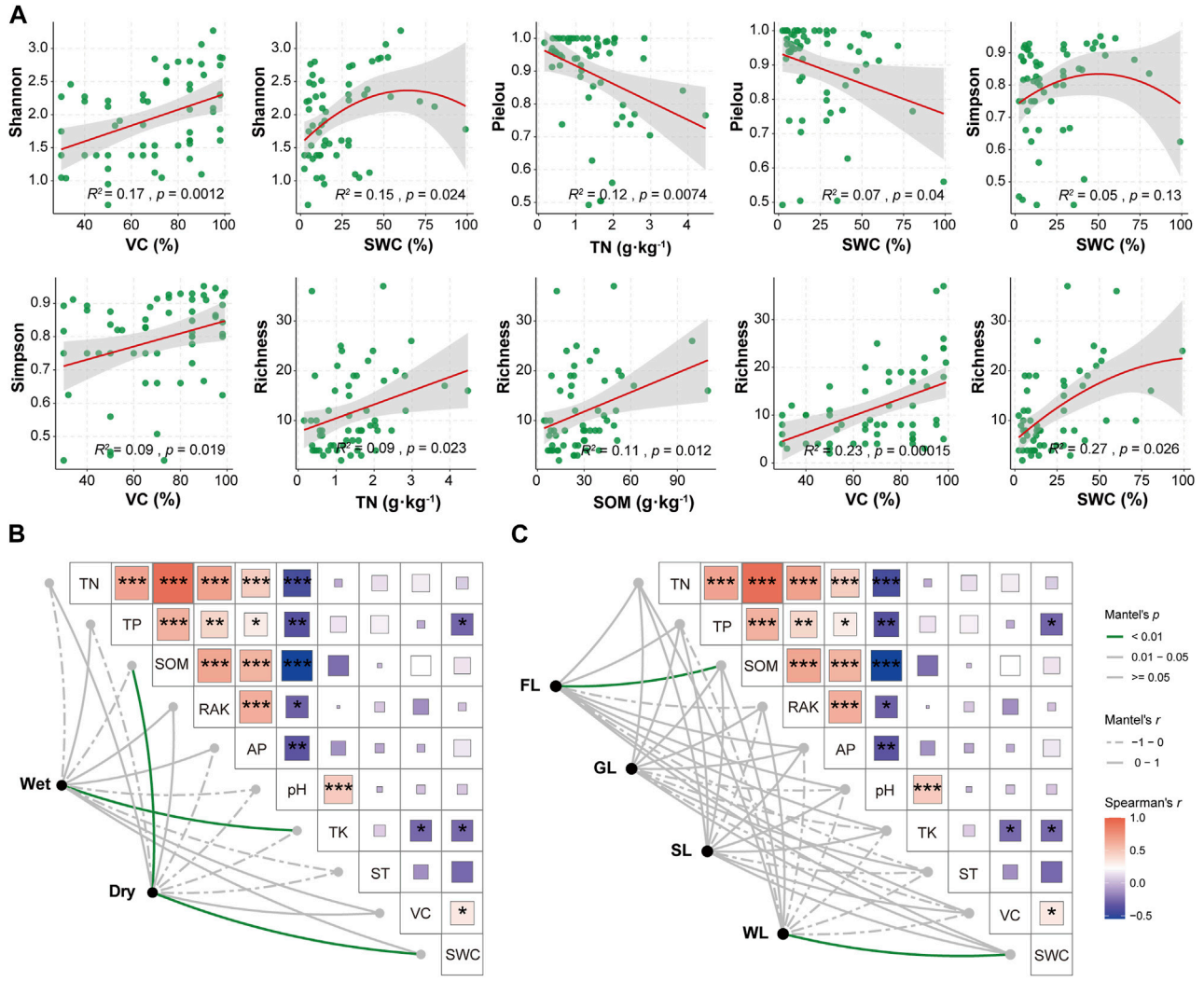

FIGURE 5
Relationship between soil ciliate communities and environmental factors. **(A)** Relationship between soil ciliate diversity and environmental factors. Environmental drivers of soil ciliate communities, as evaluated by Mantel tests in two seasons **(B)** and four habitat types **(C)**. Notes: SL: Shrubland; GL: Grassland; FL: Forestland; WL: Wetland; TN: Total nitrogen; TP: Total phosphorus; SOM: Soil organic matter; RAK: Rapidly available potassium; AP: Available phosphorus; TK: Total potassium; ST: Soil temperature; VC: Vegetation coverage; SWC: Soil water content.

community are more complex in wetland and forestland than in grassland and shrubland types.

4 Discussion

4.1 Comprehensive analysis of soil ciliate diversity in the Yarlung Zangbo River

Ciliates, as a major group of protists, play important roles in microorganism communities, exhibiting high diversity in various environments, including rivers, lakes, and soil ecosystems (Bahram et al., 2018; Oshima et al., 2020). In this study, we identified 138 soil ciliate species across two seasons and four habitat types in the middle reaches of the Yarlung Zangbo River. While previous research has reported on the biodiversity of protist in the river environment, there has been relatively limited research on soil ciliates in this region (Zhang et al., 2022; Yang Q. et al., 2023). To our knowledge, this is the first study to investigate protist diversity using morphological methods and to explore the diversity, composition, and seasonal and biogeographic dynamics in the Yarlung Zangbo River. Our findings revealed that soil ciliate diversity was slightly higher in the wet season compared to the dry season, although the differences were not statistically significant, this is consistent with previous studies on soil ciliates communities in the Gannan, which also found higher soil ciliates diversity in wet season than in dry season (Yang C. et al., 2023). The middle reaches of the Yarlung Zangbo River is an arid area with great seasonal temperature variation. Temperature is an important environmental factor regulating the biochemical processes of terrestrial ecosystems (Leavit, 1998). The accumulation and decomposition of litter, soil respiration and CO_2 release, and the feeding activities and metabolism of soil animals are all

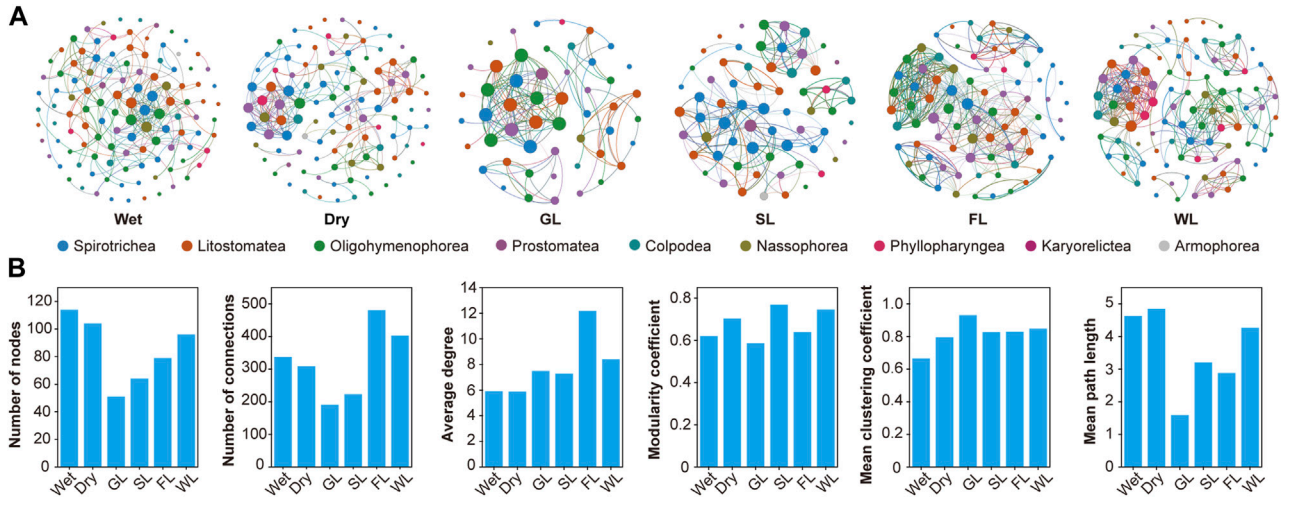

FIGURE 6
Co-occurrence network analysis. Co-occurrence ecological network of ciliates communities in middle of Yarlung Zangbo River **(A)**, and network topological parameters **(B)**. Notes: SL: Shrubland; GL: Grassland; FL: Forestland; WL: Wetland. The nodes in Figure 6A represent the different classes of ciliates.

regulated by soil temperature (Kardol et al., 2011; AlSayed et al., 2018). In the seasonal changes, more precipitation in wet season, abundant nutrients available to soil ciliates, frequent feeding activities of soil ciliates, and higher soil temperature in wet season lead to increased metabolic rate of soil ciliates and rapid reproduction, which may be the main reason for the higher diversity of soil ciliates community in wet season than in dry season (Reth et al., 2005). However, this seasonal pattern differs from the biodiversity of protists found in the aquatic environment of the middle reaches of the Yarlung Zangbo River, suggesting significant seasonal variations in the region's biodiversity (Zhang et al., 2022; Yang Q. et al., 2023). Additionally, our research indicated that soil ciliate diversity varies significantly across different habitat types, with the highest diversity in wetlands, followed by farmland and forestland, and the lowest in grasslands. These findings align with the conclusions of previous studies. Furthermore, we observed substantial variations in soil ciliate diversity among sampling points, indicating the significant environmental variations in the middle reaches of the Yarlung Zangbo River, closely related to the large and dynamic environmental conditions in the region. Despite the relatively high diversity of soil ciliates in the middle reaches of the Yarlung Zangbo River, our use of morphological identification methods may inevitably underestimate their diversity (Li et al., 2021). In today's era of rapid development in high-throughput sequencing technologies, we propose that future research should comprehensively explore the diversity of soil ciliates in the Yarlung Zangbo River's middle reaches using environmental DNA (eDNA) techniques such as metagenomics and metabarcoding (Bello et al., 2018; Ke et al., 2022). This research will significantly contribute to our understanding of the biodiversity patterns and maintenance mechanisms of the largest river basin in the Tibetan Plateau—the Yarlung Zangbo River—and hold crucial importance in the context of global biodiversity studies.

4.2 Spatiotemporal patterns of soil ciliate in Yarlung Zangbo River

Ciliates communities form large and highly diverse groups of microbiotas in soil ecosystems (Watson, 1943; Gabilondo, 2018). Our study gives a clear picture of the spatiotemporal patterns of soil ciliates communities in the Yarlung Zangbo River. Significant fluctuations in community composition were found between wet and dry seasons. Similarly, seasonal differences in soil ciliates communities have been reported for other areas (Jousset et al., 2010; Li et al., 2010; Kumar and Foissner, 2016). During the wet season, Colpodea exhibits the highest relative abundance at the class level, whereas in the dry season, Spirotrichea dominates with the highest relative abundance at the class level. This finding aligns with the results observed in Yang et al. 's study conducted in the Gannan region (Yang C. et al., 2023). Additionally, we observed that species unique of ciliate community to the wet season outnumber those unique to the dry season, consistent with the findings in Kumar et al.'s research (Kumar and Foissner, 2016). This indicates a higher complexity in the ciliate community during the wet season. These seasonal patterns were also revealed by our analysis of co-occurrence networks. The wet network had the highest node number and network connectivity, indicating that the soil ciliates community is more complex in wet than in dry. Soil ciliates have a complex relationship with their living environment, and they can promote the circulation of nutrients in litter and soil system through their life activities (Schulz-Bohm et al., 2017; Fiore-Donno et al., 2019), especially in the circulation of soil nutrients, especially nitrogen and phosphorus (Adl and Gupta, 2006). In this study, soil TN in wet season was higher than that in dry season (Supplementary Figure S1A). Correlation analysis showed that soil ciliate community richness was significantly positively correlated with TN, while negatively correlated with Pielou index (Figure 5A). The greater the richness and the less the uniformity of the community, the higher the complexity and stability of the co-occurrence network,

indicating that the stability of the soil ciliate community in the middle reaches of the Yarlung Zangbo River in the wet season is higher than that in the dry season, and the seasonal difference of TN is the main reason for this phenomenon. In diffident habitat types, significant differences exist in the composition of soil ciliate communities, potentially linked to ecological niche variations among different ciliate taxa in response to soil conditions. The research results of Zhang et al. showed that the species, quantity and biomass of soil ciliates were positively correlated with the content of soil organic matter (Zhang et al., 1999; Abraham et al., 2019). In this study, soil ciliate richness showed a significant positive correlation with SOM (Figure 5A), while SOM showed significant differences in different habitat types (Supplementary Figure S1B), indicating that SOM was a key factor affecting the community structure characteristics of soil ciliates in different habitats. We observed the least divergence in soil ciliate community composition between wetlands and shrubland habitats, while the most significant differences were found between grassland and wetland communities. This divergence may be associated with the heterogeneity of soil physicochemical properties across different habitat types (Bahram et al., 2018; Philippot et al., 2023). For instance, *Plagiocampa longis* are saprotrophic and exhibit a higher prevalence in wetland environments, whereas *Colpoda inflata* thrive in dry conditions, leading to a more abundant distribution in grassland habitats (Robinson et al., 2002; Li et al., 2005).

4.3 SWC is an important determinant of soil ciliate composition and diversity

Determining the relationship between soil ciliate composition and diversity and environmental factors is key to understanding the spatiotemporal distribution patterns of the soil ciliate community (Li et al., 2013; Shi et al., 2013; Gabilondo et al., 2015). The diversity of soil ciliate was significantly affected by several water environmental factors, including VC, SWC, SOM and TN. This finding is consistent with the results of previous studies, which showed that SWC is important ecological factor for structuring ciliates community diversity, this is consistent with previous findings in Li et al. and Robinson et al. (Robinson et al., 2002; Li et al., 2013). In addition, we found that SWC seems to limit the diversity of ciliates communities. This discrepancy may be attributed to the predominantly soil moisture conditions in the Yarlung Zangbo River area during the wet season. The combination of low precipitation and high evaporation leads to reduced soil moisture, consequently resulting in decreased diversity (Gui et al., 2023; Roy et al., 2023). This also elucidates the observed pattern of diversity, wherein soil ciliate diversity is highest in wetland habitats and lowest in grassland habitats. Soil water content is the main limiting factor for the survival, reproduction and distribution of soil protozoa (Zou et al., 2009). Most soil organisms live in soil pores and their activities depend on the availability of water (Lee and Foster, 1991; Lavelle and Spain, 2001). In this study, SWC was significantly different in different seasons. Due to more rainfall in the wet season, soil water content was higher, soil ciliates could obtain sufficient water for their own metabolism, and the reproductive ability of the community was enhanced, which may lead to the survival of some species limited by soil water content, and the diversity of the community increased accordingly. Among different habitat types, SWC of wetland was significantly higher than that of the other three types (Supplementary Figure S1B), and the Shannon diversity index, Simpson dominance index and richness index of soil ciliate community of wetland type were higher than those of the other three types (Figure 2B). SWC and soil ciliate abundance and diversity index were significantly positively correlated (Figure 5), indicating that SWC differences affected the spatial and temporal distribution characteristics of soil ciliates and shaped the diversity pattern of soil ciliate community in the middle reaches of Yarlung Zangbo River.

In summary, our study provides a comprehensive examination of the spatiotemporal dynamics of soil ciliates diversity and composition in the Yarlung Zangbo River, enhancing our understanding of the environmental adaptation of ciliates inhabiting soil habitats at the high altitude of the Tibetan Plateau.

5 Conclusion

In conclusion, our study firstly investigated the seasonal and biogeographic dynamics of the soil ciliates community in the Yarlung Zangbo River. The results show that soil ciliates communities and environmental factors exhibited significant seasonal and geographic variations. The alpha diversity of soil ciliates was highest in wet and declined in dry season. Moreover, alpha diversity was much higher in the wetland than in the grassland. The co-occurrence network analysis showed that soil ciliate community was more complex in wet season than in dry season, and the stability of soil ciliate community in wet season was higher than that in dry season. The stability of soil ciliate community in wetland was higher than that in forestland, shrubland and grassland, and the anti-interference ability was stronger. ST, TN, SOM and SWC are important factors affecting the structure of soil ciliate community. By influencing the metabolic rate and nutrient acquisition of soil ciliates, the distribution pattern of soil ciliate community diversity in the middle reaches of Yarlung Zangbo River is shaped. This study may be a valuable contribution to advance the understanding of the global biogeographic diversity of soil ciliates communities.

Data availability statement

The original contributions presented in the study are included in the article/Supplementary Material, further inquiries can be directed to the corresponding author.

Author contributions

QH: Data curation, Writing–original draft, Methodology. ML: Software, Writing–original draft. TL: Resources, Writing–review and editing. SZ: Project administration, Writing–review and editing. WZ: Formal Analysis, Project

administration, Writing–review and editing. BP: Conceptualization, Data curation, Methodology, Project administration, Writing–review and editing.

Funding

The author(s) declare that financial support was received for the research, authorship, and/or publication of this article. This work was supported by the 2021 Special Funds for the Basic Research and Development Program in the Central Nonprofit Research Institutes of China [Tibetan Finance, Science and Edu-cation Guidance (2021) No. 1].

Acknowledgments

We thank Jinlong Cui and Fuyuan Mai (Tibet University) for their assistance in sample collection. We thank Qing Yang and Peng Zhang (Tibet University) for their assistance in data analysis.

Conflict of interest

The authors declare that the research was conducted in the absence of any commercial or financial relationships that could be construed as a potential conflict of interest.

Publisher's note

Supplementary material

The Supplementary Material for this article can be found online at: https://www.frontiersin.org/articles/10.3389/fenvs.2024.1360015/full#supplementary-material

References

Abraham, J. S., Sripoorna, S., Dagar, J., Jangra, S., Kumar, A., Yadav, K., et al. (2019). Soil ciliates of the Indian Delhi Region: their community characteristics with emphasis on their ecological implications as sensitive bio-indicators for soil quality. *Saudi J. Biol. Sci.* 26, 1305–1313. doi:10.1016/j.sjbs.2019.04.013

Acosta-Mercado, D., and Lynn, D. H. (2004). Soil ciliate species richness and abundance associated with the rhizosphere of different subtropical plant species. *J. Eukaryot. Microbiol.* 51, 582–588. doi:10.1111/j.1550-7408.2004.tb00295.x

Adl, M. S., and Gupta, V. S. (2006). Protists in soil ecology and forest nutrient cycling. *Can. J. For. Res.* 36, 1805–1817. doi:10.1139/x06-056

AlSayed, A., Fergala, A., and Eldyasti, A. (2018). Influence of biomass density and food to microorganisms ratio on the mixed culture type I methanotrophs enriched from activated sludge. *J. Environ. Sci.* 70, 87–96. doi:10.1016/j.jes.2017.11.017

Azam, F., Fenchel, T., Field, J., Gray, J., Meyer-Reil, L., and Thingstad, F. (1983). The ecological role of water-column microbes in the sea. *Mar. Ecol. Prog. Ser.* 10, 257–263. doi:10.3354/meps010257

Bahram, M., Hildebrand, F., Forslund, S. K., Anderson, J. L., Soudzilovskaia, N. A., Bodegom, P. M., et al. (2018). Structure and function of the global topsoil microbiome. *Nature* 560, 233–237. doi:10.1038/s41586-018-0386-6

Bamforth, S. S., Wall, D. H., and Virginia, R. A. (2005). Distribution and diversity of soil protozoa in the McMurdo Dry Valleys of Antarctica. *Polar Biol.* 28, 756–762. doi:10.1007/s00300-005-0006-4

Bello, M. G. D., Knight, R., Gilbert, J. A., and Blaser, M. J. (2018). Preserving microbial diversity. *Science* 362, 33–34. doi:10.1126/science.aau8816

Bonkowski, M. (2004). Protozoa and plant growth: the microbial loop in soil revisited. *New Phytol.* 162, 617–631. doi:10.1111/j.1469-8137.2004.01066.x

Bremner, J. M. (1960). Determination of nitrogen in soil by the Kjeldahl method. *J. Agric. Sci.* 55, 11–33. doi:10.1017/S0021859600021572

Chen, X., Li, T., Lu, D., Cheng, L., Zhou, J., and Wang, H. (2020). Estimation of soil available potassium in Chinese agricultural fields using a modified sodium tetraphenyl boron method. *Land Degrad. Dev.* 31, 1737–1748. doi:10.1002/ldr.3535

Davidson, E. C. A., Belk, E., and Boone, R. D. (1998). Soil water content and temperature as independent or confounded factors controlling soil respiration in a temperate mixed hardwood forest. *Glob. Change Biol.* 4, 217–227. doi:10.1046/j.1365-2486.1998.00128.x

Debastiani, C., Meira, B. R., Lansac-Tôha, F. M., Velho, L. F. M., and Lansac-Tôha, F. A. (2016). Protozoa ciliates community structure in urban streams and their environmental use as indicators. *Braz. J. Biol.* 76, 1043–1053. doi:10.1590/1519-6984.08615

Domonell, A., Brabender, M., Nitsche, F., Bonkowski, M., and Arndt, H. (2013). Community structure of cultivable protists in different grassland and forest soils of Thuringia. *Pedobiologia* 56, 1–7. doi:10.1016/j.pedobi.2012.07.001

Fiore-Donno, A. M., Richter-Heitmann, T., Degrune, F., Dumack, K., Regan, K. M., Marhan, S., et al. (2019). Functional traits and spatio-temporal structure of a major group of soil protists (rhizaria: cercozoa) in a temperate grassland. *Front. Microbiol.* 10, 1332. doi:10.3389/fmicb.2019.01332

Foissner, W. (1992). *Estimating the species richness of soil protozoa using the non-flooded petri dish method*. Netherlands: Springer.

Foissner, W. (1999). Soil protozoa as bioindicators: pros and cons, methods, diversity, representative examples. *Agric. Ecosyst. Environ.* 74, 95–112. doi:10.1016/s0167-8809(99)00032-8

Foissner, W. (2005). Two new "flagship" ciliates (Protozoa, Ciliophora) from Venezuela: sleighophrys pustulata and Luporinophrys micelae. *Eur. J. Protistology* 41, 99–117. doi:10.1016/j.ejop.2004.10.002

Gabilondo, R., Blanco, S., Fernández-Montiel, I., García, D., and Bécares, E. (2018). Ciliates as bioindicators of CO2 in soil. *Ecol. Indic.* 85, 1192–1203. doi:10.1016/j.ecolind.2017.11.060

Gabilondo, R., Fernández-Montiel, I., García-Barón, I., and Bécares, E. (2015). The effects of experimental increases in underground carbon dioxide on edaphic protozoan communities. *Int. J. Greenh. Gas Control* 41, 11–19. doi:10.1016/j.ijggc.2015.06.015

Geisen, S., Mitchell, E. A. D., Adl, S., Bonkowski, M., Dunthorn, M., Ekelund, F., et al. (2018). Soil protists: a fertile frontier in soil biology research. *FEMS Microbiol. Rev.* 42, 293–323. doi:10.1093/femsre/fuy006

Geisen, S., Tveit, A. T., Clark, I. M., Richter, A., Svenning, M. M., Bonkowski, M., et al. (2015). Metatranscriptomic census of active protists in soils. *ISME J.* 9, 2178–2190. doi:10.1038/ismej.2015.30

Gui, H., Breed, M., Li, Y., Xu, Q., Yang, J., Wanasinghe, D. N., et al. (2023). Continental-scale insights into the soil microbial co-occurrence networks of Australia and their environmental drivers. *Soil Biol. Biochem.* 186, 109177. doi:10.1016/j.soilbio.2023.109177

Heger, T. J., Straub, F., and Mitchell, E. A. D. (2012). Impact of farming practices on soil diatoms and testate amoebae: a pilot study in the DOK-trial at Therwil, Switzerland. *Eur. J. Soil Biol.* 49, 31–36. doi:10.1016/j.ejsobi.2011.08.007

Jousset, A., Lara, E., Nikolausz, M., Harms, H., and Chatzinotas, A. (2010). Application of the denaturing gradient gel electrophoresis (DGGE) technique as an efficient diagnostic tool for ciliate communities in soil. *Sci. Total Environ.* 408, 1221–1225. doi:10.1016/j.scitotenv.2009.09.056

Kardol, P., Reynolds, W. N., Norby, R. J., and Classen, A. T. (2011). Climate change effects on soil microarthropod abundance and community structure. *Appl. Soil Ecol.* 47, 37–44. doi:10.1016/j.apsoil.2010.11.001

Ke, S., Weiss, S. T., and Liu, Y.-Y. (2022). Dissecting the role of the human microbiome in COVID-19 via metagenome-assembled genomes. *Nat. Commun.* 13, 5235. doi:10.1038/s41467-022-32991-w

Kumar, S., and Foissner, W. (2016). High cryptic soil ciliate (Ciliophora, Hypotrichida) diversity in Australia. *Eur. J. Protistology* 53, 61–95. doi:10.1016/j.ejop.2015.10.001

Lavelle, P., and Spain, A. V. (2001). Soil organisms. *Soil Ecol.*, 201–356. doi:10.1007/978-94-017-5279-4_3

Leavit, S. W. (1998). Biogeochemistry, an analysis of global change. *Eos, Trans. Am. Geophys. Union* 79, 20. doi:10.1029/98EO00015

Lee, K. E., and Foster, R. C. (1991). Soil fauna and soil structure. *Soil Res.* 29, 745–775. doi:10.1071/sr9910745

Li, F., Xing, Y., Li, J., Al-Rasheid, K. A. S., He, S., and Shao, C. (2013). Morphology, morphogenesis and small subunit rRNA gene sequence of a soil hypotrichous ciliate, *P erisincirra paucicirrata* (C iliophora, K ahliellidae), from the shoreline of the Y ellow river, north C hina. *J. Eukaryot. Microbiol.* 60, 247–256. doi:10.1111/jeu.12029

Li, F., Zhang, Y., Altermatt, F., and Zhang, X. (2021). Consideration of multitrophic biodiversity and ecosystem functions improves indices on river ecological status. *Environ. Sci. Technol.* 55, 16434–16444. doi:10.1021/acs.est.1c05899

Li, J., Liao, Q., Li, M., Zhang, J., Tam, N. F., and Xu, R. (2010). Community structure and biodiversity of soil ciliates at dongzhaigang mangrove forest in hainan island, China. *Appl. Environ. Soil Sci.* 2010, 1–8. doi:10.1155/2010/103819

Li, Q., Mayzlish, E., Shamir, I., Pen-Mouratov, S., Sternberg, M., and Steinberger, Y. (2005). Impact of grazing on soil biota in a Mediterranean grassland. *Land Degrad. Dev.* 16, 581–592. doi:10.1002/ldr.680

Li, S., Dong, G., Shen, J., Yang, P., Liu, X., Wang, Y., et al. (1999). Formation mechanism and development pattern of aeolian sand landform in Yarlung Zangbo River valley. *Sci. China Ser. D-Earth Sci.* 42, 272–284. doi:10.1007/BF02878964

Liu, H., Ning, Y., Yang, Y., Yang, H., Wang, L., Chen, L., et al. (2022). Use of ciliate communities for monitoring ecological restoration of grain for the green in northwestern China. *Soil Ecol. Lett.* 4, 264–275. doi:10.1007/s42832-021-0105-3

Liu, W., Sun, F., Li, Y., Zhang, G., Sang, Y.-F., Lim, W. H., et al. (2018). Investigating water budget dynamics in 18 river basins across the Tibetan Plateau through multiple datasets. *Hydrol. Earth Syst. Sci.* 22, 351–371. doi:10.5194/hess-22-351-2018

Liu, Y.-X., Qin, Y., Chen, T., Lu, M., Qian, X., Guo, X., et al. (2021). A practical guide to amplicon and metagenomic analysis of microbiome data. *Protein Cell* 12, 315–330. doi:10.1007/s13238-020-00724-8

Ning, Y. Z., Yang, Y. Q., Dong, W. H., Zhang, H. R., and Ma, J. Y. (2018). Response of soil ciliate community to ecological restoration of different return patterns. *Acta Ecol. Sin.* 38, 3628–3638. doi:10.5846/stxb201710161852

Nóbrega, G. N., Ferreira, T. O., Artur, A. G., de Mendonça, E. S., Leão, R. A., Teixeira, A. S., et al. (2015). Evaluation of methods for quantifying organic carbon in mangrove soils from semi-arid region. *J. Soils Sediments* 15, 282–291. doi:10.1007/s11368-014-1019-9

Oshima, T., Shinohara, Y., Asakawa, S., and Murase, J. (2020). Susceptibility and resilience of the soil ciliate community to high temperatures. *Soil Sci. Plant Nutr.* 66, 870–877. doi:10.1080/00380768.2020.1819148

Philippot, L., Chenu, C., Kappler, A., Rillig, M. C., and Fierer, N. (2023). The interplay between microbial communities and soil properties. *Nat. Rev. Microbiol.* doi:10.1038/s41579-023-00980-5

Reth, S., Reichstein, M., and Falge, E. (2005). The effect of soil water content, soil temperature, soil pH-value and the root mass on soil CO2 efflux – a modified model. *Plant Soil* 268, 21–33. doi:10.1007/s11104-005-0175-5

Robinson, B. S., Bamforth, S. S., and Dobson, P. J. (2002). Density and diversity of Protozoa in some arid Australian soils. *J. Eukaryot. Microbiol.* 49, 449–453. doi:10.1111/j.1550-7408.2002.tb00227.x

Roy, S., Karapurkar, J., Baidya, P., Jose, M., and Bagchi, S. (2023). Community composition, and not species richness, of microbes influences decomposer functional diversity in soil. *Soil Biol. Biochem.* 187, 109225. doi:10.1016/j.soilbio.2023.109225

Schulz-Bohm, K., Geisen, S., Wubs, E. R. J., Song, C., De Boer, W., and Garbeva, P. (2017). The prey's scent – volatile organic compound mediated interactions between soil bacteria and their protist predators. *ISME J.* 11, 817–820. doi:10.1038/ismej.2016.144

Shi, X., Zhang, F., Lu, X., Wang, Z., Gong, T., Wang, G., et al. (2018). Spatiotemporal variations of suspended sediment transport in the upstream and midstream of the Yarlung Tsangpo River (the upper Brahmaputra), China. *Earth Surf. Process. Landf.* 43, 432–443. doi:10.1002/esp.4258

Shi, Y., Lu, Y., Meng, F., Guo, F., and Zheng, X. (2013). Occurrence of organic chlorinated pesticides and their ecological effects on soil protozoa in the agricultural soils of North Western Beijing, China. *Ecotoxicol. Environ. Saf.* 92, 123–128. doi:10.1016/j.ecoenv.2013.03.006

Thunjai, T., Boyd, C. E., and Dube, K. (2001). Poind soil pH measurement. *J. World Aquac. Soc.* 32, 141–152. doi:10.1111/j.1749-7345.2001.tb01089.x

Tian, P., Lu, H., Feng, W., Guan, Y., and Xue, Y. (2020). Large decrease in streamflow and sediment load of Qinghai–Tibetan Plateau driven by future climate change: a case study in Lhasa River Basin. *CATENA* 187, 104340. doi:10.1016/j.catena.2019.104340

Watson, J. M. (1943). Anabiosis in a soil ciliate. *Nature* 152, 693–694. doi:10.1038/152693b0

Wu, Y., Fang, H., He, G., Huang, L., and Wang, J. (2021). Climate-driven changes in hydrological and hydrodynamic responses in the Yarlung Tsangpo River. *J. Hydrology* 598, 126267. doi:10.1016/j.jhydrol.2021.126267

Xiong, W., Jousset, A., Guo, S., Karlsson, I., Zhao, Q., Wu, H., et al. (2018). Soil protist communities form a dynamic hub in the soil microbiome. *ISME J.* 12, 634–638. doi:10.1038/ismej.2017.171

Xu, R., Zhang, M., Lin, H., Gao, P., Yang, Z., Wang, D., et al. (2022). Response of soil protozoa to acid mine drainage in a contaminated terrace. *J. Hazard. Mater.* 421, 126790. doi:10.1016/j.jhazmat.2021.126790

Xue, G., Liu, Q., Ren, X., and Han, Y. (2004). Determination of fifteen metal elements in Cynomorium songaricum by flame atomic absorption spectrophotometry (FAAS). *Guang Pu Xue Yu Guang Pu Fen Xi* 24, 1461–1463. doi:10.1016/j.saa.2004.03.004

Yang, C., Liu, M., and Wang, X. (2023a). Species-abundance distributions of soil ciliates on different aspects in alpine meadows of gannan, China. *Eurasian Soil S. C.* 56, S325–S336. doi:10.1134/S1064229323602044

Yang, Q., Zhang, P., Li, X., Yang, S., Chao, X., Liu, H., et al. (2023b). Distribution patterns and community assembly processes of eukaryotic microorganisms along an altitudinal gradient in the middle reaches of the Yarlung Zangbo River. *Water Res.* 239, 120047. doi:10.1016/j.watres.2023.120047

You, Q., Kang, S., Wu, Y., and Yan, Y. (2007). Climate change over the Yarlung Zangbo River Basin during 1961–2005. *J. Geogr. Sci.* 17, 409–420. doi:10.1007/s11442-007-0409-y

Zhang, G., Yao, T., Xie, H., Zhang, K., and Zhu, F. (2014). Lakes' state and abundance across the Tibetan Plateau. *Chin. Sci. Bull.* 59, 3010–3021. doi:10.1007/s11434-014-0258-x

Zhang, P., Xiong, J., Qiao, N., An, R., Da, Z., Miao, W., et al. (2022). Spatiotemporal distribution of protists in the Yarlung Zangbo River, Tibetan plateau. *Water Biol. Secur.* 1, 100064. doi:10.1016/j.watbs.2022.100064

Zhang, X., Li, C., Yin, X., and Chen, P. (1999). Relation between soil animals and nutrients in the differently used forest lands. *Chin. J. Appl. Environ. Biol.* 5, 26–31. doi:10.3321/j.issn:1006-687X.1999.01.006

Zhang, Z., Hu, G., and Ni, J. (2013). Effects of topographical and edaphic factors on the distribution of plant communities in two subtropical karst forests, southwestern China. *J. Mt. Sci.* 10, 95–104. doi:10.1007/s11629-013-2429-7

Zheng, W., Wang, C., Yan, Y., Gao, F., Doak, T. G., and Song, W. (2018). Insights into an extensively fragmented eukaryotic genome: *de novo* genome sequencing of the multinuclear ciliate uroleptopsis citrina. *Genome Biol. Evol.* 10, 883–894. doi:10.1093/gbe/evy055

Zou, T., Shen, H., Ning, Y., and Ma, Z. (2009). Community characteristics of soil ciliates in the mayan forest region of xiaolong mountains, gansu. *Chin. J. Zoology* 44, 64–73. doi:10.1360/972009-782

frontiers | Frontiers in Microbiology

TYPE Original Research
PUBLISHED 14 March 2024
DOI 10.3389/fmicb.2024.1365234

OPEN ACCESS

EDITED BY
Yang Yang,
Chinese Academy of Sciences (CAS), China

REVIEWED BY
Huan Cheng,
Sichuan Agricultural University, China
Shaokun Wang,
Chinese Academy of Sciences (CAS), China

*CORRESPONDENCE
Xin Sui
✉ suixin@iwhr.com

RECEIVED 04 January 2024
ACCEPTED 05 March 2024
PUBLISHED 14 March 2024

CITATION
Luo Z, Luo J, Wu S, Luo X and Sui X (2024) Soil bacterial community in a photovoltaic system adopted different survival strategies to cope with small-scale light stress under different vegetation restoration modes. *Front. Microbiol.* 15:1365234. doi: 10.3389/fmicb.2024.1365234

Soil bacterial community in a photovoltaic system adopted different survival strategies to cope with small-scale light stress under different vegetation restoration modes

Zhongxin Luo[1,2], Jiufu Luo[1,2], Sainan Wu[1,2], Xiaolin Luo[1,2] and Xin Sui[1,2]*

[1]China Institute of Water Resources and Hydropower Research, Beijing, China, [2]National Research Center for Sustainable Hydropower Development, Beijing, China

Solar photovoltaic (PV) power generation is a major carbon reduction technology that is rapidly developing worldwide. However, the impact of PV plant construction on subsurface microecosystems is currently understudied. We conducted a systematic investigation into the effects of small-scale light stress caused by shading of PV panels and sampling depth on the composition, diversity, survival strategy, and key driving factors of soil bacterial communities (SBCs) under two vegetation restoration modes, i.e., *Euryops pectinatus* (*EP*) and *Loropetalum chinense* var. *rubrum* (*LC*). The study revealed that light stress had a greater impact on rare species with relative abundances below 0.01% than on high-abundance species, regardless of the vegetation restoration pattern. Additionally, PV shadowing increased SBCs' biomass by 20–30% but had varying negative effects on the numbers of Operational Taxonomic Unit (OTU), Shannon diversity, abundance-based coverage estimator (ACE), and Chao1 richness index. Co-occurrence and correlation network analysis revealed that symbiotic relationships dominated the key SBCs in the *LC* sample plots, with Chloroflexi and Actinobacteriota being the most ecologically important. In contrast, competitive relationships were significantly increased in the *EP* sample plots, with Actinobacteriota having the most ecological importance. In the EP sample plot, SBCs were found to be more tightly linked and had more stable ecological networks. This suggests that EP is more conducive to the stability and health of underground ecosystems in vulnerable areas when compared with LC. These findings offer new insights into the effects of small-scale light stress on subsurface microorganisms under different vegetation restoration patterns. Moreover, they may provide a reference for optimizing ecological restoration patterns in fragile areas.

KEYWORDS

photovoltaic, small-scale light stress, soil bacterial communities, vegetation restoration, survival strategies, semi-arid vulnerable areas

1 Introduction

The atmospheric level of the main greenhouse gas (CO_2) has reached new record highs in 2021. It has increased by more than 49% from pre-industrial levels (278.3 ppb) to 415.7 ppb, primarily due to emissions from the combustion of fossil fuels and cement production, according to the Global Greenhouse Gas Bulletin from the World Meteorological Organization (WMO). Carbon neutrality is becoming a global consensus for green development (He et al., 2023). Renewable energy is a crucial strategy for reducing CO_2 emission over time (Chen et al., 2019). Solar energy is a clean and renewable energy source with numerous advantages, including zero carbon emissions, no liquid or solid waste, and widespread availability (Liu et al., 2019). Therefore, solar photovoltaic power (SPP) generation technology is rapidly becoming one of the major carbon reduction technologies (Choi et al., 2020).

Global installed solar photovoltaic (PV) capacity has rapidly expanded, reaching 843.086 GW in 2021. According to the International Energy Agency, global installed solar power capacity is expected to approach 1,700 GW by 2030 (He et al., 2023). However, land constraints will be a major limitation to PV expansion. Arid and semi-arid regions are vast and rich in solar energy resources, making them ideal for PV application. Numerous SPP stations have been constructed in these areas due to the rapid expansion of the PV industry (Liu et al., 2019).

The deployment of large-scale SPP will have a significant impact on the local ecosystem by affecting environmental factors such as the temperature, photosynthetically active radiation, precipitation, evaporation, wind speed, surface albedo, soil heat flux, humidity and temperature, etc. (Broadbent et al., 2019; Yue et al., 2021a). Solar panels partially shading have been shown to delay bloom and increase floral abundance for pollinators in a dryland, agri-voltaic ecosystem (Graham et al., 2021). Nonetheless, most studies have focused on the impact of PV on above-ground macro-ecosystems, and the impact of PV on below-ground micro-ecosystems has not been well studied.

Bacteria are the most prevalent type of soil microorganism and play a crucial role in the material cycling and energy flow. Due to their abundance and high reproductive capacity, bacteria are frequently used as sensitive indicators to evaluate changes in soil ecosystems and characterize soil quality (Trivedi et al., 2016). Light can affect soil temperature, moisture, and nutrient cycling, thus leading to environmental heterogeneity that can impact the composition, distribution, and functional features of soil bacterial communities (SBCs) (Del Pino et al., 2015; Helbach et al., 2022). However, investigations into the effects of light on soil microbial communities have primarily focused on large-scale circumstances, such as the impact of light differences caused by latitude gradients on soil microorganisms (Maestre et al., 2015; Ochoa-Hueso et al., 2018). There are only a few studies on how small-scale light heterogeneity caused by PV arrays affects soil microbial communities, particularly in karst regions with very sensitive geology and heavy human disturbance. A study conducted by Wu et al. (2016) investigated the impact of fluoride and chloride pollution on microbial communities in soils surrounding a solar PV facility. The results indicated a strong correlation between the population size and total biological activity of the SBCs and different levels of fluoride and chloride pollution. The analysis of microbial communities between and under various types of PV panels at Gonghe PV power station, Qinghai Province, has allowed researchers to examine the community abundance, diversity, structure, and distribution characteristics of soil bacteria and archaea. The conclusion drawn from this analysis is that PV stations have minimal impact on the community structure of soil bacteria and archaea (Wu C. et al., 2022; Wu W. et al., 2022; Yuan et al., 2022). However, none of the previous studies have examined the response of soil microbial communities to small-scale light gradients caused by shading from PV modules under different vegetation restorations, nor have they investigated the vertical distribution of bacterial communities. The impact of light changes on soil microbial communities may vary depending on the land use type and vegetation restoration measures employed. This is due to variations in the structure, richness, and diversity of soil microbial communities (Qiang et al., 2015; Lu et al., 2022). Deeper soil microbes play a crucial role in soil formation, nutrient cycling, and carbon storage capacity (Li et al., 2022). However, it is currently unknown how microbial taxa respond to varying soil depths and vegetation restoration in the PV field located in the karst areas of southwest China.

In view of this, this study systematically investigated the influence of light heterogeneity caused by PV panels shading on the diversity and composition of SBCs at different depths (0–20 cm, 20–40 cm, and 40–60 cm) under two vegetation restoration patterns, i.e., *Euryops pectinatus* (*EP*) and *Loropetalum chinense* var. *rubrum* (*LC*), and explored the survival strategies and key driving factors of SBC. The objectives of this study were: (1) to compare the response of SBCs' composition and diversity to small-scale light stress under different vegetation restoration patterns; (2) to explore the network relationship and survival strategy of SBCs at different depths in the sample plots under different vegetation restoration patterns; and (3) to analyze the key driving factors of the SBCs through correlation network analysis and the Mantel test. This research aims to provide new insights into the effects of small-scale light gradient variation on microorganisms and provide a reference for ecological restoration models in vulnerable areas.

2 Materials and methods

2.1 Study sites

This study is carried out at the PV Demonstration Base (103° 8′ 30.56″ E, 26° 9′ 55.70″ N) in Dongchuan District (Yunnan, southwest of China) in the semi-arid, vulnerable areas. It has an altitude of about 1,280 m, is in the subtropical monsoon climate zone, and has a characteristic karst terrain. The average annual temperature, rainfall, and evaporation are 14.9°C, 1000.5 mm, and 1856.4 mm, respectively. This zone has a distinct rainy season (from May to September) and a dry season (from October to April). Additionally, the area is rich in solar energy resources, with an annual sunshine duration of over 2,300 h and an annual solar radiation of over 5,000 MJ/m^2. This PV Demonstration Base covers an area of approximately 18,000 m^2 with an installed capacity of 1.04 MW. It was officially commissioned in 2020. For the PV arrays, the highest point of the front eaves and rear eaves is 2.5 m and 4.5 m above the ground, respectively. The width of each row of PV panels is 4.2 m, with a tilt angle of 28°and a distance of 2.6 m between two rows. The soil type at the SPP site is predominantly red soil. During the construction process, the soil in the SPP was artificially leveled. After construction, the affected areas

were replanted with native plants to mitigate the degradation of the fragile ecosystem.

2.2 Sample collection and pretreatment

To account for the effects of PV shading on SBCs, the space between two rows of PV panels was considered the control area (CK), and the spaces in the front eaves, back eaves, and under the PV panels were referred to as FP, RP, and UP, respectively. Soil samples were taken from two artificial vegetation plots, i.e., *EP* and *LC*, in October 2021. The litter layer was discarded, and soil samples were collected randomly at the 0–20 cm, 20–40 cm, and 40–60 cm levels from five subplots in each line. The three soil layers, from top to bottom, denoted as D1, D2, and D3, respectively (Figure 1). All the samples were collected at five random sampling sites with three replicates for each location and layer. Samples from the same layer and location in each vegetation plot were mixed and sieved using a 2 mm mesh sieve. Each soil sample was divided into two subsamples: one was air-dried and used for physicochemical analyses, while the other was stored and transported at 4°C and used as soon as possible for soil DNA extraction and high-throughput sequencing.

2.3 Soil property measurements

In the flat area of the PV field, a light sensor (FM-G2A, China) was used to monitor the illumination intensity of the top layer of vegetation in 4 locations between and under the PV modules, and temperature and humidity sensors (FM-3A, China) buried at different depths were used to monitor soil temperature and humidity. The heat flux probe (FM-R5, China) is used to monitor changes in soil heat flux in the surface layer of the soil. The monitoring period was the whole month of October 2021, and the monitoring frequency was 30 min each time.

The soil properties, such as soil humidity, pH, electrical conductivity (EC), total nitrogen (TN), total carbon (TC), microbial biomass carbon (MBC), water-soluble organic carbon (WSOC), available phosphorus (AP), and available potassium (AK), are tested with reference to the corresponding standards or previous studies (Lu et al., 2014; Xiao et al., 2017; Pang et al., 2018).

2.4 DNA extraction and high-throughput sequencing

Total soil DNA was extracted using a Fast®DNA SPIN Kit (MP Biomedicals, Santa Ana, CA, United States) and the method described in the instructions. DNA purity was assessed by agarose (1.0%) gel electrophoresis, and DNA concentrations were quantified using a Nanodrop-2000 device (Thermo Scientific, United States). Universal primers 515F (5′-GTGCCAGCMGCCGCGG-3′) and 909R (5′-CCGTCAA TTCMTTTRAGTTT-3′) were used to amplify the V4-V5 hypervariable regions of the 16S rRNA genes by PCR (95°C for 3 min, followed by 35 cycles at 95°C for 30 s, annealing at 55°C for 30 s, and extension at 72°C for 45 s and then a final extension at 72°C for 10 min) (Li et al., 2014). The PCR product was visually confirmed by agarose gel electrophoresis before purification using AMPure XP beads (Beckman Coulter Inc., Brea, CA, United States). After purification, the PCR products were used to construct libraries and sequenced at Major Bio on an Illumina MiSeq platform (Illumina, United States).

Fastp version 0.20.0 was employed to demultiplex the raw 16S rRNA gene sequencing reads, and FLASH version 1.2.7 was utilized

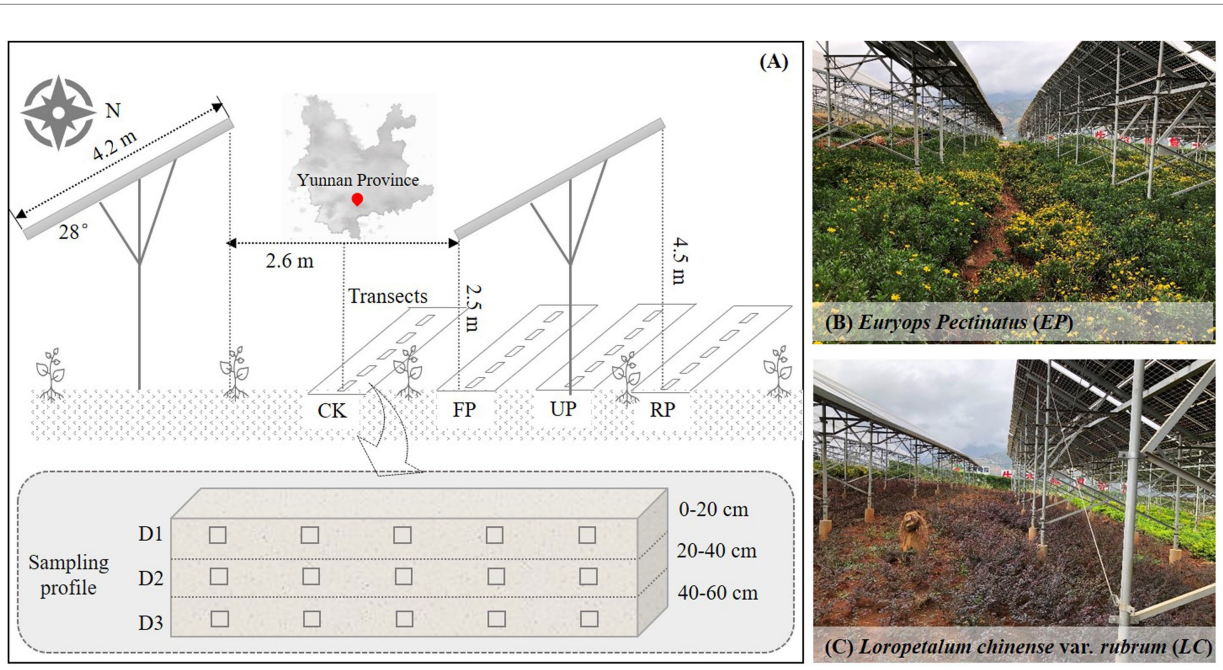

FIGURE 1
(A) Schematic diagram of experimental sampling position in the study area, CK: intervals of PV panels, FP: front of panel eaves, RP: rear of panel eaves, UP: under neath of PV panels; **(B)** *Euryops pectinatus* (*EP*) sample plot; **(C)** *Loropetalum chinense* var. *rubrum* (*LC*) sample plot.

to merge them. UPARSE version 7.1[1] was used to group operational taxonomic units (OTUs) with a 97% similarity criterion and to detect and remove chimeric sequences. RDP Classifier version 2.2 was applied to compare the taxonomy of each OTU representative sequence to the 16S rRNA database (e.g., Silva v138) with a confidence threshold of 0.7 (Li X. et al., 2023). OTUs were eliminated if they did not contain three reads in at least two samples or were not assigned to a bacterial phylum (Yang et al., 2022). Finally, 2,946 OTUs were used for further analysis.

2.5 Statistical analysis

One-way ANOVA and Tukey's test were applied to the results for the soil properties. The *OTU table* package and the *vegan* package in R software (version 3.5.1) were used to calculate the alpha diversity, and the least significant difference (LSD) was employed to compare the variations in diversity between different subgroups. The significance of changes in the structure of SBCs was examined using non-metric multidimensional scaling (NMDS) analysis, the Wilcoxon rank-sum test, and the Kruskal-Wallis H test, all performed using various functions in the *vegan* package. Correlation analyses and Mantel tests were carried out using the *vegan* package and *ggplot2* package in the R software to examine the association between bacterial diversity and abundance and various environmental factors (R Core Team, 2018). Based on the Random Matrix Theory (RMT), network analysis was performed using the molecular ecological network analysis pipeline. Collinear network analysis was used to show the relationships between different ecological groups and to ensure that only OTU sequences that co-occurred in more than 50% of the sample sites were included in the analysis. The collinear network was constructed using edges with statistical significance ($p < 0.05$). Gephi software was used for visual inspection of the collinear network as well as a computational study of the network properties (Liao et al., 2022).

3 Results

3.1 Variation of microhabitat in the PV field

The light intensity at different locations was markedly different ($p < 0.05$) in the order: CK > FP > RP > UP, indicating that the shading of the PV panels significantly reduced the light intensity and showed a gradient change at different locations (Figure 2A). The soil temperature in different soil layers showed a similar trend, first increasing and then decreasing along the light gradient and being highest at the FP position (Figure 2B). The soil heat fluxes in the shaded area of the PV panels all increased significantly, and the fluctuation range was noticeably larger in FP and RP (Figure 2C). The soil humidity at different depths also showed a similar trend, which followed an N-shaped trend with the light gradient and increased considerably at FP and UP positions (Figure 2D).

The soil properties exhibited varying trends along the light gradient under two vegetation restoration patterns, as shown in Supplementary Table S1. TC, WSOC, pH, EC, AK, and AP were not notably different ($p > 0.05$), while TN, NO_3^--N, MBC, and soil humidity exhibited considerable differences ($p < 0.05$). TN was found to be highest in the RP location of the *EP* sample plots at 1.18 g/kg and was significantly different from the RP and UP locations of the *LC* sample plots. The NO_3^--N content decreased in the *EP* sample site as the light intensity decreased. The difference between the CK and UP sites was considerable. Additionally, it decreased significantly in the RP and UP locations of the *LC* plot ($p < 0.05$). The soil humidity in this study area ranged from 13.53 to 21.25%. The average soil humidity in the shaded area of the PV panels is about 10% higher than the CK position. The variation trend observed was consistent with the long-term monitoring of soil humidity by the meteorological probe. The FP and UP positions showed a pronounced increase. The MBC was lowest at the CK location in both planted sample plots. The PV shadowing boosted SBCs' biomass by 20–30%, indicating a significant increase in the microbial biomass of the soil due to the PV shading.

3.2 Response of SBCs' composition to environmental heterogeneity

Following quality filtering, high-throughput sequencing was performed on distinct soil bacterial 16S rRNAs in the PV field, resulting in 979,402 clean reads. The number of genuine high-quality bacterial reads ranged from 32,978 to 47,325, with a corresponding library coverage rate varying from 98.0 to 98.6%. This indicated that the sample libraries in this investigation contained the majority of bacterial taxa and accurately reflected the structural makeup of the bacterial community in the samples. The SBCs comprised 12 prominent phyla, each with a relative abundance of over 2% (Figure 3A). The five most abundant phyla were Actinobacteriota, Proteobacteria, Acidobacteriota, Chloroflexi, and Gemmatimonadota, which accounted for 24.38–48.33%, 11.79–25.31%, 8.05–22.00%, 6.94–17.21%, and 1.85–7.51% of total reads, respectively.

The Venn diagram reveals that 608 genera occurred in both the *LC* and *EP* sample plots, 16 genera were endemic to the *LC* sample plot with relative abundances ranging from 0.027 to 0.564%, and 8 genera were endemic to the *EP* sample plot with relative abundances ranging from 0.004 to 0.244% (Figure 3B). In the LC sample plot, 463 genera co-occurred in different light gradients. The CK had 7 endemic genera, while the FP, RP, and UP had 5, 5, and 9 endemic genera, respectively (Figure 3C). In the *EP* sample plot, 437 genera co-occurred in different light gradients. The CK had 7 endemic genera, while the FP, RP, and UP had 7, 8, and 7 endemic genera, respectively (Figure 3D).

At the phylum level, Proteobacteria, Planctomycetota, and Myxococcota demonstrated notable variations ($p < 0.05$) between the two vegetation sample plots (Supplementary Figure S1). The abundance of Proteobacteria was much higher in the *LC* sample plots than in the EP sample plots, while Planctomycetota and Myxococcota showed the opposite trend. Gammaproteobacteria ($p < 0.05$), Planctomycetes ($p < 0.01$), and Anaerolineae ($p < 0.001$) exhibited significant differences between the two vegetation sample plots. The *LC* sample plots had a significantly higher abundance of Gammaproteobacteria compared to the *EP* sample plots. Conversely, Planctomycetes and Anaerolineae showed the opposite pattern (Figure 3E). The Kruskal-Wallis H test revealed significant differences in the abundance of Proteobacteria and Bacteroidota at varying depths

1 http://drive5.com/uparse/

10.3389/fmicb.2024.1365234

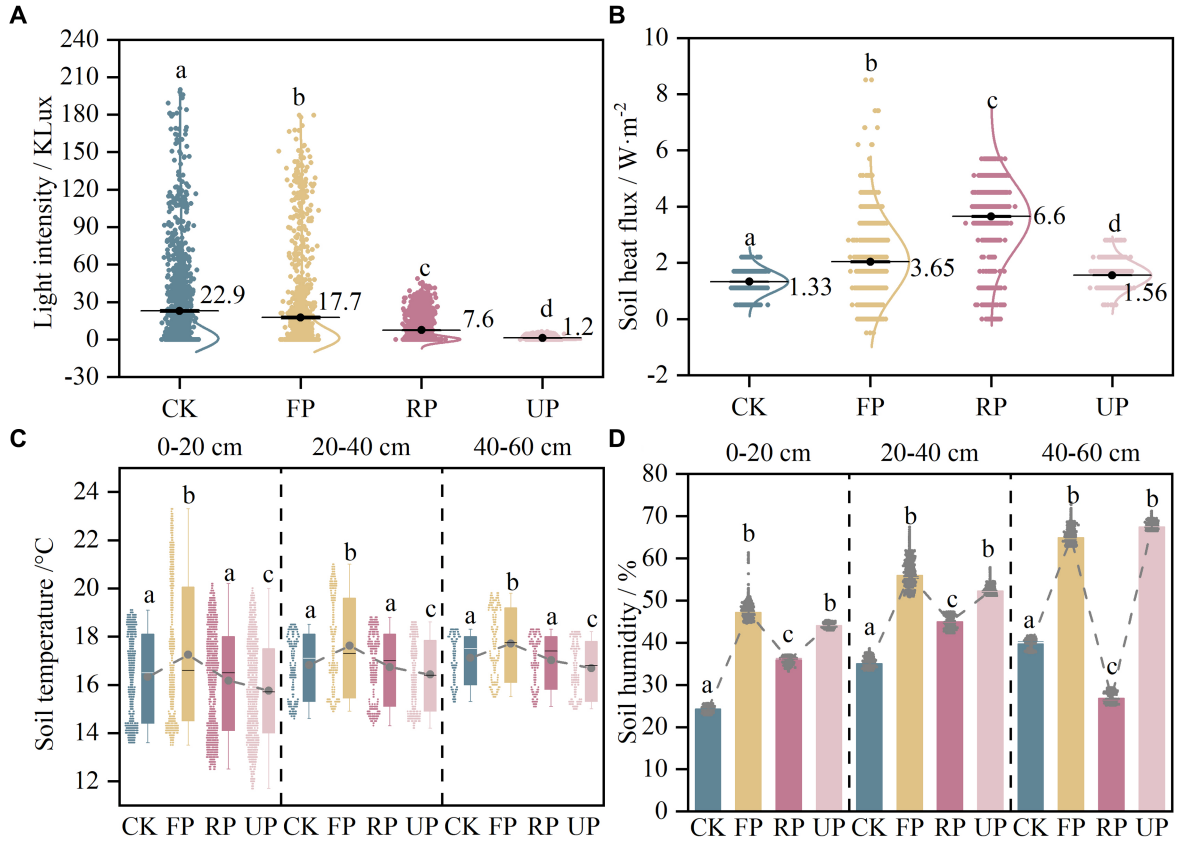

FIGURE 2
The variation of field monitoring parameters in different positions of the PV field: **(A)** light intensity; **(B)** soil heat flux; **(C)** soil temperature; **(D)** soil humidity. Different lowercase letters indicate significant difference among different location in the PV field (one-way ANOVA, $p < 0.05$).

in the *EP* plots, and Chloroflexi, Gemmatimonadota, and Methylomirabilota in the *LC* plots (Supplementary Figure S1). This highlighted that vegetation type can not only influence the composition of the SBCs in the surface layer through differences in litter quality and quantity, but also the distribution of soil bacteria in the deep layer through root exudates and their effects on soil structure.

Figures 3F,G shows Kruskal-Wallis H test bar plots for two sample plots at phylum and class levels along the light gradient. In the *LC* sample plot, Spirochaetota was only present in the RP position, indicating a strict light requirement. Polyangla varied significantly with the light gradient at the class level ($p < 0.05$), while Spirochaetiaj occurred only at the RP position with a relative abundance of less than 0.01%. The *EP* sample plot showed a decrease in the relative abundance of Firmicutes with increasing light gradient. In the PV shade area, Sumeriaeota had a 30 to 90% lower relative abundance compared to CK, while MBNT15 had the highest relative abundance at the RP position. At the class level, Bacilli, Mycococcia, Chthonomonadetes, Sumerlaeia, and norank_ MBNT15 revealed substantial variations with light gradients ($p < 0.05$).

3.3 Response of alpha and beta diversity of SBCs to environmental heterogeneity

The OTU numbers, Shannon diversity index, ACE evenness index, and Chao1 richness index were calculated to compare the α-diversity of SBCs. The results revealed inconsistent changing patterns along the light gradient in the LC and EP sample plots (Figure 4A). Although the α-diversity index of the *EP* plot was higher than that of the *LC plot*, there was no significant difference ($p > 0.05$). There were no noticeable changes in the numbers of OTU and Shannon diversity index across sampling sites in both *EP* and *LC* sample plots. In the EP sample plots, PV shade reduced both the OTU numbers and Shannon diversity index of SBC compared to CK. However, there was no clear pattern of influence of PV shading in *LC* sample plots. Both the ACE and Chao1 indices decreased gradually as the light gradient decreased, but there was no significant difference between different sampling locations within the same sample plots ($p > 0.05$). It is worth noting that PV shading increased soil microbial biomass by 20–30% (MBC content in Supplementary Table S1), but the OTU numbers, Shannon diversity, ACE and Chao1 richness index decreased to varying degrees.

The bacterial community diversity was reasonably affected by different sampling depths, as shown in Supplementary Figure S2. In the *LC* sample plot, the layer of 20–40 cm layer exhibited the highest bacterial richness and diversity, while in the *EP* sample plot, the bottom layer (40–60 cm) had the highest bacterial richness and diversity. The ACE and Chao1 indices in the layer of 40–60 cm differed significantly between the *LC* and *EP* sample plots ($p < 0.05$). NMDS analysis was conducted on the composition of SBCs at different light gradients in two vegetation plots based on Bray-Curtis distance (Figures 4B,C). The composition of SBCs changed considerably ($p = 0.003$) between the *LC* and *EP* plots, but not significantly ($p = 0.117$) at different light gradients. This indicates that the influence of light intensity on SBC's composition

10.3389/fmicb.2024.1365234

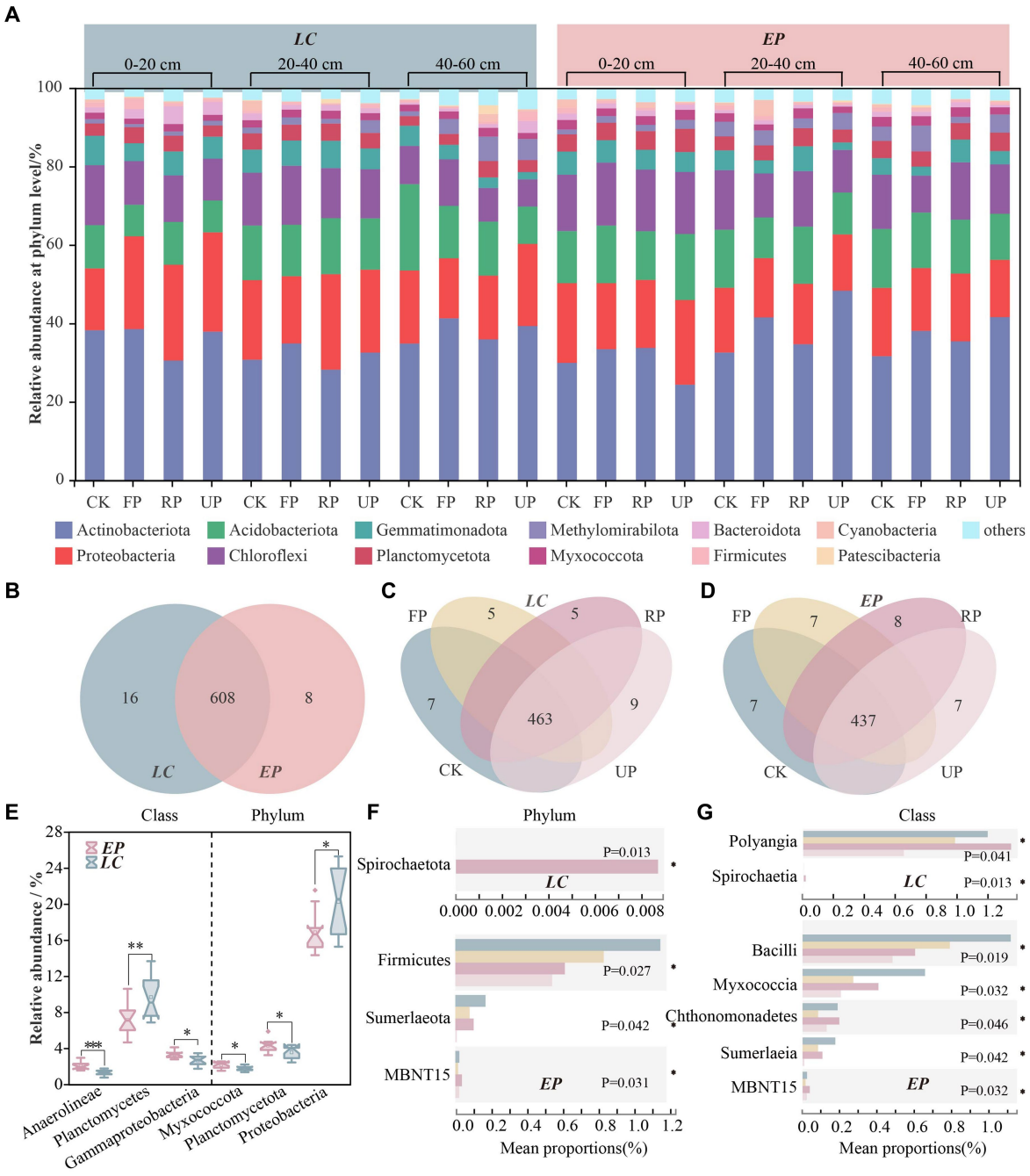

FIGURE 3
The composition of SBC at the phylum level in two vegetation sample plots **(A)**; Venn diagram at the genus level between *LC* and *EP* sample plots **(B)**; Venn diagrams at genus level along four light gradients of *LC* **(C)** and *EP* **(D)**; A Wilcoxon Rank-Sum Test box plot was used to compare LC and EP plots at the phylum and class level, and only bacteria taxonomic with significant differences are shown **(E)**; A Kruskal-Wallis H test bar plot along light gradient in LC and EP plots at phylum level **(F)** and class level **(G)**.

differed significantly under two vegetation restoration patterns. The bacterial community showed less variability in the layers of 0–20 cm and 20–40 cm compared to the layer of 40–60 cm, particularly in the *LC* sample plot. The vertical distribution of SBCs was most noticeable at the CK site in the *LC* sample plot, while in the *EP* sample plot, the difference was greatest at the UP position. Furthermore, the sample points that represent the composition of SBCs at various locations and depths were more closely clustered in the *EP* sample plot than in the *LC* sample plot.

3.4 Comparison of the co-occurrence networks of SBCs

The co-occurrence of SBCs in two vegetation plots was described using the molecular ecological network (MEN) based on random matrix theory (RMT) (Figure 5A). Networks for *LC* (755 nodes connected by 1,744 links) and *EP* were built in various sizes (779 nodes connected with 1,941 links). The created MEN had modular

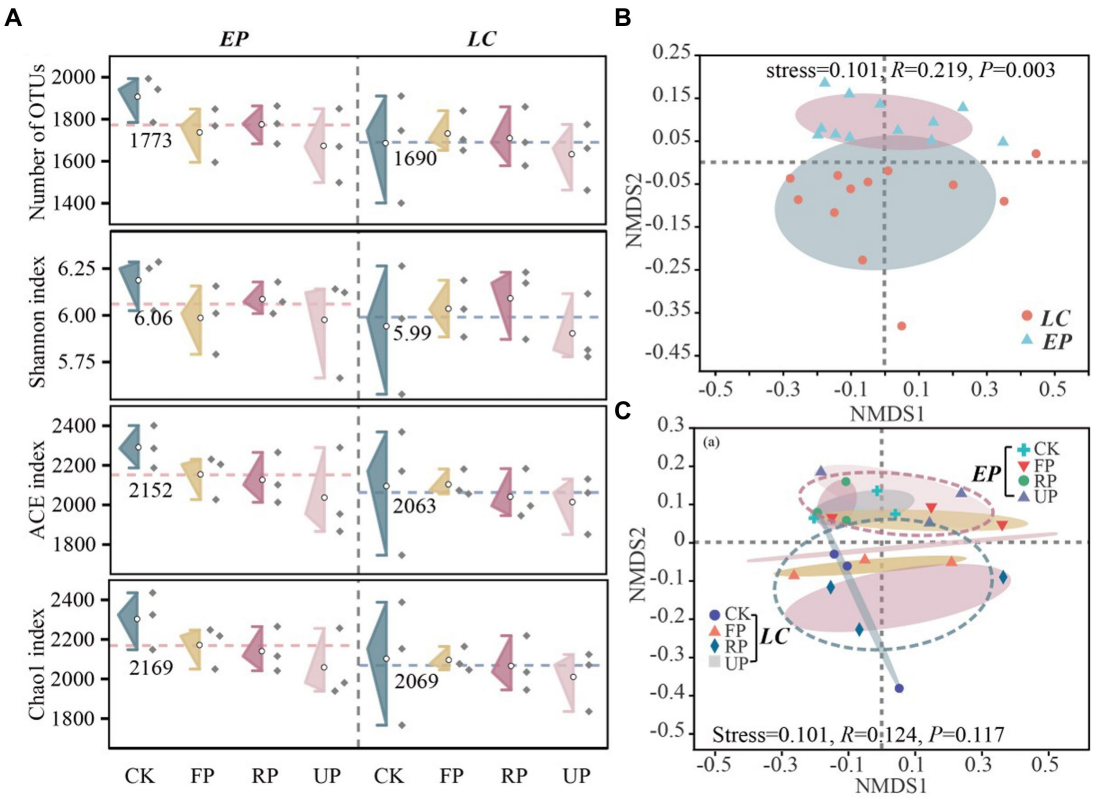

FIGURE 4
(A) Alpha diversity analysis of SBC in different soil location types and layers in two vegetation sample plots. The number of OTUs, Shannon diversity index, ACE evenness index, and Chao1 richness index are shown, with the red and blue dotted lines representing the average diversity index of EP and LC plots, respectively. **(B)** Beta diversity of bacterial community based on Bray-Curtis distance (on OTU level) analyzed by NMDS in two vegetation sample plots, and **(C)** different location along a light gradient.

architectures, as evidenced by modularity values higher than 0.4 in both the LC and EP sample plots (Newman, 2003). The integration of one network module's nodes suggested that the group was tightly knit, with few nodes affiliated with it outside of the module (Williams et al., 2014). The average path distance in the EP plots was smaller, indicating that the nodes were more closely connected to networks (Table 1). However, the *LC* and *EP* plots did not show any discernible difference in betweenness or degree (one-way ANOVA, $p > 0.05$) (Figure 5B).

In the *LC* sample plot, the core OTUs (degree > 30) were mainly primarily composed of Chloroflexi, Methylomirabilota, Actinobacteriota, Proteobacteria, Gemmatimonadota, and Acidobacteriota. Among these, the ecological niches of Chloroflexi and Actinobacteriota were the most significant, and all species exhibited positive correlations, primarily in symbiotic relationships. In the *EP* sample plot, the core OTUs (degree > 30) were mainly Actinobacteriota, Acidobacteriota, Methylomirabilota, Gemmatimonadota, Plancto mycetota, and Proteobacteria. Actinobacteria had the most ecological importance. Planctomycetota and Actinobacteriota became more important in the *EP* plot comparison to the *LC* plot, while Chloroflexi became less important (Figure 5C).

The network nodes were classified into four groups using the fast-greedy approach to determine the primary populations that impact the co-occurrence of SBCs. These groups include network hubs ($Z_i > 2.5$, $P_i > 0.62$), module hubs ($Z_i > 2.5$, $P_i < 0.62$), peripherals ($Z_i < 2.5$, $P_i < 0.62$) and non-hub connectors ($Z_i < 2.5$, $P_i > 0.62$). The classification was based on the within-module connection (Z_i) and among-module connectivity (P_i). The module hubs were classified as either provincial hubs ($Z_i > 2.5$, $P_i < 0.3$) or connectors ($Z_i > 2.5$, $0.3 < P_i < 0.62$) based on the value of P_i.

The Z_i-P_i plot reveals that approximately 98.20% of the OTUs were peripheral, implying that most OTUs had fewer linkages outside of their modules. The majority of the peripherals ($P_i = 0$) in the *LC* (75.2%) and *EP* (80.9%) plots were exclusively connected within their respective modules. Both the *EP* and *LC* sample plots had 14 module hubs, most of which belonged to Actinobacteriota. In the *EP* sample plot, there was only one connector hub belonging to Proteobacteria, while in the *LC* sample plot, there were three connector hubs, one belonging to Acidobacteriota and two belonging to Actinobacteriota. As keystone taxa, these hubs are crucial for maintaining the structure and functional integrity of the microbial community (Wu et al., 2023). Additionally, there were 14 non-collector connectors in the *EP* sample plot, five of which belonged to Chloroflexi. In comparison, there was only one non-collector connector in the LC sample plots, belonging to Gemmatimonadota (Figure 5D).

3.5 Key environmental drivers of SBCs

The Mantel test and correlation analysis were used to examine the relationships between soil properties and dominant SBCs (Figure 6A). The results showed that light intensity had a significant positive

10.3389/fmicb.2024.1365234

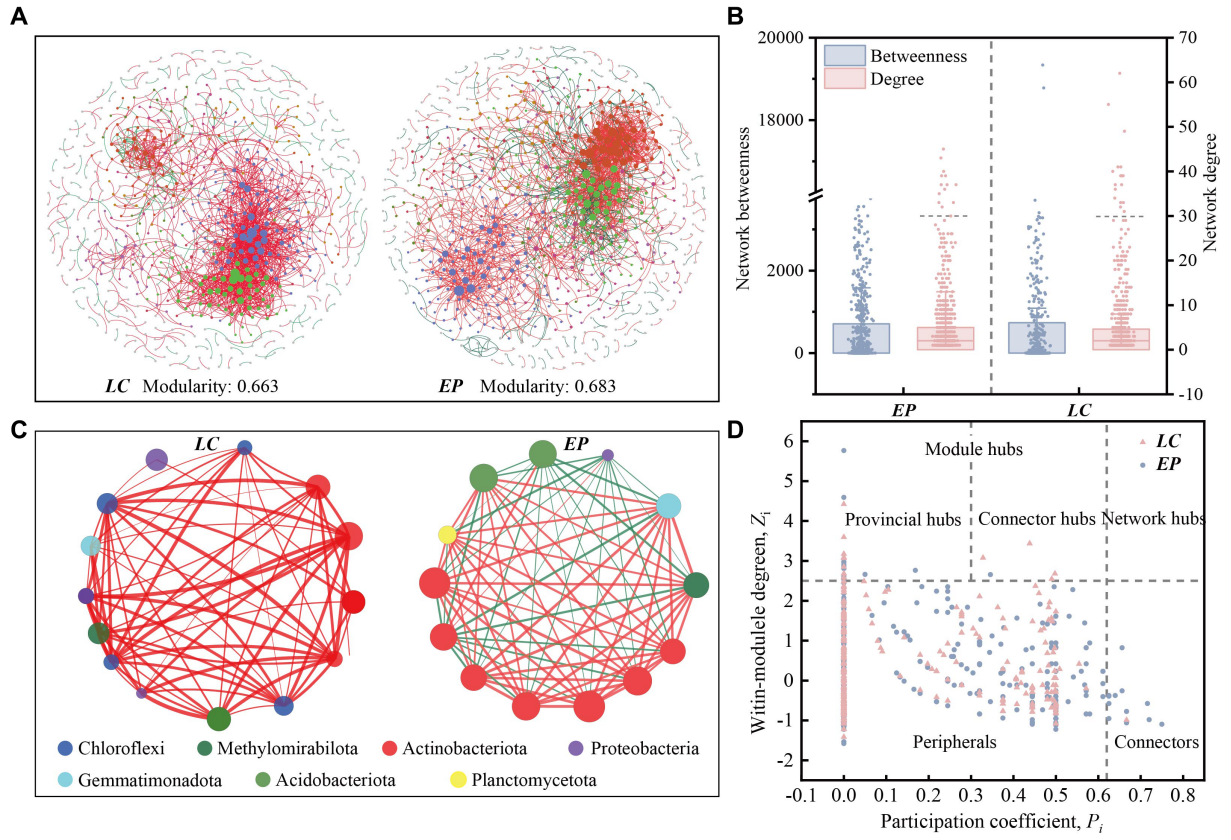

FIGURE 5
(A) Co-occurring network of SBCs at OTU level in the *LC* and *EP* plots. The nodes in network are colored by modularity class. A group of OTUs in one module indicates that these OTUs have more interactions among themselves and fewer associations with other modules. The node sizes reflect their degree of connection; **(B)** Betweenness and node-normalized degree of bacterial networks; **(C)** Network structures of the core genus (Degree >30) in the *LC* and *EP* plots. The nodes in network are colored by phylum. Red edges indicate significant positive Spearman's correlations, while green edges indicate significant negative Spearman's correlations; **(D)** The Zi-pi plots of OTUs in bacterial co-occurrence networks are based on topological interactions.

TABLE 1 **Bacterial network properties under two vegetation restoration modes.**

Network parameter		*LC*	*EP*
Node	Number of nodes	754	779
	Average degree	4.626	4.983
	Average path distance	6.692	4.978
	Average clustering coefficient	0.305	0.209
	Modularity	0.663	0.683
Edge	Number of edges	1744	1941
	Negative (proportion)	175 (10.0%)	362 (18.7%)
	Positive (proportion)	1,569 (90.0%)	1,579 (81.3%)

correlation with TN, TC, and NO_3^--N, as well as AP, but a negative correlation with MBC in the *LC* sample plot.

Actinobacteriota was significantly correlated with NO_3^--N, AK, and EC; Chloroflexi and Gemmatimonadota were both strongly correlated with AP, and Proteobacteria was highly associated with TC. In the *EP* sample plots, the soil temperature and humidity exhibited a marked negative correlation with soil nutrients. The interaction between dominant bacteria and environmental factors was considerably enhanced, and light intensity was also significantly negatively correlated with MBC. Actinobacteriota showed significant correlation with TC, WSOC, AP, and AK, whereas Chloroflexi was exhibited a strong correlation with TN, TC, and MBC. Collectively, soil nutrients were the main drivers of soil dominant community changes.

Two-factor correlation analysis (Figure 6B) revealed that the core species of soil bacteria had a significant negative correlation with soil nutrients in the *EP* sample plots Conversely, in the *LC* sample plot, they were mainly positively correlated, and light intensity was significantly positively correlated with *Gaiellales*.

4 Discussion

4.1 Effects of shading of the PV panels on soil properties

The large-scale construction of PV panels can cause heterogeneity in environmental factors, such as light, precipitation, and wind speed. This can lead to microhabitat climate changes that may affect ecosystems (Li C. et al., 2023; Li X. et al., 2023). The study found that light intensity varied significantly ($p < 0.05$) across different locations, with the order

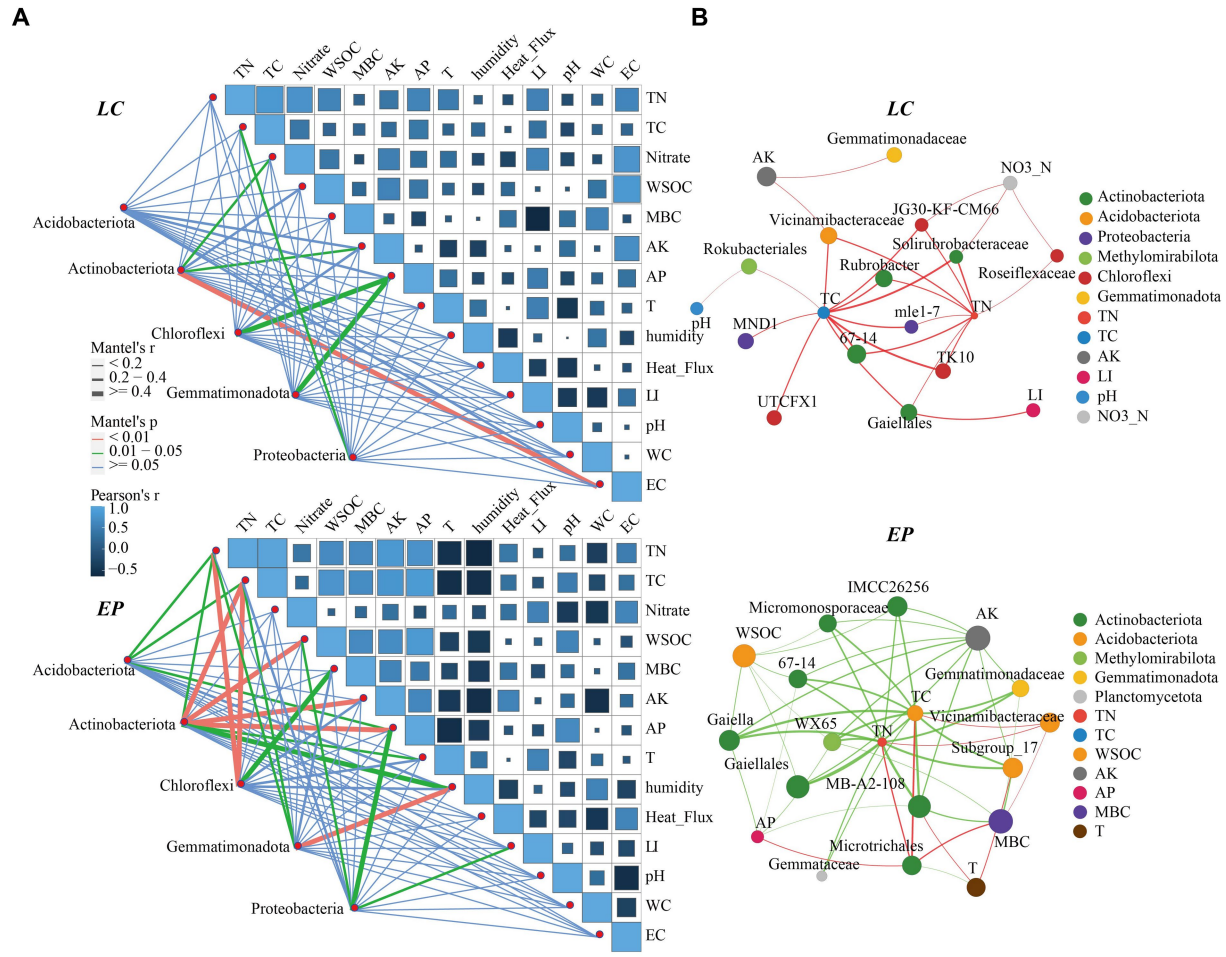

FIGURE 6
(A) Correlation analysis and the Mantel test of soil properties and dominant SBCs in the genus *LC* and *EP* plots; **(B)** Two-factor correlation network analysis of core genera (Degree > 30) and environmental factors in the *EP* and *LC* plots; TC, total carbon; TN, total nitrogen; WSOC, water-soluble organic carbon; MBC, microbial carbon; AK, available potassium; AP, available phosphorus; EC, electric conductivity. LI, Light Intensity.

being CK > FP > RP > UP. PV panel shielding reduces the amount of solar radiation by limiting the duration and area of direct exposure to the ground. Additionally, fixed-axis PV modules have varying angles, causing changes in the duration and amount of solar radiation at different locations (Marrou et al., 2013; Broadbent et al., 2019; Wu C. et al., 2022; Wu W. et al., 2022). The soil humidity in FP is higher due to the pooling effect of precipitation caused by PV modules (Choi et al., 2020). In the UP position, the shielding effect of PV panels reduces wind speed and solar radiation, increasing air humidity and hindering water evaporation to some extent (Amaducci et al., 2018). Meanwhile, the shading effect of vegetation can effectively reduce surface water evaporation and improve soil water holding capacity (Liu et al., 2019; Yue et al., 2021b).

Soil characteristics are widely acknowledged as crucial indicators of soil fertility and their ability to sustain plant production has been well documented (Zhao et al., 2019). Previous studies have demonstrated that the construction of PV power plants can alter the microclimate environment for vegetation growth by directly or indirectly impacting local airflow, precipitation, solar radiation, air temperature, humidity, and other factors. These changes can indirectly affect soil nutrient conditions (Armstrong et al., 2016; Yue et al., 2021a). Soil humidity is an environmental variable that combines the effects of climate, vegetation, and soil on the dynamics of water-stressed ecosystems. Soil humidity fluctuations can significantly impact plant development in PV fields, especially in dry areas where even small changes in water availability can have major effects on plant growth (D'Odorico et al., 2007). As a consequence, depending on the water requirements of the plants, the environmental heterogeneity provided by PV modules may offer certain advantages (Del Pino et al., 2015). MBC is the active component of the soil organic pool, which is an easily accessible pool of nutrients in the soil and the driving force for organic matter decomposition and nitrogen mineralization, acting as a key source and reservoir in the carbon and nitrogen cycling processes (Lu et al., 2022). Soil MBC is frequently used to estimate the magnitude of soil microbial biomass and is important for soil organic matter and nutrient cycling (Chen et al., 2023). In both vegetation restoration models, shading by PV panels increased the MBC content, i.e., the biomass of microorganisms in the below-ground microbial system. This might be because soil microorganisms in karst areas are prone to high temperature and drought stress, and shading by PV modules decreases soil temperature and increases soil humidity, and then the SBC may thrive and reproduce under optimal temperature and moisture conditions (Tuo et al., 2023).

4.2 Effects of shading of PV panels on composition and diversity of SBCs

Bacteria are the most abundant microorganisms in soil and play a crucial role in material cycling, energy flow, and maintaining ecological balance in terrestrial ecosystems. Their activities and interactions are vital for soil fertility, plant health, and ecosystem stability (Zhang et al., 2022; Liu et al., 2023c). The study area revealed five prominent phyla: Actinobacteriota, Proteobacteria, Acidobacteriota, Chloroflexi, and Gemmatimonadota. These findings are consistent with those reported for global drylands, although there are noticeable variations in relative abundance (Ochoa-Hueso et al., 2018).

The relative abundances of SBCs can serve as a biological indicator of environmental health (Lee et al., 2020). The abundance of Proteobacteria, Planctomycetota, and Myxococcota differed significantly between the LC and EP sample plots. This suggests that vegetation restoration regulates SBCs to some extent and that different vegetation types have a significant impact on the dominant microbial community (Liu et al., 2023a). The relative abundance of dominant phylum remained relatively constant across the light gradient in both vegetation plots. However, the sampling depth did vary. This suggests that the impact of light heterogeneity on the soil's abundant microorganisms was less significant than the soil depth under two different vegetation restoration patterns. The Venn diagram reveals that the endemic genera are relatively less abundant in different positions and vegetation plots, all being less than 1%, indicating that rare species are more responsive to environmental heterogeneity due to higher environmental filtering and dispersal limitations (Luan et al., 2023). These SBCs that produce significant differences under small-scale light heterogeneity, are likely to be photosensitive bacteria, and their functional characteristics deserve in-depth study in the future.

Light has both direct and indirect effects on the abundance and structure of soil microbial communities. Shading of PV panels at PV sites affects the amount of irradiation and energy received by the soil at different locations, which in turn affects the structure of soil microbial communities (Bai et al., 2022). PV shading increased soil microbial biomass by 20–30%. However, the numbers of OTU, Shannon diversity, ACE and Chao1 richness index decreased to varying degrees. This may be due to a decrease in light intensity, which reduced the number of sun-loving microbial species while promoting the growth and reproduction of shade-loving microbial species due to decreased competition (Davies et al., 2013).

4.3 SBCs adopt different survival strategies under two vegetation restoration models

In natural ecosystems, microorganisms do not exist as isolated individuals, but form complex networks of co-occurrence through direct or indirect interactions (Fan et al., 2017; Wu et al., 2021). Species interactions are represented by links in co-occurrence networks. Co-colonization, cross-feeding, niche overlap, and co-aggregation in microorganisms lead to positive species correlations, whereas predator–prey associations, misfeeding, improper feeding, and competition lead to negative species correlations (Yang et al., 2021). In the molecular ecological network of the LC plot, 90% of the correlations between species were positive, whereas in the EP plot, the positive correlations decreased significantly to 81.3% (Table 1). Furthermore, the core genera with a degree greater than 30 in the *LC* plot exhibited positive correlations. In contrast, the core genera in the *EP* sample plot showed a significant increase in negative correlations, suggesting an increase in competitive relationships between species and a more stable ecological network. These indicate that the SBCs in the *LC* plot was mainly in symbiotic relationships, while the competitive relationship between species increased and the ecological network became more stable in the *EP* plot (Liao et al., 2022; Liu et al., 2023b). That is to say, SBCs adopt different survival strategies to cope with small-scale light stress under two vegetation restoration modes.

Non-hub connections are responsible for managing the flow of information between modules that are otherwise inadequately or not at all linked to one another. Therefore, deleting non-hub connector species may significantly impact the functional connection of various network modules (Guimera and Nunes, 2005). The higher number of non-collector connectors in the *EP* sample plots, compared to the *LC* sample plots, suggests that the functions of SBCs in the *EP* sample plots were more closely linked and the ecological network was more stable (Liao et al., 2022). This could facilitate better adaptation to the small-scale light stress in the PV site area.

4.4 Factors driving SBCs under two vegetation restoration models

The construction and operation of SPP can promote the development of biological soil crust and vegetation growth, leading to an improvement in soil texture and nutrition (Luo et al., 2023). The study found that the relationships between soil properties, light intensity, and dominant bacterial communities varied between the two modes of vegetation restoration. In the *LC* sample plot, light intensity had a significant positive correlation with TN, TC, and NO_3^--N, as well as AP, but a negative correlation with MBC in the *LC* sample plot. These findings suggest that PV panel shading not only facilitates the accumulation of soil nutrients but also the increase of soil microorganisms. The *EP* sample plot showed a significant positive correlation between light intensity and nitrate-nitrogen and a negative correlation with MBC. The interaction between dominant bacteria and environmental factors was also significantly enhanced. This was attributed to differences in plant inter-root secretions and the nutrient cycling of plant litter in different vegetation types, which affect the soil environment and further influence the structure and diversity of SBCs (Lu et al., 2022).

In some small-scale habitats, light may be a key factor driving bacterial community aggregation (Li C. et al., 2023; Li X. et al., 2023). The correlation between the relative abundance of Proteobacteria and light intensity was significant in the EP sample plot. Shading by PV panels resulted in a reduction of its relative abundance, which contradicts the findings of another PV site (Bai et al., 2022). This difference may be attributed to variations in environmental factors and vegetation types in PV sites. The Mantel test and correlation analysis results showed soil nutrients were the key drivers of changes in soil dominant communities, while light had a less direct role in changes in soil dominant bacterial communities, and it indirectly shaped the microbial community through its effects on the plant community (Li C. et al., 2023). The two-factor correlation network

analysis revealed that the core SBCs in the *EP* sample plot were mainly negatively correlated with soil nutrients, while the core soil bacteria species in the *LC* sample plot were positively correlated with soil nutrients. This suggests that the different types of vegetation restoration have significant impacts on the soil environment and subsurface micro-ecosystems.

5 Conclusion

This study used high-throughput sequencing technology to investigate the effects of light gradient and soil depth on the composition and diversity of SBCs. It also explored survival strategies and key drivers of SBCs under two vegetation restoration modes. The results showed significant differences in light intensity among different locations ($p < 0.05$) with the order as follows: CK > FP > RP > UP. PV shading led to a 20–30% increase in soil microbial biomass. However, the OTU numbers, Shannon diversity, ACE, and Chao1 richness indices all decreased to varying degrees. The sampling depth had a greater effect on the diversity and relative abundance of SBCs than light intensity. The five most dominant phyla were Actinobacteria, Proteobacteria, Acidobacteria, Chlorobacteria, and Dimonobacteria. Species with a relative abundance of less than 0.01% were significantly more affected by light intensity than those with a high relative abundance. Network analysis revealed that symbiotic relationships dominated critical SBCs in the *LC* sample plot, whereas competitive interactions increased significantly in the *EP* sample plot, meaning that the ecological network was more stable and better adapted to light stress in the PV plots. *EP* is more conducive to maintaining the stability and health of subsurface ecosystems in vulnerable areas compared to *LC*. Soil nutrients are the key driving factor for changes in the dominant soil community.

Data availability statement

The datasets presented in this study can be found in online repositories. The names of the repository/repositories and accession number(s) can be found at: https://www.ncbi.nlm.nih.gov/, PRJNA913967.

Author contributions

ZL: Conceptualization, Data curation, Formal analysis, Investigation, Methodology, Writing – original draft, Writing – review & editing. JL: Data curation, Investigation, Writing – review & editing. SW: Investigation, Writing – review & editing. XL: Investigation, Writing – review & editing. XS: Conceptualization, Funding acquisition, Resources, Supervision, Writing – review & editing. All authors contributed to the article and approved the submitted version.

Funding

The author(s) declare that financial support was received for the research, authorship, and/or publication of this article. This work was supported by the National Natural Science Foundation of China (U22A20557) and the Technical Service Project (No. SS0203242022).

Conflict of interest

The authors declare that the research was conducted in the absence of any commercial or financial relationships that could be construed as a potential conflict of interest.

Publisher's note

Supplementary material

The Supplementary material for this article can be found online at: https://www.frontiersin.org/articles/10.3389/fmicb.2024.1365234/full#supplementary-material

References

Amaducci, S., Yin, X., and Colauzzi, M. (2018). Agrivoltaic systems to optimise land use for electric energy production. *Appl. Energy* 220, 545–561. doi: 10.1016/j.apenergy.2018.03.081

Armstrong, A., Ostle, N. J., and Whitaker, J. (2016). Solar park microclimate and vegetation management effects on grassland carbon cycling. *Environ. Res. Lett.* 11:74016. doi: 10.1088/1748-9326/11/7/074016

Bai, Z., Jia, A., Bai, Z., Qu, S., Zhang, M., Kong, L., et al. (2022). Photovoltaic panels have altered grassland plant biodiversity and soil microbial diversity. *Front. Microbiol.* 13:1065899. doi: 10.3389/fmicb.2022.1065899

Broadbent, A. M., Krayenhoff, E. S., Georgescu, M., and Sailor, D. J. (2019). The observed effects of utility-scale photovoltaics on near-surface air temperature and energy balance. *J. Appl. Meteorol. Climatol.* 58, 989–1006. doi: 10.1175/JAMC-D-18-0271.1

Chen, D., Li, Q., Huo, L., Xu, Q., Chen, X., He, F., et al. (2023). Soil nutrients directly drive soil microbial biomass and carbon metabolism in the sanjiangyuan alpine grassland. *J. Soil Sci. Plant Nutr.* 23, 3548–3560. doi: 10.1007/s42729-023-01270-y

Chen, Y., Liu, Y., Tian, Z., Dong, Y., Zhou, Y., Wang, X., et al. (2019). Experimental study on the effect of dust deposition on photovoltaic panels. *Energy Procedia* 158, 483–489. doi: 10.1016/j.egypro.2019.01.139

Choi, C. S., Cagle, A. E., Macknick, J., Bloom, D. E., Caplan, J. S., and Ravi, S. (2020). Effects of revegetation on soil physical and chemical properties in solar photovoltaic infrastructure. *Front. Environ. Sci.* 8:140. doi: 10.3389/fenvs.2020.00140

Davies, L. O., Schafer, H., Marshall, S., Bramke, I., Oliver, R. G., and Bending, G. D. (2013). Light structures phototroph, bacterial and fungal communities at the soil surface. *PLoS One* 8:e69048. doi: 10.1371/journal.pone.0069048

Del Pino, G. A., Brandt, A. J., and Burns, J. H. (2015). Light heterogeneity interacts with plant-induced soil heterogeneity to affect plant trait expression. *Plant Ecol.* 216, 439–450. doi: 10.1007/s11258-015-0448-x

D'Odorico, P., Caylor, K., Okin, G. S., and Scanlon, T. M. (2007). On soil moisture-vegetation feedbacks and their possible effects on the dynamics of dryland ecosystems. *J. Geophys. Res. Biogeosci.* 112:10. doi: 10.1029/2006JG000379

Fan, K., Cardona, C., Li, Y., Shi, Y., Xiang, X., Shen, C., et al. (2017). Rhizosphere-associated bacterial network structure and spatial distribution differ significantly from bulk soil in wheat crop fields. *Soil Biol. Biochem.* 113, 275–284. doi: 10.1016/j.soilbio.2017.06.020

Graham, M., Ates, S., Melathopoulos, A. P., Moldenke, A. R., DeBano, S. J., Best, L. R., et al. (2021). Partial shading by solar panels delays bloom, increases floral abundance during the late-season for pollinators in a dryland, agrivoltaic ecosystem. *Sci. Rep.* 11:7452. doi: 10.1038/s41598-021-86756-4

Guimera, R., and Nunes, A. L. (2005). Functional cartography of complex metabolic networks. *Nature* 433, 895–900. doi: 10.1038/nature03288

He, B., Lu, H., Zheng, C., and Wang, Y. (2023). Characteristics and cleaning methods of dust deposition on solar photovoltaic modules-a review. *Energy* 263:126083. doi: 10.1016/j.energy.2022.126083

Helbach, J., Frey, J., Messier, C., Morsdorf, M., and Scherer-Lorenzen, M. (2022). Light heterogeneity affects understory plant species richness in temperate forests supporting the heterogeneity-diversity hypothesis. *Ecol. Evol.* 12:e8534. doi: 10.1002/ece3.8534

Lee, S. A., Kim, J. M., Kim, Y., Joa, J. H., Kang, S. S., Ahn, J. H., et al. (2020). Different types of agricultural land use drive distinct soil bacterial communities. *Sci. Rep.* 10:17418. doi: 10.1038/s41598-020-74193-8

Li, Y., Gong, J., Liu, J., Hou, W., Moroenyane, I., Liu, Y., et al. (2022). Effects of different land use types and soil depth on soil nutrients and soil bacterial communities in a karst area, Southwest China. *Soil Syst.* 6:20. doi: 10.3390/soilsystems6010020

Li, C., Liu, J., Bao, J., Wu, T., and Chai, B. (2023). Effect of light heterogeneity caused by photovoltaic panels on the plant–soil–microbial system in solar park. *Land* 12:367. doi: 10.3390/land12020367

Li, X., Rui, J., Mao, Y., Yannarell, A., and Mackie, R. (2014). Dynamics of the bacterial community structure in the rhizosphere of a maize cultivar. *Soil Biol. Biochem.* 68, 392–401. doi: 10.1016/j.soilbio.2013.10.017

Li, X., Tan, Q., Zhou, Y., Chen, Q., Sun, P., Shen, G., et al. (2023). Synergic remediation of polycyclic aromatic hydrocarbon-contaminated soil by a combined system of persulfate oxidation activated by biochar and phytoremediation with basil: a compatible, robust, and sustainable approach. *Chem. Eng. J.* 452:139502. doi: 10.1016/j.cej.2022.139502

Liao, Y., Jiang, Z., Li, S., Dang, Z., Zhu, X., and Ji, G. (2022). Archaeal and bacterial ecological strategies in sediment denitrification under the influence of graphene oxide and different temperatures. *Sci. Total Environ.* 838:156549. doi: 10.1016/j.scitotenv.2022.156549

Liu, S., Gao, Y., Chen, J., Li, J., and Zhang, H. (2023c). Responses of soil bacterial community structure to different artificially restored forests in open-pit coal mine dumps on the loess plateau, China. *Front. Microbiol.* 14:1198313. doi: 10.3389/fmicb.2023.1198313

Liu, L., Ma, L., Zhu, M., Liu, B., Liu, X., and Shi, Y. (2023a). Rhizosphere microbial community assembly and association networks strongly differ based on vegetation type at a local environment scale. *Front. Microbiol.* 14:1129471. doi: 10.3389/fmicb.2023.1129471

Liu, Y., Zhang, R. Q., Huang, Z., Cheng, Z., López Vicente, M., Ma, X. R., et al. (2019). Solar photovoltaic panels significantly promote vegetation recovery by modifying the soil surface microhabitats in an arid sandy ecosystem. *Land Degrad. Dev.* 30, 2177–2186. doi: 10.1002/ldr.3408

Liu, L., Zhang, Z., Wang, X., Zhang, R., Wang, M., Wurzburger, N., et al. (2023b). Urbanization reduces soil microbial network complexity and stability in the megacity of shanghai. *Sci. Total Environ.* 893:164915. doi: 10.1016/j.scitotenv.2023.164915

Lu, X., Toda, H., Ding, F., Fang, S., Yang, W., and Xu, H. (2014). Effect of vegetation types on chemical and biological properties of soils of karst ecosystems. *Eur. J. Soil Biol.* 61, 49–57. doi: 10.1016/j.ejsobi.2013.12.007

Lu, Z., Wang, P., Ou, H., Wei, S., Wu, L., Jiang, Y., et al. (2022). Effects of different vegetation restoration on soil nutrients, enzyme activities, and microbial communities in degraded karst landscapes in Southwest China. *For. Ecol. Manag.* 508:120002. doi: 10.1016/j.foreco.2021.120002

Luan, L., Shi, G., Zhu, G., Zheng, J., Fan, J., Dini Andreote, F., et al. (2023). Biogeographical patterns of abundant and rare bacterial biospheres in paddy soils across east asia. *Environ. Microbiol.* 25, 294–305. doi: 10.1111/1462-2920.16281

Luo, L., Zhuang, Y., Liu, H., Zhao, W., Chen, J., Du, W., et al. (2023). Environmental impacts of photovoltaic power plants in Northwest China. *Sustain Energy Technol Assess* 56:103120. doi: 10.1016/j.seta.2023.103120

Maestre, F. T., Delgado-Baquerizo, M., Jeffries, T. C., Eldridge, D. J., Ochoa, V., Gozalo, B., et al. (2015). Increasing aridity reduces soil microbial diversity and abundance in global drylands. *Proc. Natl. Acad. Sci. USA* 112, 15684–15689. doi: 10.1073/pnas.1516684112

Marrou, H., Dufour, L., and Wery, J. (2013). How does a shelter of solar panels influence water flows in a soil–crop system? *Eur. J. Agron.* 50, 38–51. doi: 10.1016/j.eja.2013.05.004

Newman, M. E. J. (2003). The structure and function of complex networks. *SIAM Rev.* 45, 167–256. doi: 10.1137/S003614450342480

Ochoa-Hueso, R., Collins, S. L., Delgado-Baquerizo, M., Hamonts, K., Pockman, W. T., Sinsabaugh, R. L., et al. (2018). Drought consistently alters the composition of soil fungal and bacterial communities in grasslands from two continents. *Glob. Change Biol.* 24, 2818–2827. doi: 10.1111/gcb.14113

Pang, D., Cao, J., Dan, X., Guan, Y., Peng, X., Cui, M., et al. (2018). Recovery approach affects soil quality in fragile karst ecosystems of Southwest China: implications for vegetation restoration. *Ecol. Eng.* 123, 151–160. doi: 10.1016/j.ecoleng.2018.09.001

Qiang, L., Qingjing, H., Chaolan, Z., Mueller, W. E. G., Schroeder, H. C., Zhongyi, L., et al. (2015). The effect of toxicity of heavy metals contained in tailing sands on the organic carbon metabolic activity of soil microorganisms from different land use types in the karst region. *Environ. Earth Sci.* 74, 6747–6756. doi: 10.1007/s12665-015-4684-0

R Core Team (2018). A language and environment for statistical computing. R Foundation for Statistical Computing, Available at: https://www.R-project.org

Trivedi, P., Delgado-Baquerizo, M., Anderson, I. C., and Singh, B. K. (2016). Response of soil properties and microbial communities to agriculture: implications for primary productivity and soil health indicators. *Front. Plant Sci.* 7:990. doi: 10.3389/fpls.2016.00990

Tuo, Y., Wang, Z., Zheng, Y., Shi, X., Liu, X., Ding, M., et al. (2023). Effect of water and fertilizer regulation on the soil microbial biomass carbon and nitrogen, enzyme activity, and saponin content of panax notoginseng. *Agric. Water Manag.* 278:108145. doi: 10.1016/j.agwat.2023.108145

Williams, R. J., Howe, A., and Hofmockel, K. S. (2014). Demonstrating microbial co-occurrence pattern analyses within and between ecosystems. *Front. Microbiol.* 5:358. doi: 10.3389/fmicb.2014.00358

Wu, D., Bai, H., Zhao, C., Peng, M., Chi, Q., Dai, Y., et al. (2023). The characteristics of soil microbial co-occurrence networks across a high-latitude forested wetland ecotone in China. *Front. Microbiol.* 14:1160683. doi: 10.3389/fmicb.2023.1160683

Wu, S., Li, Y., Wang, P., Zhong, L., Qiu, L., and Chen, J. (2016). Shifts of microbial community structure in soils of a photovoltaic plant observed using tag-encoded pyrosequencing of 16s rrna. *Appl. Microbiol. Biotechnol.* 100, 3735–3745. doi: 10.1007/s00253-015-7219-4

Wu, C., Liu, H., Yu, Y., Zhao, W., Liu, J., Yu, H., et al. (2022). Ecohydrological effects of photovoltaic solar farms on soil microclimates and moisture regimes in arid Northwest China: a modeling study. *Sci. Total Environ.* 802:149946. doi: 10.1016/j.scitotenv.2021.149946

Wu, X., Yang, J., Ruan, H., Wang, S., Yang, Y., Naeem, I., et al. (2021). The diversity and co-occurrence network of soil bacterial and fungal communities and their implications for a new indicator of grassland degradation. *Ecol. Indic.* 129:107989. doi: 10.1016/j.ecolind.2021.107989

Wu, W., Yuan, B., Zou, P., Yang, R., and Zhou, X. (2022). Distribution characteristics of bacterial communities in photovoltaic industrial parks in Northwest China. *IOP Conf. Ser. Earth Environ. Sci.* 983:012093. doi: 10.1088/1755-1315/983/1/012093

Xiao, K., He, T., Chen, H., Peng, W., Song, T., Wang, K., et al. (2017). Impacts of vegetation restoration strategies on soil organic carbon and nitrogen dynamics in a karst area, Southwest China. *Ecol. Eng.* 101, 247–254. doi: 10.1016/j.ecoleng.2017.01.037

Yang, Y., Shi, Y., Kerfahi, D., Ogwu, M. C., Wang, J., Dong, K., et al. (2021). Elevation-related climate trends dominate fungal co-occurrence network structure and the abundance of keystone taxa on mt. Norikura, Japan. *Sci. Total Environ.* 799:149368. doi: 10.1016/j.scitotenv.2021.149368

Yang, H., Wu, J., Huang, X., Zhou, Y., Zhang, Y., Liu, M., et al. (2022). Abo genotype alters the gut microbiota by regulating galnac levels in pigs. *Nature* 606, 358–367. doi: 10.1038/s41586-022-04769-z

Yuan, B., Wu, W., Yue, S., Zou, P., Yang, R., and Zhou, X. (2022). Community structure, distribution pattern, and influencing factors of soil archaea in the construction area of a large-scale photovoltaic power station. *Int. Microbiol.* 25, 571–586. doi: 10.1007/s10123-022-00244-x

Yue, S., Guo, M., Zou, P., Wu, W., and Zhou, X. (2021a). Effects of photovoltaic panels on soil temperature and moisture in desert areas. *Environ. Sci. Pollut. Res. Int.* 28, 17506–17518. doi: 10.1007/s11356-020-11742-8

Yue, S., Wu, W., Zhou, X., Ren, L., and Wang, J. (2021b). The influence of photovoltaic panels on soil temperature in the gonghe desert area. *Environ. Eng. Sci.* 38, 910–920. doi: 10.1089/ees.2021.0014

Zhang, R., Li, Y., Zhao, X., Allan Degen, A., Lian, J., Liu, X., et al. (2022). Fertilizers have a greater impact on the soil bacterial community than on the fungal community in a sandy farmland ecosystem, Inner Mongolia. *Ecol. Indic.* 140:108972. doi: 10.1016/j.ecolind.2022.108972

Zhao, S., Qiu, S., Xu, X., Ciampitti, I. A., Zhang, S., and He, P. (2019). Change in straw decomposition rate and soil microbial community composition after straw addition in different long-term fertilization soils. *Appl. Soil Ecol.* 138, 123–133. doi: 10.1016/j.apsoil.2019.02.018

frontiers | Frontiers in Microbiology

TYPE Original Research
PUBLISHED 08 April 2024
DOI 10.3389/fmicb.2024.1394104

OPEN ACCESS

EDITED BY
Yang Yang,
Chinese Academy of Sciences (CAS), China

REVIEWED BY
Zhang Guogang,
Tianjin Normal University, China
Guangzhou Wang,
China Agricultural University, China

*CORRESPONDENCE:
Zhen Wang
✉ wangzhen0318@126.com
Ke Jin
✉ jinke@caas.cn

†These authors have contributed equally to this work

RECEIVED 01 March 2024
ACCEPTED 18 March 2024
PUBLISHED 08 April 2024

CITATION
Li J, Jia L, Struik PC, An Z, Wang Z, Xu Z, Ji L, Yao Y, Lv J, Zhou T and Jin K (2024) Plant and soil responses to tillage practices change arbuscular mycorrhizal fungi populations during crop growth.
Front. Microbiol. 15:1394104.
doi: 10.3389/fmicb.2024.1394104

Plant and soil responses to tillage practices change arbuscular mycorrhizal fungi populations during crop growth

Jing Li[1,2†], Lijuan Jia[1†], Paul C. Struik[3], Zhengfeng An[4], Zhen Wang[1*], Zhuwen Xu[2], Lei Ji[1], Yuqing Yao[5], Junjie Lv[5], Tao Zhou[6] and Ke Jin[1*]

[1]Institute of Grassland Research, Chinese Academy of Agricultural Sciences, Hohhot, China, [2]School of Ecology and Environment, Inner Mongolia University, Hohhot, China, [3]Department of Plant Sciences, Centre for Crop Systems Analysis, Wageningen University and Research, Wageningen, Netherlands, [4]Department of Renewable Resources, University of Alberta, Edmonton, AB, Canada, [5]Luoyang Academy of Agriculture and Forestry Sciences, Luoyang, China, [6]Ningxia Academy of Agriculture and Forestry Sciences, Shizuishan, China

Background: Tillage practices can substantially affect soil properties depending on crop stage. The interaction between tillage and crop growth on arbuscular mycorrhizal fungi (AMF) communities remains unclear. We investigated the interactions between four tillage treatments (CT: conventional tillage, RT: reduced tillage, NT: no tillage with mulch, and SS: subsoiling with mulch), maintained for 25 years, and two wheat growth stages (elongation stage and grain filling stage) on AMF diversity and community composition.

Results: The AMF community composition strongly changed during wheat growth, mainly because of changes in the relative abundance of dominant genera *Claroideoglomus*, *Funneliformi*, *Rhizophagu*, *Entrophospora*, and *Glomus*. Co-occurrence network analysis revealed that the grain filling stage had a more complex network than the elongation stage. Redundancy analysis results showed that keystone genera respond mainly to changes in soil organic carbon during elongation stage, whereas the total nitrogen content affected the keystone genera during grain filling. Compared with CT, the treatments with mulch, i.e., NT and SS, significantly changed the AMF community composition. The change of AMF communities under different tillage practices depended on wheat biomass and soil nutrients. NT significantly increased the relative abundances of *Glomus* and *Septoglomus*, while RT significantly increased the relative abundance of *Claroideoglomus*.

Conclusion: Our findings indicate that the relative abundance of dominant genera changed during wheat growth stages. Proper tillage practices (e.g., NT and SS) benefit the long-term sustainable development of the Loess Plateau cropping systems.

KEYWORDS

tillage practices, arbuscular mycorrhizal fungi, wheat growth stages, co-occurrence, Loess Plateau

1 Introduction

Agricultural practices affect not only crop production (Singh et al., 2016) but also soil quality (Zhang et al., 2015). Excessive tillage practices, as common in conventional tillage, increase the bare soil area, intensify soil erosion, destroy soil structure, and reduce soil organic matter, resulting in a yield decline (Kabiri et al., 2016; Yan et al., 2020). In order to maintain the sustainable development of agriculture, improving nutrient use efficiency is crucial to increase crop yields (Yan et al., 2020). Thus, many studies have focused on increasing crop yield through conservation tillage practices (e.g., no tillage, reduced tillage, and subsoiling with mulch) (Jin et al., 2008; Chen et al., 2019; Jia et al., 2022). Conservation tillage practices with minimal soil disturbance improve agricultural sustainability by reducing soil erosion and enhancing the diversity of microorganisms (Zuber et al., 2015; Xiao et al., 2019). Among them, arbuscular mycorrhizal fungi (AMF), as important rhizosphere microorganisms, were affected by tillage practices (Balota et al., 2016; Oehl and Koch, 2018). However, the linkages between the responses of plant–soil-AMF to conservation tillage practices, especially the timing and duration of tillage practices are still unclear.

AMF can create symbioses with the roots of more than 80% of terrestrial plant species, which enhances the ability of plants to overcome the adverse impacts of and to ameliorate plant performance under environmental stress (such as drought, extreme temperature and changes in land management) (Walder and van der Heijden, 2015; Gu et al., 2020). The mechanisms of vascular plants to resist environmental change involve forming symbiotic relationships with AMF, which allows the AMF to acquire plant-synthesized carbon (C) as well as enhance the nutrient supply (mainly N and P) to the host plants as shown by many previous studies (e.g., Augé et al., 2015; Wang et al., 2017). Conventional tillage can decrease the diversity and activity of AMF, which negatively affects the symbiotic relationship between AMF and plants and results in the decline of crop yield and soil quality (Jansa et al., 2003; Avio et al., 2013). For example, long-term conventional tillage decreased the AMF richness and induced a marked shift in the community composition by changing the functional quality of AMF (e.g., spore density or hyphal networks) (Schnoor et al., 2011; Säle et al., 2015).

Conservation tillage (reduced tillage, no tillage, and subsoiling with mulch) is considered to be an effective technology improving the stability of soil and AMF attributes, which can help maintain a more complex interaction network and increase the resilience of soil to interference (Carballar-Hernández et al., 2017; Gu et al., 2020). For instance, no tillage enhanced AMF activity and diversity by improving soil fertility, storing and conserving water, and reducing soil erosion (Bowles et al., 2017). Subsoiling with mulch also increased AMF activity and diversity by stimulating water infiltration and increasing soil carbon and nitrogen concentrations (Gu et al., 2020; Wang Z. et al., 2020; Wang S. L. et al., 2020). However, long-term conservation tillage, e.g., no tillage, may lead to problems such as soil surface hardening and more limited O_2 supply for soil organisms, which may be detrimental to the distribution of AMF propagules (Curaqueo et al., 2011). Although previous studies have shown that different tillage practices alter the composition of AMF communities, the direction and extent of the impact of different tillage practices on the composition of AMF communities are highly uncertain.

At different stages of crop growth, the community composition of AMF presents a dynamic change process (Hu et al., 2015; Wang Z. et al., 2020; Wang S. L. et al., 2020). Plant roots recruit rhizosphere AMF by secreting and absorbing different chemicals, leading to a shift in the rhizosphere AMF community across the different crop growth stages (Edwards et al., 2015; Hamonts et al., 2018). In addition, the interaction between the host and AMF regulates the growth of the AMF community in the root system (Yang et al., 2015). For example, during different phenological stages, the colonization by AMF of the plant roots changes, further affecting the community composition of AMF across crop growth stages (Merryweather and Fitter, 1998; Schalamuk et al., 2004). At present, most studies focus on the effect of tillage practices or crop growth stages on the community composition of AMF, while few studies investigate the interaction of tillage practices and crop growth stages to mediate AMF communities (Hu et al., 2015). Therefore, further research is essential to assess the temporal dynamics of AMF communities and the impact of tillage practices on AMF communities throughout crop growth and development.

As one of the largest and most important food crops in the Loess Plateau, winter wheat (*Triticum aestivum* L.) plays an important role in food security and contributes more than 70% of the agricultural production in northern China (Xue et al., 2019; Xia et al., 2020). Our previous studies have found that tillage practices affect winter wheat production, soil physicochemical properties, and microbial community composition (Jin et al., 2008; Jia et al., 2022). However, there is little information about the impact of tillage practices on the species richness and composition of AMF in the winter wheat production systems, especially at different winter wheat growth stages. Here, we assessed a 22-year field experiment examining the potential impacts of four contrasting tillage practices at two growth stages (elongation and grain filling) on AMF dynamics in the semi-arid agricultural ecosystem. We hypothesized that (1) long-term tillage practices create particular populations of AMF by altering the species diversity of AMF and the abundance of keystone operational taxonomic units or genera; (2) the effect of long-term tillage practices on AMF communities relies on the shifts in the rhizosphere environment and on biomass accumulation during winter wheat production; and (3) conservation tillage can develop particular groups of AMF by enhancing soil fertility and winter wheat productivity.

2 Materials and methods

2.1 Study sites and experimental design

The experiment started in 1999 in the eastern part of the Loess Plateau, Songzhuang Village (34°58′N, 113°08 E), Henan Province, China. The area had previously been conventionally tilled for more than 30 years before the experimental plot was established. The thickness of the Quaternary loess layer is 50 to 100 m in this area. The soil in the study area is silt loam and is classified as Inceptisol according to soil taxonomy (Soil Survey Staff, 2003). The basic soil properties were analyzed to assess plot homogeneity based on their contribution to crop performance and soil quality in previous studies (Jin et al., 2009).

Four tillage practices, conventional tillage (CT), no tillage with mulch (NT), reduced tillage (RT), and subsoiling with mulch (SS),

were set up at four nearby sites. For example, for the CT treatment, there was still 10–15 cm of stubble after harvest (May 25 to June 1), but the straw and ears had been removed from the site at harvest. In the first week of July, the soil was turned to a depth of 20 cm. Around October 1, before winter wheat was sown, the soil was turned again to a depth of 20 cm, fertilizer was mixed in, and then the soil was harrowed to prepare the seedbed. Winter wheat sowing occurred around October 5. For the RT treatment, 10–15 cm of stubble was left in the field after winter wheat harvest (May 25 to June 1), and the straw was returned to the field after harvest. Around July 15, deep plowing (25–30 cm) was combined with harrowing (5–8 cm) and compaction with a roller. Winter wheat was sown directly around October 5. Therefore, this practice only required one plowing instead of two under the CT. For the NT treatment, 30 cm of stubble was left in the field after harvest (May 25 to June 1), and the straw was returned to the field after threshing. Fertilization was carried out from September 25 to October 5. For the SS treatment, 25–35 cm of stubble remained in the field after harvest (May 25–June 1). Around July 1, subsoiling was carried out at 60 cm intervals to a depth of 30 to 35 cm. Sowing with fertilizer application was performed from September 2 to October 5. The set-up of the experiment was subject to pseudo-replication due to space-for-time substitution limitations (Blois et al., 2013). However, the four experimental sites appeared topographically similar and generally suffered little disturbance in previous studies regarding frequency and severity (Jia et al., 2022). Therefore, the tillage practices were considered the only important change factor across sites.

2.2 Plant and soil sampling

Winter wheat biomass and soil samples were collected on March 28 and May 20 (i.e., at the elongation and grain filling stages of winter wheat) in 2023. We randomly established six plots (0.5 × 0.5 m) in winter wheat crops grown in each tillage treatment. Twenty winter wheat plants were sampled and combined into one sample for each plot. The roots of winter wheat were collected from 0 to 20 cm in each plot. We shook all roots of each plot vigorously to remove soil that was not tightly adhered and used a sterile scalpel to separate the rhizosphere soil from the root surface carefully (Song et al., 2007; Liu et al., 2022). Two soil cores with a diameter of 7.5 cm were collected and then mixed with one soil sample (0–20 cm layer) per plot; thus, six AMF soil samples were collected for each treatment. A total of 48 AMF soil samples were collected (two growth stages × four tillage treatments × six AMF soil samples/tillage treatment).

2.3 Sample processing and measuring biotic and abiotic variables

Twenty winter wheat plants from each plot were separated into above-ground biomass and below-ground biomass, oven-dried at 65°C for 48 h and weighed to assess dry biomass (Jia et al., 2022). Each composite soil sample from each plot was divided into three subsamples. One subsample was air-dried to determine physicochemical properties. The second subsample was stored at 4°C and analyzed within a week to measure soil ammonium (NH_4^+) and nitrate (NO_3^-) content, microbial C and N biomass. The third subsample was immediately stored at −80 °C for DNA extraction and Miseq sequencing analysis within two days. The gravimetric method was used to measure soil water content (SWC). Soil pH was measured using a 1:2.5 soil: water mixture. The dichromate oxidation method was used to determine the soil organic carbon (SOC) (Nelson and Sommers, 1983), and total nitrogen (TN) was measured using an Elemental Analyzer (vario MACRO cube, Elementar, Germany). Soil NO_3^- and NH_4^+ were extracted from the soil samples using a 2 mol L^{-1} KCl solution and were measured using a continuous flow analyzer (Auto Analyzer 3, Seal, Germany). Soil dissolved organic carbon (DOC) was measured using a TOC-L-ASI analyzer (Analytik Jena AG, Jena, Germany) by adding 0.5 M K_2SO_4 and shaking for 1 h. The total P (TP) concentration was determined using an Astoria auto-analyzer (Clackamas, OR). The available phosphorus (AP) content was determined using the Olsen method. Soil microbial biomass C (MBC) and N (MBN) were measured using fumigation extractions (Vance et al., 1987).

2.4 AMF root colonization

Fifty fine root fragments (approximately 1 cm long) from each sample were stained with trypan blue, and the percentage of AM root colonization was measured by the line intersection method at 200-fold magnification (McGonigle et al., 1990). Total AM root colonization was determined as the percentage of root length colonized by AM fungi.

2.5 DNA extraction and high-throughput sequencing

DNA Extraction Total genomic DNA samples were extracted from 0.5 g of each soil sample using the OMEGA Soil DNA Kit (M5635-02) (Omega Bio-Tek, Norcross, GA, United States), following the manufacturer's instructions. The quantity and quality of extracted DNAs were measured using a NanoDrop NC2000 spectrophotometer (Thermo Fisher Scientific, Waltham, MA, United States) and agarose gel electrophoresis, respectively.

PCR amplification of the AMF genes region performed using the forward primer AMV4.5NF (5′-AAGCTCGTAGTTGAATTTCG-3′) AMDGR (5′-CCCAACTATCCCTATTAATCAT-3′) (Van Geel et al., 2014; Suzuki et al., 2020). Sample-specific 7-bp barcodes were incorporated into the primers for multiplex sequencing. The PCR components contained 5 μL of buffer (5×), 0.25 μL of Fast pfu DNA Polymerase (5 U/μl), 2 μL (2.5 mM) of dNTPs, 1 μL (10 uM) of each Forward and Reverse primer, 1 μL of DNA Template, and 14.75 μL of ddH_2O. Thermal cycling consisted of initial denaturation at 98°C for 5 min, followed by 30 cycles consisting of denaturation at 98°C for 30 s, annealing at 53°C for 45 s, and extension at 72°C for 45 s, with a final extension of 5 min at 72°C. PCR amplicons were purified with Vazyme VAHTSTM DNA Clean Beads (Vazyme, Nanjing, China) and quantified using the Quant-iT PicoGreen dsDNA Assay Kit (Invitrogen, Carlsbad, CA, United States). After the individual quantification step, amplicons were pooled in equal amounts, and pair-end 2 × 250 bp sequencing was performed using the Illlumina NovaSeq platform with NovaSeq 6000 SP Reagent Kit (500 cycles) at Shanghai Personal Biotechnology Co., Ltd. (Shanghai, China).

Sequence data analyses were mainly performed using QIIME2. After quality filtering and removing chimeras, high-quality sequences were also clustered into operational taxonomic units (OTUs) using USEARCH at 97% sequence identity (v2.13.4).[1] We selected one representative sequence for each OTU and aligned all representative sequences using PyNAST (Panneerselvam et al., 2020) with a minimum identity threshold of 0.8. The sequences were assigned to virtual taxa using the MaarjAM database (Koljalg et al., 2013).

2.6 Co-occurrence network construction and analyses

The "microeco" package was used to construct microbial ecological networks (Liu et al., 2021). We created the microtable class and performed basic preprocessing operations. The operational taxonomic unit (OTU) table was reduced so that sequence numbers were the same between samples (10,000 sequences in each sample). We calculated the taxa abundance for the downstream analysis. In a network, betweenness centrality (BC) calculates the fraction of the shortest paths through a given microbial taxon to another microbial taxon, which reflects the degree of control that a taxon exerts over the interactions between other taxa in the network (Lupatini et al., 2014). A valid interaction event is determined to have a robust correlation if the Pearson correlation coefficient is equal to or greater than 0.8 or equal to or lower than −0.8 and is statistically significant (p-value equal to or smaller than 0.05) (Liu et al., 2021). The gephi interactive platform[2] was used to explore and visualize the network structure. Undirected networks and Fruchterman-Reingold are used for layout.

2.7 Statistical analyses

Statistical analyses of differences between treatments were conducted using R (v. 3.2.0). Two-way ANOVAs were used to examine the effects of two growth stages and four tillage practices on the winter wheat biomass (AB and BB), soil properties (pH, SWC, SOC, TN, TP, DOC, NH_4^+, NO_3^-, and AP) and microbial C (MBC) and N (MBN). Microbial diversity was examined using diversity metrics to analyze species diversity with QIIME, including Chao1, Observed_species, PD_whole, and Shannon's diversity. Chao1 and Observed species indices represent richness, and Shannon indices represent diversity. Tukey's HSD test was used to test pairwise comparisons. The statistically significant difference was defined at $p < 0.05$.

AMF community composition across the treatments was evaluated by principal coordinate analyses (PCoA) based on the Bray-Curtis distance. Permutational multivariate analyses of variance (PERMANOVA) with the "adonis" function in the "vegan" package were performed to examine the effect of growth stage and tillage treatment on AMF community composition. Correlation analysis was performed between each biotic and abiotic variable and AMF community composition at the OTU level (Sunagawa et al., 2015). Spearman correlations were used to examine the relationship between the abundance of dominant genera and each biotic and abiotic variable. Redundancy analysis (RDA) was used to visualize the relationships between environmental variables and soil microbial communities. The "envfit" function in the "vagan" package was used to test the correlation between each biotic and abiotic variable and AMF communities to determine the important environmental variables that can explain the variation in the composition of AMF communities (Lavergne et al., 2020).

3 Results

3.1 Wheat biomass and soil properties

Compared with the elongation stage, AB, BB, soil TN content, soil MBC and MBN content all were significantly higher in the grain filling stage ($p < 0.001$); The SOC decreased significantly in the grain filling stage ($p = 0.002$; Table 1). Compared with CT, the NT and SS treatments (both including mulching) were associated with a significant increase in AB, BB, soil pH, SOC, soil TN content, DOC, and soil MBC content, but with a significant reduction in soil AP content ($p < 0.05$; Table 1). The soil NO_3^- content and soil MBN content were higher only in the NT treatment than in the CT treatment ($p < 0.05$; Table 1).

3.2 Variation in soil AMF communities

AMF root colonization was significantly influenced by the growth stage ($F = 10.87$, $p = 0.002$) and tillage practice ($F = 58.47$, $p < 0.001$; Supplementary Figure S1). Root colonization by AMF was significantly more advanced at the grain filling stage than at the elongation stage ($p < 0.05$; Supplementary Figure S1). AMF root colonization was stronger in both NT and SS (the two tillage treatments with mulch) than in CT at both growth stages ($p < 0.05$; Supplementary Figure S1).

AMF alpha diversity, as measured by the Chao1 ($F = 22.95$, $p < 0.001$), the Observed_species ($F = 23.01$, $p < 0.001$), PD_whole ($F = 24.64$, $p < 0.001$), and Shannon diversity indexes ($F = 34.21$, $p < 0.001$), was significantly higher in the grain filling stage than in the elongation stage (Figure 1). The Chao1, the Observed_species, and PD_whole index were higher in the NT treatment than in the CT treatment at elongation ($p < 0.05$; Figure 1).

The PCoA ordination showed that the AMF community composition was clearly different among different tillage practices at elongation based on the Adonis (PERMANOVA) test ($R^2 = 0.48$, $p < 0.001$; Figure 2A). CT was clearly separated from NT and RT (Figure 2A). Similarly, the PCoA also showed that the AMF community composition was clearly different among different tillage practices for the grain filling stage based on the Adonis (PERMANOVA) test ($R^2 = 0.34$, $p < 0.001$; Figure 2B). CT was similar to RT, but was clearly separated from NT and SS (Figure 2B).

During winter wheat development, the following changes occurred in four dominant genera: the relative abundance of *Claroideoglomus* ($p = 0.011$), *Rhizophagus* ($p = 0.001$), and *Entrophospora* ($p < 0.001$) increased, whereas the relative abundance of *Funneliformis* decreased ($p < 0.001$; Figure 3). Compared with the CT treatment, the RT treatment significantly increased the relative abundance of *Claroideoglomus*, while NT and SS decreased the relative

1 https://github.com/torognes/vsearch/wiki/VSEARCH-pipeline

2 https://gephi.org

TABLE 1 Wheat above-ground biomass (AB), below-ground biomass (BB), 0–20 cm soil gravimetric water content (SWC), soil pH value, soil organic carbon content (SOC), soil total nitrogen content (TN), soil total phosphorus content (TP), soil NH_4^+ and NO_3^- content, soil dissolved organic carbon (DOC), soil available phosphorus content (AP), soil microbial C (MBC) and N (MBN) biomass in response to two crop growth stages and tillage practices.

	Stage		Tillage practices				*p*-value		
	Elongation	Grain filling	CT	RT	NT	SS	S	T	S × T
AB ($g m^{-2}$)	137b	246a	162b	168b	214a	222a	**<0.001**	**<0.001**	0.540
BB ($g m^{-2}$)	45.4b	56.8a	42.0b	44.4b	57.2a	60.8a	**<0.001**	**<0.001**	0.256
SWC (%)	6.00	6.27	5.57b	6.38ab	6.72a	5.74ab	0.415	**0.007**	0.986
pH	8.13	8.19	7.98b	8.17a	8.27a	8.23a	0.098	**<0.001**	0.375
SOC ($g kg^{-1}$)	8.40a	7.72b	7.27b	6.22b	9.02a	9.74a	**0.002**	**<0.001**	0.526
TN ($g kg^{-1}$)	0.78b	0.83a	0.72b	0.63c	0.91a	0.96a	**0.003**	**<0.001**	**0.046**
TP ($g kg^{-1}$)	1.02	1.06	0.98b	0.86c	1.12a	1.19a	0.181	**<0.001**	0.253
AP ($mg kg^{-1}$)	22.48	22.17	28.58a	21.05b	18.27b	21.42b	0.832	**<0.001**	0.472
NO_3^- ($mg kg^{-1}$)	3.56	3.92	3.26b	3.42b	4.41a	3.87ab	0.138	**0.005**	0.788
NH_4^+ ($mg kg^{-1}$)	1.91	2.38	2.52	2.37	2.22	1.47	0.093	0.056	0.845
DOC ($mg kg^{-1}$)	17.7	16.9	11.0b	9.7b	21.9a	26.6a	0.297	**<0.001**	**0.001**
MBC ($mg kg^{-1}$)	89.2b	264.5a	168.0c	117.2d	198.6b	223.7a	**<0.001**	**<0.001**	**0.001**
MBN ($mg kg^{-1}$)	9.97b	14.49a	8.18c	12.53b	19.30a	8.91c	**<0.001**	**<0.001**	**<0.001**

Bold values are significant ($p < 0.05$). S is crop stage effect; T is tillage treatment effect.
For each parameter, data in a row followed by a different lowercase letter indicates significant difference at the 0.05 probability level based on protected HSD tests.
Values for elongation stage and grain filling stage are averaged across tillage treatments ($n = 24$).
Values for tillage practices are averaged across crop stages ($n = 12$). CT, conventional tillage; NT, no tillage with mulch; RT, reduced tillage; SS, subsoiling with mulch.

abundance of *Claroideoglomus* ($p < 0.05$; Figure 3). NT significantly increased the relative abundance of *Glomus* and *Septoglomus* ($p < 0.05$; Figure 3).

Key taxa were shown based on the high betweenness centrality score of the network (Figure 4). The total AMF network was composed of 59 nodes and 81 significant edges at elongation (Figure 4A). The clustering coefficient and the average number of neighbors was 0.752 and 0.638, respectively (Figure 4A). The core groups included the OTU_120, OTU_51, OTU_122, and OTU_67 belonging to the genus *Glomus* (Figure 4A). Another taxon (OUT_231) belonged to the genus *Claroideoglomus*. The total AMF network consisted of 81 nodes, and 112 significant edges were detected at grain filling (Figure 4B). The clustering coefficient and the average number of neighbors were 0.849 and 0.661, respectively (Figure 4B). OTU_8, OTU_19, OTU_140, and OTU_175 were characterized as keystone taxa, which belonged to the genus *Glomus* (Figure 4B). OTU_28 belonged to genus *Rhizophagus* (Figure 4B).

3.3 AMF community composition was related to wheat biomass and soil environmental variables

The AMF communities were influenced by winter wheat biomass and soil properties (Figure 5). BB, SOC, TN, TP, and DOC were highly correlated with AMF community composition (Figure 5). Spearman correlation showed that significant negative correlations were found for the relative abundance of dominant genera (e.g., *Claroideoglomus* and *Funneliformis*) and plant and soil properties, whereas positive relationships were found between dominant genera (e.g., *Glomus* and *Rhizophagus*) and plant and soil properties (Figure 6). The redundancy analysis (RDA) showed significant correlations between winter wheat biomass, soil properties and dominant genera under tillage practices at different growth stages ($p < 0.05$; Figure 7). For dominant genera, the RDA1 and RDA2 explained 41.9 and 27.5% of the variance at the elongation stage, respectively (Figure 7A). At grain filling, the first two axes of the RDA analysis explained 73.9% of the total variance, with RDA1 and RDA2 explaining 59.2 and 14.7% of the variance for dominant genera, respectively (Figure 7B). The envfit function showed that environmental variables explained 64.6 and 71.5% of the differences in dominant genera at different growth stages, respectively (Figures 7C,D). SOC was the primary environmental variable affecting the dominant genera at elongation, whereas TN was the primary variable affecting the dominant genera at grain filling (Figures 7C,D).

4 Discussion

4.1 Crop stage affects the AMF composition

The change in the dominant genera during crop growth affected the community composition of AMF. In this study, the change of dominant genera, including *Claroideoglomus*, *Funneliformis*, *Rhizophagus*, *Entrophospora*, and *Glomus*, altered the community composition of AMF. In addition, our co-occurrence network demonstrated that changes in network complexity could also explain seasonal changes in AMF community structure. The change in keystone OTUs (belongs to the dominant genera *Glomus*, *Claroideoglomus*, and *Rhizophagus*) related to winter wheat growth stage further influenced AMF community composition. In addition, we also found that the relationships between dominant genera

10.3389/fmicb.2024.1394104

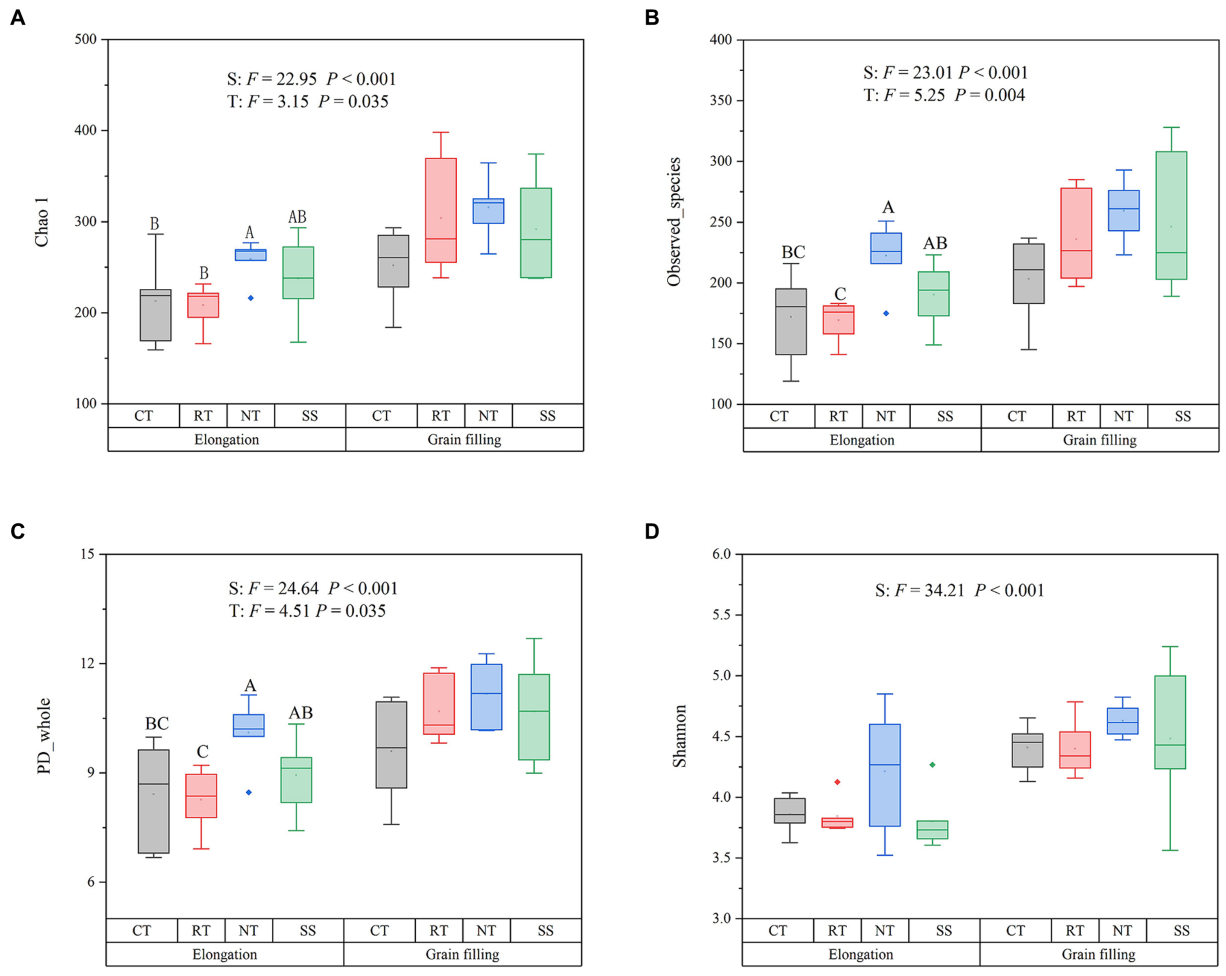

FIGURE 1
Responses of the alpha diversity of AMF to different tillage practices at two growth stages. Chao 1 **(A)**; Observed_species **(B)**; PD_whole **(C)**; Shannon **(D)**. Results are reported as the mean ± standard error ($n = 6$). For each parameter, a different letter indicates a significant difference at the 0.05 probability level ($p < 0.05$) based on Tukey's honest test. CT, conventional tillage ($n = 6$); NT, no tillage with mulch ($n = 6$); RT, reduced tillage ($n = 6$); SS, subsoiling with mulch ($n = 6$).

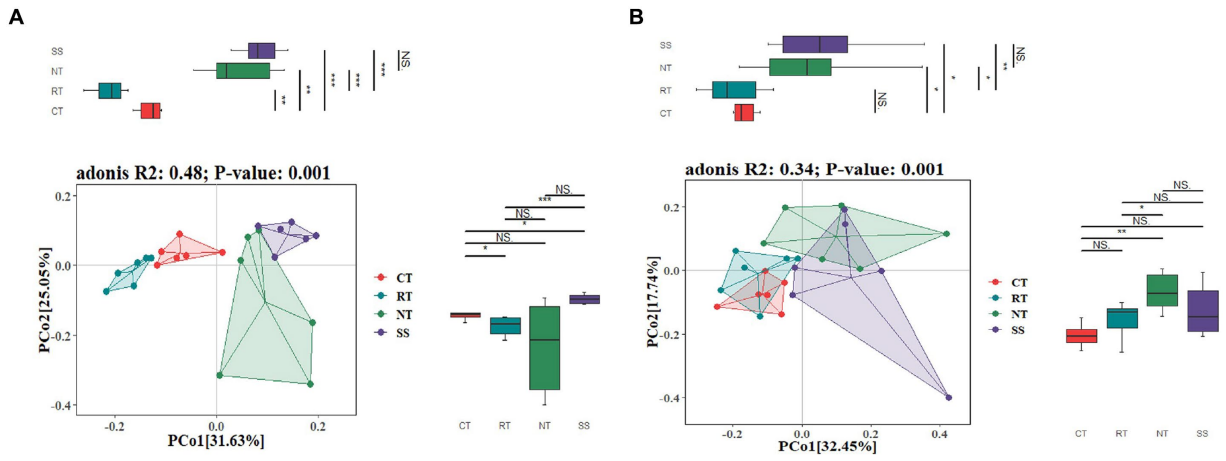

FIGURE 2
Principal coordinate analysis (PCoA) of the dissimilarity of AMF based on the Bray–Curtis distance at elongation stage **(A)** and grain filling stage **(B)**. CT, conventional tillage ($n = 6$); NT, no tillage with mulch ($n = 6$); RT, reduced tillage ($n = 6$); SS, subsoiling with mulch ($n = 6$).

10.3389/fmicb.2024.1394104

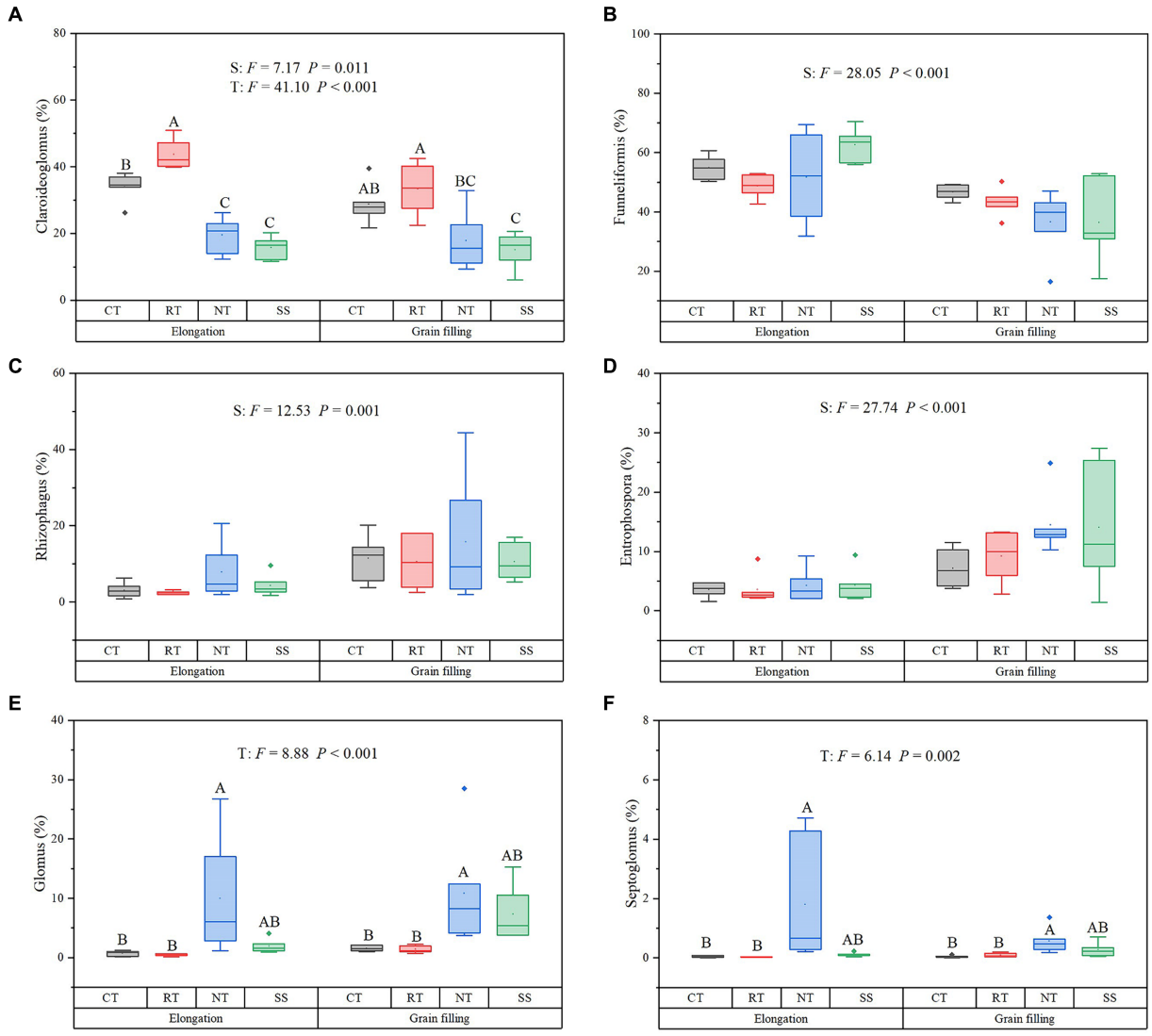

FIGURE 3
Response of dominant genera to different tillage practices at two growth stages. For each parameter, a different letter indicates a significant difference at the 0.05 probability level ($p < 0.05$) based on Tukey's honest test. Shown are the dominant genera: *Claroideoglomus* **(A)**, *Funneliformis* **(B)**, *Rhizophagus* **(C)**, *Entrophospora* **(D)**, *Glomus* **(E)**, and *Septoglomus* **(F)**. CT, conventional tillage ($n = 6$); NT, no tillage with mulch ($n = 6$); RT, reduced tillage ($n = 6$); SS, subsoiling with mulch ($n = 6$).

(negative relationship: *Claroideoglomus*, *Funneliformis*; positive relationship: *Rhizophagus*, *Entrophospora*, *Glomus*, and *Septoglomus*) and plant biomass altered AMF community composition. This means that growth dynamics could have mediated the relationship between AMF community structure and tillage practices in our study.

Soil nutrients alter AMF communities at different crop stages (Ma et al., 2019). In our study, the mycorrhizal colonization at grain filling was significantly more advanced than elongation (Supplementary Figure S1). A higher mycorrhizal infection could help plants increase their uptake of nutrients (e.g., N and P), thereby promoting plant growth (Gu et al., 2020; Liu et al., 2022). As a result, the change in wheat yield during different crop stages resulted in alterations in AMF communities.

Our results were consistent with previous studies (Abu-Elsaoud et al., 2017), in which the AMF was able to deliver more nutrients during grain filling due to the high nutrient requirement. In addition, MRT results also indicated that soil nitrogen utilization efficiency (TN and NO_3^-) played an important role in determining AMF community composition. Moreover, carbon requirements and photosynthetic capacity also affect the community composition of AMF (Louise et al., 2007). Previous studies have shown that the photosynthetic carbon allocation to soil decreased from approximately 10% at elongation to 5% at grain filling in wheat (Sun et al., 2018). In our study, the change of SOC from the elongation stage to the grain filling stage indicated that soil organic carbon affected the AMF community composition. Therefore, the higher SOC at elongation than at grain filling led to the change in the community composition of AMF in our study.

4.2 Long-term tillage shifts AMF composition

Long-term conservation tillage (e.g., NT or SS) increased root mycorrhizal colonization. Our results support that the formation of a

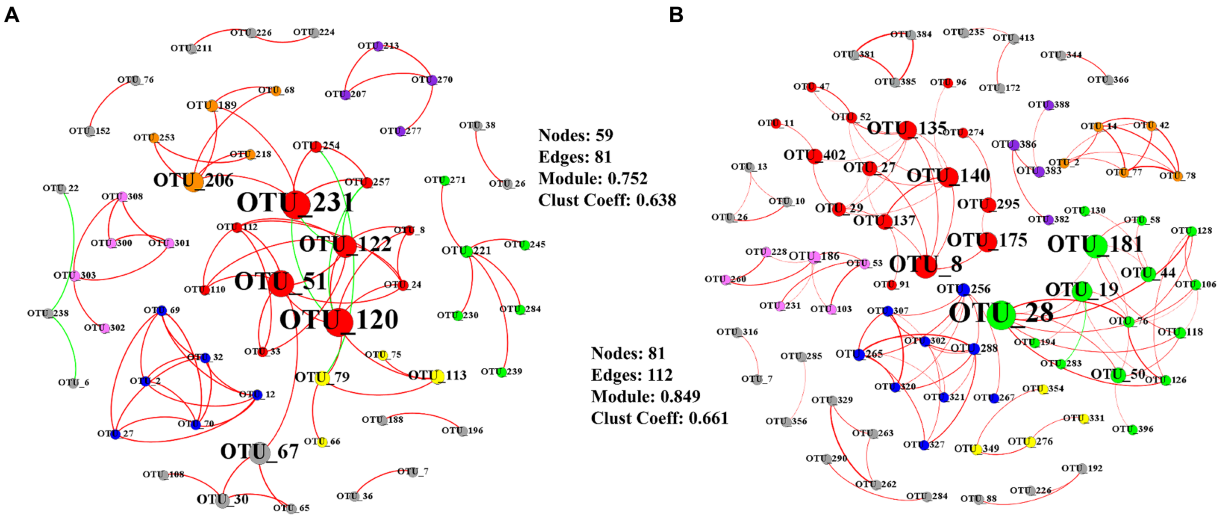

FIGURE 4
Co-occurrence networks of AMF at elongation stage **(A)** and grain filling stage **(B)**. Only Pearson's correlation coefficients ($r > 0.8$ or $r < -0.8$ significant at $p < 0.05$) are shown. Node sizes are proportional to the value of betweenness centrality. Red edges represent positive correlations and green edges represent negative correlations. The colors of the nodes represent the AMF modules.

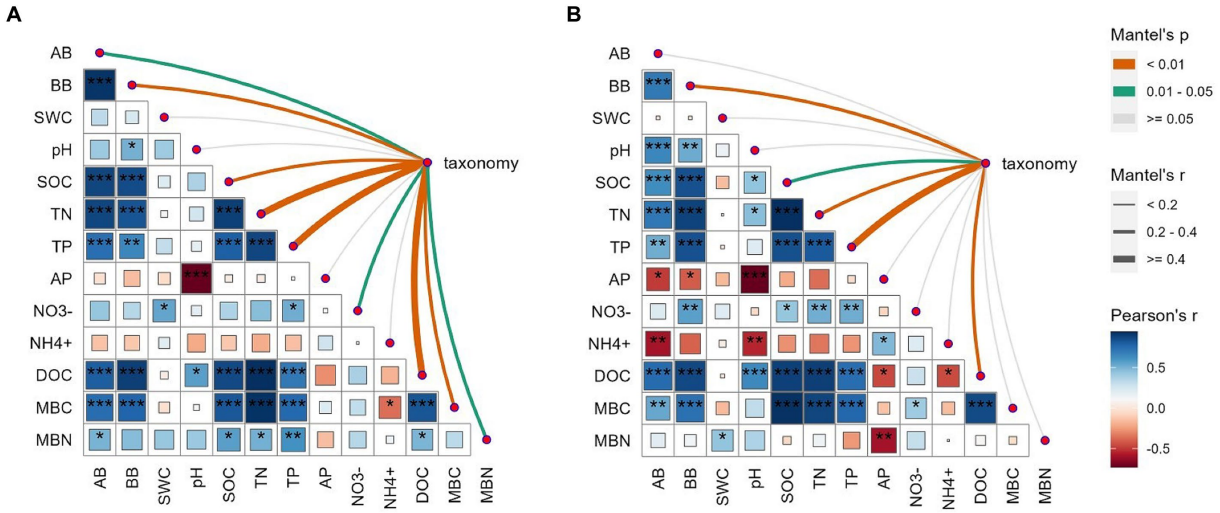

FIGURE 5
Correlation analysis between measured variables (wheat biomass and soil physicochemical properties) and AMF community composition at the OTU level under elongation stage **(A)** and grain filling stage **(B)**. Circle colors and sizes represent Spearman's correlation coefficient (r) values, while *, **, and *** indicate statistically significant differences at $p < 0.05$, $0.01 \leq p \leq 0.05$, and $p < 0.01$, respectively. The color and edge widths of the association lines represent Mantel r values, while red and gray lines represent $p < 0.05$ and $p > 0.05$ statistical significance values, respectively.

high colonization rate is linked to plants with rich roots and rapid growth (Ma et al., 2019). Increased contact between roots and AMF propagules under NT or SS can enhance the ability of plants to provide photosynthetic products to fungi, such as grass root systems. Moreover, the NT or SS did not disrupt or weakly interfere with the hyphal networks and dilution of AMF propagules (Kabir, 2005), which is more beneficial to the symbiosis between plants and AMF. We found that the AMF diversity was significantly increased under NT compared to conventional tillage. The results are in agreement with those of previous studies, in which NT versus conventional tillage markedly changed Chao 1, observed species, and PD_whole of AMF at elongation in a greenhouse experiment in Chile (Aguilera et al., 2021), a field experiment in north China (Hu et al., 2015), and a field experiment in Spain (Gu et al., 2020).

In the present study, significant differences in AMF community structure between conservation tillage (NT and SS) and conventional tillage practices can be attributed to changes in the relative abundance of *Claroideoglomus*, *Glomus*, and *Septoglomus*. The genus *Claroideoglomus* can be found in dry or extreme habitats (Al-Yahyáei et al., 2022; Ng et al., 2023). *Claroideoglomus* produces low-radical propagules, which are internal root structures consistent with stress tolerance strategies (Chagnon et al., 2013). As the most abundant

10.3389/fmicb.2024.1394104

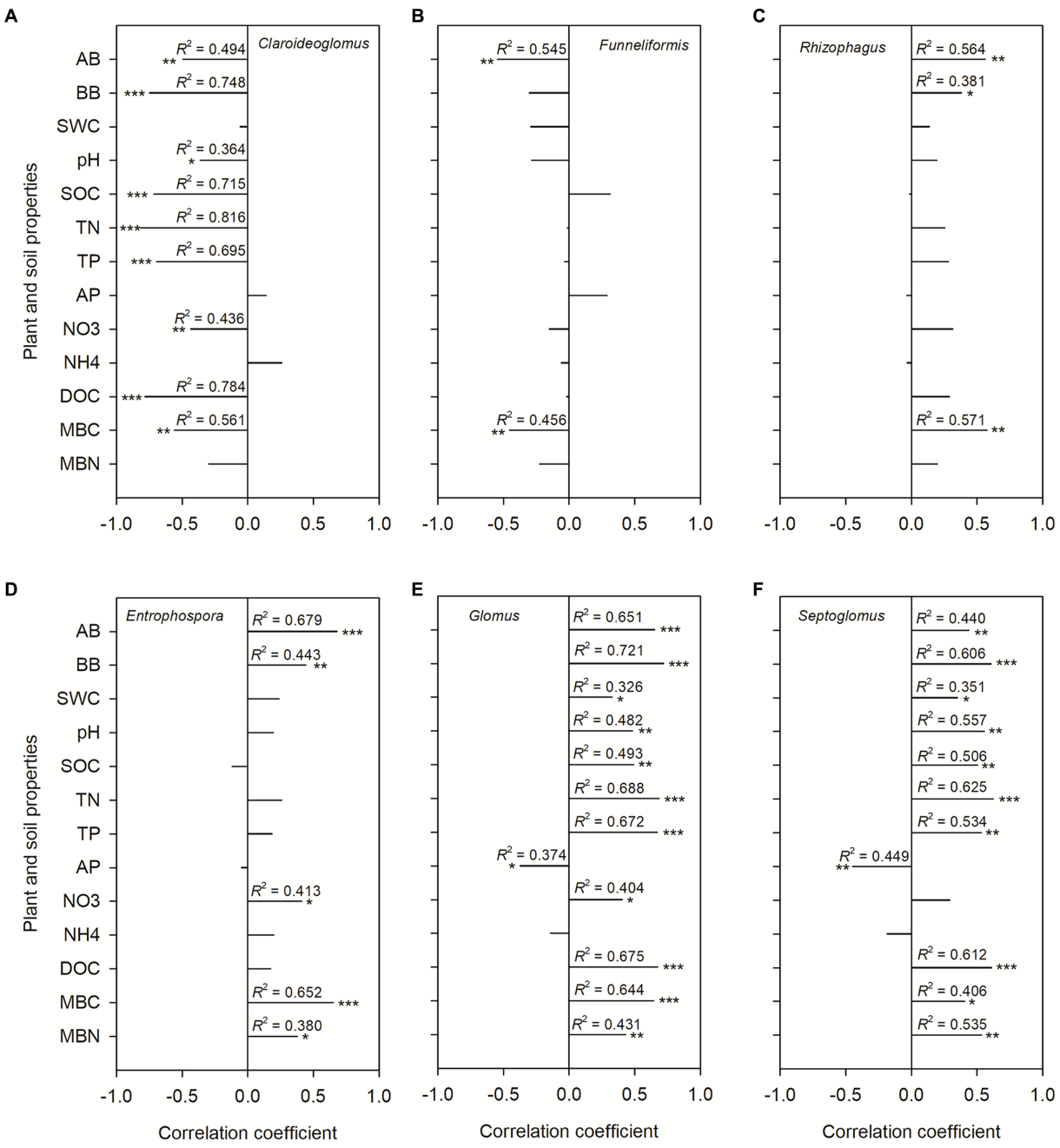

FIGURE 6
The Spearman correlation coefficients between dominant genera and plant and soil properties. Shown are the dominant genera: *Claroideoglomus* **(A)**, *Funneliformis* **(B)**, *Rhizophagus* **(C)**, *Entrophospora* **(D)**, *Glomus* **(E)**, and *Septoglomus* **(F)**. The correlations were derived for above-ground biomass (AB), below-ground biomass (BB), 0–20 cm soil gravimetric water content (SWC), soil pH value, soil organic carbon content (SOC), soil total nitrogen content (TN), soil total phosphorus content (TP), soil NH4 (NH_4^+) and NO3 (NO_3^-) content, soil dissolved organic carbon (DOC), soil available phosphorus content (AP), soil microbial C (MBC) and N (MBN) biomass.

genus of AMF across all four treatments, this functional trait may be useful in reducing the impact of abiotic stress factors on the growth of symbiotic plants in conventional tillage practices. In addition, the change in *Glomus* abundance also affects the community composition of AMF through the differences in network complexity. The higher abundance of *Glomus* in NT than in CT is attributed to *Glomus* and may be a legacy of land use due to the tillage history of all experimental plots (Liu et al., 2022). Once conventional tillage practices are suspended, the dominance of highly competitive *Glomus* species may further increase (Sangabriel-Conde et al., 2015). Our results are also in line with a previous study in Mediterranean agroecosystems (Avio et al., 2013), in which *Glomus* species were strong indicators of no-till management and were prevalent in no-till soils.

We observed that wheat biomass and soil properties were negatively correlated with the abundance of *Claroideoglomus*. We attribute the high abundance of *Claroideoglomus* under CT and

10.3389/fmicb.2024.1394104

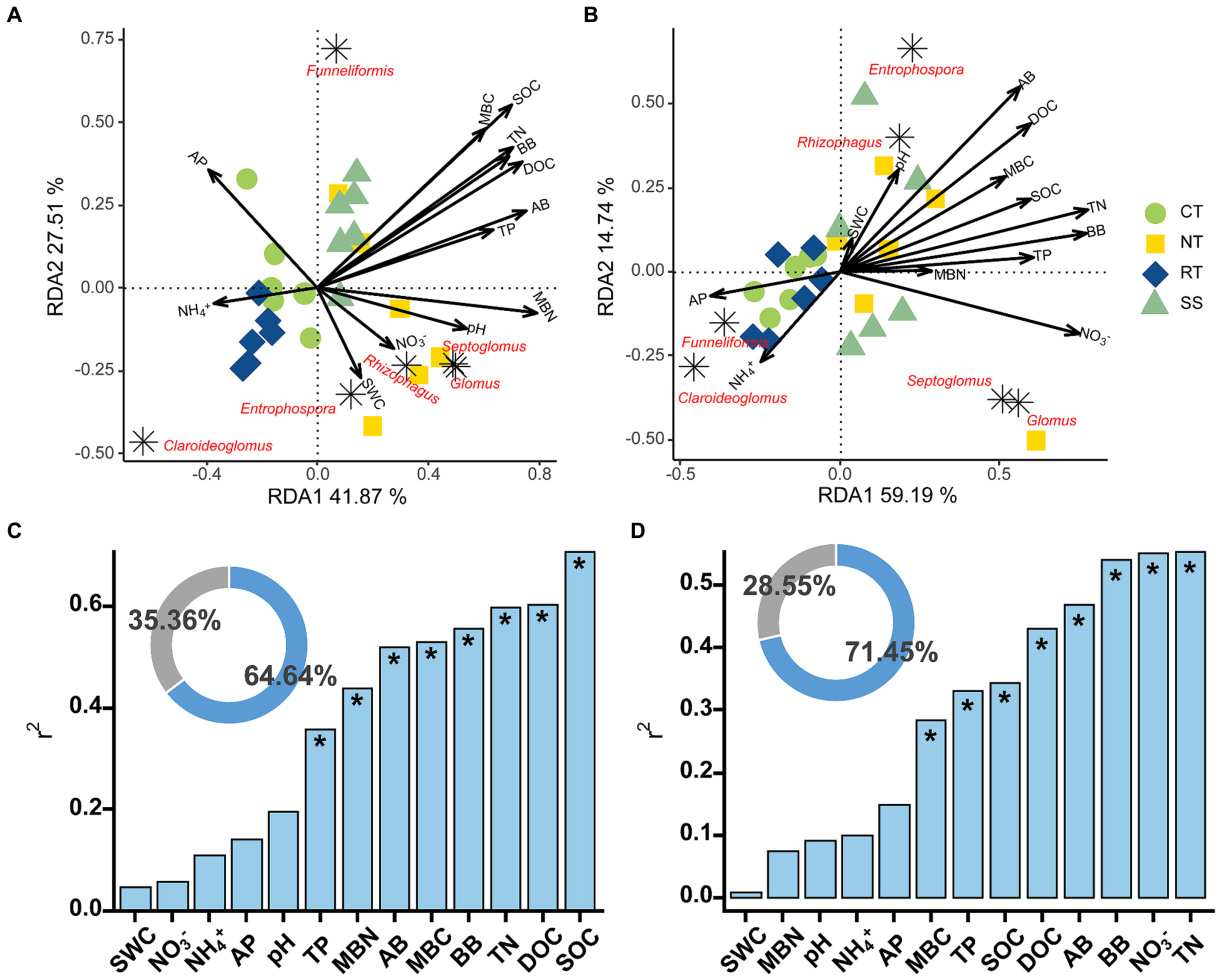

FIGURE 7
Redundancy analysis (RDA) of AMF dominant genera and environmental variables at elongation stage **(A)** and grain filling stage **(B)**. The Envfit function was used to identify important environmental variables associated with order under elongation stage **(C)** and grain filling stage **(D)**. The blue part of the circle diagram represents the degree of explanation of community composition differences by environmental variables, while the gray part represents the part of community structure differences that are unexplained by environmental variables. Significance level is as follows: $*p < 0.05$.

RT mainly to the adaptation to scarce resources with stress-tolerant life history traits (Silvani et al., 2017). The positive correlation between wheat biomass and *Glomus* abundance indicates that NT and SS can promote soil AMF communities by increasing soil fertility, thereby establishing a mutually beneficial symbiotic relationship with wheat plants and gradually increasing wheat yield (Bunn et al., 2015). In addition, higher TP in the NT and SS treatment also agreed with a previous study where higher soil P content was positively correlated with the relative abundance of *Glomus* and *Septoglomus* (Song et al., 2019; Liu et al., 2022).

5 Conclusion

Our results indicate that AMF communities change through the increase or decrease of dominant genera effectively buffering the impact of the ecosystem on environmental changes, thereby improving the overall resilience of the dry environment. No significant difference in AMF community was detected between RT and CT, whereas NT and SS significantly changed the AMF community composition at both growth stages. The CT treatment had higher proportions of the genus *Claroideoglomus*, whereas a higher proportion of the genera *Glomus* and *Septoglomus* was found under NT. Our further study confirmed that NT and SS affected the composition of key genera by changing plant biomass and soil characteristics, thereby affecting the AMF community composition. Our results highlight the importance of wheat biomass and soil properties in modulating the AMF communities. NT and SS are proper tillage practices, which may contribute to the development of sustainable agricultural production in Loess Plateau environments.

Data availability statement

The data presented in this study are deposited in the online repositories: https://www.ncbi.nlm.nih.gov/sra, accession number PRJNA1090622.

Author contributions

JiL: Data curation, Methodology, Software, Writing – original draft, Writing – review & editing. LiJ: Data curation, Software, Writing

– review & editing. PS: Writing – review & editing. ZA: Writing – review & editing. ZW: Conceptualization, Data curation, Writing – review & editing. ZX: Writing – review & editing. LeJ: Data curation, Software, Writing – review & editing. YY: Data curation, Writing – review & editing. JuL: Data curation, Software, Writing – review & editing. TZ: Data curation, Writing – review & editing. KJ: Project administration, Resources, Writing – review & editing.

Funding

The author(s) declare that financial support was received for the research, authorship, and/or publication of this article. This work was financially supported by the Program of the National Key R&D Program of China (2022YFD1900300) and the National Natural Science Foundation of China (32071861 and 32201408).

Acknowledgments

We thank Shaopeng Wang and many others for setting up the experiments.

Conflict of interest

The authors declare that the research was conducted in the absence of any commercial or financial relationships that could be construed as a potential conflict of interest.

Publisher's note

Supplementary material

The Supplementary material for this article can be found online at: https://www.frontiersin.org/articles/10.3389/fmicb.2024.1394104/full#supplementary-material

References

Abu-Elsaoud, A. M., Nafady, N. A., and Abdel-Azeem, A. M. (2017). Arbuscular mycorrhizal strategy for zinc mycoremediation and diminished translocation to shoots and grains in wheat. *PLoS One* 12:e0188220. doi: 10.1371/journal.pone.0188220

Aguilera, P., Romero, J. K., Becerra, N., Martínez, O., Vilela, R., Borie, F., et al. (2021). Phenological stages and Aluminum presence influences arbuscular mycorrhizal fungi communities in roots of plant cereals. *J. Soil Sci. Plant Nutr.* 21, 1467–1473. doi: 10.1007/s42729-021-00453-9

Al-Yahyáei, M. N., Błaszkowski, J., Al-Hashmi, H., Al-Farsi, K., Al-Rashdi, I., Patzelt, A., et al. (2022). From isolation to application: a case study of arbuscular mycorrhizal fungi of the Arabian peninsula. *Symbiosis* 86, 123–132. doi: 10.1007/s13199-021-00824-x

Augé, R. M., Toler, H. D., and Saxton, A. M. (2015). Arbuscular mycorrhizal symbiosis alters stomatal conductance of host plants more under drought than under amply watered conditions: a meta-analysis. *Mycorrhiza* 25, 13–24. doi: 10.1007/s00572-014-0585-4

Avio, L., Castaldini, M., Fabiani, A., Bedini, S., Sbrana, C., Turrini, A., et al. (2013). Impact of nitrogen fertilization and soil tillage on arbuscular mycorrhizal fungal communities in a Mediterranean agroecosystem. *Soil Biol. Biochem.* 67, 285–294. doi: 10.1016/j.soilbio.2013.09.005

Balota, E. L., Machineski, O., Honda, C., Yada, I. F. U., Barbosa, G. M. C., Nakatani, A. S., et al. (2016). Response of arbuscular mycorrhizal fungi in different soil tillage systems to long-term swine slurry application. *L. Degrad. Dev.* 27, 1141–1150. doi: 10.1002/ldr.2304

Blois, J. L., Williams, J. W., Fitzpatrick, M. C., Jackson, S. T., and Ferrier, S. (2013). Space can substitute for time in predicting climate change effects on biodiversity. *Proc. Natl. Acad. Sci. USA* 110, 9374–9379. doi: 10.1073/pnas.1220228110

Bowles, T. M., Jackson, L. E., Loeher, M., and Cavagnaro, T. R. (2017). Ecological intensification and arbuscular mycorrhizas: a meta-analysis of tillage and cover crop effects. *J. Appl. Ecol.* 54, 1785–1793. doi: 10.1111/1365-2664.12815

Bunn, R. A., Ramsey, P. W., Lekberg, Y., and van der Heijden, M. (2015). Do native and invasive plants differ in their interactions with arbuscular mycorrhizal fungi? A meta-analysis. *J. Ecol.* 103, 1547–1556. doi: 10.1111/1365-2745.12456

Carballar-Hernández, S., Hernández-Cuevas, L. V., Montaño, N. M., Larsen, J., FerreraCerrato, R., Taboada-Gaytán, O. R., et al. (2017). Native communities of arbuscular mycorrhizal fungi associated with *Capsicum annuum L.* respond to soil properties and agronomic management under field conditions. *Agric. Ecosyst. Environ.* 245, 43–51. doi: 10.1016/j.agee.2017.05.004

Chagnon, P., Bradley, R. L., Maherali, H., and Klironomos, J. N. (2013). A trait-based framework to understand life history of mycorrhizal fungi. *Trends Plant Sci.* 18, 484–491. doi: 10.1016/j.tplants.2013.05.001

Chen, H., Liang, Q., Gong, Y., Kuzyakov, Y., Fan, M., and Plante, A. F. (2019). Reduced tillage and increased residue retention increase enzyme activity and carbon and nitrogen concentrations in soil particle size fractions in a long-term field experiment on loess plateau in China. *Soil Tillage Res.* 194:104296. doi: 10.1016/j.still.2019.104296

Curaqueo, G., Barea, J. M., Acevedo, E., Rubio, R., Cornejo, P., and Borie, F. (2011). Effects of different tillage system on arbuscular mycorrhizal fungal propagules and physical properties in a Mediterranean agroecosystem in Central Chile. *Soil Tillage Res.* 113, 11–18. doi: 10.1016/j.still.2011.02.004

Edwards, J., Johnson, C., Santos-Medellín, C., Lurie, E., Podishetty, N. K., Bhatnagar, S., et al. (2015). Structure, variation, and assembly of the root-associated microbiomes of rice. *Proc. Natl. Acad. Sci. USA* 112, E911–E920. doi: 10.1073/pnas.1414592112

Gu, S., Wu, S., Guan, Y., Zhai, C., Zhang, Z., Bello, A., et al. (2020). Arbuscular mycorrhizal fungal community was affected by tillage practices rather than residue management in black soil of Northeast China. *Soil Tillage Res.* 198:104552. doi: 10.1016/j.still.2019.104552

Hamonts, K., Trivedi, P., Garg, A., Janitz, C., Grinyer, J., Holford, P., et al. (2018). Field study reveals core plant microbiota and relative importance of their drivers. *Environ. Microbiol.* 20, 124–140. doi: 10.1111/1462-2920.14031

Hu, J., Yang, A., Zhu, A., Wang, J., Dai, J., Wong, M. H., et al. (2015). Arbuscular mycorrhizal fungal diversity, root colonization, and soil alkaline phosphatase activity in response to maize-wheat rotation and no-tillage in North China. *J. Microbiol.* 53, 454–461. doi: 10.1007/s12275-015-5108-2

Jansa, J., Mozafar, A., Kuhn, G., Anken, T., Ruh, R., Sanders, I. R., et al. (2003). Soil tillage affects the community structures of mycorrhizal fungi in maize roots. *Ecol. Appl.* 13, 1164–1176. doi: 10.1890/1051-0761(2003)13[1164:statcs]2.0.co;2

Jia, L., Wang, Z., Ji, L., De Neve, S., Struik, P. C., Yao, Y., et al. (2022). Keystone microbiome in the rhizosphere soil reveals the effect of long-term conservation tillage on crop growth in the Chinese loess plateau. *Plant Soil* 473, 457–472. doi: 10.1007/s11104-022-05297-5

Jin, K., De Neve, S., Moeskops, B., Lu, J. J., Zhang, J., Gabriels, D., et al. (2008). Effects of different soil management practices on winter wheat yield and N losses on a dryland loess soil in China. *Soil Res.* 46, 455–463. doi: 10.1071/sr07134

Jin, K., Sleutel, S., Buchan, D., De Neve, S., Cai, D. X., Gabriels, D., et al. (2009). Changes of soil enzyme activities under different tillage practices in the Chinese loess plateau. *Soil Tillage Res.* 104, 115–120. doi: 10.1016/j.still.2009.02.004

Kabiri, V., Raiesi, F., and Ghazavi, M. A. (2016). Tillage effects on soil microbial biomass, SOM mineralization and enzyme activity in a semi-arid Calcixerepts. *Agric. Ecosyst. Environ.* 232, 73–84. doi: 10.1016/j.agee.2016.07.022

Kabir, Z. (2005). Tillage or no-tillage: impact on mycorrhizae. *Can. J. Plant Sci.* 85, 23–29. doi: 10.4141/p03-160

Koljalg, U., Nilsson, R. H., Abarenkov, K., Tedersoo, L., Taylor, A. F. S., Bahram, M., et al. (2013). Towards a unified paradigm for sequence-based identification of fungi. *Mol. Ecol.* 22, 5271–5277. doi: 10.1111/mec.12481

Lavergne, C., Bovio-Winkler, P., Etchebehere, C., and Garcia-Gen, S. (2020). Towards centralized biogas plants: co-digestion of sewage sludge and pig manure maintains process performance and active microbiome diversity. *Bioresour. Technol.* 297:122442. doi: 10.1016/j.biortech.2019.122442

Liu, C., Cui, Y. M., Li, X. A., and Yao, M. J. (2021). Microeco: an R package for data mining in microbial community ecology. *FEMS Microbiol. Ecol.* 97:fiaa255. doi: 10.1093/femsec/fiaa255

Liu, W., Ma, K., Wang, X., Wang, Z., and Negrete-Yankelevich, S. (2022). Effects of no-tillage and biologically-based organic fertilizer on soil arbuscular mycorrhizal fungal communities in winter wheat field. *Appli. Soil Ecol.* 178:104564. doi: 10.1016/j.apsoil.2022.104564

Louise, M., Egerton-Warburto, N. C. J., and Allen, E. B. (2007). Mycorrhizal community dynamics following nitrogen fertilization: a cross-site test in five grasslands. *Ecol. Monogr.* 77, 527–544. doi: 10.1890/06-1772.1

Lupatini, M., Suleiman, A. K. A., Jacques, R. J. S., Antoniolli, Z. I., de Siqueira, F. A., Kuramae, E. E., et al. (2014). Network topology reveals high connectance levels and few key microbial genera within soils. *Front. Environ. Sci.* 2:10. doi: 10.3389/fenvs.2014.00010

Ma, X., Luo, W., Li, J., and Wu, F. (2019). Arbuscular mycorrhizal fungi increase both concentrations and bioavailability of Zn in wheat (*Triticum aestivum* L) grain on Zn-spiked soils. *Appl. Soil Ecol.* 135, 91–97. doi: 10.1016/j.apsoil.2018.11.007

McGonigle, T. P., Miller, M. H., Evans, D. G., Fairchild, G. L., and Swan, J. A. (1990). A new method which gives an objective measure of colonization of roots by vesicular-arbuscular mycorrhizal fungi. *New Phytol.* 115, 495–501. doi: 10.1111/j.1469-8137.1990.tb00476.x

Merryweather, J., and Fitter, A. (1998). The arbuscular mycorrhizal fungi of *Hyacinthoides nonscripta* II. Seasonal and spatial patterns of fungal populations. *New Phytol.* 138, 131–142. doi: 10.1046/j.1469-8137.1998.00889.x

Nelson, D. W., and Sommers, L. E. (1983). Total carbon, organic carbon, and organic matter. *Methods of soil analysis: Part 2 chemical and microbiological properties*, 9, 539–579. doi: 10.2136/sssabookser5.3.c34

Ng, A., Wilson, B. A. L., and Frew, A. (2023). Belowground crop responses to root herbivory are associated with the community structure of native arbuscular mycorrhizal fungi. *Appl. Soil Ecol.* 185:104797. doi: 10.1016/j.apsoil.2022.104797

Oehl, F., and Koch, B. (2018). Diversity of arbuscular mycorrhizal fungi in no-till and conventionally tilled vineyards. *J. Appl. Bot. Food Qual.* 91, 56–60. doi: 10.5073/JABFQ.2018.091.008

Panneerselvam, P., Kumar, U., Senapati, A., Parameswaran, C., Anandan, A., Kumar, A., et al. (2020). Influence of elevated CO_2 on arbuscular mycorrhizal fungal community elucidated using illumina MiSeq platform in subhumid tropical paddy soil. *Appl. Soil Ecol.* 145:103344. doi: 10.1016/j.apsoil.2019.08.006

Säle, V., Aguilera, P., Laczko, E., Mäder, P., Berner, A., Zihlmann, U., et al. (2015). Impact of conservation tillage and organic farming on the diversity of arbuscular mycorrhizal fungi. *Soil Biol. Biochem.* 84, 38–52. doi: 10.1016/j.soilbio.2015.02.005

Sangabriel-Conde, W., Maldonado-Mendoza, I. E., Mancera-Lopez, M. E., Cordero-Ramírez, J. D., Trejo-Aguilar, D., and Negrete-Yankelevich, S. (2015). Glomeromycota associated with Mexican native maize landraces in Los Tuxtlas, Mexico. *Appl. Soil Ecol.* 87, 63–71. doi: 10.1016/j.apsoil.2014.10.017

Schalamuk, S., Velásquez, H., Chidichimo, H., and Cabello, M. (2004). Effect of no-till and conventional tillage on mycorrhizal colonization in spring wheat. *Bol. Soc. Argent. Bot.* 18, 13–20. doi: 10.22370/bolmicol.2003.18.0.375

Schnoor, T. K., Lekberg, Y., Rosendahl, S., and Olsson, P. A. (2011). Mechanical soil disturbance as a determinant of arbuscular mycorrhizal fungal communities in semi-natural grassland. *Mycorrhiza* 21, 211–220. doi: 10.1007/s00572-010-0325-3

Silvani, V. A., Colombo, R. P., Scorza, M. V., Bidondo, L. F., Rothen, C. P., Scotti, A., et al. (2017). Arbuscular mycorrhizal fungal diversity in high-altitude hypersaline Andean wetlands studied by 454-sequencing and morphological approaches. *Symbiosis* 72, 143–152. doi: 10.1007/s13199-016-0454-3

Singh, K., Mishra, A. K., Singh, B., Singh, R. P., and Patra, D. D. (2016). Tillage effects on crop yield and physicochemical properties of sodic soils. *L. Degrad. Dev.* 27, 223–230. doi: 10.1002/ldr.2266

Soil Survey Staff, (2003). *Keys to soil taxonomy*, *9th* USDA Handbook, NRCS, Washington, DC

Song, J., Han, Y., Bai, B., Jin, S., He, Q., and Ren, J. (2019). Diversity of arbuscular mycorrhizal fungi in rhizosphere soils of the Chinese medicinal herb *Sophora flavescens* ait. *Soil Tillage Res.* 195:104423. doi: 10.1016/j.still.2019.104423

Song, Y. N., Zhang, F. S., Marschner, P., Fan, F. L., Gao, H. M., Bao, X. G., et al. (2007). Effect of intercropping on crop yield and chemical and microbiological properties in rhizosphere of wheat (*Triticum aestivum L.*), maize (*Zea mays L.*), and faba bean (*Vicia faba L.*). *Biol. Fertil. Soils* 43, 565–574. doi: 10.1007/s00374-006-0139-9

Sunagawa, S., Coelho, L. P., Chaffron, S., Kultima, J. R., Labadie, K., Salazar, G., et al. (2015). Structure and function of the global ocean microbiome. *Science* 348:1261359. doi: 10.1126/science.1261359

Sun, Z., Chen, Q., Han, X., Bol, R., Qu, B., and Meng, F. (2018). Allocation of photosynthesized carbon in an intensively farmed winter wheat– soil system as revealed by $^{14}CO_2$ pulse labelling. *Sci. Rep.* 8, 1–10. doi: 10.1038/s41598-018-21547-y

Suzuki, K., Takahashi, K., and Harada, N. (2020). Evaluation of primer pairs for studying arbuscular mycorrhizal fungal community compositions using a MiSeq platform. *Biol. Fertil. Soils* 56, 853–858. doi: 10.1007/s00374-020-01431-6

Vance, E. D., Brookes, P. C., and Jenkinson, D. (1987). An extraction method for measuring microbial biomass carbon. *Soil Biol. Biochem.* 19, 703–707. doi: 10.1016/0038-0717(87)90052-6

Van Geel, M., Busschaert, P., Honnay, O., and Lievens, B. (2014). Evaluation of six primer pairs targeting the nuclear rRNA operon for characterization of arbuscular mycorrhizal fungal (AMF) communities using 454 pyrosequencing. *J. Microbiol. Methods* 106, 93–100. doi: 10.1016/j.mimet.2014.08.006

Walder, F., and van der Heijden, M. (2015). Regulation of resource exchange in the arbuscular mycorrhizal symbiosis. *Nat. Plants* 1:15159. doi: 10.1038/nplants.2015.159

Wang, S. L., Wang, H., Muhammad, B. H., Zhang, Q., Yu, Q., Wang, R., et al. (2020). No-tillage and subsoiling increased maize yields and soil water storage under varied rainfall distribution: a 9-year site-specific study in a semiarid environment. *Field Crop Res.* 255, 107867–107869. doi: 10.1016/j.fcr.2020.107867

Wang, W. X., Shi, J. C., Xie, Q. J., Jiang, Y. N., Yu, N., and Wang, E. T. (2017). Nutrient exchange and regulation in arbuscular mycorrhizal symbiosis. *Mol. Plant* 10, 1147–1158. doi: 10.1016/j.molp.2017.07.012

Wang, Z., Li, Y., Li, T., Zhao, D., and Liao, Y. (2020). Tillage practices with different soil disturbance shape the rhizosphere bacterial community throughout crop growth. *Soil Tillage Res.* 197:104501. doi: 10.1016/j.still.2019.104501

Xia, Q., Liu, X., Gao, Z., Wang, J., and Yang, Z. (2020). Responses of rhizosphere soil bacteria to 2-year tillage rotation treatments during fallow period in semiarid southeastern Loess Plateau. *Peerj* 8:e8853. doi: 10.7717/peerj.8853

Xiao, D., Xiao, S., Ye, Y., Zhang, W., He, X., and Wang, K. (2019). Microbial biomass, metabolic functional diversity, and activity are affected differently by tillage disturbance and maize planting in a typical karst calcareous soil. *J. Soils Sediments* 19, 809–821. doi: 10.1007/s11368-018-2101-5

Xue, L. Z., Khan, S., Sun, M., Anwar, S., Ren, A. X., Gao, Z. Q., et al. (2019). Effects of tillage practices on water consumption and grain yield of dryland winter wheat under different precipitation distribution in the loess plateau of China. *Soil Tillage Res.* 191, 66–74. doi: 10.1016/j.still.2019.03.014

Yang, Y., Song, Y., Scheller, H. V., Ghosh, A., Bai, Y., Chen, H., et al. (2015). Community structure of arbuscular mycorrhizal fungi associated with *Robinia pseudoacacia* in uncontaminated and heavy metal contaminated soils. *Soil Biol. Biochem.* 86, 146–158. doi: 10.1016/j.soilbio.2015.03.018

Yan, S. S., Song, J. M., Fan, J. S., Yan, C., Dong, S. K., Ma, C. M., et al. (2020). Changes in soil organic carbon fractions and microbial community under rice straw return in Northeast China. *Glob. Ecol. Conserv.* 22, e00962–e00912. doi: 10.1016/j.gecco.2020.e00962

Zhang, S., Li, Q., Lü, Y., Sun, X., Jia, S., Zhang, X., et al. (2015). Conservation tillage positively influences the microflora and microfauna in the black soil of Northeast China. *Soil Tillage Res.* 149, 46–52. doi: 10.1016/j.still.2015.01.001

Zuber, S. M., Behnke, G. D., Nafziger, E. D., and Villamil, M. B. (2015). Crop rotation and tillage effects on soil physical and chemical properties in Illinois. *Agron. J.* 107, 971–978. doi: 10.2134/agronj14.0465

frontiers | Frontiers in Environmental Science

TYPE Original Research
PUBLISHED 09 April 2024
DOI 10.3389/fenvs.2024.1362366

OPEN ACCESS

EDITED BY
Peng Shi,
Xi'an University of Technology, China

REVIEWED BY
Bayram Yuksel,
Giresun University, Türkiye
Yuanpeng Wang,
Xiamen University, China
Jiang Yu,
Sichuan University, China

*CORRESPONDENCE
Tingting Liu,
liusha@zju.edu.cn

RECEIVED 28 December 2023
ACCEPTED 25 March 2024
PUBLISHED 09 April 2024

CITATION
Liu T, Ni SY and Wang Z (2024), Contamination and health risk assessment of heavy metals in soil surrounding an automobile industry factory in Jiaxing, China.
Front. Environ. Sci. 12:1362366.
doi: 10.3389/fenvs.2024.1362366

Contamination and health risk assessment of heavy metals in soil surrounding an automobile industry factory in Jiaxing, China

Tingting Liu[1]*, Sheng Yue Ni[2] and Zhen Wang[1]

[1]Institute of Environmental Engineering, Department of Ecological Health, Hangzhou Vocational and Technical College, Hangzhou, China, [2]Department of Design, Zongsheng Design Group Ltd. of Zhejiang Province, Wenzhou, China

The auto parts industry occupies an important strategic position in our national economy, which brings about the pollution problem in the processing of auto parts, particularly in soil polluted by heavy metals. Soil samples were collected from an automobile parts company in Jiaxing, China, and the data were evaluated using the land accumulation index method. The study found that the heavy metal pollution in the downwind direction of the Automobile Parts Co., Ltd. is mainly As, CD, and Zn mixed heavy metal pollution, and the distribution is uneven. The coefficient of variation of As was the largest, and the regional variation amplitude was large. The coefficient of variation of CD, Cr, and Ni is 50%, that of Zn is 39.38%, and that of PB is the lowest. The accumulative index of AS and CD was 6, which was a very serious pollution level. The content of As was 1994.7 mg/kg, exceeding the standard by more than 44 times, and the distribution of As in soil was uneven. The pollution level of Zn is 3, which belongs to the moderate level. The pollution degree of heavy metals in the soil decreases as the distance from the downwind outlet of the plant increases. According to the health risk assessment, the main route of heavy metals entering the body is through the mouth by breathing. Among exposure routes, oral exposure to heavy metals is the most harmful, so we need to pay special attention to farmland soil heavy metal pollution.

KEYWORDS

automobile industry, heavy metal contamination, index of geoaccumulation, human health risk assessment, risk assessment

1 Introduction

Automotive parts are one of the automotive service industries, which have various units that make up the entire automobile and products that serve the automobile, collectively referred to as automotive parts. The upstream of the automotive parts industry includes the production of raw materials, such as steel, plastic, and rubber, whereas the downstream mainly targets the supporting market of the main engine factory and the after-sales service market (Liang et al., 2022). The automotive parts industry has many upstream- and downstream-related industries, particularly upstream, so this industry occupies an important strategic position in China's national economy. In recent years, with the improvement of the living standards of Chinese residents, small cars have spread throughout every household. However, toxic metals, such as Pb, Hg, Cd^{6+}, and Cr are found in automotive parts (Diwa et al., 2022). Lead is the most commonly used substance in automobiles among the four toxic metals. Lead mainly exists in seven forms in automotive materials, for example, instrument pointers for counterweights, seat

belt sensors, and lead used as alloy components (Chen et al., 2019). The main applications of Hg in automobiles are lighting in instrument clusters, fluorescent lamps in cars, and others. Cd^{6+} can be used as an alloy material or as a coating component.

The harm of lead (Liverpool, 2021). Lead in automotive parts can enter the environment in multiple ways. Lead in automotive parts (1) evaporates into the atmosphere through steam and particles and (2) enters rivers and soil with rainwater after electrochemical corrosion. When people breathe lead-containing air or drink lead-containing water, lead enters the human body, which will lead to chronic lead poisoning.

The harm of mercury (Cheng et al., 2023). Mercury in scrapped car parts can quickly evaporate and enter the atmosphere and also be deposited in rivers and soil through electrochemical corrosion with rainwater. Mercury can enter the alveoli through the human respiratory tract, which can be completely absorbed by the human body. Long-term accumulation will lead to mercury poisoning.

Hazards of hexavalent chromium. The chromium metal in end-of-life auto parts can easily enter rivers and soil with rainwater through electrochemical corrosion, and sodium dichromate–containing hexavalent chromium will corrode sewers. When hexavalent chromium significantly exceeds the standard (Liverpool, 2021; Adotey et al., 2022), it will also lead to lung cancer.

The harm of cadmium. Cadmium metal in scrapped cars enters the atmosphere in the form of particles, and after electrochemical corrosion, it can also enter rivers and soil with rainwater. When people inhale air or consume water and food with a high cadmium content, cadmium metal accumulates in the human body, which can cause cancer over time. Therefore, high-pollution, low-end manufacturing enterprises will not be able to survive, and the development of the automotive parts industry must take the path of energy-saving, green, and sustainable development. Automotive parts contain considerable heavy metals, and waste automotive parts factories should promptly recycle them to avoid secondary pollution.

At present, some scholars have conducted investigations and studies on the heavy metal content in soil (LI et al., 2012; Lu et al., 2012; Shen et al., 2017; Zhao et al., 2017). However, no comprehensive and systematic investigations and studies exist on the heavy metal pollution situation in the soil around automobile parts factories. Hence, our research group systematically explores the current situation of heavy metal pollution in the surrounding agricultural land soil of automobile parts companies. This study also conducts risk assessments using considerable measured data to provide a basis for early warning of soil environmental quality. Starting from evaluating the ecological and environmental effects of heavy metal pollution in soil, this study uses the ground accumulation index and potential ecological hazard index of heavy metals in soil as pollution evaluation indicators to evaluate the level of heavy metal pollution in agricultural soil in the study area. This study contributes to controlling and regulating heavy metals in farmland soil and has guiding significance.

2 Materials and methods

2.1 Overview of the study area

The auto parts company was located in the Jiaxing Asia Pacific Science and Technology Industrial Park, Nanhu District, Jiaxing, Zhejiang Province, in the center of the Yangtze Delta metropolitan area. The downtown of Jiaxing was 25 km or 1 h from Shanghai, Hangzhou, and Suzhou. Zha Jia Su Expressway was connected to 07 km, 01 Provincial Highway through the town and Hangzhou Bay Bridge. The traffic was very convenient. The main business includeed producing and selling key automotive components, metal, and plastic handicrafts for automotive decoration (excluding gold jewelry). This company was a professional production and processing enterprise specializing in designing, researching, and developing key automotive components (excluding engines). The factory covered an area of 2000 m^2 and specializes in processing services for various automotive components. The factory not only contributeed to the local economy but also had a significant impact on the surrounding environment. To make reasonable use of land resources and protect human health, this study focused on residents' health and selects seven typical heavy metals (i.e., Cr, As, Pb, Ni, Cu, Zn, and Cd) for pollution assessment and health risk assessment.

2.2 Sample collection and determination

2.2.1 Soil sampling and pretreatment

In this study, the grid method was used to arrange sampling points to investigate the pollution status of the topsoil in this block, and to determine the distribution of heavy metal pollution concentration in this key block. In addition, further investigation had be conducted on the depth of heavy metal pollution in the soil through additional cross-sectional sampling. Specifically, the southeast downwind area along the perennial wind direction of the factory was 100 m from the edge of the factory. We collected a total of 30 soil samples from top to bottom at vertical depths of 0–10, 10–20, and 20–30 cm, as shown in Figure 1. When sampling, we collected 1-2 kg of soil samples, placed them in a sampling bag, and labeled the sample information and quantity. We brought the samples back to the laboratory and place'd them in a well-ventilated place to dry naturally in the shade. The samples were ground and passed through a 100-m mesh nylon sieve before digestion.

2.2.2 Soil testing

The method of plate digestion was used to measure the total amount of metals in soil. Ground and sieved soil weighing accurately 0.2000 g was placed in a polytetrafluoroethylene crucible. The soil was wet with several drops of deionized water and added with 10 mL of HCl. Then, the soil was heated on an electric heating plate at medium temperature until it was almost dry, and 5 mL HNO_3, 5 mL HF, and 3 mL $HClO_4$ were added. The soil was heated at a high temperature until it was almost dry; if there was any residue left, we repeated adding three acids until the solution in the crucible was clear and transparent. Then, the soil was transferred to a 50-mL volumetric flask for constant volume filtration, and an inductively coupled plasma spectrometer was used to analyze soil elements (Xu et al., 2020). The reagents used in the experiment were of superior purity. Heavy metal content was analysis by ICP-MAS measurement. All experimental samples were soaked in 10% dilute nitric acid overnight and then washed with ultrapure water. Blank and parallel samples were conducted throughout the

FIGURE 1
Sampling distribution map.

process as control. The recovery rates of each metal were within the allowable range of national standard reference substances. Detection and quality control methods for heavy metals in soil samples were shown in the reference (Hao, 2010; Heng, 2016).

2.3 Evaluation method

2.3.1 Index of geo-accumulation method

This method was proposed by Muller, a German scientist, and is used to quantitatively evaluate the degree of heavy metal pollution in sediments (LI et al., 2012; Lu et al., 2012). In addition to human pollution factors and environmental geochemical background values, the factors of background value changes caused by natural diagenesis are also considered in the evaluation process (Delplace et al., 2022; Zheng et al., 2023).

Where

$$\textbf{Index of geo-accumulation } I_{geo} = \log_2\left[\frac{C_s^i}{K \times C_n^i}\right]$$

in the equation:

C_s^i Is the content of element i in sediment;

C_n^i Is the geochemical background value of this element in the sediment (Kwon et al., 2012; Bábek et al., 2015; Xu et al., 2016; Pojar et al., 2021; Sun et al., 2021; Arisekar et al., 2022; Delplace et al., 2022; Siddique et al., 2023; Zhang et al., 2023);

TABLE 1 Criteria for index of geo-accumulation (I_{geo}) (Förstner et al., 1993).

Project	Grade	Pollution level
I_{geo}	0	Non-pollution
$0<I_{geo}\leqq 1$	1	Mild poisoning pollution
$1<I_{geo}\leqq 2$	2	Moderate pollution
$2<I_{geo}\leqq 3$	3	Moderate to strong pollution
$3<I_{geo}\leqq 4$	4	Strong pollution
$4<I_{geo}\leqq 5$	5	Strong pollution—extremely severe pollution
$5<I_{geo}\leqq 10$	6	Extreme pollution

K is a factor that takes into account possible changes in background values due to differences in rocks in different regions (usually taken as 1.5).

The calculation results are divided into pollution levels according to the evaluation criteria of the index of geo-accumulation (Table 1) (Muller, 1969).

2.3.2 Human health risk assessment method

Heavy metals in soil pose a threat to human health through three main pathways: direct inhalation of soil dust into the air through oral and nasal breathing; transferred in the food chain, such as through fruits, vegetables, and grains, through contaminated soil;

TABLE 2 The values of exposure parameter (Means, 1989; Palash et al., 2020; Sun et al., 2021).

Parameter	Value	
	Children	Adult
IRsoil/(m^3/d)	200	100
IRair/(m^3/d)	7.5	15
EF/(d/a)	350	350
ED/a	6	30
SA/(cm^2/d)	1600	5,000
AF/(mg/cm^2)	0.07	0.2
ABS	0.001	0.001
PEF/(m^3/kg)	1.36×10^9	1.36×10^9
BW/kg	15.9	55.9
AT/d	carcinogenic70 × 365	noncarcinogenic30 × 365

direct skin contact with contaminated soil with heavy metals (Arisekar et al., 2022; Siddique et al., 2023). The industrial process of surface treatment of this metal generates considerable smoke and dust, which is close to farmlands. All three pathways mentioned above may become the main pathways endangering human health. Therefore, in this study, the non-carcinogenic and carcinogenic risk assessments of heavy metals on human health are all included in the model (Goher et al., 2021).

2.3.2.1 Exposure assessment calculation

The amount of pollution ingested by inhaling soil dust through respiration:

$$EDI_{\text{breathe}} = \frac{\text{CS} \times \text{IR}_{air} \times \text{EF} \times \text{ED}}{\text{PEF} \times \text{BW} \times \text{AT}}$$

Amount of pollution ingested through direct skin contact with soil:

$$EDI_{skin} = \frac{\text{CS} \times \text{SA} \times \text{AF} \times \text{ABS} \times \text{EF} \times \text{ED}}{\text{BW} \times \text{AT}} \times 10^{-6}$$

Direct oral intake of soil pollution:

$$EDI_{mouth} = \frac{\text{CS} \times \text{IR}_{\text{soil}} \times \text{EF} \times \text{ED}}{\text{BW} \times \text{AT}} \times 10^{-6}$$

Total exposure:

$$EDI_{\text{total}} = EDI_{\text{breathe}} + EDI_{\text{skin}} + EDI_{mouth}$$

In the formula, EDI_{breathe}, EDI_{skin}, and EDI_{mouth} refer to the total amount of pollutants in soil ingested through respiratory inhalation, skin contact, and direct oral intake, respectively, mg/kg per day; CS is the heavy metal content in the soil, mg/kg; IR soil refers to the soil intake rate, m^3/d; IR air is the intake rate of air, m^3/d; PEF is the soil dust generation factor m^3/kg; SA is the skin contact surface area, cm^2/d; AF is the skin's adsorption coefficient, mg/cm^2; ABS is the skin absorption rate, %; EF is the exposure frequency, d/a; ED is the exposure period/a; BW is the body mass, kg; AT is the average action time, d.

The environmental risk assessment standards for adults and children are quite different when conducting exposure assessments. Table 2 shows the values of each exposure assessment parameter in this assessment according to China's site environmental assessment guidelines, the USEPA health risk assessment method, and the actual research conclusions at home and abroad in recent years (Hasanzadeh et al., 2022; Aly-Eldeen et al., 2023; Hou et al., 2023; Jin et al., 2023; Pandion et al., 2023; Siddique et al., 2023; Zheng et al., 2023).

2.3.2.2 Toxicity assessment and risk characterization

Toxicity assessment estimates the relationship between population exposure to pollutants and the likelihood of negative effects (Bandara and Pathiratne, 2023; Ghosh et al., 2023; Wang et al., 2023). Among the six heavy metals studied in this article, Cu, Pb, Cd, and Ni all have non-carcinogenic health risks, and Pb, Cd, and Ni also have carcinogenic risks (Sharma et al., 2022; Zheng et al., 2023). Table 3 presents the non-carcinogenic and carcinogenic toxicity parameters of four heavy metals, that is, Cu, Pb, Cd, and Ni. The non-carcinogenic toxicity parameters are the reference dose (RfDj) of heavy metals under each exposure pathway, and the carcinogenic effect reference number (SF) is the carcinogenic slope factor of Cd and Ni.

Each exposure route has carcinogenic and non-carcinogenic risks. The non-carcinogenic risk level can be calculated by dividing the daily exposure of heavy metals by the chronic reference dose of three routes, namely, oral, skin, and respiratory. The calculation formula is as follows:

$$HI = \sum HQ_i$$

where HI is the total non-carcinogenic risk level of soil heavy metals under three exposure routes: oral, respiratory, and skin contact; HQi represents the non-carcinogenic risk level of different intake pathways; EDIj is the average daily intake of pollutants from different pathways, mg/(kg·d), whereas RfDj is the chronic reference dose for each pathway, mg/(kg·d) (Table 3). When HQi <1 or HI <1, no significant non-carcinogenic health risk exists. When HQi >1 or HI >1, a non-carcinogenic health risk exists, and the higher the value, the more severe the risk.

The level of cancer risk is calculated by multiplying the average daily intake to the entire life cycle by the slope coefficient of carcinogenicity through oral, skin, or respiratory inhalation. The calculation formula is as follows:

$$Risk_i = EDI_i \times SF_i$$

$$(Risk)_T = \sum Risk_i$$

where Riski is the carcinogenic risk index of soil heavy metals under different pathways; (Risk) T is the comprehensive risk index of heavy metal carcinogenesis in soil; EDI is the average daily intake of different pollutants, mg/(kg·d); SFi is the slope coefficient of cancer risk for various pathways, (kg·d)/mg (Table 3). Risk is the carcinogenic health index, usually represented by a certain number of recognized cancer patients. The acceptable risk value of carcinogens defined by the U.S. Environmental Protection Agency is 10^{-4}–10^{-6}, and the risk of cancer incidence in a lifetime exceeds the normal value. When the risk is $< 1 \times 10^{-6}$ h, no risk of cancer exists. When the risk is $> 1 \times 10^{-4}$ h, a risk of cancer

TABLE 3 RfD and SF of heavy metals for different exposure routes (Huang et al., 2022; Jin et al., 2023).

Heavymetal	RfD mouth/ [mg/(kg.d)]	RfD breath/ [mg/(kg.d)]	RfD skin/ [mg/(kg.d)]	SF/ [(kg.d)/mg]
Cd	1.02×10^{-2}	1.14×10^{-3}	1.38×10^{-5}	3.56×10^{-1}
Ni	2.12×10^{-2}	2.06×10^{-2}	5.21×10^{-3}	8.75×10^{-1}
As	3.14×10^{-4}	3.83×10^{-6}	3.21×10^{-4}	1.93×10^{0}
Zn	3.05×10^{-1}	0	3.02×10^{-1}	

TABLE 4 Heavy metal content of soil at the sampling site of Jiaxing Minhui Auto Parts Co., Ltd.

Heavy metal	Detection range (mg/kg)	Average value (mg/kg)	Coefficient of variation (%)	Average number of exceedances	Average exceedance rate (%)	Standard value (mg/kg)	Coefficient of variation (%)
Cd	1~11.25	5.13	8.54	100	0.6	2.78	54.26
As	88.25~1994.75	857.18	34.29	100	25	543.30	63.38
Pb	91~244.75	157.28	0	63	140	34.64	22.03
Cr	85.75~532.50	201.45	0	10	300	102.37	50.82
Cu	66.25~3,682.50	274.39	0	13	200	645.76	235.35
Ni	58.25~318.25	125.40	0	57	100	65.34	52.10
Zn	265.25~1437	611.242	0	100	250	240.70	39.38

exists. Then, when $1 \times 10^{-6} \leq$ risk $\leq 1 \times 10^{-4}$ h, the risk of cancer is considered within an acceptable range.

3 Results and discussion

3.1 Current situation and source analysis of heavy metal pollution

In this survey, the downwind soil around the auto parts company in Jiaxing was collected in three layers, and a total of 30 sampling data were analyzed regionally. According to the average value of the soil in the Hangzhou–Jiaxing–Huzhou Plain as the background value and the standard values of various elements (Meng et al., 2022; Shao-cheng et al., 2023; Xu et al., 2023), specified in the secondary standard of the Soil Environmental Quality Standard GB 15618-1995 (pH < 6.5), the pollution degree of heavy metals can be simply and intuitively displayed by using the multiple of exceeding the standard. The coefficient of variation reflects the interference of human activities on heavy metal content (Xiaogang, 2014). The average values of heavy metal content in the downwind direction of the study area and the heavy metal content at three different sampling depths were measured (Halim, 2023). The objective is to investigate the overall pollution status of heavy metals around Jiaxing Automotive Parts Company and the impact of their location and distance from the pollution source. Table 4; Figure 2 show the results.

Table 4 shows that, compared with the soil environmental quality table issued in 2018, Cd, As, Pb, Cr, Cu, Ni, and Zn have all exceeded the standard, with exceeding rates of 100%, 100%, 63%, 10%, 13%, 57%, and 100%, respectively. Among them, the maximum coefficient of variation of As reached 63.38%, indicating that the distribution of As in the study area is very uneven and that the amplitude changes are significant. Second, the coefficient of variation of Cd, Cr, and Ni also reached 50%, whereas that of Zn was 39.38%. The distribution of several heavy metals was also uneven, whereas the coefficient of variation of Pb was the lowest. Relatively speaking, the distribution was relatively uniform.

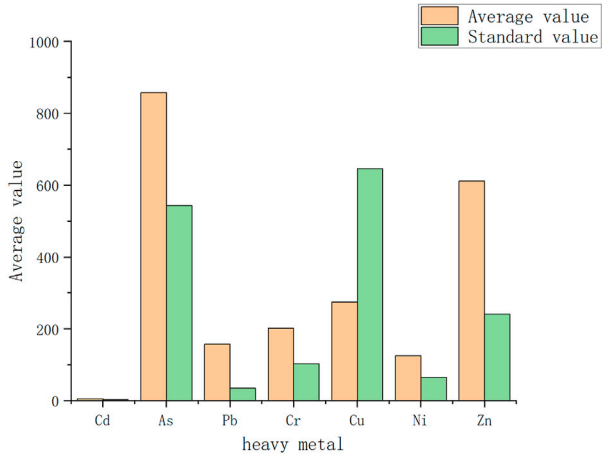

FIGURE 2
Heavy metal content in different soil layer (mg/kg).

Research has shown that heavy metals in soil are not only related to species but also to the relative location and distance of pollution

sources. In this study, the As content of sampling points 1, 2, 3, 4, and 5 is particularly high, and these five points are located approximately 1 km below the air outlet of the factory area. On this basis, the closer you are to the factory area, the higher the concentration of heavy metals deposited in the soil. The content of As in all directions and locations exceeds the background value of soil in Jiaxing City (LI et al., 2012; Shen et al., 2017). Moreover, the content of As in the middle layer of 10–20-cm soil reaches the maximum value, with an average exceeding the standard of 79.39 times. This case may be caused by the disordered discharge of arsenic-containing wastewater and the atmospheric sedimentation of exhaust gas generated by the nearby automobile beauty enterprises in the production process. In addition, using organic arsenic pesticides to control rice diseases has caused a large amount of arsenic residue. The simple substance arsenic is non-toxic, and Arsenic compounds are toxic. Trivalent arsenic is approximately 60 times more toxic than pentavalent arsenic. The toxicity of organic arsenic is similar to that of inorganic arsenic. Moreover, long-term inhalation or oral administration in small amounts can lead to chronic poisoning (Li et al., 2023). Meanwhile, breathing arsenic-containing air for 5–10 min can lead to fatal poisoning. The presence of arsenic in agricultural soil is a major environmental and public health issue. Arsenic, an element that occurs naturally, can be introduced into soils by human activities such as mining, pesticide application, and industrial operations. Arsenic, when found in the soil, has the ability to build up in crops, posing a threat to the safety of our food. Prolonged exposure to arsenic through tainted agricultural produce has been associated with many health problems, such as dermatological abnormalities, cardiovascular disorders, and specific types of cancer (Dong-Yan, 2018). Arsenic pollution can cause toxicity in the gastrointestinal tract, liver, and kidneys and induce cancer. Hence, effective measures must be taken to prevent and treat it. In addition to As, the average value of Cd also exceeded 8.54 times, exhibiting the same distribution pattern as As, reaching its peak in the soil layer at 10–20 cm. Cd is a non-biological essential element that can enter the human body through the food chain and accumulate in the body, causing chronic poisoning, liver and kidney damage, and bone metabolism obstruction (Jin et al., 2023). Therefore, special attention is also needed. The exceeding standard rate of Zn reached 100%, which was higher than the soil background value in Jiaxing City. This situation may be due to proximity to highways, vehicle exhaust emissions, forum wear and tear, and corporate exhaust emissions exceeding the standard. Pb and Cu are similar in average bidding multiples, similar to the soil background values of Jiaxing City (Gao et al., 2023; Siddique et al., 2023). Cr has the lowest exceeding standard rate and average exceeding standard multiple among the seven tested heavy metals, which may be related to the layout of drainage channels (Zheng et al., 2023). The dominant wind direction in Jiaxing is southeast wind all year round, and in this study, the overall direction of heavy metal production and enrichment is 100 m southwest rather than in the downwind region. Zhao Renxin et al. (Zhao et al., 2017) concluded that the influence of wind direction on the distribution of heavy metals is not significant. The main reasons for this phenomenon may be threefold: interference from other enterprises' emissions, interference from agricultural pesticides, and atmospheric sedimentation caused by wind power. The airflow disturbance caused by vehicles traveling to the west of the factory area weakens the role of natural wind direction.

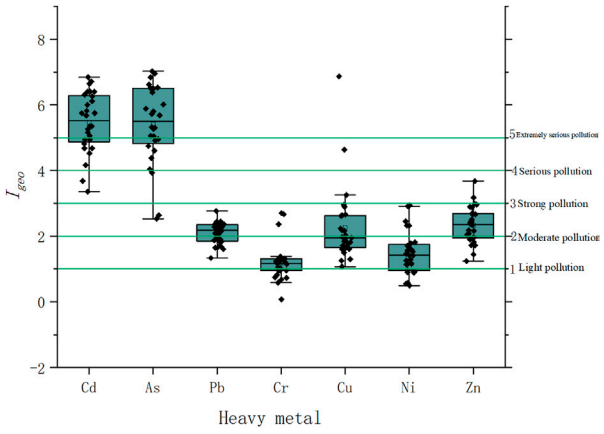

FIGURE 3
Soil heavy metal cumulative index vertical distribution of the study area.

3.2 Index of geo-accumulation

Figure 3 shows the overall evaluation of six heavy metals in the soil around the metal factory using the land accumulation index method and the evaluation results of each metal at different vertical depths.

From Figure 3, the cumulative index (Igeo) of heavy metals around the metal surface treatment plant is Cd > As > Cu > Zn > Pb > Ni > Cr in descending order. The ground accumulation index of the middle soil layer (10–20 cm) is mostly at a high level, which may be the result of surface infiltration downward. Many deep soil layers (20–30 cm) have a higher ground accumulation index than the surface soil, indicating that the deep soil is also severely polluted. The highest ground accumulation index of As and Cd is above 5.8, and all soils are contaminated with varying degrees of As and Cd. Surface and deep soils are at extremely severe pollution levels. Second, the overall pollution of Cu and Zn is between strong and moderate pollution levels, with a high degree of soil pollution in the layer (10–20 cm). The overall pollution level of Pb is at a moderate level. Compared with other heavy metals, the pollution level of Cr is the lightest. The pollution decreases with the deepening of soil depth, which may be because of the adsorption and diffusion of soil particles (Pandion et al., 2023). As shown in Figure 3, out of the seven heavy metals measured in this study, six are all at a moderate or higher pollution level. Considering their potential harm to surrounding residents, As, Zn, and Cd were selected as risk factors for human health risk assessment.

3.3 Health risk assessment

3.3.1 Exposure assessment analysis

The exposure assessment of As, Zn, and Cd on children and adults on non-carcinogenic days was carried out in this study, and Table 5 shows the results. From Table 5, the intake of heavy metals through oral intake is much higher than that through skin contact and respiratory inhalation. The daily intake of heavy metals in soil through the three pathways is in descending order: EDI through

TABLE 5 Dailyexxposure doses of heavy metals in soil mg/(kg d).

metals	classification	$EDI_{breathe}$		EDI_{skin}		EDI_{mouth}		EDI_{total}	
		children	adult	children	adult	children	adult	children	adult
As	maximum	5.69E-08	1.62E-07	1.15E-06	5.15E-05	3.05E-03	1.47E-03	3.05E-03	1.47E-03
	minimum	2.52E-09	7.16E-09	5.11E-08	2.28E-06	2.05E-03	6.49E-05	2.05E-03	6.49E-05
	Average	2.44E-08	6.95E-08	4.96E-07	2.21E-05	8.83E-04	6.30E-04	8.83E-04	6.30E-04
Zn	maximum	4.10E-08	1.17E-07	8.32E-07	3.71E-05	1.48E-03	1.06E-03	1.48E-03	1.06E-03
	minimum	7.56E-09	2.15E-08	1.54E-07	6.84E-06	2.73E-04	1.95E-04	2.73E-04	1.95E-04
	Average	1.74E-08	4.96E-08	3.54E-07	1.58E-05	6.30E-04	4.49E-04	6.30E-04	4.49E-04
Cd	maximum	3.21E-11	9.12E-10	6.51E-09	2.90E-07	1.16E-05	8.27E-06	1.16E-05	8.27E-06
	minimum	2.85E-11	8.11E-11	5.79E-10	2.58E-08	1.03E-06	7.35E-07	1.03E-06	7.35E-07
	Average	1.46E-10	4.16E-10	2.97E-09	1.32E-07	5.28E-06	3.77E-06	5.28E-06	3.77E-06

TABLE 6 The index of health risk.

Risk index	Classification	As	Zn	Cd
$Risk_{mouth}$	Child	8.83E-04	6.30E-04	5.28E-06
	Adult	6.30E-04	4.49E-04	3.77E-06
$Risk_{breathe}$	Child	2.44E-08	1.74E-08	1.46E-10
	Adult	6.95E-08	4.96E-08	4.16E-10
$Risk_{skin}$	Child	4.96E-07	3.54E-07	2.97E-09
	Adult	2.21E-05	1.58E-05	1.32E-07
$Risk_{total}$	Child	8.83E-04	6.30E-04	5.28E-06
	Adult	6.30E-04	4.50E-04	3.77E-06

mouth > EDI through skin > EDI through respiration. Children's intake of heavy metals through oral intake is higher than that of adults, but the content of heavy metals through skin contact and respiratory inhalation is lower than that of adults. The exposure dose reaches its maximum when children ingest As through mouth, 3.05×10^{-3} mg/(kg/d), and the minimum exposure dose appears in children who inhale Cd through breathing, with a minimum value of 2.85×10^{-11} mg/(kg/d). The doses of the other two metals Zn and Cd ingested by mouth, skin contact, and respiratory inhalation in adults are greater than those in children.

3.3.2 Healthy risk assessment

In this study, non-carcinogenic daily exposure assessment of three heavy metals, As, Zn, and Cd, to children and adults was carried out, and the results are shown in Table 6. From Table 6, the non-carcinogenic risk index (HQi) of the surrounding soil of Jiaxing Minhui Automotive Parts Company is partially greater than 1. Relatively speaking, the risk of oral intake is the highest, and the non-carcinogenic risk of direct skin contact and respiratory inhalation is relatively small. These results are consistent with the health risk assessment conclusion of heavy metals in subway station dust, which is the research background of Yang Xiaozhi (Yang et al., 2022). The maximum occurrence of HQi is in children's oral intake of As, with a maximum value of 12.34, whereas the minimum value is the respiratory intake of heavy metal Zn by children, with a minimum value of 7.56×10^{-9}. In addition, the doses of Cd and Zn for oral intake, skin contact, and respiratory inhalation in adults are higher than those in children. This result is consistent with the conclusions of the exposure assessment, indicating that the non-carcinogenic risk index is related to the exposure route (Meng et al., 2022). Regardless of the exposure pathway, the non-carcinogenic health risk assessment of As is higher than that of the other two heavy metals. Therefore, As has the greatest potential for carcinogenic health risk, with a total HQi of 12 for non-carcinogenic health risks, followed by Zn. Therefore, the prevention and control of these two elements should be strengthened. In addition, the total non-carcinogenic health risk HQi of Cd for adults and children is less than 1, indicating that these elements do not pose a non-carcinogenic health risk to residents around the factory area. Fadel et al. (Fadel et al., 2022) studied the soil pollution situation around electroplating plants and also found that the carcinogenic risk of As and Cr in the soil was greater than 10^{-4}, which was higher than the maximum acceptable risk level, similar to the results of this study.

The maximum values of the carcinogenic health risk index (RISK) of As for adults and children under the exposure pathway of oral intake are 6.30×10^{-4} and 8.83×10^{-4}, with a risk of cancer. The minimum value of the carcinogenic health risk index of Cd is 1.46×10^{-10}, occurring in children through respiratory exposure pathways, within an acceptable range of carcinogenic risk. The maximum values of Cd all occur through the oral intake pathway in children, with values of 5.28×10^{-6}. Zn does not have a carcinogenic risk. Overall, the total cancer risk index of As through three pathways is relatively high, and risks in children are higher than in adults, which should be highly valued and strengthened for prevention and control. The excessive levels of As may be related to the application of pesticides in farmland or to nearby agricultural companies (Fan et al., 2022; Hou et al., 2023; Shao-cheng et al., 2023). As for Cd, risks in adults are higher than those in children, which is consistent with the results of the non-carcinogenic risk index. The health risk index for cancer caused by oral intake in adults is 5.28×10^{-6}, has exceeded the warning value,

and if not controlled, will pose a threat to the health of surrounding residents.

4 Conclusion

1) Many kinds of heavy metal pollution were detected in the leeward soil of Jiaxing Minhui Auto Parts Factory; the soil was extremely polluted by As and Cd, and the exceeding standard rates are 100% and 37%, respectively. Moreover, the As content can reach 1994.7 mg/kg, exceeding the standard by 34.287 times. Such pollution is unevenly distributed in the soil. The pollution level of Zn is 3, belonging to the moderate pollution level. The average exceeding multiple of Zn is not high, but the exceeding rate reaches 100%. The level of heavy metal pollution in the soil decreases as the distance from the downwind mouth of the factory increases, but some do not follow this pattern. Overall, this area is polluted by a mixture of As, Cd, and Zn, similar to the heavy metal pollution in agricultural soil in Zhejiang Province. The coefficient of variation of As reached 63.38%, possibly because of the use of arsenic-containing fertilizers and pesticides causing metal residues.
2) The conclusion drawn from the ground accumulation index method is that As and Cd pollution is the most severe, with a grading result of 6 levels, belonging to the extremely strong pollution level. Pb, Cu, and Zn are at levels 3, 4, and 3, respectively, belonging to the medium strong pollution level. The ground accumulation index of Cr and Ni is at level 2, belonging to the moderate pollution level. When the distance between the lower air vents in the factory area is close and the pollution level high, the soil in this area is highly polluted with As and Cd, accompanied by moderate to high levels of Pb, Cu, and Zn pollution. Moreover, the relevant parts should be taken seriously, and efforts should be made to address the pollution of heavy metals on the soil to ensure people's lives and health.
3) The daily intake of heavy metals in the soil through three pathways, in descending order, is EDI through mouth > EDI through skin > EDI through respiration. The non-carcinogenic risk index is related to the exposure pathway. The total carcinogenic risk index of As in the study area through three exposure pathways is relatively high, whereas the carcinogenic harm of Zn is within an acceptable range. However, a potential carcinogenic risk that should be highly valued and prevented already exists.

Data availability statement

The original contributions presented in the study are included in the article/Supplementary material, further inquiries can be directed to the corresponding author.

Author contributions

TTL: Writing–original draft, Writing–review and editing. SYN: Data curation, Formal Analysis, Methodology, Writing–review and editing. ZW: Funding acquisition, Investigation, Resources, Visualization, Writing–review and editing.

Funding

The author(s) declare that financial support was received for the research, authorship, and/or publication of this article. I would like to express my gratitude to the supported by the Open Fund of the Key Laboratory of Waste minimisation technology Research of Zhejiang Province (No. 2021ZEKL10).

Conflict of interest

Author SN was employed by Zongsheng Design Group Ltd. of Zhejiang Province.

The remaining authors declare that the research was conducted in the absence of any commercial or financial relationships that could be construed as a potential conflict of interest.

Publisher's note

References

Adotey, E. K., Burkutova, L., Tastanova, L., Bekeshev, A., Balanay, M. P., Sabanov, S., et al. (2022). Quantification and the sources identification of total and insoluble hexavalent chromium in ambient PM: a case study of Aktobe, Kazakhstan. *Chemosphere* 307, 136057. doi:10.1016/j.chemosphere.2022.136057

Aly-Eldeen, M. A., Shreadah, M. A., and Abdel Ghani, S. A. (2023). Distribution, bioavailability, and ecological risk assessment of potentially toxic heavy metals in El-Burullus Lake sediments, Egypt. *Mar. Pollut. Bull.* 191, 114984. doi:10.1016/j.marpolbul.2023.114984

Arisekar, U., Shakila, R. J., Shalini, R., Jeyasekaran, G., Keerthana, M., Arumugam, N., et al. (2022). Distribution and ecological risk assessment of heavy metals using geochemical normalization factors in the aquatic sediments. *Chemosphere* 294, 133708. doi:10.1016/j.chemosphere.2022.133708

Bábek, O., Grygar, T. M., Faměra, M., Hron, K., Nováková, T., and Sedláček, J. (2015). Geochemical background in polluted river sediments: how to separate the effects of sediment provenance and grain size with statistical rigour? *CATENA* 135, 240–253. doi:10.1016/j.catena.2015.07.003

Bandara, S., and Pathiratne, A. (2023). Concentrations of trace metals in Siganus javus captured in Negombo estuary, Sri Lanka: human health risk assessment through dietary exposure. *Mar. Pollut. Bull.* 188, 114639. doi:10.1016/j.marpolbul.2023.114639

Chen, Y., Zhang, Q., Luo, T., Xing, L., and Xu, H. (2019). Occurrence, distribution and health risk assessment of organophosphate esters in outdoor dust in Nanjing, China: urban vs rural areas. *Chemosphere* 231, 41–50. doi:10.1016/j.chemosphere.2019.05.135

Cheng, S., Liu, P., Hou, X., Guo, X., Li, G., Yang, F., et al. (2023). Copper and mercury exposure alters rectum microbiota in female adult mice. *J. King Saud Univ. - Sci.* 35 (6), 102776. doi:10.1016/j.jksus.2023.102776

Delplace, G., Viers, J., and Oliva, P. (2022). This letter is a response to the comment submitted to chemosphere by Melleton et al. on our paper (Delplace et al., 2022),

entitled "pedo-geochemical background and sediment contamination of metal(loid)s in the old mining-district of Salsigne (Orbiel valley, France)" by Gauthier Delplace, Jérôme Viers, Eva Schreck, Priscia Oliva and Philippe Behra (2022), published online in Chemosphere in September 2021. *Chemosphere* 307, 135766. doi:10.1016/j.chemosphere.2022.135766

Diwa, R. R., Elvira, M. V., Deocaris, C. C., Fukuyama, M., and Belo, L. P. (2022). Transport of toxic metals in the bottom sediments and health risk assessment of Corbicula fluminea (Asiatic clam) collected from Laguna de Bay, Philippines. *Sci. Total Environ.* 838, 156522. doi:10.1016/j.scitotenv.2022.156522

Dong-Yan, R. (2018). Association between arsenic exposure and diabetes mellitus in rats. *J. Environ. Occup. Med.* 2018.

Fadel, M., Ledoux, F., Afif, C., and Courcot, D. (2022). Human health risk assessment for PAHs, phthalates, elements, PCDD/Fs, and DL-PCBs in PM2.5 and for NMVOCs in two East-Mediterranean urban sites under industrial influence. *Atmos. Pollut. Res.* 13 (1), 101261. doi:10.1016/j.apr.2021.101261

Fan, T., Pan, J., Wang, X., Wang, S., and Lu, A. (2022). Ecological risk assessment and source apportionment of heavy metals in the soil of an Opencast mine in xinjiang. *Int. J. Environ. Res. Public Health* 19 (23), 15522. doi:10.3390/ijerph192315522

Förstner, U., Ahlf, W., and Calmano, W. (1993). Sediment quality objectives and criteria development in Germany. *Water Sci. Technol.* 28 (8-9), 307–316. doi:10.2166/wst.1993.0629

Gao, X., Zhou, Y., Fan, M., Jiang, M., Zhang, M., Cai, H., et al. (2023). Environmental risk assessment near a typical spent lead-acid battery recycling factory in China. *Environ. Res.* 233, 116417. doi:10.1016/j.envres.2023.116417

Ghosh, S., Banerjee, S., Prajapati, J., Mandal, J., Mukherjee, A., and Bhattacharyya, P. (2023). Pollution and health risk assessment of mine tailings contaminated soils in India from toxic elements with statistical approaches. *Chemosphere* 324, 138267. doi:10.1016/j.chemosphere.2023.138267

Goher, M. E., Mangood, A. H., Mousa, I. E., Salem, S. G., and Hussein, M. M. (2021). Ecological risk assessment of heavy metal pollution in sediments of Nile River, Egypt. *Environ. Monit. Assess.* 193 (11), 703. doi:10.1007/s10661-021-09459-3

Halim, T. (2023). Comments on "Economics of natural disasters and technological innovations in Africa: an empirical evidence" by Okolo, Chukwuemeka et al., DOI (10.1007/s11356-022-22989-8). *Environ. Sci. Pollut. Res. Int.* 30 (10), 122974–122975. doi:10.1007/s11356-023-30873-2

Hao, C. (2010). The monitoring process of heavy metals in soils and its quality control measures. *Environ. Monit. China*. doi:10.3724/SP.J.1088.2010.00432

Hasanzadeh, M., Malakootian, M., Nasiri, A., Oliveri Conti, G., Ferrante, M., and Faraji, M. (2022). Ecological and probabilistic health risk assessment of heavy metals in topsoils, southeast of Iran. *Bull. Environ. Contam. Toxicol.* 108 (4), 737–744. doi:10.1007/s00128-021-03389-z

Heng, C. (2016). Monitoring process and quality control of heavy metals in soil. *Constr. Des. Eng.*

Hou, Y., Zhao, Y., Lu, J., Wei, Q., Zang, L., and Zhao, X. (2023). Environmental contamination and health risk assessment of potentially toxic trace metal elements in soils near gold mines – a global meta-analysis. *Environ. Pollut.* 330, 121803. doi:10.1016/j.envpol.2023.121803

Huang, Y., Han, R., Qi, J., Duan, H., Chen, C., Lu, X., et al. (2022). Health risks of industrial wastewater heavy metals based on improved grey water footprint model. *J. Clean. Prod.* 377, 134472. doi:10.1016/j.jclepro.2022.134472

Jin, J., Zhao, X., Zhang, L., Hu, Y., Zhao, J., Tian, J., et al. (2023). Heavy metals in daily meals and food ingredients in the Yangtze River Delta and their probabilistic health risk assessment. *Sci. Total Environ.* 854, 158713. doi:10.1016/j.scitotenv.2022.158713

Kwon, J. C., Lee, J., and Jung, M. C. (2012). Arsenic contamination in agricultural soils surrounding mining sites in relation to geology and mineralization types. *Appl. Geochem.* 27 (5), 1020–1026. doi:10.1016/j.apgeochem.2011.11.015

Li, N., Li, Y., Wei, J., Liu, K., Wang, G., Zhang, H., et al. (2023). Source-oriented ecological risk assessment of heavy metals in sediments of West Taihu Lake, China. *Environ. Sci. Pollut. Res. Int.* 30 (6), 13909–13919. doi:10.1007/s11356-022-24766-z

Liang, Q., Tian, K., Li, L., He, Y., Zhao, T., Liu, B., et al. (2022). Ecological and human health risk assessment of heavy metals based on their source apportionment in cropland soils around an e-waste dismantling site, Southeast China. *Ecotoxicol. Environ. Saf.* 242, 113929. doi:10.1016/j.ecoenv.2022.113929

Liverpool, L. (2021). Legal levels of lead in US tap water can still cause harm. *New Sci.* 251 (3344), 21. doi:10.1016/s0262-4079(21)01285-9

Li, X., Yin, H., and Su, J. (2012). An attempt to quantify Cu-resistant microorganisms in a paddy soil from jiaxing, China. *Pedosphere* 22 (2), 201–205. doi:10.1016/s1002-0160(12)60006-x

Lu, J., Jiang, L., Chen, D., Toyota, K., Strong, P. J., Wang, H., et al. (2012). Decontamination of anaerobically digested slurry in a paddy field ecosystem in Jiaxing region of China. *Agric. Ecosyst. Environ.* 146 (1), 13–22. doi:10.1016/j.agee.2011.10.011

Means, B. (1989). Risk-assessment guidance for superfund. *Human Health Evaluation Manual. Part A. Interim report (Final)* 1. Available at: https://www.osti.gov/biblio/350784.

Meng, C., Wang, P., Hao, Z., Gao, Z., Li, Q., Gao, H., et al. (2022). Ecological and health risk assessment of heavy metals in soil and Chinese herbal medicines. *Environ. Geochem Health* 44 (3), 817–828. doi:10.1007/s10653-021-00978-z

Muller, G. (1969). Index of geoaccumulation in sediments of the rhine river. *GeoJournal* 2 (3), 109–118.

Palash, M. A. U., Islam, M. S., Bayero, A. S., Taqui, S. N., and Koki, I. B. (2020). Evaluation of trace metals concentration and human health implication by indigenous edible fish species consumption from Meghna River in Bangladesh. *Environ. Toxicol. Pharmacol.* 80, 103440. doi:10.1016/j.etap.2020.103440

Pandion, K., Arunachalam, K. D., Rajagopal, R., Ali, D., Alarifi, S., Chang, S. W., et al. (2023). Health risk assessment of heavy metals in the seafood at Kalpakkam coast, Southeast Bay of Bengal. *Mar. Pollut. Bull.* 189, 114766. doi:10.1016/j.marpolbul.2023.114766

Pojar, I., Kochleus, C., Dierkes, G., Ehlers, S. M., Reifferscheid, G., and Stock, F. (2021). Quantitative and qualitative evaluation of plastic particles in surface waters of the Western Black Sea. *Environ. Pollut.* 268, 115724. doi:10.1016/j.envpol.2020.115724

Shao-cheng, S., Yu-cheng, W., Yuan, L., Shuai, Y., Xiao-hong, P., and Yong-ming, L. (2023). Divergent soil health responses to long-term inorganic and organic fertilization management on subtropical upland red soil in China. *Ecol. Indic.* 154, 110486. doi:10.1016/j.ecolind.2023.110486

Sharma, K., Janardhana Raju, N., Singh, N., and Sreekesh, S. (2022). Heavy metal pollution in groundwater of urban Delhi environs: pollution indices and health risk assessment. *Urban Clim.* 45, 101233. doi:10.1016/j.uclim.2022.101233

Shen, L., Wang, H., Lü, S., Zhang, X., Yuan, J., Tao, S., et al. (2017). Influence of pollution control on air pollutants and the mixing state of aerosol particles during the 2nd World Internet Conference in Jiaxing, China. *J. Clean. Prod.* 149, 436–447. doi:10.1016/j.jclepro.2017.02.114

Siddique, S., Chaudhry, M. N., Ahmad, S. R., Nazir, R., Zhao, Z., Javed, R., et al. (2023). Ecological and human health hazards; integrated risk assessment of organochlorine pesticides (OCPs) from the Chenab River, Pakistan. *Sci. Total Environ.* 882, 163504. doi:10.1016/j.scitotenv.2023.163504

Sun, X., Zhang, L., and Lv, J. (2021). Spatial assessment models to evaluate human health risk associated to soil potentially toxic elements. *Environ. Pollut.* 268, 115699. doi:10.1016/j.envpol.2020.115699

Wang, J., Chen, Y., Pan, D., Zhang, J., Zhang, Y., and Lu, Z. (2023). Source and health risk assessment of soil polycyclic aromatic hydrocarbons under straw burning condition in Changchun City, China. *Sci. Total Environ.* 894, 165057. doi:10.1016/j.scitotenv.2023.165057

Xiaogang, Y. (2014). Variation of heavy metal concentrations in hyporheic sediments for the Weihe River of Shaanxi Province. *Acta Sci. Circumstantiae*.

Xu, D., Chen, S., Xu, H., Wang, N., Zhou, Y., and Shi, Z. (2020). Data fusion for the measurement of potentially toxic elements in soil using portable spectrometers. *Environ. Pollut.* 263, 114649. doi:10.1016/j.envpol.2020.114649

Xu, G., Liu, J., Pei, S., Hu, G., and Kong, X. (2016). Sources and geochemical background of potentially toxic metals in surface sediments from the Zhejiang coastal mud area of the East China Sea. *J. Geochem. Explor.* 168, 26–35. doi:10.1016/j.gexplo.2016.06.003

Xu, H., Huang, Y., Xiong, X., Zhu, H., Lin, J., Shi, J., et al. (2023). Changes in soil Cd contents and microbial communities following Cd-containing straw return. *Environ. Pollut.* 330, 121753. doi:10.1016/j.envpol.2023.121753

Yang, J., Sun, F., Su, H., Tao, Y., and Chang, H. (2022). Multiple risk assessment of heavy metals in surface water and sediment in taihu lake, China. *Int. J. Environ. Res. Public Health* 19 (20), 13120. doi:10.3390/ijerph192013120

Zhang, J., Peng, W., Lin, M., Liu, C., Chen, S., Wang, X., et al. (2023). Environmental geochemical baseline determination and pollution assessment of heavy metals in farmland soil of typical coal-based cities: a case study of Suzhou City in Anhui Province, China. *Heliyon* 9 (4), e14841. doi:10.1016/j.heliyon.2023.e14841

Zhao, B., Han, L., Pilz, J., Wu, J., Khan, F., and Zhang, D. (2017). Metallogenic efficiency from deposit to region–A case study in western Zhejiang Province, southeastern China. *Ore Geol. Rev.* 86, 957–970. doi:10.1016/j.oregeorev.2016.10.003

Zheng, X., Lu, Y., Xu, J., Geng, H., and Li, Y. (2023). Assessment of heavy metals leachability characteristics and associated risk in typical acid mine drainage (AMD)-contaminated river sediments from North China. *J. Clean. Prod.* 413, 137338. doi:10.1016/j.jclepro.2023.137338

frontiers | Frontiers in Microbiology

TYPE Original Research
PUBLISHED 17 April 2024
DOI 10.3389/fmicb.2024.1381891

OPEN ACCESS

EDITED BY
Yang Yang,
Institute of Earth Environment (CAS), China

REVIEWED BY
Huan Cheng,
Sichuan University, China
Jiwei Li,
Northwest A&F University, China
Rongxiao Che,
Yunnan University, China
Lichao Fan,
Northwest A&F University, China

*CORRESPONDENCE
De Kejia
dekejia1002@163.com

RECEIVED 04 February 2024
ACCEPTED 29 March 2024
PUBLISHED 17 April 2024

CITATION
Xuemei X, Kejia D, Weishan L, Tingxu F, Fei L and Xijie W (2024) Indirect influence of soil enzymes and their stoichiometry on soil organic carbon response to warming and nitrogen deposition in the Tibetan Plateau alpine meadow.
Front. Microbiol. 15:1381891.
doi: 10.3389/fmicb.2024.1381891

Indirect influence of soil enzymes and their stoichiometry on soil organic carbon response to warming and nitrogen deposition in the Tibetan Plateau alpine meadow

Xiang Xuemei, De Kejia*, Lin Weishan, Feng Tingxu, Li Fei and Wei Xijie

College of Animal Husbandry and Veterinary Science, Qinghai University, Xining, China

Despite extensive research on the impact of warming and nitrogen deposition on soil organic carbon components, the response mechanisms of microbial community composition and enzyme activity to soil organic carbon remain poorly understood. This study investigated the effects of warming and nitrogen deposition on soil organic carbon components in the Tibetan Plateau alpine meadow and elucidated the regulatory mechanisms of microbial characteristics, including soil microbial community, enzyme activity, and stoichiometry, on organic carbon components. Results indicated that both warming and nitrogen deposition significantly increased soil organic carbon, readily oxidizable carbon, dissolved organic carbon, and microbial biomass carbon. The interaction between warming and nitrogen deposition influenced soil carbon components, with soil organic carbon, readily oxidizable carbon, and dissolved organic carbon reaching maximum values in the W0N32 treatment, while microbial biomass carbon peaked in the W3N32 treatment. Warming and nitrogen deposition also significantly increased soil Cellobiohydrolase, β-1,4-N-acetylglucosaminidase, leucine aminopeptidase, and alkaline phosphatase. Warming decreased the soil enzyme C: N ratio and C:P ratio but increased the soil enzyme N:P ratio, while nitrogen deposition had the opposite effect. The bacterial Chao1 index and Shannon index increased significantly under warming conditions, particularly in the N32 treatment, whereas there were no significant changes in the fungal Chao1 index and Shannon index with warming and nitrogen addition. Structural equation modeling revealed that soil organic carbon components were directly influenced by the negative impact of warming and the positive impact of nitrogen deposition. Furthermore, warming and nitrogen deposition altered soil bacterial community composition, specifically *Gemmatimonadota* and *Nitrospirota*, resulting in a positive impact on soil enzyme activity, particularly soil alkaline phosphatase and β-xylosidase, and enzyme stoichiometry, including N:P and C:P ratios. In summary, changes in soil organic carbon components under warming and nitrogen deposition in the alpine meadows of the Tibetan Plateau primarily depend on the composition of soil bacterial communities, soil enzyme activity, and stoichiometric characteristics.

KEYWORDS

warming, nitrogen deposition, soil organic carbon, enzyme activity, microbial community, Tibetan Plateau, alpine meadows

Introduction

The alpine grasslands of the Qinghai-Tibet Plateau encompass approximately 40% of China's grassland area. This region holds global ecological significance, serving as a repository for unique biodiversity and genetic resources crucial for high-altitude organisms. Additionally, it plays a vital role in providing ecosystem services such as biodiversity maintenance, regulation of nutrient cycling, hydrological function, and carbon storage (Fu et al., 2021). Among the grassland types in this area, alpine meadows are prominent, especially in high-altitude regions, which are particularly susceptible to the effects of climate change (Liu S. B. et al., 2018). Projections indicate that temperatures on the Qinghai-Tibet Plateau are expected to rise by 1.5–2.9°C between 2030 and 2099, with nitrogen deposition averaging 8.7–13.8 kg N ha^{-1} $yr.^{-1}$ (Liu X. D. et al., 2009; Pang et al., 2019). Climate warming and nitrogen deposition are intertwined components of global climate change (Sun et al., 2021). Climate warming can escalate the emission of reactive nitrogen into the atmosphere, resulting in lower nitrogen use efficiency and atmospheric pollution (Li et al., 2024). However, the increase in atmospheric reactive nitrogen can directly or indirectly contribute to further climate warming (Ma et al., 2022). Extensive experimentation has demonstrated that climate warming and nitrogen deposition significantly impact the structure and function of grassland ecosystems, leading to declines in biodiversity, alterations in carbon cycling, and changes in grassland multifunctionality (Su et al., 2022).

Soil carbon storage represents the largest carbon reservoir in terrestrial ecosystems, surpassing vegetation and atmospheric carbon reservoirs by 2–3 times (Delgado-Baquerizo et al., 2017). Soil organic carbon constitutes the primary component of soil carbon storage and can be categorized into the biologically active, unstable organic carbon pool, and the long-term stable organic carbon pool based on its decomposition degree and turnover rate (Li et al., 2018). Unstable organic carbon, including labile organic carbon, soluble organic carbon, microbial carbon, and other carbon fractions, plays a crucial role in regulating soil nutrient flow and carbon-nitrogen fluxes (Cong et al., 2020). Minor changes in grassland soil carbon storage, such as increased soil respiration, can significantly impact atmospheric carbon dioxide production, thereby exacerbating global climate warming through positive feedback mechanisms (Nottingham et al., 2020). Therefore, understanding the response of soil organic carbon fractions to warming is crucial for exploring the carbon cycle in grassland ecosystems. Evidence suggests that experimental warming can have negative effects (Wang et al., 2019), positive effects (Zheng et al., 2020), or no effect (Tian et al., 2021) on soil organic carbon fractions. Due to the fundamental coupling of carbon and nitrogen cycles in terrestrial ecosystems, enhanced nitrogen availability can alter ecosystem carbon cycling and accumulation processes (Yang et al., 2011). Previous studies have indicated that nitrogen deposition may increase (Wang et al., 2022), decrease (Zhong et al., 2017), or have no effect on organic carbon content (Balesdent et al., 2000). Variations in grassland vegetation types, nitrogen addition rates, warming magnitudes, and experimental durations can influence soil organic carbon fractions (Lu et al., 2011; Luo et al., 2019). While most previous research on organic carbon fractions has focused solely on individual climatic factors, few studies have investigated the effects of multiple climate factors on organic carbon fractions. Therefore, exploring differences in soil organic carbon fractions in response to nitrogen deposition and warming is a crucial direction for increasing soil carbon storage and reducing greenhouse gas emissions under future climate change conditions.

Soil microbes represent indispensable components of terrestrial ecosystems, fulfilling crucial roles in promoting soil organic matter turnover and enhancing soil nutrient mineralization rates in the soil carbon cycle (Van Der Heijden et al., 2008). Research indicates that under elevated temperatures and nitrogen deposition, soil microbes not only release carbon into the air through heterotrophic decomposition but also metabolize exogenous carbon into certain substances and sequester them in the soil through synthetic processes (Tamura and Tharayil, 2014). Additionally, soil microbes can influence soil aggregate stability by secreting carbon-transforming enzymes (Trivedi et al., 2016). Consequently, any alterations in the diversity, composition, and potential functions of microbial communities may affect the direction of carbon mineralization (Ibrahim et al., 2021). Soil microbial extracellular enzymes serve as potential indicators of microbial function, playing critical roles in the degradation, transformation, and mineralization of soil organic matter in the carbon cycle (Nannipieri et al., 2018). Studies indicate that soil enzymes produced by soil microbes, such as β-glucosidase and β-xylosidase activities, regulate carbon transformation processes by degrading different molecules or depolymerizing large molecular substrates (Duan et al., 2021). Furthermore, nitrogen enrichment and climate warming may disrupt soil element balances, affecting the limited resources available for soil microbial metabolism (Steinweg et al., 2013). Microbial enzyme stoichiometry is recognized as an effective tool for assessing the environmental drivers of microbial metabolism. Research has demonstrated that changes in soil organic carbon induced by warming are associated with microbial enzyme stoichiometry (Stark et al., 2018). Therefore, microbial enzyme stoichiometry plays a pivotal role in controlling soil carbon cycling (Buchkowski et al., 2015). While there is abundant research on the response of soil organic carbon fractions to warming and nitrogen deposition (Ding et al., 2019; Chen et al., 2020), most studies overlook the regulatory mechanisms of soil microbial characteristics on soil carbon fractions.

Investigating the changes in soil organic carbon fractions and their regulatory mechanisms under nitrogen deposition and climate warming in the alpine meadows of the Qinghai-Tibet Plateau is crucial for enhancing our understanding of organic carbon cycling mechanisms in these ecosystems under future climate change. We hypothesize the following: (1) Both warming and nitrogen deposition will significantly affect soil organic carbon fractions, enzyme activity, stoichiometry, microbial diversity, and composition. However, soil enzyme stoichiometry will respond differently to warming and nitrogen deposition. (2) Soil organic carbon fractions will experience distinct impacts from warming and nitrogen deposition, with soil bacterial communities exerting a greater influence than fungi. Additionally, soil enzyme activity and stoichiometry are pivotal in regulating organic carbon composition.

Materials and methods

Study area overview

The study was conducted at the Chengdu Zi Station of the Three-River Source Grassland Ecosystem National Field Scientific

Observation and Research Station in Qinghai Province (33° 24′30″N, 97° 18′00″E), situated at an elevation of 4,270 m. The area exhibits a typical plateau continental climate, characterized by an annual average temperature ranging from −5.6°C to 3.8°C and an average annual precipitation of 562.2 mm. The majority of the precipitation, approximately 75% of the annual total, falls during the peak growing season for grasses from July to September. Dominant vegetation species include *Kobresia humilis* (C.A.Mey ex Trauvt) Serg., *Kobresia pygmaea* Clarke, *Elymus nutans* Griseb., and *Poa annua* L.

Experimental design

The field experiment for this study was conducted in May 2023 within a fenced flat area measuring 50 × 50 m^2. Projections suggest that the Qinghai-Tibet Plateau will face additional warming of up to 2.0°C by 2035 and up to 4.9°C by 2100 (Peng et al., 2017). Consequently, the study comprised four temperature treatments (non-warming and three warming treatments) established within plots. Three temperature gradients were created using Open-Top Chambers (OTCs) to mitigate the volume effect (Table 1; Figure 1). Soil and air temperatures were continuously monitored using HOBOS-TMB-M006 Temperature Smart Sensors (HOBO, United States).

Environmental nitrogen deposition on the Qinghai-Tibet Plateau is estimated to be approximately 8 kg N ha^{-1} $yr.^{-1}$, predominantly in the form of NH4-N and NO3-N (Zhan et al., 2019). Hence, three nitrogen deposition levels were chosen to simulate future atmospheric N deposition: N0 (0 kg ha^{-1} $yr.^{-1}$), N16 (16 kg N ha^{-1} $yr.^{-1}$), and N32 (32 kg N ha^{-1} $yr.^{-1}$). Ammonium nitrate was utilized to simulate nitrogen deposition during the growing season, dissolved in water, and uniformly sprayed onto the plots, with an equivalent amount of water sprayed in the control. The experiment followed a randomized complete block design, with four replicates in each plot and 12 treatment levels per subplot, including W0N0 (no warming or nitrogen addition, CK), W0N8, W0N32, W1N0, W1N8, W1N32, W2N0, W2N8, W2N32, W3N0, W3N8, and W3N32, resulting in a total of 48 plots.

Sample collection

Sampling was conducted during the plant growing season in August 2023, with samples randomly taken from each treatment within 0.5 × 0.5 m quadrats. From each quadrat, five soil cores with a diameter of 3 cm and a depth of 30 cm were randomly collected. These cores were combined to create one soil sample. Plant roots and stones were eliminated using a 2 mm mesh sieve. The sample was then divided into two subsamples: one stored at −80°C for subsequent microbial analysis, and the other air-dried naturally for determining physicochemical properties.

Soil sample analysis

Soil organic carbon components

Soil organic carbon (SOC) was quantified employing the potassium dichromate oxidation method with external heating. Microbial biomass carbon (MBC) was extracted using the chloroform fumigation method and analyzed using a carbon and nitrogen analyzer. Dissolved organic carbon (DOC) was determined via a TOC analyzer following deionized water extraction. The content of readily oxidizable carbon (ROC) in soil was measured utilizing the potassium permanganate oxidation method with UV spectrophotometry.

TABLE 1 Specifications and performance of warming facility.

Warming gradient (°C)	Top diameter (m)	Bottom diameter (m)	Height (m)	Temperature (°C)	
				10 cm above ground air temperature	5 cm below ground soil temperature
W1	1.5	1.95	0.4	0.47	0.61
W2	1	1.45	0.4	0.92	1.09
W3	0.5	0.95	0.4	1.44	1.95

W1, W2, and W3 denote the warming conditions relative to W0.

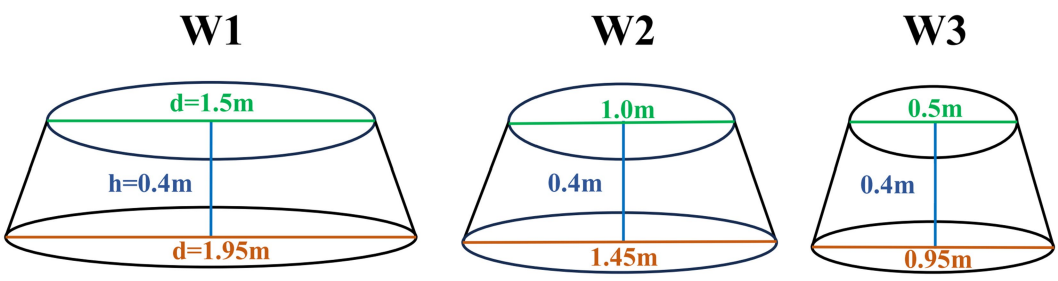

FIGURE 1
Schematic diagram of warming facility specifications.

Soil enzyme activity and stoichiometry

Enzymes involved in carbon cycling [cellobiohydrolase (CBH), β-xylosidase (βX)], nitrogen cycling [β-1,4-N-acetylglucosaminidase (NAG), leucine aminopeptidase (LAP)], and phosphorus cycling [alkaline phosphatase (AKP/ALP)] were measured using a 96-well microplate fluorescence assay (Peng and Wang, 2016). After incubating soil with substrates for 4 h, 10 μL of NaOH was added to adjust the pH of the reaction mixture for optimal fluorescence values. Fluorescence values were then detected using a multifunctional enzyme analyzer (Tecan Infinite M200, Austria), with excitation and emission wavelengths of 365 nm and 450 nm, respectively. Enzyme activity was expressed as $\mu mol \cdot g^{-1} \cdot h^{-1}$. Soil extracellular enzyme C: N, C:P, and N:P stoichiometric ratios were calculated as ln (CBH + βX): ln (NAG + LAP), ln (CBH + βX): ln (AKP/ALP), and ln (NAG + LAP): ln (AKP/ALP), respectively (Xu et al., 2020).

Soil microbial community composition

Approximately 0.5 g of refrigerated soil samples were utilized for total DNA extraction following the manufacturer's protocol of the DNA extraction kit (Omega Bio-tek, Norcross, GA, United States). The concentration and purity of DNA were assessed using the NanoDrop 2000 spectrophotometer (Thermo Scientific Inc., Waltham, MA, United States). PCR amplification targeting the V3-V4 region of bacterial 16S rRNA (with primers 341F: 5′-CCTACGGGNGGCWGCAG-3′ and 805R: 5′-GACTACHVGGGTATCTAATCC-3′) and the ITS2 region of fungal ITS (with primers ITS-1F: 5′-GTGARTCATCRARTYTTTG-3′ and ITS-2: 5′-TCCTSCGCTTATTGATATGC-3′) was conducted using the ABI GeneAmp®9700 PCR thermal cycler (ABI, CA, United States). The PCR reaction system (20 μL) included 4 μL of 5 × TransStartFastPfu buffer, 0.8 μL of each primer, 2 μL of 2.5 mM dNTPs, 0.4 μL of TransStart FastPfu DNA polymerase, 10 ng of template DNA, and sterilized ddH2O to make up the volume. The PCR program comprised an initial denaturation at 95°C for 3 min, followed by 32 cycles of denaturation at 95°C for 30 s, annealing at 56°C for 30 s, extension at 72°C for 45 s, and a final extension at 72°C for 10 min. Each sample was run in triplicate. PCR products were purified from 2% agarose gels using the AxyPrep DNA Gel Extraction Kit (Axygen Biosciences, Union City, CA, United States) following the manufacturer's instructions and quantified using the Quantus™ Fluorometer (Promega, United States). The Illumina NovaSeq 6000 platform was employed for paired-end sequencing (PE250) of 16S and ITS amplicons to generate raw data. To assess sample diversity, clean data were imported into QIIME2 for DADA2-based filtering, quality control, chimera removal, merging of paired-end reads, and denoising to generate amplicon sequence variants (ASVs). For taxonomic classification, the bacterial classifier was trained using the Silva138 99% clustered sequences of the V3-V4 region, while the fungal classifier was trained using the UNITE database (version 8.0). The trained classifiers were then used to assign taxonomic information to the ASVs, resulting in the microbial community composition of each sample.

Statistical analysis

To assess the impacts of warming, nitrogen deposition, and their interaction on soil organic carbon fractions, enzyme activities, and the diversity and richness of soil bacterial and fungal communities, a linear mixed-effects model was employed, with warming and nitrogen deposition as fixed factors and site as a random factor. Furthermore, one-way analysis of variance (ANOVA) with Tukey's test was utilized to compare differences between nitrogen and warming treatments, with a significance level set at $p < 0.05$. All results are expressed as mean ± standard deviation. Chao1 and Shannon diversity indices were calculated using Qiime software (Version 1.9.0). Soil microbial beta diversity was assessed using the Anosim test to determine if between-group differences were greater than within-group differences, indicating the significance of grouping. *R*-values, ranging from −1 to 1, were obtained, with $R > 0$ indicating greater between-group differences and $R < 0$ indicating the opposite. Larger |R| values denote greater differences, with *p*-values indicating the confidence level of statistical analysis ($p < 0.05$ indicates significance). Canoco 5 was utilized to explore the principal factors affecting soil organic carbon under nitrogen deposition and warming conditions, incorporating soil microbial diversity and composition. A structural equation model (SEM) in SPSS Amos 22 software was employed to establish links among soil enzyme activities, microbial diversity, dominant bacterial phyla, and soil organic carbon fractions under warming and nitrogen deposition conditions. Variables for SEM were selected based on Monte Carlo permutation tests conducted in redundancy analysis, with model fit assessed using CMIN/Df, *p*-values, goodness-of-fit index (GFI), and root mean square error of approximation (RMSEA) to determine the optimal-fit model.

Results

Soil organic carbon fractions

Warming significantly affects soil organic carbon, readily oxidizable organic carbon content, dissolved organic carbon, and microbial biomass carbon. Similarly, nitrogen deposition also significantly impacts these soil carbon fractions. Moreover, the interaction between warming and nitrogen deposition influences all soil carbon fractions (Figure 2). Compared to the control group (W0), soil organic carbon increased significantly by 1.40 and 9.30% in the W1 and W3 treatments, respectively. Readily oxidizable organic carbon content increased by 1.27% in the W2 treatment, while dissolved organic carbon increased by 9.56% in the W3N0 treatment. Microbial carbon increased by 1.27 and 15.75% in the W2 and W3 treatments, respectively. Similarly, compared to the control group (N0), soil organic carbon increased significantly by 1.40 and 21.59% in the N16 and N32 treatments, respectively. Readily oxidizable organic carbon content increased by 21.18% in the N32 treatment, and dissolved organic carbon increased by 18.92% in the N36 treatment. Microbial carbon increased by 12.48% in the N32 treatment (Figure 2). Notably, soil organic carbon, readily oxidizable organic carbon content, dissolved organic carbon, and microbial carbon reached their maximum values in the W0N32 treatment, whereas microbial carbon peaked in the W3N32 treatment. The proportions of dissolved organic carbon, microbial biomass carbon, and readily oxidizable carbon in total soil organic carbon were significantly influenced by warming, nitrogen deposition, and their interaction. Particularly, readily oxidizable carbon constituted the main part (26.5–18.0%) of soil organic carbon, while dissolved organic carbon comprised the least (0.41–0.21%) (Supplementary Table S1).

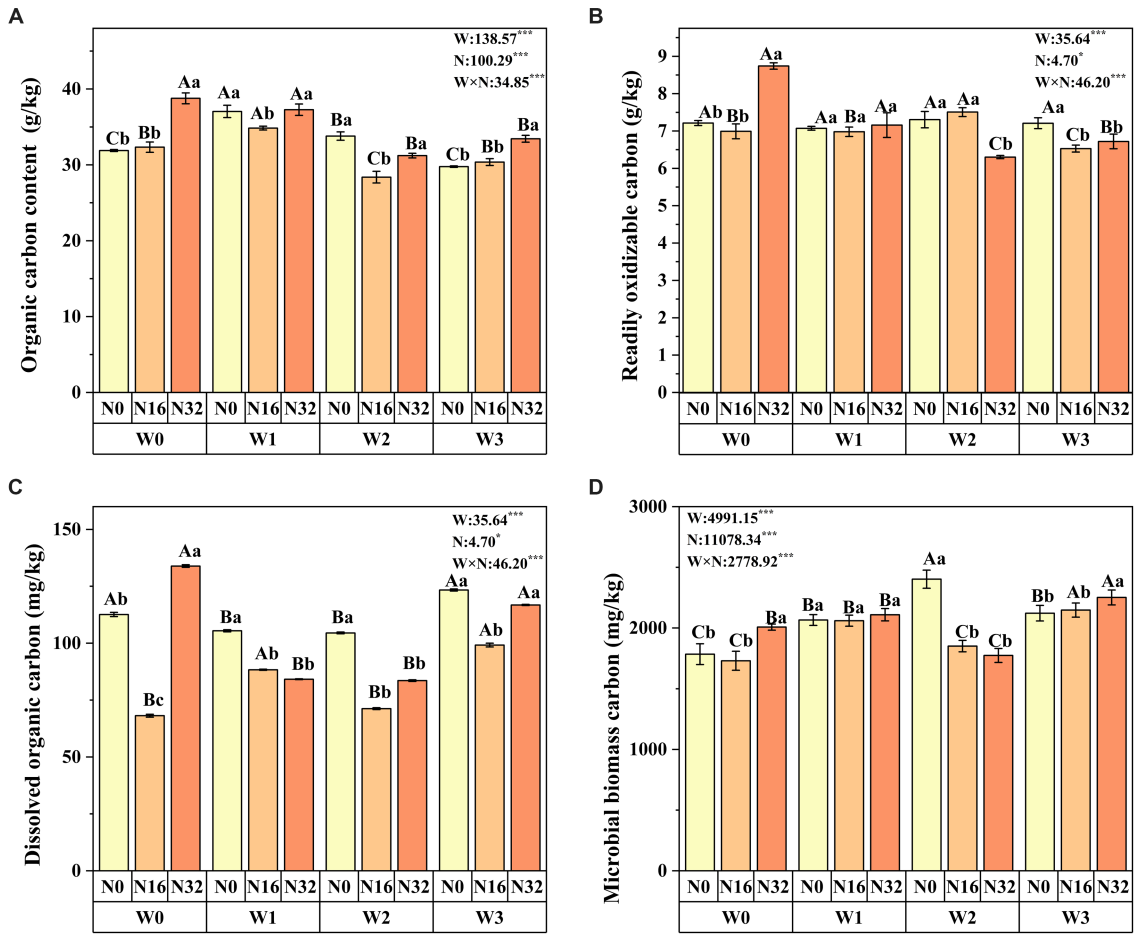

FIGURE 2
Impact of warming, nitrogen deposition, and their interaction on soil carbon fractions. **(A–D)** respectively soil organic carbon, readily oxidizable organic carbon content, dissolved organic carbon and microbial biomass carbon. Lowercase letters indicate significant differences among nitrogenlevels within the same warming treatment, whereas uppercase letters denote significant differences among warming treatment nitrogen level (n = 4). W represents the effect of the warming treatment,N represents the effect of the nitrogen treatment, and W*N represents the interaction effect of warming and nitrogen treatment. *$p < 0.05$; **$p < 0.01$; ***$p < 0.001$; ns indicates not significant.

Soil enzyme activity and stoichiometry

Warming significantly affects soil leucine aminopeptidase, soil cellobiohydrolase, soil alkaline phosphatase, soil β-1,4-N-acetylglucosaminidase, and soil β-xylosidase, while nitrogen deposition also significantly impacts these enzyme levels (Figure 3). Compared to the control group (W0), soil leucine aminopeptidase increased by 36.81, 7.10, and 8.97% in the W1, W2, and W3 treatments, respectively. Soil cellobiohydrolase increased by 11.42% in the W1 treatment, while soil alkaline phosphatase increased by 24.73% in the W1 treatment. Soil β-1,4-N-acetylglucosaminidase increased by 55.57, 22.34, and 32.13% in the W1, W2, and W3 treatments, respectively, and β-xylosidase levels increased by 52.68, 18.90, and 20.81% in the W1, W2, and W3 treatments, respectively. Similarly, compared to the control group (N0), soil leucine aminopeptidase increased by 10.13% in the N32 treatment, while soil cellobiohydrolase increased by 4.09 and 54.62% in the N16 and N32 treatments, respectively. Soil alkaline phosphatase increased by 27.10 and 23.18% in the N16 and N32 treatments, respectively, and soil β-1,4-N-acetylglucosaminidase increased by 16.20 and 3.20% in the N16 and N32 treatments, respectively. Additionally, the interaction between warming and nitrogen deposition significantly influences soil enzyme activity, with soil leucine aminopeptidase reaching its maximum in the W1N0 treatment, while soil cellobiohydrolase and soil alkaline phosphatase reach their peak levels in the W0N32 treatment. Soil β-1,4-N-acetylglucosaminidase reaches its maximum in the W2N32 treatment, and β-xylosidase levels peak in the W1N16 treatment.

Both warming and nitrogen deposition significantly influence soil enzyme C: N, C:P, and N:P ratios. Compared to the control group (W0), soil enzyme C: N ratios decreased significantly by 5.69, 11.69, and 4.73% in the W1, W2, and W3 treatments, respectively, while soil enzyme N:P ratios increased significantly by 2.47, 4.63, and 4.26%. Soil enzyme C:P ratios also decreased significantly by 3.37 and 7.60% in the W1 and W2 treatments, respectively. Similarly, compared to the control group (N0), soil enzyme C: N ratios increased significantly by 2.30 and 9.77% in the N16 and N32 treatments, respectively, while soil enzyme N:P ratios decreased significantly by 8.36 and 4.59%. Additionally, the interaction between warming and nitrogen deposition significantly influences soil enzyme carbon, nitrogen, and phosphorus stoichiometry. Soil enzyme C: N and C:P ratios reach

10.3389/fmicb.2024.1381891

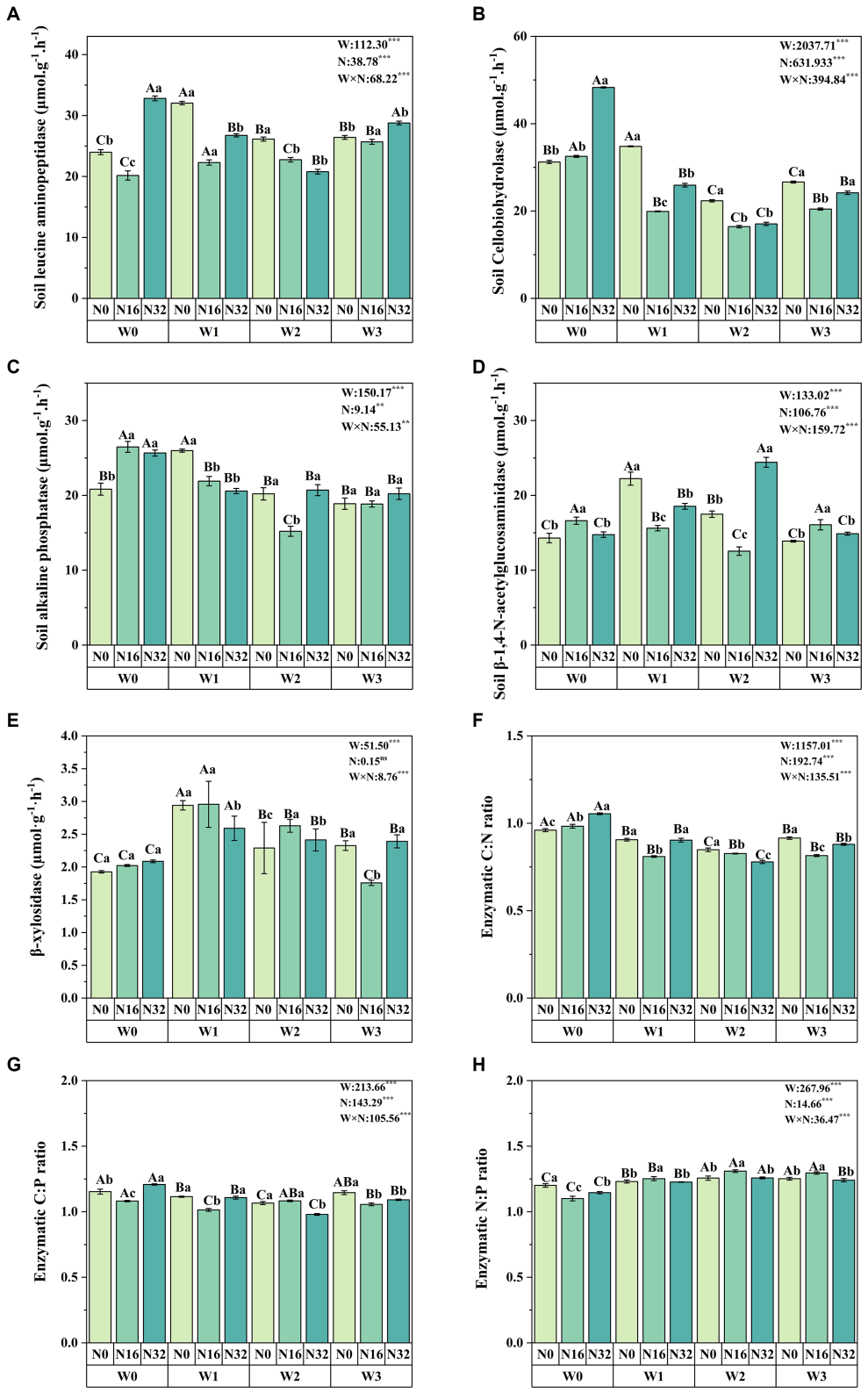

FIGURE 3
Impact of warming and nitrogen deposition on soil enzyme activity. **(A–E)** Extracellular enzyme activities related to carbon, nitrogen, and phosphorus (soil leucine aminopeptidase, soil cellobiohydrolase, soil alkaline phosphatase, soil β-1,4-N-acetylglucosaminidase, and β-xylosidase). **(F–H)** Soil enzyme stoichiometry (C: N, C:P, and N:P). Values represent the mean ± standard error of the mean for replicated plots ($n = 4$). Duncan's test indicates significant differences, where different lowercase letters denote significant differences at the same warming level with different nitrogen levels, and different uppercase letters denote significant differences at the same nitrogen level with different warming treatments ($p < 0.05$). W: effect of warming treatment; N: effect of nitrogen treatment; W*N: interaction effect of warming and nitrogen treatments. Asterisks indicate significant differences at different levels (***$p < 0.001$).

their maximum in the W0N32 treatment, while the soil enzyme N:P ratio reaches its peak in the W2N16 treatment (Figures 3F,G,H).

Soil microbial diversity and composition

To elucidate the differences in soil microbial diversity and community, we investigated bacterial and fungal diversity and community composition across various levels of warming and nitrogen deposition. Under warming treatment, both the bacterial Chao1 index and Shannon index exhibited significant increases ($p < 0.05$) (Supplementary Figures S1A,B). Specifically, there were notable increases of 2.65 and 0.56% in the W1 treatment, 12.71 and 4.44% in the W2 treatment, and 26.88 and 5.37% in the W3 treatment, respectively. In the N32 treatment, the bacterial Chao1 index and Shannon index increased significantly by 2.30 and 1.25%, respectively. Moreover, the interaction between warming and nitrogen deposition significantly affected the soil bacterial Chao1 index. However, there were no significant changes in the fungal Chao1 index and Shannon index with warming and nitrogen addition (Supplementary Figures S1C,D). ANOSIM results with $R > 0$ indicate that inter-group differences surpass intra-group differences, with $p < 0.05$ denoting statistical significance. This implies that both warming and nitrogen deposition exert significant influence on soil microbial community structure (Supplementary Figures S2).

Differences in bacterial community composition are evident under warming and nitrogen deposition (Figure 4A). The dominant phyla of soil bacteria include *Acidobacteriota*, *Proteobacteria*, and *Bacteroidota*. With warming, the relative abundance of *Acidobacteriota* declined by 8.40–30.10%, whereas Proteobacteria increased from 16.42 to 21.12%, and *Bacteroidota* increased by 10.44–20.04%. Under nitrogen deposition, the relative abundance of *Acidobacteriota* decreased by 4.68–7.37%, while Proteobacteria increased from 16.42 to 18.30%, and *Bacteroidota* increased by 7.09–13.40%. The dominant phyla of soil fungi were *Ascomycota*, *Basidiomycota*, and *Mortierellomycota* (Figure 4B). With warming, the relative abundance of Ascomycota decreased by 21.14–24.34%, while *Basidiomycota* increased from 13.91 to 41.48%. The relative abundance of *Mortierellomycota* decreased by 57.46–74.09%. Under nitrogen addition, the relative abundance of *Ascomycota* initially increased followed by a decrease, Basidiomycota initially decreased followed by an increase, while the relative abundance of *Mortierellomycota* gradually decreased.

Linkages between soil microbial community, enzyme activity, and carbon fractions

Redundancy analysis (RDA) results reveal that 57.89% of soil carbon fractions can be elucidated by soil enzyme activity (Figure 5A). Notably, factors such as C/P, S-LAP, S-AKP/ALP, βX, S-NAG, and N/P significantly influence soil organic carbon (Table 2). Furthermore, soil microbial community diversity and structure account for 38.79% of soil organic carbon dynamics (Figure 5B). Within the top 10 microbial taxa at the phylum level, *Gemmatimonadota*, *unidentified*, *Crenarchaeota*, and *Nitrospirota* emerge as pivotal microbial groups (Table 2).

The results of the structural equation model indicate that changes in soil carbon fractions are directly and indirectly influenced by nitrogen deposition, warming, soil enzyme activity, and soil microbial composition (Figure 6A). Climate warming has a significant positive effect on *Gemmatimonadota*, *Nitrospirota*, and N/P ratio, while it negatively impacts soil carbon fractions. Conversely, nitrogen deposition negatively affects LAP but positively influences soil carbon fractions. In summary, climate warming and nitrogen deposition alter soil microbial composition (such as *Gemmatimonadota*, and *Nitrospirota*), thereby affecting soil microbial enzyme activity (including S-AKP/ALP, βX) and enzyme stoichiometry (N/P ratio, C/P ratio), ultimately leading to changes in soil carbon fractions. The main factors influencing soil carbon fractions under climate warming and nitrogen deposition include S-AKP/ALP, enzyme N/P ratio, nitrogen deposition, enzyme C/P ratio, and βX. The direct effects of

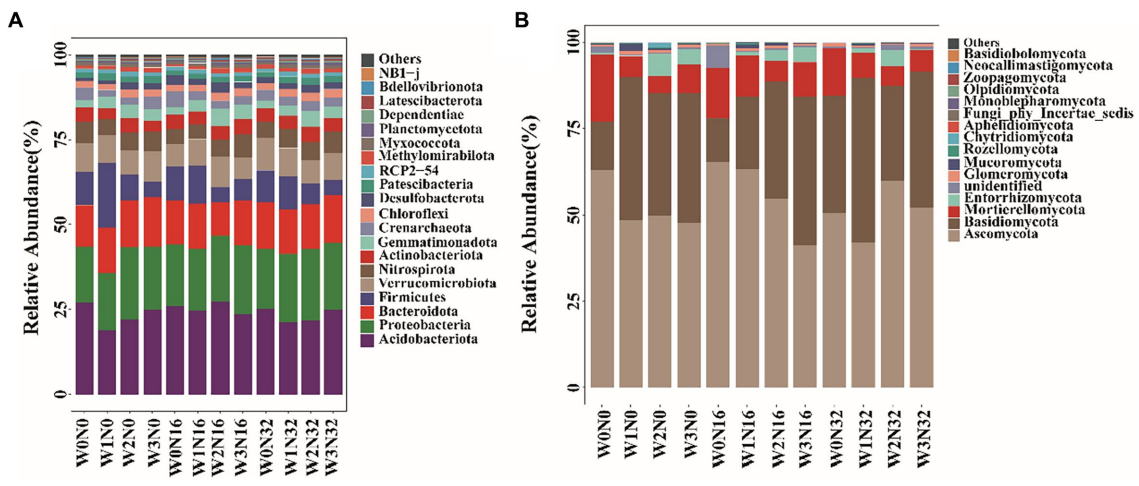

FIGURE 4
The composition of soil microbial community structure on phylum level under different treatments. **(A)** The situation of soil bacteria. **(B)** The situation of soil fungal.

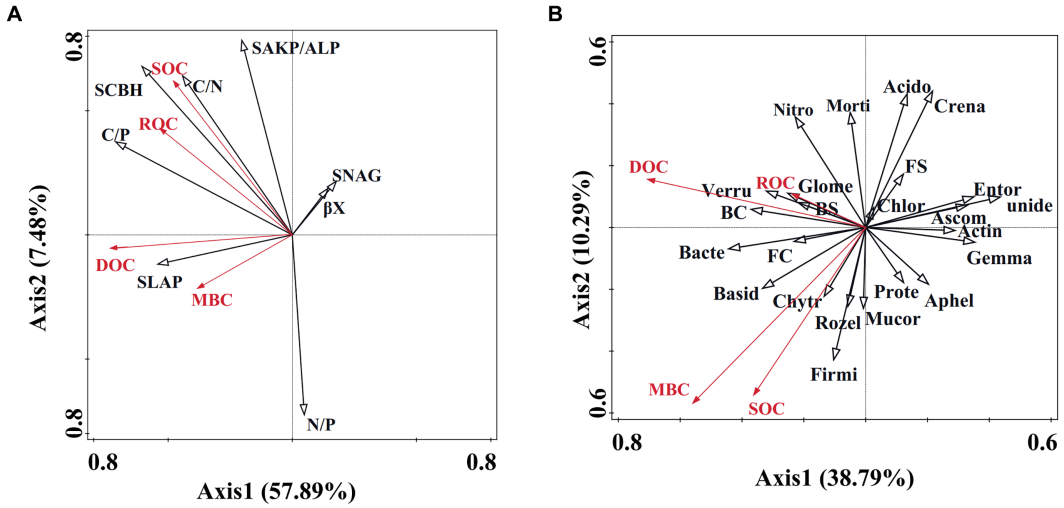

FIGURE 5
Redundancy analysis of soil microbial community and enzyme activity regarding organic carbon dynamics. **(A)** Redundancy analysis illustrating the correlation between enzyme activity and organic carbon dynamics. SOC, ROC, DOC, and MBC denote soil organic carbon, readily oxidizable carbon, dissolved organic carbon, and microbial biomass carbon, respectively. S-LAP, SCBH, S-AKP/ALP, S-NAG, and cc represent soil leucine aminopeptidase, soil cellobiohydrolase, soil alkaline phosphatase, soil β-1,4-N-acetylglucosaminidase, and β-xylosidase, respectively. **(B)** Redundancy analysis demonstrating the association between soil microbial community and organic carbon dynamics. Unide, Gemma, Crena, Nitros, BC, Chlor, Verru, Ascom, Bacter, Chytr, FC, FS, Entor, Morti, Rozel, Aphel, Acido, Mucor, Firmi, Prote, Actin, Glome, BS, Basid represent unidentified, Gemmatimonadota, Crenarchaeota, Nitrospirota, Bacteria chao, Chloroflexi, Verrucomicrobiota, Ascomycota, Bacteroidota, Chytridiomycota, Fungus chao, Fungus Shannon, Entorrhizomycota, Mortierellomycota, Rozellomycota, Aphelidiomycota, Acidobacteriota, Mucoromycota, Firmicutes, Proteobacteria, Actinobacteria, Glomeromycota, Bacteria Shannon, Basidiomycota.

TABLE 2 **Monte Carlo permutation test results for redundancy analysis.**

Factor	Explains %	*p*	Factor	Explains %	*p*
C/P	31.7	0.002	N/P	7.9	0.002
S-LAP	17.5	0.002	Gemmatimonadota	8.6	0.048
S-AKP/ALP	6.1	0.012	Unidentified	7.8	0.048
βX	3.6	0.021	Crenarchaeota	5.2	0.049
S-NAG	4.0	0.016	Nitrospirota	4.9	0.049

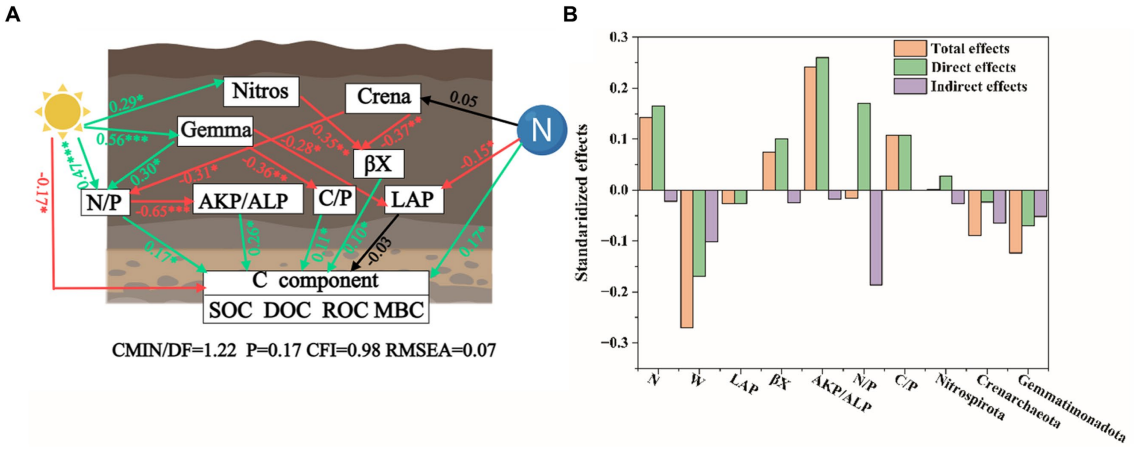

FIGURE 6
Structural equation model analysis of soil enzyme activity and microbial community on organic carbon under warming and nitrogen deposition. **(A)** Schematic representation of the structural model (Created with MedPeer.com). Green, red, and black colors indicate positive, negative, and no effects, respectively. Asterisks denote significance at probability levels of $p < 0.01$ and $p < 0.001$ (represented as ** and ***). **(B)** Direct and indirect effects of different factors on soil organic carbon fractions.

temperature increase and nitrogen deposition on soil organic carbon are −0.17 and 0.17, respectively (Figure 6B).

Discussion

Impact of warming and nitrogen deposition on soil organic carbon fractions

This study illustrates that nitrogen deposition fosters an increase in soil organic carbon, consistent with findings in the Qinghai-Tibetan Plateau (Xiao et al., 2020) and the Yellow River Delta region (Qu et al., 2020). Nitrogen addition stimulates plant growth and microbial decomposition in nitrogen-limited environments, thereby influencing soil microbial communities and plant decomposition patterns, ultimately affecting soil organic carbon retention (Frey et al., 2013). Temperature is a critical limiting factor in high-altitude ecosystems (Duan et al., 2019). Our study found that warming increases soil organic carbon. Other studies have shown that changes in microbial community structure induced by warming can promote carbon release (Chen et al., 2021). This is mainly due to plant inputs, such as rhizosphere exudates and litter, being significant pathways for soil organic carbon formation. Research suggests that enhanced nitrogen availability can amplify warming's effects on microbial-mediated litter and organic matter decomposition (Chen et al., 2017b). In our study, soil organic carbon reached its maximum in the W0N32 treatment, indicating that the response of soil organic carbon to nitrogen deposition and warming is not simply additive. A comprehensive assessment of various climatic factors is crucial for understanding changes in soil carbon storage.

Soil microbial biomass carbon serves as an indicator of the microbial biomass involved in decomposition processes and is considered a reliable indicator of soil nutrient cycling potential (Fan et al., 2021). This study demonstrates that elevated temperature and nitrogen deposition significantly influence soil microbial biomass carbon, reaching its peak in the W3N32 treatment. This suggests that warming and nitrogen deposition increase the availability of nutrients in the soil, creating a favorable environment for microbial survival and promoting microbial growth and metabolism, thereby enhancing soil microbial biomass carbon (Chen et al., 2014). Soil-dissolved organic carbon, the most readily utilizable portion of carbon substrates for microbes, is crucial for microbial metabolic maintenance (Fungo et al., 2017). Studies have shown that warming can increase soil dissolved organic carbon by boosting the production of dissolved organic compounds by plants or microbial communities (Bai et al., 2020). Conversely, excessive nitrogen addition can reduce aboveground biomass and microbial activity, impairing microbial decomposition of litter, and leading to a decrease in soil dissolved organic carbon (Zhong et al., 2015). In our study, we found that soil dissolved organic carbon reached its maximum in the W0N32 treatment. This is primarily because nitrogen addition increases plant biomass, with plant residues and secretions being the main sources of soil dissolved organic carbon. Additionally, nitrogen addition promotes plants to provide carbon sources for soil microbes, enhancing microbial activity in the soil, thereby accelerating the decomposition of plant residues, releasing more nutrients, improving soil structure, and promoting soil dissolved organic carbon (Yang et al., 2016). The migration and transformation of soil readily oxidizable organic carbon content also play a crucial role in carbon cycling in grassland ecosystems (Liu F. et al., 2018; Liu H. Y. et al., 2018). Our study found that soil readily oxidizable organic carbon content reached its maximum in the W0N32 treatment, and soil readily oxidizable organic carbon content is the main component of soil organic carbon. A higher ROC/SOC ratio indicates stronger soil organic carbon activity, while a lower ratio indicates more stable soil (Han et al., 2022). Since soil readily oxidizable organic carbon content is mostly composed of recently fallen plant residues, nitrogen addition promotes the decomposition of surface litter by soil microbes, accelerating soil organic carbon turnover rates (Liu F. et al., 2018; Liu H. Y. et al., 2018).

Impact of warming and nitrogen deposition on soil enzyme activity and stoichiometry

Soil enzymes play a crucial role in regulating key processes such as microbial decomposition of organic matter and soil nutrient cycling (Liu et al., 2021). Previous studies have consistently demonstrated the positive effects of nitrogen addition on C-acquiring, especially β-glucosidase (BG), and P-acquiring, particularly alkaline phosphatase (AP), and hydrolases (Xiao et al., 2018). Our study also observed significant increases in β-xylosidase activity and soil AP in response to nitrogen addition, suggesting that nitrogen stimulates microbial demand for carbon and phosphorus (Yang et al., 2022). Furthermore, nitrogen addition enhances the activity of nitrogen-acquiring enzymes, such as soil leucine aminopeptidase and soil N-acetylglucosaminidase. However, it has been documented that nitrogen addition significantly reduces the activity of soil microbial enzymes involved in carbon, nitrogen, and phosphorus acquisition, thereby impeding the transformation of chemical elements and the decomposition and release of nutrients in the soil (Li et al., 2021). Consequently, the response of soil enzyme activity to nitrogen deposition is multifaceted and should take into account soil nutrient status, microbial conditions, nitrogen addition forms, plant community composition, and grassland type (Margalef et al., 2021).

Elevated temperature also impacts soil enzyme activity in various ways. Firstly, it promotes the binding of soil enzymes to substrates, thereby altering their activity. Secondly, temperature influences the mineralization of soil organic matter, accelerates litter decomposition, and induces changes in microbial communities, indirectly affecting enzyme activity (Morrison et al., 2019). Our study observed significant effects of warming on soil leucine aminopeptidase, soil cellobiohydrolase, soil alkaline phosphatase, soil β-1,4-N-acetylglucosaminidase, and β-xylosidase. Prior research has also noted increased activities of β-glucosidase (βG) and cellobiohydrolase (CBH) under elevated temperatures (Jiang et al., 2018). This can be attributed to the facilitation of microbial mobility, nutrient movement, and enzyme-substrate binding in soil solutions under higher temperatures, provided there is sufficient water availability (Alvarez et al., 2018). Studies have shown that the interaction between temperature and nitrogen addition significantly enhances the activity of soil acid phosphatase (aG), βG, CBH, and alkaline phosphatase (ACP) (Huang et al., 2022). In our investigation, β-xylosidase and soil alkaline phosphatase peaked in the W0N32 treatment, while soil N-acetylglucosaminidase reached its maximum in the W2N32 treatment. Additionally, minimal or insignificant changes in soil phosphatase, urease, and β-glucosidase activity have been reported due to climate warming (Pold et al., 2017; Souza et al., 2017).

Furthermore, elevated temperatures exacerbate transpiration, leading to reduced soil moisture content, which hampers the effectiveness of soil enzyme substrates (Liu W. X. et al., 2009). This indicates that different enzymes have distinct optimal temperature ranges, with excessively high temperatures causing denaturation and excessively low temperatures reducing activity.

Ecological enzyme stoichiometry, derived from soil carbon, nitrogen, and phosphorus extracellular enzyme activities, serves as a valuable tool for elucidating microbial resource constraints across various ecosystems (Xu et al., 2022). Our findings reveal that nitrogen deposition leads to a significant increase in soil enzyme C: N ratios, coupled with a notable decrease in soil enzyme N:P ratios. This trend suggests that warming and nitrogen deposition exacerbate microbial phosphorus limitation (Ma et al., 2020). The intensified microbial phosphorus limitation is linked to nitrogen addition fostering plant growth, consequently heightening plant demand for and uptake of phosphorus, thereby intensifying nutrient competition between plants and microbes (Liu et al., 2022). Concurrently, increased soil temperature modifies soil nutrient turnover and microbial activity, consequently influencing soil extracellular enzyme stoichiometry. Specifically, our results indicate that under warming conditions, soil enzyme C: N and C:P ratios exhibit significant decreases, while soil enzyme N:P ratios register significant increases. This pattern arises from elevated temperatures accelerating cell membrane maintenance and lipid turnover, thereby augmenting microbial demand for nitrogen and phosphorus (Fang et al., 2016). Moreover, our study demonstrates that soil enzyme C: N and C:P ratios peak in the W0N32 treatment, while soil enzyme N:P ratios reach their maximum in the W2N16 treatment. This phenomenon may stem from soil microbial communities adjusting their extracellular enzyme production to achieve chemical stoichiometric balance in response to changes in nutrient availability. To maintain elemental stability, microbes can flexibly modulate the production of their extracellular enzymes by maximizing the mobilization of substrates abundant in limiting elements (Mooshammer et al., 2014).

Impact of warming and nitrogen deposition on soil microbial composition and structure

Microorganisms play a pivotal role in ecosystem functions, including soil nutrient cycling and organic matter decomposition (Luo et al., 2020). This study illustrates the influence of warming and nitrogen deposition on soil bacterial community diversity, as measured by Shannon and Chao1 indices, while soil fungal diversity remains largely unchanged. These findings suggest that bacterial communities undergo sustained alterations under climate change, whereas soil fungi exhibit relative stability. This phenomenon can be attributed to two main factors: (1) Direct modification of soil microbial community composition by climate warming, driven by the diverse optimal growth temperatures of different microbial species (Fukasawa, 2018). (2) Indirect impacts of warming and nitrogen deposition on plant communities and soil nutrient status, thereby influencing soil microbial community diversity (Liu F. et al., 2018; Liu H. Y. et al., 2018). Bacteria and fungi demonstrate variations in metabolic adaptability, resulting in diverse impacts on soil microbial activity (Begum et al., 2019).

Research indicates that nitrogen addition can lead to a decrease in the abundance of specific bacterial phyla, including *Actinobacteria*, *Proteobacteria*, and *Acidobacteria* (Freedman et al., 2016). According to the oligotrophic symbiotic nutrition theory, symbiotic taxa exhibit high nutrient requirements and growth rates, whereas oligotrophic taxa can survive in environments with low organic carbon availability (Xie et al., 2019). *Acidobacteria* are recognized as oligotrophic microbes, while Proteobacteria are categorized as copiotroph microbes (Fierer et al., 2007). In this investigation, both nitrogen addition and temperature elevation resulted in a decreased abundance of *Acidobacteriota* and an increased abundance of Proteobacteria. Consequently, the ratios of oligotrophic to copiotrophic (o: c) and acidobacteria to proteobacteria (a: P) remained unchanged under warming and nitrogen treatments. This study reveals that both warming and nitrogen deposition significantly diminished the relative abundance of *Mortierellomycota* but had no discernible impact on soil fungal microbiota. Previous research has similarly indicated that warming did not affect soil fungal diversity but did reduce the complexity of soil fungal communities (Yu et al., 2024). Nitrogen enrichment can also influence soil microbial community structure, although its effects on diversity and abundance are minimal (Wang et al., 2023). These findings suggest that the response of soil microbial communities to the altered soil environment resulting from climate warming and nitrogen deposition is intricate (Mitchell et al., 2015).

Impact of soil microbes and enzyme activity on carbon composition under climate warming and nitrogen deposition

Soil microbes represent a significant portion of global biodiversity and play essential roles in carbon sequestration, organic matter decomposition, and nutrient cycling (Luo et al., 2020). Their extracellular enzymes are pivotal in regulating the rate of organic matter decomposition (Yang et al., 2022). Studies have shown that elevated soil temperatures can enhance the activity of soil N-acetylglucosaminidase and alkaline phosphatase by altering the microbial community composition, thus influencing soil carbon decomposition and transformation (Zhou et al., 2013). The findings of this study reveal that climate warming and nitrogen deposition reshape soil microbial composition, notably affecting soil microbial enzyme activity, such as AKP/ALP and βX, and enzyme stoichiometry, including the N/P ratio and C/P ratio, consequently altering soil carbon composition. This is attributed to the selection of different soil microbial communities under climate warming and nitrogen deposition, which further reshapes soil ecosystem processes and functions (Li et al., 2018). Enzymes related to carbon, nitrogen, and phosphorus are primarily produced by microbes, and variations in microbial quantity and types can lead to changes in enzyme activity levels. Elevated extracellular enzyme activity levels can degrade both unstable and recalcitrant carbon substances, thereby influencing the biotransformation processes of organic carbon (Sardans et al., 2017).

This study reveals that soil organic carbon composition significantly decreases with climate warming, attributed to changes in microbial community composition or substrate utilization efficiency, accelerating microbially mediated organic matter degradation and reducing soil organic carbon content (Chen et al., 2017a). Additionally, soil organic carbon composition is directly influenced by nitrogen. This is due to two main reasons: firstly, nitrogen can enhance soil organic carbon accumulation by promoting plant growth, increasing litterfall, and inhibiting microbial

degradation of soil organic matter (Xia et al., 2017). Secondly, the nitrogen addition threshold for grasslands on the Qinghai-Tibet Plateau is 272 kg N ha^{-1} $year^{-1}$ (He et al., 2024). Studies indicate that nitrogen inputs below this critical level can suppress soil respiration by inhibiting soil microbial growth, reducing root biomass, and litter decomposition, thus fostering soil carbon sequestration (Xiao et al., 2021). Therefore, nitrogen inputs ranging from 16 to 32 kg N ha^{-1} $year^{-1}$ may promote carbon sequestration in alpine meadows on the Qinghai-Tibet Plateau.

Conclusion

Both climate warming and nitrogen deposition significantly increased soil organic carbon components, including organic carbon content, readily oxidizable carbon, dissolved organic carbon, and microbial biomass carbon. Moreover, soil enzyme activity, such as Soil Cellobiohydrolase, β-1,4-N-acetylglucosaminidase, leucine aminopeptidase, and alkaline phosphatase, was enhanced under these conditions. Similarly, soil bacterial diversity, as indicated by the Chao1 index and Shannon index, also showed significant increments. Additionally, climate warming led to a decrease in the soil enzyme C: N ratio and C:P ratio, while increasing the soil enzyme N:P ratio. Conversely, nitrogen deposition resulted in a significant increase in the soil enzyme C: N ratio and a decrease in the soil enzyme N:P ratio. The soil organic carbon components were directly influenced by the negative impact of climate warming and the positive impact of nitrogen deposition. Furthermore, climate warming and nitrogen deposition altered soil bacterial, particularly *Gemmatimonadota*, and *Nitrospirota*, leading to a positive impact on soil enzyme activity, particularly soil alkaline phosphatase and β-xylosidase, and enzyme stoichiometry, including C:P and N:P ratios.

Data availability statement

The datasets presented in this study can be found in online repositories. The raw sequence reads can be found at: https://www.ncbi.nlm.nih.gov/bioproject/PRJNA1096318.

Author contributions

XX: Data curation, Formal analysis, Investigation, Software, Writing – original draft. DK: Funding acquisition, Writing – review & editing. LW: Formal analysis, Investigation, Writing – review & editing. FT: Formal analysis, Investigation, Writing – review & editing. LF: Formal analysis, Investigation, Writing – review & editing. WX: Formal analysis, Investigation, Writing – review & editing.

Funding

The author(s) declare financial support was received for the research, authorship, and/or publication of this article. This study was supported by the National Key Research and Development Program (2022YFD1602302) and the Qinghai Provincial Science and Technology Department Project (K9922050).

Conflict of interest

The authors declare that the research was conducted in the absence of any commercial or financial relationships that could be construed as a potential conflict of interest.

Publisher's note

Supplementary material

The Supplementary material for this article can be found online at: https://www.frontiersin.org/articles/10.3389/fmicb.2024.1381891/full#supplementary-material

References

Alvarez, G., Shahzad, T., Andanson, L., Bahn, M., Wallenstein, M. D., and Fontaine, S. (2018). Catalytic power of enzymes decreases with temperature: new insights for understanding soil C cycling and microbial ecology under warming. *Glob. Chang. Biol.* 24, 4238–4250. doi: 10.1111/gcb.14281

Bai, T. S., Wang, P., Hall, S. J., Wang, F. W., Ye, C. L., Li, Z., et al. (2020). Interactive global change factors mitigate soil aggregation and carbon change in a semi-arid grassland. *Glob. Chang. Biol.* 26, 5320–5332. doi: 10.1111/gcb.15220

Balesdent, J., Chenu, C., and Balabane, M. (2000). Relationship of soil organic matter dynamics to physical protection and tillage. *Soil Till. Res.* 53, 215–230. doi: 10.1016/S0167-1987(99)00107-5

Begum, N., Qin, C., Ahanger, M. A., Raza, S., Khan, M. I., Ashraf, M., et al. (2019). Role of arbuscular mycorrhizal fungi in plant growth regulation: implications in abiotic stress tolerance. *Front. Plant Sci.* 10:1068. doi: 10.3389/fpls.2019.01068

Buchkowski, R. W., Schmitz, O. J., and Bradford, M. A. (2015). Microbial stoichiometry overrides biomass as a regulator of soil carbon and nitrogen cycling. *Ecology* 96, 1139–1149. doi: 10.1890/14-1327.1

Chen, J., Luo, Y. Q., Li, J. W., Zhou, X. H., Cao, J. J., Wang, R. W., et al. (2017a). Costimulation of soil glycosidase activity and soil respiration by nitrogen addition. *Glob. Chang. Biol.* 23, 1328–1337. doi: 10.1111/gcb.13402

Chen, J., Luo, Y. Q., Xia, J. Y., Wilcox, K. R., Cao, J. J., Zhou, X. H., et al. (2017b). Warming effects on ecosystem carbon fluxes are modulated by plant functional types. *Ecosystems* 20, 515–526. doi: 10.1007/s10021-016-0035-6

Chen, Q. Y., Niu, B., Hu, Y. L., Luo, T. X., and Zhang, G. X. (2020). Warming and increased precipitation indirectly affect the composition and turnover of labile-fraction soil organic matter by directly affecting vegetation and microorganisms. *Sci. Total Environ.* 714:136787. doi: 10.1016/j.scitotenv.2020.136787

Chen, R. R., Senbayram, M., Blagodatsky, S., Myachina, O., Dittert, K., Lin, X. G., et al. (2014). Soil C and N availability determine the priming effect: microbial N mining and stoichiometric decomposition theories. *Glob. Chang. Biol.* 20, 2356–2367. doi: 10.1111/gcb.12475

Chen, W. J., Zhou, H. K., Wu, Y., Li, Y. Z., Qiao, L. L., Wang, J., et al. (2021). Plant-mediated effects of long-term warming on soil microorganisms on the Qinghai-Tibet plateau. *Catena* 204:1596. doi: 10.1016/j.catena.2021.105391

Cong, P., Wang, J., Li, Y. Y., Liu, N., Dong, J. X., Pang, H. C., et al. (2020). Changes in soil organic carbon and microbial community under varying straw incorporation strategies. *Soil Till. Res.* 204:104735. doi: 10.1016/j.still.2020.104735

Delgado-Baquerizo, M., Eldridge, D. J., Maestre, F. T., Karunaratne, S. B., Trivedi, P., Reich, P. B., et al. (2017). Climate legacies drive global soil carbon stocks in terrestrial ecosystems. *Sci. Adv.* 3:e1602008. doi: 10.1126/sciadv.1602008

Ding, X. L., Chen, S. Y., Zhang, B., Liang, C., He, H. B., and Horwath, W. R. (2019). Warming increases microbial residue contribution to soil organic carbon in an alpine meadow. *Soil Biol. Biochem.* 135, 13–19. doi: 10.1016/j.soilbio.2019.04.004

Duan, M., Li, A. D., Wu, Y. H., Zhao, Z. P., Peng, C. H., DeLuca, T. H., et al. (2019). Differences of soil CO2 flux in two contrasting subalpine ecosystems on the eastern edge of the Qinghai-Tibetan plateau: a four-year study. *Atmos. Environ.* 198, 166–174. doi: 10.1016/j.atmosenv.2018.10.067

Duan, J. J., Yuan, M., Jian, S. Y., Gamage, L., Parajuli, M., Dzantor, K. E., et al. (2021). Soil extracellular oxidases mediated nitrogen fertilization effects on soil organic carbon sequestration in bioenergy croplands. *GCB Bioenergy* 13, 1303–1318. doi: 10.1111/gcbb.12860

Fan, J., Liu, T., Liao, Y., Li, Y., Yan, Y., and Lu, X. (2021). Distinguishing stoichiometric homeostasis of soil microbial biomass in alpine grassland ecosystems: evidence from 5,000 km belt transect across Qinghai–Tibet plateau. *Front. Plant Sci.* 12:781695. doi: 10.3389/fpls.2021.781695

Fang, X., Zhou, G. Y., Li, Y. L., Liu, S. Z., Chu, G. W., Xu, Z. H., et al. (2016). Warming effects on biomass and composition of microbial communities and enzyme activities within soil aggregates in subtropical forest. *Biol. Fert. Soils* 52, 353–365. doi: 10.1007/s00374-015-1081-5

Fierer, N., Bradford, M. A., and Jackson, R. B. (2007). Toward an ecological classification of soil bacteria. *Ecology* 88, 1354–1364. doi: 10.1890/05-1839

Freedman, Z. B., Upchurch, R. A., and Zak, D. R. (2016). Microbial potential for ecosystem N loss is increased by experimental N deposition. *PLoS One*:11. doi: 10.3389/fmicb.2016.00259

Frey, S. D., Lee, J., Melillo, J. M., and Six, J. (2013). The temperature response of soil microbial efficiency and its feedback to climate. *Nat. Clim. Chang.* 3, 395–398. doi: 10.1038/NCLIMATE1796

Fu, Y. H., Gao, X. J., Zhu, Y. M., and Guo, D. (2021). Climate change projection over the Tibetan plateau based on a set of RCM simulations. *Adv. Clim. Chang. Res.* 12, 313–321. doi: 10.1016/j.accre.2021.01.004

Fukasawa, Y. (2018). Temperature effects on hyphal growth of wood-decay basidiomycetes isolated from *Pinus densiflora* deadwood. *Mycoscience* 59, 259–262. doi: 10.1016/j.myc.2018.02.006

Fungo, B., Lehmann, J., Kalbitz, K., Thiongo, M., Okeyo, I., Tenywa, M., et al. (2017). Aggregate size distribution in a biochar-amended tropical Ultisol under conventional hand-hoe tillage. *Soil Till. Res.* 165, 190–197. doi: 10.1016/j.still.2016.08.012

Han, X., Liu, X., Li, Z., Li, J., Yuan, Y., Li, H., et al. (2022). Characteristics of soil organic carbon fractions and stability along a chronosequence of *Cryptomeria japonica* var. sinensis plantation in the rainy area of Western China. *Forests* 13:1663. doi: 10.3390/f13101663

He, S., Du, J. Q., Wang, Y. F., Cui, L. Z., Liu, W. J., Xiao, Y. F., et al. (2024). Differences in background environment and fertilization method mediate plant response to nitrogen fertilization in alpine grasslands on the Qinghai-Tibetan plateau. *Sci. Total Environ.* 906:167272. doi: 10.1016/j.scitotenv.2023.167272

Huang, S. P., Cui, X. C., Xu, Z. H., Zhang, Z. S., and Wang, X. M. (2022). Nitrogen addition exerts a stronger effect than elevated temperature on soil available nitrogen and relation to soil microbial properties in the rhizosphere of *Camellia sinensis* L. seedlings. *Environ. Sci. Pollut. R.* 29, 35179–35192. doi: 10.1007/s11356-022-18748-4

Ibrahim, M. M., Zhang, H. X., Guo, L. M., Chen, Y. L., Heiling, M., Zhou, B. Q., et al. (2021). Biochar interaction with chemical fertilizer regulates soil organic carbon mineralization and the abundance of key C-cycling-related bacteria in rhizosphere soil. *Eur. J. Soil Biol.* 106:103350. doi: 10.1016/j.ejsobi.2021.103350

Jiang, M. H., Ni, M. Y., Zhou, J. C., Chen, Y. M., and Yang, Y. S. (2018). Effects of increasing temperature and decreasing rainfall on soil enzyme activity in young Chinese fir forest. *Chin. J. Ecol.* 37, 3210–3219. doi: 10.13292/j.1000-4890.201811.040

Li, G., Kim, S., Han, S. H., Chang, H., Du, D. L., and Son, Y. (2018). Precipitation affects soil microbial and extracellular enzymatic responses to warming. *Soil Biol. Biochem.* 120, 212–221. doi: 10.1016/j.soilbio.2018.02.014

Li, Z. Y., Qiu, X. R., Sun, Y., Liu, S. N., Hu, H. L., Xie, J. L., et al. (2021). C: N:P stoichiometry responses to 10 years of nitrogen addition differ across soil components and plant organs in a subtropical *Pleioblastus amarus* forest. *Sci. Total Environ.* 796:148925. doi: 10.1016/j.scitotenv.2021.148925

Li, D., Wu, C., and Wu, J. (2024). Nitrogen deposition does not change stochastic processes of soil microbial community assembly under climate warming in primary forest. *Ecol. Indic.* 158:111618. doi: 10.1016/j.ecolind.2024.111618

Liu, X. D., Cheng, Z. G., Yan, L. B., and Yin, Z. Y. (2009). Elevation dependency of recent and future minimum surface air temperature trends in the Tibetan plateau and its surroundings. *Glob. Planet. Chang.* 68, 164–174. doi: 10.1016/j.gloplacha.2009.03.017

Liu, M. H., Gan, B. P., Li, Q., Xiao, W. F., and Song, X. Z. (2022). Effects of nitrogen and phosphorus addition on soil extracellular enzyme activity and stoichiometry in Chinese fir (*Cunninghamia lanceolata*) forests. *Front. Plant Sci.* 13:834184. doi: 10.3389/fpls.2022.834184

Liu, X. W., Li, X. L., Li, X. T., Ma, W. J., Guo, Q., Zhu, X. R., et al. (2021). Dominant plant identity determines soil extracellular enzyme activities of its entire community in a semi-arid grassland. *Appl. Soil Ecol.* 161:103872. doi: 10.1016/j.apsoil.2020.103872

Liu, H. Y., Mi, Z. R., Lin, L., Wang, Y. H., Zhang, Z. H., Zhang, F. W., et al. (2018). Shifting plant species composition in response to climate change stabilizes grassland primary production. *PNAS* 115, 4051–4056. doi: 10.1073/pnas.1700299114

Liu, S. B., Zamanian, K., Schleuss, P. M., Zarebanadkouki, M., and Kuzyakov, Y. (2018). Degradation of Tibetan grasslands: consequences for carbon and nutrient cycles. *Agric. Ecosyst. Environ.* 252, 93–104. doi: 10.1016/j.agee.2017.10.011

Liu, F., Zhang, Y., and Luo, J. (2018). The effects of experimental warming and CO_2 concentration doubling on soil organic carbon fractions of a montane coniferous forest on the eastern Qinghai-Tibetan plateau. *Eur. J. For. Res.* 137, 211–221. doi: 10.1007/s10342-018-1100-9

Liu, W. X., Zhang, Z., and Wan, S. Q. (2009). Predominant role of water in regulating soil and microbial respiration and their responses to climate change in a semiarid grassland. *Glob. Chang. Biol.* 15, 184–195. doi: 10.1111/j.1365-2486.2008.01728.x

Lu, M., Zhou, X. H., Luo, Y. Q., Yang, Y. H., Fang, C. M., Chen, J. K., et al. (2011). Minor stimulation of soil carbon storage by nitrogen addition: a meta-analysis. *Agric. Ecosyst. Environ.* 140, 234–244. doi: 10.1016/j.agee.2010.12.010

Luo, R. Y., Fan, J. L., Wang, W. J., Luo, J. F., Kuzyakov, Y., He, J. S., et al. (2019). Nitrogen and phosphorus enrichment accelerates soil organic carbon loss in alpine grassland on the Qinghai-Tibetan plateau. *Sci. Total Environ.* 650, 303–312. doi: 10.1016/j.scitotenv.2018.09.038

Luo, R. Y., Luo, J. F., Fan, J. L., Liu, D. Y., He, J. S., Perveen, N., et al. (2020). Responses of soil microbial communities and functions associated with organic carbon mineralization to nitrogen addition in a Tibetan grassland. *Pedosphere* 30, 214–225. doi: 10.1016/S1002-0160(19)60832-5

Ma, W. J., Li, J., Gao, Y., Xing, F., Sun, S. N., Zhang, T., et al. (2020). Responses of soil extracellular enzyme activities and microbial community properties to interaction between nitrogen addition and increased precipitation in a semi-arid grassland ecosystem. *Sci. Total Environ.* 703:134691. doi: 10.1016/j.scitotenv.2019.134691

Ma, R. Y., Yu, K., Xiao, S. Q., Liu, S. W., Ciais, P., and Zou, J. W. (2022). Data-driven estimates of fertilizer-induced soil NH_3, NO and N_2O emissions from croplands in China and their climate change impacts. *GCB Bioenergy* 28, 1008–1022. doi: 10.1111/gcb.15975

Margalef, O., Sardans, J., Maspons, J., Molowny-Horas, R., Fernández-Martínez, M., Janssens, I. A., et al. (2021). The effect of global change on soil phosphatase activity. *Glob. Chang. Biol.* 27, 5989–6003. doi: 10.1111/gcb.15832

Mitchell, P. J., Simpson, A. J., Soong, R., and Simpson, M. J. (2015). Shifts in microbial community and water-extractable organic matter composition with biochar amendment in a temperate forest soil. *Soil Biol. Biochem.* 81, 244–254. doi: 10.1016/j.soilbio.2014.11.017

Mooshammer, M., Wanek, W., Zechmeister-Boltenstern, S., and Richter, A. (2014). Stoichiometric imbalances between terrestrial decomposer communities and their resources: mechanisms and implications of microbial adaptations to their resources. *Front. Microbiol.* 5:22. doi: 10.3389/fmicb.2014.00022

Morrison, E. W., Pringle, A., van Diepen, L. T. A., Grandy, A. S., Melillo, J. M., and Frey, S. D. (2019). Warming alters fungal communities and litter chemistry with implications for soil carbon stocks. *Soil Biol. Biochem.* 132, 120–130. doi: 10.1016/j.soilbio.2019.02.005

Nannipieri, P., Trasar-Cepeda, C., and Dick, R. P. (2018). Soil enzyme activity: a brief history and biochemistry as a basis for appropriate interpretations and meta-analysis. *Biol. Fert. Soils* 54, 11–19. doi: 10.1007/s00374-017-1245-6

Nottingham, A. T., Meir, P., Velasquez, E., and Turner, B. L. (2020). Soil carbon loss by experimental warming in a tropical forest. *Nature* 584:234. doi: 10.1038/s41586-020-2566-4

Pang, Z., Jiang, L. L., Wang, S. P., Xu, X. L., Rui, Y. C., Zhang, Z. H., et al. (2019). Differential response to warming of the uptake of nitrogen by plant species in non-degraded and degraded alpine grasslands. *J. Soils Sediments* 19, 2212–2221. doi: 10.1007/s11368-019-02255-0

Peng, Y. F., Li, F., Zhou, G. Y., Fang, K., Zhang, D. Y., Li, C. B., et al. (2017). Nonlinear response of soil respiration to increasing nitrogen additions in a Tibetan alpine steppe. *Environ. Res. Lett.* 12:024018. doi: 10.1088/1748-9326/aa5ba6

Peng, X. Q., and Wang, W. (2016). Stoichiometry of soil extracellular enzyme activity along a climatic transect in temperate grasslands of northern China. *Soil Biol. Biochem.* 98, 74–84. doi: 10.1016/j.soilbio.2016.04.008

Pold, G., Grandy, A. S., Melillo, J. M., and DeAngelis, K. M. (2017). Changes in substrate availability drive carbon cycle response to chronic warming. *Soil Biol. Biochem.* 110, 68–78. doi: 10.1016/j.soilbio.2017.03.002

Qu, W. D., Han, G. X., Eller, F., Xie, B. H., Wang, J., Wu, H. T., et al. (2020). Nitrogen input in different chemical forms and levels stimulates soil organic carbon decomposition in a coastal wetland. *Catena* 194:104672. doi: 10.1016/j.catena.2020.104672

Sardans, J., Bartrons, M., Margalef, O., Gargallo-Garriga, A., Janssens, I. A., Ciais, P., et al. (2017). Plant invasion is associated with higher plant- soil nutrient concentrations in nutrient-poor environments. *Glob. Chang. Biol.* 23, 1282–1291. doi: 10.1111/gcb.13384

Souza, R. C., Solly, E. F., Dawes, M. A., Graf, F., Hagedorn, F., Egli, S., et al. (2017). Responses of soil extracellular enzyme activities to experimental warming and CO_2

enrichment at the alpine treeline. *Plant Soil* 416, 527–537. doi: 10.1007/s11104-017-3235-8

Stark, S., Ylänne, H., and Tolvanen, A. T. (2018). Long-term warming alters soil and enzymatic N:P stoichiometry in subarctic tundra. *Soil Biol. Biochem.* 124, 184–188. doi: 10.1016/j.soilbio.2018.06.016

Steinweg, J. M., Dukes, J. S., Paul, E. A., and Wallenstein, M. D. (2013). Microbial responses to multi-factor climate change: effects on soil enzymes. *Front. Microbiol.* 4:146. doi: 10.3389/fmicb.2013.00146

Su, J. S., Zhao, Y. J., Xu, F. W., and Bai, Y. F. (2022). Multiple global changes drive grassland productivity and stability: a meta-analysis. *J. Ecol.* 110, 2850–2869. doi: 10.1111/1365-2745.13983

Sun, Y., Gu, B. J., van Grinsven, H. J. M., Reis, S., Lam, S. K., Zhang, X. Y., et al. (2021). The warming climate aggravates atmospheric nitrogen pollution in Australia. *Research* 2021:9804583. doi: 10.34133/2021/9804583

Tamura, M., and Tharayil, N. (2014). Plant litter chemistry and microbial priming regulate the accrual, composition and stability of soil carbon in invaded ecosystems. *New Phytol.* 203, 110–124. doi: 10.1111/nph.12795

Tian, J., Zong, N., Hartley, I. P., He, N. P., Zhang, J. J., Powlson, D., et al. (2021). Microbial metabolic response to winter warming stabilizes soil carbon. *Glob. Chang. Biol.* 27, 2011–2028. doi: 10.1111/gcb.15538

Trivedi, P., Delgado-Baquerizo, M., Trivedi, C., Hu, H. W., Anderson, I. C., Jeffries, T. C., et al. (2016). Microbial regulation of the soil carbon cycle: evidence from gene-enzyme relationships. *ISME J.* 10, 2593–2604. doi: 10.1038/ismej.2016.65

Van Der Heijden, M. G. A., Bardgett, R. D., and Van Straalen, N. M. (2008). The unseen majority: soil microbes as drivers of plant diversity and productivity in terrestrial ecosystems. *Ecol. Lett.* 11, 296–310. doi: 10.1111/j.1461-0248.2007.01139.x

Wang, X. D., Feng, J. G., Ao, G. K. L., Qin, W. K., Han, M. G., Shen, Y. W., et al. (2023). Globally nitrogen addition alters soil microbial community structure, but has minor effects on soil microbial diversity and richness. *Soil Biol. Biochem.* 179:108982. doi: 10.1016/j.soilbio.2023.108982

Wang, H., Liu, S., Schindlbacher, A., Wang, J. X., Yang, Y. J., Song, Z. C., et al. (2019). Experimental warming reduced topsoil carbon content and increased soil bacterial diversity in a subtropical planted forest. *Soil Biol. Biochem.* 133, 155–164. doi: 10.1016/j.soilbio.2019.03.004

Wang, H. Y., Wu, J. Q., Li, G., Yan, L. J., Wei, X. X., and Ma, W. W. (2022). Effects of simulated nitrogen deposition on soil active carbon fractions in a wet meadow in the Qinghai-Tibet plateau. *J. Soil. Sci. Plant Nutr.* 22, 2943–2954. doi: 10.1007/s42729-022-00858-0

Xia, M. X., Talhelm, A. F., and Pregitzer, K. S. (2017). Chronic nitrogen deposition influences the chemical dynamics of leaf litter and fine roots during decomposition. *Soil Biol. Biochem.* 112, 24–34. doi: 10.1016/j.soilbio.2017.04.011

Xiao, W., Chen, X., Jing, X., and Zhu, B. A. (2018). A meta-analysis of soil extracellular enzyme activities in response to global change. *Soil Biol. Biochem.* 123, 21–32. doi: 10.1016/j.soilbio.2018.05.001

Xiao, J. N., Dong, S. K., Zhao, Z. Z., Han, Y. H., Li, S., Shen, H., et al. (2021). Stabilization of soil organic carbon in the alpine meadow is dependent on the nitrogen deposition level on the Qinghai-Tibetan plateau. *Ecol. Eng.* 170:106348. doi: 10.1016/j.ecoleng.2021.106348

Xiao, D., Liu, X., Yang, R., Tan, Y. J., Zhang, W., He, X. Y., et al. (2020). Nitrogen fertilizer and *Amorpha fruticosa* leguminous shrub diversely affect the diazotroph communities in an artificial forage grassland. *Sci. Total Environ.* 711:134967. doi: 10.1016/j.scitotenv.2019.134967

Xie, L., Zhang, Q. J., Cao, J. L., Liu, X. F., Xiong, D. C., Kong, Q., et al. (2019). Effects of warming and nitrogen addition on the soil bacterial Community in a Subtropical Chinese fir Plantation. *Forests* 10:861. doi: 10.3390/f10100861

Xu, H. W., Qu, Q., Li, G. W., Liu, G. B., Geissen, V., Ritsema, C. J., et al. (2022). Impact of nitrogen addition on plant-soil-enzyme C-N-P stoichiometry and microbial nutrient limitation. *Soil Biol. Biochem.* 170:108714. doi: 10.1016/j.soilbio.2022.108714

Xu, M., Xu, L. J., Fang, H. J., Cheng, S. L., Yu, G. X., Yang, Y., et al. (2020). Alteration in enzymatic stoichiometry controls the response of soil organic carbon dynamic to nitrogen and water addition in temperate cultivated grassland. *Eur. J. Soil Biol.* 101:103248. doi: 10.1016/j.ejsobi.2020.103248

Yang, Y., Fang, H. J., Cheng, S. L., Xu, L. J., Lu, M. Z., Guo, Y. F., et al. (2022). Soil enzyme activity regulates the response of soil C fluxes to N fertilization in a temperate cultivated grassland. *Atmos.*:13. doi: 10.3390/atmos13050777

Yang, H. J., Li, Y., Wu, M. Y., Zhang, Z., Li, L. H., and Wan, S. Q. (2011). Plant community responses to nitrogen addition and increased precipitation: the importance of water availability and species traits. *Glob. Chang. Biol.* 17, 2936–2944. doi: 10.1111/j.1365-2486.2011.02423.x

Yang, Y., Li, H., Zhang, L., Zhu, J., He, H., Wei, Y., et al. (2016). Characteristics of soil water percolation and dissolved organic carbon leaching and their response to long-term fencing in an alpine meadow on the Tibetan plateau. *Environ. Earth Sci.* 75:1471. doi: 10.1007/s12665-016-6178-0

Yu, Y., Zhou, Y., Janssens, I. A., Deng, Y., He, X. J., Liu, L. L., et al. (2024). Divergent rhizosphere and non-rhizosphere soil microbial structure and function in long-term warmed steppe due to altered root exudation. *GCB Bioenergy* 30:e17111. doi: 10.1111/gcb.17111

Zhan, D. Y., Peng, Y. F., Li, F., Yang, G. B., Wang, J., Yu, J. C., et al. (2019). Trait identity and functional diversity co-drive response of ecosystem productivity to nitrogen enrichment. *J. Ecol.* 107, 2402–2414. doi: 10.1111/1365-2745.13184

Zheng, H. F., Liu, Y., Chen, Y. M., Zhang, J., Li, H. J., Wang, L. F., et al. (2020). Short-term warming shifts microbial nutrient limitation without changing the bacterial community structure in an alpine timberline of the eastern Tibetan plateau. *Geoderma* 360:113985. doi: 10.1016/j.geoderma.2019.113985

Zhong, X. L., Li, J. T., Li, X. J., Ye, Y. C., Liu, S. S., Hallett, P. D., et al. (2017). Physical protection by soil aggregates stabilizes soil organic carbon under simulated N deposition in a subtropical forest of China. *Geoderma* 285, 323–332. doi: 10.1016/j.geoderma.2016.09.026

Zhong, Y. Q. W., Yan, W. M., and Shangguan, Z. P. (2015). Soil carbon and nitrogen fractions in the soil profile and their response to long-term nitrogen fertilization in a wheat field. *Catena* 135, 38–46. doi: 10.1016/j.catena.2015.06.018

Zhou, X. Q., Chen, C. R., Wang, Y. F., Xu, Z. H., Han, H. Y., Li, L. H., et al. (2013). Warming andincreased precipitation have differential effects on soil extracellular enzyme activities in a temperate grassland. *Sci. Total Environ.* 444, 552–558. doi: 10.1016/j.scitotenv.2012.12.023

frontiers | Frontiers in Microbiology

TYPE Original Research
PUBLISHED 31 May 2024
DOI 10.3389/fmicb.2024.1394179

OPEN ACCESS

EDITED BY
Peng Shi,
Xi'an University of Technology, China

REVIEWED BY
Shankar Ganapathi Shanmugam,
Mississippi State University, United States
Baoku Shi,
Northeast Normal University, China

*CORRESPONDENCE
Gen-lin Wang
✉ wanggenlin2005@163.com
Yan Duan
✉ duanyan@iim.ac.cn

RECEIVED 01 March 2024
ACCEPTED 13 May 2024
PUBLISHED 31 May 2024

CITATION
Li Y-m, Wang Y-m, Qiu G-w, Yu H-j, Liu F-m, Wang G-l and Duan Y (2024) Conservation tillage facilitates the accumulation of soil organic carbon fractions by affecting the microbial community in an eolian sandy soil. *Front. Microbiol.* 15:1394179. doi: 10.3389/fmicb.2024.1394179

Conservation tillage facilitates the accumulation of soil organic carbon fractions by affecting the microbial community in an eolian sandy soil

Yu-mei Li[1], Yu-ming Wang[2,3], Guang-wei Qiu[4], Hong-jiu Yu[1], Feng-man Liu[1], Gen-lin Wang[1]*and Yan Duan[2]*

[1]Heilongjiang Black Soil Conservation and Utilization Research Institute, Harbin, China, [2]The Centre for Ion Beam Bioengineering Green Agriculture, Hefei Institutes of Physical Science, Chinese Academy of Sciences, Hefei, China, [3]Science Island Branch, Graduate School of USTC, Hefei, China, [4]Keshan Branch of Heilongjiang Academy of Agricultural Sciences, Qiqihar, China

Conservation tillage (CT) is an important agronomic measure that facilitates soil organic carbon (SOC) accumulation by reducing soil disturbance and plant residue mulching, thus increasing crop yields, improving soil fertility and achieving C neutrality. However, our understanding of the microbial mechanism underlying SOC fraction accumulation under different tillage practices is still lacking. Here, a 6-year *in situ* field experiment was carried out to explore the effects of CT and traditional tillage (CK) practices on SOC fractions in an eolian sandy soil. Compared with CK, CT increased the particulate OC (POC) content in the 0–30 cm soil layer and the mineral-associated OC (MAOC) content in the 0–20 cm soil layer. Moreover, tillage type and soil depth had significant influences on the bacterial, fungal and protistan community compositions and structures. The co-occurrence network was divided into 4 ecological modules, and module 1 exhibited significant correlations with the POC and MOC contents. After determining their topological roles, we identified the keystone taxa in the network. The results indicated that the most common bacterial taxa may result in SOC loss due to low C use efficiency, while specific fungal (Cephalotrichum) and protistan (Cercozoa) species could facilitate SOC fraction accumulation by promoting macroaggregate formation and predation. Therefore, the increase in keystone fungi and protists, as well as the reduction in bacteria, drove module 1 community function, which in turn promoted SOC sequestration under CT. These results strengthen our understanding of microbial functions in the accrual of SOC fractions, which contributes to the development of conservation agriculture on the Northeast China Plain.

KEYWORDS

conservation tillage, particulate organic carbon, mineral-associated organic carbon, microbial community, soil depth

1 Introduction

Soils are the largest carbon (C) pool in the global terrestrial system and contain more than 2,500 Gt of C (Banerjee et al., 2016). Global soil organic carbon (SOC) dynamics immensely influence soil productivity, greenhouse gas emissions and C neutrality (Tang et al., 2019; Duan et al., 2023). In agroecosystems, tillage practices are regarded as crucial agronomic regimes

that mediate SOC sequestration and depletion processes (Topa et al., 2021). Traditional agricultural practices involve frequent tillage to accomplish achieve high crop productivity (Zhang et al., 2019). However, high-intensity tillage not only decreases crop productivity but also leads to reduced soil fertility and sustainability and results in the loss of other agroecosystem services, causing soil erosion, water shortages or biodiversity decline (Raus et al., 2016). Hence, abundant attempts have been made to transition from traditional tillage to conservation tillage (CT) to increase the soil C stock of agroecosystems in recent years. In particular, CT practices, such as no-tillage or reduced-tillage, may minimize the degree and frequency of tillage passes and maintain an adequate soil surface covered with residues to reduce soil physical disturbance and increase the soil C sink capacity (Pearsons et al., 2023). Nevertheless, contrasting tillage practices cause changes in resource availability in the topsoil and subsoil, which leads to differences in SOC formation (Angers and Eriksen-Hamel, 2008). Therefore, elucidating the SOC sequestration mechanisms that occur under different tillage practices and at different soil depths is crucial for maintaining soil health and facilitating agroecosystem services.

Overall, the input of exogenous organic materials (i.e., manure and crop residues) is an essential prerequisite for SOC accumulation (Lehmann and Kleber, 2015). Many expert researchers have confirmed that the mechanisms underlying SOC accumulation are commonly attributed to physical protection by aggregates and chemical stabilization by soil minerals (Six et al., 2004). Correspondingly, semidecomposed exogenous large organic biopolymers are readily encapsulated by aggregates and form particulate organic carbon (POC); as biopolymers further decompose, the C monomers tend to be adsorbed by mineral surfaces and become mineral-associated organic carbon (MAOC) (Bastian et al., 2009; Herath et al., 2014). There is nearly a consensus regarding the disruption of topsoil aggregates due to frequent tillage, which leads to the loss of POC (Hewins et al., 2017). These conclusions also reflect the potential of using CT to increase SOC sequestration in agroecosystems. Several previous studies also suggested that traditional tillage practices involving straw return can transport crop residues to the subsoil, thus contributing to the accumulation of SOC in the subsoil to some extent (Zhang et al., 2013). This contradiction also illustrates the complexity of enhancing soil fertility through tillage practices. Achankeng and Cornelis (2023) found that climate, soil texture, rotation pattern, and crop type are all crucial factors to be considered under different tillage treatments in a meta-analysis, which increases the challenge for researchers in optimizing tillage practices. Therefore, to date, we still lack a comprehensive understanding of the direct associations between tillage practices and SOC fractions.

Soil microorganisms play an important role in SOC formation (Cotrufo et al., 2013; Sarker et al., 2018). Generally, when plant residues are applied, soil animal- and meso-fauna-driven fragmentation constitute the first stage of straw degradation (Gessner et al., 2010). Subsequently, bacteria and fungi successively regulate further degradation processes due to changes in C and N availability in the substrate (Wang et al., 2021). In the early stage of decomposition, adequate amounts of labile straw C and nitrogen can sustain bacterial proliferation (Huang et al., 2017). With continuous plant decomposition, the microbial community synchronously undergoes succession. Fungi may be the dominant decomposers due to their potent ability to utilize recalcitrant straw components (Clemmensen et al., 2015). Therefore, many scholars consider the ratio of bacteria to fungi to be an important indicator of the straw decomposition process (Li J. W. et al., 2020; Zhao et al., 2021). Moreover, microbial diversity and module community was the key drivers of SOC turnover. Previous study found that bacterial, fungal protistan richness was significantly correlated with carbon use efficiency, microbial biomass carbon, microbial respiration and growth rate, which changed the SOC turnover process (Ma et al., 2024). Soil microbial module community also played an important role in influencing SOC. Numerous studies have demonstrated that the core microbial module community was involved in maintaining the stability of soil microbial function, promoting soil nutrient cycling and SOC accumulation; while the keystone species were the core to achieve them (Shi et al., 2020; Jiao et al., 2022). Therefore, keystone taxa-driven the changes of microbial module communities and diversity are pivotal factors leading to SOC turnover. In particular, soil bacterial and fungal communities are extremely sensitive to tillage practices. Li Y. et al. (2020) reported that, compared with traditional tillage, minimum tillage increases fungal biomass and bacterial diversity, which may further influence residue decomposition. However, as major members of the soil microbiome, protists drive plant residue decomposition, and microbial community regulation has rarely been included in microbiome analyses associated with SOC fraction turnover (Geisen and Bonkowski, 2018). Specific protozoan taxa participate in aggregate formation and SOC turnover. According to the report of Pellegrino et al. (2021), CT increased the abundance of Alveolata and Cercozoa, which contributed to SOC accumulation by reshaping soil aggregates. Additionally, the top-down control of protists in the soil microfood web demonstrated great potential for influencing SOC turnover (Gao et al., 2019). Therefore, a thorough empirical understanding of the microbial roles (including bacterial, fungal and protist roles) in SOC fraction sequestration under different tillage practices has not been achieved.

To bridge these gaps, eolian sandy soil located in the Northeast Plain, the largest grain-producing area in China, was selected as the research object. In recent years, the Northeast Plain has been facing continuous depletion of SOC stocks since the 1980s, when straw return was widely implemented (Wang et al., 2018). Therefore, we conducted a 5-year *in situ* field experiment to reveal the effect of tillage practices on the microbial community, SOC fraction and maize yield at different soil depths. The soil samples were collected from the 0–50 cm soil profile under CT and traditional tillage practices. In this study, we determined the SOC fraction content and microbial community and attempted to explain the potential relationships between them. We hypothesized that (1) the SOC fraction content and microbial traits exhibit distinct responses to traditional and CT practices at different depths and that (2) specific microbial taxa may be involved in the turnover of SOC fractions.

2 Materials and methods

2.1 Experimental site

The experimental field was located in Dulbert Mongolian Autonomous County (46°54′N, 124°26′E), Daqing city, Heilongjiang Province, which has a semiarid monsoon continental climate. The mean annual precipitation and temperature are 400 mm and 5.6°C, respectively. According to the USDA soil taxonomy, the soils in the area are carbonate meadow soils. The basic nutrient contents of the soil before the experiment were as follows: 0.53 g kg^{-1} total nitrogen; 60.95 mg kg^{-1} alkali-hydrolyzable nitrogen; 60.22 mg kg^{-1} available phosphorus;

44.51 mg kg^{-1} available potassium; and 9.52 g kg^{-1} SOC with a pH of 5.56. The cropping system used was single spring maize (*Zea mays* L.).

2.2 Field trial design and soil sampling

The experimental trial was set up in 2017 in accordance with a randomized complete block design with three replicates. Each field plot was covering an area of 64 m^2 (4 m × 16 m). Before the experiment, all the plots were treated with N-P-K fertilizers, and straw was removed via shallow tillage to 25 cm. Traditional tillage (CK): the plots were plowed with large machinery, and a five-share turning plow tilled the soil to 25 cm after harvest at October (amount of maize stover return about 7,200 kg ha^{-1}); and CT: no-tillage with 100% straw mulch after harvest at October (amount of maize stover mulch about 7,600 kg ha^{-1}). A straw crusher was used to crush the straw into fragments with lengths less than 10 cm before mulching. Except for the field surface drilling of maize in October, the no-tillage plots remained undisturbed, and maize straw was evenly distributed over the field surface after harvest every year. Chemical fertilizers were applied in May, and the N-P_2O_5-K_2O application rates ranged from 180–115–75 kg hm^{-2}. All the other normal management practices were consistent between the treatments during the experiment.

Soil profiles were excavated at a depth of 50 cm in October 2022 in each replicate plot. Soil samples were collected at depths of 0–10, 10–20, 20–30, 30–40, and 40–50 cm. Three soil samples were collected from each plot. The three soil samples were placed into the same sterile plastic bag and mixed to create one composite sample. All the samples were immediately transported to the laboratory in an incubator with ice packs. Each soil sample was divided into two parts: one part was stored at −80°C for DNA extraction, and the remaining part was air-dried for use in the additional chemical analyses. The basic chemical properties of the soils under different tillage practices and at different depths in 2022 are shown in Supplementary Figure S1.

2.3 Basic soil properties, SOC fractionation, and soil aggregate isolation

The basic chemical properties of the soil were measured using the method described by Lu (2000). The soil pH was measured at a 1:2.5 soil: water ratio for 30 min. The SOC concentration was determined using $K_2Cr_2O_7$ digestion, and total nitrogen was determined by the Kjeldahl method. Available phosphorus and potassium were determined using molybdenum blue colorimetric and flame photometry methods, respectively.

SOC fractionation was determined using a method described by Yu et al. (2017). First, the SOC was further fractionated into POC and MAOC. Generally, 5.0 g (dry weight) of soil was dispersed by adding 30 mL of 0.5% sodium hexametaphosphate solution and centrifuging at 200 r min^{-1} for 18 h. Thereafter, the POC and MAOC fractions were obtained by passing the samples through 53-μm filters. All the fractions were dried (50°C), and POC and MAOC were measured using $K_2Cr_2O_7$ digestion.

The wet sieving method was used to separate the water-stable aggregates (Six et al., 2002). First, the soil samples were gently broken apart into small pieces along natural break points, and the fragmented samples were subsequently placed on top of a 0.25-mm sieve and soaked in deionized water for 5 min. The samples were subsequently separated at an amplitude of 3 cm and a frequency of 30 cycles per min for a duration of 2 min by a wet-sieving apparatus. Afterward, the aggregate subsamples above each sieve were obtained as follows: macroaggregates (>0.25 mm), microaggregates (0.053–0.25 mm), and silt and clay fractions (<0.053 mm). After wet sieving, all the aggregates were immediately oven-dried at 60°C and weighed.

The mean weight diameter (MWD) was used to describe the aggregate stability and was calculated by the following formula:

$$MWD = \sum Xi * Wi$$

where Xi represents the average diameter of each aggregate size and Wi represents the proportion of each aggregate weight relative to the total sample weight after wet sieving. The upper limit of the macroaggregate diameter was 2 mm.

2.4 DNA extraction and 16S, ITS and 18S amplification and sequencing

Total DNA was extracted from 0.5 g of soil using a Fast DNA Spin Kit for Soil (MP Biomedicals, CA, United States) in accordance with the manufacturer's instructions. Each treatment contained three replicates. The extracted DNA samples were stored at −80°C for molecular analysis.

High-throughput sequencing was performed using the Illumina MiSeq sequencing platform (Illumina, Inc.). Both the forward and reverse primers were tagged with adapter and linker sequences, and 8-bp barcode oligonucleotides were added to distinguish the amplicons derived from different soil samples.

The primers *515F (5′-GTGCCAGCMGCCGCGGTAA-3′)* and *907R (5′-CCGTCAATTCMTTTRAGTTT-3′)* were chosen to amplify the 16S rRNA genes in the V4–V5 hypervariable region. PCR was conducted in a 50-μL reaction mixture containing 27 μL of ddH_2O, 2 μL (5 μM) of each forward/reverse primer, 2.5 μL (10 ng) of template DNA, 5 μL (2.5 mM) of deoxynucleoside triphosphates, 10 μL of 5× Fastpfu buffer, 0.5 μL of bovine serum albumin, and 1 μL of TransStart Fastpfu polymerase (TransGen, Beijing, China). The PCR procedure was 94°C for 5 min; 30 cycles of 94°C for 30 s, 52°C for 30 s and 72°C for 30 s, followed by 72°C for 10 min (Biddle et al., 2008).

The fungal ITS1 region was amplified using the primer pair *ITS1F (CTTGGTCATTTAGAGGAAGTAA)/ITS2 (GCTGCGTTCTTCATCGATGC)*. The 50-μL reaction mixture contained 1 μL (30 ng) of DNA, 4 μL (1 μM) each of forward/reverse primer, 25 μL of PCR Master Mix, and 16 μL of ddH_2O. PCR amplification was conducted at 98°C for 3 min, followed by 30 cycles of 98°C for 45 s, 55°C for 45 s, and 72°C for 45 s, with a final extension at 72°C for 7 min (Ghannoum et al., 2010).

The eukaryotic V4 region was amplified using the primer pair V4_1f *(CCAGCASCYGCGGTAATWCC)/TAReukREV3 (ACTTTCG TTCTTGATYRA)*. PCR was performed in a 20 μL volume consisting of 4 μL of 5× reaction buffer, 2 μL of dNTPs (2.5 mM), 0.8 μL of each primer (10 μM), 0.4 μL of FastPfu Polymerase, 10 ng of DNA template, and ddH_2O to reach the final volume. PCR amplification was conducted at 95°C for 5 min, followed by 30 cycles of 95°C for 30 s, 55°C for 30 s, and 72°C for 45 s, with a final extension at 72°C for 10 min. To construct the protistan amplicon sequence variant (ASV)

table, we removed sequences belonging to Rhodophyta, Streptophyta, Metazoa, and Fungi (Stoeck et al., 2010).

Raw Illumina amplicon reads were processed using the QIIME2 Core 2019.7 distribution. The Divisive Amplicon Denoising Algorithm (DADA2) pipeline implemented in the QIIME 2 platform was used to conduct sequence quality control, which included quality filtering reads, denoising reads, merging forward and reverse reads, removing chimeric reads, and assigning reads to ASVs. The Silva 138 Bacterial 16S rRNA gene database, the UNITE Fungal ITS database, and the Protist Ribosomal Reference (PR2) database v4.14.0 were used to classify the representative sequences of ASVs (Ghannoum et al., 2010). All singletons and nonfungal ASVs were removed, and each sample was rarefied to 30,000, 36,000, and 44,000 sequences for the bacterial, fungal and eukaryotic diversity analysis. The alpha diversity and Bray–Curtis distances for principal coordinate analysis of the soil microbial community were calculated after all the samples were rarefied to the same sequencing depth.

2.5 Statistical analysis

Crop yield and soil biochemical and other relevant properties under different tillage practices were subjected to the chi-square test for independence of variance. Significant differences were determined by one-way analysis of variance (ANOVA) based on the *post hoc* Tukey test at the 5% level. Prior to ANOVA, the normality and homogeneity of variance were tested by the Kolmogorov–Smirnov test and Levene's test, respectively. If normality was not met, log or square-root transformation was carried out. One-way ANOVA was performed using SPSS 21.0 (SPSS, Inc., Chicago, IL, United States).

Principal component analysis (PCA) was used to determine and evaluate the changes in the community structure of the soil microbiome via the R (ver 4.2.3) package "vegan." To characterize the patterns of soil microbial interactions, we constructed a co-occurrence network with the "igraph" and "WGCNA" R packages. We constructed microbial networks using bacteria, fungi and protists with relative abundances greater than 0.01%; screened nodes with Pearson's correlations greater than 0.6 and $p < 0.05$; performed modular analysis based on the connectivity between nodes; visualized the network using Gephi (ver. 0.9.2); and calculated information on network topological features. The within-cluster connectivity (*Zi*) and among-cluster connectivity (*Pi*) of different clusters were calculated using the R packages "reshape2," "igraph," "ggrepel," "dplyr," and "Rcpp" and filtered for peripherals ($Zi \leq 2.5$, $Pi \leq 0.62$), connectors ($Zi \leq 2.5$, $Pi > 0.62$), cluster hubs ($Zi > 2.5$, $Pi \leq 0.62$), and network hubs ($Zi > 2.5$, $Pi > 0.62$) (Deng et al., 2012). ASVs in module hubs, connectors and network hubs may be regarded as the microbial keystone taxa of network systems (Deng et al., 2012). An interactive platform "Gephi" (default parameters set) was used to identify the modules (ecological clusters) of soil taxa strongly interacting with each other.

Linear regressions between SOC fractions and the microbial community modules were conducted to determine the relationships between microbial communities and SOC fraction contents using Origin 2018. The microbial module community variation data were quantified by the PCA 1 axis. Heatmaps were constructed to reveal the potential associations between keystone taxa richness and SOC fraction content via the "heatmap.2" function in the R package "ggplots."

3 Results

3.1 Crop yields, aggregate size distributions, and SOC fractions

Overall, CT had a positive effect on crop yield and SOC fraction content. After 5 consecutive years of different tillage practices, the maize yield, aggregate stability and SOC fraction content changed significantly (Supplementary Figures S2, S3); Figure 1). However, no significant changes were found before 2021. Compared with those in CK, the maize yields in CT significantly increased in 2021 and 2022 (Supplementary Figure S2, $p < 0.05$).

Different tillage practices changed the aggregate size distribution and stability (Supplementary Figure S3). CT significantly increased the proportion of macroaggregates at the 0–30 cm soil depth ($p < 0.05$) and decreased the proportion of microaggregates at the 0–20 cm soil depth ($p < 0.05$). However, no changes were observed in the silt and clay fractions under the different treatments. Additionally, the MWD was greater under CT than CK at 0–30 cm depth, while there were no significant changes at 40–50 cm depth.

SOC, POC, and MAOC contents were also affected by tillage practice (Figure 1). Generally, CT significantly increased the SOC, POC, and MAOC contents in the topsoil (0–20 cm layer, $p < 0.05$, except for MAOC in the 10–20 cm layer). Moreover, the POC content was significantly greater under CT than CK. No significant changes were observed in the 30–50 cm layer under the different tillage practices.

3.2 Microbial community, co-occurrence network, and keystone taxa

PCA was used to evaluate the changes in the soil microbial community under the different tillage practices (Supplementary Figures S4, S5). The results indicated that the soil communities changed significantly under the different tillage practices and at different soil depths (except for tillage practices on the protistan community). Generally, the effect of soil depth on microbial communities was observed mainly along the PCA 1 axis, while the effect of tillage practices on microbial communities was observed mainly along the PCA 2 axis.

Although soil microbial community compositions were changed after different tillage practices and depths, Proteobacteria, Acidobacteriota, Actinobacteriota, and Gemmatimonadota were the main phyla of bacteria, contributing more than 60% of the total bacterial abundance (Supplementary Figure S6A). Generally, with the increase of depth, the relative abundance of Proteobacteria decreased gradually. Ascmycota, Basidiomycota, and Mortierellomycota were the main phyla of fungi, contributing almost 80% of the total fungal abundance (Supplementary Figure S6B); while protist were composed mainly of Intramacronucleata, Cercozoa, Chlorophyta, and Apicomplexa (Supplementary Figure S6C).

A co-occurrence network was constructed to reveal the connections between specific microbial species (Figure 2). We found four dominant ecological modules (Figure 2A). Modules 1, 2, 3, and 4 contained 225, 182, 160, and 124 nodes, respectively. Among the four modules, protists and fungi accounted for the greatest proportion of microbial species in module 1, while bacteria accounted

10.3389/fmicb.2024.1394179

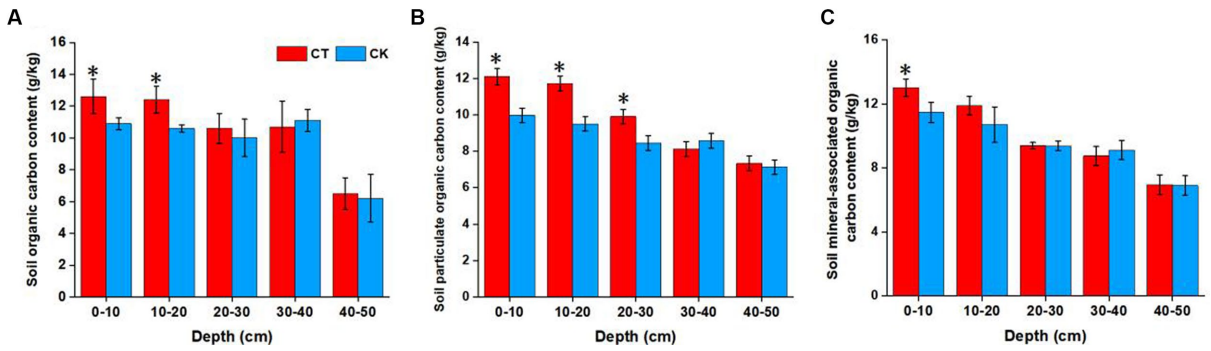

FIGURE 1
Soil organic carbon **(A)**, particulate organic carbon **(B)**, and mineral-associated organic carbon **(C)** contents at various depths under different soil tillage treatments. *$p < 0.05$; CT, conservation tillage; CK, traditional tillage.

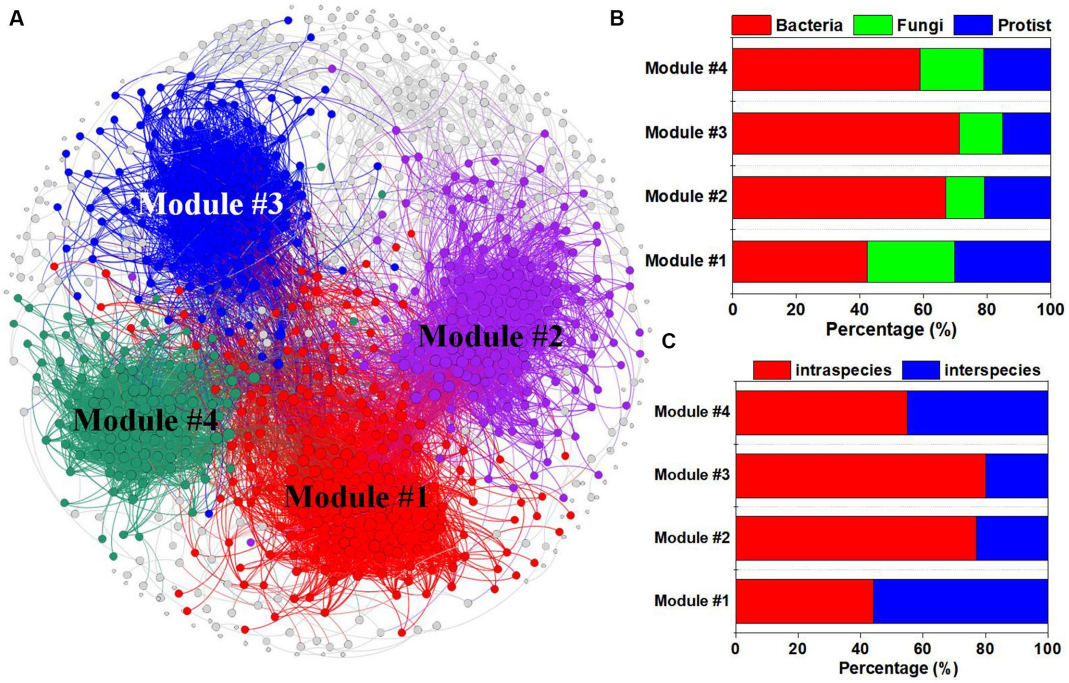

FIGURE 2
Co-occurrence network analysis of bacterial, fungal and protistan ASVs under different tillage practices and at different soil depths. **(A)** Multitrophic network including multiple ecological modules. The colors of the nodes represent different ecological modules; the percentages of bacterial, fungal and protistan ASVs **(B)**; and the intraspecies and interspecies relationships **(C)** in each module.

for the highest proportion of microbial species in module 3 (Figure 2B). Additionally, the percentage of intraspecies edges was greater in module 3 than in the other modules, while module 1 contained more interspecies edges than did the other modules (Figure 2C).

ZP plots were constructed to identify the topological roles of each node in the co-occurrence network. A total of 30 microbial taxa (including 13 bacteria, 11 fungi and 6 protists) were detected as keystone species (Figure 3). Nineteen keystone taxa belonged to module 1, and modules 2 and 3 each contained 2 keystone taxa. The information for the selected keystone taxa is displayed in Supplementary Table S1. The bacterial keystone species mainly belonged to Proteobacteria (7 taxa), the fungal keystone species mainly belonged to Ascomycota (6 taxa), and the protist keystone species mainly belonged to Cercozoa (2 taxa).

3.3 Relationships between microbial traits and SOC fractions

To determine the potential relationships between the microbial communities of specific modules and SOC fractions, we constructed

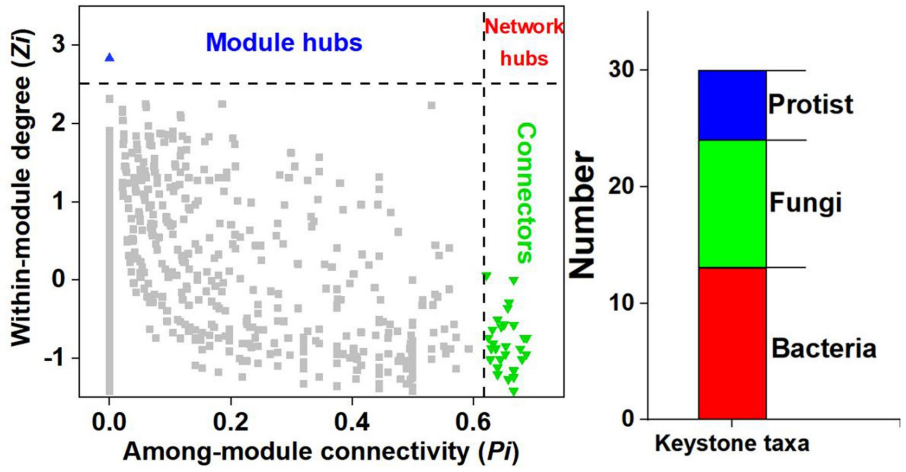

FIGURE 3
ZP plot showing the distribution of ASVs based on their module-based topological roles. The topological role of each ASV was determined according to the scatter plot of within-module connectivity (Z) and among-module connectivity (P).

correlations between the microbial community module connections and the SOC fractions. Figure 4 shows that there were significant correlations between microbial module communities and POC content ($R^2 = 0.74$ for module 1 and $R^2 = 0.68$ for module 2) and MAOC content ($R^2 = 0.51$ for module 1 and $R^2 = 0.44$ for module 2). However, no significant associations were detected between the SOC fractions and the other microbial module communities.

Heatmaps revealed close associations between the richness of keystone taxa and SOC fractions (Figure 5). Overall, the bacterial richness demonstrated significant negative correlations with the POC and MAOC contents (except for BASV 147) (Figure 5A). There were significant positive correlations between FASV945 richness and SOC fraction contents (POC and MAOC), as well as between FASV945 richness and MAOC content. FASV95 richness was negatively correlated with MAOC content (Figure 5B). Moreover, the richness of PASV45 and PASV17 was positively correlated with the POC content, and the richness of PASV45 was also positively correlated with the MAOC content (Figure 5C).

In the present study, we selected keystone species that were significantly associated with the SOC fraction content for further analysis. The richness of keystone taxa was sensitive to the different tillage practices (Supplementary Figure S7). Compared with CT, CK increased the richness of bacterial keystone taxa by 21.51–520.75%. The richness of BASV8256 decreased by 32.15% under CK compared with that under CT (Supplementary Figure S7A). Compared with CK, CT increased the richness of FASV945 and FASV95 by 58.81 and 42.81%, respectively, and decreased the richness of FASV946 by 82.61%. In addition, compared to that under CK, PASV17 and PASV45 richness increased by 97.79 and 12.97%, respectively, under CT (Supplementary Figure S7B).

4 Discussion

CT has been considered a sustainable technique for properly managing soil and hence maintaining agroecosystem services by minimizing tillage operations to effectively avoid water infiltration and erosion (Müller et al., 2009). In this study, we compared crop yields, SOC fraction contents and microbial traits under different tillage practices and investigated the relationships between SOC fractions and microbial functions. The results of this research strengthen our understanding of SOC accumulation under different tillage practices on the Northeast China Plain.

4.1 Response of SOC fractions and maize yields to different tillage practices

The effect of tillage practices on crop yields has been studied frequently; however, no consistent conclusions have been drawn. It was reported that no- or minimum-tillage practices led to a 0–30% reduction in yields in Europe, which was affected by crop type, tillage technique, soil texture and crop rotation (Alaoui et al., 2020). Another study revealed that shallow tillage (8 cm strip depth) achieved the greatest yields (Licht and Al-Kaisi, 2005). This is mainly because shallow tillage can be a neutral solution to the problem of late seed emergence due to no-tillage by reducing soil disturbance (Araya et al., 2021). Notably, based on a 17-year experiment, CT practices increased maize yields by 12.2 to 20.1% (Ren et al., 2024), which was consistent with our results (Supplementary Figure S2). This can be explained partly by the fact that the CT method is generally implemented with straw residue left on topsoil while minimizing soil disturbance, which favors soil nutrient accumulation, moisture retention and temperature increase, resulting in faster seed emergence (Licht and Al-Kaisi, 2005). In summary, although optimizing tillage practices requires consideration of factors such as crop rotation and soil texture, CT increases crop yield in maize monoculture systems in the eolian sandy soil of the Northeast China Plain.

SOC is the key to soil fertility and is sensitive to changes in tillage practices (Figure 1). Lehmann and Kleber (2015) proposed a soil continuum model indicating that the input of exogenous organic materials (such as plant residues) is a prerequisite for SOC accumulation. Thus, the finding that CT can improve topsoil OC fractions is no surprise. However, the POC and MOC contents were

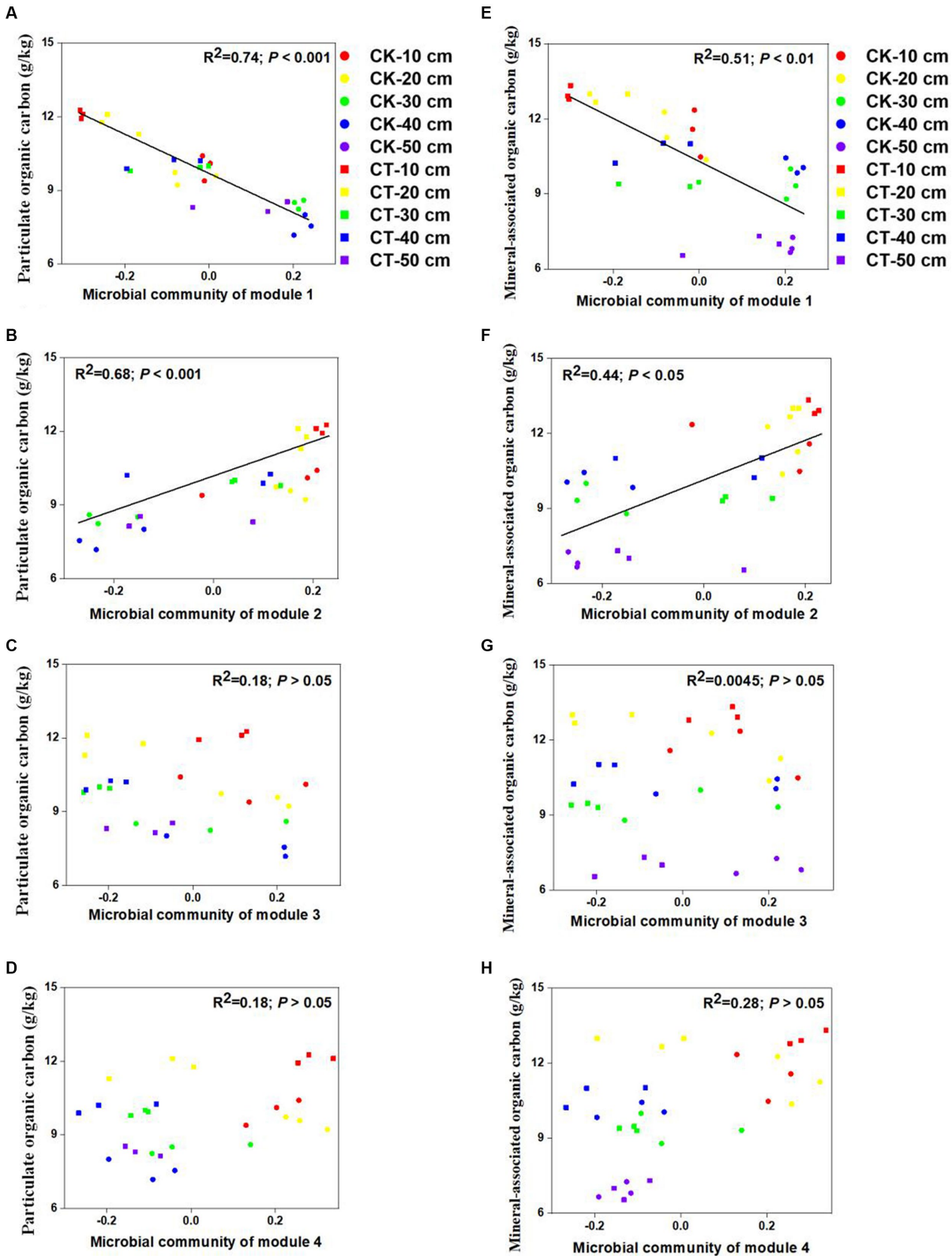

FIGURE 4
Links between the soil community of each module within the co-occurrence network and the SOC fraction content. The links between soil microbial community of module 1-4 with particulate organic carbon were sown in A-D; the links between soil microbial community of module 1-4 with mineral-associated organic carbon were sown in E-H.

not consistent. No-tillage practices improved the POC content in the 0–30 cm soil layer. Undecomposed and semidecomposed plant residues are the "core" of POC, which is encapsulated by macroaggregates (Samson et al., 2020). Therefore, the formation of macroaggregates and the accumulation of POC are generally complementary. The data on the distribution of aggregate sizes in the

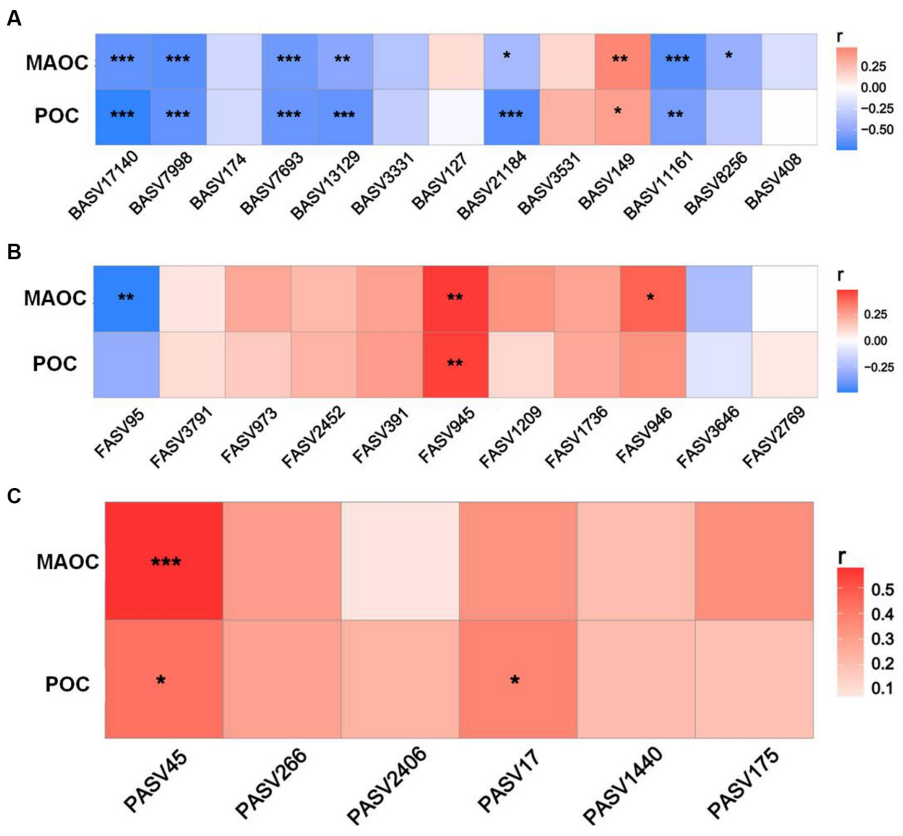

FIGURE 5
Relationships of SOC fraction contents with the richness of bacterial **(A)**, fungal **(B)**, and protistan **(C)** keystone species.

present study also validate this view (Supplementary Figure S3). An increased proportion of macroaggregates provides physical protection for POC and thus favors POC accumulation. CK practices disturb the physical structure at 0–25 cm soil depths through frequent plowing, thus destroying the formation of macroaggregate structures (Jat et al., 2019).

When the large biopolymers in the residues further decomposed, the small biopolymers and C monomers (such as root exudates and microbial necromass) can be adsorbed to the soil mineral surface and become MAOC (Lehmann and Kleber, 2015). In addition to straw return, microbial and maize biomass are important factors that cannot be ignored. As a supplementary exogenous C source in the soil, straw inevitably increases MAOC content after further degradation of residues (Vogel et al., 2014). Posteriorly, CT decreases the soil structure distribution and increases the soil density, which promotes the growth of crop roots to a certain extent (Shi et al., 2012). In addition, the crop yield data imply a well-developed root system that has secreted more organic matter (Van den Putte et al., 2010). With respect to microbial biomass, minimum tillage and residue retention increase the soil microbial population size due to the adequate energy supply and appropriate stoichiometry and result in MAOC sequestration in topsoil under CT practices (Ren et al., 2024). In summary, soil microbiomes play an irreplaceable role in straw degradation and SOC turnover. Therefore, revealing the microbial mechanisms responsible for SOC fraction accumulation under different tillage practices is crucial for improving soil fertility.

4.2 Microbial keystone species-driven SOC fraction sequestration by regulating specific module community functions

CT changed the soil microbial diversity and community, which subsequently affected SOC formation and accumulation. We found that soil depth affected the soil bacterial, fungal and protistan communities much more than did tillage practice (Supplementary Figure S4). This is partly because the soil layer has the greatest influence on the changes in nutrient accessibility and availability rather than tillage practices (Kong et al., 2011). As soil depth increases, nutrient pools decrease, and mineral protection increases, leading to increased difficulty in nutrient acquisition by soil microorganisms (Modak et al., 2019). As a result, oligotrophs may become the dominant species in the community.

Microbial communities were classified into different functional modules by identifying soil taxa strongly interacting with each other (Figure 2), which can indicate important ecological processes, different niches, and habitat preferences. Each module in a network is considered a functional unit that conducts an identifiable task (Chen et al., 2019). In the present study, strong relationships were observed between the SOC fractions and the microbial community in modules 1 and 2, which indicated the potential function of SOC turnover (Figure 4). A previous study demonstrated that microbial keystone species have great explanatory power in terms of network (module) structure and function (Delgado-Baquerizo et al., 2018). Thus, it is

necessary to explore the function of keystone species within modules 1 and 2. However, more than two-thirds of the identified keystone species belong to module 1 communities (19/30), while only two keystone species (2/30) belong to module 2 communities (Supplementary Table S1). Therefore, it is more meaningful to study the function of keystone species-driven module communities on SOC turnover in module 1 community.

Microbial keystone taxa also exhibited significant correlations with SOC fractions (Figure 5). Among the bacteria, Rhizobiales_Incertae_Sedis (BASV7693) and Reyranellaceae (BASV11161) within module 1 were identified as Proteobacteria, which encompasses typical copiotrophs with low C use efficiency that leads to straw C loss (Dove et al., 2021). A previous study demonstrated that Gaiellaceae (BASV7998) richness is recognized as an indicator of the carbon-to-nitrogen ratio due to its ability to utilize labile C (Duan et al., 2021). Therefore, the increase in the above bacterial taxa indicated negative effects on straw-derived OC accumulation. Moreover, only the Sphingomonadaceae richness exhibited a positive association with the POC and MAOC contents. This was likely because Sphingomonadaceae can consume various C sources and become major exopolysaccharide contributors, which provide a source for MAOC formation (Lan et al., 2022). Compared with bacteria, fungi generally exhibit greater C use efficiency and straw decomposition ability (Clemmensen et al., 2015). The richness of Cephalotrichum (FASV945) and Herpotrichiellaceae (FASV946) in module 1 was conducive to POC and MAOC sequestration. As typical saprophytic fungi, Cephalotrichum and Herpotrichiellaceae are often considered to play roles in straw degradation, pathogen control, and crop growth promotion and are considered important indicators of soil health (Zhang et al., 2022). Zhang et al. (2023) indicated that Cephalotrichum was enriched after straw addition and promoted straw decomposition and SOC accumulation in saline-alkaline soils. Most Cephalotrichum species are known for their saprotrophic function in decomposing plant materials (Woudenberg et al., 2017), corresponding with our results that the Cephalotrichum played a dominant role in POC and MAOC sequestration. In addition, higher abundance of Cephalotrichum led to the higher fungal diversity (Wang et al., 2023). Jin et al. (2022) found that Cephalotrichum exerted significant inhibitory effects on several pathogenic bacteria. Due to these strong abilities, Cephalotrichum abundance was also considered as the biomarker of soil health. Therefore, we speculated that the increase in the abundances of Cephalotrichum can accelerate straw degradation and that the early and late products favor the formation of POC and MAOC, respectively.

In addition, protists can influence SOC accumulation through direct or indirect effects (Pellegrino et al., 2021). Our results revealed that Cercozoa (PASV45 in module 1) may be a possible participant that was significantly positively correlated with POC ($p < 0.05$) and MAOC ($p < 0.001$). Pellegrino et al. (2021) reported that CT practices increase the abundance of Cercozoa partly via several abiotic factors, such as soil moisture, clay content and N availability. As expected, Cercozoa are important consumers of straw residues, which promotes the fragmentation of straw to facilitate further decomposition and is a prerequisite for organic carbon accumulation (Gessner et al., 2010). These authors also indicated that Cercozoa was the keystone taxon in macroaggregates and was positively correlated with SOC by promoting residue decomposition (Delgado-Baquerizo et al., 2020). Moreover, Cercozoa was also thought to have been an important driving force in the formation of macroaggregates by reshaping the pore sizes in the soil (Berisso et al., 2012). Therefore, according to the theory of interaction between SOC and aggregate structure, Cercozoa-driven straw fragments can be encapsulated by aggregates and become the core of aggregate formation. The formation of aggregates provides physical protection for POC, which is conducive to POC accumulation. This conclusion is also consistent with previous reports that Cercozoa are crucial microorganisms in macroaggregate taking part to long-term sequestration and storage of SOC (Pellegrino et al., 2021). Another study indicated that Cercozoa species exhibited the highest numbers of links with bacteria and fungi through the construction of co-occurrence networks, which implied that they were potentially vital to soil food webs (microbiome predation) (Kou et al., 2020). Cercozoa are phagotrophs that may consume Acidobacteria, Proteobacteria, and Ascomycota and consequently increase microbe-derived C. Furthermore, Ma et al. (2024) confirmed that protozoa can regulate microbial carbon use efficiency and SOC formation by regulating fungal, bacterial and keystone module communities through structural equation model analysis. Among these factors, the Cercozoa-driven protozoan community was the most influential factor. Accordingly, Cercozoa mediated POC and MAOC accumulation, mainly through macroaggregate formation and microbial necromass supply.

After comparing the richness of the selected keystone species, our results showed that C-accumulating microbes were enriched under CT. Specifically, compared with CK, CT decreased the abundances of most keystone bacterial taxa and increased the abundances of specific fungal and protistan species in module 1 of the network, which promoted the sequestration of SOC fractions by straw degradation, aggregate formation and predation effects. As a consequence, soil bacteria, fungi and protistan taxa all participate in SOC turnover under different tillage practices, while the appointed keystone species-driven community of module 1 facilitated POC and MOC accumulation under CT.

5 Conclusion

In this study, we demonstrated the associations between microbial keystone taxa and SOC fractions under different tillage practices. Compared with CK, continuous 6-year CT significantly increased maize yields, aggregate stability, and POC (0–30 cm) and MAOC (0–20 cm) contents. Tillage practice and soil depth both influence bacterial, fungal and protistan communities, which might change the turnover of SOC fractions. The co-occurrence network indicated that the connectivity of module 1 was significantly related to POC and MAOC contents CT increased the richness of specific fungal (Cephalotrichum) and protistan (Cercozoa) species and thus promoted SOC fraction accumulation through straw degradation, macroaggregate formation and predation effects. The selected bacterial taxa were enriched in the CK treatment and resulted in SOC loss due to low C use efficiency. Taken together, our results revealed that stimulating the function of keystone taxa can drive the function of the module 1 community in SOC accumulation under CT practices, which is beneficial for maintaining soil fertility and productivity in eolian sandy soils on the Northeast China Plain.

Data availability statement

Raw sequencing data were deposited in the NCBI Sequence Read Archive under accession number PRJNA1111948. The data of SOC, soil nutrients content and maize yields can be found in the article/supplementary material.

Author contributions

Y-mL: Data curation, Funding acquisition, Investigation, Methodology, Writing – original draft. Y-mW: Writing – review & editing, Data curation, Investigation. G-wQ: Writing – review & editing. H-jY: Writing – review & editing. F-mL: Writing – review & editing. G-lW: Funding acquisition, Supervision, Writing – review & editing. YD: Funding acquisition, Investigation, Methodology, Supervision, Writing – original draft, Writing – review & editing.

Funding

The author(s) declare that financial support was received for the research, authorship, and/or publication of this article. This study was funded by the National Key Research and Development Program of China (2022YFD1500704, 2022YFD1500305, 2016YFD0300806, 2023YFD1901005), the Grant of the President Foundation of Hefei Institutes of Physical Science of Chinese Academy of Sciences (YZJJ2023QN37).

Conflict of interest

The authors declare that the research was conducted in the absence of any commercial or financial relationships that could be construed as a potential conflict of interest.

Publisher's note

Supplementary material

The Supplementary material for this article can be found online at: https://www.frontiersin.org/articles/10.3389/fmicb.2024.1394179/full#supplementary-material

References

Achankeng, E., and Cornelis, W. (2023). Conservation tillage effects on European crop yields: a meta-analysis. *Field Crop Res.* 298:108967. doi: 10.1016/j.fcr.2023.108967

Alaoui, A., Barao, L., Ferreira, C. S. S., Schwilch, G., Basch, G., Garcia-Orenes, F., et al. (2020). Visual assessment of the impact of agricultural management practices on soil quality. *Agron. J.* 112, 2608–2623. doi: 10.1002/agj2.20216

Angers, D. A., and Eriksen-Hamel, N. S. (2008). Full-inversion tillage and organic carbon distribution in soil profiles: a meta-analysis. *Soil Sci. Soc. Am. J.* 72, 1370–1374. doi: 10.2136/sssaj2007.0342

Araya, T., Gebremedhin, A., Baudron, F., Hailemariam, M., Birhane, E., Nyssen, J., et al. (2021). Influence of 9 years of permanent raised beds and contour furrowing on soil health in conservation agriculture based systems in Tigray region, Ethiopia. *Land Degrad. Dev.* 32, 1525–1539. doi: 10.1002/ldr.3816

Banerjee, S., Kirkby, C. A., Schmutter, D., Bissett, A., Kirkegaard, J. A., and Richardson, A. E. (2016). Network analysis reveals functional redundancy and keystone taxa amongst bacterial and fungal communities during organic matter decomposition in an arable soil. *Soil Biol. Biochem.* 97, 188–198. doi: 10.1016/j.soilbio.2016.03.017

Bastian, F., Bouziri, L., Nicolardot, B., and Ranjard, L. (2009). Impact of wheat straw decomposition on successional patterns of soil microbial community structure. *Soil Biol. Biochem.* 41, 262–275. doi: 10.1016/j.soilbio.2008.10.024

Berisso, F. E., Schjonning, P., Keller, T., Lamandé, M., Etana, A., de Jonge, L. W., et al. (2012). Persistent effects of subsoil compaction on pore size distribution and gas transport in a loamy soil. *Soil Till. Res.* 122, 42–51. doi: 10.1016/j.still.2012.02.005

Biddle, J. F., Fitz-Gibbon, S., Schuster, S. C., Brenchley, J. E., and House, C. H. (2008). Metagenomic signatures of the Peru margin subseafloor biosphere show a genetically distinct environment. *Proc. Natl. Acad. Sci. U.S.A.* 105, 10583–10588. doi: 10.1073/pnas.0709942105

Chen, F., Yan, G. Y., Xing, Y. J., Zhang, J. H., Wang, Q. G., Wang, H. L., et al. (2019). Effects of N addition and precipitation reduction on soil respiration and its components in a temperate forest. *Agric. For. Meteorol.* 271, 336–345. doi: 10.1016/j.agrformet.2019.03.021

Clemmensen, K. E., Finlay, R. D., Dahlberg, A., Stenlid, J., Wardle, D. A., and Lindahl, B. D. (2015). Carbon sequestration is related to mycorrhizal fungal community shifts during long-term succession in boreal forests. *New Phytol.* 205, 1525–1536. doi: 10.1111/nph.13208

Cotrufo, M. F., Wallenstein, M. D., Boot, C. M., Denef, K., and Paul, E. (2013). The microbial efficiency-matrix stabilization (MEMS) framework integrates plant litter decomposition with soil organic matter stabilization: do labile plant inputs form stable soil organic matter? *Glob. Chang. Biol.* 19, 988–995. doi: 10.1111/gcb.12113

Delgado-Baquerizo, M., Oliverio, A. M., Brewer, T. E., Benavent-González, A., Eldridge, D. J., Bardgett, R. D., et al. (2018). A global atlas of the dominant bacteria found in soil. *Science* 359:320-+. doi: 10.1126/science.aap9516

Delgado-Baquerizo, M., Reich, P. B., Trivedi, C., Eldridge, D. J., Abades, S., Alfaro, F. D., et al. (2020). Multiple elements of soil biodiversity drive ecosystem functions across biomes. *Nat. Ecol. Evol.* 4, 210–220. doi: 10.1038/s41559-019-1084-y

Deng, Y., Jiang, Y. H., Yang, Y. F., He, Z. L., Luo, F., and Zhou, J. Z. (2012). Molecular ecological network analyses. *BMC Bioinformatics* 13:113. doi: 10.1186/1471-2105-13-113

Dove, N. C., Torn, M. S., Hart, S. C., and Tas, N. (2021). Metabolic capabilities mute positive response to direct and indirect impacts of warming throughout the soil profile. *Nat. Commun.* 12:2089. doi: 10.1038/s41467-021-22408-5

Duan, Y., Chen, L., Li, Y. M., Li, J. Y., Zhang, C. Z., Ma, D. H., et al. (2023). Nitrogen input level modulates straw-derived organic carbon physical fractions accumulation by stimulating specific fungal groups during decomposition. *Soil Tillage Res.* 225:105560. doi: 10.1016/j.still.2022.105560

Duan, Y., Chen, L., Li, Y. M., Wang, Q. Y., Zhang, C. Z., Ma, D. H., et al. (2021). N, P and straw return influence the accrual of organic carbon fractions and microbial traits in a Mollisol. *Geoderma* 403:115373. doi: 10.1016/j.geoderma.2021.115373

Gao, Z. L., Karlsson, I., Geisen, S., Kowalchuk, G., and Jousset, A. (2019). Protists: puppet masters of the rhizosphere microbiome. *Trends Plant Sci.* 24, 165–176. doi: 10.1016/j.tplants.2018.10.011

Geisen, S., and Bonkowski, M. (2018). Methodological advances to study the diversity of soil protists and their functioning in soil food webs. *Appl. Soil Ecol.* 123, 328–333. doi: 10.1016/j.apsoil.2017.05.021

Gessner, M. O., Swan, C. M., Dang, C. K., Mckie, B. G., Bardgett, R. D., Wall, D. H., et al. (2010). Diversity meets decomposition. *Trends Ecol. Evol.* 25, 372–380. doi: 10.1016/j.tree.2010.01.010

Ghannoum, M. A., Jurevic, R. J., Mukherjee, P. K., Cui, F., Sikaroodi, M., Naqvi, A., et al. (2010). Characterization of the Oral fungal microbiome (Mycobiome) in healthy individuals. *PLoS Pathog.* 6:e1000713. doi: 10.1371/journal.ppat.1000713

Herath, H. M. S. K., Camps-Arbestain, M., Hedley, M., Van Hale, R., and Kaal, J. (2014). Fate of biochar in chemically- and physically-defined soil organic carbon pools. *Org. Geochem.* 73, 35–46. doi: 10.1016/j.orggeochem.2014.05.001

Hewins, D. B., Sinsabaugh, R. L., Archer, S. R., and Throop, H. L. (2017). Soil-litter mixing and microbial activity mediate decomposition and soil aggregate formation in a

sandy shrub-invaded Chihuahuan Desert grassland. *Plant Ecol.* 218, 459–474. doi: 10.1007/s11258-017-0703-4

Huang, R., Lan, M. L., Liu, J., and Gao, M. (2017). Soil aggregate and organic carbon distribution at dry land soil and paddy soil: the role of different straws returning. *Environ. Sci. Pollut. R.* 24, 27942–27952. doi: 10.1007/s11356-017-0372-9

Jat, S. L., Parihar, C. M., Singh, A. K., Nayak, H. S., Meena, B. R., Kumar, B., et al. (2019). Differential response from nitrogen sources with and without residue management under conservation agriculture on crop yields, water-use and economics in maize-based rotations. *Field Crop Res.* 236, 96–110. doi: 10.1016/j.fcr.2019.03.017

Jin, Q., Zhang, Y., Ma, Y., Sun, H., Guan, Y., Liu, Z., et al. (2022). The composition and function of the soil microbial community and its driving factors before and after cultivation of Panax ginseng in farmland of different ages. *Ecol. Indic.* 145:109748. doi: 10.1016/j.ecolind.2022.109748

Kong, A. Y. Y., Scow, K. M., Córdova-Kreylos, A. L., Holmes, W. E., and Six, J. (2011). Microbial community composition and carbon cycling within soil microenvironments of conventional, low-input, and organic cropping systems. *Soil Biol. Biochem.* 43, 20–30. doi: 10.1016/j.soilbio.2010.09.005

Lan, J. C., Wang, S. S., Wang, J. X., Qi, X., Long, Q. X., and Huang, M. Z. (2022). The shift of soil bacterial community after afforestation influence soil organic carbon and aggregate stability in karst region. *Front. Microbiol.* 13:901126. doi: 10.3389/fmicb.2022.901126

Lehmann, J., and Kleber, M. (2015). The contentious nature of soil organic matter. *Nature* 528, 60–68. doi: 10.1038/nature16069

Li, J. W., Li, M. Y., Dong, L. B., Wang, K. B., Liu, Y. L., Hai, X. Y., et al. (2020). Plant productivity and microbial composition drive soil carbon and nitrogen sequestrations following cropland abandonment. *Sci. Total Environ.* 744:140802. doi: 10.1016/j.scitotenv.2020.140802

Li, Y., Zhang, Q. P., Cai, Y. J., Yang, Q., and Chang, S. X. (2020). Minimum tillage and residue retention increase soil microbial population size and diversity: implications for conservation tillage. *Sci. Total Environ.* 716:137164. doi: 10.1016/j.scitotenv.2020.137164

Licht, M. A., and Al-Kaisi, M. (2005). Strip-tillage effect on seedbed soil temperature and other soil physical properties. *Soil Tillage Res.* 80, 233–249. doi: 10.1016/j.still.2004.03.017

Lu, R. K. (2000). *The analysis method of soil agricultural chemistry*. Beijing: Chinese Agricultural Sciences and Technology Press (in Chinese).

Ma, L., Zhou, G., Zhang, J., Jia, Z., Zou, H., Chen, L., et al. (2024). Long-term conservation tillage enhances microbial carbon use efficiency by altering multitrophic interactions in soil. *Sci. Total Environ.* 915:170018. doi: 10.1016/j.scitotenv.2024.170018

Modak, K., Ghosh, A., Bhattacharyya, R., Biswas, D. R., Das, T. K., Das, S., et al. (2019). Response of oxidative stability of aggregate-associated soil organic carbon and deep soil carbon sequestration to zero-tillage in subtropical India. *Soil Till. Res.* 195:104370. doi: 10.1016/j.still.2019.104370

Müller, E., Wildhagen, H., Quintern, M., Hess, J., Wichern, F., and Joergensen, R. G. (2009). Spatial patterns of soil biological and physical properties in a ridge tilled and a ploughed Luvisol. *Soil Till. Res.* 105, 88–95. doi: 10.1016/j.still.2009.05.011

Pearsons, K. A., Omondi, E. C., Zinati, G., Smith, A., and Rui, Y. C. (2023). A tale of two systems: does reducing tillage affect soil health differently in long-term, side-by-side conventional and organic agricultural systems? *Soil Till. Res.* 226:105562. doi: 10.1016/j.still.2022.105562

Pellegrino, E., Piazza, G., Helgason, T., and Ercoli, L. (2021). Eukaryotes in soil aggregates across conservation managements: major roles of protists, fungi and taxa linkages in soil structuring and C stock. *Soil Biol. Biochem.* 163:108463. doi: 10.1016/j.soilbio.2021.108463

Raus, L., Jitareanu, G., Ailincai, C., Pârvan, L., and Topa, D. (2016). Impact of different soil tillage systems and Organo-mineral fertilization on physical properties of the soil and on crops yield in Pedoclimatical conditions of Moldavian plateau. *Rom. Agric. Res.* 33, 111–123,

Ren, Z. J., Han, X. J., Feng, H. X., Wang, L. F., Ma, G., Li, J. H., et al. (2024). Long-term conservation tillage improves soil stoichiometry balance and crop productivity based on a 17-year experiment in a semi-arid area of northern China. *Sci. Total Environ.* 908:168283. doi: 10.1016/j.scitotenv.2023.168283

Samson, M. E., Chantigny, M. H., Vanasse, A., Menasseri-Aubry, S., Royer, I., and Angers, D. A. (2020). Management practices differently affect particulate and mineral-associated organic matter and their precursors in arable soils. *Soil Biol. Biochem.* 148:107867. doi: 10.1016/j.soilbio.2020.107867

Sarker, J. R., Singh, B. P., Cowie, A. L., Fang, Y. Y., Collins, D., Dougherty, W. J., et al. (2018). Carbon and nutrient mineralisation dynamics in aggregate-size classes from different tillage systems after input of canola and wheat residues. *Soil Biol. Biochem.* 116, 22–38. doi: 10.1016/j.soilbio.2017.09.030

Shi, X. H., Yang, X. M., Drury, C. F., Reynolds, W. D., McLaughlin, N. B., and Zhang, X. P. (2012). Impact of ridge tillage on soil organic carbon and selected physical properties of a clay loam in southwestern Ontario. *Soil Till. Res.* 120, 1–7. doi: 10.1016/j.still.2012.01.003

Six, J., Bossuyt, H., Degryze, S., and Denef, K. (2004). A history of research on the link between (micro)aggregates, soil biota, and soil organic matter dynamics. *Soil Till. Res.* 79, 7–31. doi: 10.1016/j.still.2004.03.008

Six, J., Conant, R. T., Paul, E. A., and Paustian, K. (2002). Stabilization mechanisms of soil organic matter: implications for C-saturation of soils. *Plant Soil* 241, 155–176. doi: 10.1023/A:1016125726789

Stoeck, T., Bass, D., Nebel, M., Christen, R., Jones, M. D. M., Breiner, H. W., et al. (2010). Multiple marker parallel tag environmental DNA sequencing reveals a highly complex eukaryotic community in marine anoxic water. *Mol. Ecol.* 19, 21–31. doi: 10.1111/j.1365-294X.2009.04480.x

Tang, Q., Ti, C. P., Xia, L. L., Xia, Y. Q., Wei, Z. J., and Yan, X. Y. (2019). Ecosystem services of partial organic substitution for chemical fertilizer in a peri-urban zone in China. *J. Clean. Prod.* 224, 779–788. doi: 10.1016/j.jclepro.2019.03.201

Topa, D., Cara, I. G., and Jitareanu, G. (2021). Long term impact of different tillage systems on carbon pools and stocks, soil bulk density, aggregation and nutrients: a field meta-analysis. *Catena* 199:105102. doi: 10.1016/j.catena.2020.105102

Van den Putte, A., Govers, G., Diels, J., Gillijns, K., and Demuzere, M. (2010). Assessing the effect of soil tillage on crop growth: a meta-regression analysis on European crop yields under conservation agriculture. *Eur. J. Agron.* 33, 231–241. doi: 10.1016/j.eja.2010.05.008

Vogel, C., Mueller, C. W., Höschen, C., Buegger, F., Heister, K., Schulz, S., et al. (2014). Submicron structures provide preferential spots for carbon and nitrogen sequestration in soils. *Nat. Commun.* 5:2947. doi: 10.1038/ncomms3947

Wang, J., Li, H., Cheng, Z., Yin, F., Yang, L., and Wang, Z. (2023). Changes in soil bacterial and fungal community characteristics in response to long-term mulched drip irrigation in oasis agroecosystems. *Agric. Water Manage.* 279:108178. doi: 10.1016/j.agwat.2023.108178

Wang, C., Qu, L. R., Yang, L. M., Liu, D. W., Morrissey, E., Miao, R. H., et al. (2021). Large-scale importance of microbial carbon use efficiency and necromass to soil organic carbon. *Glob. Chang. Biol.* 27, 2039–2048. doi: 10.1111/gcb.15550

Wang, S. C., Zhao, Y. W., Wang, J. Z., Zhu, P., Cui, X., Han, X. Z., et al. (2018). The efficiency of long-term straw return to sequester organic carbon in Northeast China's cropland. *J. Integr. Agric.* 17, 436–448. doi: 10.1016/S2095-3119(17)61739-8

Woudenberg, J., Sandoval-Denis, M., Houbraken, J., Seifert, K. A., and Samson, R. A. (2017). Cephalotrichum and related synnematous fungi with notes on species from the built environment. *Stud. Mycol.* 88, 137–159. doi: 10.1016/j.simyco.2017.09.001

Yu, Z. H., Zhang, J. B., Zhang, C. Z., Xin, X. L., and Li, H. (2017). The coupling effects of soil organic matter and particle interaction forces on soil aggregate stability. *Soil Till. Res.* 174, 251–260. doi: 10.1016/j.still.2017.08.004

Zhang, Y., Li, X. J., Gregorich, E. G., McLaughlin, N. B., Zhang, X. P., Guo, Y. F., et al. (2019). Evaluating storage and pool size of soil organic carbon in degraded soils: tillage effects when crop residue is returned. *Soil Till. Res.* 192, 215–221. doi: 10.1016/j.still.2019.05.013

Zhang, S. X., Li, Q., Lü, Y., Zhang, X. P., and Liang, W. J. (2013). Contributions of soil biota to C sequestration varied with aggregate fractions under different tillage systems. *Soil Biol. Biochem.* 62, 147–156. doi: 10.1016/j.soilbio.2013.03.023

Zhang, X. P., Li, Q. L., Zhong, Z. K., Huang, Z. Y., Bian, F. Y., Yang, C. B., et al. (2022). Changes in soil organic carbon fractions and fungal communities, subsequent to different management practices in Moso bamboo plantations. *J. Fungi (Basel)* 8:8. doi: 10.3390/jof8060640

Zhang, L., Tang, C., Yang, J., Yao, R., Wang, X., Xie, W., et al. (2023). Salinity-dependent potential soil fungal decomposers under straw amendment. *Sci. Total Environ.* 891:164569. doi: 10.1016/j.scitotenv.2023.164569

Zhao, R. D., He, M., Jiang, C. L., Li, C. L., and Liu, F. (2021). Microbial community structure in rhizosphere soil rather than that in bulk soil characterizes aggregate-associated organic carbon under long-term forest conversion in subtropical region. *Rhizosphere* 20:100438. doi: 10.1016/j.rhisph.2021.100438

frontiers | Frontiers in Environmental Science

TYPE Original Research
PUBLISHED 01 August 2024
DOI 10.3389/fenvs.2024.1417949

OPEN ACCESS

EDITED BY
Peng Shi,
Xi'an University of Technology, China

REVIEWED BY
Hao Yang,
Guangxi Normal University, China
Yongfu Li,
Zhejiang Agriculture and Forestry University, China

*CORRESPONDENCE
Xianfei Huang,
hxfswjs@gznu.edu.cn

RECEIVED 15 April 2024
ACCEPTED 24 June 2024
PUBLISHED 01 August 2024

CITATION
Wang X, Huang X, Zhu X, Wu N, Zhang Z, Liu Y, Huang Y and Hu J (2024), Spatial distribution characteristics of soil organic matter in different land uses and its coupling with soil animals in the plateau basin in the South China Karst basin. *Front. Environ. Sci.* 12:1417949. doi: 10.3389/fenvs.2024.1417949

Spatial distribution characteristics of soil organic matter in different land uses and its coupling with soil animals in the plateau basin in the South China Karst basin

Xingfu Wang[1,2], Xianfei Huang[3]*, Xun Zhu[1], Nayiyu Wu[1], Zhenming Zhang[4], Yi Liu[1], Yu Huang[1] and Jiwei Hu[3]

[1]School of Health Management, Guiyang Healthcare Vocational University, Guiyang, China, [2]Guizhou Provincial Engineering Research Center of Medical Resourceful Healthcare Products, Guiyang Healthcare Vocational University, Guiyan, China , [3]Guizhou Provincial Key Laboratory for Information Systems of Mountainous Areas and Protection of Ecological Environment, Guizhou Normal University, Guiyang, China, [4]College of Resources and Environmental Engineering, Guizhou University, Guiyang, China

Karst landforms are widely distributed in southern China. The terrain and soil properties in karst basins are complex, which results in high spatial heterogeneity of the ecological environment and soil organic matter (SOM) in karst watersheds. To investigate the spatial distribution characteristics of SOM in different land uses in the karst plateau basin, a total of 3,816 soil samples were taken from 568 soil profiles. The soil animals and different soil properties were recorded, and the concentration of SOM was tested using the potassium dichromate method in the laboratory. Then, the changes in the SOM content associated with soil animals and the soil properties associated with the different land use types were analyzed. The results showed a large discrepancy in SOM in the karst plateau basin. The average values of SOM in different soil layers were between 9.23 g kg^{-1} and 59.39 g kg^{-1}. The SOM decreased in the following order: forestland > grassland > barren land > cultivated land > garden land. The SOM in soil in which soil animals are present is generally greater than that in the absence of soil animals, and the SOM partially increases with soil species diversity. *Agrotis segetum* is the main soil animal species that positively affects the distribution of organic matter in the surface soil layer. The SOM in soil with the phylum Annelida is much greater than that in soils with other animals, and earthworms are the main contributor. The structure of soil animal species is complex, and the change trend of SOM is stable. The major positive factors affecting soil animal diversity are soil thickness, soil humidity and soil structure, and rock outcrops are the main negative factor. In summary, good land use can increase animal diversity and abundance in soil, which promotes soil organic matter accumulation. Moreover, microtopography is an important factor that influences soil organic matter accumulation in karst basins and further affects the restructuring of the spatial distribution of soil organic matter.

KEYWORDS

soil organic matter, spatial heterogeneity, soil animals, land use, effect mechanism, Karst basin

1 Introduction

Soil organic matter (SOM) refers to all the carbonaceous organic matter existing in soil, including the residual organic matter of plants and animals, microorganisms, and humus (Jurgensen et al., 1997; Kaiser et al., 2002; Di et al., 2015; Zhang J. et al., 2023). It is an important resource used in many processes, including carbon cycling in terrestrial ecosystems (Mcdonagh et al., 2001; Six et al., 2007). Because the main component of SOM is carbon, SOM is crucial for the global carbon cycle (Caspersen et al., 2000; Schime et al., 2000; Zhang X. et al.f, 2023). There are some interactions between the processes of carbon cycling and climate change (Ding et al., 2002; West and Post, 2002; Li et al., 2024). According to the transition relationship between SOM and soil organic carbon, the global SOM reserve in the 0–100 cm soil layer is approximately 2,517 Pg (Weissert et al., 2016; Wang et al., 2022). This indicates that the global SOM reserve is a large carbon reservoir. Small changes in SOM may lead to great changes in atmospheric CO_2, further resulting in global climate change (Lin and Zhang, 2012; Bieluczyk et al., 2023; Wang et al., 2023). SOM is an important part of the terrestrial carbon pool that affects the carbon balance (Pouyat et al., 2002; Freitas et al., 2022). In addition, SOM is an essential factor in agricultural productivity and soil fertility. SOM can improve the physical structure and chemical composition of soil. It is not only a main index of soil quality but also the basis of sustainable development (Wang et al., 2005; Smith et al., 2013). It is beneficial to soil aggregate formation and can promote plant nutrient absorption from soil (Di et al., 2015; Poffenbarger et al., 2020; Street et al., 2020; Li et al., 2024). In summary, the reserves and spatial heterogeneity of SOM directly impact the carbon cycle in terrestrial ecosystems, plant growth, soil fertility maintenance, and agricultural output and quality (Niu et al., 2015; Wang et al., 2022). Therefore, research on SOM has become a popular field worldwide (Cheshire, 1987; Li et al., 2019; Zhang et al., 2019).

Although SOM reserves are essential in terrestrial ecosystems, they are not constant in soil but constitute a long-term dynamic balance system of input and output (Yan et al., 2011; Aaltonen et al., 2019; Zhou et al., 2024). There is high spatial distribution heterogeneity of SOM because the exchange processes between SOM and other materials in different ecosystems are complex, and SOM is influenced by multivariate factors (Huang et al., 2018). The influence of multifactor coupling on SOM is complex, which leads to the key factors being different in various areas (Huang et al., 2018; Wang et al., 2022). Therefore, many scholars have studied SOM from different perspectives and in different ways. For example, Li et al. researched the relationships between SOM and soil pH and soil bulk density (SBD), and the results showed that there was a negative correlation between these indices; the higher the soil pH and soil bulk density are, the lower the SOM concentration is (Li D. C. et al., 2020). In another instance, Zhang et al. researched the spatiotemporal variation mechanism of SOM in farmland by different abandoned tillage practices and noted that the decreasing order of SOM under different abandoned tillage practices is season abandonment > adjustment abandonment > annual ring abandonment > long-term abandonment > long-term cultivation (Zhang T. Y. et al., 2020). The conversion of natural pasture to dryland farming results in a notable decrease in SOM. This decrease in SOM is quantified as a reduction of 24.7% at the first site and 44.2% at the second site within the top 30 cm of soil (Haghighi et al., 2010). These results indicate that land use patterns and soil properties are important factors affecting SOM and that fertilizer and green manure inputs to soil and straw return to farmland can promote SOM accumulation (Zhang W. J. et al., 2012; Zhang et al., 2015; Qaswar et al., 2019). In addition, Shen et al. noted a positive correlation between SOM and the species and number of soil animals (Shen et al., 2009). Zhang et al. suggested that land use change greatly impacts soil animal diversity. He noted that forestland supports a more diverse and complex soil animal community than farmland or grassland, and the composition and number of these soil animals vary across different sampling plots (Zhang J. E. et al., 2011). SOM is highly heterogeneous in soil, and the SOM process and its impacts are complex.

Karst basins are a typical landform type in karst mountainous areas, and farmland, forestland, barren land, etc., are widely distributed in karst basins. The special ecosystem of karst landforms is different from that of nonkarst regions (Zhang et al., 2016). Because soil erosion in karst areas is severe, karst areas exhibit low stability, poor self-regulation, and low environmental capacity (Yang et al., 2010; Zhang X. B. et al., 2011). Therefore, the microenvironments and land use types of karst landforms are more complex than those of other landforms (Wang et al., 2022). The soil quality of different land uses in karst basins varies greatly, which can directly affect agricultural yield and carbon sequestration. These factors result in high spatial distribution heterogeneity of SOM in karst areas, and SOM is impacted by major factors in different karst regions (Huang et al., 2018; Zhang et al., 2019). SOM is an important index of soil quality, fertility, and carbon balance (Freitas et al., 2022; Wang et al., 2023). We ask the following question: What is the mechanism of the relationships among soil animals, land use, and SOM in karst basins? This main issue is not clearly understood for karst basins in general or, more specifically, for the South China Karst.

In summary, SOM is critical for global carbon circulation; changes in SOM can influence the carbon balance, which partially responds to soil structure and fertility. However, no researchers have reported on the response of SOM to soil animals in karst basin areas with different land uses. Therefore, the distribution characteristics of soil animals in karst plateau basin soils were analyzed, and the coupling mechanisms among land use, soil animals, and SOM were further investigated. The aim of this study was to provide a reference for carbon sequestration management and land use, thereby promoting soil quality and production in karst areas.

2 Materials and methods

2.1 Study region

The research region was set in Puding County, which is a typical plateau basin in the central region of the South China Karst with geographic coordinates of 105°27′49″–105°58′51″E and 26°26′36″–26°31′42″N. It is in the belt of the translation zone between the Sichuan Basin and the Yun-Gui Plateau and extends to the Hunan Hills. The elevation is approximately 800–1900 m. The topography of the southern and northern regions is greater than that

of the central region, and its karst landform characteristics are abundant, widely distributed, distinctly discrepant, and seriously rocky desertification. Severe soil erosion has occurred due to the karst landform development and the number of underground rivers. The region is a subtropical region with a humid monsoon climate, and this region is affected by the quasistationary Guiyang–Kunming front. The average annual temperature is 15.1°C, the average annual sunshine duration is 1,164.9 h, and the average annual rainfall reaches 1,378.2 mm. The research area is one of three major core rainfall regions in Guizhou Province, and it belongs to the Yangzi River ecosystem. The survey and statistics revealed three types of soils, Leptosols, Ferralsols, and Anthrosols, in the area of interest (IUSS Working Group WRB, 2014). The vegetation mostly includes walnut, *Quercus glauca*, pine trees, strawberry trees, plum trees, and Chinese pear. The land use mostly includes paddy fields, dry land, forestland, sloped farmland, and grassland. The major crops and grasses are sweet potato, paddy rice, corn, pepper, soybean, and foxtail grass. The soil animals mostly include ants (Formicidae, Arthropoda, and Hymenoptera), earthworms (Lumbricus and Annelida), centipedes (Chilopoda and Arthropoda), crickets (Gryllidae and Arthropoda), and spiders (Araneae and Arthropoda).

2.2 Sampling design

To research the relationship between SOM and soil animals in different land uses, samples containing traces of soil animal activity were collected from different locations. The number of soil animal species was counted in an approximate square with a length of approximately 1.7 m and a depth of 0–20 cm, and the sampling sites were in the center of each sampling grid. The sampling site was sampled at a depth of 100 cm according to the design, and the soil profile of each sampling site was divided into 12 layers (0–5 cm, 5–10 cm, 10–15 cm, 15–20 cm, 20–30 cm, 30–40 cm, 40–50 cm, 50–60 cm, 60–70 cm, 70–80 cm, 80–90 cm, and 90–100 cm). Other information, such as soil thickness, rock outcrop, soil animal, SBD, soil moisture, soil structure, soil genus, soil color, slope position, slope gradient, and vegetation, was also recorded.

2.3 Soil sample collection and test

In fact, the soil thicknesses of many sampling sites were less than 100 cm. Therefore, the number of collected soil samples was lower than the theoretical sample number. Finally, a total of 3,816 soil samples were taken from 568 soil profiles. The soil samples were taken to the laboratory, air-dried at room temperature, ground, and sieved to remove the gravel fraction (>2 mm). The resulting materials were ground into powders and saved for SOM analysis. The SOM concentration in the soil samples was determined using the potassium dichromate method with $K_2Cr_2O_7$ oxidation at 170°C–180°C, followed by titration with Fe_3O_4 (Wang et al., 2010; Zhang et al., 2019). The soil thickness at each site was measured by inserting an iron rod with a length of either 60 cm or 120 cm. The SBD was determined via the cutting ring method (Huang et al., 2018; Zhang et al., 2019; Wang et al., 2022), and the soil moisture was tested via the oven method (Sharaya and Van, 2022). The rock outcrop rate at each sampling site was assessed via the line-transect method, and the line length was set to 10 m (Zhang et al., 2019; Wang et al., 2022).

2.4 Calculations and statistical analysis

The SBD ($g•cm^{-3}$) was tested in the field by the cylindrical core method. The formula is as follows (Huang et al., 2018; Wang et al., 2022):

$$SBD = \frac{M_2 - M_1,}{V} \quad (1)$$

where M_1 is the weight of the cutting ring (g), M_2 is the weight of the cutting ring with dry soil (g), and V is the volume of the cutting ring (cm^3).

The species diversity index of the local environment was determined via the following formula (Zeng et al., 2018):

$$D = S/\ln A, \quad (2)$$

where D is the species diversity index, S is the species number of soil animals, and A is the area of the sampling site (m^2).

Factor analysis was carried out via principal component analysis (PCA) and redundancy analysis (RDA). PCA analyzes the similarity and diversity among factors and distinguishes the significant impact factors from all samples. RDA is an important method of constrained ordination that can sort species and environmental factor datasets and sort the environmental factors under constrained species (Wang et al., 2020).

The data were managed and organized using Microsoft Excel 2003 (Microsoft, Redmond, WA, USA). Statistical analysis was performed with IBM SPSS 18.0 and Origin 8.6 software.

3 Results and analysis

3.1 Descriptive statistics of the major soil properties

The soil properties are more complex in karst mountainous areas, and there is high spatial heterogeneity in the major soil properties, such as soil thickness, SBD, rock outcrop, and soil moisture, which are important factors that affect SOM in karst areas (Zhang W. et al., 2012; Zhang et al., 2019). According to the information in Table 1, the average values of soil thickness, SBD, rock outcrop, and moisture content were 61.70 cm, 1.17 g cm^{-3}, 16%, and 23%, respectively, and their coefficients of variation were 0.53, 0.18, 1.38, and 0.57, respectively. The changes in soil thickness, rock outcrop, and soil moisture content were highly variable, and the SBD was moderately variable (Shang et al., 2018). The skewness of both the soil thickness and the SBD was lower than 0, which indicated that the skewness exhibited a certain degree of left-sided bias. This result showed that the soil thickness and SBD were generally lower than the average values, which indicated that the soil layer in a typical karst basin was thinner and nonuniform and that there was high spatial heterogeneity in the soil thickness and SBD in the karst basin.

TABLE 1 Descriptive statistics of the major soil properties in the karst basin.

Soil properties	Maximum	Minimum	Mean	C.V. (%)	Skewness	Kurtosis
Soil thickness (cm)	100	5	61.70	0.53	−0.07	−1.56
SBD (g·cm^{-3}) (Eq. 1)	1.84	0.39	1.17	0.18	−0.19	−0.36
Rock outcrop rate (%)	0.95	0	0.16	1.38	1.33	−0.79
Moisture content (%)	5.36	46.73	0.23	0.57	2.57	−1.33

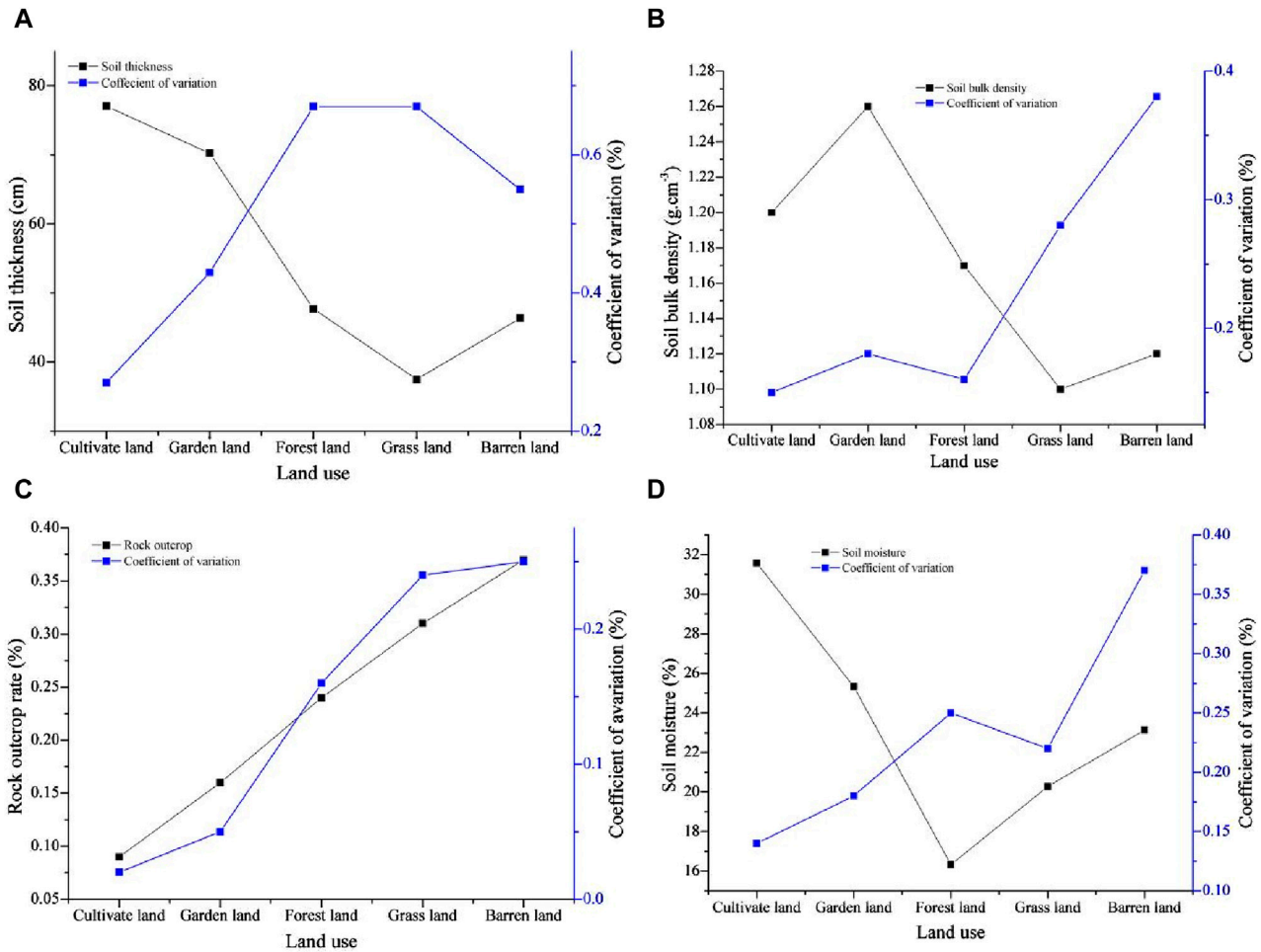

FIGURE 1
Information characteristics on soil properties in different land uses: **(A)** soil thickness, **(B)** SBD, **(C)** rock outcrop, and **(D)** soil moisture.

The skewness values of the rock outcrops and moisture content were greater than 0, which indicated that the rock outcrops and moisture content had a degree of right-sided bias and that there was high rock desertification in the karst basins. Moreover, the kurtosis values of the soil thickness, SBD, rock outcrop cover, and moisture content were lower than 0, and the peak distributions were gradual. This indicated that the spatial distributions of soil thickness, SBD, rock outcrop cover, and moisture content were diverse.

There was a greater discrepancy in the soil properties among the land use types (Figure 1). The soil thickness under the different land uses ranged between 37.48 and 77.06 cm, and the soil thickness decreased in the following order: cultivated land > garden land > forestland > barren land > grassland. The soil layer thickness of cultivated land and garden land was much greater than that of the other land uses. The coefficient of variation of soil thickness in all land use types reached high levels, with forests and grasslands having the highest values and being similar (Figure 1A). The average SBD values for all land uses were between 1.10 g cm^{-3} and 1.26 g cm^{-3}, and the SBD values decreased in the following order: garden land > cultivated land > forestland > barren land > grassland. Moreover, the differences in SBD among the land use types were greater. The coefficient of variation of SBD in cultivated land and forestland was low, while that in garden land was moderately variable. However, the

TABLE 2 The statistics of soil animals in the karst basin.

Soil animal/Species	Number (n)	Order (n)	Class (n)	Phylum (n)
Ground beetle (*D. dispar Chanisso et Eysenhard*)	18	*Blattaria* (18)	*Insecta* (862)	*Arthropoda* (897)
Agrotis segetum (*Denis et Schiffermüller*)	19	*Lepidoptera* (22)		
Caterpillar (*Caterpillar*)	17			
Ant (*Monomorium pharaonis L.*)	791	*Hymenoptera* (791)		
Cicada (*Cryptotympana atrata Fabricius*)	7	*Hemiptera* (7)		
Cricket (*Gryllulus; Gryllus*)	24	*Orthoptera* (24)		
Coccinella septempunctata	15	*Coleoptera* (15)		
Spider (*Araneida*)	10	*Araneae* (10)	*Arachnida* (10)	
Centipede (*Scolopendra subspinipes*)	25	*Chilopoda* (25)	*Myriapoda* (25)	
Frog (*Rana nigromaculata*)	11	*Anura* (11)	*Amphibian* (11)	*Chordata* (11)
Earthworm (*Earthworm*)	331	*Haplotaxida* (331)	*Clitellata* (331)	*Annelida* (331)

values for grassland and barren land reached highly variable levels, and the value for barren land was the greatest (Figure 1B).

The rock outcrop rate under the different land uses ranged between 0.09 and 0.37, and its coefficient of variation ranged between 0.02 and 0.25. The spatial distribution characteristics of rock outcrops and their coefficients of variation for all land use types were similar, and their descending order was barren land > grassland > forestland > garden land > cultivated land. The distribution of rock outcrops among different land uses followed a regular gradient pattern. In addition, the coefficient of variation of rock outcrops in cultivated land and garden land was low; however, those values in forestland, grassland, and barren land had a high degree of variation (Figure 1C).

The average soil moisture content under the different land uses ranged from 16.33% to 31.57%, and the moisture content decreased in the following order: cultivated land > garden land > barren land > grassland > forestland. The distribution characteristics of soil moisture under the different land use types revealed a type of "V." There were few differences in the soil moisture content among garden land, grassland, and barren land. The descending order of the coefficient of variation for different land uses was barren land > forestland > grassland > garden land > cultivated land. The coefficient of variation for cultivated land was low, but that for garden land, forestland, and grassland varied moderately. The coefficient of variation for barren land was significantly greater than that for other land uses (Figure 1D).

3.2 Statistics on the number of soil animals in the sampled spots

The number of soil animals in the sampling sites was counted, and the sites were divided into different levels of species, order, class, and phylum. There were many different soil animals in the soil samples, such as ground beetles, *Agrotis segetum*, caterpillars, ants, cicadas, crickets, *Coccinella septempunctata*, spiders, centipedes, frogs, and earthworms. Among them, *Agrotis segetum* and its caterpillars can be classified as Lepidoptera, and other soil animals belong to the Blattaria, Hymenoptera, Hemiptera, Orthoptera, Coleoptera, Araneae, Chilopoda, Anura, and Haplotaxida orders. These animal orders can be divided into five animal classes: Insecta, Arachnida, Myriapoda, Amphibian, and Clitellata and further divided into three animal phyla, Arthropoda, Chordata, and Annelida (Table 2).

At the species level, the top two soil animal species were ants and earthworms, and their numbers were far greater than those of other soil animal species. Their accumulation proportion was 89.5%, and the number of ants was more than double that of earthworms. This indicated that ants and earthworms were the dominant species in the study area and were widely distributed in the karst plateau basin. At the order level, the top two soil animals were *Hymenoptera* and *Haplotaxida,* and the distribution characteristics among all the soil animal orders were similar to the trend at the species level. However, there were few differences in number among the other soil animal orders. At the class level, the top two most abundant were *Insecta* and *Clitellata,* and their accumulation proportion reached 96.3%. At the phylum level, the abundance of *Arthropoda* was close to three times greater than that of *Annelida,* and *Annelida* was far more abundant than *Chordata*, and their percentages were 72.5%, 26.7%, and 0.9%, respectively. This indicated that the major soil animal phyla *Arthropoda* and *Annelida* were widely distributed in the karst basin, and there were fewer *Chordata*. This may be because the mass of *Chordata* is much larger than that of other soil animals, and *Chordata* occupy more places in the food chain; for example, ants are a food source for frogs.

3.3 The spatial distribution characteristics of SOM in different land uses

There was a greater discrepancy in the SOM in each soil layer among the different land use types, and their spatial distribution characteristics are shown in Table 3. The average SOM concentration in all soil layers under the different land use types ranged between 8.98 g kg^{-1} and 69.25 g kg^{-1}. In the 0–5 cm, 5–10 cm, 10–15 cm, and 15–20 cm soil layers, the SOM distributions in the

TABLE 3 The soil organic matter content characteristics in different land uses (g·kg^{-1}).

Soil layers	Cultivate land	Garden land	Forest land	Grassland	Barren land
0–5	43.73 ± 18.13	42.97 ± 18.44	69.25 ± 35.34	63.76 ± 31.07	63.60 ± 33.29
5–10	38.64 ± 16.18	36.71 ± 17.98	58.3 ± 30.94	53.21 ± 27.37	52.71 ± 28.82
10–15	34.17 ± 15.52	31.5 ± 18.95	50.96 ± 28.36	46.82 ± 26.10	44.55 ± 23.51
15–20	28.54 ± 14.97	27.23 ± 18.21	44.91 ± 27.20	41.28 ± 24.78	39.71 ± 22.80
20–30	22.40 ± 13.50	21.85 ± 15.86	33.54 ± 20.39	33.56 ± 20.62	33.94 ± 22.37
30–40	17.15 ± 10.54	16.95 ± 11.14	22.52 ± 12.88	25.15 ± 14.92	27.59 ± 19.30
40–50	15.02 ± 10.42	14.18 ± 8.30	18.54 ± 10.88	18.45 ± 10.29	21.5 ± 15.25
50–60	12.76 ± 9.76	13.85 ± 7.83	14.68 ± 7.60	15.91 ± 8.64	14.89 ± 8.97
60–70	11.36 ± 8.96	12.26 ± 7.90	13.15 ± 7.39	15.18 ± 7.80	12.25 ± 6.83
70–80	10.45 ± 8.91	9.18 ± 6.29	12.43 ± 7.82	12.44 ± 6.31	11.34 ± 6.12
80–90	9.28 ± 9.06	9.52 ± 7.73	11.98 ± 8.03	12.09 ± 5.32	10.21 ± 5.44
90–100	8.89 ± 7.43	9.00 ± 4.05	11.09 ± 8.29	11.57 ± 5.78	8.98 ± 3.88

different land use types were similar and exhibited a pattern of forestland > grassland > barren land > cultivated land > garden land. The differences between barren land and grassland and between cultivated land and garden land were small, and the SOM content in forestland was significantly greater than that in the other land types. In the 20–30 cm and 30–40 cm soil layers, the SOM concentration decreased in the following order: barren land > grassland > forestland > cultivated land > garden land. The values in barren land, grassland, and forestland were similar, and the discrepancy in the SOM content between cultivated land and garden land was small. In the 40–50 cm soil layer, the SOM concentration decreased in the following order: barren land > forestland > grassland > cultivated land > garden land. In the 50–60 cm, 60–70 cm, and 80–90 cm soil layers, the spatial distribution characteristics of the SOM concentration under the different land use types exhibited the following pattern: grassland > barren land > forestland > garden land > cultivated land. In the 70–80 cm soil layer, the descending order was grassland > forestland > barren land > cultivated land > garden land. However, the distribution of SOM in the 90–100 cm soil layer decreased in the following order: grassland > forestland > garden land > barren land > cultivated land.

In addition, in the vertical direction, the discrepancy in the SOM concentration from the surface soil layer to the subsurface soil among the different land use types was great. The descending order was forestland > barren land > grassland > cultivated land > garden land, and their ranges were 58.19 g kg^{-1}, 54.62 g kg^{-1}, 52.19 g kg^{-1}, 34.84 g kg^{-1}, and 33.97 g kg^{-1}, respectively. In the 0–5 cm to 50–60 cm soil layers, the SOM concentration declined quickly; however, its decrease from the 60–100 cm soil layers was relatively slow. Moreover, the differences in SOM among the soil layers with different land use types were highly variable, and the coefficient of variation ranged from 0.39 to 0.85. In summary, the distribution regularity of the SOM concentration in the upper soil layers was distinctly better than that in the subsoil, and the depth of 60 cm could be considered the boundary of the distribution characteristics of the SOM in the upper soil layers and subsoil layers.

3.4 The spatial distribution characteristics of SOM in response to soil animals

Information on the spatial distribution characteristics of SOM under coupled soil conditions is listed in Figure 2. The SOM concentrations in the samples with soil animals were generally greater than those in the soil without soil animals, and the SOM gradually decreased with increasing soil thickness. There was less difference between the SOM concentrations of soil samples containing animals and those with no animals in the upper soil layer, but this difference gradually increased with soil thickness. In addition, there was a distribution pattern of SOM in the vertical direction in which the SOM rapidly decreased in the soil layer from the surface to 50 cm, and the decrease rate of SOM in the 50 cm–100 cm layer was relatively slower and more stable. Furthermore, the coefficients of SOM variation in different soil layers were highly variable; these changes in non-animal-soil samples were generally greater than those in animal-soil samples, and this difference gradually increased in the subsoil layer (Figure 2A). There was no significant regular distribution of SOM in soils with different soil animals, but there was a larger discrepancy in SOM in soils with different soil animals in the 0 cm–60 cm soil layers, and this difference in the 60 cm–100 cm subsoil layer was relatively slight (Figure 2B).

To further analyze the differences in SOM in soils with different soil animals, the soil animals were classified into three different soil phyla: *Arthropoda*, *Chordata*, and *Annelida*. In the upper soil layers from 0 cm to 20 cm, the descending order of SOM concentration in soils with different soil animal phyla was *Annelida* > *Chordata* > *Arthropoda*, and the SOM in soils with *Annelida* was significantly greater than that in soils with *Chordata* and *Arthropoda*. In the subsoil layer from 20 cm to 100 cm, the descending order of SOM concentration in soils with different animal phyla was *Annelida* > *Arthropoda* > *Chordata*. Obviously, the SOM concentration in each soil layer under the coupling of the *Annelida* animal phylum was the highest, and it was significantly greater than that under the coupling of the other two animal phyla. In addition, there was a slight

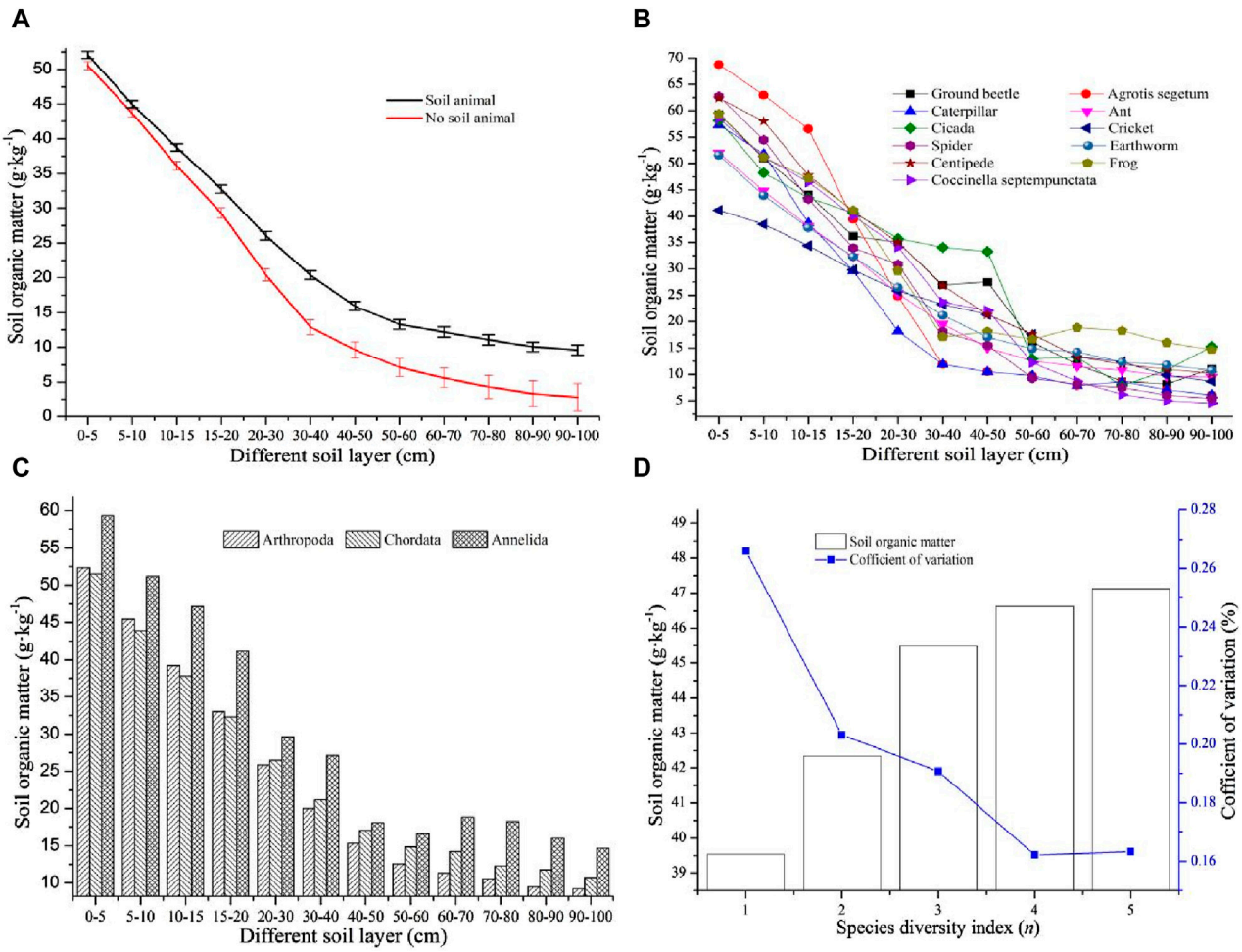

FIGURE 2
Distribution characteristics of SOM under the coupling of soil animals: **(A)** Spatial distribution of SOM with soil animals and no soil animals, **(B)** SOM distribution with different soil animals, **(C)** different soil phylum effects on SOM, and **(D)** the spatial distribution characteristics of SOM response to the species diversity index.

difference in the SOM in the different soil layers with the animal phyla *Chordata* and *Arthropoda* (Figure 2C). This indicated that *Annelida* animals could promote SOM sequestration in soil more than other soil animals, which could improve soil quality in nature. The species diversity was calculated by Eq. 2. To better understand how species diversity affects SOM, the relationship between the average value of SOM in the 0 cm–20 cm soil layer and the change in the species diversity index was analyzed. The results showed that the SOM concentration gradually increased with increasing species diversity index, and there was a significant increase in the value of SOM when the species diversity index was between 1 and 3. When the species diversity index was between 3 and 5, the difference in SOM decreased. The variation coefficient of SOM at different levels of the species diversity index indicated moderate variation, and these values were between 0.16 and 0.26. The change in the SOM concentration gradually decreased with increasing species diversity index. Thus, when the species diversity index was relatively lower, the SOM concentration was lower, but there was a larger discrepancy in the SOM. When the species diversity index gradually increased, not only was the SOM concentration higher but also the difference in SOM was slight. This indicated that species diversity could promote SOM sequestration and maintain stable soil fertility (Figure 2D).

3.5 The spatial distribution characteristics of SOM in response to soil thickness

To analyze the distribution characteristics of SOM at different soil thickness levels, the SOM concentrations in each soil layer in the upper and bottom soil layers under different soil thicknesses were compared. Because the soil animals were mainly distributed in the 20-cm soil layer, the soil thickness at most sampling sites was less than 30 cm. Therefore, comparisons were conducted for the 5 cm, 10 cm, and 20 cm soil layers and in the subsoil (Figure 3). The SOM in the topsoil layer of 5 cm at different soil thicknesses gradually decreased with increasing soil thickness, and the SOM concentration ranged between 37.01 g kg^{-1} and 89.93 g kg^{-1}. The maximum value was 2.43 times greater than the minimum, which indicated that there was a greater discrepancy in the SOM in the topsoil layer

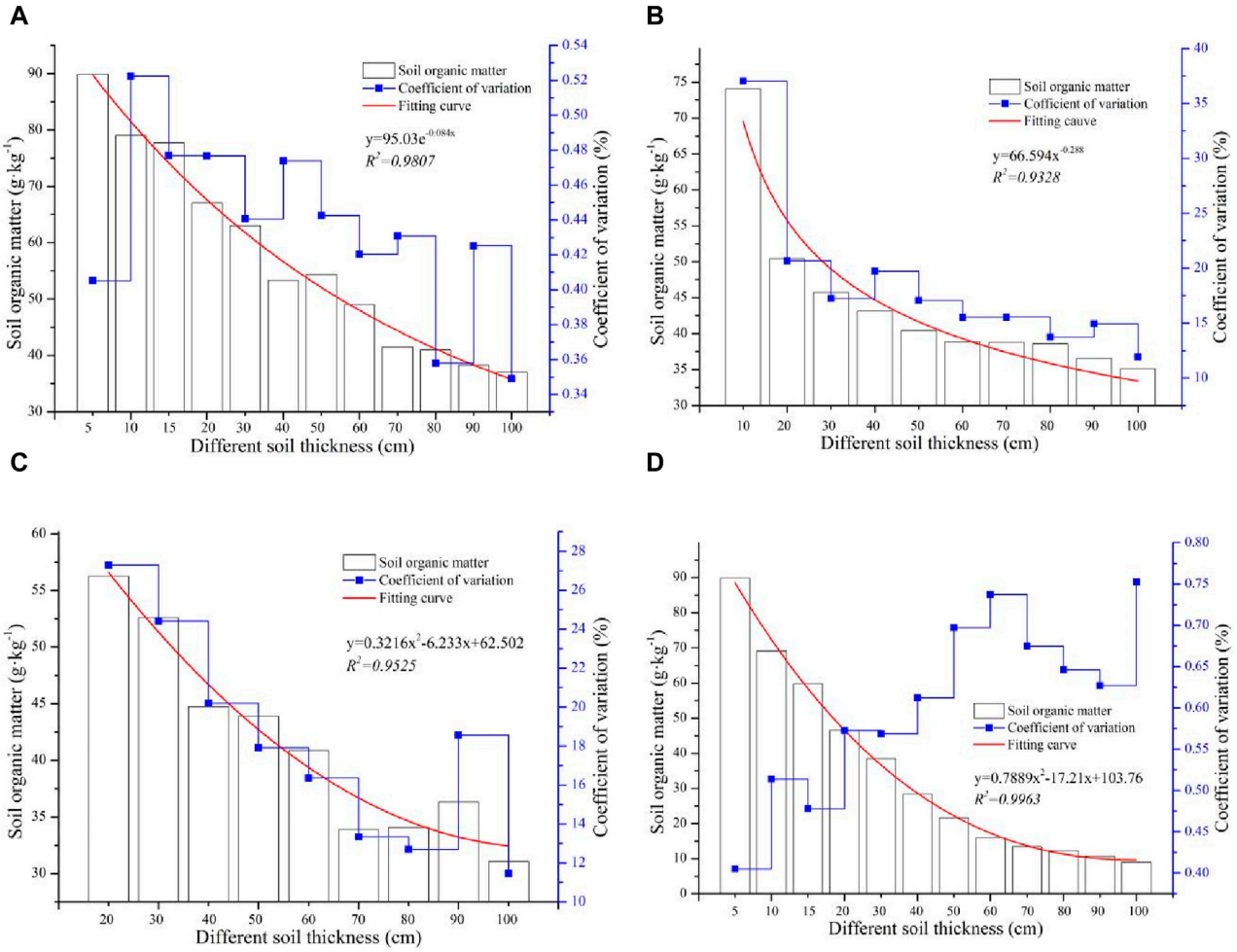

FIGURE 3
The soil thickness effects of the SOM concentration: **(A)** the SOM in the 5 cm surface soil layer at different soil thicknesses, **(B)** the SOM in the 10 cm upper soil layer at different soil thicknesses, **(C)** the SOM in the 20 cm upper soil layer at different soil thicknesses, and **(D)** the SOM in the subsoil layer at different soil thicknesses.

among the different soil thickness levels. In addition, the change in SOM in the topsoil layer at each soil thickness level was highly variable except at the 80 cm and 100 cm soil thickness levels. The change trend of SOM at different soil thickness levels fit an exponential function curve ($y = 95.03e^{-0.084x}$, $R^2 = 0.9807$) (Figure 3A). In the 10 cm soil layer, the SOM concentration gradually decreased with increasing soil thickness. However, the average SOM concentration at the 10 cm soil thickness level was much greater than that at the other soil thickness levels, and the largest value of SOM was 2.11 times the lowest value. There was little difference in SOM at different soil thicknesses from 20 cm to 100 cm, and the SOM concentration at different soil thickness levels fit a power function curve ($y = 66.59x^{-0.288}$, $R^2 = 0.9328$). Only the coefficient of variation of SOM at a soil thickness level of 10 cm indicated high variation; those at soil thickness levels of 20 cm, 30 cm, 40 cm, and 50 cm indicated moderate variation, and the change in SOM at soil thickness levels from 60 cm to 100 cm indicated low variation (Figure 3B).

The distribution characteristics of the average concentration of SOM in the upper 20 cm soil layer at different soil thickness levels from 20 cm to 100 cm were similar to those in the 10 cm soil layer (Figure 3C). As the soil thickness increased, the SOM concentration decreased, and the change in SOM also decreased. The change trend of SOM at different soil thicknesses fit a polynomial function curve ($y = 0.3216x^2 - 6.233x + 62.502$, $R^2 = 0.9525$). Moreover, all the changes in SOM at different soil thickness levels exhibited low and moderate variations, which indicated that when the soil thickness was greater, the SOM was more stable. There was a significant regular distribution of SOM in the bottom soil layer at different soil thickness levels. The SOM concentration gradually decreased with increasing soil thickness, and the change trend of SOM at different soil thickness levels fit a polynomial function curve ($y = 0.7889x^2 - 17.21x + 103.76$, $R^2 = 0.9963$). The SOM concentration in the bottom soil layer at the different soil thickness levels ranged between 9.05 g kg^{-1} and 89.93 g kg^{-1}, and the maximum was approximately 10 times the minimum. In addition, the degree of change in the SOM concentration in the bottom soil layer gradually increased with increasing soil thickness, and all the coefficients of variation were highly

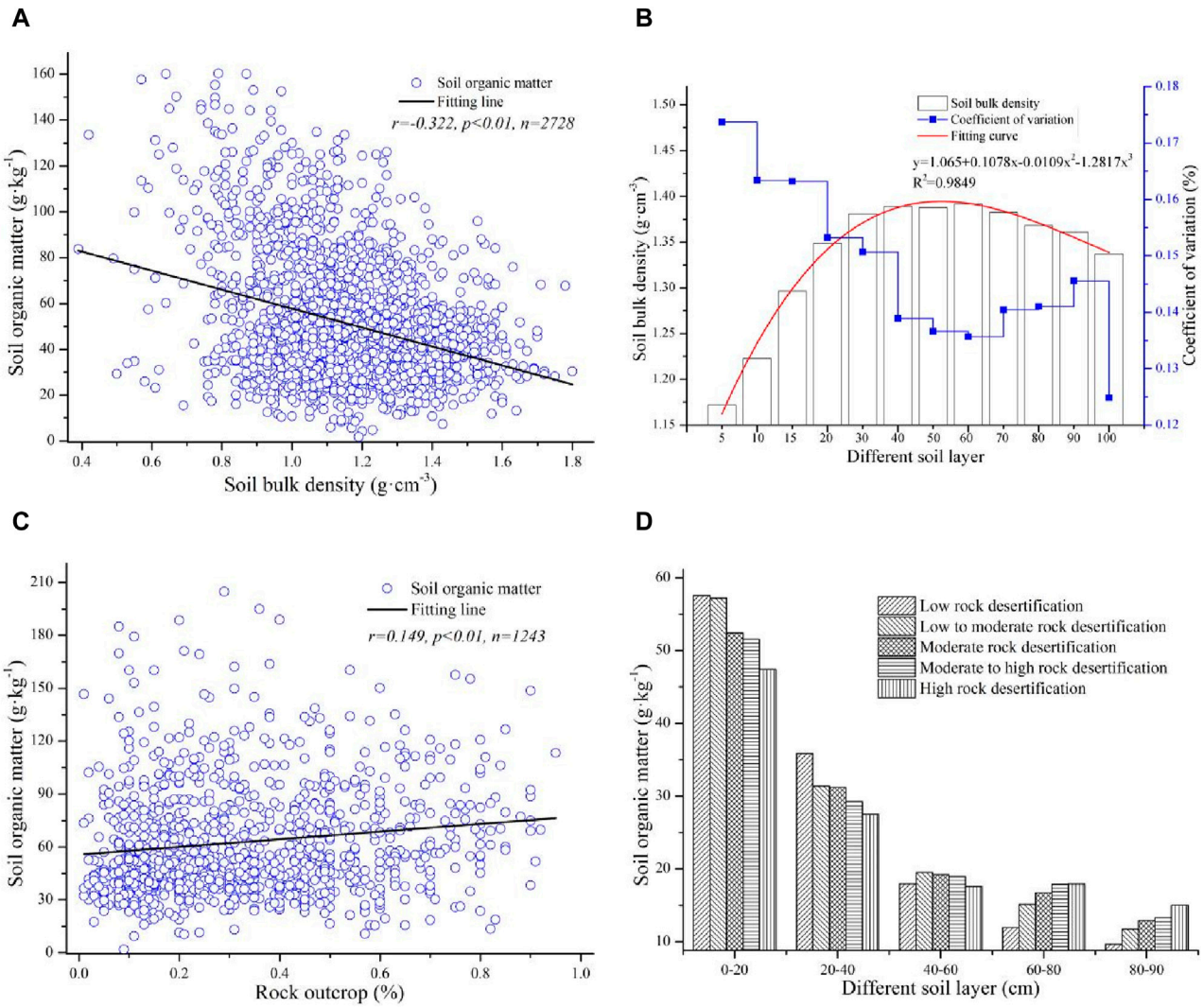

FIGURE 4
The SBD and rock outcrop affected the SOM concentration: **(A)** the relationship between SBD and SOM, **(B)** the spatial distribution of SBD in the vertical direction, **(C)** the relationship between SOM and rock outcrop, and **(D)** rocky desertification affected SOM in different soil layers.

variable (Figure 3D). This indicated a high discrepancy in SOM in the bottom soil layer at different soil thickness levels.

In summary, the soil thickness greatly influenced the SOM, and this influencing mechanism can be summarized as follows: The SOM concentration in each soil layer at the different soil thicknesses gradually decreased with increasing soil thickness, and the change in SOM in the upper soil layer gradually decreased with increasing soil thickness. However, the change in SOM in the bottom soil layer differed from that in the upper soil layer, which gradually increased with increasing soil thickness.

3.6 The spatial distribution characteristics of SOM in response to SBD and rock outcrops

The relationships between SOM and SBD and between SOM and rock outcrops were analyzed, and the results are shown in Figure 4. The large discrepancies in the SBD and rock outcrops were important properties of the soil in karst basins, and there were important factors that affected the SOM to varying degrees. The SOM and SBD were negatively correlated ($r = -0.332$, $p < 0.01$, $n = 2,728$), which indicated that the higher the SBD was, the lower the SOM (Figure 4A). Moreover, the SBD quickly increased with soil thickness in the upper 0–40 cm soil layer, there was a slight difference in the SBD in the 40–60 cm soil layer, and then the SBD gradually decreased with increasing soil thickness in the 60–100 cm soil layer. In addition, the change trend of the SBD from the surface soil layer to the bottom soil layer fit a polynomial curve ($y = 1.065 + 0.1078x - 0.0109x^2 - 1.2817x^3$, $R^2 = 0.9849$), which revealed that the effects of the SBD on the SOM mainly occurred in the upper 0–40 cm of the soil layer, and this influence in the subsoil layer was relatively lower. Furthermore, there was a large change in the SBD in the upper soil layer, and this change was relatively lower in the subsoil layer. All the coefficients of variation of the SBD in the different

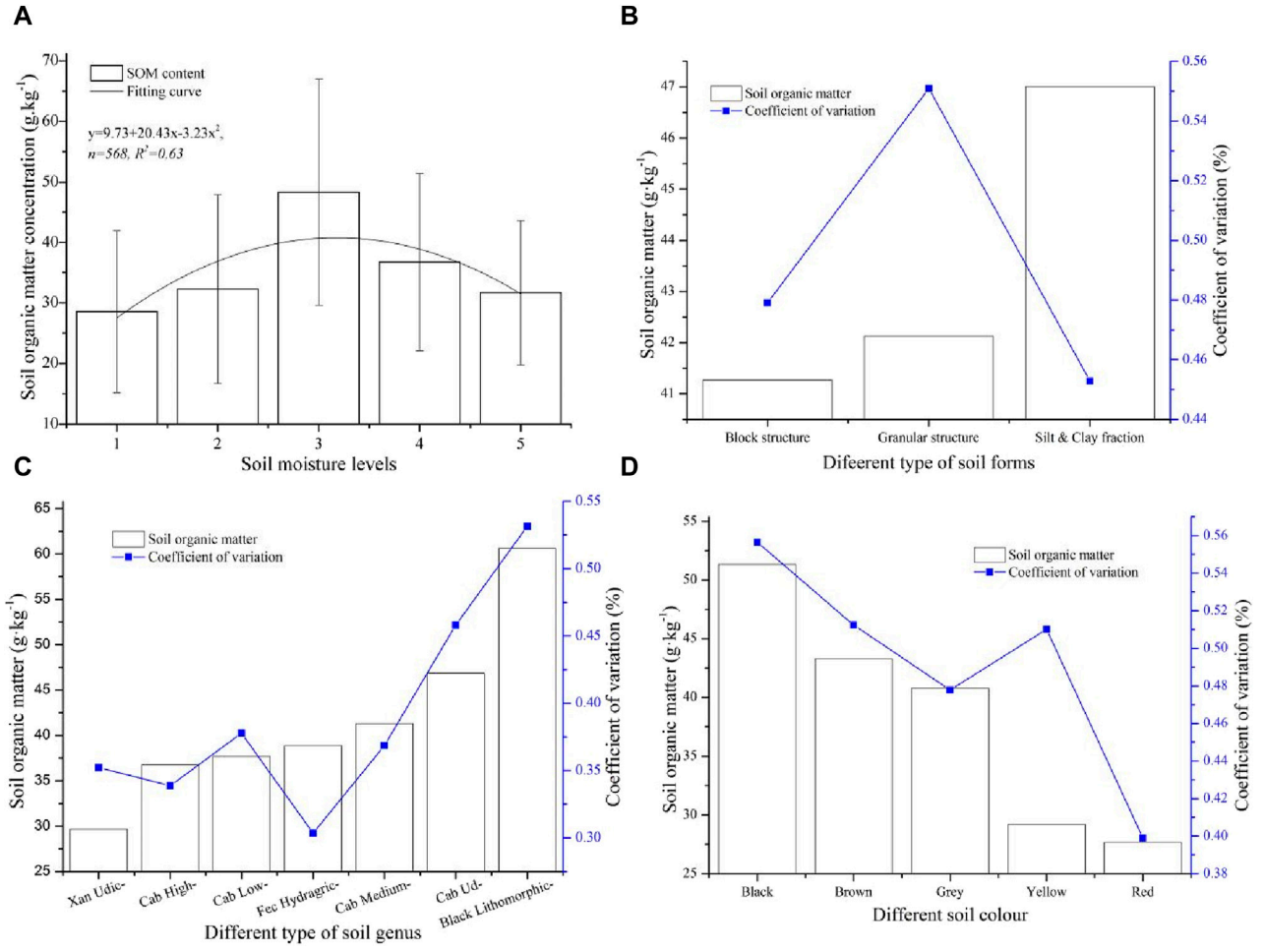

FIGURE 5
The relationship between SOM and soil properties: **(A)** the relationship between SOM and soil moisture, **(B)** the relationship between SOM and soil structures, **(C)** the relationship between SOM and soil genus, and **(D)** the relationship between SOM and soil color.

soil layers exhibited low variation, except for that in the 0–5 cm soil layer (Figure 4B).

Rock outcrops could partially promote SOM accumulation, and the relationships between the SBD and rock outcrops were positively correlated ($r = 0.194$, $p < 0.01$, $n = 1{,}243$) (Figure 4C). To further analyze the effects of rock outcrops on different soil layers, the rock outcrops were divided into different rocky desertification areas according to the rock outcrop rate, after which the changes in SOM among the different rocky desertification areas in the different soil layers were analyzed. The results showed that the SOM gradually decreased with increasing rocky desertification in the upper soil layers of 0–40 cm, and there was little change in the SOM at different rocky desertification degrees in the middle soil layer of 40–60 cm. In contrast, the SOM gradually increased with increasing rocky desertification degree, but the average value of SOM in the bottom soil layer was lower than that in the upper soil layer (Figure 4D). This indicated that lower rocky desertification mainly affected the SOM in the upper soil layer, and higher rocky desertification had a greater effect on the SOM in the subsoil layer.

3.7 The spatial distribution characteristics of SOM responded to other soil properties

Soil moisture, soil structure, soil genus, and soil color are additional important soil characteristics in karst basins. To analyze the relationship between these soil properties and SOM, the average SOM concentration in the upper 0–20 cm layer was determined under the coupling of different soil properties, and the information is listed in Figure 5. To analyze the response of the SOM concentration to soil moisture more clearly, the soil moisture was divided into five categories according to the soil moisture content, which ranged from 5.67% to 43.25%. The soil moisture had a greater effect on the SOM concentration, and there was a larger discrepancy in the SOM content at the different soil humidity levels. The lowest value of SOM occurred at a soil moisture level of 1, and the maximum value of SOM occurred at a soil moisture level of 3. The SOM concentration was between 28.56 g kg^{-1} and 48.29 g kg^{-1}, and the largest value was 1.69 times the minimum value. There was a slight difference in the SOM content at levels 2 and 5, and the SOM content at level 3 was much greater than that at the other soil moisture levels. The change trend of the SOM value coupled with the

soil moisture level fit a polynomial curve ($y = 9.73 + 20.43x - 3.23x^2$, $R^2 = 0.63$). This revealed that the effect of soil moisture on SOM mainly exists in moderately humid soil, and this influence in dry soil and wetter soil is relatively less. Furthermore, all the changes in SOM at different degrees of soil moisture were highly variable, which indicated that there was a large discrepancy in SOM with the change in soil moisture (Figure 5A). There was a significant change in the SOM in the different soil structures, and the SOM gradually increased with decreasing soil structure. The content of SOM in the different soil structures ranged between 41.27 g kg^{-1} and 47.01 g kg^{-1}, and its coefficient of variation ranged between 0.45 and 0.55. The SOM concentrations in the block structure and granular structure were relatively lower, and the difference in SOM in the two soil structures was also smaller. The SOM content in the soil structure of the silt and clay fraction was the highest, and its change was the lowest (Figure 5B). Thus, the smaller the soil structure was, the more easily the accumulation of SOM was promoted, and the SOM accumulation was relatively stable.

The descending order of SOM in the upper soil layer at 0–20 cm in the different soil types was *Black Lithomorphic Isohumisols* (Black Lithomorphic) > *Cab Udi Orthic Entisols* (Cab Udi) > *Cab Medium Fertility Orthic Anthrosols* (Cab Medium) > *Fec Hydragric Anthrosols* (Fec Hydragric) > *Cab Low Fertility Orthic Anthrosols* (Cab Low) > *Cab High Fertility Orthic Anthrosols* (Cab High) > *Xan Udic Fernalisols* (Xan Udic), and their average values were 29.67 g kg^{-1}, 36.75 g kg^{-1}, 37.67 g kg^{-1}, 38.85 g kg^{-1}, 41.32 g kg^{-1}, 46.86 g kg^{-1}, and 60.64 g kg^{-1}, respectively. The SOM gradually increased from Cab High to Cab Udi, and there were smaller differences in the SOM values among them. Moreover, the SOM values in Black Lithomorphic soil were greater than those in the other soils, and the values in Xan Udic soil were lower than those in the other soil types. In addition, there was a regular distribution of the coefficient of variation for SOM changes in different soil types, which was similar to the change trend of SOM content in different soil types. In general, the higher the SOM content was, the greater the coefficient of variation in the different soil types. The changes in SOM in the Xan Udic, Cab High, and Fec Hydragric soils exhibited moderate variation, and those in the Black Lithomorphic, Cab Udi, Cab Medium, and Cab High soils exhibited high variation (Figure 5C). This indicated that the SOM in calcareous soil was generally greater than that in other soils. The descending order of SOM in the different soil colors was black > brown > gray > yellow > red, and the SOM content ranged between 27.67 g kg^{-1} and 51.32 g kg^{-1}. The concentration of SOM in the different soil colors could be divided into three different levels. The SOM content in the black soil was the highest, the SOM content in the brown and gray soils was the second highest, and the SOM content in the yellow and red soils was the third highest. There were smaller differences in SOM at the second level, and these differences at the third level were similar. Furthermore, there was a greater discrepancy in SOM at different levels, and the change presented a significant ladder. The coefficient of variation of SOM in different soil colors gradually decreased with decreasing SOM content, but all the coefficients of variation were highly variable (Figure 5D). Obviously, the SOM in dark-colored soil was generally greater than that in bright-colored soil, and the degree of change in SOM in dark-colored soil was also relatively greater.

4 Discussion

4.1 Coupling mechanism between soil properties and soil animals in the karst plateau basin

According to the information in Figure 2, which indicates that the relationship between SOM and soil animals is positively correlated, the number of soil animals and the species of soil animals can partially promote the accumulation of organic matter in soil. The many soil animal species in karst basins can be divided into different animal orders, classes, and phyla; this information is listed in Table 2. There is a larger discrepancy in the spatial distribution characteristics of soil animals in karst basins, which results in the spatial heterogeneity of soil animals in karst basins being more complex. Because the ecological environment in karst regions is more fragmented, the coupling mechanism between soil animals and different soil properties is more complex. Therefore, to research the relationship between SOM and soil animals, the spatial distribution characteristics of soil animals impacted by different soil properties must be investigated. The relationships between the soil animals and soil properties are listed in Figure 6.

Soil thickness is an important soil property; it is a site where energy and matter are stored and translated, which is the basis of sustainable development (Keesstra et al., 2018; Visser et al., 2019). The soil layer in the center of the intersection of the lithosphere, biosphere, hydrosphere, and atmosphere is an important reservoir of organic matter (Hobley et al., 2014). Moreover, the soil layer is an important habitat for organisms, and changes in the soil environment may influence species structure and number. Soil thickness significantly impacts soil animals; the thicker the soil is, the more soil animal species there are. In addition, thicker soil can promote the structural stability of living soil because the coefficient of variation of species diversity tends to gradually decrease with increasing soil thickness. Then, the species diversity gradually increased with soil thickness, and the change fit a polynomial formula curve ($y = 2.6760.16x - 0.02x^2 - 0.95x3$, $R^2 = 0.861$) (Figure 6A). The main range of SBD values in the karst basin was between 0.8 and 1.6, and the SBD in this range was 94.59%. The relationship between soil animals and SBD fits a polynomial formula curve ($y = 0.93x^2 + 1.95x + 2.19$, $R^2 = 0.786$). The species diversity index gradually increased with increasing SBD before the top site, and then, the species index gradually decreased with increasing SBD (Figure 6B). This indicated that a moderate range of SBD is an advantage for soil animal survival, and both too-high and too-low SBDs are not good environments for organisms living in soil. This can further influence the spatial distribution characteristics of SOM.

There was a significant regular distribution of soil species diversity under the impact of rocky desertification, which showed that the species diversity index increased from low rocky desertification to low–moderate rocky desertification, after which the species diversity in the soil quickly decreased with increasing rocky desertification. This trend in soil species diversity was coupled with the change in rocky desertification, which fit a curve of the Gauss formula ($y = 2.67+(2.02\cdot\mathrm{sqrt}\ (PI/2))\cdot e^{(-2((x-1.64)/2.02)2)}$, $R^2 = 0.998$). In addition, the change in species diversity in soil gradually increased with rocky desertification in general, and the

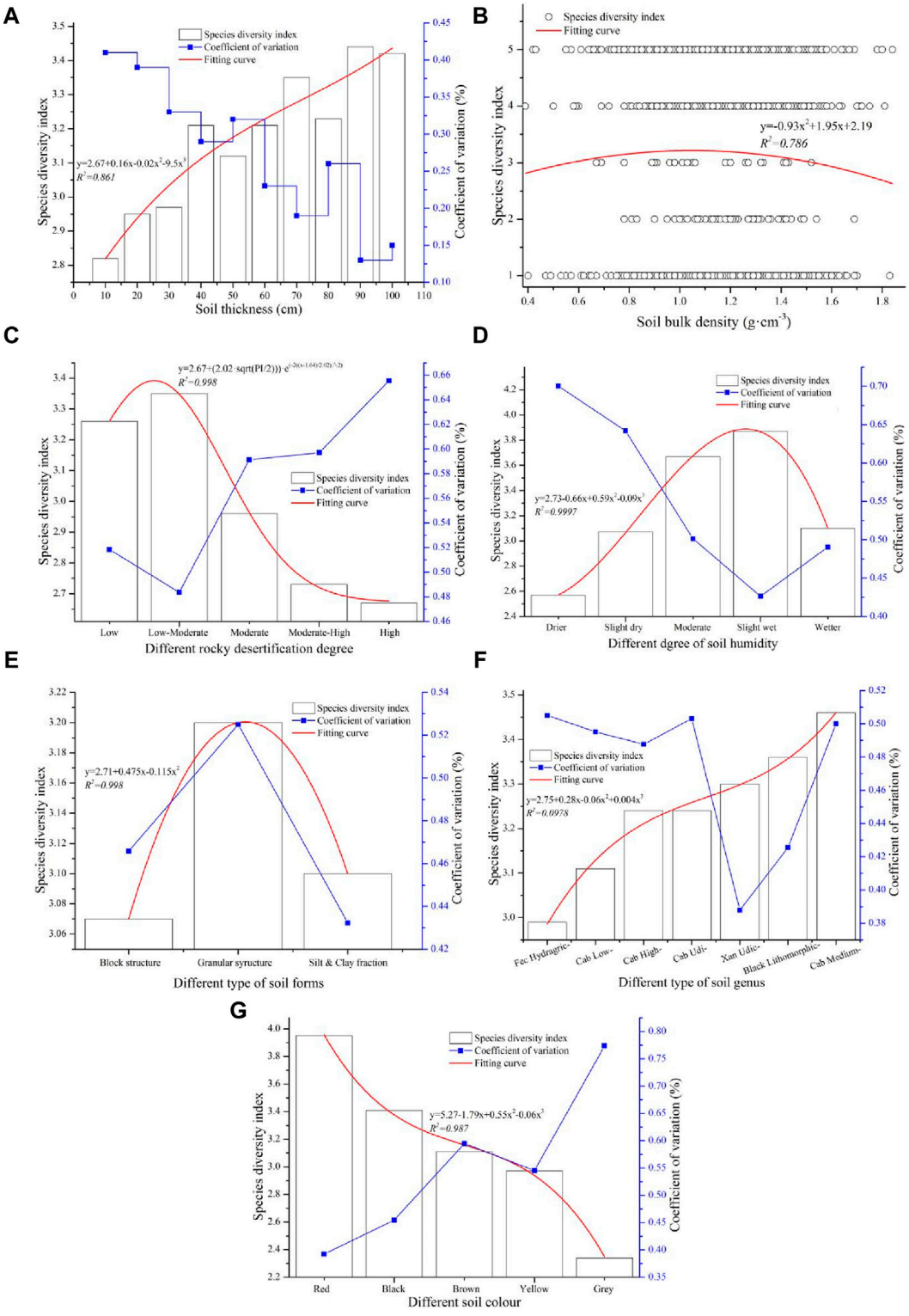

FIGURE 6
The relationship between soil animals and soil properties: **(A)** the relationship between soil animals and soil thickness, **(B)** the relationship between soil animals and SBD, **(C)** the relationship between soil animals and rocky desertification, **(D)** the relationship between soil animals and soil humidity, **(E)** the relationship between soil animals and soil structures, **(F)** the relationship between soil animals and soil types, and **(G)** the relationship between soil animals and soil color.

coefficients of variation of the species diversity index at low and low–moderate levels of rocky desertification were relatively lower than those at other degrees of rocky desertification. However, all the degrees of change in soil species diversity at different levels of rocky desertification were highly variable (Figure 6C), which indicated that low and moderate levels of rocky desertification could promote soil living, and there was a large discrepancy in the number of animal species in the soil.

The main soil dry humidity conditions in the karst basin include moderate, slightly wet, and slightly dry conditions, and drier soil is relatively less abundant. At first, the soil species diversity gradually increased with soil humidity until the soil humidity level was slightly wet, and then the species diversity quickly decreased with increasing soil humidity. The change trend of soil species diversity under the coupling of soil dry humidity fits a polynomial formula curve ($y = 2.73 - 0.66x + 0.59x^2 - 0.09x^3$, $R^2 = 0.9997$). Furthermore, the coefficient of variation of soil species diversity in the karst basin gradually decreased with soil humidity in general, but all the changes in species diversity at different soil humidities exhibited high variation (Figure 6D). This indicated that moderate and slight degrees of soil humidity are beneficial to soil life, and drier and wetter levels of soil humidity are not favorable sites for different soil animals. In addition, the main soil animals in wetter soil were *Annelida*, such as earthworms. The soil species diversity index in the granular structure of the soil in the karst basin was the largest, followed by that in the block structure, and the soil species diversity in the granular structure was significantly greater than that in the other soil structures. The regular distribution of soil species diversity from a larger structure to a smaller structure of soil fit a polynomial formula curve ($y = 2.71 + 0.48x - 0.12x^2$, $R^2 = 0.998$), and the coefficient of variation of soil species diversity in the granular structure was the highest (Figure 6E). This revealed that the granular structure of soil is an advantage for the survival of living organisms in soil, and there is a large discrepancy in soil species diversity among different soil structures.

The difference in soil species diversity among the different soil types was not large, and the species diversity indices among the different soil types ranged between 2.99 and 3.46. The descending order of species diversity in the different soil types was Cab Medium > Black Lithomorphic > Xan Udic > Cab Udi > Cab High > Cab Low > Fec Hydragric. According to the order of the different soil types, the relationships between the soil types and the species diversity indices of the soil animals fit a polynomial curve ($y = 2.75 + 0.28x - 0.06x^2 + 0.04x^3$, $R^2 = 0.978$). In summary, the species diversity in calcareous soil was greater than that in loamy soil, and all the changes in species diversity exhibited high variation among the different soil types (Figure 6F). This indicated that there is no significant regular distribution of soil animals in different soil types, and there is a slight trend that the soil animals in black limestone soil and yellow limestone are relatively more prevalent than in other soils. There was a great difference in species diversity among the different soil colors, and the species diversity indices under the different soil colors ranged between 2.34 and 3.95. The largest species diversity index value was in red soil, the lowest was in gray soil, and the change trend fit a polynomial curve ($y = 5.27 - 1.79x + 0.55x^2 - 0.06x^3$, $R^2 = 0.987$). The trend of the coefficient of variation of species diversity in different soil colors was the opposite of the change in species diversity in different soil colors; the species diversity in red soil was the highest, but the change was the lowest, and the opposite was the case in gray soil (Figure 6G). In summary, the qualities of soils with bright colors can promote soil life more than the qualities of soils of other colors. The abundance of organisms in gray soil is lower, which may be the result of gray soil having properties similar to those of limestone bedrock.

4.2 Relationships among SOM, soil animals, and land use in the karst plateau basin

Because of the main distribution of soil animals in surface soil layers (Li X. D. et al., 2020), the relationships among SOM, soil animals, and land use changes are discussed mainly for the 0–20 cm soil layer. According to the information from Tables 2, 3 and Figures 1, 2, the distribution characteristics of SOM in different land uses showed a regular stepwise decrease. Among them, forestland was at the first level, significantly higher than other land uses, followed by grassland and barren land, and cultivated land and garden land were at the third level. This was because the SOM concentrations in the soil samples containing animals are generally greater than those in the soil without soil animals (Figure 2A). Moreover, the soil animal diversity of forestland, barren land, and grassland is generally greater than that of garden land and cultivated land. The diversity forestland and cultivated land are significantly greater and less than those of other land uses, respectively (Figure 7A). This result is similar to that of Lu et al.'s research, which showed a significant correlation between soil animals and SOM ($p < 0.01$), and the SOM concentration increases with the increasing number of soil animal species (Lu et al., 2016). In addition, the microtopography of stone basins, stone grooves, stone crevices, etc., is widely distributed in barren land grasslands, and humus is generally intercepted in these microtopographies (Huang et al., 2018; Wang et al., 2022). In forestland, there is an abundant SOM resource, and the surface soil is not washed by rainfall because of the buffering effect of tree crowns (Wang et al., 2022). According to Figure 2B, the SOM concentrations in the 0–20 cm layer of soil with *Agrotis segetum* are greater than those in the soil with other soil animals (Figure 7B). Moreover, the average numbers of *Agrotis segetum* in barren land and grassland are much greater than those in other land uses. The SOM concentrations in cultivated land and garden land are lower than those in other land uses, but their earthworm numbers are generally high (Figure 7C). This is because earthworms positively or negatively affect SOM. They can promote the accumulation and decomposition of humus and SOM (Crowther et al., 2014; Kang and Wu, 2021). Although earthworms are considered major soil animals that affect SOM conversion, it is unclear how much and how quickly they can protect SOM content (Shan et al., 2013; Tu et al., 2020). In addition, cultivated land, including paddy fields and dry land, is more disturbed by productive activities, resulting in easier loss of SOM (Wang et al., 2022; Gao et al., 2023). According to the relationships between land use types, soil animals can be summarized as two loop lines, Line A and Line B, in the karst basin area. Among these factors, land use is crucial in the cyclical process. In line A, land use affects the soil animal species and subsequently affects the SOM distribution. In line B, the distribution characteristics of SOM in the different land use types greatly differ in

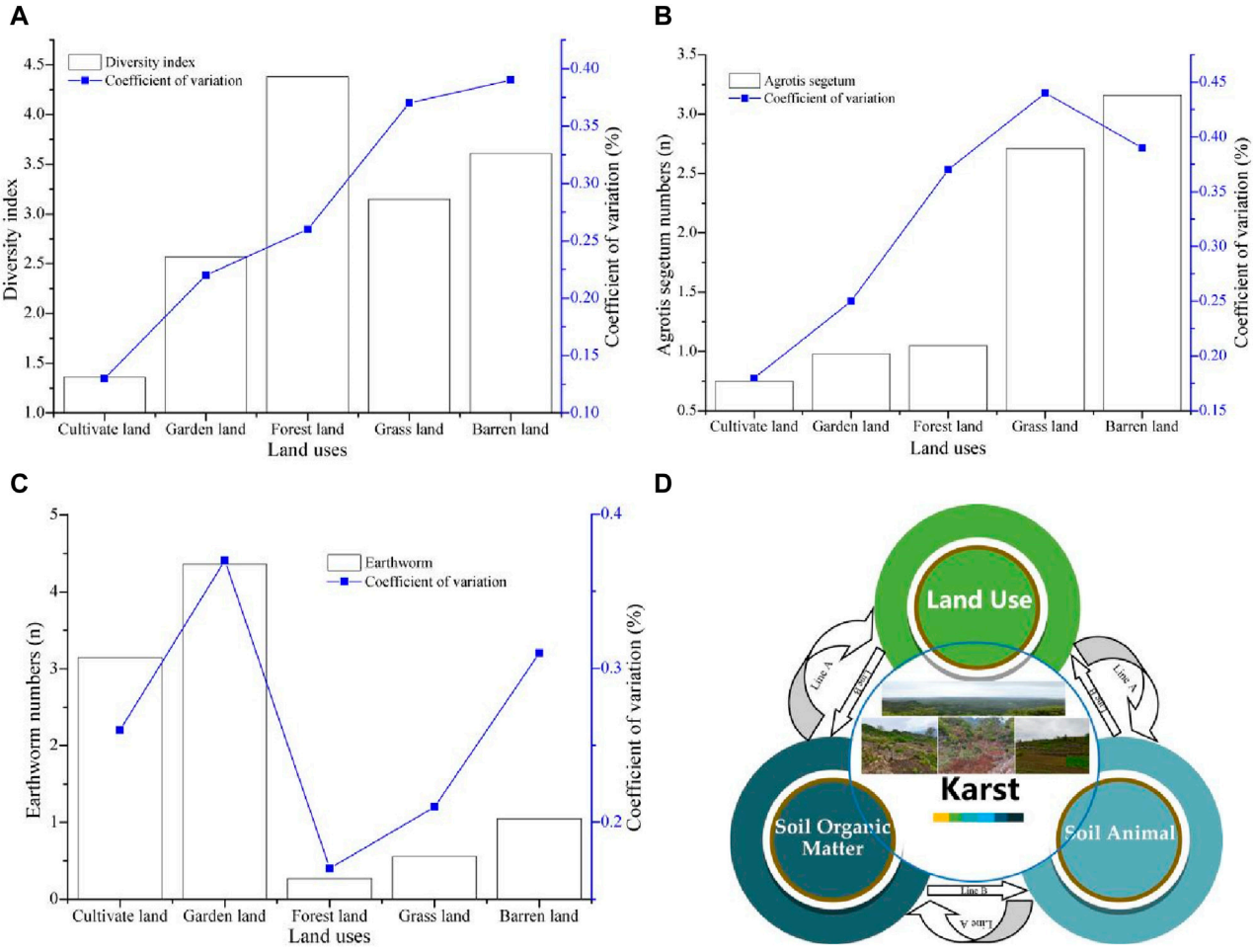

FIGURE 7
The relationship between SOM, soil animals, and land use: **(A)** the relationship between soil animals and land use; **(B, C)** the relationship between *Agrotis segetum* and land use and earthworms and land use; **(D)** the relationship cycle of land use, soil animals, and soil organic matter in karst.

all the soil layers, which further affects the spatial distribution of the number of soil animals in the different soil layers (Figure 7D). For these reasons, the SOM concentrations in those land use types are greater than those in other land use types. However, the SOM concentrations in cultivated land and garden land are relatively low, but the distribution of SOM is more uniform. In summary, the coupling mechanism among land use, soil animals, and SOM in karst areas is complex, and there are multiple relationships among them. Their relationships show not only positive promotion but also negative restraint. A good land type may increase the number and abundance of soil animal species and SOM. However, microtopography, such as stone grooves and stone crevices, can affect the restructuring of the spatial distribution of SOM in karst basin areas (Huang et al., 2018; Zhang et al., 2019).

4.3 Major factors impacting soil animals in the karst plateau basin

Figures 2, 3, 6 show the complexity of the relationships between SOM, soil animals, and different influencing factors. The distribution characteristics of each impact factor in the karst plateau basin are also complex, which means the multiple factors influencing the SOM in the karst plateau basin are complicated (Zhang et al., 2019; Wang et al., 2022). To more accurately analyze the response model of factors that affect soil animals, the key factors in karst plateau basins should be discussed (Huang et al., 2018; Zhang et al., 2019). The dimensions of the multiple factors were reduced using PCA via SPSS software (Table 4).

The first three principal components represented 82.063% of the correlation between different factors. The contribution rates of the first, second, and third principal components were 49.778%, 17.162%, and 15.123%, respectively. Among those impact factors, soil thickness and soil humidity had high positive loads on the first principal axis, and soil structure and SBD had high positive loads on the second principal axis; however, the rock outcrop and soil type had high negative loads on the third principal axis. These factors were critical on each principal axis, which revealed two positive alliance models—soil thickness-soil humidity and soil structure-SBD—and a negative alliance of rock outcrop-soil type that has a greater influence on soil animals in the karst plateau basin. According to the RDA results, the major positive impact factors of soil animal diversity mostly include soil thickness, soil

TABLE 4 Principal component analysis (PCA) of environmental factors via the maximum variance method.

Factors	First principal component	Second principal component	Third principal component
SBD	−0.160	0.430	0.048
Soil color	−0.028	0.068	−0.105
Rock outcrop	−0.459	−0.021	−0.392
Soil genus	−0.042	0.235	−0.218
Soil structure	0.120	0.868	−0.015
Soil humidity	0.236	0.122	0.042
Soil thickness	0.991	−0.050	−0.118
Contribution rate of variance (%)	49.778	17.162	15.123
Accumulate contribution rate (%)	49.778	66.940	82.063

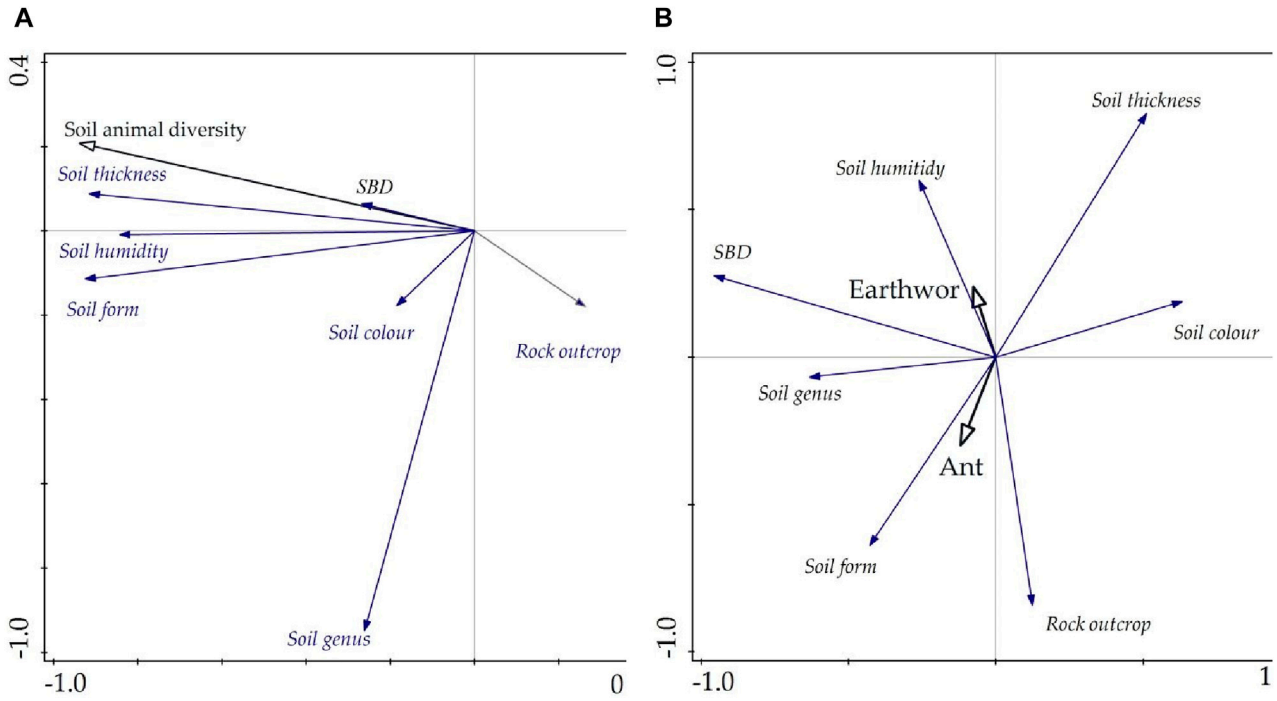

FIGURE 8
The key impact factors of soil animals: **(A)** soil animal diversity in response to different factors in all samples and **(B)** the dominant species response to different factors.

humidity, and soil form, and the negative impact factor is rock outcrops (Figure 8A). The dominant species of soil animals in the study area are ants and earthworms. Among them, soil form positively influences ants, and soil humidity positively affects earthworms (Figure 8B). These results were consistent with those of Han et al. and Ye et al., who reported that the soil animal community positively responds to soil humidity, and the relationship between SOM and soil animals exhibits a significant positive correlation (Han et al., 2017; Ye et al., 2019). Zhang et al. noted that soil moisture has a significant control effect on earthworm reproduction (Zhang X. H. et al., 2020). In summary, the soil animal community was positively influenced by soil thickness, soil humidity, and soil form and negatively influenced by rock outcrop cover. In addition, the dominant species affecting the spatial distribution of SOM are ants and earthworms, which are impacted to a greater degree by soil form and soil humidity, respectively.

4.4 Reliability of SOM assessment under the influence of soil animals in the karst plateau basin

Soil animals are an important component of the soil ecological system and affect the translation of nutrients and energy in soil. Soil animals are often treated as mini-pulverizers of litterfall that can impact the conversion of SOM and the formation of humus. The comprehensive interaction between soil animals and soil

microorganisms can stimulate the activity of soil enzymes and promote the decomposition of soil humus (Dong et al., 2016). The activities of soil animals can improve soil air permeability, soil structure, and soil fertility. For example, ants and earthworms burrow, nest, and obtain food in soil and can mix different soil layers that increase soil porosity, reduce SBD, improve soil aggregation, and promote soil nutrient cycling (Mbau et al., 2015). In addition, soil animal feces and exudation can increase the effectiveness of soil nutrients, influencing the spatial distribution characteristics of SOM in profiled soil and simultaneously impacting soil properties in direct and indirect ways (Frouz et al., 2008; Dong et al., 2016). Figure 7 shows that soil properties promote an increase in soil animals, which indicates a synergistic effect between soil animals and soil properties. The soil thickness, SBD, rock outcrop, soil structure, and soil humidity are particularly important factors affecting soil animals, and there is a significant regular distribution between soil animals under the coupling of these soil properties. There is a significant correlation between soil animals and soil properties in karst basins, and the interaction is similar to the findings of Frouz et al. (2008) and Mbau et al. (2015). Moreover, based on Figure 2, the organic matter in soil with soil animals was generally greater than that in soil with no soil animals, and the coupling mechanism was consistent with the work by Dong et al. (2016). In addition, soil properties are impacted by the synergism between different soil animals and other factors in general, and different soil animals affect SOM in different ways (Wright and Covich, 2005). The organic matter in soil with earthworms (phylum *Annelida*) is much greater than that in soil with other soil animals (Figure 2C), which is consistent with the results of Kisand and Tanmmert (2000), Scullion and Malik (2000), and Bradford et al. (2002). Furthermore, soil species diversity can partially promote soil quality, and the higher the species diversity index is, the better the soil structure (Figure 6E), which is consistent with the results of Berg and Mcclaugherty (2013). According to the information in Figure 3D, species diversity is a major factor promoting SOM; the higher the species diversity index is, the greater the SOM value, and the regular relationship between species diversity and SOM is consistent with studies by BjΦrnlund and Christensen (2005), and Wang et al., (2009).

In summary, there is a significant correlation between soil animals, soil properties and SOM, and soil animals not only impact different soil properties but also influence SOM. Moreover, the soil thickness, SBD, rock outcrop, soil humidity, and soil aggregates are important soil properties in karst basins (Huang et al., 2018; Li et al., 2019; Zhang et al., 2019), and the regular relationships between soil animals and SOM in karst basins are obvious. Thus, soil animal distribution characteristics are important factors that affect SOM in karst basins, and the mechanism of SOM distribution under the coupling of soil animals is partially reliable.

5 Conclusion

The average concentration of soil organic matter (SOM) in the Puding Basin varies between 9.23 g kg^{-1} and 59.39 g kg^{-1} across the different land uses and is ranked in descending order as follows: forestland, grassland, barren land, cultivated land, and garden land. The SOM distribution in the upper soil layers is more pronounced than that in the subsoil layers, with a notable change at a depth of approximately 60 cm. Soils containing soil animals generally have higher SOM concentrations than those without. Higher SOM levels are associated with greater species diversity, and both diversity and SOM decrease with increasing soil depth. Large variability in SOM was observed under the influence of different soil animal phyla. Soils with *Annelida*, particularly earthworms, exhibited higher SOM concentrations than did the other soils. Soils with *Agrotis segetum* also have elevated SOM levels. *Annelida* greatly improved soil quality, fertility, and nutrient availability in karst basins. The major species influencing the SOM distribution were *Agrotis segetum*, which affects surface layers, and earthworms, which facilitate deeper organic matter penetration. Earthworms thrive at relatively high soil humidity and thickness but are negatively impacted by rock outcrops. The spatial distribution of soil animals is positively influenced by interactions between soil thickness, humidity, structure, and bulk density and is negatively influenced by rock outcrops and soil types. Soil animal diversity is mostly affected by soil thickness, humidity, and structure. Land use type is also crucial in influencing SOM distribution; beneficial land use increases soil animal diversity and abundance, promoting SOM accumulation. Microtopography greatly impacts SOM in karst basins by altering its spatial distribution. Overall, land use and soil animals are critical factors affecting SOM, with complex relationships influenced by spatial heterogeneity in karst environments. Therefore, more accurate methods are needed to assess SOM in these areas for further study.

Data availability statement

The original contributions presented in the study are included in the article/Supplementary Material; further inquiries can be directed to the corresponding author.

Ethics statement

The manuscript presents research on animals that do not require ethical approval for their study.

Author contributions

XW: data curation, formal analysis, funding acquisition, investigation, software, writing–original draft, and writing–review and editing. XH: conceptualization, investigation, project administration, software, and writing–review and editing. XZ: investigation, software, and writing–original draft. NW: data curation, software, and writing–original draft. ZZ: conceptualization, funding acquisition, investigation, and writing–original draft. YL: data curation, software, and writing–original draft. YH: data curation, software, and writing–original draft. JH: writing–review and editing.

Funding

The author(s) declare that financial support was received for the research, authorship, and/or publication of this article. This research was supported by the Doctoral Research Fund of Guiyang Healthcare Vocational University (No. K2023-8), the Planning

Project of Guiyang City (no. Zhukehe [2023]3-11), the Guizhou Provincial Key Technology R&D Program (QKHZC [2023]-141), the Collaborative Innovation Center of Biology and Information Technology in Karst Plateau Area of Guizhou Province (no. QJJ[2022] 010), the Central Guidance Local Science and Technology Development Fund (Qianke Zhongyin [2022] 4035), the Guiyang Science and Technology Plan Project (Zhuke Contract [2022] No. 3–7), and the Tongren City Science and Technology Support Project ([2021] No.24).

Conflict of interest

The authors declare that the research was conducted in the absence of any commercial or financial relationships that could be construed as a potential conflict of interest.

Publisher's note

Supplementary material

The Supplementary Material for this article can be found online at: https://www.frontiersin.org/articles/10.3389/fenvs.2024.1417949/full#supplementary-material

References

Aaltonen, H., Palviainen, M., Zhou, X., Köster, E., Berninger, F., Pumpanen, J., et al. (2019). Temperature sensitivity of soil organic matter decomposition after forest fire in Canadian permafrost region. *J. Environ. Manag.* 241, 637–644. doi:10.1016/j.jenvman.2019.02.130

Berg, B., and Mcclaugherty, C. (2013). *Plant litter: decomposition, humus formation, carbon sequestration*. Berlin Heidelberg: Springer. doi:10.1007/978-3-642-38821-7

Bieluczyk, W., Asselta, F. O., Navroski, D., Júlia, B. G., Venturini, A. M., Mendes, L. W., et al. (2023). Linking above and belowground carbon sequestration, soil organic matter properties, and soil health in brazilian atlantic forest restoration. *J. Environ. Manag.* 344, 118573. doi:10.1016/j.jenvman.2023.118573

BjΦrnlund, L., and Christensen, S. (2005). How does litter quality and site heterogeneity interact on decomposer food webs of a semi-natural forest. *Soil Biol. Biochem.* 37, 203–213. doi:10.1016/j.soilbio.2004.07.030

Bradford, M. A., Jones, T. H., Bardgett, R. D., Black, H. I. J., Boag, B., Bonkowski, M., et al. (2002). Impacts of soil faunal community composition on model grassland ecosystems. *Science* 298, 615–618. doi:10.1126/science.1075805

Caspersen, J. P., Pacala, S. W., Jenkins, J. C., Hurtt, G. C., and Birdsey, R. A. (2000). Contributions of land-use history to carbon accumulation in U.S. forests. *Science* 290, 1148–1151. doi:10.1126/science.290.5494.1148

Cheshire, M. V. (1987). Soil organic matter. *Soil Sci.* 144 (4), 304–305. doi:10.1097/00010694-198710000-00011

Crowther, T. W., Maynard, D. S., Leff, J. W., Oldfield, E. E., Mcculley, R. L., Fierer, N., et al. (2014). Predicting the responsiveness of soil biodiversity to deforestation: a cross-biome study. *Glob. change Biol.* 20 (9), 2983–2994. doi:10.1111/gcb.12565

Di, X. Y., An, X. J., Dong, H., Tang, H. M., and Xiao, B. H. (2015). The distribution and evolution of soil organic matter in the Karst region, Guizhou Province, Southwestern China. *Earth Environ.* 43, 697–708. doi:10.14050/j.cnki.1672-9250.2015.06.014

Ding, G., Novak, J. M., Amarasiriwardena, D., Hunt, P. G., and Xing, B. (2002). Soil organic matter characteristics as affected by tillage management. *Soil Sci. Soc. Am. J.* 66, 421–429. doi:10.2136/sssaj2002.4210

Dong, W. H., Li, X. Q., and Song, Y. (2016). Role of soil fauna on soil organic matter formation. *Soils* 48, 211–218. doi:10.13758/j.cnki.tr.2016.02.001

Freitas, V., Babos, D. V. D., Guedes, W. N., Silva, F. P., Tozo, M. L. D. L., Martin-Neto, L., et al. (2022). "Assessing soil organic matter quality with laser-induced fluorescence (lifs) and its correlation to soil carbon stock," in Latin America Optics and Photonics (LAOP) Conference 2022, Technical Digest Series (Optica Publishing Group, 2022), ppaper W3B.5. doi:10.1364/laop.2022.w3b.5

Frouz, J., Lobinske, R., Kalcík, J., and Ali, A. (2008). Effects of the exotic crustacean, *Armadillidium vulgare* (Isopoda), and other macrofauna on organic matter dynamics in soil microcosms in a hardwood forest in central Florida. *Fla. Entomol.* 91, 328–331. doi:10.1653/0015-4040(2008)91[328:eoteca]2.0.co;2

Gao, L., Zhang, D. S., Long, H. Y., Chen, X. Y., and Lin, C. H. (2023). Characteristics and influencing factors of soil organic carbon in different land use types in Ningxia. *J. lanzhou Univ. Nat. Sci.* 59 (6), 749–758. doi:10.13885/j.issn.0455-2059.2023.06.006

Haghighi, F., Gorji, M., and Shorafa, M. (2010). A study of the effects of land use changes on soil physicalproperties and organic matter. *Land Degrad. Dev.* 26, 496–502. doi:10.1002/ldr.999

Han, H. Y., Yin, X. Q., and Kou, X. C. (2017). Community characteristics of soil fauna in the low-mountain of the Changbai mountains and its respond to the change of environmental factors. *Acta Ecol. sin.* 37, 2197–2205. doi:10.5846/stxb201511232368

Hobley, E. U., Willgoose, G. R., Frisia, S., and Jacobsen, G. (2014). Stability and storage of soil organic carbon in a heavy-textured karst soil from south-eastern Australia. *Soil Res.* 52, 476–551. doi:10.1071/SR13296

Huang, X. F., Zhou, Y. C., and Zhang, Z. M. (2018). Carbon sequestration anticipation response to land use change in a mountainous karst basin in China. *J. Environ. Manag.* 228, 40–46. doi:10.1016/j.jenvman.2018.09.017

Jurgensen, M. F., Harvey, A. E., Graham, R. T., Page-Dumroese, D. S., Tonn, J. R., Larson, M. J., et al. (1997). Impacts of timber harvesting on soil organic matter, nitrogen, productivity and health of inland Northwest forests. *For. Sci.* 43, 234–251. doi:10.1093/forestscience/43.2.234

Kaiser, K., Guggenberger, G., Haumaier, L., and Zech, W. (2002). The composition of dissolved organic matter in forest soil solutions: changes induced by seasons and passage through the mineral soil. *Org. Geochem.* 33, 307–318. doi:10.1016/S0146-6380(01)00162-0

Kang, Y. J., and Wu, H. T. (2021). Effects and mechanism of earthworms on soil organic carbon and nitrogen cycling: a review. *Soils crops* 10 (2), 150–162. doi:10.11689/j.issn.2095-2961.2021.02.004

Keesstra, S., Mol, G., Leeuw, J. D., Okx, J., Molenaar, C., Margot, D. C., et al. (2018). Soil-related sustainable development goals: four concepts to make land degradation neutrality and restoration work. *Land* 7, 133. doi:10.3390/land7040133

Kisand, V., and Tanmmert, H. (2000). Bacterioplankton strategies for leucine and glucose uptake after a cyanobacterial bloom in an eutrophic shallow lake. *Soil Biol. Biochem.* 32, 1965–1972. doi:10.1016/S0038-0717(00)00171-1

Li, D. C., Huang, J., Ma, C. B., Xue, Y. D., Gao, J. S., Wang, B. R., et al. (2020a). Soil organic matter content and its relationship with pH and bulk density in agriculture areas of China. *J. soil water conservation* 34, 252–258. doi:10.13870/j.cnki.stbcxb.2020.06.035

Li, H. W., Wang, S. J., Bai, X. Y., Cao, Y., and Wu, L. H. (2019). Spatiotemporal evolution of carbon sequestration of limestone weathering in China. *Sci. China earth Sci.* 62, 974–991. doi:10.1007/s11430-018-9324-2

Li, X. D., Jiang, Y. F., Rong, W. T., Qin, G. L., Yuan, B. D., and Qin, W. G. (2020b). The community structure and composition of soil fauna under different crops in Karst area. *J. changzhou Inst. Technol.* 33 (3), 1–6. Available at: https://czgb.cbpt.cnki.net/WKE2/WebPublication/paperDigest.aspx?paperID=700405b9-fee7-44ad-b0ef-b5932f0dd18b.

Li, Y. F., Fang, Y. Y., Hui, D. F., Tang, C. X., Van Zwieten, L., Zhou, J. S., et al. (2024). Nitrogen deposition-induced stimulation of soil heterotrophic respiration is counteracted by biochar in a subtropical forest. *Agric. For. Meteorology* 349, 109940. doi:10.1016/j.agrformet.2024.109940

Lin, Z. B., and Zhang, R. D. (2012). Dynamics of soil organic carbon under uncertain climate change and elevated atmospheric CO_2. *Pedosphere* 22, 489–496. doi:10.1016/S1002-0160(12)60033-2

Lu, S. W., Li, X. W., and Zhang, X. G. (2016). Cupressus inefficient forest in hilly area of central Sichuan basin after transformation of afforestation with gap. *Mod. Agric. Sci. Technol.* 10, 125–129. Available at: https://kns.cnki.net/kcms2/article/abstract?v=9CXCstbk-ttXWEVDbkrkigVYMAx6UpCnlYTiAwQSKuzoQs0s83R-CKD6LLh2giltVRXTolE5bd9_teDYsj_gPE73wJAhJs1SXQ8nQsSE9YOorLbPQUoDgkxtpS16QDcjSFZ9xclhpa0xidqtiZNVzA==&uniplatform=NZKPT&language=CHS.

Mbau, S. K., Karanja, N., and Ayuke, F. (2015). Short-term influence of compost application on maize yield, soil macrofauna diversity and abundance in nutrient deficient soils of Kakamega County, Kenya. *Plant Soil* 387 (1-2), 379–394. doi:10.1007/s11104-014-2305-4

Mcdonagh, J. F., Thomsen, T. B., and Magid, J. (2001). Soil organic matter decline and compositional change associated with cereal cropping in southern Tanzania. *Land Degrad. Dev.* 12, 13–26. doi:10.1002/ldr.419

Niu, X., Gao, P., Li, Y. X., and Li, X. (2015). Impact of different afforestation systems on soil organic carbon distribution characteristics of limestone mountains. *Pol. J. Environ. Stud.* 24, 2543–2552. doi:10.15244/pjoes/59235

Poffenbarger, H., Olk, D. C., Cambardella, C., Kersey, J., Castellano, M. J., Mallarino, A., et al. (2020). Whole-profile soil organic matter content, composition, and stability under cropping systems that differ in belowground inputs. *Agric. Ecosyst. Environ.* 291, 106810. doi:10.1016/j.agee.2019.106810

Pouyat, T. R., Grofman, P., Yesilonis, I., and Hernandez, L. (2002). Soil carbon pools and fluxes in urban ecosystems. *Environ. Pollut.* 116, S107–S118. doi:10.1016/S0269-7491(01)00263-9

Qaswar, M., Jing, H., Ahmed, W., Li, D. C., Liu, S. J., Ali, S., et al. (2019). Long-term green manure rotations improve soil biochemical properties, yield sustainability and nutrient balances in acidic paddy soil under a rice-based cropping system. *Agronomy* 9, 780. doi:10.3390/agronomy9120780

Schime, D., Melillo, J., Tian, H. Q., McGuire, A. D., Kicklighter, D., Kittel, T., et al. (2000). Contribution of increasing CO_2 and climate to carbon storage by ecosystems in the United States. *Science* 287, 2004–2006. doi:10.1126/science.287.5460.2004

Scullion, M. J. A., and Malik, A. (2000). Earthworm activity affecting organic matter, aggregation and microbial activity in soils restored after opencast mining for coal. *Soil Biol. Biochem.* 32, 119–126. doi:10.1016/S0038-0717(99)00142-X

Shan, J., Liu, J., Wang, Y. F., Yan, X. Y., Guo, H. Y., Li, X. Z., et al. (2013). Digestion and residue stabilization of bacterial and fungal cells, protein, peptidoglycan, and chitin by the geophagous earthworm Metaphire guillelmi. *Soil Biol. Biochem.* 64, 9–17. doi:10.1016/j.soilbio.2013.03.009

Shang, M. J., Zhou, Z. F., Wang, X. Y., Huang, D. H., and Zhang, S. S. (2018). Evaluation of soil environmental quality in karst mountain area based on support vector machine: a case study of a tea plantation in northern Guizhou. *Carsologica Sin.* 37, 575–583. doi:10.11932/karst20180411

Sharaya, L. S., and Van, P. S. (2022). Regular changes in soil moisture content in coniferous forests of the udyly state nature reserve, lower amur river region. *Contemp. problems Ecol.* 15 (7), 863–871. doi:10.1134/S1995425522070198

Shen, Q. X., Ran, J. C., Rong, L., Lan, H. B., Lu, C. W., and Guo, Y. L. (2009). Spatial variability of soil organic matter in maolan Karst forest. *World For. Res.* 22, 110–114. Available at: https://kns.cnki.net/kcms2/article/abstract?v=9CXCstbk-tuU31pCL7me3Cv9-eEv3ZjwbrzCwh563whb9n4U5wAQLoMt2bCVXXHj3JhY7EjTkIpq58Pu89J9G_6kq1PclChaOjO08J_7xaGmF7m9lMx9AKJTnts2WT1gOCUy3vqVeujm0jft_KrjRg==&uniplatform=NZKPT&language=CHS.

Six, J., Callewaert, P., Lenders, S., Gryze, S. D., Morris, S. J., Gregorich, E. G., et al. (2007). Measuring and understanding carbon storage in afforested soils by physical fractionation. *Soil Sci. Soc. Am. J.* 66, 1981–1987. doi:10.2136/sssaj2002.1981

Smith, P., Haberl, H., Popp, A., Erb, K., Lauk, C., Harper, R., et al. (2013). How much land-based green-house gas mitigation can be achieved without compromising food security and environmental goals. *Glob. change Biol.* 19, 2285–2302. doi:10.1111/gcb.12160

Street, L. E., Garnett, M. H., Subke, J. A., Baxter, R., and Wookey, P. A. (2020). Plant carbon allocation drives turnover of old soil organic matter in permafrost tundra soils. *Glob. change Biol.* 26, 4559–4571. doi:10.1111/gcb.15134

Tu, T. T. N., Vidal, A., Katell, Q., Mercedes, M. M., and Derenne, S. (2020). Influence of earthworms on apolar lipid features in soils after 1 year of incubation. *Biogeochemistry* 147 (3), 243–258. doi:10.1007/s10533-020-00639-w

Visser, S., Keesstra, S., Maas, G., Cleen, M. C., and Molenaar, C. (2019). Soil as a basis to create enabling conditions for transitions towards sustainable land management as a key to achieve the SDGs by 2030. *Sustainability* 11, 6792. doi:10.3390/su11236792

Wang, Q. K., Wang, S. L., Feng, Z. W., and Huang, Y. (2005). Active soil organic matter and its relationship with soil quality. *Acta Ecol. sin.* 25, 513–519. Available at: https://www.researchgate.net/publication/285838318_Active_soil_organic_matter_and_its_relationship_with_soil_quality.

Wang, S. J., Ruan, H. H., and Wang, B. (2009). Effects of soil microarthropods on plant litter decomposition across an elevation gradient in the Wuyi Mountains. *Soil Biol. Biochem.* 41 (5), 891–897. doi:10.1016/j.soilbio.2008.12.016

Wang, X. F., Huang, X. F., Hu, J. W., and Zhang, Z. M. (2020). The spatial distribution characteristics of soil organic carbon and its effects on topsoil under different karst landforms. *Int. J. Environ. Res. Public Health* 17, 2889. doi:10.3390/ijerph17082889

Wang, X. F., Huang, X. F., Xiong, K. N., Hu, J. W., Zhang, Z. M., and Zhang, J. C. (2022). Mechanism and evolution of soil organic carbon coupling with rocky desertification in South China Karst. *Forests* 13, 28. doi:10.3390/f13010028

Wang, Y. G., Li, Y., Ye, X. H., Chu, Y., and Wang, X. P. (2010). Profile storage of organic/inorganic carbon in soil: from forest to desert. *Sci. total Environ.* 408, 1925–1931. doi:10.1016/j.scitotenv.2010.01.015

Wang, Z. Q., Lin, Y. H., Cai, L., Wu, G. L., Zheng, K., Zhrng, K., et al. (2023). Substantial uncertainties in global soil organic carbon simulated by multiple terrestrial carbon cycle models. *Land Degrad. Dev.* 34, 3225–3249. doi:10.1002/ldr.4679

Weissert, L. F., Salmond, J. A., and Schwendenmann, L. (2016). Variability of soil organic carbon stocks and soil CO_2 efflux across urban land use and soil cover types. *Geoderma* 271, 80–90. doi:10.1016/j.geoderma.2016.02.014

West, T. O., and Post, W. M. (2002). Soil Organic carbon sequestration rates by tillage and crop rotation: a global data analysis. *Soil Sci. Soc. Am. J.* 66, 1930–1946. doi:10.2136/SSSAJ2002.1930

Wright, M. S., and Covich, A. P. (2005). Relative importance of bacteria and fungi in a tropical headwater stream: leaf decomposition and invertebrate feeding preference. *Microb. Ecol.* 49, 536–546. doi:10.1007/s00248-004-0052-4

Yan, J. H., Zhou, C. Y., Wen, A. B., Liu, X. Z., Chu, G. W., and Li, K. (2011). Relationship between soil organic carbon and soil bulk density in the rocky desertification process of Karst ecosystem in Guizhou. *J. Trop. subtropical Bot.* 19, 273–278. doi:10.3969/j.issn.1005-3395.2011.03.013

Yang, D. W., Kanae, S., Oki, T., Koike, T., and Musiake, K. (2010). Global potential soil erosion with reference to land use and climate changes. *Hydrol. Process.* 17, 2913–2928. doi:10.1002/hyp.1441

Ye, Y., Jiang, Y. X., and Chen, H. (2019). Responses of functional groups of large soil fauna to niche environmental factors. *Jiangsu Agric. Sci.* 47, 253–257. doi:10.15889/j.issn.1002-1302.2019.03.060

Zeng, W. H., Shi, W., Tang, Y. S., Zhen, W. Y., and Cao, K. F. (2018). Comparison of the species diversity and phylogenetic structure of tree communities in karst and non-karst mountains in Guangxi. *Acta Ecol. sin.* 38 (24), 8708–8716. doi:10.5846/stxb201808021643

Zhang, J., Wei, R., and Guo, Q. (2023a). Impacts of mining activities on the spatial distribution and source apportionment of soil organic matter in a karst farmland. *Sci. total Environ.* 882, 163627. doi:10.1016/j.scitotenv.2023.163627

Zhang, J. E., Qin, Z., and Li, Q. F. (2011a). Clustering and ordination of soil animal community under different land-use types. *Chin. J. Ecol.* 30, 2849–2856. doi:10.1097/RLU.0b013e3181f49ac7

Zhang, L., Wu, W. L., Wei, Y. P., and Hu, K. (2015). Effects of straw return and regional factors on spatio-temporal variability of soil organic matter in a high-yielding area of northern China. *Soil tillage Res.* 145, 78–86. doi:10.1016/j.still.2014.08.003

Zhang, T., Wu, X. Q., Dai, E. F., and Zhao, D. S. (2016). SOC storage and potential of grasslands from 2000 to 2012 in central and eastern Inner Mongolia, China. *J. arid land* 8, 364–374. doi:10.1007/s40333-016-0041-8

Zhang, T. Y., Hu, Y. M., Ren, X. N., Chen, F. X., and Feng, X. K. (2020a). Study on the spatiotemporial variation of soil organic matter induced by abandoned tillage behavior. *J. Agric. Resour. Environ.* 37, 805–817. doi:10.13254/j.jare.2020.0480

Zhang, W., Wang, K. L., Chen, H., He, X., and Zhang, J. (2012b). Ancillary information improves kriging on soil organic carbon data for a typical karst peak cluster depression landscape. *J. Sci. food Agric.* 92, 1094–1102. doi:10.1002/jsfa.5593

Zhang, W. J., Xu, M. G., Wang, X. J., Huang, Q. H., Nie, J., Li, Z., et al. (2012a). Effects of organic amendments on soil carbon sequestration in paddy fields of subtropical China. *J. soil sediments* 12, 457–470. doi:10.1007/s11368-011-0467-8

Zhang, X., Li, D., Liu, Y., Li, J., and Hu, H. (2023b). Soil organic matter contents modulate the effects of bacterial diversity on the carbon cycling processes. *J. Soils Sediments* 23, 911–922. doi:10.1007/s11368-022-03336-3

Zhang, X. B., Bai, X. Y., and He, X. B. (2011b). Soil creeping in the weathering crust of carbonate rocks and underground soil losses in the karst mountain areas of Southwest China. *Carbonate evaporites* 26, 149–153. doi:10.1007/s13146-011-0043-8

Zhang, X. H., Zhang, Z. S., and Wu, H. T. (2020b). Effects of ant disturbance on soil organic carbon cycle: a review. *Chin. J. Appl. Ecol.* 31, 4301–4311. doi:10.13287/j.1001-9332.202012.033

Zhang, Z. M., Zhou, Y. C., Wang, S. J., and Huang, X. F. (2019). The soil organic carbon stock and its influencing factors in a mountainous karst basin in P. R. China. *Carbonates Evaporites* 34, 1031–1043. doi:10.1007/s13146-018-0432-3

Zhou, J. S., Zhang, S. B., Hui, D. F., Vancov, T., Fang, Y. Y., Tang, C. X., et al. (2024). Pyrogenic organic matter decreases while fresh organic matter increases soil heterotrophic respiration through modifying microbial activity in a subtropical forest. *Biol. Fertil. Soils* 60, 509–524. doi:10.1007/s00374-024-01815-y

frontiers | Frontiers in Microbiology

TYPE Original Research
PUBLISHED 04 September 2024
DOI 10.3389/fmicb.2024.1463291

OPEN ACCESS

EDITED BY
Yang Yang,
Chinese Academy of Sciences (CAS), China

REVIEWED BY
Nan Ma,
Zhejiang Agriculture and Forestry University, China
Xianheng Ouyang,
Northwest A and F University, China
Liu Haitao,
Henan Agricultural University, China

*CORRESPONDENCE
Zhengxiang Wu
✉ 20131138@nynu.edu.cn

RECEIVED 11 July 2024
ACCEPTED 14 August 2024
PUBLISHED 04 September 2024

CITATION
Wu Z, Zhou Y and Wang M (2024) Spatial differentiation and influencing factors of effective phosphorus in cultivated soil in the water source area of the mid-route of South-to-North water transfer project. *Front. Microbiol.* 15:1463291. doi: 10.3389/fmicb.2024.1463291

Spatial differentiation and influencing factors of effective phosphorus in cultivated soil in the water source area of the mid-route of South-to-North water transfer project

Zhengxiang Wu[1,2,3]*, Yang Zhou[1,2,3] and Miao Wang[1,2,3]

[1]Key Laboratory of Natural Disaster and Remote Sensing of Henan Province, Nanyang Normal University, Nanyang, Henan, China, [2]Rural Revitalization Institute, Nanyang Normal University, Nanyang, Henan, China, [3]Nanyang Development Strategy Institute, Nanyang Normal University, Nanyang, Henan, China

The long-term application of phosphate fertilizers in agricultural production leads to a large accumulation of phosphorus in the soil. When it exceeds a certain limit, phosphorus will migrate to surrounding water bodies through surface runoff and other mechanisms, potentially causing environmental risks such as eutrophication of water bodies and increasing the risk of water source pollution. This study takes Shiyan City, the water resources area of the mid-route of the South-to-North Diversion Project (MSDP), as the study area. Based on 701 sampling points of topsoil, geostatistics and geodetectors were used to explore the spatial heterogeneity and influencing factors of available phosphorus (AP) in the topsoil of the area. The results show that the effective phosphorus content in the topsoil of the study area ranges from 0.30 to 146.00 mg/kg, with an average value of 14.28 mg/kg, showing strong variability characteristics. Geostatistical analysis shows that among all theoretical models, the exponential model has the best fitting effect, with a lump gold effect of 0.447 and a range of 82,000 m. The soil available phosphorus content shows an increasing trend from the Central Valley lowlands to the surrounding mountainous hills. Among them, elevation is the main controlling factor for the spatial variation of available phosphorus in the topsoil, followed by soil types, planting systems, annual precipitation, and organic matter. The non-linear enhancement or dual-factor enhancement among various environmental factors reveals the diversity and complexity of spatial heterogeneity affecting available phosphorus content in cultivated soil. This study could provide scientific references for maintaining ecological security in the water source area of the MSDP, improving the precise management of AP, and enhancing cultivated land quality.

KEYWORDS

available phosphorus, cultivated soil, spatial differentiation, geostatistics, geodetectors

1 Introduction

Available phosphorus (AP) in cultivated soil is an important factor that characterizes the abundance and deficiency of soil phosphorus nutrition and quality of the environment (Liu et al., 2022; Zhang et al., 2021). As one of the three essential nutrients for plants, phosphorus plays an irreplaceable role in their life cycle. The lack of soil AP can

limit crop growth and affect crop yield (Bieluczyk et al., 2024; Zicker et al., 2018). With the continuous improvement of land use intensity, the application of phosphorus fertilizers has become widespread in agricultural production to ensure the quality and yield of agricultural production. Compared to nitrogen and potassium, phosphorus fertilizer is easily adsorbed and converted into insoluble phosphate that is difficult for crops to absorb by the surface of soil particles or iron and aluminum oxides in the soil after being applied to the soil (Du et al., 2021). Therefore, the seasonal utilization rate of phosphorus fertilizer is low, ranging from 10 to 25% (Rowe et al., 2015). At the same time, farmers are accustomed to using phosphorus fertilizers that often exceed the actual phosphorus requirements of crops. Long-term fertilization leads to a large accumulation of phosphorus in the soil (Yang et al., 2017; Khan et al., 2018). Although phosphorus accumulation can improve the soil's phosphorus supply capacity to crops, when it exceeds a certain limit, phosphorus may migrate to surrounding water bodies through surface runoff and other mechanisms. This not only results in fertilizer wastage but also increases environmental risks, such as eutrophication of water bodies, posing significant threats to ecological health and the sustainable development of agriculture (Holger et al., 2018; Liu et al., 2016). Therefore, fully understanding the spatial layout characteristics of soil AP in regional farmland is crucial for optimizing farmland management measures, applying phosphorus fertilizers more effectively, and reducing phosphorus loss and non-point source pollution in water bodies.

The application of soil AP plays an important role in ensuring food yield increase and sustainable development of soil phosphorus fertility, which have attracted widespread attention from scholars both at home and abroad. Scholars have conducted extensive research on the spatial distribution characteristics of AP from the perspective of soil properties (Sattari et al., 2012), crop types (Lv et al., 2022), crop rotation systems (Chen et al., 2024; Lü et al., 2022), topography (Hua et al., 2020), and soil types (Bai et al., 2013; Wang et al., 2023). Some scholars have also explored the spatiotemporal evolution characteristics (Ma et al., 2016), AP enrichment effects, and potential ecological risk assessment of farmland utilization and have achieved fruitful results (Chen et al., 2022; Schoumans et al., 2015; Reijneveld et al., 2010). Most studies show that meteorological and topographic variables are the most important influencing factors on the spatial distribution of soil available phosphorus content (Hua et al., 2020; Miller et al., 2001; Cao et al., 2022). In different regions, the spatial variation of available phosphorus is closely related to soil properties and planting systems (Cao et al., 2012; Chad and James, 2019). Previous research mainly focused on certain administrative regions, crops, soil types, and land use types. There is still limited research on the spatial variation characteristics and influencing factors of soil AP in the cultivated layers of the water source area of the South-to-North Water Diversion Project (Tan et al., 2021; Wu, 2024). Previous studies have focused on describing or qualitatively analyzing the spatial differentiation of soil AP, often neglecting the exploration of interactions and the degree of influence among various factors. There has been a lack of quantitative analysis regarding these influencing factors and their interactions. Geodetectors are new statistical methods used to detect the spatial heterogeneity of events and reveal the driving factors behind them. These methods address the shortcomings of traditional approaches and provide a more comprehensive understanding of how influencing factors explain the spatial differentiation of soil nutrients.

The mid-route of the South-to-North Diversion Project (MSDP) is a strategic cross-basin water transfer project that alleviates the severe shortage of water resources in northern China (Yu et al., 2021). The water source area bears the arduous task of supplying water to the South-to-North Diversion Project, and water quality safety issues determine the success or failure of the entire project. The proportion of the agricultural population in this region is relatively high, and the vast rural areas are relatively backward, making it highly susceptible to ecological negative impacts caused by improper human development activities. It is a typical ecologically sensitive area, and the protection of the ecological environment in this region is the foundation and key measure to ensure good water quality. Based on this approach, the study uses Shiyan City, a key water source area of the MSDP, as a case area. It employs geostatistical methods to explore the spatial distribution characteristics of AP in the cultivated layers. By integrating geodetectors, the study investigates the main control factors and their interactions, aiming to reveal their inherent patterns and driving forces. The findings provide a theoretical basis for soil AP regulation and the improvement of farmland quality in the research area.

2 Materials and methods

2.1 Study area

Shiyan City is located in the northwest Hubei Province and is the core water source area of the MSDP (109°29′-111°16′E, 31°30–33°16′N) (Figure 1). It is known as the "Green Lung of Central China" and the "Water Well of North China," with an area of 23,680 km^2. This region has a northern subtropical continental monsoon climate, with an average annual temperature of 15.4°C, an average annual precipitation of 870 mm, 1,650 h of sunshine, and a frost-free period of 224 days. At an altitude of 83–2,571 m, there are over 2,000 rivers. The landform types are hills, low mountains, middle mountains, and high mountains, suitable for the growth of various water and drought crops. The farming types are mainly wheat, corn, and rice. The main planting systems include rotation, monoculture, and intercropping, and yellow-brown soil, lime soil, and paddy soil are the main soil types.

2.2 Data sources and preprocessing methods

2.2.1 Soil sample data

The soil sample data were sourced from the farmland quality survey and evaluation project in Shiyan City (Figure 1). After the autumn harvest of crops in 2020, sampling points were arranged according to the utilization conditions of cultivated land in each county and city. Five soil samples were collected from the top 0–20 cm layer using a "star" or "S" shape, according

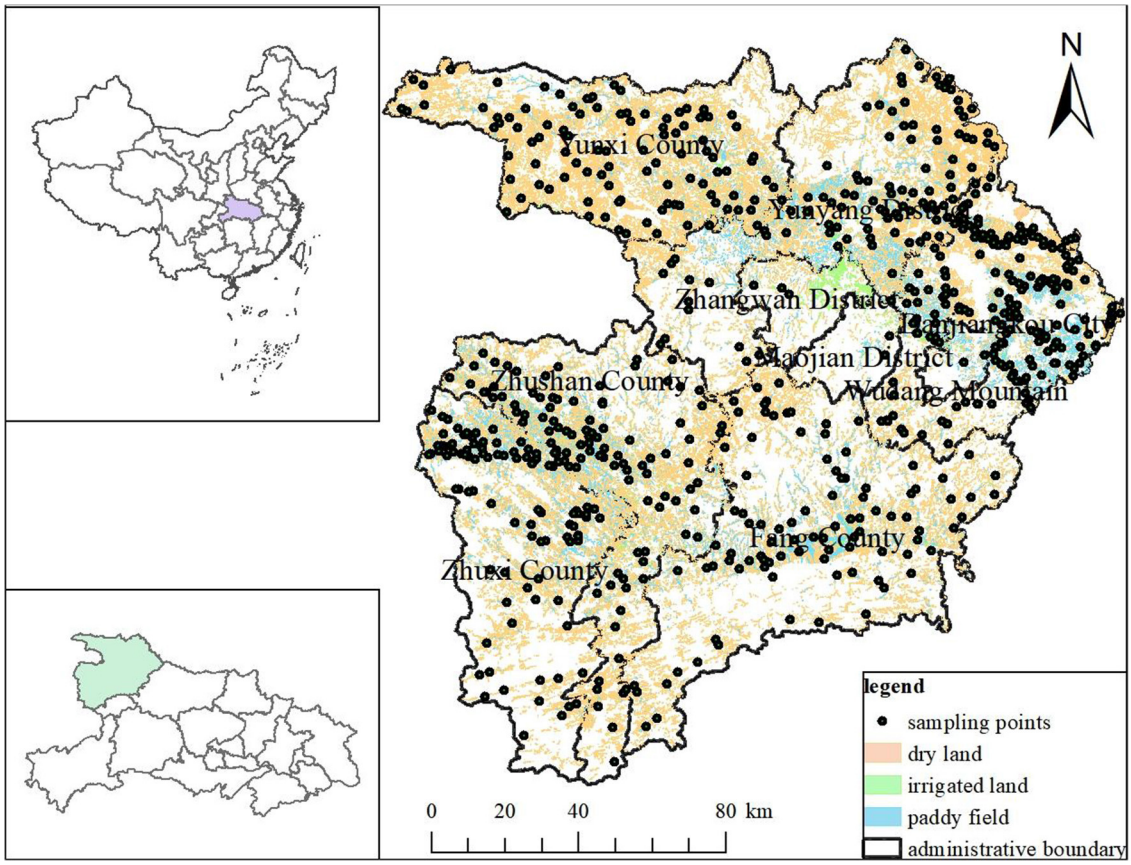

FIGURE 1
Distribution of sampling sites in the study area.

to the actual situation of the plot (Fink et al., 2016). After collection, the samples were mixed, and 1 kg was kept for further analysis. After air drying, grinding, and sieving, the soil sample was subjected to a sodium bicarbonate extraction molybdenum antimony colorimetric method to determine soil AP, a potassium dichromate volumetric method to determine soil organic matter, and a 2.5:1 soil water ratio extraction pH meter method to determine soil pH (National Agricultural Technology Extension Service Center, 2006). During sampling, GPS positioning was used to obtain the geographical location and altitude of each sampling point, and over 40 types of environmental background information were recorded and investigated, including soil parent materials, soil types, crop rotations, and land use. At the same time, geographical coordinates and altitude were recorded for each sampling point. Finally, 701 representative sample points were selected for research (Figure 1).

2.2.2 Impact factor data

Based on existing research, the impact of soil AP spatial variation is mainly concentrated in eight aspects: terrain (Liu et al., 2022, 2016; Hua et al., 2020; Li et al., 2016), climate (Liu et al., 2022), soil type (Liu et al., 2022; Khan et al., 2018; Ma et al., 2016), soil pH (Liu et al., 2022; Zhao et al., 2011), soil organic matter (Khan et al., 2018), soil parent materials (Liu et al., 2022; Hua et al., 2020), land use (Liu et al., 2022; Khan et al., 2018; Hua et al., 2020), and soil management (Liu et al., 2022; Bieluczyk et al., 2024; Khan et al., 2018; Holger et al., 2018). Based on existing achievements, this research selected the following influencing factors:

- Structural factors: elevation (Elev), slope (Slope), mean annual temperature (Mat), mean annual precipitation (Map), soil type (Soil type), soil pH (Soil pH), and soil organic matter (SOM).
- Randomness factors: land use and planting system.

The elevation and slope data were calculated using ArcGIS 10.7 using digital elevation data with a horizontal resolution of 30 on the geospatial cloud platform. Climate data were obtained from the Resource and Environmental Science and Data Center, with a resolution of 500 m × 500 m. The data on soil type, land use status, and planting system were sourced from the land parcel survey.

2.2.3 Data preprocessing

All vector data and raster data were converted to a unified projection coordinate system. According to the requirements of geographical exploration input variables, the land use data were categorized. Continuous data, including elevation, slope, temperature, and precipitation were classified into seven categories

TABLE 1 Types of interaction detection.

Judgment criteria	Interaction results
$q(X_i \cap X_j) < \text{Min}(q(X_i)), (q(X_j))$	Non-linear attenuation
$\text{Min}(q(X_i)), (q(X_j)) < q(X_i \cap X_j) < \text{Max}(q(X_i)), (q(X_j))$	Single-factor non-linear attenuation
$q(X_i \cap X_j) > \text{Max}(q(X_i)), (q(X_j))$	Dual-factor enhancement
$q(X_i \cap X_j) = (q(X_i)) + q(X_j)$	Independence
$q(X_i \cap X_j) > (q(X_i)) + q(X_j)$	Non-linear enhancement

TABLE 2 Classification standard of soil available phosphorous and frequency distribution of each class.

Grade	Range (mg/kg)	Sample size	Ratio
I (extremely rich)	>40	42	5.99%
II (rich)	20–40	100	14.27%
III (upper-middle)	10–20	176	25.11%
IV (middle-lower)	5–10	242	34.52%
V (less lacking)	3–5	100	14.27%
VI (extremely lacking)	<3	41	5.85%

using the natural breakpoint method. The semi-variance function of soil AP was fitted using GS+9.0 software.

2.3 Research methods

2.3.1 Geostatistical methods

The semi-variance function is the theoretical basis of geostatistics and is used in this study to reflect the spatial variation and correlation degree of the regionalized variable AP in the study area. The calculation formula is as follows:

$$r(h) = \frac{1}{2N(h)} \sum_{i=1}^{n} [z(x_i) - Z(x_i + i)]^2$$

2.3.2 Geodetectors

Geodetectors are new statistical methods that detect spatial differentiation of geographical phenomena and reveal their underlying driving forces. They include several key factors: factor detection, interaction detection, risk detection, and ecological detection (Chad and James, 2019). Among them, factor detection uses a q-value to measure the explanation of factor X for the spatial differentiation of attribute Y, with a range of q-values of [0, 1]. The bigger the q-value, the stronger the explanatory power of the independent variable X for attribute Y, and vice versa.

The interaction detector is used to measure whether the interaction between two influencing factors will increase or decrease the explanatory power of soil AP spatial variation. If the q-value is closer to 1, it indicates that the interaction between the two factors is more significant (Table 1). Based on the results of factor detection and interaction detection, this article identified the dominant factors and dual-factor interaction results that affect the spatial variation of soil AP in Shiyan City.

3 Results and analysis

3.1 AP descriptive statistical analysis

According to the soil AP classification method in the second soil survey, the soil AP in the study area was classified (Li et al., 2016) (Table 2), with a sample size of 5.99%, 14.27%, 25.11%, 34.52%, 14.27%, and 5.85% for levels I–VI, respectively. The AP content in the study area is concentrated in two moderate levels, accounting for 59.63% of the total. Table 3 shows that the AP content of 701 sample points in the study area ranges from 0.30 to 146.00 mg/kg, with an average value of 14.28 mg/kg. According to the AP classification of the second soil survey, the overall AP is in a moderate state, with a standard deviation of 14.96 mg/kg, reflecting the heterogeneity of the sample data. The coefficient of variation of AP is 104.76%, belonging to a strong degree of variation. The AP content changes greatly, with many extreme values and a relatively scattered distribution. In the process of soil management, targeted fertilization plans should be formulated according to local conditions and cannot be generalized.

3.2 Analysis of spatial variation structure characteristics of AP

The semi-variance function of soil AP in the study area was fitted (Table 4). The optimal model was selected based on the following criteria: maximizing the coefficient of determination (R^2) to approach 1, minimizing the residual sum of squares (RSS) to approach 0, and prioritizing the RSS value. The results show that the exponential model has the best fitting effect and can better reflect the good spatial structure of soil AP.

Spatial variation mainly includes two parts: random variation and structural variation. In Table 3, C0/(C0 + C) is referred to as the block gold coefficient, which represents the degree of spatial heterogeneity. A high ratio indicates a significant degree of spatial variation caused by random parts (Xiaolan et al., 2007). On the contrary, a higher degree of spatial variation due to spatial autocorrelation is observed. It is generally believed that variables smaller than 0.25 have strong spatial autocorrelation. Variables with moderate spatial autocorrelation have coefficients between 0.25 and 0.75. Variables above 0.75 have weak spatial autocorrelation (Cambardella et al., 1994). For such variables, the variation is mainly random, which is not suitable for using spatial interpolation methods for prediction (Goovaerts, 1999). The lump gold value (C0) of soil AP is 0.430, indicating the presence of random factors causing variation at the current sampling density. The nugget coefficient is 0.447, showing a moderate degree of spatial autocorrelation, indicating that the spatial variation of soil AP in the study area is influenced by both structural and random factors. The range of the study area is 82,000 m, with a step size of 7,050.29 m, indicating that the sampling spacing set up in the study

TABLE 3 Descriptive statistic of soil available phosphorous.

Soil property	Sample size	Minimum	Maximum	Mean	Median	Standard deviation	Skewness	Kurtosis	Coefficient of variation (%)
AP	701	0.30	146.00	14.28	9.24	14.96	0.09	15.58	104.76%

TABLE 4 Semivariogram model and its parameters of soil available phosphorous.

Theoretic models	Nugget (C_0)	Sill ($C_0 + C$)	Nugget/sill ($C_0/C_0 + C$)	Range/m	R^2	RSS
Spherical	0.001	0.675	0.001	8,600	0.296	0.0834
Exponential	0.430	0.961	0.447	82,000	0.955	7.561E-03
Gaussian	0.079	0.675	0.117	7,447	0.299	0.0832
Linear	0.517	0.797	0.649	102,458	0.874	0.0149

area is smaller than the range of soil AP, which can meet the needs of spatial variability evaluation in the study area.

3.3 AP Kriging interpolation mapping and analysis

The optimal parameters of Kriging interpolation were simulated using GS$^+$9.0 software and then input into ArcGIS 10.7. The spatial distribution map of soil AP was created using ordinary Kriging interpolation. Figure 2 shows that the distribution area of extremely rich grade areas is relatively small, mainly distributed in the southwest of Zhuxichuan County and the southeast of Fang County, with a relatively high terrain; The lack of hierarchy is mainly distributed in the faulted basin centered around the Malan River Valley in the northern part of Fang County, where the granaries are located and the terrain is relatively low. The spatial distribution of soil AP shows an increasing trend from the Central Valley lowlands to the surrounding mountainous hills, which is strongly consistent with the terrain changes in the study area (Figure 3). According to the soil AP grading standards in the second soil survey, the soil AP content in the vast majority of the study area is mainly at levels III and IV, indicating that the average level of soil AP content in the study area is moderate and can meet the requirements of crop growth.

3.4 Analysis of geodetectors

3.4.1 Factor detection analysis

The factor detector reflects the influence of geographical environmental factors on the spatial distribution pattern of soil AP and is measured by the magnitude of the *q*-value. The results show (Table 5) that the *q*-values of each influencing factor are arranged in descending order as elevation (0.1459), soil type (0.0707), planting system (0.0622), annual precipitation (0.0612), organic matter (0.0623), annual average temperature (0.0456), soil pH (0.0301), slope (0.0264), and farmland use (0.0104). Among them, the q-value of elevation is bigger than 0.1 and has the strongest explanatory power through a 1% significance test, which is the main controlling factor determining the spatial distribution pattern of AP in Shiyan City. The following factors are soil types, planting systems, annual precipitation, and organic matter. The *q*-values of other factors are relatively small and have weak explanatory power, which are secondary factors affecting the spatial heterogeneity of soil AP. Comparing the explanatory power of structural factors and random factors, it can be found that the *q*-values of structural factors such as terrain and climate factors are slightly higher than those of random factors such as planting systems and land use, indicating that structural factors have a relatively large driving force on the spatial variation of AP in cultivated land in Shiyan City, which is consistent with previous analysis.

3.4.2 Interaction detection analysis

This study used interaction detectors to analyze the degree of interaction between nine factors and the spatial distribution of soil AP content in the study area (Table 5). In terms of dual-factor interaction, both factors exhibit non-linear enhancement or dual-factor enhancement effects. The maximum interaction factor is elevation slope (0.3224), followed by elevation organic matter (0.3161), elevation planting system (0.2905), slope planting system (0.2621), and elevation soil pH (0.2604). The explanatory power of the interaction is bigger than 0.25. In terms of comprehensive interaction, the strongest is elevation synthesis (total 1.9997), followed by planting system synthesis (1.6114), slope synthesis (1.3502), annual precipitation (1.2904), organic matter (1.1830), soil type (1.1502), annual average temperature (1.1057), soil pH (1.0459), and farmland utilization (0.7151). Overall, the interaction between elevation, planting system, and slope with other factors is quite prominent, which means that areas with significant differences in elevation, planting system, and slope often have significant differences in AP. The distribution of other factors will enhance the impact of elevation, planting system, and slope on the spatial distribution of AP in the cultivated layers.

4 Discussion

To further investigate the impact of various environmental variables on the differentiation of soil AP in cultivated land in the study area, a correlation analysis was conducted between soil AP and environmental variables (Table 6). It was found that soil AP was negatively correlated with altitude, field slope, annual precipitation,

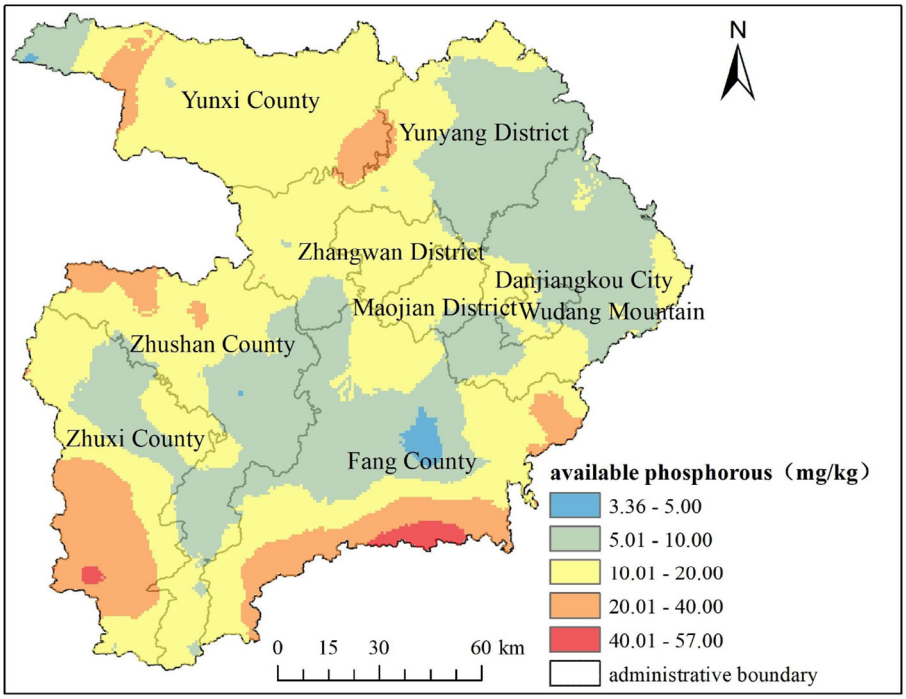

FIGURE 2
Spatial distribution of soil available phosphorous in the study area.

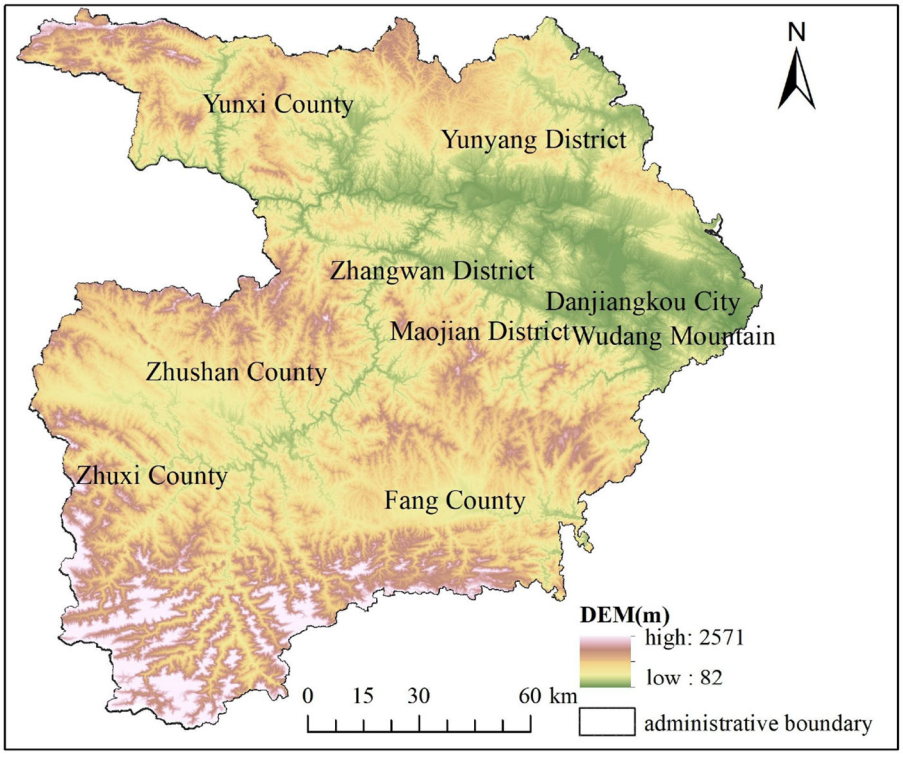

FIGURE 3
Elevation map of the research area.

TABLE 5 Geographical detection of the factors affecting the soil available phosphorous spatial variation.

Factor type	Factor detects *q*-value	Interactive detection *q*-value							
			X2	X3	X4	X5	X6	X7	X8	X9
X_1	0.1459*	0.1459								
X_2	0.0264*	0.3224#	0.0264							
X_3	0.0456*	0.2042#	0.1299#	0.0456						
X_4	0.0612*	0.2301#	0.1440#	0.1425#	0.0612					
X_5	0.0707*	0.2155	0.1943#	0.1346#	0.1537#	0.070				
X_6	0.0301*	0.2604#	0.1012#	0.1361#	0.1756#	0.1637#	0.0301			
X_7	0.0623*	0.3161#	0.1462#	0.1150#	0.1474#	0.1770#	0.1280#	0.0623		
X_8	0.0104***	0.1605#	0.0501#	0.0724#	0.0884#	0.0888#	0.0605#	0.1028#	0.0104	
X_9	0.0622*	0.2905#	0.2621#	0.1710#	0.2085#	0.1762#	0.1840#	0.2274#	0.0916#	0.0622

X1, X2, X3, X4, X5, X6, X7, X8, and X9, respectively, represent elevation, slope, mean annual temperature, mean annual precipitation, soil type, soil pH, soil organic matter, land use, and planting system; *** and * significant at the 1% and 10% levels, respectively. #Indicating non-linear enhancement.

TABLE 6 Correlation analysis of soil available phosphorous and environmental variables.

Environmental variables	pH	SOM	Map	Mat	Elev	Slope
Pearson	−0.149**	0.235**	0.179**	−0.166**	0.339**	0.089*
P-value	0.000	0.000	0.000	0.000	0.000	0.018

**At the 0.01 level (double-tailed), the correlation is significant.
*At the 0.05 level (two-tailed), the correlation is significant.

and soil organic matter content in the study area and negatively correlated with annual average temperature and soil pH.

4.1 The impact of terrain factors on AP variation

Terrain factors affect the available phosphorus content in soil by influencing water and thermal conditions and the redistribution of soil-forming materials (Li et al., 2016). Table 6 shows that the AP content in the study area is significantly positively correlated with altitude and slope. The low-value areas of AP in the research area are mainly distributed in low-terrain areas, such as the Han River and its tributaries, the Duhe River, and the Malan River valley. The terrain is relatively flat and suitable for crop cultivation, making it a concentrated production area for vegetables and grain crops. Compared to areas with higher elevations, the intensity of land development and utilization in this area is higher, resulting in significant interference from farming activities. Crops are densely planted, and the phosphorus carried away by crop growth is relatively high, resulting in lower available phosphorus content in the soil. The high-value areas are mainly distributed in the northern, central, and southern regions with high elevations and steep slopes. Due to the vertical zonality of the climate, agricultural production in this area exhibits strong seasonality and a low rate of multiple cropping. The transportation convenience is poor, and there is no comparative advantage in output level. In addition, to increase household income, a large number of young and middle-aged people in the region have migrated for work, resulting in a shortage of rural labor and leading to the abandonment of cultivated land. In Shiyan City, where the climate is characterized by favorable rainy and hot conditions, these factors facilitate self-restoration of the ecological environment of this abandoned cultivated land, resulting in a high AP content. In addition, in areas with higher elevations, the slope of sampling points is relatively gentle, making it easier for phosphorus to accumulate in the soil and increasing the available phosphorus content. Dong et al. (2016) studied the spatial distribution of available phosphorus in tea garden soil and found that the higher the terrain and the greater the slope, the higher the phosphorus content, and vice versa. Hua et al. (2020) found a positive correlation between soil AP and elevation through research, which is consistent with the results of this study. Zhao et al. (2011) found that terrain and landforms are the main structural factors affecting the spatial differentiation of soil AP, but they found a significant negative correlation between soil AP content and altitude and slope. Wang Y. H. et al. (2016) found through their research on the tobacco growing areas in northern Sichuan in southwest China that due to the loss of available phosphorus in high-altitude areas and the enrichment of available phosphorus in low-altitude areas, soil AP is negatively correlated with elevations. From this, it can be seen that the impact of terrain factors on AP is very complex, which may be caused by differences in location conditions and research scales of different research areas, and the specific reasons may need further analysis.

4.2 The impact of climate factors on AP variation

The impact of climate on soil AP is mainly reflected in two aspects: temperature and precipitation. Previous studies have shown that fluctuations in soil temperature and moisture caused

by changes in temperature and precipitation affect the conversion of phosphorus components within the soil through non-biological factors such as soil pH, nutrient content, and moisture content, as well as biological factors such as soil microorganisms and vegetation types, thereby affecting the available phosphorus content in the soil (Santos et al., 2019; Wang et al., 2019; Wu et al., 2020; Mei et al., 2019). High temperatures and precipitation make phosphorus in the soil easily weathered and released (Lin et al., 2009). Due to the influence of terrain, for every 100 m increase in altitude in the study area, the average temperature decreases by 0.55°C, and precipitation increases with altitude, with an increase of 35 mm for every 100 m increase (Wu et al., 2021). It is generally believed that the annual precipitation mainly affects the spatial distribution of soil AP through soil leaching. The more annual precipitation there is, the stronger the soil leaching effect, leading to the loss of available phosphorus in the soil (Miller et al., 2001). Precipitation mainly changes soil moisture and soil aggregate structure, causing soil leaching and reducing soil phosphorus content. It can also affect the migration and transformation of phosphorus elements, as well as the composition and availability of soil phosphorus elements, by controlling the biochemical processes of organic phosphorus mineralization (Wang R. Z. et al., 2016). Lambers et al. (2006) believe that under higher moisture conditions, the diffusion rate of soil phosphorus increases with the increase of soil moisture, accelerating the rate of plant and microbial uptake of phosphorus, resulting in lower available phosphorus content in the soil.

The annual average temperature mainly indirectly affects the availability of soil phosphorus by affecting the weathering rate of phosphorus-containing minerals and the activity of microorganisms in the soil during the soil formation process, thereby affecting the content of soil available phosphorus (Cao et al., 2022). Warming promotes the increase of dissolved phosphorus in soil by affecting the phosphorus content of litter, causing it to adsorb and precipitate with calcium carbonate, fixing dissolved phosphorus in the soil surface, and increasing the effective phosphorus content of the soil (Siebers et al., 2017). Wang et al. (2022) found that an increase in temperature may lead to a decrease in acid phosphatase activity and microbial biomass phosphorus content in cultivated land, reducing microbial activity and their ability to retain phosphorus. However, in this study, the AP content in the study area was significantly positively correlated with annual precipitation and negatively correlated with annual average temperature (Table 6). The areas with higher AP content in the study area were distributed in the southwest of Zhuxichuan County and the southeast of Fang County, which show higher precipitation and lower temperatures. Cao et al. (2022) found that in hilly areas of south China, high values of soil available phosphorus are mainly distributed in areas with low annual precipitation and high annual average temperature, which is inconsistent with the results of this study. According to the study by Wu et al. (2021), the soil organic matter content in Shiyan City shows a continuous decreasing trend with the decrease of elevation, the status of available phosphorus in soil is closely related to the content of soil organic matter, and in agricultural practice, increasing the content of soil organic matter can increase the desorption of solid phosphorus, enhance phosphorus activity, and increase the content of available phosphorus (Shen et al., 2014; Fei et al., 2021). Perhaps due to the lower temperature and weak soil microbial activity in high-altitude areas, the decomposition of organic matter is slow, which is conducive to the accumulation of organic matter. There are more nutrient elements accumulated in the soil, and the content of soil organic matter is significantly positively correlated with the content of available phosphorus, resulting in a higher content of AP in the soil. It is also possible that other factors such as elevation have a bigger impact on the spatial variation of soil AP in the study area than climate factors, leading to the masking of the impact of climate factors.

4.3 The impact of soil type on AP variation

Different soils in the study area have a significant impact on soil AP content ($F = 9.849$, $P < 0.05$), with brown soil having the highest content (64.18 mg/kg) and purple soil having the lowest content (10.55 mg/kg). The coefficients of variation for paddy soil and tidal soil are 123.49% and 103.07%, respectively, indicating strong variation, while others show moderate variation. The brown soil in the research area is acidic brown soil, and the developed parent material is mainly weathered mudstone, with a slightly acidic soil (Table 7). As shown in Table 6, there is a negative correlation between soil pH and soil AP content in the study area. Soil pH affects soil phosphorus availability by affecting the adsorption and fixation of soil phosphorus (Fei et al., 2021). The lower the soil pH, the stronger the acidity, and the bigger the adsorption and fixation effect of phosphorus by iron and aluminum oxides. It exists in the form of phosphate, and phosphorus fertilizers used in agricultural management are also easily adsorbed and fixed in large quantities, thereby increasing the content of available phosphorus in the soil (Chad and James, 2019). The moisture soil contains abundant carbonates and iron aluminum oxides, with high clay content and strong adsorption of phosphorus. The terrain of purple soil is hilly and undulating, with strong soil erosion, making it easy to lose effective phosphorus. The development degree of this soil type is relatively low, and good soil ventilation makes it difficult to accumulate organic matter. In addition, the utilization intensity of this soil type is relatively low, and the application amount of phosphorus fertilizer is also relatively low, resulting in a significantly lower accumulation rate of effective phosphorus in purple soil than in other soils. The average content of available phosphorus in the soil of this study is ranked as follows: brown soil > fluvo-aquic soil > paddy soil > yellow-brown soil > calcareous soil > yellow cinnamon soil>purple soil. Wang Y. H. et al. (2016) studied the spatial variation characteristics of soil available phosphorus in the tobacco growing areas of northern Sichuan of China and found that the average content of available phosphorus in five soil types was as follows: paddy soil > purple soil > yellow-brown soil > new soil > yellow soil. In both regions, the AP content of paddy soil is relatively high, but the AP content of yellow-brown soil in the study area is higher than that of purple soil, while the AP content of purple soil in northern Sichuan is higher than that of yellow-brown soil. It can be seen that the content of soil AP in different regions is complex and has regional characteristics.

10.3389/fmicb.2024.1463291

TABLE 7 Descriptive statistic characteristics of available phosphorous in different soil parent materials.

Soil type	Sample size	Minimum/ (mg/kg)	Maximum/ (mg/kg)	Mean/ (mg/kg)	Standard deviation	Coefficient of variation /(%)
Fluvo-aquic soil	12	4.10	55.10	16.31	16.81	103.07
Yellow cinnamon soil	30	2.50	40.80	12.20	8.89	72.90
Yellow-brown Soil	454	0.74	98.80	14.15	13.46	95.15
Calcareous soil	36	2.10	39.20	12.41	10.60	85.36
Paddy soil	119	0.30	146.00	15.46	19.09	123.49
Purple soil	46	3.10	52.67	10.55	9.24	87.58
Brown soil	4	5.50	105.40	64.18	49.26	76.76

TABLE 8 Descriptive statistic characteristics of soil available phosphorous in different cropping systems.

Cropping system	Sample size	Minimum/ (mg/kg)	Maximum/ (mg/kg)	Mean/ (mg/kg)	Standard deviation	Coefficient of variation (%)
Tea and orchard planting	79	0.91	82.73	12.34	13.90	112.66
Vegetable planting	15	5.91	105.40	27.06	24.29	89.78
Rice monoculture	55	0.30	51.70	9.89	9.50	96.02
Rapeseed rice rotation	28	2.38	55.87	19.47	15.09	77.50
Wheat rice rotation	24	2.00	146.00	21.97	32.48	147.88
Wheat corn rotation	106	2.00	51.10	15.28	11.50	75.30
Corn rice rotation	43	3.60	40.00	12.05	9.45	78.41
Potato corn intercropping	71	1.25	71.77	16.02	16.40	102.39
Rapeseed corn rotation	193	0.74	66.20	11.17	10.33	92.49
Corn monoculture	87	2.36	104.40	18.22	19.07	104.69

4.4 The impact of the planting system on AP variation

Due to the wide area, complex terrain, significant local climate differences, and complex planting system of Shiyan City, water and drought crops in the region are planted in rotation, intercropping, and monoculture. This complex planting system affects the availability of phosphorus in the soil through factors such as land use intensity, management measures, and crop growth habits. The cultivation system significantly affects the soil's available phosphorus content, and there are significant differences in AP content among different planting systems in the study area ($P < 0.05$, $F = 9.849$). As shown in Table 8, the highest AP content is in vegetable cultivation (27.06 mg/kg), and the lowest is in rice cultivation (9.89 mg/kg). From the perspective of coefficient of variation, the coefficient of variation of AP content under different planting systems ranges from 75.30 to 147.88%, all showing moderate degree of variation. The high AP content in vegetable cultivation is due to the high replanting index and good economic benefits of vegetable cultivation. The local farmers cultivate diligently, actively apply farm manure, and invest in more production materials. According to a questionnaire survey, a large amount of phosphorus fertilizer was input in the local vegetable planting season [with an average annual phosphorus fertilizer input of 6.05 kg/hm^2 (calculated as P_2O_5)], resulting in a higher rate of phosphorus accumulation. In addition, to improve economic benefits, local governments introduced policies that benefit farmers and actively promoted the implementation of organic fertilizers instead of chemical fertilizers to improve vegetable quality. On the one hand, organic fertilizers themselves contain a large amount of available phosphorus. On the other hand, the mineralization and decomposition of organic matter release available phosphorus. The increase in organic matter content promotes the release of adsorbed phosphorus from iron and aluminum oxides in the soil due to competition, increasing the content of available phosphorus in the soil (Fink et al., 2016). Rice monoculture results in lower AP uptake during crop harvest and higher soil AP content. However, among all planting methods, rice monoculture has the lowest AP content, which may be due to long-term flooding of the rice field, resulting in the loss or transformation of available phosphorus in the soil. Wheat corn rotation, corn rice rotation, and rapeseed corn rotation may be due to the lower economic benefits of grain crops and the more extensive cultivation and management practices employed by farmers. On the other hand, crops may deplete more soil nutrients more rapidly than they are replenished, leading to nutrient imbalances in the cultivated land. Although the amount of straw returned to the field is relatively large and contributes to improving the AP content in the soil, the relatively low phosphorus content in straw leads to a lower AP content. In future agricultural production, it is necessary to adjust the

cultivation methods and fertilization measures in a timely manner according to the different planting systems and spatial distribution characteristics of soil nutrients in the study area and pay attention to soil fertilization management.

4.5 The impact of interaction factors on AP spatial variation

The purpose of an interaction detector is to test whether the interaction between each factor increases, decreases, or is independent of the dependent variable, to better explain the driving mechanism. From the interaction results of influencing factors on the spatial differentiation of soil available potassium in the study area, it can be seen that the interaction of various environmental factors is bigger than their individual effects, and there is a non-linear or dual-factor enhancement between various environmental factors. Lin et al. (2023) used a geodetic instrument to analyze the spatial heterogeneity of pH values in cultivated land in Anhui Province and found that the interactions between various factors mainly manifested as non-linear enhancement and dual-factor enhancement. Liu et al. (2018) used a geographical detector to analyze the spatial differentiation and influencing factors of soil phosphorus loss in the Bailongjiang River Basin in Gansu Province, China, and found that the factors showed a synergistic enhancement effect on phosphorus loss, and the interaction relationship was a coexistence of non-linear enhancement and dual-factor enhancement, which is similar to the results of this study.

5 Conclusion

(1) The average AP content in the topsoil of the study area is 14.96 mg/kg, indicating a moderate level of phosphorus availability. The spatial distribution of AP content exhibits a notable degree of variability. The spatial structure is well-fitted using an exponential model, and the AP content indicates a moderate degree of spatial autocorrelation. Structural and random factors jointly affect the spatial variation of AP. The AP enrichment of the cultivated soil is mainly distributed in the southwest of Zhuxichuan County and the southeast of Fangxian County, where the terrain is relatively high. The lack of hierarchy is mainly distributed in the faulted basins in the northern part of Fang County. The spatial distribution of soil AP shows an increasing trend from the Central Valley lowlands to the surrounding mountainous hills, which is strongly consistent with the terrain changes.

(2) The operation results of the factor detector show that the q-value descending order of the impact factors on the spatial heterogeneity of soil AP is elevation (0.1459), soil type (0.0707), planting system (0.0622), annual precipitation (0.0612), organic matter (0.0623), annual average temperature (0.0456), soil pH (0.0301), slope (0.0264), and farmland use (0.0104). Elevation is the main controlling factor determining the spatial distribution pattern of soil AP in Shiyan City.

(3) The interaction detection results indicate that both factors exhibit non-linear enhancement or dual-factor enhancement effects, showing an increased influence when combined than when considered as single factors. The interaction between various influencing factors is bigger than their individual effects, and the synergistic effect of the two influencing factors will enhance the explanatory power of SOM spatial variation. The maximum interaction factor is elevationnslope (0.3224), followed by elevationnorganic matter (0.3161), elevationnplanting system (0.2905), slopenplanting system (0.2621), and elevationnsoil pH (0.2604), all of which have explanatory power >0.25. In terms of interactive comprehensive effects, elevation has the strongest interactive comprehensive effect (total 1.9997), followed by planting system comprehensive effect (1.6114), slope comprehensive effect (1.3502), annual precipitation (1.2904), organic matter (1.1830), soil type (1.1502), annual average temperature (1.1057), and soil pH (1.0459). The explanatory power of interactive comprehensive effects is > 1. Overall, the interaction between elevation, planting system, slope, and other factors is quite prominent. This means that areas with significant differences in elevation, planting system, and slope often have significant differences in AP. The distribution of other factors will enhance the influence of elevation, planting system, and slope on the spatial distribution of AP in the plow layers. This study provides a scientific reference for maintaining ecological security in the water source area of the MSDP, improving the precise management of AP, and enhancing the quality of cultivated land.

Data availability statement

The original contributions presented in the study are included in the article/supplementary material, further inquiries can be directed to the corresponding author.

Author contributions

ZW: Conceptualization, Writing – original draft. YZ: Investigation, Writing – review & editing. MW: Methodology, Writing – review & editing.

Funding

The author(s) declare financial support was received for the research, authorship, and/or publication of this article. This study was supported by the Key R&D and Promotion Project of Henan Province (Soft Science Research) (232400411098), the Doctoral Program of Nanyang Normal University (2022ZX042), the National Social Sciences Cultivation Project of Nanyang Normal University in 2022 (2022PY018), the Key Project of the Open Project of Nanyang Branch of Henan Academy of Social Sciences in 2022 (YJY202205), the Key project of 2022 bidding project of Rural Revitalization Research Institute of Nanyang Normal University (2022sczx04), the Key Project of the Open Project of Nanyang Branch of Henan Academy of Social Sciences in 2023 (YJY202301),

and the 2024 Nanyang Normal University STP Project (2024STP011; 2023STP009).

Conflict of interest

The authors declare that the research was conducted in the absence of any commercial or financial relationships that could be construed as a potential conflict of interest.

Publisher's note

References

Bai, Z. H., Li, H. G., Yang, X. Y., Zhou, B. K., Shi, X. J., Wang, B., et al. (2013). The critical soil P levels for crop yield, soil fertility and environmental safety in different soil types. *Plant Soil*. 372, 27–37. doi: 10.1007/s11104-013-1696-y

Bieluczyk, W., Piccolo, C. D. M., Gonçalves, M. V. J., Pereira, M. G., Lambais, G., De Camargo, P. B., et al. (2024). Fine root production and decomposition of integrated plants under intensified farming systems in Brazil. *Rhizosphere* 31:100930. doi: 10.1016/j.rhisph.2024.100930

Cambardella, C. A., Moorman, T. B., Novak, J. M., Parkin, T. B., Karlen, D. L., Turco, R. F., et al. (1994). Field-scalevariability of soil properties in central Iowa soils. *Soil Sci. Soc. Am. J.* 58, 1501–1511. doi: 10.2136/sssaj1994.03615995005800050033x

Cao, J. P., Zhang, L. M., Qiu, L. X., Xing, S. H., and Ma, D. (2022). Ping soil available phosphorus of cultivated land in hilly region of southern China based on sparse samples. *Chin. J. Eco Agric*. 30, 290–301. doi: 10.12357/cjea.20210565

Cao, N., Chen, X. P., Cui, Z. L., and Zhang, F. S. (2012). Change in soil available phosphorus in relation to the phosphorus budget in China. *Nutr. Cycling Agroecosyst.* 94, 161–170. doi: 10.1007/s10705-012-9530-0

Chad, J. P., and James, J. C. (2019). A critical review on soil chemical processes that control how soil pH affects phosphorus availability to plants. *Agriculture* 9:120. doi: 10.3390/agriculture9060120

Chen, L., Kou, X. Y., Dang, Y. A., NIiu, Y. N., Bao, S. S., and Shen, Y. F. (2024). Effects of phosphorus application rates in wheat season on wheat-maize rotation yield and available phosphorus in soil. *J. Triticeae Crops* 44, 85–194.

Chen, Z. X., Qiu, L. X., Chen, H. Y., Fan, X. Y., Wu, T., Shen, J. Q., et al. (2022). Enrichment and ecological risk assessment of available phosphorus in paddy soil of Fujian Province Over Past 40 years. *Environ. Sci.* 43, 3741–3751. doi: 10.13227/j.hjkx.202108140

Dong, L. K., Fang, B., Shi, L. B., Ma, X. Y., and Zheng, J. (2016). Camparative analysis of spatial heterogeneity of soil available phosphorus at the township scale-taking the high quality tea planting area in Jiangsu and Zhejiang as examples. *Resour. Environ. Yangtze Basin* 25, 576–1584. doi: 10.11870/cjlyzyyhj201610012

Du, J. X., Liu, K. L., Huang, J., Han, T. F., Wang, Y. P., Li, D. C., et al. (2021). Spatio-temporal evolution characteristics of soil available phosphorus and its response to phosphorus balance in paddy soil in China. *Acta Pedol. Sin.* 58, 476–486. doi: 10.11766/trxb201911040381

Fei, C., Zhang, S. R., Feng, X. H., and Ding, X. D. (2021). Organic material with balanced C-nutrient stoichiometry and P addition could improve soil P availability with low C cost. *J. Plant Nutr. Soil Sci*. 184, 360–366. doi: 10.1002/jpln.202100108

Fink, J. R., Inda, A. V., Tiecher, T., and Barrón, V. (2016). Iron oxides and organic matter on soil phosphorus availability. *Ciênc. Agrotec.* 40, 369–379. doi: 10.1590/1413-70542016404023016

Goovaerts, P. (1999). Geostatistics in soil science: state-of-the-art and perspectives. *Geoderma* 89, 1–45. doi: 10.1016/S0016-7061(98)00078-0

Holger, R., Ralph, M., and Peter, L. (2018). Plant available phosphorus in soil as predictor for the leaching potential: insights from long-term lysimeter studies. *Ambio* 47(1S), 103–113. doi: 10.1007/s13280-017-0975-x

Hua, D. W., Xu, J., and, Li, Y. (2020). Influence of topographical factors on spatial distribution characteristics of soil nutrients in Qinba Mountain Area. *IOP Conf. Ser. Earth Environ. Sci.* 558:032025. doi: 10.1088/1755-1315/558/3/032025

Khan, A., Lu, G. Y., Ayaz, M., Zhang, H. T., Wang, R. J., Lv, F. L., et al. (2018). Phosphorus efficiency, soil phosphorus dynamics and critical phosphorus level under long-term fertilization for single and double cropping systems. *Agric. Ecosyst. Environ.* 256, 1–11. doi: 10.1016/j.agee.2018.01.006

Lambers, H., Shane, M. W., Cramer, M. D., Pearse, S. J., and Veneklaas, E. J. (2006). Root structure and functioning for efficient acquisition of phosphorus: matching morphological and ph ysiological traits. *Ann. Bot.* 98, 693–713. doi: 10.1093/aob/mcl114

Li, Q., Liu, X. Y., Wang, P., Duan, W. J., Cheng, C. X., Luo, W., et al. (2016). Spatial variation of available Phosphorus in tobacco-planting soil and evaluation of its potential risks to leaf quality and surface pollution in Luliang county of Yunnan province. *Acta Tabacaria Sin*. 22, 79–87. doi: 10.16472/j.chinatobacco.2015.504

Lin, J. S., Shi, X. Z., Lu, X. X., Yu, D. S., Wang, H. J., Zhao, Y. C., et al. (2009). Storage and spatial variation of phosphorus in paddy soils of China. *Pedosphere* 19, 790–798. doi: 10.1016/S1002-0160(09)60174-0

Lin, Y. S., Ma, K., Zhou, H., Lliu, W. B., Fang, F. M., and Zhi, J. J. (2023). Spatial variation and driving factors of soil pH in cultivated land of Anhui Province based on geomorphic unit. *Acta Sci. Circumstantiae* 43, 318–330. doi: 10.13671/j.hjkxxb.2022.044

Liu, D.Q., Zhang, J. X., Li, H. Y., Cao, E. J., and Gong, J. (2018). Impact factors of soil phosphorus loss in watershed based on geographical detector. *Acta Sci. Circumstantiae* 38, 4814–4822. doi: 10.13671/j.hjkxxb.2018.0313

Liu, P., Yan, H. H., Xu, S. N., Lin, X., Wang, W. Y., Wang, D., et al. (2022). Moderately deep banding of phosphorus enhanced winter wheat yield by improving phosphorus availability, root spatial distribution, and growth. *Soil Tillage Res.* 220:105388. doi: 10.1016/j.still.2022.105388

Liu, X., Sheng, H., Jiang, S. Y., Yuan, Z. W., Zhang, C. S., Elser, J. J., et al. (2016). Intensification of phosphorus cycling in China since the 1600s. *Proc. Natl. Acad. Sci. USA*. 113, 2609–2614. doi: 10.1073/pnas.1519554113

Lü, C. L., Chen, Y. H., He, W. T., Zhang, S. Y., Jiang, N., Fan, D. J., et al. (2022). Response of soil phosphorus availability to long-term application of organic fertilizer under maize cropping system: a meta-analysis. *J. Agro Environ. Sci*. 41:2. doi: 10.11654/jaes.2022-0015

Lv, Z. W., Sun, H. R., Zhang, J. P., Lv, Y. C., Cheng, W. Z., Dong, W. L., et al. (2022). Abundance-deficiency index of soil available phosphorus and the appropriate amount of phosphorus fertilizer application for cotton in China. *Soil Fert. Sci. China* 197–206.

Ma, J. C., He, P., Xu, X. P., He, W. T., Liu, Y. X., Yang, F. Q., et al. (2016). Temporal and spatial changes in soil available phosphorus in China (1990-2012). *Field Crops Res.* 192, 13–20. doi: 10.1016/j.fcr.2016.04.006

Mei, L. L., Yang, X., Zhang, S. Q., Zhang, T., and Guo, J. X. (2019). Arbuscular mycorrhizal fungi alleviate phosphorus limitation by reducing plant N:P ratios under warming and nitrogen addition in a temperate meadow ecosystem. *Sci. Total Environ.* 686, 1129–1139. doi: 10.1016/j.scitotenv.2019.06.035

Miller, A. J., Schuur, E. A. G., and Chadwic, K. O. A. (2001). Redox control of phosphorus pools in *Hawaiian montane* forest soils. *Geoderma* 102, 219–237. doi: 10.1016/S0016-7061(01)00016-7

National Agricultural Technology Extension and Service Center (2006). *Technical Specification for Soil Analysis*. Beijing: Chinese Agricultural Publishing House, 73–75.

Reijneveld, J. A., Ehlert, P. A. I., Termorshuizen, A. J., and Oenema, O. (2010). Changes in the soil phosphorus status of agricultural land in the Netherlands during the 20th century. *Soil Use Manag.* 26, 399–411. doi: 10.1111/j.1475-2743.2010.00290.x

Rowe, H., Withers, P. J. A., Baas, P., Chan, N. L., Doody, D., Holiman, J., et al. (2015). Integrating legacy soil phosphorus into sustainable nutrient management strategies for future food, bioenergy and water security. *Nutr. Cycling Agroecosyst.* 104, 393–412. doi: 10.1007/s10705-015-9726-1

Santos, F., Abney, R., Barnes, M., Bogie, N., Ghezzehei, T. A., Jin, L., et al. (2019). "The role of the physical properties of soil in determining biogeochemical responses to soil warming," in *Ecosystem Consequeces of Soil Warming*, ed. J. E. Mohan (Salt Lake City, UT: Academic Press), 209–244. doi: 10.1016/B978-0-12-813493-1.00010-7

Sattari, S. Z., Bouwman, A. F., Giller, K. E., and Van, I. M. K. (2012). Residual soil phosphorus as the missing piece in the global phosphorus crisis puzzle. *Proc. Natl. Acad. Sci. USA*. 109, 6348–6353. doi: 10.1073/pnas.1113675109

Schoumans, O. F., Bouraoui, F., Kabbe, C., Oenema, O., and Van, D. K. C. (2015). Phosphorus management in Europe in a changing world. *Ambio* 44, 180–192. doi: 10.1007/s13280-014-0613-9

Shen, P., He, X. H., Xu, M. i. G., Zhang, H. M., Peng, C., Gao, H. J., et al. (2014). Soil organic carbon accumulation increases percentage of soil available phosphorus to total P at two 15-year mono-cropping systems in Northern China. *J. Integr. Agric*. 13, 597–603. doi: 10.1016/S2095-3119(13)60717-0

Siebers, N., Sumann, M., Kaiser, K., and Amelung, W. (2017). Climatic effects on phosphorus fractions of native and cultivated North American grassland soils. *Soil Sci. Soc. Am. J.* 81, 299–309. doi: 10.2136/sssaj2016.06.0181

Tan, L., Wang, Z. Q., Xue, Z. B., and Yang, B. (2021). Spatial variability and pollution risk assessment of soil fluorine in the core area of the middle route of the South- to-North Water Transfer Project. *Resour. Sci.* 4, 368–379. doi: 10.18402/resci.2021.02.14

Wang, H., Liu, S., Schindlbacher, A., Wang, J., Yang, Y., Song, Z., et al. (2019). Experimental warming reduced topsoil carbon content and increased soil bacterial diversity in a subtropical planted forest. *Soil Biol. Biochem.* 133, 155–164. doi: 10.1016/j.soilbio.2019.03.004

Wang, R. Z., Creamer, C. A. A., Wang, X., He, P., Xu, Z., Jiang, Y., et al. (2016). The effects of a 9-year nitrogen and water addition on soil aggregat phosphorus and sulfur availability in a semi-arid grassland. *Ecol. Indic.* 61, 806–814. doi: 10.1016/j.ecolind.2015.10.033

Wang, W., Li, Y. H., Guan, P. T., Chang, C., Zhu, X., Zhang, P., et al. (2022). How do climate warming affect soil aggregate stability and aggregate-associated phosphorus storage under natural restoration? *Geoderma* 420:115891. doi: 10.1016/j.geoderma.2022.115891

Wang, Y. H., Wang, C., Li, Q., Li, Q. Q., He, B., Jin, Y. T., et al. (2016). Spatial variation characteristics of soil available phosphorus and key controlling factors in northern of Sichuan Province. *J. Nuclear Agric. Sci.* 30, 2425–2433. doi: 10.11869/j.issn.100-8551.2016.12.2425

Wang, Y. K., Cai, Z. J., and Feng, G. (2023). Effects of different phosphorus application techniques on phosphorus availability in a rape system in a Red Soil. *Acta Pedol. Sin.* 60, 235–246. doi: 10.11766/trxb202104210207

Wu, M. (2024). Spatial-temporal variation and driving factors of grey water footprint loading coefficient in water-receiving area of central route of the South-to-North Water Diversion Project. *Resour. Environ. Yangtze Basin* 33, 971–981. doi: 10.11870/cjlyzyyhj202405006

Wu, T., Liu, S. Z., Lie, Z. Y., Zheng, M. H., Duan, H. L., Chu, G. W., et al. (2020). Divergent effects of a 6-year warming experiment on the nutrient productivities of subtropical tree species. *For. Ecol. Manage.* 461:117952. doi: 10.1016/j.foreco.2020.117952

Wu, Z. X., Zhou, Y., Liu, J. Y., and Xi, T. (2021). Spatial variability of soil organic matter and its influencing factors in mountain areas of northwestern Hubei Province. *Resour. Environ. Yangtze Basin* 30, 1141–1152. doi: 10.11870/cjlyzyyhj202105011

Xiaolan, Z., Shenglu, Z., Jiangtao, L., and Qiguo, Z. (2007). Heavy metals contamination in the Yangtze River Delta-a case study of Taicang City, Jiangsu Province. *Acta Pedol. Sin*. (2007) 44, 33–40. doi: 10.11766/trxb200508260106 (In Chinese).

Yang, X. L., Lu, Y. L., Ding, Y., Yin, X. F., Raza, S., Tong, Y. A., et al. (2017). Optimising nitrogen fertilisation: a key to improving nitrogen-use efficiency and minimising nitrate leaching losses in an intensive wheat/maize rotation (2008-2014). *Field Crops Res.* 206, 1–10. doi: 10.1016/j.fcr.2017.02.016

Yu, T. S., Zheng, S. N., Zhu, J. Y., Tang, M. F., Dong, R. C., Wang, Y. (2021). Evaluation on the ecological security status in Nanyang city, the water source region of the middle route of South-to-North Water Diversion Project in China. *Acta Ecol. Sin.* 41, 7292–7300. doi: 10.5846/stxb202003260701

Zhang, Z., Zhu, L., and Li, D. (2021). *In situ* root phenotypes of cotton seed lings under phosphorus stress revealed through rhizopot. *Front. Plant Sci.* 12:716691. doi: 10.3389/fpls.2021.716691

Zhao, Y. T., Chang, Q. R., Chen, X. X., and Ma, Y. G. (2011). Study on the spatial pattern of available Potassium in county farmland-Wugong county as an example. *J. Northwest A&F Univ.* 39, 157–162+167. doi: 10.13207/j.cnki.jnwafu.2011.03.016

Zicker, T., Tucher, V. S., Kavka, M., and Eichler-Löbermann, B. (2018). Soil test phosphorus as affected by phosphorus budgets in two long-term field experiments in Germany. *Field Crops Res.* 218, 158–170. doi: 10.1016/j.fcr.2018.01.008

frontiers | Frontiers in Microbiology

TYPE Original Research
PUBLISHED 06 September 2024
DOI 10.3389/fmicb.2024.1458777

OPEN ACCESS

EDITED BY
Yang Yang,
Institute of Earth Environment (CAS), China

REVIEWED BY
Zhengfeng An,
University of Alberta, Canada
Qiang Lu,
Nanjing Forestry University, China
Zhen Wang,
Institute of Grassland Research (CAAS), China

*CORRESPONDENCE
Mengli Zhao
✉ nmgmlzh@126.com

RECEIVED 03 July 2024
ACCEPTED 23 August 2024
PUBLISHED 06 September 2024

CITATION
Qiao J, Zheng J, Li S, Zhang F, Zhang B and Zhao M (2024) Impact of climate warming on soil microbial communities during the restoration of the inner Mongolian desert steppe.
Front. Microbiol. 15:1458777.
doi: 10.3389/fmicb.2024.1458777

Impact of climate warming on soil microbial communities during the restoration of the inner Mongolian desert steppe

Jirong Qiao, Jiahua Zheng, Shaoyu Li, Feng Zhang, Bin Zhang and Mengli Zhao*

Key Laboratory of Grassland Resources of the Ministry of Education, Key Laboratory of Forage Cultivation, Processing and High Efficient Utilization of the Ministry of Agriculture and Rural Affairs, Inner Mongolia Key Laboratory of Grassland Management and Utilization, College of Grassland, Resources and Environment, Inner Mongolia Agricultural University, Hohhot, China

Introduction: Grazer exclosure is widely regarded as an effective measure for restoring degraded grasslands, having positive effects on soil microbial diversity. The Intergovernmental Panel on Climate Change (IPCC) predicts that global surface temperatures will increase by 1.5–4.5°C by the end of the 21st century, which may affect restoration practices for degraded grasslands. This inevitability highlights the urgent need to study the effect of temperature on grassland soil microbial communities, given their critical ecological functions.

Methods: Here, we assessed the effects of heavy grazing (control), grazer exclosure, and grazer exclosure plus warming by 1.5°C on soil microbial community diversity and network properties as well as their relationships to soil physicochemical properties.

Results and discussion: Our results showed that grazer closure increased soil microbial richness relative to heavy grazing controls. Specifically, bacterial richness increased by 7.9%, fungal richness increased by 20.2%, and the number of fungal network nodes and edges increased without altering network complexity and stability. By contrast, grazer exclosure plus warming decreased bacterial richness by 9.2% and network complexity by 12.4% compared to heavy grazing controls, while increasing fungal network complexity by 25.8%. Grazer exclosure without warming increased soil ammonium nitrogen content, while warming increased soil nitrate nitrogen content. Soil pH and organic carbon were not affected by either exclosure strategy, but nitrate nitrogen was the dominant soil factor explaining changes in bacterial communities.

Conclusion: Our findings show that grazer exclosure increases soil microbial diversity which are effective soil restoration measures for degraded desert steppe, but this effect is weakened under warming conditions. Thus, global climate change should be considered when formulating restoration measures for degraded grasslands.

KEYWORDS

climate change, degraded grassland restoration, soil microbial diversity, microbial network complexity, microbial network stability

1 Introduction

Soil microbial communities play a critical role in maintaining the functioning of grassland ecosystems (Liu et al., 2020; Coban et al., 2022). These microbes facilitate plant and soil restoration by influencing litter decomposition, organic substrate transformation, and mineral nutrient supply (Lindsay and Cunningham, 2009; Coban et al., 2022; Pedrinho et al., 2024), with bacteria and fungi dominating these processes due to their high biodiversity, complex taxonomic composition, and ubiquitous influence on biogeochemical cycles (Zhou et al., 2023). However, their diversity, species composition, and network properties face serious threats due to human activities and global climate change (Pedrinho et al., 2024). Grazing is the traditional method of grassland management in Inner Mongolia; specifically, the desert steppe ecosystem is ecologically fragile compared to other grasslands, and its microbial diversity is very sensitive to grazing disturbance (Zhang et al., 2021). In recent years, overgrazing and continuous climate warming have escalated ecological challenges to the desert steppe, making the restoration of degraded grasslands a pressing issue (Zhou et al., 2010; Wu Y. et al., 2022; He et al., 2022). Grazer exclosure is a widely employed grassland management method for restoring degraded grasslands, by introducing a physical barrier against unwanted grazing animals (Medina-Roldán et al., 2012; Tang et al., 2016; Yao et al., 2018; Zhang M. X. et al., 2023). Therefore, studying the effects of grazer exclosure on soil microbial diversity, especially fungal and bacterial diversity, under global climate change will help improve the diversity and restoration of degraded grasslands.

Grazing affects soil microbial community composition and diversity primarily through livestock excreta deposition and trampling (Yang et al., 2019), and grazer exclosure might mitigate these grazing effects (Fan et al., 2020). Previous studies have shown that compared to free-grazed areas, grazer exclosure promotes the colonization of eutrophic microbial taxa (Cao et al., 2022), alters soil microbial community composition (Yang et al., 2019), and increases microbial richness and soil network connectivity (Morriën et al., 2017). However, long-term grazer exclosure may harm soil microbial network stability (Chen et al., 2023). Several studies have shown that soil moisture, pH, and nutrients (including organic carbon and nitrogen) are key drivers of microbial composition and structure (Lauber et al., 2009; Yao et al., 2018; Wang et al., 2019). Specifically, microbial communities tend to be more richly structured under higher soil moisture and nutrient content, with bacterial diversity greater in neutral soils than in acidic ones (Kang et al., 2021; Philippot et al., 2024). Grazer exclosure significantly increases aboveground vegetation cover (Yang et al., 2016) and the abundance of plant-derived food resources (e.g., leaf litter and roots) entering the soil (Chen and Chen, 2018). This leads to higher soil moisture and nutrient levels (Chen et al., 2023), particularly organic carbon content, which, in turn, enhances microbial diversity and network stability (Kang et al., 2021; Wu et al., 2021). Additionally, the concentration of nitrate nitrogen is crucial in shaping bacterial and fungal communities (Wang et al., 2019; Zhang et al., 2024). Grazer exclosure reduces the input of livestock waste and consequently affects the effectiveness and distribution of soil nitrogen, which leads to changes in microbial composition. Importantly, the IPCC predicts global surface temperatures will increase between 1.5 and 4.5°C by the end of the 21st century (IPCC, 2013). According to the metabolic theory of ecology (MTE), higher temperatures will stimulate interactions among various species, leading to the formation of more complex microbial networks (Brown et al., 2004; Guo et al., 2019; Yuan et al., 2021). However, rising temperatures are also expected to reduce soil microbial alpha diversity and alter beta diversity (Wu L. et al., 2022; Zhao et al., 2024). Previous studies have shown that the impact of global warming on the soil microbial community is mediated by changes in soil water availability and nutrient availability (Weedon et al., 2012; Zhang et al., 2015), largely, by changes in soil nitrogen availability (Li et al., 2024).

Taken together, both grazer exclosure and warming have varying impacts on soil microbial communities. However, the influence of global warming on the recovery processes of these communities under grazer exclosure remains unclear. Understanding this will aid in the development of effective grassland management and conservation strategies to mitigate the effects of climate change (Guo et al., 2019). Therefore, this study investigates changes in soil microbial alpha diversity, beta diversity, network complexity, and network stability in the desert steppe under three conditions: free grazing (CK), grazer exclosure (GE), and grazer exclosure plus warming by 1.5°C (GE + W). We tested two hypotheses: (1) Grazer exclosure normally promotes soil microbial restoration, but this effect is limited under warming conditions, and (2) warming-induced changes in soil nutrient content are a key factor limiting the recovery of soil microbial communities in degraded arid and semi-arid grassland ecosystems.

2 Materials and methods

2.1 Study sites and experimental design

The experimental site is located in the desert steppe of Siziwangqi (41°46′43″ N, 111°53′42″ E, at 1450 m above sea level), Inner Mongolia, China. This region is characterized by aridity and low rainfall, with an average annual temperature of 4.15°C, mean annual precipitation of 229 mm, and sandy loam soil (FAO soil classification). This area is mainly used for grazing, and the dominant plant species are *Stipa breviflora*, *Cleistogenes songorica*, and *Artemisia frigida* (Zhang F. et al., 2023).

The experiments were conducted on a long-term (20-year) grazing platform that included no grazing, light grazing, moderate grazing, and heavy grazing treatment. The stocking rates were based on the results of Wei et al. (2000) with 0, 0.91, 1.82, and 2.71 sheep ha^{-1} $year^{-1}$, respectively, grazed from 6 a.m. to 6 p.m. from June to November each year. Each plot covered an area of 4.4 ha and was replicated three times.

In May 2020, we selected the heavy grazing plots as the experimental area of degraded grassland (CK). In each plot, two 10 m × 10 m fences were set up for grazer exclosure treatment (natural restoration, GE); at the same time, traditional open-top chambers (OTC) were deployed in each of the grazer exclosure areas to simulate warming (GE + W). These chambers, surrounded by Plexiglas fiberboards, featured a bottom area of 1.50 m^2, a height of 0.51 m, and a top opening area of 0.79 m^2. By 2023, the OTCs had effectively increased the mean temperature of the topsoil (0–10 cm) by 1.5°C.

2.2 Soil sampling and assaying

In mid-August 2023, topsoil samples were collected from each experimental plot (CK, GE, and GE + W) using the 5-point sampling method, totaling 18 soil samples (3 treatments × 3 blocks × 2

fences) = 18 soil samples. The soil samples were further divided into two, one of which was stored at −80°C for DNA extraction and amplicon sequencing, and the other immediately transported to the laboratory in a cooler for the determination of soil physicochemical properties.

The dichromate oxidation method was used to determine soil organic carbon (SOC) content, and a flow analyzer (AA3, SEAL Analytical, Germany) was used to determine ammonium nitrogen (NH_4^+-N) and nitrate nitrogen (NO_3^--N) contents (Nelson and Sommers, 2018). Finally, soil pH was measured by a pH meter (BPH-7100, BELL Analytical Instruments, Dalian, China).

2.3 Soil microbial diversity assaying

Total soil DNA was extracted from fresh soil samples using the PowerSoil DNA Isolation Kit (MO BIO Laboratories, Carlsbad, United States). A NanoDrop UV–Vis spectrophotometer (ND-2000c, Nano Technologies, DE, United States) was used to measure the concentration and purity of soil DNA. The primers 515-forward (5′-GTGCCAGCMGCCGCGGTAA-3′) and 806-reverse (5′-GGACTACHVGGGTWTCTAAT-3′) were used to amplify bacterial 16S rDNA. The fungal primer sets ITS5-1737-forward and ITS2-2043-reverse were used to amplify the ITS1 variable region. Libraries were constructed using the TruSeq® DNA PCR-Free Sample Preparation Kit. Sequencing was performed by Novogold Bioinformatics Ltd., Beijing, China. After training the naïve Bayes classifier based on the primer sequences, the ASVs were taxonomically annotated using the feature-classifier module based on the SILVA database release 138 (Liu D. et al., 2024).

2.4 Microbial network analysis

First, raw microbial ASVs were screened to exclude those with less than 15 occurrences in the 18 soil samples, where the number of ASVs represents microbial richness. Then, the microbial co-occurrence network was constructed in R software with the "Hmisc" package (R Core Development Team, R Foundation for Statistical Computing, Vienna, Austria), and sub-network parameters for each sample were extracted using the "igraph" package, including the numbers of nodes, edges, and network complexity. Network parameters were visualized using Gephi 0.10.1 software.[1] The stability of the microbial network was quantified using the ratio of negative to positive cohesion, which represents the competitive and cooperative interactions between species in the community, respectively (Faust and Raes, 2012).

$$cohesion = \sum_{i=1}^{n} r_i \times c_i$$

where n is the number of taxa in the community, and r_i and c_i are the abundance and connectivity of taxa, respectively.

1 http://gephi.github.io/

2.5 Statistical analysis

Significant differences in microbial diversity, composition, and network parameters between treatments were detected using one-way ANOVA and Duncan's test with $p = 0.05$ indicating significance. The results were visualized using OriginLab 2022 software. The Shapiro–Wilk test was used to test for normality prior to the ANOVA. Treatment effects on microbial community composition were assessed using non-metric multidimensional scaling (NMDS) analysis of different distance matrices using the "vegan" package. The degree and significance of each treatment on microbial community structure were quantified by analysis of similarities (ANOSIM), and significance was verified by the dispersion test. Then, correlations between soil physicochemical factors and microbial diversity, composition, and network parameters were assessed using Pearson's correlation. To better determine which soil properties were correlated with microbial composition, we performed redundancy analyses (RDA) using Canoco 5.0 software (Ithaca, NY, United States). We used a linear fit of prominent soil impact factors and the relative abundance of microbial dominant species using OriginLab 2022 software.

3 Results

3.1 Variation in soil microbial communities

Compared to CK, the GE treatment increased bacterial and fungal richness by 63 and 28, respectively, and the GE + W treatment significantly decreased bacterial richness by 62 ($p < 0.05$, Figures 1A,D). The NMDS analyses showed that bacterial communities differed significantly in ordinal spatial clustering, while fungal communities did not show significant differences (Figures 1B,E). The ANOSIM analysis further confirmed this result. Bacterial variability was significantly higher in the GE + W group than in the GE treatments ($R^2 = 0.11$, Figure 1B), whereas fungal community variability under each treatment was not significant differences (Figure 1E).

The dominant bacterial phyla in each treatment were Actinobacteria, Proteobacteria, and Bacteroidota, with the GE + W treatment significantly decreasing the relative abundance of Proteobacteria compared to CK and the GE treatment increasing the relative abundance of Chloroflexi ($p < 0.05$, Figure 1C). Ascomycota and Basidiomycota were the dominant fungal phyla, and the fungal relative abundance of fungal species was not significantly different among the treatments ($p > 0.05$, Figure 1F).

3.2 Co-occurrence networks of microbial communities

Soil microbial co-occurrence networks were constructed based on Spearman's correlation between ASVs to explore interconnections between microbes after short-term grazer exclosure (Figures 2A,B). Overall, the GE + W treatment reduced the number of nodes and edges of the bacterial network compared to the CK treatment, and the degree of the network was reduced by 22.15 and 33.84%, respectively. The GE + W treatment also reduced

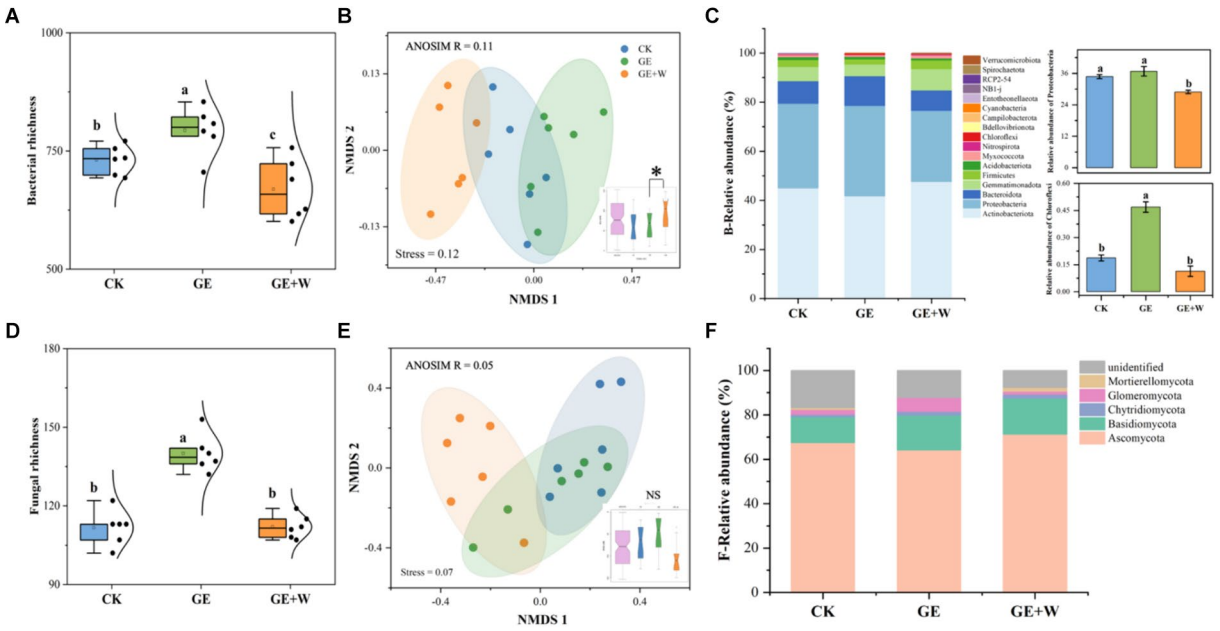

FIGURE 1
Variations in soil bacterial and fungal richness and abundance under different treatments (mean ± SE). **(A)** Bacterial richness, **(B)** bacterial beta-diversity, **(C)** bacterial phyla relative abundance, **(D)** fungal richness, **(E)** fungal beta-diversity, and **(F)** fungal phyla relative abundance. The lowercase letters indicate significant differences between means at $p < 0.05$ after *post-hoc* comparisons using Duncan's test. CK, heavy grazing; GE, grazer exclosure; GE + W, grazer exclosure plus warming by 1.5°C.

the bacterial network complexity without changing stability (Figure 2C). The GE treatment increased the number of bacterial network edges relative to the CK control, but other properties were not changed. Compared with CK treatment, GE and GE + W treatments increased the number of fungal nodes and edges, but GE treatment did not affect fungal network complexity, while GE + W increased it (Figure 2B).

3.3 Relationship between the microbial community and soil properties

Compared to the CK group, the GE treatment increased NH_4^+-N contents ($p < 0.05$), the GE + W treatment significantly increased NH_4^+-N, and NO_3^--N contents ($p < 0.05$), but other soil properties did not differ significantly between treatments (Table 1). The soil content of NO_3^--N was negatively correlated with bacterial richness, composition, and bacterial network complexity, and positively correlated with fungal network complexity, while SOC showed the opposite trend for each of these variables (Figure 3A; Supplementary Table S1).

The RDA of microbial community composition with soil environmental factors showed that bacterial community composition on axis 1 showed differences with decreasing soil organic carbon and increasing nitrate nitrogen content (Figure 3B), where soil nitrate nitrogen content was the main influence factor influencing bacterial community composition ($p < 0.05$, Supplementary Table S2). Soil fungal community composition was not affected by environmental factors (Figure 3C). The relative abundance of both Proteobacteria (Figure 3D) and Chloroflexi (Figure 3E) declined with increasing nitrate nitrogen content.

4 Discussion

4.1 Grazer exclosure increases microbial richness without affecting network complexity, but this effect is impaired during warming

Consistent with hypothesis 1 and previous findings (Ding et al., 2019; Eldridge et al., 2017; Zhang M. X. et al., 2023), our results demonstrate that grazer exclosure treatment increased soil bacterial and fungal richness and altered the soil microbial community structure. Prior research by Shu et al. (2024) and Yang et al. (2022) supports the notion that grazer exclosure enhances soil microbial community structure and function by mitigating the disturbances caused by grazing. Similarly, Geng et al. (2023) found that grazer exclosure in desert steppe regions increased the relative abundance of key microbial taxa such as Actinobacteria, Proteobacteria, and Chloroflexi, thereby enhancing overall soil microbial diversity and metabolic activity. In our study, we observed a significant increase in the relative abundance of Chloroflexi, while the relative abundance of many dominant taxa did not change significantly during the 3-year restoration period. This finding contrasts with Yao et al. (2018), who reported a decrease in the relative abundance of Chloroflexi after the restoration of degraded desert steppe via fencing. This discrepancy may be attributed to the longer duration of exclosure in their study, as long-term grazing exclosure likely leads to an increase in soil nutrients, which is detrimental to the survival of oligotrophic bacterial communities. Concurrently, the increased nutrient availability enhances the reproductive rate and resource competitiveness of eutrophic bacteria, placing additional competitive pressure on oligotrophic bacteria and further reducing their diversity and relative abundance (Cheng et al., 2016; Cao et al., 2022; Chen et al., 2023).

10.3389/fmicb.2024.1458777

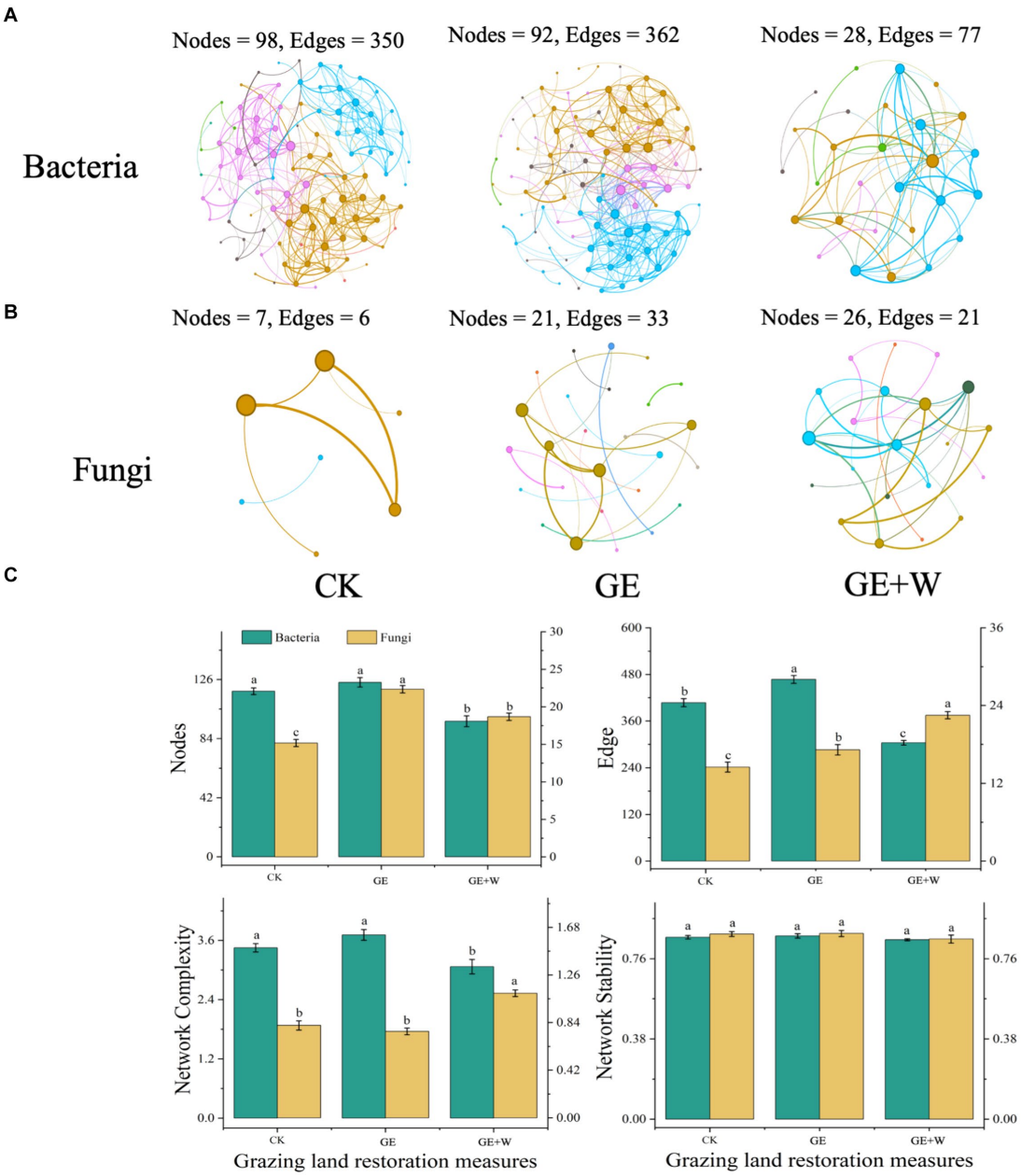

FIGURE 2
Network co-occurrence, complexity, and stability of soil bacterial and fungal communities. **(A)** Bacterial co-occurrence network, **(B)** fungal co-occurrence network, and **(C)** summary of bacterial and fungal network nodes, edges, network complexity, and network stability. The lowercase letters indicate significant differences between means at $p < 0.05$ after *post-hoc* comparisons using Duncan's test. CK, heavy grazing; GE, grazer exclosure; GE + W, grazer exclosure plus warming by 1.5°C.

TABLE 1 Variations in soil microbial diversity under different treatments (mean ± standard error).

	CK	GE	GE + W
Organic carbon ($g\,kg^{-1}$)	15.19 ± 0.01 a	15.20 ± 0.01 a	15.16 ± 0.01 a
Ammonium nitrogen ($mg\,kg^{-1}$)	4.46 ± 0.02 c	5.97 ± 0.16 a	4.78 ± 0.09 b
Nitrate nitrogen ($mg\,kg^{-1}$)	9.99 ± 0.30 b	9.64 ± 0.10 b	10.85 ± 0.15 a
pH	7.89 ± 0.07 a	7.88 ± 0.03 a	7.94 ± 0.03 a

Different lowercase letters indicate significant differences between different treatments at $p < 0.05$.
CK, heavy grazing; GE, grazer exclosure; GE + W, grazer exclosure plus warming by 1.5°C.

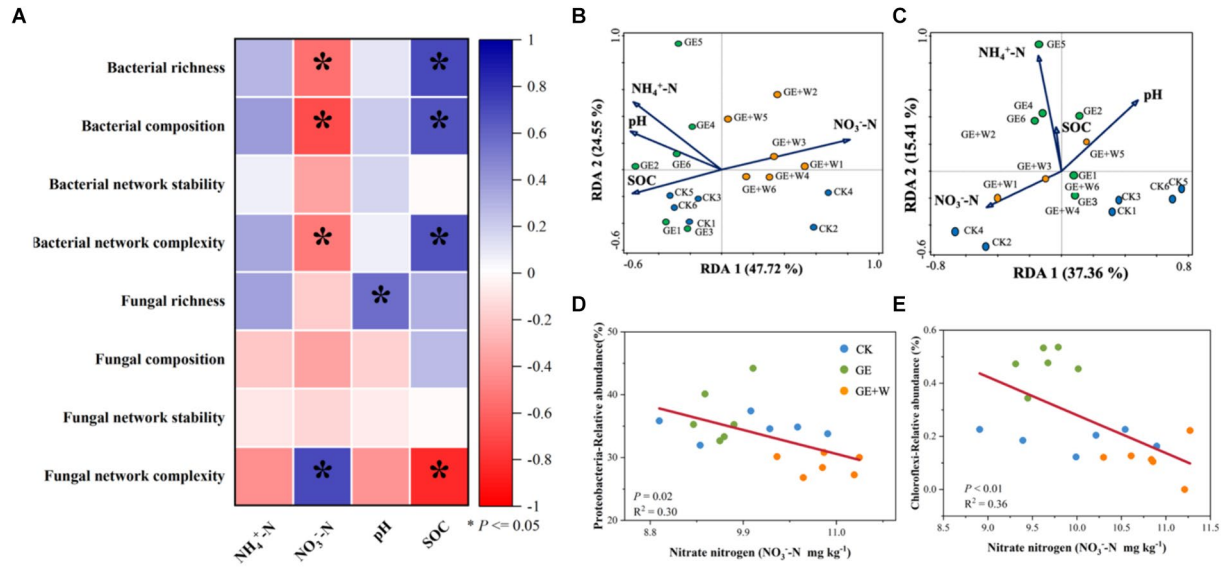

FIGURE 3
Relationships between microbial diversity, composition, network parameters, and soil properties. **(A)** Pearson correlation analysis of soil bacterial and fungal properties with soil properties. **(B)** Redundancy analysis of soil bacterial composition and soil properties. **(C)** Redundancy analysis of soil fungal composition and soil properties. **(D)** Linear fitting of soil nitrate nitrogen to Proteobacteria. **(E)** Linear fitting of soil nitrate nitrogen to Chloroflexi. NH_4^+-N: ammonium nitrogen, NO_3^-N, nitrate nitrogen; SOC, soil organic carbon. The blue color indicates a positive correlation, and the red color indicates a negative correlation; $*p < 0.05$.

Moreover, the benefits of grazer exclosure on soil microbial communities can be modulated by other environmental factors, such as climate warming (Li et al., 2016; Guo et al., 2018, 2019). For example, the positive effect of exclosure on bacterial α-diversity is weakened by warming (Wu L. et al., 2022; He et al., 2022). Our findings corroborate this, as we observed that grazer exclosure plus warming treatment had a negative impact on bacterial richness. This is likely because increased temperatures exacerbate the metabolic costs for soil bacteria, leading to competitive displacement and reduced survival rates of temperature-sensitive species (Söllinger et al., 2022) such as Proteobacteria (Zhang et al., 2015; Zhao et al., 2024). Similarly, we found that warming treatment of exclosure areas reduced the relative abundance of Proteobacteria but did not affect the structure and composition of the fungal community. Fungi are more resistant to environmental changes and disturbances than bacteria because of their active dispersal traits (Roper et al., 2010; Liu Y. et al., 2024).

Our results demonstrate that grazer exclosure without warming treatment increased the number of soil microbial network nodes and edges but did not change bacterial network complexity or stability. In contrast, grazer exclosure with warming treatment had the same effect on the number of microbial network nodes, edges, and stability, but significantly decreased bacterial network complexity and increased fungal network complexity. These results suggest that soil networks become more connected as natural restoration proceeds (Morriën et al., 2017), whereas grazer exclosure under climate warming enhances the competitive advantage of fungi and adversely affects the stability of bacterial communities (Jia et al., 2023; Zhou et al., 2023; Zhu et al., 2023). Our results are consistent with previous research conducted in coastal areas (Zhou et al., 2021) and the Loess Plateau (Wang et al., 2024), which suggests that warming leads to bacterial community instability due to shrinking soil microbial ecological niches (Yang et al., 2013; Wu et al., 2021). However, studies conducted in the tallgrass prairie (Yuan et al., 2021) and the Tibetan Plateau (Chen et al., 2023) found that warming enhances the complexity and stability of bacterial networks. These inconsistent observations may result from differences in ecosystem vulnerability and sensitivity (Zhang M. et al., 2023). The desert steppe responds strongly to climate change due to its arid climate, infertile soils, and ecological fragility (Yang et al., 2020); in which case, microbial networks may loosen or even collapse with warming (Ullah et al., 2018).

4.2 Grazer exclosure impacts bacterial microbial communities by influencing nitrate nitrogen content under warming

As expected, our experiment revealed that soil nitrate nitrogen content influenced microbial community composition, evidenced by a decrease in the relative abundance of soil metazoans and green curvilinear bacteria with increasing nitrate nitrogen content. We found that grazer exclosure treatment increased soil ammonium nitrogen content, while grazer exclosure plus warming increased nitrate nitrogen content, in line with previous studies indicating that grazer exclosure would allow soil nutrients to recover (Cheng et al., 2016; Wang et al., 2019; Liu et al., 2019). Climate warming affects soil nitrogen availability and subsequently impacts the microbial community (Li et al., 2024; Bai et al., 2013). As temperatures rise, microbial activity and metabolism increase, stimulating the mineralization of organic nitrogen compounds into inorganic forms such as ammonium (NH_4^+) and nitrate (NO_3^-), which are more readily available to microorganisms (Liu et al., 2022). Additionally, climate warming enhances nitrification in grassland soils, accelerating the conversion of ammonium to nitrate. Higher nitrate nitrogen content consequently inhibits microbes with lower nitrogen requirements (Shi et al., 2023). Zhou et al. (2015) also found that soil nitrate nitrogen

content has a major influence on microbial community structure, with high nitrate nitrogen content resulting in lower Pedosphaerae abundance. We also observed that soil nitrate nitrogen content was negatively correlated with bacterial richness and network complexity and had a negative effect on bacterial community composition. In contrast, there was a positive correlation with fungal complexity and no significant correlation to fungal community composition and diversity. Indeed, bacterial community composition is primarily regulated by soil factors, whereas fungal community composition is regulated by plants (Su et al., 2023). A recent meta-analysis showed that shifts in microbial α-diversity under global change were mainly explained by soil pH (Zhou et al., 2020). Kang et al. (2021) also found changes in soil microbial diversity and community structure were caused by pH and organic carbon content. This is inconsistent with our findings in which soil pH and organic carbon content were not found to affect the microbial community, which might be due to a shorter period of grazer exclosure in our study.

5 Conclusion

Overall, we showed that grazer exclosure is effective in increasing soil microbial diversity without affecting the stability of their networks. These benefits may be affected by climate warming, which reduces bacterial diversity and network complexity by increasing nitrate nitrogen contents. Our study demonstrated that the recovery of soil microbial communities in degraded grasslands through grazing exclosure may be slow under future warming scenarios. Moreover, long-term grazing exclosure may reduce the income of herders and, consequently, regional and national economies. Therefore, land managers need to consider the environmental as well as social and economic implications of degraded grassland restoration measures. Developing climate change-adapted grassland management measures, such as rotational grazing, could be a suitable option for maintaining grassland sustainability.

Data availability statement

The original contributions presented in the study are included in the article/Supplementary material, further inquiries can be directed to the corresponding author.

Author contributions

JQ: Conceptualization, Data curation, Formal analysis, Methodology, Software, Visualization, Writing – original draft, Writing – review & editing. JZ: Data curation, Software, Visualization, Writing – review & editing. SL: Data curation, Software, Visualization, Writing – review & editing. FZ: Data curation, Writing – review & editing. BZ: Writing – review & editing. MZ: Funding acquisition, Supervision, Writing – review & editing.

Funding

The author(s) declare that financial support was received for the research, authorship, and/or publication of this article. This study was supported by the Inner Mongolia Nature Foundation Major Project (2020ZD03) and the Natural Science Foundation of Inner Mongolia (2024QN03049).

Conflict of interest

The authors declare that the research was conducted in the absence of any commercial or financial relationships that could be construed as a potential conflict of interest.

Publisher's note

Supplementary material

The Supplementary material for this article can be found online at: https://www.frontiersin.org/articles/10.3389/fmicb.2024.1458777/full#supplementary-material

References

Bai, E., Li, S. L., Xu, W. H., Li, W., Dai, W., and Jiang, P. (2013). A meta-analysis of experimental warming effects on terrestrial nitrogen pools and dynamics. *New Phytol.* 199, 441–451. doi: 10.1111/nph.12252

Brown, J. H., Gillooly, J. F., Allen, A. P., Savage, V., and West, G. (2004). Toward a metabolic theory of ecology. *Ecology* 85, 1771–1789. doi: 10.1890/03-9000

Cao, J., Jiao, Y., Che, R., Holden, N. M., Zhang, X., Biswas, A., et al. (2022). The effects of grazer exclosure duration on soil microbial communities on the Qinghai-Tibetan plateau. *Sci. Total Environ.* 839:156238. doi: 10.1016/j.scitotenv.2022.156238

Chen, X., and Chen, H. Y. H. (2018). Global effects of plant litter alterations on soil CO_2 to the atmosphere. *Glob. Chang. Biol.* 24, 3462–3471. doi: 10.1111/gcb.14147

Chen, K., Xing, S., Shi, H., Tang, Y., Yang, M., Gu, Q., et al. (2023). Long-term fencing can't benefit plant and microbial network stability of alpine meadow and alpine steppe in Three-River-source National Park. *Sci. Total Environ.* 902:166076. doi: 10.1016/j.scitotenv.2023.166076

Cheng, J., Jing, G., Wei, L., and Jing, Z. (2016). Long-term grazing exclusion effects on vegetation characteristics, soil properties and bacterial communities in the semi-arid grasslands of China. *Ecol. Eng.* 97, 170–178. doi: 10.1016/j.ecoleng.2016.09.003

Coban, O., De Deyn, G. B., and Van Der Ploeg, M. (2022). Soil microbiota as game-changers in restoration of degraded lands. *Science* 375:abe0725. doi: 10.1126/science.abe0725

Ding, X., Zhang, B., Filley, T. R., Tian, C., Zhang, X., and He, H. (2019). Changes of microbial residues after wetland cultivation and restoration. *Biol. Fertil. Soils.* 55, 405–409. doi: 10.1007/s00374-019-01341-2

Eldridge, D. J., Delgado-Baquerizo, M., Travers, S. K., Val, J., Oliver, I., Hamonts, K., et al. (2017). Competition drives the response of soil microbial diversity to increased grazing by vertebrate herbivores. *Ecology.* 98, 1922–1931. doi: 10.1002/ecy.1879

Fan, D., Kong, W., Wang, F., Yue, L., and Li, X. (2020). Fencing decreases microbial diversity but increases abundance in grassland soils on the Tibetan plateau. *Land Degrad. Dev.* 31, 2577–2590. doi: 10.1002/ldr.3626

Faust, K., and Raes, J. (2012). Microbial interactions: from networks to models. *Nat. Rev. Microbiol.* 10, 538–550. doi: 10.1038/nrmicro2832

Geng, M., Wang, X., Liu, X., and Lv, P. (2023). Effects of grazing exclusion on microbial community diversity and soil metabolism in desert grasslands. *Sustain. For.* 15:11263. doi: 10.3390/su151411263

Guo, X., Feng, J., Shi, Z., Zhou, X., Yuan, M., Tao, X., et al. (2018). Climate warming leads to divergent succession of grassland microbial communities. *Nat. Clim. Change* 8, 813–818. doi: 10.1038/s41558-018-0254-2

Guo, X., Zhou, X., Hale, L., Yuan, M., Ning, D., Feng, J., et al. (2019). Climate warming accelerates temporal scaling of grassland soil microbial biodiversity. *Nat. Ecol. Evol.* 3, 612–619. doi: 10.1038/s41559-019-0848-8

He, M., Pan, Y., Zhou, G., Barry, K. E., Fu, Y., and Zhou, X. (2022). Grazing and global change factors differentially affect biodiversity-ecosystem functioning relationships in grassland ecosystems. *Glob. Chang. Biol.* 28, 5492–5504. doi: 10.1111/gcb.16305

IPCC (2013) in Climate Change 2013: The physical science basis. eds. T. F. Stocker, D. Qin, G.-K. Plattner, M. Tignor, S. K. Allen and J. Boschunget al. (Cambridge: Cambridge University Press).

Jia, M., Gao, Z., Huang, J., Li, J., Liu, Z., Zhang, G., et al. (2023). Soil bacterial community is more sensitive than fungal community to nitrogen supplementation and climate warming in inner Mongolian desert steppe. *J. Soils Sediments* 23, 405–421. doi: 10.1007/s11368-022-03283-z

Kang, E., Li, Y., Zhang, X., Yan, Z., Wu, H., Li, M., et al. (2021). Soil pH and nutrients shape the vertical distribution of microbial communities in an alpine wetland. *Sci. Total Environ.* 774:145780. doi: 10.1016/j.scitotenv.2021.145780

Lauber, C. L., Hamady, M., Knight, R., and Fierer, N. (2009). Pyrosequencing-based assessment of soil pH as a predictor of soil bacterial community structure at the continental scale. *Appl. Environ. Microbiol.* 75, 5111–5120. doi: 10.1128/AEM.00335-09

Li, Y., Lin, Q., Wang, S., Li, X., Liu, W., Luo, C., et al. (2016). Soil bacterial community responses to warming and grazing in a Tibetan alpine meadow. *FEMS Microbiol. Ecol.* 92:fiv152. doi: 10.1093/femsec/fiv152

Li, S., Tang, S., Chen, H., and Jin, K. (2024). Soil nitrogen availability drives the response of soil microbial biomass to warming. *Sci. Total Environ.* 917:170505. doi: 10.1016/j.scitotenv.2024.170505

Lindsay, E. A., and Cunningham, S. A. (2009). Livestock grazing exclusion and microhabitat variation affect invertebrates and litter decomposition rates in woodland remnants. *For. Ecol. Manag.* 258, 178–187. doi: 10.1016/j.foreco.2009.04.005

Liu, J., Bian, Z., Zhang, K., Ahmad, B., and Khan, A. (2019). Effects of different fencing regimes on community structure of degraded desert grasslands on mu us desert, China. *Ecol. Evol.* 9, 3367–3377. doi: 10.1002/ece3.4958

Liu, Y., Delgado-Baquerizo, M., Bing, H., Wang, Y., Wang, J., Chen, J., et al. (2024). Warming-induced shifts in alpine soil microbiome: an ecosystem-scale study with environmental context-dependent insights. *Environ. Res.* 255:119206. doi: 10.1016/j.envres.2024.119206

Liu, D., Fei, Y., Peng, Y., Zhu, S., Lu, J., Luo, Y., et al. (2024). Genotype of pioneer plant *Miscanthus* is not a key factor in the structure of rhizosphere bacterial community in heavy metal polluted sites. *J. Hazard. Mater.* 477:135242. doi: 10.1016/j.jhazmat.2024.135242

Liu, J., Jia, X., Yan, W., Zhong, Y., and Shangguan, Z. (2020). Changes in soil microbial community structure during long-term secondary succession. *Land Degrad. Dev.* 31, 1151–1166. doi: 10.1002/ldr.3505

Liu, W. L., Jiang, Y. L., Su, Y., Smoak, J. M., and Duan, B. L. (2022). Warming affects soil nitrogen mineralization via changes in root exudation and associated soil microbial communities in a subalpine tree species *Abies fabri*. *J. Soil Sci. Plant Nutr.* 22, 406–415. doi: 10.1007/s42729-021-00657-z

Medina-Roldán, E., Paz-Ferreiro, J., and Bardgett, R. D. (2012). Grazing exclusion affects soil and plant communities, but has no impact on soil carbon storage in an upland grassland. *Agric. Ecosyst. Environ.* 149, 118–123. doi: 10.1016/j.agee.2011.12.012

Morriën, E., Hannula, S. E., Snoek, L. B., Helmsing, N. R., Zweers, H., de Hollander, M., et al. (2017). Soil networks become more connected and take up more carbon as nature restoration progresses. *Nat. Commun.* 8:14349. doi: 10.1038/ncomms14349

Nelson, D. W., and Sommers, L. E. (2018). "Total carbon, organic carbon, and organic matter" in SSSA Book Series. Soil Science Society of America. eds. D. L. Sparks, A. L. Page, P. A. Helmke, R. H. Loeppert, P. N. Soltanpour and M. A. Tabatabaiet al. (Madison, WI: American Society of Agronomy), 961–1010.

Pedrinho, A., Mendes, L. W., De Araujo Pereira, A. P., Araujo, A., Vaishnav, A., Karpouzas, D., et al. (2024). Soil microbial diversity plays an important role in resisting and restoring degraded ecosystems. *Plant Soil* 500, 325–349. doi: 10.1007/s11104-024-06489-x

Philippot, L., Chenu, C., Kappler, A., Rillig, M. C., and Fierer, N. (2024). The interplay between microbial communities and soil properties. *Nat. Rev. Microbiol.* 22, 226–239. doi: 10.1038/s41579-023-00980-5

Roper, M., Seminara, A., Bandi, M. M., Cobb, A., Dillard, H. R., and Pringle, A. (2010). Dispersal of fungal spores on a cooperatively generated wind. *Proc. Natl. Acad. Sci. USA* 107, 17474–17479. doi: 10.1073/pnas.1003577107

Shi, Y., Religieux, E., Kuzyakov, Y., Wang, J., Hu, J., and le Roux, X. (2023). Local climate conditions explain the divergent climate change effects on (de) nitrification across the grassland biome: A meta-analysis. *Soil Biol. Biochem.* 187:109218. doi: 10.1016/j.soilbio.2023.109218

Shu, X., Ye, Q., Huang, H., Xia, L., Tang, H., Liu, X., et al. (2024). Effects of grazing exclusion on soil microbial diversity and its functionality in grasslands: a meta-analysis. *Front. Plant Sci.* 15:1366821. doi: 10.3389/fpls.2024.1366821

Söllinger, A., Séneca, J., Borg Dahl, M., Motleleng, L. L., Prommer, J., Verbruggen, E., et al. (2022). Down-regulation of the bacterial protein biosynthesis machinery in response to weeks, years, and decades of soil warming. *Sci. Adv.* 8:eabm3230. doi: 10.1126/sciadv.abm3230

Su, J., Ji, W., Sun, X., Wang, H., Kang, Y., and Yao, B. (2023). Effects of different management practices on soil microbial community structure and function in alpine grassland. *J. Environ. Manag.* 327:116859. doi: 10.1016/j.jenvman.2022.116859

Tang, J., Davy, A. J., Jiang, D., Musa, A., Wu, D., Wang, Y., et al. (2016). Effects of excluding grazing on the vegetation and soils of degraded sparse-elm grassland in the Horqin Sandy land, China. *Agric. Ecosyst. Environ.* 235, 340–348. doi: 10.1016/j.agee.2016.11.005

Ullah, H., Nagelkerken, I., Goldenberg, S. U., and Fordham, D. A. (2018). Climate change could drive marine food web collapse through altered trophic flows and cyanobacterial proliferation. *PLoS Biol.* 16:e2003446. doi: 10.1371/journal.pbio.2003446

Wang, X., Wang, Z., Chen, F., Zhang, Z., Fang, J., Xing, L., et al. (2024). Deterministic assembly of grassland soil microbial communities driven by climate warming amplifies soil carbon loss. *Sci. Total Environ.* 923:171418. doi: 10.1016/j.scitotenv.2024.171418

Wang, Z., Zhang, Q., Staley, C., Gao, H., Ishii, S., Wei, X., et al. (2019). Impact of long-term grazing exclusion on soil microbial community composition and nutrient availability. *Biol. Fertil. Soils* 55, 121–134. doi: 10.1007/s00374-018-01336-5

Weedon, J. T., Kowalchuk, G. A., Aerts, R., van Hal, J., van Logtestijn, R., Taş, N., et al. (2012). Summer warming accelerates sub-arctic peatland nitrogen cycling without changing enzyme pools or microbial community structure. *Glob. Chang. Biol.* 18, 138–150. doi: 10.1111/j.1365-2486.2011.02548.x

Wei, Z., Han, G., Yang, J., and Lv, X. (2000). The response of *Stipa breviflora* community to stocking rate. *Grassland of China* 6, 1–5. doi: 10.3321/j.issn:1673-5021.2000.06.001

Wu, M.-H., Chen, S.-Y., Chen, J.-W., Xue, K., Chen, S. L., Wang, X. M., et al. (2021). Reduced microbial stability in the active layer is associated with carbon loss under alpine permafrost degradation. *Proc. Natl. Acad. Sci. USA* 118:e2025321118. doi: 10.1073/pnas.2025321118

Wu, Y., Chen, D., Delgado-Baquerizo, M., Liu, S., Wang, B., Wu, J., et al. (2022). Long-term regional evidence of the effects of livestock grazing on soil microbial community structure and functions in surface and deep soil layers. *Soil Biol. Biochem.* 168:108629. doi: 10.1016/j.soilbio.2022.108629

Wu, L., Zhang, Y., Guo, X., Ning, D., Zhou, X., Feng, J., et al. (2022). Reduction of microbial diversity in grassland soil is driven by long-term climate warming. *Nat. Microbiol.* 7, 1054–1062. doi: 10.1038/s41564-022-01147-3

Yang, Z., Gao, J., Zhao, L., Xu, X. L., and Ouyang, H. (2013). Linking thaw depth with soil moisture and plant community composition: effects of permafrost degradation on alpine ecosystems on the Qinghai-Tibet plateau. *Plant Soil* 367, 687–700. doi: 10.1007/s11104-012-1511-1

Yang, F., Huang, M., Li, C., Wu, X., and Fang, L. (2022). Vegetation restoration increases the diversity of bacterial communities in deep soils. *Appl. Soil Ecol.* 180:104631. doi: 10.1016/j.apsoil.2022.104631

Yang, F., Niu, K., Collins, C. G., Yan, X., Ji, Y., Ling, N., et al. (2019). Grazing practices affect the soil microbial community composition in a Tibetan alpine meadow. *Land Degrad. Dev.* 30, 49–59. doi: 10.1002/ldr.3189

Yang, Y., Wang, K., Liu, D., Zhao, X., and Fan, J. (2020). Effects of land-use conversions on the ecosystem services in the agro-pastoral ecotone of northern China. *J. Clean. Prod.* 249:119360. doi: 10.1016/j.jclepro.2019.119360

Yang, Z., Xiong, W., Xu, Y., Jiang, L., Zhu, E., Zhan, W., et al. (2016). Soil properties and species composition under different grazing intensity in an alpine meadow on the eastern Tibetan plateau, China. *Environ. Monit. Assess.* 188:678. doi: 10.1007/s10661-016-5663-y

Yao, M., Rui, J., Li, J., Wang, J., Cao, W., and Li, X. (2018). Soil bacterial community shifts driven by restoration time and steppe types in the degraded steppe of Inner Mongolia. *Catena* 165, 228–236. doi: 10.1016/j.catena.2018.02.006

Yuan, M. M., Guo, X., Wu, L., Zhang, Y., Xiao, N., Ning, D., et al. (2021). Climate warming enhances microbial network complexity and stability. *Nat. Clim. Chang.* 11, 343–348. doi: 10.1038/s41558-021-00989-9

Zhang, F., Bennett, J. A., Zhang, B., Wang, Z., Li, Z., Li, H., et al. (2023). Cessation of grazing stabilizes productivity through effects on species asynchrony and stability of shrub/semi-shrub plants in arid grasslands. *Agric. Ecosyst. Environ.* 348:108411. doi: 10.1016/j.agee.2023.108411

Zhang, M., Delgado-Baquerizo, M., Li, G., Isbell, F., Wang, Y., Hautier, Y., et al. (2023). Experimental impacts of grazing on grassland biodiversity and function are explained by aridity. *Nat. Commun.* 14:5040. doi: 10.1038/s41467-023-40809-6

Zhang, N. L., Wan, S. Q., Guo, J. X., Hang, G. D., Gutknecht, J., Schmid, B., et al. (2015). Precipitation modifies the effects of warming and nitrogen addition on soil microbial communities in northern Chinese grasslands. *Soil Biol. Biochem.* 89, 12–23. doi: 10.1016/j.soilbio.2015.06.022

Zhang, R., Wang, Z., Niu, S., Tian, D., Wu, Q., Gao, X., et al. (2021). Diversity of plant and soil microbes mediates the response of ecosystem multifunctionality to grazing disturbance. *Sci. Total Environ.* 776:145730. doi: 10.1016/j.scitotenv.2021.145730

Zhang, B., Zhang, F., Wang, X., Chen, D., Tian, Y., Wang, Y., et al. (2024). Secondary succession of soil, plants, and bacteria following the recovery of abandoned croplands in two semi-arid steppes. *Land Degrad. Dev.* 35, 296–307. doi: 10.1002/ldr.4916

Zhang, M.-X., Zhao, L.-Y., Hu, J.-P., Khan, A., Yang, X. X., Dong, Q. M., et al. (2023). Different grazers and grazing practices alter the growth, soil properties, and rhizosphere soil bacterial communities of *Medicago ruthenica* in the Qinghai-Tibetan plateau grassland. *Agric. Ecosyst. Environ.* 352:108522. doi: 10.1016/j.agee.2023.108522

Zhao, J., Xie, X., Jiang, Y., Li, J., Fu, Q., Qiu, Y., et al. (2024). Effects of simulated warming on soil microbial community diversity and composition across diverse ecosystems. *Sci. Total Environ.* 911:168793. doi: 10.1016/j.scitotenv.2023.168793

Zhou, J., Guan, D., Zhou, B., Zhao, B., Ma, M., Qin, J., et al. (2015). Influence of 34-years of fertilization on bacterial communities in an intensively cultivated black soil in Northeast China. *Soil Biol. Biochem.* 90, 42–51. doi: 10.1016/j.soilbio.2015.07.005

Zhou, S., Lie, Z., Liu, X., Liu, X., Zhu, Y.-G., Peñuelas, J., et al. (2023). Distinct patterns of soil bacterial and fungal community assemblages in subtropical forest ecosystems under warming. *Glob. Chang. Biol.* 29, 1501–1513. doi: 10.1111/gcb.16541

Zhou, Y., Sun, B., Xie, B., Feng, K., Zhang, Z., Zhang, Z., et al. (2021). Warming reshaped the microbial hierarchical interactions. *Glob. Chang. Biol.* 27, 6331–6347. doi: 10.1111/gcb.15891

Zhou, X., Wang, J., Hao, Y., and Wang, Y. (2010). Intermediate grazing intensities by sheep increase soil bacterial diversities in an inner Mongolian steppe. *Biol. Fertil. Soils* 46, 817–824. doi: 10.1007/s00374-010-0487-3

Zhou, Z., Wang, C., and Luo, Y. (2020). Meta-analysis of the impacts of global change factors on soil microbial diversity and functionality. *Nat. Commun.* 11:3072. doi: 10.1038/s41467-020-16881-7

Zhu, L., Chen, Y., Sun, R., Zhang, J., Hale, L., Dumack, K., et al. (2023). Resource-dependent biodiversity and potential multi-trophic interactions determine belowground functional trait stability. *Microbiome* 11:95. doi: 10.1186/s40168-023-01539-5

frontiers | Frontiers in Microbiology

TYPE Original Research
PUBLISHED 06 November 2024
DOI 10.3389/fmicb.2024.1481044

OPEN ACCESS

EDITED BY
Yan Xing Dou,
Institute of Soil and Water Conservation, Chinese Academy of Sciences (CAS), China

REVIEWED BY
Ludmila Chistoserdova,
University of Washington, United States
Junjie Lin,
Zhejiang University of Science and Technology, China

*CORRESPONDENCE
Zhongjun Jia
jia@issas.ac.cn

RECEIVED 15 August 2024
ACCEPTED 18 October 2024
PUBLISHED 06 November 2024

CITATION
Zheng Y, Cai Y and Jia Z (2024) Role of methanotrophic communities in atmospheric methane oxidation in paddy soils.
Front. Microbiol. 15:1481044.
doi: 10.3389/fmicb.2024.1481044

Role of methanotrophic communities in atmospheric methane oxidation in paddy soils

Yan Zheng[1], Yuanfeng Cai[2] and Zhongjun Jia[2]*

[1]College of Food and Bioengineering, Zhengzhou University of Light Industry, Zhengzhou, Henan, China, [2]State Key Laboratory of Soil and Sustainable Agriculture, Institute of Soil Science, Chinese Academy of Sciences, Nanjing, Jiangsu, China

Wetland systems are known methane (CH_4) sources. However, flooded rice fields are periodically drained. The paddy soils can absorb atmospheric CH_4 during the dry seasons due to high-affinity methane-oxidizing bacteria (methanotroph). Atmospheric CH_4 uptake can be induced during the low-affinity oxidation of high-concentration CH_4 in paddy soils. Multiple interacting factors control atmospheric CH_4 uptake in soil ecosystems. Broader biogeographical data are required to refine our understanding of the biotic and abiotic factors related to atmospheric CH_4 uptake in paddy soils. Thus, here, we aimed to assess the high-affinity CH_4 oxidation activity and explored the community composition of active atmospheric methanotrophs in nine geographically distinct Chinese paddy soils. Our findings demonstrated that high-affinity oxidation of 1.86 parts per million by volume (ppmv) CH_4 was quickly induced after 10,000 ppmv high-concentration CH_4 consumption by conventional methanotrophs. The ratios of 16S rRNA to rRNA genes (rDNA) for type II methanotrophs were higher than those for type I methanotrophs in all acid-neutral soils (excluding the alkaline soil) with high-affinity CH_4 oxidation activity. Both the 16S rRNA:rDNA ratios of type II methanotrophs and the abundance of ^{13}C-labeled type II methanotrophs positively correlated with high-affinity CH_4 oxidation activity. Soil abiotic factors can regulate methanotrophic community composition and atmospheric CH_4 uptake in paddy soils. High-affinity methane oxidation activity, as well as the abundance of type II methanotroph, negatively correlated with soil pH, while they positively correlated with soil nutrient availability (soil organic carbon, total nitrogen, and ammonium-nitrogen). Our results indicate the importance of type II methanotrophs and abiotic factors in atmospheric CH_4 uptake in paddy soils. Our findings offer a broader biogeographical perspective on atmospheric CH_4 uptake in paddy soils. This provides evidence that periodically drained paddy fields can serve as the dry-season CH_4 sink. This study is anticipated to help in determining and devising greenhouse gas mitigation strategies through effective farm management in paddy fields.

KEYWORDS

atmospheric methane oxidation, high-affinity methanotrophs, methanotrophic biogeography, paddy soils, stable isotope probing

1 Introduction

The atmospheric concentration of methane (CH_4), a significant greenhouse gas, has increased from 0.82 parts per million volume (ppmv) in 1841 to over 1.86 ppmv in 2019 (Etheridge et al., 1992; IPCC, 2021). Wetlands are known CH_4 sources with high global warming potential (IPCC, 2021). However, flooded paddy soils (Conrad, 2007), Arctic wetlands (Voigt et al., 2023), and mire-wetlands (Wang et al., 2023), known as CH_4 emitters, act as CH_4 sinks during dry periods. Multiple interacting factors control the atmospheric CH_4 concentrations in wetlands (Maucieri et al., 2017). Hence, an investigation of potential soil factors that increase wetland soil CH_4 sinks is needed to mitigate the greenhouse effect.

Water content plays a critical role in controlling CH_4 emissions in wetlands by regulating the relative proportions of anaerobic zones for CH_4 production and aerobic zones for CH_4 oxidation within the soil column (Schultz et al., 2023). Soil drying promotes atmospheric CH_4 uptake in Arctic soils (Voigt et al., 2023). Higher CH_4 uptake is linked to increased availability of soil nutrients (Lee et al., 2023; Voigt et al., 2023). The soil CH_4 sink increases with enhanced soil nitrogen (Voigt et al., 2023). Nitrogen promotes CH_4 oxidation by stimulating the growth of methane-oxidizing bacteria (methanotroph) in paddy soils (Zheng et al., 2014; Nijman et al., 2021). Soil organic carbon (SOC) decomposition can provide an alternative carbon substrate that promotes the growth of methanotrophs, thereby mediating the atmospheric CH_4 uptake (Lee et al., 2023). SOC decomposition responds to various complex factors in soil ecosystems (Lin et al., 2023). Increased temperatures can stimulate SOC decomposition (Zhao et al., 2023; Nazir et al., 2024). Temperature positively affects soil CH_4 sink (Lee et al., 2023). Soil pH may also influence the CH_4 oxidation activity by regulating the methanotrophic community (Shiau et al., 2018; Zhao et al., 2020).

Methane-oxidizing bacteria-based microbial CH_4 oxidation is the sole known biological sink of atmospheric CH_4 (Saunois et al., 2020). Almost all cultivated aerobic methanotrophs belong to *Proteobacteria* and are divided into two major subgroups: type I methanotrophs (*Gammaproteobacteria*) and type II methanotrophs (*Alphaproteobacteria*) (Dedysh and Knief, 2018). Established type II methanotrophs, such as *Methylocystis*, *Methylosinus*, and *Methylocapsa* (Baani and Liesack, 2008; Tveit et al., 2019; Tikhonova et al., 2021) and certain conventional type I methanotrophs can oxidize atmospheric CH_4 (Benstead et al., 1998). Type I and type II methanotrophs predominate under different environmental conditions, owing to their distinct life strategies (Ho et al., 2013). Type I methanotrophs are generally favored by high nutrient availability (Steenbergh et al., 2010; Zheng et al., 2014), whereas type II methanotrophs are more competitive under oligotrophic conditions (Cai et al., 2016). Abiotic factors affect soil atmospheric CH_4 levels by regulating the methanotrophic community (Conrad, 2007; Lee et al., 2023; Voigt et al., 2023). Therefore, understanding the roles of different methanotrophic taxa in atmospheric CH_4 uptake will provide deeper insights into the mitigation capacity of methanotrophic communities.

Rice fields play a central role in determining the global CH_4 budget (IPCC, 2021). The varying water content in the rice fields results in notable fluctuations in soil CH_4 concentrations (Conrad, 2007). A nature wetland conversation to the upland can turn a CH_4 source into a CH_4 sink (Wang et al., 2023). The rice fields are similar to aerated upland soils during the dry seasons (Conrad, 2007). The paddy soil CH_4 source under flooded conditions turns into an atmospheric CH_4 sink during the dry seasons (Singh et al., 1996). Paddy soils oxidize atmospheric CH_4 only after incubation under conditions involving high CH_4 (Yan and Cai, 1997). Conventional methanotrophs in a typical paddy soil can rapidly induce high-affinity CH_4 oxidation (1.86 ppmv) when exposed to high CH_4 concentrations (Cai et al., 2016). The aforementioned previous studies provide evidence that periodically drained paddy fields can act as an atmospheric CH_4 sink. Therefore, the investigation of broader biogeographical data is needed to improve our understanding of the factors related to atmospheric CH_4 uptake in paddy soils. This study will help determine effective farm management strategies to enhance atmospheric CH_4 sink in paddy fields, providing a climate mitigation strategy.

Here, we aimed to assess high-affinity CH_4 oxidation activity and explore the community composition of active atmospheric methanotrophs. To this end, we selected nine paddy soils across three climate zones from the primary rice production areas in China. The potential activity of the methanotrophic community in the paddy soils was explored using the 16S rRNA:rDNA ratios of methanotrophs based on high-throughput sequencing and documenting their $^{13}CH_4$-labeled relative abundance complemented by DNA- and RNA-based stable isotope probing (SIP). The 16S rRNA:rDNA ratios may offer deeper insights into bacterial community activity than those of abundance alone (Campbell and Kirchman, 2013). In combination with high-throughput sequencing, DNA- and RNA-based SIP can target active methanotrophic communities by providing the growth substrate $^{13}CH_4$ (Dumont et al., 2011). To our best knowledge, this is the first large-scale study to analyze the potential atmospheric CH_4 uptake activity and ecological roles of different methanotrophs in atmospheric methane oxidation in paddy soils.

2 Materials and methods

2.1 Sampling sites

Paddy soils were sampled from nine different sites across the primary rice production areas in China (Figure 1A). The annual mean temperatures (AMT) ranged from 3.0 to 24.1°C at the sampling sites (Supplementary Table 1). All the sites have been used for rice cultivation for over 50 years. Soils were collected from each site immediately after the rice harvest, when the paddy fields had been drained. Five soil blocks, 20 meters apart from each other, were collected, and mixed to obtain a composite soil sample from each site. For each soil block, bulk soil from a depth of 0–15 cm was collected using a stainless-steel corer with an inner diameter of 7 cm. The composite soils were transported on ice to the laboratory and stored at 4°C for the analysis of soil environmental factors and

Abbreviations: ppmv, parts per million by volume; methanotroph, methane-oxidizing bacteria; GC-FID, gas chromatography-flame ionization detector; SIP, stable isotope probing; ANOVA, analysis of variance; RDA, redundancy analysis; PHB, polyhydroxybutyrate; SOC, soil organic carbon; TN, total nitrogen; RPCs, rice paddy clusters.

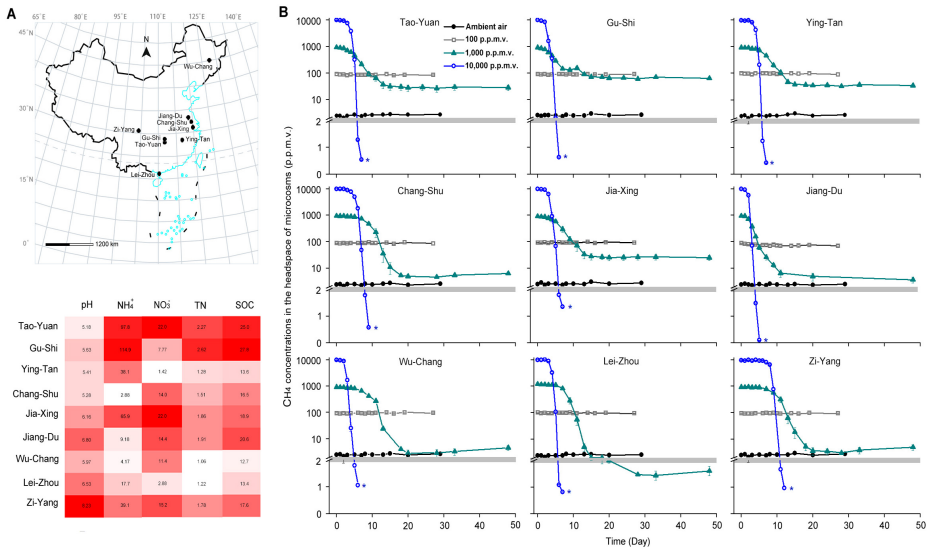

FIGURE 1
Emergence of high-affinity methane (CH_4) oxidation in paddy soils sampled from China. **(A)** The sampling locations and soil abiotic factors of paddy soils in China. **(B)** CH_4 consumption of paddy soils during incubation with various initial CH_4 concentrations in the headspace of microcosms. The blue asterisks indicate the soil samples used to verify high-affinity CH_4 oxidation activity in Figure 2 and to explore methanotrophic activity in Figure 3. The error bars represent standard deviations of triplicate microcosms. NO_3^-, nitrate (μg N g^{-1} dry weight soil [*d.w.s.*]); NH_4^+, ammonium (μg N g^{-1} *d.w.s.*); TN, total nitrogen (mg g^{-1} *d.w.s.*); and SOC, soil organic carbon (mg g^{-1} *d.w.s.*).

incubation experiments. The soils were passed through a 2-mm sieve prior to incubation.

2.2 Soil variables

Soil pH was measured in a 1:2.5 (w/v) soil-to-water suspension using a Mettler Toledo 320-S pH meter (Mettler Toledo Instruments, Shanghai, China). Soil inorganic nitrogen, extracted using 2 mol/L KCl, was determined using a Skalar San Plus segmented flow analyser (Skalar, Breda, Netherlands). Soil total nitrogen (TN) and SOC were measured using a Vario Max CN element analyser (Elementar, Langenselbold, Germany). The total quantity of water absorbed by the soil is estimated using the water-holding capacity, which can be measured by the soil-cutting ring method (Yang et al., 2023). Briefly, the soil samples were oven-dried at 105°C for 8 h and then placed into a container. The dried soils were treated with water absorption. After soaking in water for 24 h, the weights of soaked soil samples were measured. The soaked soils were oven-dried at 105°C for 8 h until a constant weight was recorded. The weights of dry soil were recorded to determine the water content, which was then used to calculate the maximum water-holding capacity. The maximum water-holding capacity for each paddy soil is described in Supplementary Table 1.

2.3 Microcosm construction

The soil moisture of each 300 g of soil sample was adjusted to 60% maximum water-holding capacity and preincubated in an incubator for four days under ambient air conditions at 28°C in the dark. The incubator temperature (28°C) was monitored throughout the preincubation period. The fluctuation of temperature was within ± 0.1°C. Preincubated paddy soils were used as the initial soils (day 0). Before the development of a microcosm, water loss was replenished to maintain 60% maximum water-holding capacity in each soil.

The microcosms were constructed by adding 6.0 g (dry weight) of preincubated soil to a serum bottle (120 mL) capped with a gas-tight butyl rubber stopper. Identical microcosms were created using initial CH_4 concentrations of 10,000, 1,000, 100, and 2 ppmv (ambient air) to mimic the fluctuating CH_4 concentrations in periodically drained rice fields. The microcosms were placed into the incubator. The treatments were conducted at 60% maximum water holding capacity and 28°C in the dark throughout the incubation. Water loss could be generated as tiny droplets of water on the inner walls of the microcosm bottles during incubation. To maintain the soil moisture, we gently shook the bottles 3–5 times using our hands to return the water to the soil.

For the 10,000 ppmv CH_4-amended soils, the $^{12}CH_4$ (control) and $^{13}CH_4$ SIP treatments were incubated with $^{12}CH_4$ and $^{13}CH_4$ (99 atom % ^{13}C; Sigma–Aldrich Co., St Louis, MO, USA), respectively, with six replicates. The $^{12}CH_4$ and $^{13}CH_4$ SIP treatments were incubated with a 60% maximum water-holding capacity and were maintained at 28°C in the dark throughout the incubation. When the headspace CH_4 concentrations were reduced to < 1.40 ppmv in the SIP microcosms, destructive sampling was performed in triplicate for $^{12}CH_4$ and $^{13}CH_4$ treatments. The incubated soils were dug using a stainless-steel sampling spoon from each bottle and divided into subsamples. For nucleic acid extraction, 3.0 g of the soils was immediately suspended in RNA*later* (Ambion, Austin, TX, USA), stored at 4°C overnight, and frozen at −80°C. The remaining subsamples were stored at −20°C for further analysis.

The headspace gas in the remaining 10,000 ppmv CH_4-amended microcosms was replaced with ambient air (~1.86 ppmv CH_4) to monitor the high-affinity CH_4 oxidation activity. The microcosms were incubated at a 60% maximum water-holding capacity and 28°C in the dark throughout the incubation. The gas samples were immediately analyzed when the bottles were closed with gas-tight butyl rubber stoppers (hour 0). After 3 h of incubation, the gas samples were immediately analyzed (hour 3). The high-affinity CH_4 oxidation activity was determined by calculating the amount of atmospheric CH_4 that can be oxidized in the first 3 h (Cai et al., 2016).

CH_4 concentration in the headspace was measured using a gas chromatography-flame ionization detector (GC-FID) (Shimadzu GC12-A, Kyoto, Japan). The column oven, injection, and FID detector temperatures were 40, 75, and 250, respectively. The flow rate of the carrier gas (N_2) was 30 mL min^{-1}. The injection volume was 200 μL, and the samples were analyzed twice. The equipment was calibrated as previously described (Preuss et al., 2013). CH_4 standard gases at concentrations of 1.7, and 200 ppmv, 1, 10, and 50 vol % were used. The uncertainty due to manual injection onto the column was < 10% for the 1.7 ppmv standard and < 1% for the standards above 200 ppmv.

2.4 Nucleic acid extraction and SIP gradient fractionation

Total nucleic acids were extracted from paddy soils using the protocol developed by Mettel et al. (2010), with slight modifications (Cai et al., 2016). Soil samples stored at −80 °C in RNA*later* were thawed on ice. Subsequently, the samples were pelleted at 20,000 × *g* for 1 min to remove the supernatants. The pellets were mixed with 0.5 g of glass beads (0.5 mm: 0.1 mm = 3:2) and resuspended in acidic lysis buffers. The mixture was shaken using two rounds of bead-beating. The supernatant was obtained at 20,000 × *g* for 1 min, and successively extracted using water-saturated phenol (pH 4.5), phenol-chloroform–isoamyl alcohol (25:24:1 [vol/vol/vol], pH 4.5), and chloroform–isoamyl alcohol (24:1 [v/v], pH 5.5). The resulting aqueous phase was mixed with two volumes of PEG–NaCl (30% PEG-6000, 1.6 M NaCl). After incubation at 25°C for 5 min, the mixture was centrifuged at 20,000 × *g* for 30 min to obtain the nucleic acid pellet. The pellets were washed with 400 μL of 70% ethanol and resuspended in 50 μL of nuclease-free H_2O. DNA was isolated from the total nucleic acid through RNase I digestion (Ambion, Austin, TX, USA). RNA was separated from the total nucleic acid through DNase I digestion (Ambion, Austin, TX, USA) and purified using an RNeasy Mini Kit (Qiagen, Hilden, Germany). Contaminating DNA in the RNA samples was assessed through PCR for 16S rRNA genes (Cai et al., 2016).

The quantity and purity of the nucleic acid were assessed using NanoDrop ND-1000 spectrophotometer (NanoDrop Technologies, USA). The purity of nucleic acid was represented by the absorbance ratio between nucleic acid (260 nm) and both humic acids and salts (230 nm) (A260/A230) and between nucleic acid (260 nm) and both humic acids and proteins (280 nm) (A260/A280). The DNA and RNA levels were in the range of 2.61–22.4 and 0.58–8.43 μg g^{-1} dry weight soil (*d.w.s.*) for the nine soils, respectively (Supplementary Table 2). The A260/A230 and A260/280 for DNA were in the range of 1.19–1.59 and 1.50–1.94, respectively. The A260/A230 and A260/280 for RNA were in the range of 1.14–1.62 and 1.48–1.87, respectively.

DNA-SIP (Zheng et al., 2014) and RNA-SIP fractionation (Dumont et al., 2011) in the $^{12}CH_4$ and $^{13}CH_4$ treatments were performed. RNA was reverse-transcribed into complementary DNA (cDNA) using a PrimeScript 1st Strand cDNA Synthesis Kit (Takara, Beijing, China) and random hexamers (Cai et al., 2016).

2.5 Real-time quantitative PCR of the *pmoA* genes

Total DNA from day 0 and $^{13}CH_4$ treatment and fractionated DNA from the $^{12}CH_4$ and $^{13}CH_4$ treatments were selected for the real-time quantitative PCR (qPCR) of the *pmoA* genes using the primer pair A189F/mb661r (Costello and Lidstrom, 1999) on a CFX96 Optical Real-Time Detection System (Bio-Rad, Hercules, CA, USA). Real-time qPCR was performed as described previously (Zheng et al., 2014). The cycling conditions were set as follows: 3 min at 95°C, followed by 40 cycles of 95°C for 10 s, 55°C for 30 s, 72°C for 30 s, and 80°C for 5 s with the plate read. The melt curve analysis was monitored from 65 to 95°C. One representative cloning containing *pmoA* genes was used to generate standards. The plasmid DNA was extracted from the clone and then diluted to create a series of standard templates. The standard curve of bacteria *pmoA* genes covered 10^2 to 10^8 copies of template per assay. The amplification efficiencies for the *pmoA* genes were 93–99%, with R^2 values of 0.991–0.999. A serial dilution of the DNA template in paddy soils was performed to assess whether the PCR was inhibited during the amplification. For quantifying the *pmoA* gene in the paddy soils, the fractionated DNA was undiluted, and the total DNA was diluted by 20-fold. The amplification specificity was investigated using melting curve analysis and standard agarose gel electrophoresis at the end of a PCR run.

2.6 High-throughput sequencing of the *pmoA* genes

Total DNA from day 0 and $^{13}CH_4$ treatment and fractionated ^{13}C-DNA containing the peak *pmoA* gene copies from the heavy fraction of the $^{13}CH_4$ treatment were selected for high-throughput sequencing of *pmoA* genes using the barcode primer pair A189F/mb661r (Costello and Lidstrom, 1999) on a Roche 454 GS FLX Titanium sequencer (Roche Diagnostics Corporation, Branford, CT, USA). Raw sequence files were processed using the mothur software for quality control (Schloss et al., 2009). Low-quality sequence reads (read with lengths < 200 bp, ambiguous bases > 0, homopolymers > 6, primer mismatches, and average quality scores < 30) were removed. Subsequently, these sequences were processed with the online version of FunGene pipelines to remove the chimera using USEARCH 6.0 (Cai et al., 2016). The *pmoA* gene sequences were classified using a naïve classifier implemented with the mothur software (Zhao et al., 2020).

2.7 High-throughput sequencing of 16S rDNA and rRNA

Total DNA and cDNA from day 0 and $^{13}CH_4$ treatment and fractionated DNA and cDNA from $^{12}CH_4$ and $^{13}CH_4$ treatments were selected for sequencing the 16S rDNA and rRNA, respectively, using the barcode primer pair 515F/907R (Zheng et al., 2014) on a Roche 454 GS FLX Titanium sequencer (Roche Diagnostics Corporation, Branford, CT, USA). Raw sequence files were processed using the mothur software for quality control (Schloss et al., 2009). Low-quality sequence reads (read with lengths < 200 bp, ambiguous bases > 0, homopolymers > 6, primer mismatches, and average quality scores < 30) were filtered for quality. Subsequently, the UCHIME algorithm was used to remove the chimeric sequences with a chimera-free reference database using the USEARCH tool (Ren et al., 2015). High-quality 16S rDNA and rRNA sequences were taxonomically classified using the Ribosomal Database Project classifier (Cai et al., 2016).

2.8 Statistical analysis

The methanotrophic communities in the paddy soils were compared using a one-way analysis of variance, followed by Tukey's *post-hoc* test ($p < 0.05$). Statistical analyses were performed using SPSS version 24.0 (IBM Corporation, Armonk, NY, USA). Soil microbial co-occurrence network structures were constructed based on 16S rRNA sequencing data in R software using the SpiecEasi package (Cao et al., 2022) and visualized using the Gephi interactive platform (Barberán et al., 2012). Spearman's rank correlations were calculated at the genus level for all taxa in the paddy soils on day 0 and when the soils can oxidize atmospheric CH_4. Correlations with $\rho > 0.6$ and $p < 0.05$ were considered robust correlations (Gao et al., 2022). A redundancy analysis (RDA) was applied to investigate the influence of abiotic factors on the methanotrophic community composition in the paddy soils. Methanotrophic community composition was based on the *pmoA* gene in the paddy soils with high-affinity methane oxidation activity. The abundance of methanotrophic genera was expressed as the *pmoA* gene copies of total methanotrophs based on qPCR multiplied by the relative abundance of the targeted methanotrophic genera-related *pmoA* genes based on high-throughput sequencing. Detrended correspondence analysis (DCA) was used to analyze the data matrix, suggesting that the best-fit mathematical model was the RDA. Permutational multivariate analysis of variance (PERMANOVA) was used to test whether the different abiotic factors harbored significantly different methanotrophic communities (Kaupper et al., 2022). The RDA analysis was implemented in the R package vegan v4.2.1 function.

3 Results

3.1 High-affinity oxidation of atmospheric CH_4 in paddy soils

CH_4 could not be oxidized under conditions involving 2 or 100 ppmv concentrations in the microcosms (Figure 1B). In contrast, the headspace CH_4 concentrations were significantly reduced during the incubation with CH_4 concentrations of 1,000 and 10,000 ppmv. CH_4 concentrations in the 10,000 ppmv CH_4-amended microcosms reduced to < 1.40 ppmv for 4–11 days in paddy soils (Figure 1B), indicating the widespread potential to use atmospheric CH_4 in paddy soils.

Following the consumption of 10,000 ppmv CH_4, the headspace gas of the microcosms was renewed with ambient air (~1.86 ppmv CH_4) (Figure 2). The atmospheric CH_4 concentrations were rapidly reduced in all paddy soils. The high-affinity CH_4 oxidation activity, assessed based on the amount of atmospheric CH_4 oxidized in the first 3 h, varied from 0.07 to 0.23 nmol of CH_4 h^{-1} g^{-1} dry weight soil (Supplementary Table 3). However, the headspace CH_4 concentrations in the 1,000 ppmv CH_4-amended microcosms did not reduce to < 1.86 ppmv in all paddy soils except in Lei-Zhou (Figure 1B). These results indicate that the threshold of CH_4 concentrations that induce high-affinity CH_4 oxidation activity for atmospheric CH_4 varies among different paddy soils.

3.2 Active methanotrophs responsible for high-affinity CH_4 oxidation in paddy soils

Following the consumption of 10,000 ppmv CH_4, the paddy soils possessed high-affinity CH_4 oxidation activity (Figure 1B). The paddy soils were collected and then used to investigate methanotrophic community based on a high-throughput sequencing of *pmoA* genes, 16S rDNA, and 16S rRNA (Supplementary Tables 4, 5). Compared with the soils on day 0, a substantial growth of total methanotrophs was observed in all paddy soils with high-affinity CH_4 oxidation activity (Supplementary Figures 1A–C).

The 16S rRNA:rDNA ratios of type I methanotrophs varied in different paddy soils with high-affinity CH_4 oxidation activity, as well as type II methanotrophs (Figure 3A). The 16S rRNA:rDNA ratios of type II methanotrophs were 1.27–12.5-fold higher than those of type I methanotrophs in each paddy soil with high-affinity CH_4 oxidation activity, except in Zi-Yang. In contrast, 16S rRNA:rDNA ratio of type II methanotrophs in the alkaline paddy soil in Zi-Yang, was 3.61-fold lower than that of type I methanotrophs. Notably, the eight paddy soils, possessing higher 16S rRNA:rDNA ratios for type II methanotrophs than that for type I methanotrophs, exhibited acid-neutral soils with a pH of 5.18–6.80. This indicates the higher potential activity of type II methanotrophs compared to that of type I methanotrophs in high-affinity CH_4 oxidation in acid-neutral paddy soils. We observed a positive correlation between the 16S rRNA:rDNA ratios of type II methanotrophs and high-affinity CH_4 oxidation activity (Figure 3B) but not for type I methanotrophs (Supplementary Table 6). The 16S rRNA:rDNA ratios of type II methanotroph *Methylocystis* were higher than those of any type I methanotrophic genus in each acid-neutral soil (Supplementary Figure 2A). Additionally, we observed a significant positive relationship between the 16S rRNA:rDNA ratios of type II methanotroph *Methylocystis* and high-affinity CH_4 oxidation activity in paddy soils (Supplementary Figure 2B).

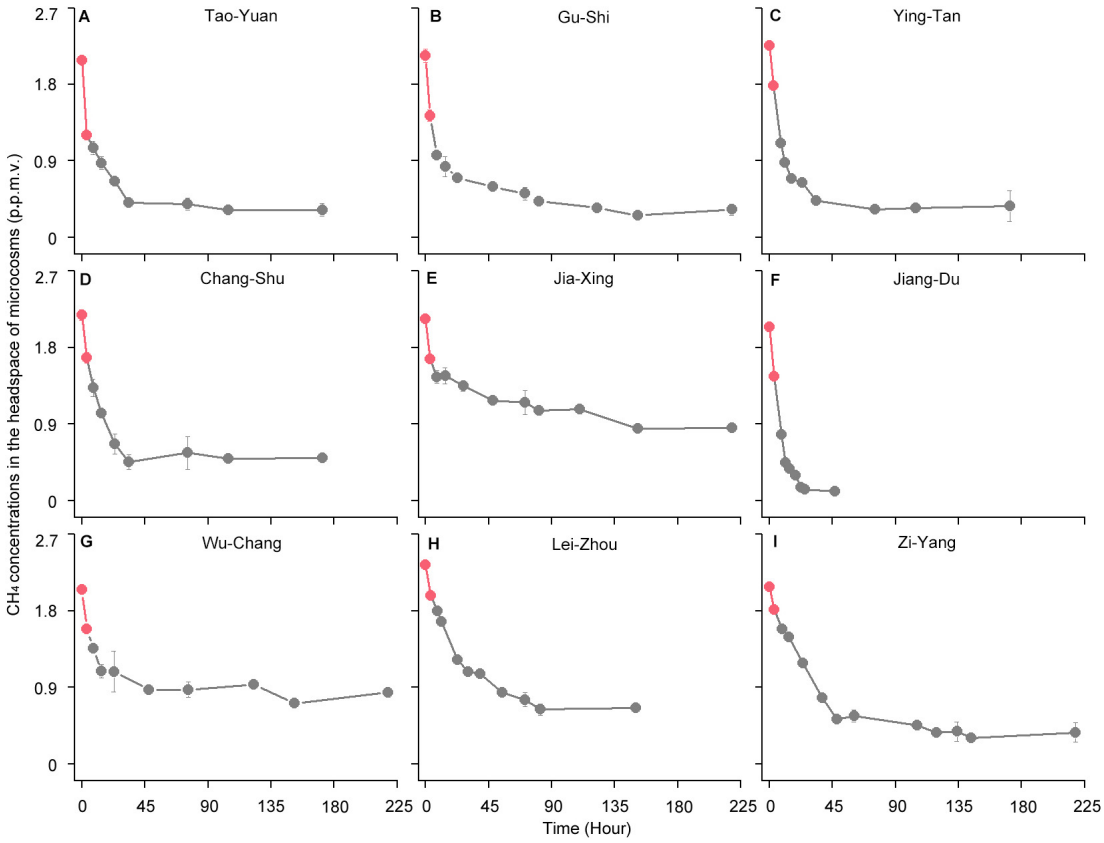

FIGURE 2
High-affinity methane (CH_4) oxidation dynamics of paddy soils under atmospheric CH_4 concentrations **(A–I)**. **(A)** Tao-Yuan; **(B)** Gu-Shi; **(C)** Ying-Tan; **(D)** Chang-Shu; **(E)** Jia-Xing; **(F)** Jiang-Du; **(G)** Wu-Chang; **(H)** Lei-Zhou; **(I)** Zi-Yang. After the complete depletion of 10,000 parts per million by volume (ppmv) CH_4, the headspace of microcosms is renewed with ambient air (~1.86 ppmv CH_4). The circles indicate time points for analyzing CH4 concentrations in the microcosms. The two red circles for each soil sample represent time points at 0 and 3 h, respectively. The amount of atmospheric CH4 oxidized in the first 3 h was used to assess the high-affinity CH_4 oxidation activity, as described in Supplementary Table 3. The error bars represent standard deviations of triplicate microcosms.

Additionally, 10,000 ppmv $^{13}CH_4$ can target active methanotrophs, which can help in exploring the relative role of individual methanotrophic taxa in soil CH_4 oxidation (Figure 3C). The highly enriched *pmoA* gene, methanotrophic 16S rDNA, and methanotrophic 16S rRNA were observed in heavy fractions from the $^{13}CH_4$ treatment (Figure 3C and Supplementary Tables 7, 8). It indicates that both the genomes and transcriptomes of methanotrophic cells were strongly labeled in the $^{13}CH_4$-treated soils. ^{13}C-labeled 16S rRNA reads revealed a significantly higher proportion of type I methanotrophs than that of type II methanotrophs in each paddy soil, except in the most acidic soil, in Tao-Yuan (Figure 3C). A similar trend, a higher proportion of type I methanotrophs compared to that of type II methanotrophs, was observed using ^{13}C-labeled *pmoA* genes and 16S rDNA in these eight paddy soils. The results indicate that type II methanotrophs displayed a lower growth rate compared with type I methanotrophs during the low-affinity oxidation of 10,000 ppmv high-CH_4 in most paddy soils. However, we observed a significant positive relationship between the relative abundance of ^{13}C-labeled type II methanotrophs and high-affinity CH_4 oxidation activity (Figure 3D) but not for ^{13}C-labeled type I methanotrophs (Supplementary Table 6).

Almost all type II methanotrophs were phylogenetically related to *Methylocystis* in the paddy soils (Figure 3E). Although ^{13}C-labeled *Methylocystis* constituted a lower fraction of methanotrophs than the type I methanotrophic genera (*Methylosarcina*, *Methylobacter*, or *Methylocaldum*), it was positively correlated with high-affinity CH_4 oxidation activity in paddy soils (Figure 3F). We also observed a positive correlation between the high-affinity CH_4 oxidation activity and *pmoA* gene copy numbers of *Methylocystis* (Supplementary Table 6). For type II methanotroph *Methylosinus*, a very low abundance was detected in all paddy soils (Figure 3E); however, it was positively correlated with the high-affinity CH_4 oxidation activity (Supplementary Table 6).

3.3 Biotic interactions of methanotrophs and other prokaryotic taxa

Co-occurring network analysis indicated that the number of links (degree) among methanotrophs and other prokaryotic taxa was higher in the paddy soil with high-affinity CH_4 oxidation activity (degree = 227) than in the paddy soils on day 0 (degree = 162) (Figure 4A and Supplementary Figure 4A). This indicates that atmospheric CH_4 oxidation enhanced the possible

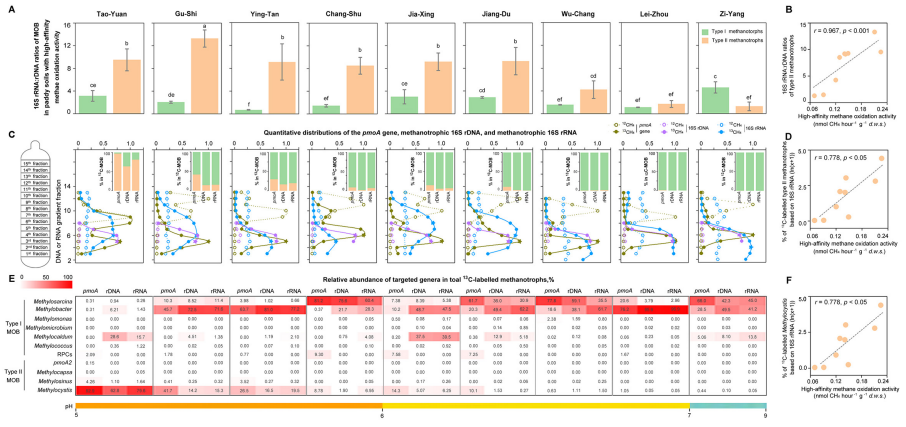

FIGURE 3
Activity of methanotrophs by assessing the 16S rRNA:16S rDNA ratios and documenting the relative abundance of ^{13}C-labeled methanotrophs in paddy soils. **(A)** The ratios of 16S rRNA to 16S rDNA of methanotrophic subgroups (type I and type II) in paddy soils with high-affinity CH_4 oxidation activity. The 16S rRNA:rDNA ratios of methanotrophs are expressed as the ratios of the relative abundance of targeted methanotrophic 16S rRNA in total 16S rRNA to the relative abundance of targeted methanotrophic 16S rDNA in total 16S rDNA based on high-throughput sequencing in each sample. The error bars represent standard deviations of triplicate microcosms. Different letters above the columns indicate a significant difference (analysis of variance [ANOVA], $p < 0.05$). **(B)** Relationship between high-affinity CH_4 oxidation activity and the 16S rRNA:16S rDNA ratios of type II methanotrophs in paddy soils ($n = 9$). There is no significant correlation between high-affinity CH_4 oxidation activity and the 16S rRNA:rDNA ratios of type I methanotrophs. Statistical analysis is performed using Spearman's rank-based correlation. **(C)** Quantitative distributions of the *pmoA* gene, methanotrophic 16S rDNA, and methanotrophic 16S rRNA in paddy soils with high-affinity CH_4 oxidation activity. $^{13}CH_4$ and $^{12}CH_4$ represent the paddy soils incubated with 10,000 parts per million by volume (ppmv) $^{12}CH_4$ and 10,000 ppmv $^{13}CH_4$, respectively. The *pmoA* gene and methanotrophic 16S rDNA are across the buoyant density gradient of the DNA fractions, and methanotrophic 16S rRNA is across the buoyant density gradient of the RNA fractions. For *pmoA* genes, the normalized data are the ratios of gene copy number in each DNA fraction to the maximum quantities from each treatment based on real-time quantitative PCR. The abundance of methanotrophs based on high-throughput sequencing is expressed as the proportion of methanotrophic 16S rDNA to the total 16S rDNA in each DNA fraction and the proportion of methanotrophic 16S rRNA to the total 16S rRNA in each RNA fraction. The pentagrams in olive, purple, and blue indicate the ^{13}C-labeled *pmoA* genes, ^{13}C-labeled 16S rDNA, and ^{13}C-labeled 16S rRNA that are used for the analysis of active methanotrophic community composition using high-throughput sequencing, respectively. The columns indicate the ^{13}C-labeled methanotrophic community composition that is expressed as the percentage of the targeted methanotrophic subgroup to the total ^{13}C-labeled methanotrophs based on the ^{13}C-*pmoA* gene, ^{13}C-16S rDNA, and ^{13}C-16S rRNA. **(D)** Relationship between high-affinity CH_4 oxidation activity and relative abundance of ^{13}C-labeled type II methanotrophs based on 16S rRNA in paddy soils ($n = 9$). The correlations between high-affinity CH_4 oxidation activity and the relative abundance of ^{13}C-labeled methanotrophs based on the *pmoA* gene and 16S rDNA are also significant and positive, as described in Supplementary Table 6. The relative abundance of ^{13}C-labeled methanotrophs is log-transformed before statistical testing. Statistical analysis is performed using Spearman's rank-based correlation. **(E)** The community composition of ^{13}C-labeled methanotrophs at the genus level. The numbers indicate the percentage of the targeted methanotrophic genus to total methanotrophs based on the ^{13}C-labeled *pmoA*, ^{13}C-labeled 16S rDNA, and ^{13}C-labeled 16S rRNA. **(F)** Relationship between high-affinity CH_4 oxidation activity and the relative abundance of ^{13}C-labeled *Methylocystis* based on 16S rRNA in paddy soils ($n = 9$). The correlations between high-affinity CH_4 oxidation activity and the relative abundance of ^{13}C-labeled *Methylocystis* based on the *pmoA* gene and 16S rDNA are also significant and positive (Supplementary Table 6). The relative abundance of ^{13}C-labeled *Methylocystis* is log-transformed before statistical testing. Statistical analysis is performed using Spearman's rank-based correlation.

biotic interactions between methanotrophs and other prokaryotic taxa in the paddy soils. The significant correlation between methanotroph and prokaryotic taxa involved in the nitrogen cycle, such as diazotrophs (e.g., *Bradyrhizobium*, *Burkholderia*, *Acidisoma*, and *Mesorhizobium*), and nitrifying bacteria (e.g., *Nitrobacter*, and *Nitrospira*), was observed during CH_4 oxidation (Supplementary Figure 4B). Notably, *Methylocystis* exhibited the highest degree in the network when the paddy soil could oxidize atmospheric CH_4 (Figure 4A).

3.4 Abiotic factors and their association with methanotrophic community and high-affinity methane oxidation activity in the paddy soils

The RDA integrated the abiotic factors to methanotrophic community composition in the paddy soils with high-affinity methane oxidation activity (Figure 4B). Among the abiotic factors, soil pH and soil nutrient availability (SOC, TN, NH_4^+, and NO_3^-) significantly affected the methanotrophic community composition (Figure 4B). The abundant type I methanotrophs (*Methylosarcina*, *Methylobacter*, *Methylocaldum*, and rice paddy clusters [RPCs]) and type II methanotrophs (*Methylocystis*, and *Methylosinus*) exhibited different responses to environmental factors. Type II methanotrophs were commonly found in more acidic paddy soils compared to type I methanotrophs. The abundance of type II methanotrophs, especially *Methylocystis*, were positively correlated to soil nutrient availability (SOC, TN, and NH_4^+) in the paddy soils, whereas type I methanotroph RPCs were positively correlated with soil NO_3^-. The high-affinity methane oxidation activity exhibited a negative correlation with soil pH and a positive correlation with nutrient availability (SOC, TN, and NH_4^+) (Figure 4C), similar to the correlations between abiotic factors and type II methanotrophs. Contrary to our expectations, the annual mean temperature had no significant effect on the methanotrophic community

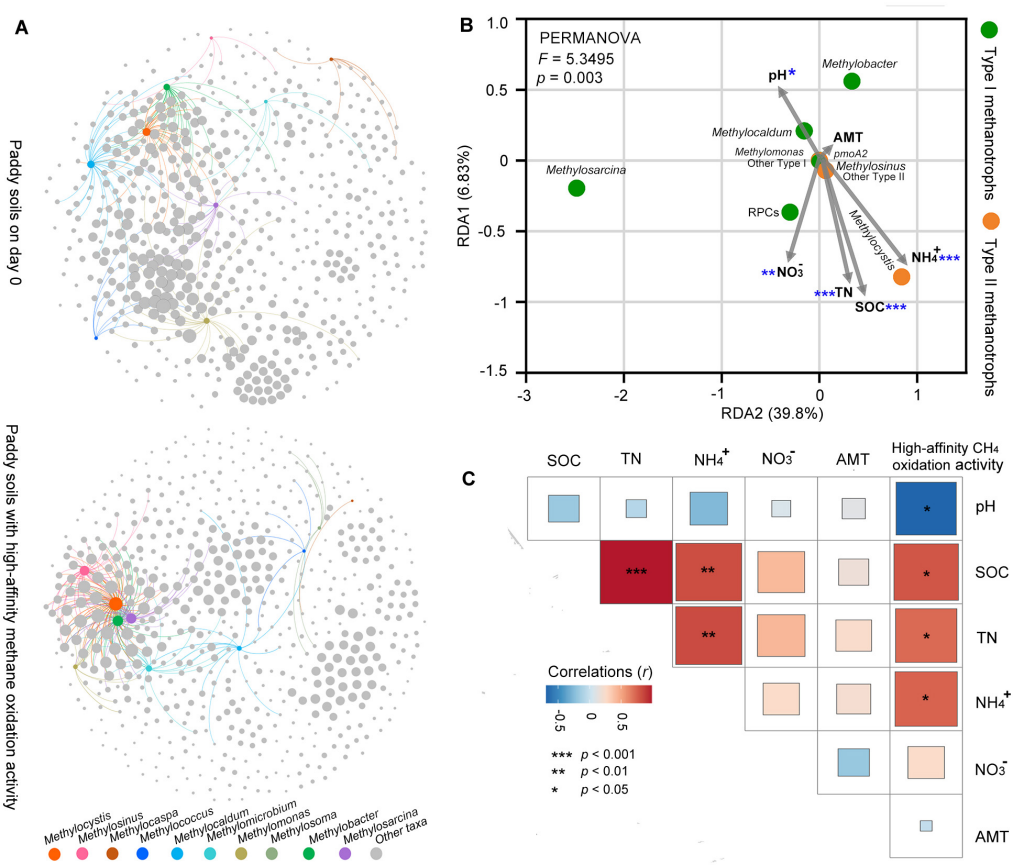

FIGURE 4
Biotic interactions of methanotrophs and other prokaryotic taxa, and abiotic factors and their association with methanotrophic community and high-affinity methane oxidation activity in paddy soils. **(A)** Co-occurrence network analysis demonstrating the associations among all prokaryotic genera in the paddy soils. The nodes represent the prokaryotic microorganisms at the genus level based on 16S rRNA. Links between the nodes indicate a significant correlation (correlation > 0.6, $p < 0.05$). For visual clarity, only links among methanotrophs-other prokaryotic taxa are illustrated. The bigger the node, the higher the degree (the number of network links for the node). Details of the network among all prokaryotic genera are listed in Supplementary Figure 4. **(B)** Redundancy analysis (RDA) showing the abiotic factors (pH, SOC, TN, NH_4^+, NO_3^-, and AMT) affecting the methanotrophic community as constraints. Significant abiotic factors affecting the methanotrophic community composition are marked with asterisks (*$p < 0.05$; **$p < 0.01$; ***$p < 0.001$). **(C)** Correlations between abiotic factors and high-affinity methane oxidation activity. Statistical analysis is performed using Pearson's rank-based correlation ($n = 9$). The abbreviation AMT represents annual mean temperature in the soil sampling site. All other abbreviations are the same as those in Figure 1.

composition (Figure 4B) or high-affinity methane oxidation (Figure 4C).

4 Discussion

Wetlands are typically considered CH_4 sources (IPCC, 2021). However, some periodically drained wetland ecosystems, such as the flooded paddy soils (Conrad, 2007), Arctic wetlands (Voigt et al., 2023), and mire-wetlands (Wang et al., 2023), serve as CH_4 sinks during the dry periods. In this study, we selected paddy soils across three climate zones from the primary rice production areas in China to obtain extensive spatial coverage of atmospheric CH_4 uptake in paddy soils.

The CH_4 concentrations in flooded rice fields vary with alterations in water content (Conrad, 2007). We constructed identical microcosms with various initial CH_4 concentrations to assess the occurrence of high-affinity CH_4 oxidation in periodically draining paddy soils, where CH_4 availability fluctuated. All tested paddy soils can oxidize atmospheric CH_4 following the consumption of CH_4 at high concentrations (10,000 ppmv) (Figure 1B). The estimated atmospheric CH_4 consumption rate in paddy soils varied from 1.87 to 6.03 kg CH_4 ha^{-1} per year (Supplementary Table 3), consistent with the values reported for soil ecosystems (Aronson et al., 2013). Our experiments indicate that paddy soils can serve as a CH_4 sink if drained after periodic flooding in rice fields with high concentrations of CH_4.

In contrast to microcosms with 10,000 ppmv of CH_4, we did not observe high-affinity oxidation of atmospheric CH_4 in all paddy soils incubated with CH_4 at concentrations ranging from 2 to 1,000 ppmv, except in Lei-Zhou soil incubated with 1,000 ppmv CH_4 (Figure 1B). A threshold amount of CH_4 consumption for the induction of atmospheric CH_4 uptake may vary greatly among different soils; however, the underlying mechanism remains elusive (Cai et al., 2016). The lower threshold in Lei-Zhou could not be attributed to the abiotic and biotic factors noted in our study. We hypothesize that it may be explained by the influence of unmeasured environmental factors. For instance, soil texture

can influence gas diffusion and soil aeration (Wang et al., 2022). The gas diffusion may regulate the CH_4 and O_2 availability and methanotrophic activity (Lee et al., 2023). Hence, further consideration of more soil factors is needed to identify the underlying mechanisms.

The ribosome content per cell follows bacterial growth (Kemp et al., 1993). rDNA can be extracted from living, dormant, and dead microbial cells (Josephson et al., 1993). rRNA is generally positively correlated with the growth rate of bacteria and degrades during certain stress conditions, such as substrate starvation (Deutscher, 2006). The 16S rRNA:rDNA ratio serves as an indicator of bacterial taxa activity in natural communities (Campbell et al., 2011; Campbell and Kirchman, 2013; Lankiewicz et al., 2016). The 16S rRNA:rDNA ratio is more informative than abundance alone in understanding the microbial activity in the environment (Campbell and Kirchman, 2013). The 16S rRNA:rDNA ratio of methanotrophs indicated that type II methanotrophs exhibited higher potential activity than type I methanotrophs during high-affinity CH_4 oxidation in most paddy soils (Figure 3A). Additionally, 16S rRNA:rDNA ratios of type II methanotrophs positively correlated with the high-affinity CH_4 oxidation activity (Figure 3B).

Notably, significant positive relationships were observed between the 16S rRNA:rDNA ratios and potential growth rates, as determined by assessing the relative abundance of ^{13}C-labeled methanotrophs for type II methanotrophs (Supplementary Figure 3). This indicates that type II methanotrophs can survive under CH_4-starvation conditions without markedly rRNA degradation. Although type II methanotrophs was not found to dominate in most paddy soils (Figure 3C), its abundance was positively correlated with high-affinity methane oxidation activity (Figure 3D). This finding was particularly noted *Methylocystis* (Figure 3F). Some rare taxa may exhibit higher microbial activity compared with the abundant taxa in the environment (Campbell et al., 2011). These findings support a better adaptation of type II methanotrophs, especially *Methylocystis*, to atmospheric CH_4 than that of type I methanotrophs in paddy soils.

High-affinity CH_4 oxidation activity is due to the consumption of high concentrations of CH_4 in paddy soils (Yan and Cai, 1997; Cai et al., 2016). Theoretically, atmospheric CH_4 does not provide adequate energy for the survival of cultured methanotrophs (Dunfield, 2007). High-affinity methanotrophs living in atmospheric CH_4 can obtain energy from additional sources (Baani and Liesack, 2008; Cai et al., 2016; Tveit et al., 2019). Endogenous storage compounds that have accumulated during exposure to high CH_4 concentrations, such as polyhydroxybutyrate (PHB), can potentially provide reductive power for CH_4 monooxygenase in methanotrophs during atmospheric CH_4 oxidation (Pieja et al., 2011; Cai et al., 2016). PHB production has been observed in type II methanotrophs, such as *Methylocystis* and *Methylosinus*, whereas type I methanotrophs may not be able to produce PHB (Pieja et al., 2011). Culturable methanotrophs sustain atmospheric methane oxidation if supplied with formate (Jensen et al., 1998). Formate oxidation reaction could provide the donor electron for particulate methane monooxygenase (pMMO) to sustain high-affinity methane oxidation (Le and Lee, 2023). Type II methanotrophs can transform acetate to acetyl-CoA (Singleton et al., 2018). Acetate as a source of carbon and energy allows methanotrophs to maintain methane oxidation activity under CH_4 starvation conditions (Belova et al., 2011; Singleton et al., 2018). Some type II methanotrophs harvest additional energy from aerobic respiration of hydrogen (H_2) at atmospheric concentrations (Tveit et al., 2019).

In addition to the known type of pMMO1 responsible for high CH_4 concentrations, most type II methanotrophs possess pMMO2 to oxidize CH_4 at atmospheric concentrations (Baani and Liesack, 2008). However, pMMO2 may not be detected in any known type I methanotrophs (Tchawa Yimga et al., 2003). In this study, *pmoA2* genes that encode pMMO2 were observed in the acid-neutral paddy soils (Jiang-Du, Gu-Shi, Ying-Tan, Tao-Yuan, and Chang-Shu) that can oxidize atmospheric CH_4 (Supplementary Table 4). Moreover, the type II methanotroph *Methylocapsa*, whose ^{13}C-labeled 16S rRNA was observed in Tao-Yuan (Figure 3E), encoded a single PMMO responsible for CH_4 oxidation at high and atmospheric concentrations (Tveit et al., 2019). The coexistence of high- and low-affinity CH_4 oxidation activities may be advantageous for type II methanotrophs to thrive in paddy soils, where CH_4 concentrations fluctuate significantly. Therefore, in type II methanotrophs, the capacity for PHB production, acetate and hydrogen uptake, and high-affinity pMMO expression provides a selective advantage for survival under CH_4 starvation conditions in paddy soils.

Type I methanotrophs may also play a role in the high-affinity CH_4 oxidation, specifically in the alkaline Zi-Yang soil (pH 8.23). The 16S rRNA:rDNA ratio (Figure 3A) and the abundance (Figure 3C) were remarkably higher for type I methanotrophs than that for type II methanotrophs in Zi-Yang. Numerous strains within type I methanotrophs can oxidize atmospheric CH_4 after incubation with high CH_4 concentrations (Schnell and King, 1995; Benstead et al., 1998). Type I methanotrophic *pmoA* transcripts are observed in a paddy soil with atmospheric CH_4 oxidation activity (Cai et al., 2016).

CH_4 oxidation enhanced a complex network of microbial interactions among the methanotrophs and other prokaryotic taxa, as illustrated in Figure 4A. In addition, linkages between *Methylocystis* and other taxa occurred at the highest proportion in the paddy soils with high-affinity CH_4 oxidation activity (Figure 4A). Organic carbon derived from a source of CH_4 via the assimilation of methanotrophs facilitates the growth of non-methanotrophs (Kaupper et al., 2022). For instance, type II methanotrophs *Methylocystis* and *Methylosinus* were positively correlated with *Methylobacterium* (Supplementary Figure 4B). *Methylobacterium* can use methanol as an energy and carbon source (Tani et al., 2021). Cross-feeding might drive their positive correlations via the methanol from the oxidation of methane by methanotrophs. In addition, methanotrophs-nitrifying bacteria and methanotrophs-diazotrophs interactions linked carbon and nitrogen cycling in paddy soils (Supplementary Figure 4B). Nitrifying bacteria are chemoautotrophs (Xia et al., 2011), and CH_4-derived CO_2 can be incorporated by chemoautotrophs (Kaupper et al., 2022). Diazotrophs can contribute reactive nitrogen to natural ecosystems (Hu et al., 2024). The available nitrogen from diazotrophs might drive the positive links between diazotrophs and *Methylocystis*.

The methanotrophic community (Figure 4B) and methane oxidation uptake (Figure 4C) respond to various abiotic factors in the paddy fields, such as CH_4 content, pH, nutrient availability and temperature. The variations in soil moisture attributed to periodic drainage in rice fields could result in significant fluctuations in soil CH_4 concentrations (Conrad, 2007). The rice fields are

similar to aerated upland soils during the dry seasons (Conrad, 2007). Our paddy soils were collected in the drained rice fields, where CH_4 availability was limited. The dominance of type II methanotrophs on day 0 (Supplementary Figure 1D) aligns with a K-type life strategy, characterized by an investment in survival and longevity (Steenbergh et al., 2010; Ho et al., 2013). This strategy may be advantageous for type II methanotrophs that can occupy niches under resource limiting conditions. It helps explain why the type II methanotrophic activity (based on 16S rRNA:rDNA ratios) was higher than that of type I methanotrophs during atmospheric methane oxidation in most paddy soils (Figure 3A). We incubated the paddy soils with CH_4 at a concentration of 10,000 ppmv to mimic the high availability of CH_4 noted under flooded conditions. The faster growth of type I methanotrophs in most paddy soils (Figure 3C) is an indication of an r-type life strategy that emphasizes high reproductive success, which is instantaneous under favorable conditions (Qiu et al., 2008; Steenbergh et al., 2010). Type I and II methanotrophs possess distinct life strategies, offering them a selective advantage under various environmental conditions (Ho et al., 2013).

Soil pH significantly regulated methanotrophic community composition (Figure 4B) and negatively influenced CH_4 uptake (Figure 4C) in paddy soils. To date, most known type II methanotrophs cannot survive above pH 8.0; however, cultivated type I methanotrophs are more tolerant to high pH conditions than type II methanotrophs (Kalyuzhnaya et al., 2019; Yao et al., 2022). This finding helps explain why higher 16S rRNA:rDNA ratios for type I methanotrophs, compared to type II methanotrophs, were only observed in the alkaline paddy soil of Zi-Yang (pH 8.23) under methane-starvation conditions (Figure 3A). A majority of acidophilic methanotrophs are type II (Hwangbo et al., 2023). In paddy soils with pH values ranging from 5.0 to 8.0, type II methanotrophs are more widespread in low pH conditions than in high pH conditions (Shiau et al., 2018; Zhao et al., 2020). A pH value of less than 5.2 is a key driving force for the selection of type II over type I methanotrophs in paddy soils at a high-methane condition (Shiau et al., 2018). It helps explain that faster growth of type II than type I methanotrophs during the low-affinity oxidation of high-methane was only detected in the acidic soil Tao-Yuan (pH 5.18) (Figure 3C). Type II methanotrophs had positive effect on atmospheric CH_4 take (Figures 3B, D). Soil pH was negatively correlated with the abundance of type II methanotrophs, especially *Methylocystis* (Figure 4B), thereby, influencing the atmospheric CH_4 uptake (Figure 4C). A high influence of soil pH on atmospheric CH_4 uptake was also observed in Arctic soils, where CH_4 uptake increased with lower soil pH (Voigt et al., 2023).

Soil nutrient availability, such as SOC, TN, and NH_4^+, positively affected the abundance of type II methanotrophs, especially *Methylocystis* (Figure 4B), and atmospheric CH_4 uptake (Figure 4C) in paddy soils. Higher SOC content results in increased atmospheric CH_4 uptake in forest soils (Lee et al., 2023). SOC increases the soil pore space and, therefore, diffuses atmospheric CH_4 into the soil (Lee et al., 2023). In addition, SOC can facilitate atmospheric methanotrophic activity by providing alternative carbon substrates, such as formate and acetate, during CH_4 starvation (Jensen et al., 1998, West and Schmidt, 1999, Lee et al., 2023). The capability of using acetate as a carbon and energy source is a common trait in *Methylocystis* (Belova et al., 2011; Singleton et al., 2018). It may be advantageous for *Methylocystis* under CH_4-limited conditions.

Nitrogen interacts with atmospheric methane uptake in the soil ecosystems (Bodelier and Steenbergh, 2014; Voigt et al., 2023). Nitrogen as a nutrient stimulates the growth of methanotrophs and promotes methanotrophic oxidation activity (Zheng et al., 2014; Peng et al., 2019; Nijman et al., 2021). Nitrogen is the main limiting nutrient for methanotrophs in rice fields (Bodelier and Steenbergh, 2014). Enhanced nitrogen promotes CH_4 uptake in N-limiting soils (Bodelier and Steenbergh, 2014; Peng et al., 2019; Voigt et al., 2023). In contrast to type I methanotrophs, type II methanotrophs can fix atmospheric nitrogen to assimilable nitrogen forms (Ho et al., 2013). Therefore, type II methanotrophs possess an advantage when nitrogen is limited. Soil NO_3^- content showed no significant effect on atmospheric CH_4 uptake (Figure 4C). In addition to acting as a nutrient, NO_3^- exerts a toxic effect that could inhibit methane uptake (Ho et al., 2013). It adds to the complexity of methane oxidation-nitrogen assimilation interactions.

CH_4 sink is enhanced with increasing temperature in forest soils (Lee et al., 2023). However, the temperature has no significant effect on the composition of methanotrophic community (Figure 4B) and atmospheric oxidation activity (Figure 4C) in paddy soils. Temperature might influence atmospheric CH_4 uptake via other soil variables (Lee et al., 2023; Lin et al., 2023). For instance, increased temperature accelerates soil organic carbon decomposition (Zhao et al., 2023; Nazir et al., 2024) and, therefore the methanotrophic activity (Lee et al., 2023). We cannot observe a significant correlation between the temperature and SOC content (Figure 4C), probably due to the influence of unmeasured environmental factors on SOC and methanotrophic activity.

Overall, we observed higher atmospheric CH_4 oxidation activity in paddy soils with lower soil pH, higher nutrient availability (SOC, TN, and NH_4^+), and higher type II methanotrophic activity, especially *Methylocystis*. Abiotic factors could influence the methanotrophic community and, hence, the atmospheric CH_4 oxidation activity. This large-scale study examining atmospheric CH_4 sink in paddy soils will facilitate an understanding of the relationships between atmospheric CH_4 uptake, environmental factors, and microbial community. These results help understand how biotic and abiotic factors affect the atmospheric CH_4 uptake in paddy soils. Our study helps explore the potential farm management (e.g., field fertilization and irrigation strategies) to promote CH_4 uptake in paddy soils, providing avenues to develop strategies to mitigate global climate change.

The large-scale field sites investigated here were located within a wide range of climates, soil conditions, and microbial communities; however, certain special conditions cannot be explained by the measured factors in our study. Therefore, it is important to consider the limitations of this study. (1) The threshold amount of methane consumption for the induction of high-affinity methane oxidation was lower in Lei-Zhou (1,000 ppmv) than in other soils (10,000 ppmv). However, the underlying mechanism remains elusive according to the measured biotic factors and abiotic factors. To understand the underlying mechanisms, we should investigate more detailed biotic factors via advanced methods, such as metatranscriptomics and metaproteomics, and analyze more abiotic factors (e.g., soil texture). (2) Increasing temperature can enhance atmospheric

methane uptake in forest soils. However, temperature did not influence atmospheric methane uptake in paddy soils. The range of annual mean temperature was narrow in our study, in the range of 16–19°C in most sampling sites. In addition, temperature might influence the atmospheric CH_4 uptake via unmeasured environmental factors. Therefore, more soil samples from a wider temperature range and more soil factors are needed to provide deeper mechanistic insights into the underlying mechanisms. (3) The higher activity of type I methanotrophs (the ratio of 16S rRNA:rDNA) in "high-affinity" soils was observed only in one alkaline soil. We should examine more soil samples to determine whether the trait is widespread in alkaline soils. (4) The selection of type II over type I methanotrophs was observed under high-methane conditions only in Tao-Yuan, which is not consistent with the life strategy for methanotrophs. Low pH condition (pH < 5.2) is the possible driving factor; however, the unknown potential environmental factors are of significant interest. More paddy soils, especially acidic soils, and more abiotic factors should be considered to refine our understanding of the underlying mechanisms in the future. Taken together, more paddy soils with broader environmental conditions (e.g., wider soil pH range and annual mean temperature range), more soil factors (e.g., soil texture), and more advanced methodologies for analyzing methanotrophic activity (e.g., metatranscriptomics and metaproteomics approaches) are needed to validate and expand upon our findings in the future.

5 Conclusion

High-affinity CH_4 oxidation induced by high CH_4 concentrations is widespread in paddy soils, as indicated by the large spatial coverage of atmospheric CH_4 uptake measurements. In acid-neutral paddy soils capable of oxidizing atmospheric CH_4, type II methanotrophs exhibited higher 16S rRNA:rDNA ratios and, therefore, higher potential activity than type I methanotrophs. Additionally, the methanotrophic activity was analyzed by examining the relative abundance of ^{13}C-labeled methanotrophs using both DNA- and RNA-SIP. Significant positive relationships were observed between the high-affinity CH_4 oxidation activity and 16S rRNA:rDNA ratios of type II methanotrophs and the relative abundance of ^{13}C-labeled type II methanotrophs. The microbial co-occurrence network indicated that CH_4 oxidation enhanced biotic interactions between methanotrophs and other prokaryotic taxa. Soil pH and nutrient availability can significantly affect the methanotrophic community and high-affinity CH_4 oxidation activity. The abundance of type II methanotrophs, especially *Methylocystis*, as well as the high-affinity methane oxidation activity, showed a negative correlation with soil pH and a positive correlation with soil nutrient availability (SOC, TN and NH_4^+). Our results offer a wide biogeographical perspective on atmospheric CH_4 uptake in paddy soils and help to explore the mitigation strategy for global climate change via optimal farm management (e.g., field fertilization and irrigation strategies) in paddy fields. Future research should investigate a broader range of paddy soil samples and soil factors to further elucidate the underlying mechanisms unidentified in our study, providing a deeper insight into greenhouse gas mitigation strategies.

Data availability statement

The raw sequence data reported in this article are available in the NCBI Sequence Read Archive under BioProject PRJNA1030075.

Author contributions

YZ: Data curation, Formal analysis, Methodology, Software, Validation, Visualization, Writing – original draft, Writing – review and editing. YC: Writing – review and editing. ZJ: Conceptualization, Investigation, Writing – original draft, Writing – review and editing.

Funding

The authors declare that financial support was received for the research, authorship, and/or publication of this article. This work was supported by the National Natural Science Foundation of China [grant numbers 92251305, 41501276, and 41877062] and the Open Fund for State Key Laboratory of Soil and Sustainable Agriculture [grant number Y812000008].

Acknowledgments

We thank Jing Xu and Wanmeng Wang for their help in sampling the soils.

Conflict of interest

The authors declare that the research was conducted in the absence of any commercial or financial relationships that could be construed as a potential conflict of interest.

Publisher's note

Supplementary material

The Supplementary Material for this article can be found online at: https://www.frontiersin.org/articles/10.3389/fmicb.2024.1481044/full#supplementary-material

References

Aronson, E. L., Allison, S. D., and Helliker, B. R. (2013). Environmental impacts on the diversity of methane-cycling microbes and their resultant function. *Front. Microbiol.* 4:225. doi: 10.3389/fmicb.2013.00225

Baani, M., and Liesack, W. (2008). Two isozymes of particulate methane monooxygenase with different methane oxidation kinetics are found in *Methylocystis* sp. strain SC2. *Proc. Natl. Acad. Sci. U.S.A.* 105, 10203–10208. doi: 10.1073/pnas.0702643105

Barberán, A., Bates, S. T., Casamayor, E. O., and Fierer, N. (2012). Using network analysis to explore co-occurrence patterns in soil microbial communities. *ISME J.* 6, 343–351. doi: 10.1038/ismej.2013.236

Belova, S. E., Baani, M., Suzina, N. E., Bodelier, P. L. E., Liesack, W., and Dedysh, S. N. (2011). Acetate utilization as a survival strategy of peat-inhabiting Methylocystis spp. *Environ. Microbiol. Rep.* 3, 36–46. doi: 10.1111/j.1758-2229.2010.00180.x

Benstead, J., King, G. M., and Williams, H. G. (1998). Methanol promotes atmospheric methane oxidation by methanotrophic cultures and soils. *Appl. Environ. Microbiol.* 64, 1091–1098. doi: 10.1128/AEM.64.3.1091-1098.1998

Bodelier, P. L. E., and Steenbergh, A. K. (2014). Interactions between methane and the nitrogen cycle in light of climate change. *Curr. Opin. Env. Sustain.* 9, 26–36. doi: 10.1016/j.cosust.2014.07.004

Cai, Y. F., Zheng, Y., Bodelier, P. L. E., Conrad, R., and Jia, Z. (2016). Conventional methanotrophs are responsible for atmospheric methane oxidation in paddy soils. *Nat. Commun.* 7:11728. doi: 10.1038/ncomms11728

Campbell, B. J., and Kirchman, D. L. (2013). Bacterial diversity, community structure and potential growth rates along an estuarine salinity gradient. *ISME J.* 7, 210–220. doi: 10.1038/ismej.2012.93

Campbell, B. J., Yu, L., Heidelberg, J. F., and Kirchman, D. L. (2011). Activity of abundant and rare bacteria in a coastal ocean. *Proc. Natl. Acad. Sci. U.S.A.* 108, 12776–12781. doi: 10.1073/pnas.1101405108

Cao, W., Cai, Y., Bao, Z., Wang, S., Yan, X., and Jia, Z. (2022). Methanotrophy alleviates nitrogen constraint of carbon turnover by rice root-associated microbiomes. *Front. Microbiol.* 13:885087. doi: 10.3389/fmicb.2022.885087

Conrad, R. (2007). Microbial ecology of methanogens and methanotrophs. *Adv. Agron.* 96, 1–63. doi: 10.1016/S0065-2113(07)96005-8

Costello, A. M., and Lidstrom, M. E. (1999). Molecular characterization of functional and phylogenetic genes from natural populations of methanotrophs in lake sediments. *Appl. Environ. Microbiol.* 65, 5066–5074. doi: 10.1128/AEM.65.11.5066-5074.1999

Dedysh, S. N., and Knief, C. (2018). "Diversity and phylogeny of described aerobic methanotrophs," in *Methane biocatalysis: Paving the way to sustainability*, eds M. Kalyuzhnaya and X. H. Xing (Cham: Springer), 17–42. doi: 10.1007/978-3-319-74866-5_2

Deutscher, M. P. (2006). Degradation of RNA in bacteria: Comparison of mRNA and s table RNA. *Nucleic Acids Res.* 34, 659–666. doi: 10.1093/nar/gkj472

Dumont, M. G., Pommerenke, B., Casper, P., and Conrad, R. (2011). DNA-, rRNA- and mRNA-based stable isotope probing of aerobic methanotrophs in lake sediment. *Environ. Microbiol.* 13, 1153–1167. doi: 10.1111/j.1462-2920.2010.02415.x

Dunfield, P. F. (2007). "The soil methane sink," in *Greenhouse gas sinks*, eds. D. S. Reay, C. N. Hewitt, and J. Grace (Wallingford: Cambridge University Press), 152–170. doi: 10.1079/9781845931896.0152

Etheridge, D. M., Pearman, G. I., and Fraser, P. J. (1992). Changes in tropospheric methane between 1841 and 1978 from a high accumulation-rate Antarctic ice core. *Tellus B.* 44, 282–294. doi: 10.3402/tellusb.v44i4.15456

Gao, C., Xu, L., Montoya, L., Madera, M., Hollingsworth, J., Chen, L., et al. (2022). Co-occurrence networks reveal more complexity than community composition in resistance and resilience of microbial communities. *Nat. Commun.* 13:3867. doi: 10.1038/s41467-022-31343-y

Ho, A., Kerckhof, F. M., Luke, C., Reim, A., Krause, S., Boon, N., et al. (2013). Conceptualizing functional traits and ecological characteristics of methane-oxidizing bacteria as life strategies. *Environ. Microbiol. Rep.* 5, 335–345. doi: 10.1111/j.1758-2229.2012.00370.x

Hu, W., Wang, X., Xu, Y., Wang, X., Guo, Z., Pan, X., et al. (2024). Biological nitrogen fixation and the role of soil diazotroph niche breadth in representative terrestrial ecosystems. *Soil Biol. Biochem.* 189:109261. doi: 10.1016/j.soilbio.2023.109261

Hwangbo, M., Shao, Y., Hatzinger, P. B., and Chu, K. H. (2023). Acidophilic methanotrophs: Occurrence, diversity, and possible bioremediation applications. *Environ. Microbiol. Rep.* 15, 265–281. doi: 10.1111/1758-2229.13156

IPCC (2021). "The physical science basis: Contribution of working group I to the sixth assessment report of the intergovernmental panel on climate change. Summary for policymakers," in *Climate change*, eds V. Masson-Delmotte, P. Zhai, A. Pirani, S.L. Connors, C. Péan, S. Berger, et al. (New York, NY: Cambridge University Press), 3–32. doi: 10.1017/9781009157896.001

Jensen, S., Priemé, A., and Bakken, L. (1998). Methanol improves methane uptake in starved methanotrophic microorganisms. *Appl. Environ. Microbiol.* 64, 1143–1146. doi: 10.1128/AEM.64.3.1143-1146.1998

Josephson, K. L., Gerba, C. P., and Pepper, I. L. (1993). Polymerase chain reaction detection of nonviable bacterial pathogens. *Appl. Environ. Microbiol.* 59, 3513–3515. doi: 10.1128/AEM.59.10.3513-3515.1993

Kalyuzhnaya, M. G., Gomez, O. A., and Murrell, J. C. (2019). "The methane-oxidizing bacteria (methanotrophs)," in *Taxonomy, genomics and ecophysiology of hydrocarbon-degrading microbes. Handbook of hydrocarbon and lipid microbiology*, ed. T. McGenity (Cham: Springer), 245–278. doi: 10.1007/978-3-030-14796-9_10

Kaupper, T., Mendes, L. W., Poehlein, A., Frohloff, D., Rohrbach, S., Horn, M. A., et al. (2022). The methane-driven interaction network in terrestrial methane hotspots. *Environ. Microb.* 17:15. doi: 10.1186/s40793-022-00409-1

Kemp, P. F., Lee, S., and LaRoche, J. (1993). Estimating the growth rate of slowly growing marine bacteria from RNA content. *Appl. Environ. Microbiol.* 59, 2594–2601. doi: 10.1128/AEM.59.8.2594-2601.1993

Lankiewicz, T. S., Cottrell, M. T., and Kirchman, D. L. (2016). Growth rates and rRNA content of four marine bacteria in pure cultures and in the Delaware estuary. *ISME J.* 10, 823–832. doi: 10.1038/ismej.2015.156

Le, H. T. Q., and Lee, E. Y. (2023). Methanotrophs: Metabolic versatility from utilization of methane to multi-carbon sources and perspectives on current and future applications. *Bioresour. Technol.* 384:129296. doi: 10.1016/j.biortech.2023.129296

Lee, J., Oh, Y., Lee, S. T., Seo, Y. O., Yun, J., Yang, Y., et al. (2023). Soil organic carbon is a key determinant of CH4 sink in global forest soils. *Nat. Commun.* 14:3110. doi: 10.1038/s41467-023-38905-8

Lin, J., Hui, D., Kumar, A., Yu, Z., and Huang, Y. (2023). Editorial: Climate change and/or pollution on the carbon cycle in terrestrial ecosystems. *Front. Environ. Sci.* 11:1253172. doi: 10.3389/fenvs.2023.1253172

Maucieri, C., Barbera, A. C., Vymazal, J., and Borin, M. (2017). A review on the main affecting factors of greenhouse gases emission in constructed wetlands. *Agric. For. Meteorol.* 236, 175–193. doi: 10.1016/j.agrformet.2017.01.006

Mettel, C., Kim, Y., Shrestha, P. M., and Liesack, W. (2010). Extraction of mRNA from soil. *Appl. Environ. Microbiol.* 76, 5995–6000. doi: 10.1128/AEM.03047-09

Nazir, M. J., Li, G., Nazir, M. M., Zulfiqar, F., Siddique, K. H. M., Iqba, B., et al. (2024). Harnessing soil carbon sequestration to address climate change challenges in agriculture. *Soil Tillage Res.* 237:105959. doi: 10.1016/j.still.2023.105959

Nijman, T. P. A., Davidson, T. A., Weideveld, S. T. J., Audet, J., Esposito, C., Levi, E. E., et al. (2021). Warming and eutrophication interactively drive changes in the methane-oxidizing community of shallow lakes. *ISME Commun.* 1:32. doi: 10.1038/s43705-021-00026-y

Peng, Y., Wang, G., Li, F., Yang, G., Fang, K., Liu, L., et al. (2019). Unimodal response of soil methane consumption to increasing nitrogen additions. *Environ. Sci. Technol.* 53, 4150–4160. doi: 10.1021/acs.est.8b04561

Pieja, A. J., Rostkowski, K. H., and Criddle, C. S. (2011). Distribution and selection of poly-3-hydroxybutyrate production capacity in methanotrophic proteobacteria. *Microb. Ecol.* 62, 564–573. doi: 10.1007/s00248-011-9873-0

Preuss, I., Knoblauch, C., Gebert, J., and Pfeiffer, E. M. (2013). Improved quantification of microbial CH4 oxidation efficiency in arctic wetland soils using carbon isotope fractionation. *Biogeosciences* 10, 2539–2552. doi: 10.5194/bg-10-2539-2013

Qiu, Q., Noll, M., Abraham, W. R., Lu, Y., and Conrad, R. (2008). Applying stable isotope probing of phospholipid fatty acids and rRNA in a Chinese rice field to study activity and composition of the methanotrophic bacterial communities in situ. *ISME J.* 2, 602–614. doi: 10.1038/ismej.2008.34

Ren, G., Ren, W., Teng, Y., and Li, Z. (2015). Evident bacterial community changes but only slight degradation when polluted with pyrene in a red soil. *Front. Microbiol.* 6:22. doi: 10.3389/fmicb.2015.00022

Saunois, M., Stavert, A. R., Poulter, B., Bousquet, P., Canadell, J. G., Jackson, R. B., et al. (2020). The global methane budget 2000–2017. *Earth Syst. Sci. Data* 12, 1561–1623. doi: 10.5194/ESSD-8-697-2016

Schloss, P. D., Westcott, S. L., Ryabin, T., Hall, J. R., Hartmann, M., Hollister, E. B., et al. (2009). Introducing Mothur: Open-source, platform-independent, community-supported software for describing and comparing microbial communities. *Appl. Environ. Microbiol.* 75, 7537–7541. doi: 10.1128/AEM.01541-09

Schnell, S., and King, G. M. (1995). Stability of methane oxidation capacity to variations in methane and nutrient concentrations. *FEMS Microbiol. Ecol.* 17, 285–294. doi: 10.1111/J.1574-6941.1995.TB00153.X

Schultz, M. A., Janousek, C. N., Brophy, L. S., Schmitt, J., and Bridgham, S. D. (2023). How management interacts with environmental drivers to control greenhouse gas fluxes from Pacific Northwest coastal wetlands. *Biogeochemistry* 165, 165–190. doi: 10.1007/s10533-023-01071-6

Shiau, Y. J., Cai, Y., Jia, Z., Chen, C. L., and Chiu, C. Y. (2018). Phylogenetically distinct methanotrophs modulate methane oxidation in rice paddies across Taiwan. *Soil Biol. Biochem.* 124, 59–69. doi: 10.1016/j.soilbio.2018.05.025

Singh, J. S., Singh, S., Raghubanshi, A. S., Singh, S., and Kashyap, A. K. (1996). Methane flux from rice/wheat agroecosystem as affected by crop phenology, fertilization and water level. *Plant Soil* 183, 323–327. doi: 10.1007/BF00011448

Singleton, C. M., McCalley, C. K., Woodcroft, B. J., Boyd, J. A., Evans, P. N., Hodgkins, S. B., et al. (2018). Methanotrophy across a natural permafrost thaw environment. *ISME J.* 12, 2544–2558. doi: 10.1038/s41396-018-0065-5

Steenbergh, A. K., Meima, M. M., Kamst, M., and Bodelier, P. L. E. (2010). Biphasic kinetics of a methanotrophic community is a combination of growth and increased activity per cell. *FEMS Microbiol. Ecol.* 71, 12–22. doi: 10.1111/j.1574-6941.2009.00782.x

Tani, A., Mitsui, R., and Nakagawa, T. (2021). "Chapter One-Discovery of lanthanide-dependent methylotrophy and screening methods for lanthanide-dependent methylotrophs," in *Rare-earth element biochemistry: Methanol dehydrogenases and lanthanide biology*, Vol. 650, ed. J. A. Cotruvo (London: Academic Press), 1–18. doi: 10.1016/bs.mie.2021.01.031

Tchawa Yimga, M., Dunfield, P. F., Ricke, P., Heyer, J., and Liesack, W. (2003). Wide distribution of a novel pmoA-Like gene copy among type II methanotrophs, and its expression in Methylocystis strain SC2. *Appl. Environ. Microbiol.* 69, 5593–5602. doi: 10.1128/AEM.69.9.5593-5602.2003

Tikhonova, E. N., Grouzdev, D. S., Avtukh, A. N., and Kravchenko, I. K. (2021). *Methylocystis silviterrae* sp. nov., a high-affinity methanotrophic bacterium isolated from the boreal forest soil. *Int. J. Syst. Evol. Microbiol.* 71, 5166. doi: 10.1099/ijsem.0.005166

Tveit, A. T., Hestnes, A. G., Robinson, S. L., Schintlmeister, A., Dedysh, S. N., Jehmlich, N., et al. (2019). Widespread soil bacterium that oxidizes atmospheric methane. *Proc. Natl. Acad. Sci. U.S.A.* 116, 8515–8524. doi: 10.1073/pnas.1817812116

Voigt, C., Virkkala, A. M., Gosselin, G. H., Bennett, K. A., Black, T. A., Detto, M., et al. (2023). Arctic soil methane sink increases with drier conditions and higher ecosystem respiration. *Nat. Clim. Change* 13, 1095–1104. doi: 10.1038/s41558-023-01785-3

Wang, N., Zhu, X., Zuo, Y., Liu, J., Yuan, F., Guo, Z., et al. (2023). Microbial mechanisms for methane source-to-sink transition after wetland conversion to cropland. *Geoderma* 429:116229. doi: 10.1016/j.geoderma.2022.116229

Wang, Y., Zhang, Z., Guo, Z., Xiong, P., and Peng, X. (2022). The dynamic changes of soil air-filled porosity associated with soil shrinkage in a Vertisol. *Eur. J. Soil Sci.* 73:3313. doi: 10.1111/ejss.13313

West, A. E., and Schmidt, S. K. (1999). Acetate stimulates atmospheric CH4 oxidation by an alpine tundra soil. *Soil Biol. Biochem.* 31, 1649–1655. doi: 10.1016/S0038-0717(99)00076-0

Xia, W., Zhang, C., Zeng, X., Feng, Y., Weng, J., Lin, X., et al. (2011). Autotrophic growth of nitrifying community in an agricultural soil. *ISME J.* 5, 1226–1236. doi: 10.1038/ismej.2011.5

Yan, X. Y., and Cai, Z. C. (1997). Laboratory study of methane oxidation in paddy soils. *Nutr. Cycling Agroecosyst.* 49, 105–109. doi: 10.1023/a:1009788507536

Yang, Y., Jing, L., Li, Q., Liang, C., Dong, Q., Zhao, S., et al. (2023). Big-sized trees and higher species diversity improve water holding capacities of forests in northeast China. *Sci. Total Environ.* 880:163263. doi: 10.1016/j.scitotenv.2023.163263

Yao, X., Wang, J., and Hu, B. (2022). How methanotrophs respond to pH: A review of ecophysiology. *Front. Microbiol.* 13:1034164. doi: 10.3389/fmicb.2022.1034164

Zhao, J., Cai, Y., and Jia, Z. (2020). The pH-based ecological coherence of active canonical methanotrophs in paddy soils. *Biogeosciences* 17, 1451–1462. doi: 10.5194/bg-17-1451-2020

Zhao, Y., Lin, J., Cheng, S., Wang, K., Kumar, A., Yu, Z. G., et al. (2023). Linking soil dissolved organic matter characteristics and the temperature sensitivity of soil organic carbon decomposition in the riparian zone of the Three Gorges Reservoir. *Ecol. Indic.* 154:110768. doi: 10.1016/j.ecolind.2023.110768

Zheng, Y., Huang, R., Wang, B. Z., Bodelier, P. L. E., and Jia, Z. J. (2014). Competitive interactions between methane- and ammonia-oxidizing bacteria modulate carbon and nitrogen cycling in paddy soil. *Biogeosciences* 11, 3353–3368. doi: 10.5194/bg-11-3353-2014

frontiers | Frontiers in Microbiology

TYPE Original Research
PUBLISHED 27 November 2024
DOI 10.3389/fmicb.2024.1477571

OPEN ACCESS

EDITED BY
Yang Yang,
Chinese Academy of Sciences (CAS), China

REVIEWED BY
Chuck Randall Smallwood,
Sandia National Laboratories, United States
Xibin Sun,
Sun Yat-sen University, China
Min Yuan,
Sichuan Academy of Natural Resource Sciences, China

*CORRESPONDENCE
Changjun Ding
changjund@126.com
Qiwu Sun
sqw@caf.ac.cn

†These authors have contributed equally to this work

RECEIVED 08 August 2024
ACCEPTED 09 October 2024
PUBLISHED 27 November 2024

CITATION
Liu X, Hou L, Ding C, Su X, Zhang W, Pang Z, Zhang Y and Sun Q (2024) Effects of stand age and soil microbial communities on soil respiration throughout the growth cycle of poplar plantations in northeastern China. *Front. Microbiol.* 15:1477571. doi: 10.3389/fmicb.2024.1477571

Effects of stand age and soil microbial communities on soil respiration throughout the growth cycle of poplar plantations in northeastern China

Xiangrong Liu[1,2†], Lingyu Hou[1,2†], Changjun Ding[1,2*], Xiaohua Su[1,2], Weixi Zhang[1,2], Zhongyi Pang[3], Yanlin Zhang[1,2] and Qiwu Sun[1,2*]

[1]State Key Laboratory of Tree Genetics and Breeding, Key Laboratory of Tree Breeding and Cultivation of State Forestry Administration, Research Institute of Forestry, Chinese Academy of Forestry, Beijing, China, [2]State Key Laboratory of Efficient Production of Forest Resource, Research Institute of Forestry, Chinese Academy of Forestry, Beijing, China, [3]State-Owned Xinmin City Machinery Forest Farm, Shenyang, China

Introduction: Many studies have identified stand age and soil microbial communities as key factors influencing soil respiration (Rs). However, the effects of stand age on Rs and soil microbial communities throughout the growth cycle of poplar (*Populus euramevicana* cv.'I-214') plantations remain unclear.

Methods: In this study, we adopted a spatial approach instead of a temporal one to investigate Rs and soil microbial communities in poplar plantations of 15 different ages (1–15 years old).

Results: The results showed that Rs exhibited clear seasonal dynamics, with the highest rates observed in the first year of stand age (1-year-old). As stand age increased, Rs showed a significant decreasing trend. We further identified r-selected microbial communities (copiotrophic species) as key biological factors influencing the decline in Rs with increasing stand age. Other abiotic factors, such as soil temperature (ST), pH, soil organic carbon (SOC), nitrate nitrogen (NO_3^--N), and the C/N ratio of plant litter (Litter C/N), were also significantly correlated with Rs. Increased stand age promoted fungal community diversity but suppressed bacterial community diversity. Bacterial and fungal communities differed significantly in abundance, composition, and function, with the Litter C/N ratio being a key variable affected by microbial community changes.

Conclusion: This study provides crucial empirical evidence on how stand age affects Rs, highlighting the connection between microbial community assemblages, their trophic strategies, and Rs over the growth cycle of poplar plantations.

KEYWORDS

soil respiration, stand age, soil microbial community structure and function, poplar plantation, microbial r-K selection theory

1 Introduction

Soil respiration (Rs) is the process through which plant roots, fungi, and bacteria in the soil consume organic matter and produce carbon dioxide (CO_2) (Bond-Lamberty and Thomson, 2010). It is a crucial component of the carbon cycle in terrestrial ecosystems and represents the second largest flux of carbon exchange with the atmosphere (Ma et al., 2023). Rs significantly influences atmospheric CO_2 concentrations. It has been reported that soil

respiration releases 10 times more CO_2 into the atmosphere annually than fossil fuel combustion (Masson-Delmotte et al., 2021). Consequently, even small changes in Rs can substantially impact atmospheric CO_2 levels and the global terrestrial ecosystem carbon cycle (Feng et al., 2018). Since the industrial revolution, atmospheric CO_2 concentrations have surged, leading to a rise in global temperatures. In the context of global warming, understanding the characteristics of Rs and the factors influencing it is vital for estimating changes in atmospheric CO_2 concentrations. This understanding is crucial for accurately assessing regional carbon balances (Huang et al., 2020; Ma et al., 2014).

In terrestrial ecosystems, forests act as important natural carbon sinks and have a negative feedback effect on global warming (Bonan, 2008; Pan et al., 2011). Forests comprise roughly half of the biomass in terrestrial ecosystems and exert a significant and indispensable influence on the global soil carbon pool (Dixon et al., 1994). Stand age is a crucial indicator of forest developmental succession and carbon dynamics, with significant amounts of organic matter accumulating in the surface layer of forest soils over time (Bastida et al., 2019; Tang et al., 2009). Whether forest ecosystems act as carbon sources or sinks largely depends on the balance between photosynthetic carbon sequestration and respiration. Consequently, many studies have focused on the mechanisms of Rs changes and the factors influencing them. Previous studies on the impact of stand age on Rs has yielded three primary findings. First, Rs increases with stand age, mainly due to the growth and accumulation of soil organic carbon (SOC), roots, and microbial biomass (Wiseman and Seiler, 2004; Xiao et al., 2014). Second, there is an inverse relationship between Rs and stand age, attributed primarily to the decline in fine root biomass and metabolic activity (Gong et al., 2012; Yan et al., 2011; Zhao et al., 2016). Finally, some studies have found no significant linear correlation between Rs and stand age (Powers et al., 2018; Tang et al., 2009). The previous studies have selected discontinuous stand ages, and has not focused throughout the growth cycle.

Afforestation can increase carbon sequestration in terrestrial ecosystems, mitigate soil erosion, and reduce greenhouse gas emissions (Liu et al., 2013; Reay et al., 2007). Ecological restoration projects implemented in China in the late 1970s significantly contributed to carbon emissions in the 2001–2010 decade. These contributions were equivalent to 9.4 percent of the carbon emissions from fossil fuels during the same period (Fang et al., 2018; Lu et al., 2018). China's poplar plantation area reaches 7.57 Mha, ranking first in the world (National Forestry and Grassland Administration, 2019). Poplar is widely planted as pure or mixed species plantations, which has an economic value in providing wood and energy raw materials (Pilipovic et al., 2022), as well as mitigating the problem of dust storms and sandstorms in spring in northern China, which is of great significance for ecological environment protection and restoration of the areas in need of windbreaks and sand fixation. The increase in the area of poplar plantations is also due to their strong adaptability, rapid growth, and outstanding advantages in carbon sequestration (Gielen and Ceulemans, 2001). Additionally, poplars are also one of the major emitters of isoprene, a volatile organic compound (VOC) naturally released by trees, which has a significant impact on the atmospheric carbon cycle. Furthermore, the ability of poplars to emit isoprene is influenced by physiological states such as developmental stages, and is regulated by environmental factors such as temperature, light intensity, nitrogen nutrition, and atmospheric CO_2 concentration (Teuber et al., 2007). Therefore, the study of the relationship between the age of poplar plantations and carbon emissions is of great significance in addressing climate change and assessing carbon balance.. However, the relationship between Rs and throughout the growth cycle of poplar plantation has not been studied yet.

Previous research in forest ecosystems has shown that Rs is correlated with various factors, including soil temperature and moisture (ST and SM), soil physicochemical properties, and forest type (Zhao et al., 2016). In recent years, many studies have analysed microbial communities properties and carbon cycle which could improve the prediction of Rs (Liu et al., 2023; Nottingham et al., 2022; Zeng et al., 2022; Zhang and Zhang, 2016). Research has shown that Rs is correlated with soil microbial communities, particularly with Alphaproteobacteria, Acidobacteria, and Basidiomycota (Chen et al., 2021b). Additionally, in subtropical subalpine mountain ecosystems, it has been discovered that bacterial communities have a significant positive correlation with Rs. Rare bacterial phyla (e.g., Gemmatimonadetes and Cyanobacteria) are the primary driving factor, exerting a greater influence on Rs than abundant microbial communities (Han and Wang, 2023). According to the microbial trophic utilization patterns and carbon mineralization characteristics, microbial communities are usually divided into two ecological functions: r-strategists (copiotrophic) and K-strategists (oligotrophic) (Fierer et al., 2007). R-selected species grow fast and often utilize labile carbon. In contrast, k-selected species grow slowly and often utilize recalcitrant carbon. Fungi tend to grow slower than bacteria and are often classified as k-strategists (Yang et al., 2022). Related studies have reported specific roles for both copiotrophs and oligotrophs bacteria in utilizing carbon for respiration, and that the role of copiotrophs bacteria is higher than that of oligotrophs bacteria (Liu et al., 2020; Liu et al., 2018a; Liu et al., 2020b; Siles and Margesin, 2016). In summary, these findings indicate a close relationship between microbial communities and Rs.

In this study, we applied a spatial - for - temporal substitution method, focusing for the first time on poplar plantations in the Songliao Plain, Northeast China, spanning 1 to 15 years. We analyzed the link between stand age and Rs during continuous growth. This approach aims to explore the impact of stand age on Rs, providing new theoretical perspectives and empirical evidence for related research. The influence of stand age on soil respiration (Rs) was investigated from July 2022 to June 2023. The key objectives were to delve into (1) the pattern of change in Rs with stand age; (2) the dynamics of soil microbial communities with stand age; and (3) the relationship between biotic and abiotic factors and Rs.

2 Materials and methods

2.1 Site description and experimental design

The study site is located in a forest farm in Xinmin City, Liaoning Province, China (41°42′–42°17′N, 122°27′–123°20′E) (Supplementary Figure S1). The area belongs to the sandstorm area in the northern part of the Liaohe Plain, with a low terrain, gradually higher from south to north, and an average elevation of 29 metres above sea level. The study site experienced a temperate continental monsoon climate, with mean annual temperatures and precipitation of 8.2°C and 417.7 mm, respectively. It had an average frost-free period of 160 days and an annual sunshine duration averaging 2753.2 h. The soil type is brown soil.

In June 2022, based on principles such as site conditions and consistent species, we selected 15 stand ages ranging from 1 to 15 years

as the research objects. In each forest area, we randomly selected three 20 m × 20 m plots with similar growth as independent replicates, with the plots being no more than 30 meters apart from each other, establishing a total of 45 plots. All sampled plots were designated as forest land, with all previously being managed as pure artificial forests of the same species of poplar trees and subjected to identical management practices. To minimize the differences in climate, topography, and other factors among the plots, ensuring that variations in soil respiration and soil properties are attributed solely to stand age, the distance between any two stands was kept to no more than 3 km.

In October 2022, after removing surface litter, we collected 10 soil cores from each plot at a depth of 0 - 20 cm using the "S" sampling method and combined them into a single composite sample per plot. First, stones and plant roots were removed from the samples, which were then passed through 2 mm and 0.149 mm mesh sieves. The soil samples designated for physicochemical property analysis were air-dried and stored. Meanwhile, the soil samples intended for microbial community analysis were stored at - 80°C. Plant leaf litter was dried to a constant weight and then ground into powder for later use.

2.2 Field measurement of Rs rates

In June 2022, six PVC soil rings were randomly installed within each stand-age sample for Rs measurements. The PVC ring has a diameter of 20 cm and a length of 15 cm, with about 5 cm exposed above the soil surface, and remains in place throughout the entire experimental process. Before each measurement, plants within the soil ring were removed, along with the litter, to avoid the influence of plants and litter on Rs. Measurements were taken using the Li-8100a automated soil CO_2 flux system (LI-COR Inc., Lincoln, NE, United States) in the middle and end of each month from July 2022 to June 2023, respectively (no measurements were taken in December–February due to snow cover that froze the soil), with each measurement taken between 8.00 a.m. and 11.30 a.m. While measuring Rs rates, ST and SM at a depth of 5 cm in the vicinity of the soil ring were also measured.

2.3 Analysis of soil and litter samples

The soil bulk density (SBD) was measured using the cutting ring method (Wang et al., 2018). Soil pH was measured by using the soil-water (1:2.5) mixed suspension through the potential method. Soil and litter organic carbon was determined by the K_2CrO_7 oxidation method (Lefroy et al., 1993). Total soil and litter nitrogen was determined by Kjeldahl method. SOC and TN data were used to calculate soil C/N. Litter C/N was calculated using litter organic carbon and total nitrogen data. Dissolved organic carbon (DOC) was extracted with deionized water (1:4) and then measured using a TOC analyzer (Shimadzu Corp, Kyoto, Japan). Easily oxidised organic carbon (EOC) was determined after $KMnO_4$ oxidation (Zhao et al., 2018). The available phosphorus (AP) and available potassium (AK) were extracted from the soil samples using a 2% $(NH_4)_2\,CO_3$ solution at a soil-to-solution ratio of 1:5, and were subsequently determined using an ICAP instrument (Spectro Analytical Instruments, Spectro Arcos ICP, Kleve, Germany) (Wang et al., 2022). Nitrate nitrogen (NO_3^--N) and ammonium nitrogen (NH_4^+-N) were extracted from the soil using 2 M KCl and the content was determined using a continuous flow injection analyser system (AA3 Continuous Flow Analytical System).

2.4 Soil DNA extraction and sequence analysis

Soil total DNA was extracted from 0.25–0.5 g of soil samples using the TIANNamp Guide S96 kit (Beijing, China). The extracted nucleic acids were assayed for concentration using an enzyme labeler (GeneCompang Limited, synergy HTX). After passing the assay, the nucleic acids were amplified, and the amplified PCR products were then detected by electrophoresis using agarose at a concentration of 1.8%. The bacterial V3–V4 region was amplified using the 16S rRNA gene primers 338F (5′-ACTCCTACGGGAGGCAGCAG-3′) and 806R (5′-GGACTACHVGGGTWTCTAAT-3′). The fungal ITS1 region was amplified using the fungal ITS primers ITS1F (5′-CTTGGTCATT TAGAGGAAGTAA-3′) and ITS2R (5′-GCTGCGTTCTTCAT CGATGC-3′). The products were purified, quantified, and normalized on the Illumina Novaseq 6000 platform, and detected using the NovaSeq 6000 S4 Reagent Kit (San Diego). The original image data files obtained from sequencing are converted into raw sequencing sequences through base recognition analysis. The sequencing results are filtered, and then primer sequences are identified and removed to obtain effective sequences.

The soil microbial communities (bacteria and fungi) were classified as r-strategists or K-strategists based on their nutrient utilization modes. Among them, copiotrophic bacteria, such as Actinobacteriota, Bacteroidota, Firmicutes, and Gemmatimonadota, were categorized as r-strategists. The oligotrophs bacterial members, including Acidobacteriota, Chloroflexi to K-strategists. The r-strategist fungi include Ascomycota, while the K-strategist fungi include Basidiomycota (Li et al., 2021; Fierer et al., 2007; Yang et al., 2022). We also selected several microbial taxa associated with the carbon cycle, including Proteobacteria, Acidobacteriota, Actinobacteriota, Bacteroidota, Ascomycota, and Basidiomycota. We analyzed their relative abundance to investigate the potential relationship with Rs (Chen et al., 2021b; Castro et al., 2019).

2.5 Statistical analysis

Regression analyses were used to evaluate the relationship between soil properties, microbial community structure, characteristics and stand age. Pearson correlation analysis was used to determine the relationship between Rs and biotic and abiotic factors. Using the "plspm" package (Sanchez et al., 2013), the effects of stand age, climate (ST, SM), soil and plant properties (pH, SOC, DOC/SOC, EOC/SOC, AK, NO_3^--N, and litter C/N), as well as soil bacterial and fungal community structure, on Rs were evaluated through a partial least squares path model (PLS-PM). One-way analysis of variance (ANOVA) was used to compare the dominant communities of soil bacteria and fungi in stands of different stand ages. Differences in Bray–Curtis distances between stand ages for bacterial and fungal communities were analysed using non-metric multidimensional scaling (NMDS); the significance of the differences was determined by using ranked analysis of variance (PERMANOVA). The relationship

between soil and plant properties and soil bacterial and fungal diversity and community structure was analysed using the Mantel test. In addition, functional information was annotated for OTU of bacteria and fungi using FAPROTAX and FUNGuild software (Louca et al., 2016; Nguyen et al., 2016). All data analysis and figures were conducted using SPSS18.0 (IBM, United States), Origin2021 (OriginLab, United States), and R software (v4.3.2).

3 Results

3.1 Changes in Rs with stand age Changes and relationships between Rs and soil factors under stand age effects

Rs rate significantly decreased with increasing stand age ($p < 0.001$) (Figure 1). SBD, SOC, DOC, and NO_3^--N showed significant changes with stand age ($p < 0.05$) (Supplementary Figure S2). Among these, SBD and DOC generally increased with stand age, while SOC and NO_3^--N decreased. All factors except for soil pH, DOC, NH_4^+-N, and AP were significantly correlated with Rs rate ($p < 0.05$) (Supplementary Figure S3). Specifically, SOC, TN, NO_3^--N, and AK were significantly positively correlated with Rs, while SBD and EOC were significantly negatively correlated. Rs rate was significantly negatively correlated with both the DOC/SOC and EOC/SOC, and significantly positively correlated with litter C/N ($p < 0.05$), but showed no significant correlation with soil C/N (Supplementary Figure S4).

3.2 Soil bacterial community composition and its relationship with environmental factors

The bacterial community structure and diversity changed with increasing stand age. The dominant phyla across different stand ages were Proteobacteria (29.19–41.88%), Acidobacteriota (18.90–29.11%), and Actinobacteriota (6.49–12.50%), comprising 71.96–79.34% of the bacterial samples at each stand age. The relative abundance of these dominant phyla significantly changed with stand age. Notably, the relative abundance of Proteobacteria and Actinobacteriota showed a significant increasing trend with stand age ($p < 0.05$) (Figure 2A).

Functional annotation of bacterial OTUs using FAPROTAX was used to identify carbon and nitrogen transforming functional bacterial groups in poplar associated soils and to determine their relative abundance in each stand. Related to the carbon cycle are phototrophy, photoautotrophy and oxygenic photoautotrophy. Associated with the nitrogen cycle are nitrate reduction and nitrogen fixation. The results indicate that as the stands mature, there is a general decrease in the abundance of nitrate-reducing bacteria involved in nitrogen transformation, while nitrogen-fixing bacteria show an increasing trend (Supplementary Figure S5A). Concurrently, the abundance of photoautotrophic organisms involved in carbon transformation tends to decrease with stand age (Supplementary Figure S5A).

Microbial characteristics changed significantly with stand age ($p < 0.05$) (Supplementary Figure S6). Bacteria Shannon decreased significantly with stand age and bacterial NMDS1 increased significantly with stand age. Bacterial to fungal ratio Shannon, on the other hand, decreased significantly with stand age. The results of Mantel test showed that pH, litter C/N, AK, DOC/SOC and NO_3^--N were important factors affecting the structure of bacterial community ($p < 0.05$) (Figure 3A). MMDS analyses showed that bacterial community β-diversity varied considerably with stand age, and bacterial community composition was significantly segregated between different stand ages ($p < 0.05$; Supplementary Figure S7A). PERMANOVA analyses further determined significant differences

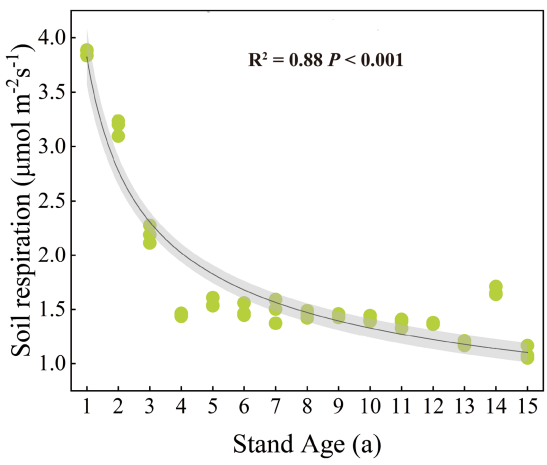

FIGURE 1
Patterns of change in soil respiration with stand age.

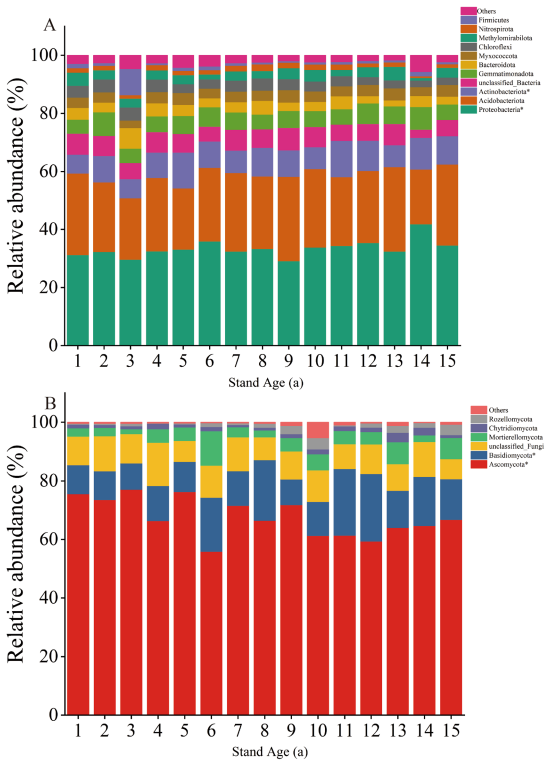

FIGURE 2
Relative abundance of dominant bacterial **(A)** and fungal **(B)** groups at the phylum level. *Significant differences ($p < 0.05$) were found between different stand ages.

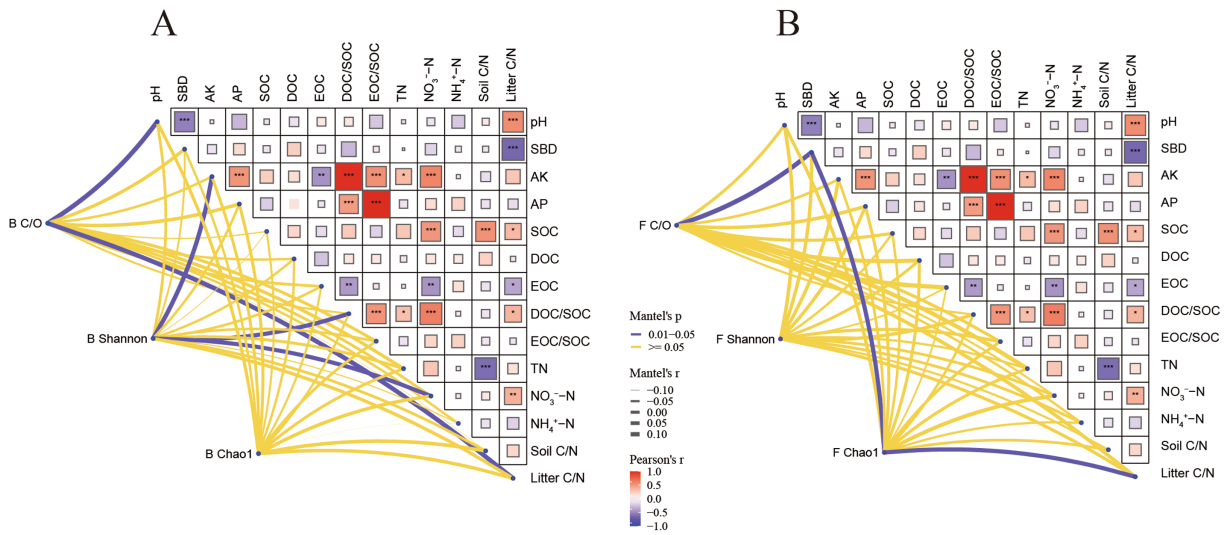

FIGURE 3
The Mantel test of the correlations analysed the relationship between soil and plant characteristics and soil bacterial **(A)** and fungal **(B)** diversity and community structure. B C/O, bacterial copiotroph/oligotroph ratio; B Shannon, bacteria Shannon; B Chao1, bacteria Chao1; F C/O, fungal copiotroph/oligotroph ratio, F Shannon, fungi Shannon; F Chao1, fungi Chao1; SBD, soil bulk density; AK, available potassium; AP, available phosphorus SOC, soil organic carbon; DOC, dissolved organic carbon; EOC, easily oxidised organic carbon; TN, total nitrogen; NO_3^--N, nitrate nitrogen; NH_4^+-N, ammonium nitrogen; litter C/N, plant litter C/N. In the figure, the heatmap colors and grid sizes are simultaneously used to map the magnitude of correlation values. Darker colors and larger grid sizes indicate larger absolute values of correlation, while lighter colors and smaller grid sizes indicate smaller absolute values of correlation. Colors closer to red indicate stronger positive correlation, while colors closer to blue indicate stronger negative correlation. The marks within the grids, *$p < 0.05$; **$p < 0.01$; ***$p < 0.001$, indicate statistically significant results. The thickness of the lines connecting the three nodes with various soil and plant factors serves as an indication of the magnitude of their correlation. Thicker lines signify stronger correlations, whereas thinner lines indicate weaker correlations. Blue lines represent significant correlations ($p < 0.05$), while yellow lines denote non-significant correlations ($p > 0.05$).

in bacterial ($p = 0.001$) community composition across the 15 stand ages.

3.3 Soil fungal community composition and its relationship with environmental factors

The primary fungal phyla were Ascomycota (55.92–77.02%) and Basidiomycota (8.83–23.08%), collectively comprising 72.88–87.17% of fungal sequences in each sample, with Ascomycota predominating. The relative abundance of these fungal communities was significantly influenced by stand age. Ascomycota exhibited an overall significant decreasing trend, while Basidiomycota showed a significant overall increasing trend ($p < 0.05$) (Figure 2B).

The FUNGuild database was used to predict the functional attributes of fungal communities, firstly by classifying fungi into three main groups based on the mode of nutrition: saprotroph, symbiotroph and pathotroph. Based on the predicted results, the saprotroph types include dung saprotroph, litter saprotroph, plant saprotroph, soil saprotroph, undefined saprotroph and wood saprotroph. Symbiotroph trophic types include ectomycorrhizal and endophyte. Pathotroph types include plant pathogen, animal pathogen and fungal parasite. Stand age significantly influenced the abundance of fungal functional communities. It is noteworthy that dung saprotroph and litter saprotroph abundance decreased significantly with stand age ($p < 0.05$) (Supplementary Figure S5B).

Fungal microbiological properties changed significantly with stand age ($p < 0.05$) (Supplementary Figure S6). Fungi Shannon increased significantly with stand age and fungal NMDS1 increased significantly with stand age. The Mantel test revealed a significant correlation between litter C/N and fungal Chao1, and highlighted SBD as a key determinant influencing fungal community structure ($p < 0.05$) (Figure 3B). NMDS analyses showed that the β-diversity of fungal communities varied considerably with stand age, and the composition of fungal communities was significantly segregated between different stand ages ($p < 0.05$) (Supplementary Figure S7B). PERMANOVA analyses further determined significant differences in fungal community composition across the 15 stand ages ($p = 0.032$).

3.4 Characterisation of Rs dynamics and its relationship with biotic and abiotic factors

Overall, Rs rates of all stand ages showed similar seasonal variations over the observation period. Rs varied markedly by stand age, with Rs rate being greatest in 1a and showing an overall decreased trend with increased stand age. ST changes were consistent with the dynamics of Rs rate, while SM dynamics were inconsistent with the pattern of Rs rate and ST changes (Figure 4).

Pearson correlation analysis revealed that Rs was significantly correlated with stand age, SBD, ST, DOC/SOC, EOC/SOC, AK, TN, NO_3^--N, and litter C/N ($p < 0.05$) (Supplementary Figure S8). To further explore the relationship between microbial diversity and Rs,

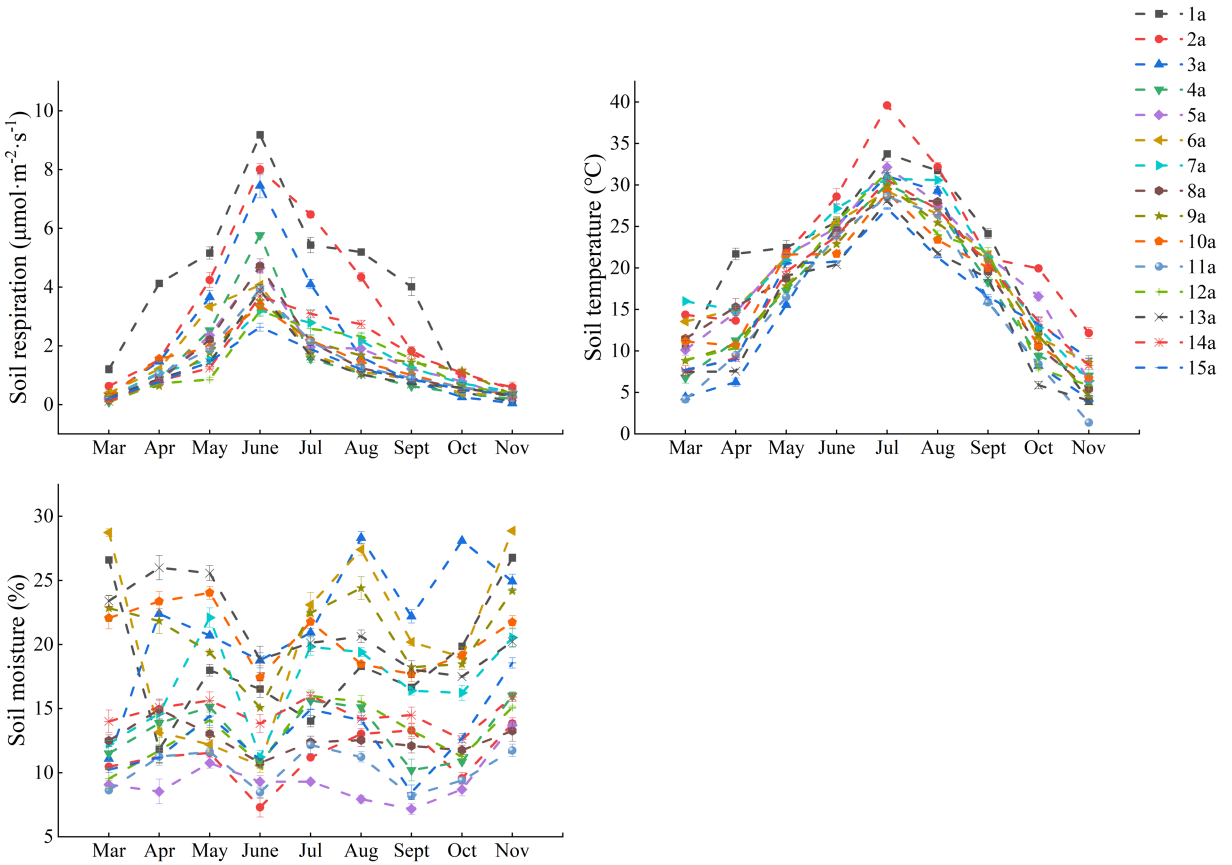

FIGURE 4
Seasonal changes in soil respiration, soil temperature and soil moisture in 15 poplar plantations of different stand ages.

we found that the shift in microbial diversity had a significant impact on Rs as the poplar plantations matured (Supplementary Figure S9). For example, changes in the relative abundance of specific microbial groups, such as Actinobacteria and Ascomycota, might alter the decomposition rate of organic matter, thereby affecting Rs (Figure 5). In addition, the balance between bacterial and fungal communities also played a crucial role in regulating Rs. This is consistent with the correlation between the bacterial Shannon index and Rs, indicating that higher bacterial diversity contributes to more efficient carbon cycling at younger stand ages.

We further analyzed the possible links between stand age, soil properties, climate, soil microbial (bacterial and fungal) community structure, and Rs using PLS-PM, as well as the direct and indirect effects they produce (Figure 6). bove all, stand age and soil properties accounted for the greatest proportion of variation in Rs (Figure 6B). Stand age had a significant indirect effect on soil bacterial community structure (path coefficient: −0.46) ($p < 0.01$), suggesting that as poplar plantations mature, shifts in microbial diversity may contribute to reduced Rs rates (path coefficient: −0.45) ($p < 0.05$). Changes in soil bacterial community structure were also directly determined by soil properties (path coefficient: 0.39). Stand age indirectly and significantly influenced Rs through soil properties (path coefficient: −0.46) ($p < 0.005$) and climate (path coefficient: 0.62) ($p < 0.01$), while changes in Rs were also directly influenced by stand age (path coefficient: −0.20), soil properties (path coefficient: 0.63), and climate (path coefficient: −0.27), respectively. Overall these variables explained 85% of the variation in Rs.

4 Discussion

4.1 Relationship between stand age and Rs

There are no existing studies that investigate the impact of stand age on Rs throughout the entire growth cycle of poplar plantations. Our research demonstrated that stand age significantly affected Rs, showing a decreasing trend in the Rs rate as stand age increased (Figure 1). The decrease trend is also reported in the *Populus balsamifera* L. and *Populus davidiana* Dode plantations in Xinjiang and Hebei in China, with the Rs rate of young forests being the highest, and the Rs significantly decreasing with the increase of stand age (Gong et al., 2012; Yan et al., 2011; Zhao et al., 2016). In contrast, there is no significant change in Rs with the increase of stand age in the hybrid poplar plantations (Saurette et al., 2008). The findings suggest that the effect of stand age on Rs can vary depending on the type of tree species and planting techniques, potentially attributed to disparities in the quality of the soil carbon pool and the amount of root biomass (Xiao et al., 2014).

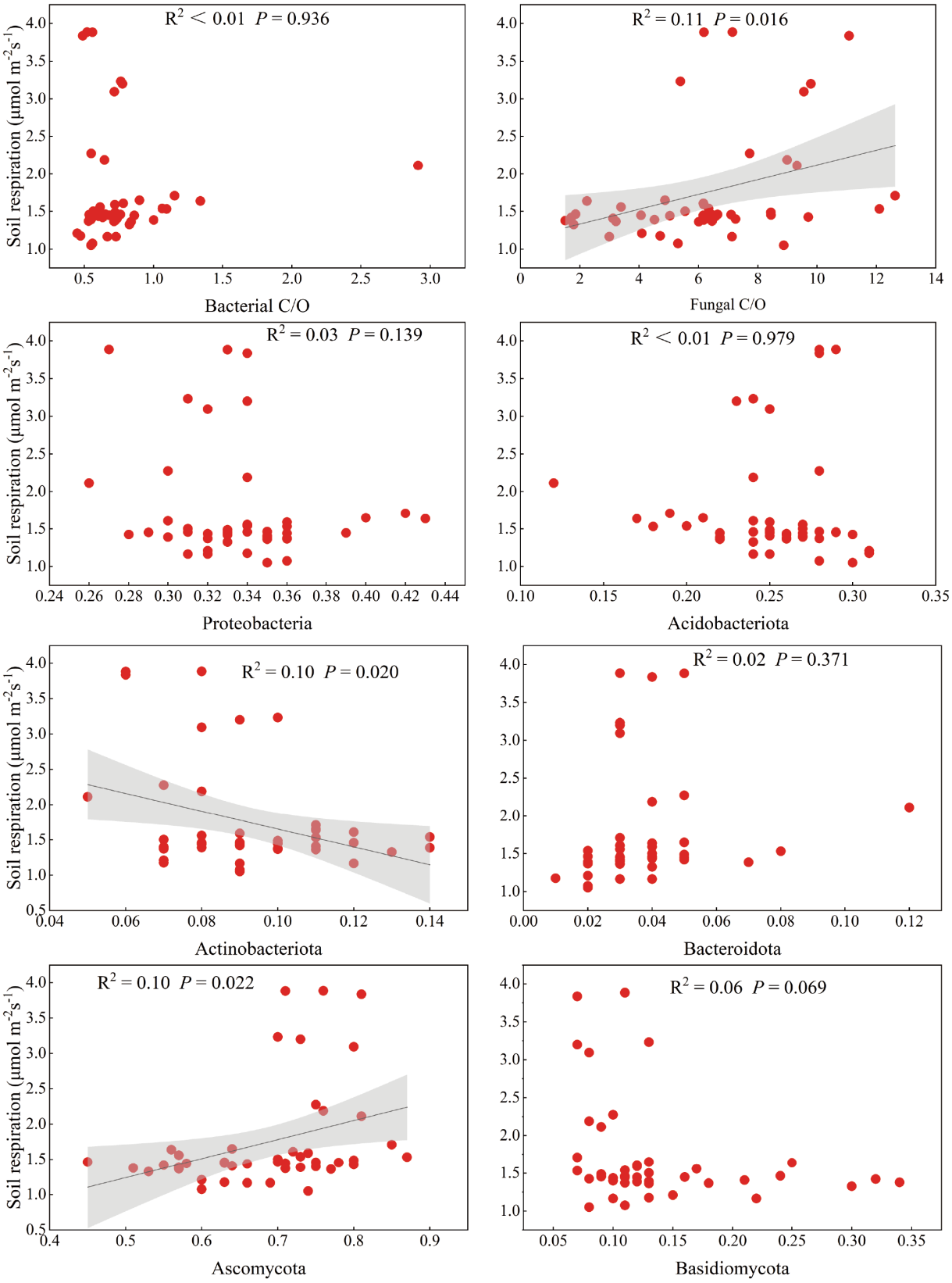

FIGURE 5
Relationship between soil respiration rate and relative abundance of major microbial taxa associated with carbon mineralisation. The solid black line indicates a significant linear relationship consistent with the regression model, and the shaded area indicates the fitted 95% confidence interval.

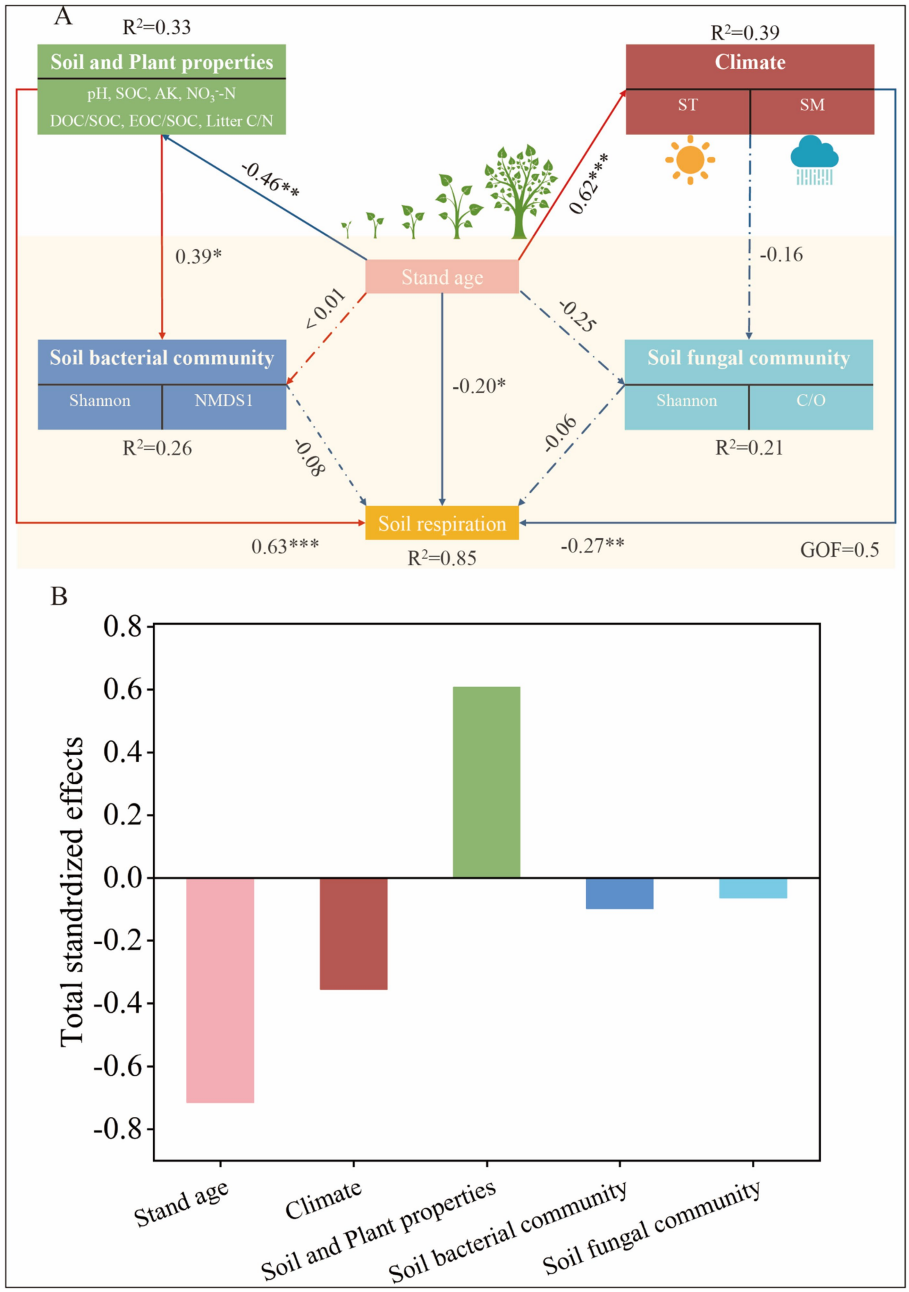

FIGURE 6
Partial least squares path modelling (PLS-PM) of soil respiration by stand age, climate, soil properties, soil bacterial and fungal communities **(A)**, and the standardised total effects of soil respiration influences **(B)**. Causal relationships are indicated by arrows and the numbers next to the arrows indicate the standardised path coefficients. Solid lines indicate significant relationships (*$p < 0.05$, **$p < 0.01$, and ***$p < 0.001$) and dashed lines indicate non-significant relationships. R^2 denotes the variance of the variables considered in the model. GOF, goodness of fit. SOC, soil organic carbon; AK, available potassium; NO_3^--N, nitrate nitrogen; EOC, Easily oxidised organic carbon; Litter C/N, plant litter C/N; ST, soil temperature; SM, soil moisture; Shannon, diversity indices of bacterial and fungal communities; C/O, copiotroph/oligotroph ratio.

In this study, stand age significantly influenced Rs by altering environmental conditions such as soil temperature and nutrients (Figure 6; Supplementary Figure S8). With the increase in stand age, the canopy structure gradually undergoes transformation. Mature forests typically possess denser canopies, reducing the amount of solar radiation reaching the ground surface and thereby modulating understory temperature and humidity (McCarthy and Brown, 2006). During warm seasons, the dense canopy mitigates direct sunlight on the soil surface, leading to lower ST. This reduced ST subsequently slows down microbial metabolic activities, resulting in decreased Rs rates. Conversely, in younger stands, the sparser canopy allows more sunlight to penetrate the soil surface, elevating ST and enhancing Rs. This study confirms this phenomenon, with significantly higher ST in 1a and 2a stands compared to older stands, and much higher Rs values in summer (June-August) than in spring (March-May) and autumn

(September-November) (Figure 4). This aligns with the positive correlation between ST and Rs observed in previous studies (Wang et al., 2023). Additionally, while SM can potentially influence Rs under extreme conditions (Raich and Potter, 1995) no significant correlation between Rs and SM was detected in this study (Supplementary Figure S8). This may be attributed to the fact that during the growing season in the study area, SM in the poplar plantations was relatively abundant, posing no constraints on microbial and root respiration (Nottingham et al., 2020).

As stand age increases, the patterns of tree absorption and utilization of soil nutrients also undergo changes, subsequently influencing Rs. Young stands grow rapidly with high nutrient demands, potentially leading to a decrease in available nutrients such as nitrogen and available potassium in the soil, both of which are crucial elements for microbial respiration. The deficiency of these nutrients can inhibit microbial activity, thereby reducing Rs. In contrast, in mature stands, tree growth slows down, reducing nutrient demands, and soil nutrient content may stabilize, supporting more stable microbial activities (Rodríguez-Soalleiro et al., 2018). Concurrently, with the increase in stand age, the accumulation of plant residues and litter in the soil enhances the organic carbon content (Yang et al., 2014), providing a substrate source for microbial respiration. However, excessive organic carbon may also impact soil aeration, potentially inhibiting microbial activity.

Changes in Rs can also be explained by substrate carbon and nitrogen effectiveness and soil carbon fractions (SOC, MBC, DOC, EOC) (Tedeschi et al., 2006; Wu et al., 2020). Compared to soil recalcitrant carbon SOC, MBC, DOC and EOC are more readily available for direct use by soil microorganisms. In this study, soil carbon fractions (SOC, ECO, DOC/SOC, EOC/SOC), TN, NO_3^--N, and Litter C/N ($p < 0.001$) were significantly correlated with Rs (Supplementary Figures S2, S4), and may be attributed to the strong response of Rs to substrate carbon and nitrogen effectiveness (Wang et al., 2017; Yang et al., 2022). Therefore, as stand age increases, changes in soil carbon-to-nitrogen ratios and litter carbon-to-nitrogen ratios both affect microbial biomass and activity, subsequently influencing Rs (Tu et al., 2013). In forest systems, inputs of litter increase SOC while decreasing soil nitrogen content, resulting in an increase in the soil C/N. Therefore, changes in both soil carbon and nitrogen, as well as litter carbon and nitrogen, affect soil microbial biomass and microbial activity, leading to changes in heterotrophic respiration, which is a component of total Rs (Tu et al., 2013). In this paper, the SOC decreased with stand age overall, it began to show a certain upward trend after 7a and 8a (Supplementary Figure S2). This may be attributed to the fact that poplars are designed to grow rapidly at younger ages, thereby absorbing large amounts of nutrient elements from the soil and accumulating biomass (Rodríguez-Soalleiro et al., 2018). After the stage of 7a and 8a, the plant growth rate slows down and nutrient uptake begins to decrease, allowing the retention and accumulation of apoplastic and root organic matter (Yang et al., 2014).

4.2 Changes of soil microbial communities with stand age

The results of our PERMANOVA analyses revealed that increased stand age significantly influenced the structure of soil bacterial and fungal communities (Supplementary Figure S7). Furthermore, our PLS-PM analyses attributed this effect to changes in soil properties brought about by increased stand age (Figure 6), which consequently altered the ecological strategies of microorganisms (Marques et al., 2014). Some studies have reported that increased root biomass stimulates secretions into the soil as a key factor contributing to increased soil microbial community diversity (Fraser et al., 2017), and if this is the case, we hypothesise that soil microbial diversity increased with stand age. However, our results showed that soil bacterial community diversity decreased with stand age, but soil fungal community diversity showed an increased trend (Supplementary Figure S6). This was possibly due to a decreased root secretion with age and the fact that the fungal community was more resistant to the effects of age than the bacterial community. Another explanation is that bacterial communities have a smaller ecological niche in the soil than fungal communities, have a smaller symbiotic relationship with plants than fungi, and provide less significant feedbacks to plants and soil than fungal communities (Sun et al., 2017). Thus fungal community diversity has a more positive direct or indirect effect on stand age. At the same time, stand age also altered the relative abundance of major bacterial phyla (Proteobacteria, Acidobacteriota, and Actinobacteriota) and fungal phyla (Ascomycota and Basidiomycota) (Figure 2). This result is similar to findings from poplar plantations in other regions (Wu et al., 2021). Proteobacteria and Actinobacteria were classified as copiotrophic bacteria, while Ascomycota was classified as copiotrophic fungi. Both copiotrophic bacteria and fungi belong to fast-growing taxa (r-strategists) and prefer nutrient-rich environments. On the other hand, Basidiomycota are classified as oligotrophic and belong to slow-growing taxa (K-strategists), which are better suited to grow in environments with lower nutrient concentrations. Meanwhile, the relative abundance of r-fungi (Ascomycota) exhibits an overall downward trend with the increase of stand age, while the relative abundance of K-fungi (Basidiomycota) displays an overall upward trend. This shift indicates that K-strategy fungi become more dominant as stand age increases.

Stand age, climate, soil properties and plant species were all important predictors of soil microbial community structure (Chen et al., 2021a; Marques et al., 2014). The structure of microbial communities is influenced by soil pH, permeability, and physicochemical properties (Krause et al., 2017; Lupwayi et al., 2017). This coincides with our finding that the diversity and structure of soil microbial communities varied significantly with stand age in relation to soil pH, and physico-chemical properties such as SBD, AK, NO_3^--N, DOC/SOC, and litter C/N (Figure 3). Vitali et al. (2016) observed that soil microbial communities in poplar plantations are influenced by pH. Our results confirmed this finding and further supported the notion that soil microbial communities in poplar plantations of varying stand ages are also affected by pH. Additionally, Ascomycota and Basidiomycota may also influence the changes in soil pH and SBD (Zhao et al., 2018).

Prediction of ecological functions of soil bacterial and fungal communities using FAPROTAX and FUNGuild showed that soil microbial functional groups changed significantly with stand age (Supplementary Figure S5). Among the bacterial functional groups, the abundance of nitrate reduction and photoautotrophy generally decreases with increasing stand age, while the abundance of nitrogen fixation generally increases with increasing stand age (Supplementary Figure S5A). However, Yan et al. (2020) study of

secondary succession in *Quercus liaotungensis* forests found that the relative abundance of microbial functional groups associated with soil carbon and nitrogen cycling increased with succession, which should be attributed to the low levels of both SOC and TN in our study area. As the understory vegetation ecosystem recovers as the stand ages, the relative abundance of nitrogen fixation bacteria increases (Blaud et al., 2018). Only dung saprotroph and litter saprotroph among the saprotrophic types showed a significant decrease with stand age (Supplementary Figure S5B). Most saprophytic bacteria are in the Ascomycetes phylum and are important decomposers of soil as they are able to break down the complex structure of organic matter in the soil (Paungfoo-Lonhienne et al., 2015). Therefore, with increasing stand age, the saprotrophic functional groups may be influenced by changes in the relative abundance of the Ascomycota phylum.

When discussing changes in soil microbial functional groups in poplar plantations with increasing stand age, we relied solely on two databases for prediction. This limitation may restrict the comprehensiveness of our conclusions, as it may not fully capture the diversity and dynamic changes of soil microbial functional groups. In order to better understand how stand age affects changes in soil microbial function, future studies should expand samples and use better sequencing methods.

4.3 Important factors affecting Rs

Based on the regression analysis model and Pearson's correlation analysis, we observed that changes in Rs depend strongly on the microbial properties at the community level (Figure 5; Supplementary Figure S8). In addition to soil properties, changes in temperature often affect the structure of soil microbial communities. For instance, fungal communities prefer cooler environments relative to bacterial communities. According to the Carbon-Quality-Temperature hypothesis, recalcitrant carbon decomposition with higher activation energy possesses higher temperature sensitivity compared to the decomposition of labile carbon (Fierer et al., 2005; Wang et al., 2018). And soil microbes are more active in carbon-rich conditions. Therefore, the reasons for the changes in Rs with stand age can be explained by the decreasing trends in soil carbon and nitrogen content and temperature with stand age. This viewpoint is well-supported by ample evidence, revealing the close relationships and interactions among stand age, soil properties, ST and bacterial community structure.

Specific microbial communities and ecological clusters are important factors in microbial prediction of Rs (Wang et al., 2021). In conclusion, microorganisms associated with carbon mineralisation (Actinobacteriota and Ascomycota) and microbial r-/K strategy ratio (fungal copiotroph/oligotroph ratio) were the main biological factors that predicted a decline in soil respiration with age in poplar plantations. Copiotrophic and oligotrophic have different ecological functions in using carbon for respiration due to different substrate utilisation strategies. R-strategy communities prefer nutrient-rich and warm environments over K-strategy communities and use the majority of the acquired energy for their own growth and reproduction, thus reducing respiration efficiency while having more efficient carbon utilisation. In contrast, K-strategy tends to preferentially utilise recalcitrant carbon, which requires a large amount of energy consumption, and so devotes the majority of its energy and resources to respiration (Liu et al., 2020b; Malik et al., 2020). The positive correlation of Ascomycota and Fungal C/O with Rs further confirmed that Rs decreased with the distribution of soil microbial r-strategies under increasing stand age.

We observed microbial r-/K strategy ratio (fungal copiotroph/oligotroph ratio), microbial community diversity (e.g., Shannon and NMDS1 for bacteria and fungi), and microbial communities associated with carbon mineralisation (Actinobacteriota and Ascomycota) as important biotic factors affecting Rs. However, soil microbial communities are often influenced by a number of other abiotic factors such as soil physico-chemical properties. Thus, such abiotic factors are also important drivers of Rs. For example, our data indicates that SOC and NO_3^--N are abiotic factors that affect soil carbon flux, consistent with the findings reported for Rs in *Pinus massoniana* plantations (Yu et al., 2019). In general, a high soil C/N ratio inhibits microbial decomposition (He et al., 2018). However, although no significant effect of soil microorganisms on Rs was observed in PLS-PM analysis, the importance of soil microorganisms was verified by both the regression analysis model and the correlation analysis. Thus, our findings emphasised the potential importance of soil microbial communities and ecological clusters in predicting Rs.

In general, the Rs rate in poplar plantations decreases with increasing stand age, as stand age influences environmental conditions such as soil temperature (ST), nutrients, and microbial communities. This suggests that with increasing stand age, the carbon sink capacity of poplar plantations may be enhanced, since lower Rs corresponds to reduced soil carbon loss. Thus, older poplar plantations may be more effective in carbon sequestration than younger ones, contributing to global carbon storage. In the context of global warming, Rs typically increases with rising temperatures, leading to higher CO_2 emissions. However, our study shows that as stand age increases, Rs decline, suggesting that older forests may act as crucial carbon sinks, mitigating climate change. A lower Rs rate may offset the adverse effects of climate change by delaying soil carbon release. Therefore, we propose extending the growth cycles of poplar plantations, particularly maintaining older stands, to aid in carbon sequestration and climate mitigation efforts. In forest management and land-use planning, focusing on preserving older forests could optimize carbon sequestration. Additionally, poplars are significant sources of volatile organic compound (VOC) emissions, which may result in carbon loss and are linked to stand age. Future research should focus on stand age's effect on the ecological carbon dynamics of poplar plantations, which is crucial for assessing ecological services across different ages.

5 Conclusion

Rs decreased with increasing stand age in poplar plantations throughout the growth cycle. The microbial r-strategies were the key biotic factors that influenced Rs in different-age poplar plantations. Other abiotic factors such as ST, pH, SOC and NO_3^--N, and litter C/N were also important drivers of Rs. Soil properties such as pH and SBD also significantly affected soil microbial

community diversity and composition, and altered the ecological strategies of microbial communities, which in turn impacted altered Rs. Our study provides new insights into understanding the changes in Rs in poplar plantations in Northeast China influenced by stand age. Meanwhile, the study highlighted the potential link between the combination of different ecological taxa of soil microbes and Rs, which is of great significance for the prediction of soil carbon dynamics in poplar plantation ecosystems in the context of global warming.

Data availability statement

The bacterial and fungal DNA sequences of the soil samples have been deposited in the SRA (Sequence Read Archive) of the NCBI database, with the accession number PRJNA1180506.

Author contributions

XL: Conceptualization, Formal analysis, Data curation, Writing – original draft, Writing – review & editing. LH: Conceptualization, Formal analysis, Data curation, Writing - original draft, Writing - review & editing. CD: Conceptualization, Investigation, Supervision, Writing – review & editing, Funding acquisition. XS: Writing – review & editing, Funding acquisition. WZ: Writing – review & editing. ZP: Investigation, Writing – review & editing. YZ: Formal analysis, Investigation, Writing – review & editing. QS: Conceptualization, Investigation, Supervision, Writing – review & editing.

Funding

The author(s) declare that financial support was received for the research, authorship, and/or publication of this article. This research was funded by the National Key Research and Development Program of China (Grant Nos. 2021YFD2201201 and 2021YFD2201205), the Basic Research Fund of CAF (Grant No. CAFYBB2023QB003).

Conflict of interest

The authors declare that the research was conducted in the absence of any commercial or financial relationships that could be construed as a potential conflict of interest.

Publisher's note

All claims expressed in this article are solely those of the authors and do not necessarily represent those of their affiliated organizations, or those of the publisher, the editors and the reviewers. Any product that may be evaluated in this article, or claim that may be made by its manufacturer, is not guaranteed or endorsed by the publisher.

Supplementary material

The Supplementary material for this article can be found online at: https://www.frontiersin.org/articles/10.3389/fmicb.2024.1477571/full#supplementary-material

References

Bastida, F., Lopez-Mondejar, R., Baldrian, P., Andres-Abellan, M., Jehmlich, N., Torres, I. F., et al. (2019). When drought meets forest management: effects on the soil microbial community of a Holm oak forest ecosystem. *Sci. Total Environ.* 662, 276–286. doi: 10.1016/j.scitotenv.2019.01.233

Blaud, A., van der Zaan, B., Menon, M., Lair, G. J., Zhang, D. Y., Huber, P., et al. (2018). The abundance of nitrogen cycle genes and potential greenhouse gas fluxes depends on land use type and little on soil aggregate size. *Appl. Soil Ecol.* 125, 1–11. doi: 10.1016/j.apsoil.2017.11.026

Bonan, G. B. (2008). Forests and climate change: forcings, feedbacks, and the climate benefits of forests. *Science* 320, 1444–1449. doi: 10.1126/science.1155121

Bond-Lamberty, B., and Thomson, A. (2010). Temperature-associated increases in the global soil respiration record. *Nature* 464, 579–582. doi: 10.1038/nature08930

Castro, S. P., Cleland, E. E., Wagner, R., Al Sawad, R., and Lipson, D. A. (2019). Soil microbial responses to drought and exotic plants shift carbon metabolism. *ISME J.* 13, 1776–1787. doi: 10.1038/s41396-019-0389-9

Chen, L. F., He, Z. B., Wu, X. R., Du, J., Zhu, X., Lin, P. F., et al. (2021a). Linkages between soil respiration and microbial communities following afforestation of alpine grasslands in the northeastern Tibetan plateau. *Appl. Soil Ecol.* 161:103882. doi: 10.1016/j.apsoil.2021.103882

Chen, L. F., He, Z. B., Zhao, W. Z., Kong, J. Q., and Gao, Y. J. (2021b). Empirical evidence for microbial regulation of soil respiration in alpine forests. *Ecol. Indic.* 126:107710. doi: 10.1016/j.ecolind.2021.107710

Dixon, R. K., Solomon, A. M., Brown, S., Houghton, R. A., Trexier, M. C., and Wisniewski, J. (1994). Carbon pools and flux of global forest ecosystems. *Science* 263, 185–190. doi: 10.1126/science.263.5144.185

Fang, J. Y., Yu, G. R., Liu, L. L., Hu, S. J., and Chapin, F. S. III (2018). Climate change, human impacts, and carbon sequestration in China. *Proc. Natl. Acad. Sci. U.S.A.* 115, 4015–4020. doi: 10.1073/pnas.1700304115

Feng, J. G., Wang, J. S., Song, Y. J., and Zhu, B. (2018). Patterns of soil respiration and its temperature sensitivity in grassland ecosystems across China. *Biogeosciences* 15, 5329–5341. doi: 10.5194/bg-15-5329-2018

Fierer, N., Bradford, M. A., and Jackson, R. B. (2007). Toward an ecological classification of soil bacteria. *Ecology* 88, 1354–1364. doi: 10.1890/05-1839

Fierer, N., Craine, J. M., McLauchlan, K., and Schimel, J. P. (2005). Litter quality and the temperature sensitivity of decomposition. *Ecology* 86, 320–326. doi: 10.1890/04-1254

Fraser, T. D., Lynch, D. H., Gaiero, J., Khosla, K., and Dunfield, K. E. (2017). Quantification of bacterial non-specific acid (*phoC*) and alkaline (*phoD*) phosphatase genes in bulk and rhizosphere soil from organically managed soybean fields. *Appl. Soil Ecol.* 111, 48–56. doi: 10.1016/j.apsoil.2016.11.013

Gielen, B., and Ceulemans, R. (2001). The likely impact of rising atmospheric CO_2 on natural and managed *Populus*: a literature review. *Environ. Pollut.* 115, 335–358. doi: 10.1016/S0269-7491(01)00226-3

Gong, J. R., Ge, Z. W., An, R., Duan, Q. W., You, X., and Huang, Y. M. (2012). Soil respiration in poplar plantations in northern China at different forest ages. *Plant Soil* 360, 109–122. doi: 10.1007/s11104-011-1121-3

Han, S., and Wang, A. (2023). Belowground bacterial communities and carbon components contribute to soil respiration in a subtropical forest. *Plant Soil* 501, 125–137. doi: 10.1007/s11104-023-06257-3

He, Z. B., Chen, L. F., Du, J., Zhu, X., Lin, P. F., Li, J., et al. (2018). Responses of soil organic carbon, soil respiration, and associated soil properties to long-term thinning in a semiarid spruce plantation in northwestern China. *Land Degrad. Dev.* 29, 4387–4396. doi: 10.1002/ldr.3196

Huang, N., Wang, L., Song, X. P., Black, T. A., Jassal, R. S., Myneni, R. B., et al. (2020). Spatial and temporal variations in global soil respiration and their relationships with climate and land cover. *Sci. Adv.* 6:eabb8508. doi: 10.1126/sciadv.abb8508

Krause, S. M. B., Johnson, T., Karunaratne, Y. S., Fu, Y. F., Beck, D. A. C., Chistoserdova, L., et al. (2017). Lanthanide-dependent cross-feeding of methane-derived carbon is linked by microbial community interactions. *Proc. Natl. Acad. Sci. U.S.A.* 114, 358–363. doi: 10.1073/pnas.1619871114

Lefroy, R. D. B., Blair, G. J., and Strong, W. M. (1993). Changes in soil organic matter with cropping as measured by organic carbon fractions and ^{13}C natural isotope abundance. *Plant Soil* 155-156, 399–402. doi: 10.1007/BF00025067

Li, H., Yang, S., Semenov, M. V., Yao, F., Ye, J., Bu, R. C., et al. (2021). Temperature sensitivity of SOM decomposition is linked with a K-selected microbial community. *Glob. Change Biol.* 27, 2763–2779. doi: 10.1111/gcb.15593

Liu, Y. R., Delgado-Baquerizo, M., Wang, J. T., Hu, H. W., Yang, Z. M., and He, J. Z. (2018a). New insights into the role of microbial community composition in driving soil respiration rates. *Soil Biol. Biochem.* 118, 35–41. doi: 10.1016/j.soilbio.2017.12.003

Liu, Y. R., Delgado-Baquerizo, M., Yang, Z. M., Feng, J., Zhu, J., and Huang, Q. Y. (2020b). Microbial taxonomic and functional attributes consistently predict soil CO_2 emissions across contrasting croplands. *Sci. Total Environ.* 702:134885. doi: 10.1016/j.scitotenv.2019.134885

Liu, S. E., Wang, H., Tian, P., Yao, X., Sun, H., Wang, Q. K., et al. (2020). Decoupled diversity patterns in bacteria and fungi across continental forest ecosystems. *Soil Biol. Biochem.* 144:107763. doi: 10.1016/j.soilbio.2020.107763

Liu, M. H., Wei, Y. Q., Lian, L., Wei, B., Bi, Y. X., Liu, N., et al. (2023). Macrofungi promote SOC decomposition and weaken sequestration by modulating soil microbial function in temperate steppe. *Sci. Total Environ.* 899:165556. doi: 10.1016/j.scitotenv.2023.165556

Liu, X. P., Zhang, W. J., Cao, J. S., Shen, H. T., Zeng, X. H., Yu, Z. Q., et al. (2013). Carbon storages in plantation ecosystems in sand source areas of North Beijing, China. *Plos One.* 8:11. doi: 10.1371/journal.pone.0082208

Louca, S., Parfrey, L. W., and Doebeli, M. (2016). Decoupling function and taxonomy in the global ocean microbiome. *Science* 353, 1272–1277. doi: 10.1126/science.aaf4507

Lu, F., Hu, H. F., Sun, W. J., Zhu, J. J., Liu, G. B., Zhou, W. M., et al. (2018). Effects of national ecological restoration projects on carbon sequestration in China from 2001 to 2010. *Proc. Natl. Acad. Sci. U.S.A.* 115, 4039–4044. doi: 10.1073/pnas.1700294115

Lupwayi, N. Z., Larney, F. J., Blackshaw, R. E., Kanashiro, D. A., and Pearson, D. C. (2017). Phospholipid fatty acid biomarkers show positive soil microbial community responses to conservation soil management of irrigated crop rotations. *Soil Tillage Res.* 168, 1–10. doi: 10.1016/j.still.2016.12.003

Ma, X. L., Jiang, S. J., Zhang, Z. Q., Wang, H., Song, C., and He, J. S. (2023). Long-term collar deployment leads to bias in soil respiration measurements. *Methods Ecol. Evol.* 14, 981–990. doi: 10.1111/2041-210x.14056

Ma, Y. C., Piao, S. L., Sun, Z. Z., Lin, X., Wang, T., Yue, C., et al. (2014). Stand ages regulate the response of soil respiration to temperature in a *Larix principis-rupprechtii* plantation. *Agric. For. Meteorol.* 184, 179–187. doi: 10.1016/j.agrformet.2013.10.008

Malik, A. A., Martiny, J. B. H., Brodie, E. L., Martiny, A. C., Treseder, K. K., and Allison, S. D. (2020). Defining trait-based microbial strategies with consequences for soil carbon cycling under climate change. *ISME J.* 14, 1–9. doi: 10.1038/s41396-019-0510-0

Marques, J. M., da Silva, T. F., Vollu, R. E., Blank, A. F., Ding, G. C., Seldin, L., et al. (2014). Plant age and genotype affect the bacterial community composition in the tuber rhizosphere of field-grown sweet potato plants. *FEMS Microbiol. Ecol.* 88, 424–435. doi: 10.1111/1574-6941.12313

Masson-Delmotte, V., Zhai, P., Pirani, S., Connors, C., Pean, S., Berger, N., et al. (2021). "IPCC, 2021: summary for policymakers" in The physical science basis. Contribution of Working Group I to the Sixth Assessment Report of the Intergovernmental Panel on Climate Change (Cambridge: Cambridge University Press).

McCarthy, D. R., and Brown, K. J. (2006). Soil respiration responses to topography, canopy cover, and prescribed burning in an oak-hickory forest in southeastern Ohio. *For. Ecol. Manag.* 237, 94–102. doi: 10.1016/j.foreco.2006.09.030

National Forestry and Grassland Administration. (2019). China forest resources assessment. China Forest Resources Report: 2014-2018. China Forestry Publishing House.

Nguyen, N. H., Song, Z. W., Bates, S. T., Branco, S., Tedersoo, L., Menke, J., et al. (2016). FUNGuild: an open annotation tool for parsing fungal community datasets by ecological guild. *Fungal Ecol.* 20, 241–248. doi: 10.1016/j.funeco.2015.06.006

Nottingham, A. T., Meir, P., Velasquez, E., and Turner, B. L. (2020). Soil carbon loss by experimental warming in a tropical forest. *Nature* 584, 234–237. doi: 10.1038/s41586-020-2566-4

Nottingham, A. T., Scott, J. J., Saltonstall, K., Broders, K., Montero-Sanchez, M., Puspok, J., et al. (2022). Microbial diversity declines in warmed tropical soil and respiration rise exceed predictions as communities adapt. *Nat. Microbiol.* 7, 1650–1660. doi: 10.1038/s41564-022-01200-1

Pan, Y. D., Birdsey, R. A., Fang, J. Y., Houghton, R., Kauppi, P. E., Kurz, W. A., et al. (2011). A large and persistent carbon sink in the world's forests. *Science* 333, 988–993. doi: 10.1126/science.1201609

Paungfoo-Lonhienne, C., Yeoh, Y. K., Kasinadhuni, N. R. P., Lonhienne, T. G. A., Robinson, N., Hugenholtz, P., et al. (2015). Nitrogen fertilizer dose alters fungal communities in sugarcane soil and rhizosphere. *Sci. Rep.* 5:8678. doi: 10.1038/srep08678

Pilipovic, A., Headlee, W. L., Zalesny, R. S. Jr., Pekec, S., and Bauer, E. O. (2022). Water use efficiency of poplars grown for biomass production in the Midwestern United States. *Glob. Change Biol. Bioenergy.* 14, 287–306. doi: 10.1111/gcbb.12887

Powers, M., Kolka, R., Bradford, J., Palik, B., and Jurgensen, M. (2018). Forest floor and mineral soil respiration rates in a northern Minnesota red pine chronosequence. *Forests* 9:15. doi: 10.3390/f9010016

Raich, J. W., and Potter, C. S. (1995). Global patterns of carbon dioxide emissions from soils. *Glob. Biogeochem. Cycles* 9, 23–36. doi: 10.1029/94GB02723

Reay, D., Sabine, C., Smith, P., and Hymus, G. (2007). Spring-time for sinks. *Nature* 446, 727–728. doi: 10.1038/446727a

Rodríguez-Soalleiro, R., Eimil-Fraga, C., Gomez-Garcia, E., Garcia-Villabrille, J. D., Rojo-Alboreca, A., Munoz, F., et al. (2018). Exploring the factors affecting carbon and nutrient concentrations in tree biomass components in natural forests, forest plantations and short rotation forestry. *For. Ecosyst.* 5:35. doi: 10.1186/s40663-018-0154-y

Sanchez, G., Trinchera, L., Sanchez, M. G., and FactoMineR, S. (2013). Package 'plspm'. State College, PA: Citeseer.

Saurette, D. D., Chang, S. X., and Thomas, B. R. (2008). Autotrophic and heterotrophic respiration rates across a chronosequence of hybrid poplar plantationsin northern Alberta. *Can. J. Soil Sci.* 88, 261–272. doi: 10.4141/CJSS07005

Siles, J. A., and Margesin, R. (2016). Abundance and diversity of bacterial, archaeal, and fungal communities along an altitudinal gradient in alpine forest soils: what are the driving factors? *Microb. Ecol.* 72, 207–220. doi: 10.1007/s00248-016-0748-2

Sun, S., Li, S., Avera, B. N., Strahm, B. D., and Badgley, B. D. (2017). Soil bacterial and fungal communities show distinct recovery patterns during forest ecosystem restoration. *Appl. Environ. Microbiol.* 83:e00966. doi: 10.1128/AEM.00966-17

Tang, J. W., Bolstad, P. V., and Martin, J. G. (2009). Soil carbon fluxes and stocks in a Great Lakes forest chronosequence. *Glob. Change Biol.* 15, 145–155. doi: 10.1111/j.1365-2486.2008.01741.x

Tedeschi, V., Rey, A., Manca, G., Valentini, R., Jarvis, P. G., Borghetti, M., et al. (2006). Soil respiration in a Mediterranean oak forest at different developmental stages after coppicing. *Glob. Change Biol.* 12, 110–121. doi: 10.1111/j.1365-2486.2005.01081.x

Teuber, M., Zimmer, I., Kreuzwiese, J., Ache, P., Polle, A., Rennenberg, H., et al. (2007). VOC emissions of Grey poplar leaves as affected by salt stress and different N sources. *Plant Biology* 10, 86–96. doi: 10.1111/j.1438-8677.2007.00015.x

Tu, L. H., Hu, T. X., Zhang, J., Li, X. W., Hu, H. L., Liu, L., et al. (2013). Nitrogen addition stimulates different components of soil respiration in a subtropical bamboo ecosystem. *Soil Biol. Biochem.* 58, 255–264. doi: 10.1016/j.soilbio.2012.12.005

Vitali, F., Mastromei, G., Senatore, G., Caroppo, C., and Casalone, E. (2016). Long lasting effects of the conversion from natural forest to poplar plantation on soil microbial communities. *Microbiol. Res.* 182, 89–98. doi: 10.1016/j.micres.2015.10.002

Wang, H. H., Huang, W. D., He, Y. Z., and Zhu, Y. Z. (2023). Effects of warming and precipitation reduction on soil respiration in Horqin sandy grassland, northern China. *Catena* 233:107470. doi: 10.1016/j.Catena.2023.107470

Wang, R., Sun, Q. Q., Wang, Y., Liu, Q. F., Du, L. L., Zhao, M., et al. (2017). Temperature sensitivity of soil respiration: synthetic effects of nitrogen and phosphorus fertilization on Chinese Loess Plateau. *Sci. Total Environ.* 574, 1665–1673. doi: 10.1016/j.scitotenv.2016.09.001

Wang, Q., Sun, Q. W., Wang, W. Z., Liu, X. R., Song, L. G., and Hou, L. Y. (2022). Effects of different native plants on soil remediation and microbial diversity in Jiulong Iron Tailings Area, Jiangxi. *Forests* 13:1106. doi: 10.3390/f13071106

Wang, C. Q., Xue, L., Dong, Y. H., Wei, Y. H., and Jiao, R. J. (2018). Unravelling the functional diversity of the soil microbial community of Chinese fir plantations of different densities. *Forests* 9:532. doi: 10.3390/f9090532

Wang, X. X., Zhang, W., Liu, Y., Jia, Z. J., Li, H., Yang, Y. F., et al. (2021). Identification of microbial strategies for labile substrate utilization at phylogenetic classification using a microcosm approach. *Soil Biol. Biochem.* 153:107970. doi: 10.1016/j.soilbio.2020.107970

Wiseman, P. E., and Seiler, J. R. (2004). Soil CO_2 efflux across four age classes of plantation loblolly pine *Pinus taeda* L. on the Virginia Piedmont. *For. Ecol. Manag.* 192, 297–311. doi: 10.1016/j.foreco.2004.01.017

Wu, N., Li, Z., Meng, S., and Wu, F. (2021). Soil properties and microbial community in the rhizosphere of *Populus alba var. pyramidalis* along a chronosequence. *Microbiol. Res.* 250:126812. doi: 10.1016/j.micres.2021.126812

Wu, X., Xu, H., Tuo, D. F., Wang, C., Fu, B. J., Lv, Y. H., et al. (2020). Land use change and stand age regulate soil respiration by influencing soil substrate supply and microbial community. *Geoderma* 359:113991. doi: 10.1016/j.geoderma.2019.113991

Xiao, W. F., Ge, X. G., Zeng, L. X., Huang, Z. L., Lei, J. P., Zhou, B. Z., et al. (2014). Rates of litter decomposition and soil respiration in relation to soil temperature and water in different-aged *Pinus massoniana* forests in the three gorges reservoir area, China. *Plos One.* 9:e101890. doi: 10.1371/journal.pone.0101890

Yan, B. S., Sun, L. P., Li, J. J., Liang, C. Q., Wei, F. R., Xue, S., et al. (2020). Change in composition and potential functional genes of soil bacterial and fungal communities with secondary succession in *Quercus liaotungensis* forests of the Loess Plateau, western China. *Geoderma* 364:114199. doi: 10.1016/j.geoderma.2020.114199

Yan, M., Zhang, X., Zhou, G., Gong, J., and You, X. (2011). Temporal and spatial variation in soil respiration of poplar plantations at different developmental stages in Xinjiang, China. *J. Arid Environ*. 75, 51–57. doi: 10.1016/j.jaridenv.2010.09.005

Yang, Q., Lei, A. P., Li, F. L., Liu, L. N., Zan, Q. J., Shin, P. K. S., et al. (2014). Structure and function of soil microbial community in artificially planted *Sonneratia apetala* and *S. Caseolaris* forests at different stand ages in Shenzhen Bay, China. *Mar. Pollut. Bull.* 85, 754–763. doi: 10.1016/j.marpolbul.2014.02.024

Yang, S., Wu, H., Wang, Z. R., Semenov, M. V., Ye, J., Yin, L. M., et al. (2022). Linkages between the temperature sensitivity of soil respiration and microbial life strategy are dependent on sampling season. *Soil Biol. Biochem.* 172:108758. doi: 10.1016/j.soilbio.2022.108758

Yu, K. Y., Yao, X., Deng, Y. B., Lai, Z. J., Lin, L. C., and Liu, J. (2019). Effects of stand age on soil respiration in *Pinus massoniana* plantations in the hilly red soil region of southern China. *Catena* 178, 313–321. doi: 10.1016/j.catena.2019.03.038

Zeng, X. M., Feng, J., Chen, J., Delgado-Baquerizo, M., Zhang, Q. G., Zhou, X. Q., et al. (2022). Microbial assemblies associated with temperature sensitivity of soil respiration along an altitudinal gradient. *Sci. Total Environ.* 820:153257. doi: 10.1016/j.scitotenv.2022.153257

Zhang, F. G., and Zhang, Q. G. (2016). Microbial diversity limits soil heterotrophic respiration and mitigates the respiration response to moisture increase. *Soil Biol. Biochem.* 98, 180–185. doi: 10.1016/j.soilbio.2016.04.017

Zhao, X., Li, F. D., Zhang, W. J., Ai, Z. P., Shen, H. T., Liu, X. P., et al. (2016). Soil respiration at different stand ages (5, 10, and 20/30 years) in coniferous (*Pinus tabulaeformis* Carriere) and deciduous (*Populus davidiana* Dode) plantations in a sandstorm source area. *Forests* 7:15. doi: 10.3390/f7080153

Zhao, F. Z., Ren, C. J., Zhang, L., Han, X. H., Yang, G. H., and Wang, J. (2018). Changes in soil microbial community are linked to soil carbon fractions after afforestation. *Eur. J. Soil Sci.* 69, 370–379. doi: 10.1111/ejss.12525

frontiers | Frontiers in Microbiology

TYPE Original Research
PUBLISHED 21 February 2025
DOI 10.3389/fmicb.2024.1462941

OPEN ACCESS

EDITED BY
Peng Shi,
Xi'an University of Technology, China

REVIEWED BY
Tatiana A. Vishnivetskaya,
The University of Tennessee, Knoxville, United States
David E. Graham,
Oak Ridge National Laboratory (DOE), United States

*CORRESPONDENCE
Chuck R. Smallwood
✉ crsmall@sandia.gov

RECEIVED 10 July 2024
ACCEPTED 12 December 2024
PUBLISHED 21 February 2025

CITATION
Smallwood CR, Hasson N, Yang J, Schambach J, Bennett H, Ricken B, Sammon J, Mascarenas M, Eberling N, Kolker S, Whiting J, Mays WD, Anthony KW and Miller PR (2025) Bioindicator "fingerprints" of methane-emitting thermokarst features in Alaskan soils. *Front. Microbiol.* 15:1462941. doi: 10.3389/fmicb.2024.1462941

Bioindicator "fingerprints" of methane-emitting thermokarst features in Alaskan soils

Chuck R. Smallwood[1]*, Nicholas Hasson[2], Jihoon Yang[3], Jenna Schambach[1], Haley Bennett[1], Bryce Ricken[1], Jason Sammon[4], Monica Mascarenas[1], Naomi Eberling[1], Stephanie Kolker[1], Joshua Whiting[4], Wittney D. Mays[5], Katey Walter Anthony[2] and Philip R. Miller[4]

[1]Department of Environmental Systems Biology, Sandia National Laboratories, Albuquerque, NM, United States, [2]Water and Environmental Research Center, University of Alaska Fairbanks, Fairbanks, AK, United States, [3]Bioresource & Environmental Security, Sandia National Laboratories, Livermore, CA, United States, [4]Biological & Chemical Sensors, Sandia National Laboratories, Albuquerque, NM, United States, [5]Systems Biology, Sandia National Laboratories, Livermore, CA, United States

Permafrost thaw increases the bioavailability of ancient organic matter, facilitating microbial metabolism of volatile organic compounds (VOCs), carbon dioxide, and methane (CH_4). The formation of thermokarst (thaw) lakes in icy, organic-rich Yedoma permafrost leads to high CH_4 emissions, and subsurface microbes that have the potential to be biogeochemical drivers of organic carbon turnover in these systems. However, to better characterize and quantify rates of permafrost changes, methods that further clarify the relationship between subsurface biogeochemical processes and microbial dynamics are needed. In this study, we investigated four sites (two well-drained thermokarst mounds, a drained thermokarst lake, and the terrestrial margin of a recently formed thermokarst lake) to determine whether biogenic VOCs (1) can be effectively collected during winter, and (2) whether winter sampling provides more biologically significant VOCs correlated with subsurface microbial metabolic potential. During the cold season (March 2023), we drilled boreholes at the four sites and collected cores to simultaneously characterize microbial populations and captured VOCs. VOC analysis of these sites revealed "fingerprints" that were distinct and unique to each site. Total VOCs from the boreholes included > 400 unique VOC features, including > 40 potentially biogenic VOCs related to microbial metabolism. Subsurface microbial community composition was distinct across sites; for example, methanogenic archaea were far more abundant at the thermokarst site characterized by high annual CH_4 emissions. The results obtained from this method strongly suggest that ~10% of VOCs are potentially biogenic, and that biogenic VOCs can be mapped to subsurface microbial metabolisms. By better revealing the relationship between subsurface biogeochemical processes and microbial dynamics, this work advances our ability to monitor and predict subsurface carbon turnover in Arctic soils.

KEYWORDS

volatile organic compounds, permafrost thaw, methanogens, methanotrophs, methane emissions, anaerobic degradation, carbon sequestration, greenhouse gases

Background

Permafrost soils, like those in interior Alaska, contain the largest terrestrial pool of temperature soil organic carbon stocks on the planet; they cover ~15% of the global land area but account for ~60% of global soil carbon storage (Schuur et al., 2015). Unfortunately, increasing duration of permafrost thaw seasons (Jorgenson et al., 2010; Smith et al., 2010), perpetuates a positive feedback loop in which gradual or abrupt thaw events cause the active (seasonally frozen) soil layer to deepen and the size of talik sites (unfrozen ground in the permafrost area) to expand (Liljedahl et al., 2016; Kokelj et al., 2017; Farquharson et al., 2022), triggering increased carbon flux, and hydrological flow (Farquharson et al., 2022). The most widespread form of abrupt thaw is the thermokarst (land surface collapse caused by the loss of ice-rich permafrost), which commonly results in the creation of ponds or lakes. In recent decades, the number of thermokarst lakes in interior Alaska has grown by ~40% (Walter Anthony et al., 2021), which is particularly concerning because these newly formed thermokarst lakes are derived mainly from the thaw of Yedoma (methane-rich, Pleistocene-aged permafrost), resulting in the highest recorded CH_4 emissions from Arctic lakes (Walter Anthony et al., 2016).

Recently, high-C flux has been observed in the Arctic, but while some ecosystem models suggest that terrestrial permafrost is currently a net CO_2 sink (range 0–0.8 Pg C-CO_2e yr^{-1}) (Walter Anthony et al., 2018), results from Arctic soil incubation studies in the laboratory suggest that permafrost soils have intrinsically short C turnover times and may switch to become a net C source in the near future, with a potential loss of 0.22–0.53 petagrams of C annually through the end of this century (Ren et al., 2024). To date, permafrost C feedback (PCF) modeling has focused on gradual, near-surface processes of C transformation in degraded permafrost (Schaefer et al., 2014; Walter Anthony et al., 2018), and these models predict that large proportions of permafrost C in Alaska are vulnerable to abrupt thaw events, on timescales of months to years (Olefeldt et al., 2016). However, our inability to consistently monitor subsurface biogeochemical cycles in the field has obscured the fine-scale biogeochemical processes that underlie thaw events (gradual or abrupt), which occur on timescales of hours to days (Turetsky et al., 2019). This gap in the experimental data significantly limits the accuracy of current PCF system models, resulting in high magnitudes of uncertainty associated with permafrost thaw (Bradford et al., 2016) and hindering our ability to predict increases in thaw depth caused by abrupt thaw events that seasonal freeze cannot overcome (Turetsky et al., 2020). To enable a detailed characterization of subsurface biogeochemical processes and constrain the uncertainty in PCF models, we urgently need more experimental data (Tao et al., 2024).

To effectively account for permafrost ecosystems, our analysis this data must effectively differentiate abiotic and biogeochemical processes, particularly because the microbes that drive biogeochemical processes often operate on shorter timescales than abiotic processes (Zolkos and Tank, 2020; Waldrop et al., 2023). Laboratory and small-scale field experiments have demonstrated that microbes respond rapidly to thaw (Mackelprang et al., 2011) and that distinct microbial species are present in frozen versus thawing permafrost (Mackelprang et al., 2011; Monteux et al., 2018; Ji et al., 2020). Although soil cores are often required to characterize microbial activity in the subsurface, the direct extraction of permafrost soil samples is destructive to fragile ecosystems. The release of unique microbial metabolites has been detected during thaw into lakes and streams, which could provide non-destructive measurements of microbial processes (Vonk et al., 2015). Moreover, volatile organic compounds (VOCs) such as methane (CH_4) can be emitted from thawing soils (PeÑUelas et al., 2014; Schulz-Bohm et al., 2017).

Biogenic VOCs are generated by microbes (e.g., bacteria, archaea, and fungi) and range from small- (< C15) to medium- (C16–C28) chain molecules with low molecular masses (< 300 Da), high vapor pressure, and a low boiling point (Schulz-Bohm et al., 2017; Franchina et al., 2019). These molecules are typically in the gas phase but may also occur dissolved in liquid phase until environmental conditions favor evaporation. VOCs are normally lipophilic compounds capable of diffusing through water and gas-filled pores in soil environments (Effmert et al., 2012; Schmidt et al., 2016; Schulz-Bohm et al., 2017). Unlike dissolved metabolites, which are often involved in short distance (< 12 cm) infochemical biological interactions, VOCs can travel and act on other biosystems even at long distances (> 2 m) (Tyc et al., 2017; Westhoff et al., 2017; Schulz-Bohm et al., 2018). An estimated 2,000 VOCs attributed to about 1,000 microbial hosts have already been identified, and more identifications are occurring daily (Lemfack et al., 2018). VOCs can be measured from soils over time to elucidate subsurface biogeochemical processes for incorporation into process-based models to predict early warning signs of thaw (Kramshøj et al., 2019; Ghirardo et al., 2020; Li B. et al., 2021).

In this study, we sought to determine whether biogenic VOCs (1) can be effectively captured in arctic environments during winter, and (2) if this approach provides more biologically relevant chemical signatures that correlate to subsurface microbial metabolic potential during winter in perennially thawed taliks. Guided by electrical resistivity (ER) maps of subsurface taliks, we sought to validate these measurements and characterize microbiomes and VOCs related to these CH_4-emitting taliks. Focused on four upland thermokarst sites characterized by wintertime CH_4-emitting taliks in interior Alaska, we quantified microbial communities using short-read sequencing metagenomics and measured corresponding borehole VOCs as a means of detecting subsurface biochemical processes.

Because the boundaries of thermokarst lakes are areas where positive feedback between permafrost thaw and atmospheric warming can be actively measured (Bradford et al., 2016; in 't Zandt et al., 2020), we took four core samples from three Yedoma-taliks north of Fairbanks, Alaska. Permafrost soil microbiomes have been shown to be dramatically different during winter, with high methanogen abundance as well as metabolic processes related to degradation of soil organic matter (Mackelprang et al., 2011; Vigneron et al., 2019), so we collected our samples in March 2023. Typically, metagenomes are used to identify microbes and genes related to carbon degradation pathways (Fierer et al., 2012). However, recent advancements in VOC collection and analysis have enabled characterization of volatile metabolite emissions from microbiomes (volatilome) (Meredith and Tfaily, 2022; Jiao et al., 2023). Thus, volatilomics can provide a means to investigate the chemical conversation between subsurface microbes in real-time and resolve the metabolic frontier of

unresolved pathways. We surmised that corresponding VOCs from these distinct talik sites could provide realistic bioindicators of subsurface biogeochemical processes related to permafrost degradation.

Materials and methods

Geophysical surveys of drilling locations, methane flux measurements, and soil cores collection

For our preliminary geophysical surveys, we employed a multi-frequency EM system (GSM-19WV, Gem Systems Inc., Ontario, Canada, 2019) based on EM induction amplitudes corresponding to electrical resistivity (Ohm-m) at angular frequencies (ω) using the controlled-source very-long-frequency-magnetotelluric (VLF-MT) bands (McNeill and Labson, 1991; Elder et al., 2021). Leveraging ER data acquired from the VLF signals emitted from US Navy transmitters (16.8–24.8 kHz), we conducted magnetotelluric analysis (Sasaki, 1989); to enhance the precision of the geophysical mapping, we employed the VLF2dmf.v2 tool (Monteiro Santos et al., 2006) and Occam's technique for 2D modeling (Constable et al., 1987). The resulting 2D-inversion models show cross-sections of permafrost for the BTL, NSY, and SKP sites (Figure 1). Following established methods (Elder et al., 2021), we measured linear methane fluxes with a portable 20 L chamber placed over each borehole. Air was briefly (120–150 s) recirculated through the chamber and a Los Gatos Research Micro-Portable Greenhouse Gas Analyzer (MGGA) (ABB Inc., Quebec City, CA) was used to measure CH_4 concentration, with a measurement frequency of 10 Hz. Diffusive fluxes were calculated from the ideal gas law using chamber volume, temperature, atmospheric pressure; a least square fit regression was applied with a minimum R^2 value of 0.95 (Elder et al., 2021). At BTL, methane fluxes were collected at four sites transecting the lake (A1, A2, A3, and A4) and at the nearby Eddy-covariance tower (A0) (Figure 1; Supplementary Figure S1).

We began by collecting four soil cores from three thermokarst systems (two well-drained thermokarst-mounds, a drained thermokarst lake, and the terrestrial margin of a recently formed thermokarst lake) (Figure 2) around Big Trail Lake (BTL), a thermokarst lake located in Goldstream valley that was formed between 1949 and 1967 (in 't Zandt et al., 2020; Pellerin et al., 2022). The samples were taken from four Yedoma-talik sites: two on the south side of BTL boundary (BTL1, closer to the terrestrial margin; and BTL2, closer to the lake); one at North Star Yedoma (NSY), a well-drained terrestrial hillslope characterized by thermokarst mounds; and one site at Skidmore Pond (SKP), a recently drained (2022) thermokarst pond in hillslope Yedoma near the well-studied Vault Creek Permafrost Tunnel (Schirrmeister et al., 2016; Heslop et al., 2020; Figure 1). Although BTL occupies only < 0.01% of the known permafrost land area it contains widespread sub-aerial taliks situated over Yedoma permafrost, which is estimated to emit between 0.1–5.2 tetragrams of CH_4 per year, roughly 4% of the entire pan-Arctic wetland budget (Elder et al., 2021).

Using a Talon Coring system (Quantum Machine Works, Whitehorse, Canada) we drilled cores during the winter, when the top ~1.2 meters of soil was frozen solid. On consecutive days, we drilled on the south boundary of the lake at site BTL1 (A2), then BTL2 (A1), NSY (B1), and SKP (C1) (Figure 1). The depth of each borehole (including depth of the active layer and transition zone) and depth profile are given in Supplementary File S1. We sought to obtain cores at least 5 m long at all talik sites; at the NSY site we were able to reach the permafrost layer ~6.8 m. After drilling, each core was extracted in half-meter increments, subsampled for plugs, and capped in ABS (acrylonitrile butadiene styrene) pipes obtained from a local hardware supplier. Active layer core increments (frozen solid in the ground) were stored frozen until analysis; cores collected from below the active layer (not fully frozen in the ground) were unfrozen when harvested and stored at 4°C. To enable sub-sampling, frozen core increments were allowed to briefly thaw at room temperature to soften the soil; all subsampled plugs were then stored in air-tight conical tubes and frozen for later microbial and chemical analysis.

Subsampling soil cores

Sampling equipment was sterilized using 10% bleach/70% ethanol or autoclaved prior to sub-sampling. For metagenomic analysis of microbial populations in the insulated layer below the frozen active layer, plugs were extracted from BTL1, BTL2, SKP, and NSY at 1.5 m depth. Each plug was sampled and sectioned with sterile 5 mL syringes (with the syringe tips excised), then each syringe was used to push a plug into separate 15 mL centrifuge tubes for each depth. Once all plugs are extracted from the core increments, the outer portion of the core increment is discarded, and the inner portion of the core is saved. This sub-sampling approach reduces contamination of the inner core with the outer core microbial fraction. In some cases, soil subsampling was done in an anaerobic chamber to prevent anerobic microbes from exposure to oxygen and other general contaminants. Soil samples were sent to Zymo Research for DNA extraction, V3-V4 16S rRNA gene sequencing, shotgun metagenomics sequencing, and data analysis (Caporaso et al., 2010; Segata et al., 2011; Callahan et al., 2016).

Elemental chemical analysis

Core samples were sent for elemental chemical analysis at ALS Global (Tucson, Arizona) to measure the percent weight of ash, carbon, hydrogen, nitrogen, and sulfur at various depths for each borehole site core (Supplementary Table S1). Prior to chemical analysis, each soil sample was dried at 60°C. Oxygen was measured using a combustion technique to pyrolyze the sample in an inert atmosphere (helium). Pyrolysis of the soils produces nitrogen, hydrogen, and carbon monoxide when they interact with a nickel-plated carbon catalyst at 1,060°C. These products were separated via a chromatographic column, and the carbon monoxide was analyzed in a thermal conductivity analyzer, providing the oxygen percentage.

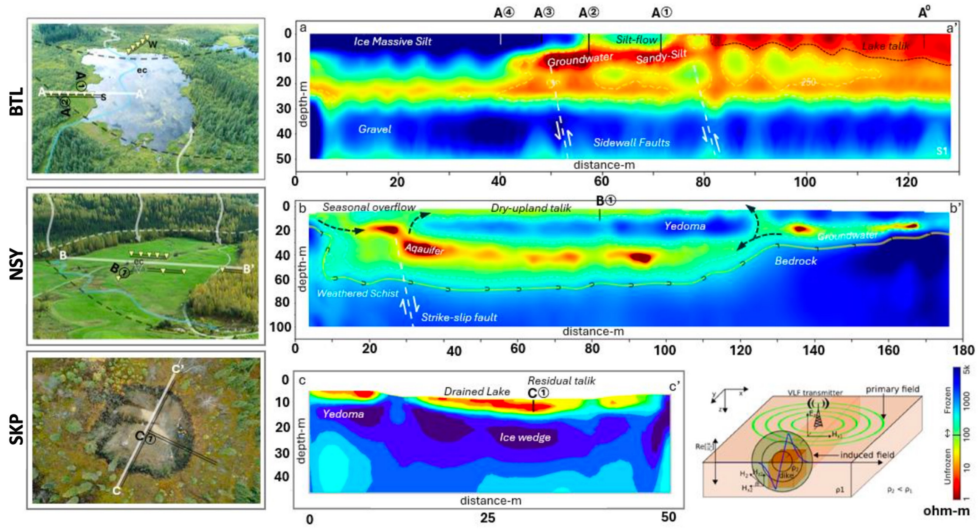

FIGURE 1
Geophysical resistivity surveys were conducted using very long frequency-magnetotelluric (VLF-MT) to generate 2D-inversion models showing cross-sections of thermokarst (TK) at Big Trail Lake (BTL) in a lowland valley, NorthStar Yedoma (NSY) on a well-drained hillslope, and Skidmore Pond SKP, now a shallow thermokarst pond. An overhead view of each site was paired with 2D-inversion models show the presence or absence of permafrost, and the color-contour plots indicates cold frozen permafrost (blue) and unfrozen features (yellow to red) conditions. The 2-D electrical resistivity (ER) profiles, supported by borehole data across transects (A-A', B-B', C-C'), indicate permafrost presence with < 100 ohm-m reflecting thawed conditions or talik. The darkest red (< 1 ohm-m) marks groundwater within talik or fault fractures. Color contours show permafrost (5,000–600 ohm-m) and thawed or water-saturated sediments (100–1 ohm-m). The BTL model shows south (A) and north (A') transecting line indicating flux site measurements (A1, A2, A3, and A4) as well as the nearby Eddy-covariance tower (A0). The NSY model shows the east (B) and west (B') transect indicating core site B1 sampled at NSY The SKP model shows the north (C) and south (C') transect indicating core site C1 sampled at SKP.

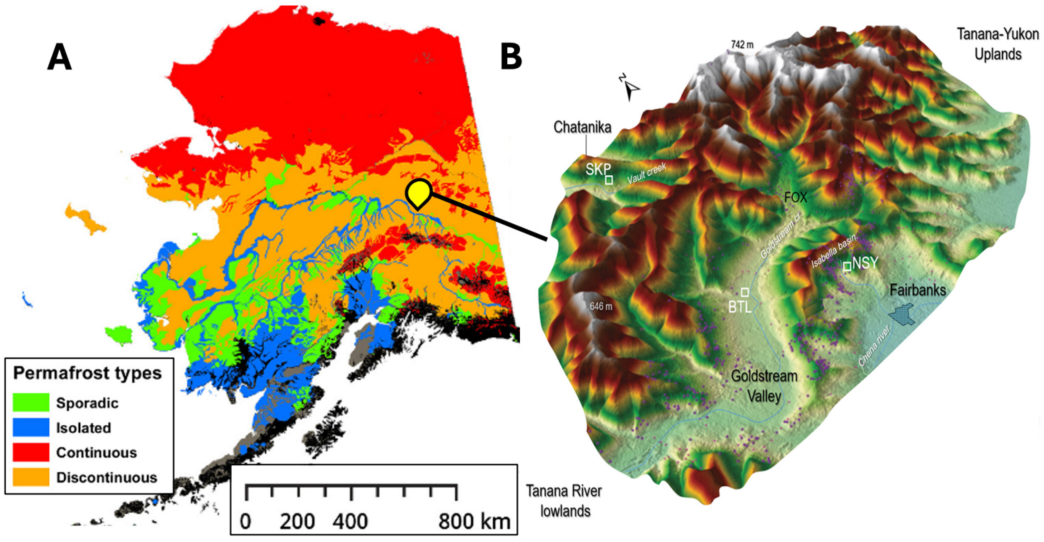

FIGURE 2
Estimates of permafrost gradients across central Alaska were adapted from Mishra and Riley (2012) showing sporadic (green), isolated (blue), continuous (red), and discontinuous (orange) permafrost generalized across Alaska **(A)**. Central Alaska Goldstream Valley area where the thermokarst sites Big Trail Lake (BTL), NorthStar Yedoma (NSY), and Skidmore Pond (SKP) sites featured in this study represent three unique watersheds near Fairbanks Alaska **(B)**.

16S rRNA sequencing and analysis of cores from various depths

For 16S rRNA sequencing, ZymoBIOMICS® -96 MagBead DNA Kit (Zymo Research, Irvine, CA) was used for DNA extraction. Positive controls included ZymoBIOMICS Microbial Community Standard (Zymo Research, Irvine, CA). For 16S rRNA sequencing, DNA libraries were prepared for using the Quick-16S Plus NGS Library Prep Kit (Zymo Research, Irvine, CA). ZymoBIOMIC 16S rRNA gene primers (forward CCTACGGGGNGGCWGCAG, reverse GACTACHVGGGTATCTAATCC) for V3–V4 regions

amplification of 16S rRNA genes. The sequencing library was prepared by PCR using real-time PCR thermocycler (QuantStudio 12K Flex, Applied Biosystems) to control cycles and limit PCR chimera formation. Quantification of final PCR products was performed using qPCR fluorescence readings before being pooled together at equal molarity. Pooled libraries were cleaned with DNA Clean & Concentrator kit (Zymo Research, Irvine, CA), and quantified with TapeStation (Agilent Technologies, Santa Clara, CA) and Invitrogen Qubit 1X dsDNA High-Sensitivity Assay Kits (Thermo Fisher Scientific, Waltham, WA). The final library was sequenced on Illumina NextSeq 2000 with a p1 (cat 20075294) reagent kit with 600 cycles. 16S amplicon sequencing was performed with 30% PhiX spike-in. Chimeric sequences were also removed with the Dada2 pipeline (Callahan et al., 2016). Taxonomy assignments were performed using Uclust from Qiime v.1.9.1 (Caporaso et al., 2010). Absolute abundance quantification was performed using qPCR conducted with a standard curve of plasmid DNA with one copy of the 16S gene region prepared in 10-fold serial dilutions (Supplementary Figure S2). Taxonomy was assigned with the Zymo 16S database (Supplementary Figure S3; Supplementary Table S2). Relative taxonomic composition was generated from samples that were sequenced to a 200M read target, and 1M reads were used in downstream processing.

Shotgun metagenomic library preparation and sequencing of soil core samples

Genomic DNA was extracted from each plug with ZymoBIOMICS® -96 MagBead DNA Kits (Zymo Research, Irvine, CA) and then subjected to shotgun metagenomic sequencing. Illumina® DNA Library Prep Kit (Illumina, San Diego, CA) with up to 500 ng DNA input following the manufacturer's protocol using unique dual-index 10 bp barcodes with Nextera® adapters (Illumina, San Diego, CA). All libraries were quantified with TapeStation® (Agilent Technologies, Santa Clara, CA) and then pooled to equal abundance. The final pool was quantified using qPCR. The final library was sequenced on an Illumina NovaSeq X (Illumina, San Diego, CA) with 2 × 150 kit (300 cycles). The metagenomic read processing summary more than 2M reads with > 75% reads surviving (Supplementary Table S4).

Metagenomic bioinformatics and microbial composition analysis

To remove low-quality features, raw sequence reads were trimmed with Trimmomatic-0.33 (Bolger et al., 2014). Quality trimming was conducted via sliding window with 6 bp window size and a quality cutoff of 20; reads with size lower than 70 bp were removed. BBduk (version 39.03) was used to filter the contaminants and adapter sequences from metagenomic raw reads (Singer et al., 2016). The artifact sequences were evaluated and trimmed off by kmer matching (k = 31). The trimmed reads were assembled using MEGAHIT (v 1.2.9) (Li et al., 2015) and the genes were called by Prodigal (v 2.6.2) (Li et al., 2015). The functional profiles were annotated by Eggnog Mapper (v2.1.12) on assembled reads to identify the presence of KOs (KEGG Orthology groups) (Cantalapiedra et al., 2021; Kanehisa et al., 2023). Taxonomy was profiled using Kraken2 (v2.1.3) against the NCBI database (Wood et al., 2019). The resulting taxonomy and abundance information were further analyzed via: (1) alpha- and beta-diversity analyses (Supplementary Figure S2); (2) microbial composition bar plots using QIIME (Caporaso et al., 2012); (3) abundance heatmaps with hierarchical clustering (based on Bray-Curtis dissimilarity); and (4) biomarker discovery with LEfSe (Segata et al., 2011) with default settings ($p > 0.05$ and LDA effect size > 2). Functional profiling was performed on assembled reads using Humann3 (Beghini et al., 2021), including the identification of UniRef gene family and MetaCyc metabolic pathways.

Gas collection and chemical desorption of VOCs from borehole sites

To capture VOC gasses in the field, we used a stainless-steel gas capture dome with a custom fitting for thermal desorption unit (TDU) tubes. For general VOCs, we used Tenax TA 60/80 from Camsco (Camsco, Houston, TX) placed in-line between a non-polar filter and a calibrated air SKC AirChek pump (SKC, Eighty Four, PA). The non-polar filter was attached between the capture device and the TDU tube to reduce water adsorption on the Tenax TDU. The pump was calibrated with using Mesa Labs 530 + DryCal calibrator (Mesa Labs Inc., Lakewood, Colorado). The capture dome was placed on the borehole immediately after the last core was extracted. At each borehole, 2 L of borehole gas was extracted over 5 min with a calibrated pump flow rate of 0.4 L/min. To provide technical replicates for analysis, triplicate TDU tubes were used to consecutively collect gas from each borehole site. The gas samples were stored at −20°C until 2D-GC-MS analysis.

2D-GC-MS instrumental parameters and standards

Samples were thermally desorbed using a Gerstel Thermal Desorption Unit 3.5 + (Gerstel GmbH, Mülheim, Germany) integrated into a gas chromatograph/mass spectrometer system and ramped at 60°C/min from 35°C to either 280°C for Tenax TA sorbent. Desorbed samples were refocused on a Gerstel CIS 4 Cryogenic Inlet, held at -50°C during desorption and ramped at 12°C/s to 300°C to inject the desorbed sample as a single bolus into the gas chromatograph/mass spectrometer system. Analysis of the samples was performed via a LECO Pegasus BT two-dimensional gas chromatograph coupled to a time-of-flight mass spectrometer (2D-GC-MS) (LECO Corp., Michigan, United States). Compound separation was conducted by two analytical gas chromatography columns, with the primary column a 15 m, 0.25 mm ID DB-WAX and secondary column a 2 m, 0.25 mm ID DB-1 (Both Agilent, California, United States), with film thickness of 0.5 μm for the primary column and 1 μm for the secondary column. The Gas Chromatograph analytical program had an initial temperature of 35°C, ramping at 10°C/min to a maximum of 230°C with a 5-minute hold. The secondary column was ramped at the same rate, but with a + 5°C offset from the primary column. Column flow was

set to 1 mL/min with an inlet flow split of 50:1. Thermal modulation between columns was set to 7 s with a hot pulse time of 2.10 s. Mass spectra were collected at a 200 spectra/s rate scanning from 20–500 m/z. A 30 kHz extraction frequency and a detector offset of -30 V were used.

Volatile compound composition and abundance analysis

Chemical identification by 2D-GC-MS detected 1,000 + different chemical features. Top-down quantitative analysis of metabolites in the hit lists was performed using the ChromaTOF TILE software (LECO Corp., St. Joseph, Michigan). TILE divides chromatographs into retention time windows "TILES" and filters these TILES based on the statistical significance (fisher ratio) for each mass identified for facile handling of complex data sets. The size of the TILE accommodates for retention time variation, which can plague other approaches for 2D gas chromatography analysis and is an industry proven tool. In practice, TILE provides the user a qualitative list of VOC chemical classification to search and compare amongst test conditions thus greatly reducing analysis time for "biomarker" hunting. TILEs are then traced to the online NIST23 library for chemical identification. TILE filtering parameters: Tile size D1 (modulations) = 3; Tile size D2 (spectra) = 44; S/N threshold = 50; Samples that must exceed S/N threshold = 2; Mass F-ratios to average = 1; Threshold type = p-value; p-value threshold = 0.05; Minimum masses per tile = 3; Minimum mass = 0; Maximum mass = 1,000; Masses to ignore: = blank.

Each individual VOC feature identified by TILES analysis was compared to the NIH PubChem database (accessed June 2024) to check for alternative chemical synonyms. From the > 400 TILES, each VOC feature was then manually compared to the KEGG database to identify related biochemical pathways, genes, and enzymes. We identified 41 unique VOCs that are potentially biogenic in origin and were unique to individual borehole sites in KEGG (Kanehisa et al., 2023), which are indicated in the Biological VOC table in Figure 1. Chemical names were from these data were aligned to a subset of VOCs abundance to gene-hit abundance of enzymes found in related metabolic pathways on KEGG (Figure 3). Triplicate samples were averaged with standard deviations (Supplementary Table S1).

For statistical analysis of VOCs compounds compared across borehole sites a one-way analysis of variance (ANOVA) was performed using GraphPad Prism 10.2.3 (GraphPad Software LLC, Boston, MA) on the triplicate VOC samples found in Supplementary File S3. We performed the ANOVA analysis using the triplicate VOC values obtained from each borehole, averaged them, and compared the variances to determine if the boreholes had significantly different expression of each VOC from Supplementary File S3. Our null hypothesis was that there was no statistical significance of VOC abundance between boreholes. (Supplementary Table S5). As part of our ANOVA summary in Supplementary Table S5 we included the Brown-Forsythe test and Bartlett's test. Brown–Forsythe test is a statistical test for the equality of group variances based on performing an Analysis of Variance (ANOVA) on a transformation of the response variable. Bartlett's test tests the hypothesis that our samples have equal variances.

Results

Profiling talik sites using geophysical surveys

To better compare corresponding microbial and VOCs signatures between talik sites, we needed to select the sites to provide contrasting examples of talik systems at various stages and magnitudes of thaw. To guide that selection, began by mapping the varying stages of permafrost thaw along hydrological gradients from uplands to lowlands, generating 2D-inversion models from geophysical resistivity surveys using very long frequency-magnetotelluric (VLF-MT) (Elder et al., 2021) for the BTL, NSY, and SKP sites (Figure 1).

Colored contour plots differentiate frozen and unfrozen subsurface features (e.g., aquifers, taliks), allowing us to identify two talik sites at BTL that were only 15 meters apart but exhibited different hydrological and CH_4-emitting properties. The BTL1 site (A2 in Figure 1) is in the terrace zone of the thermokarst; it was also more saturated than the BTL 2 site and exhibited elevated CH_4 emission in both the cold and grow season (Figure 1). In contrast, the BTL2 site (A1 in Figure 1) was < 1 m higher in elevation and was a drained-soil site in the littoral zone with a deep talik below 5 m in the soil column; this site had also exhibited natural fluxes up to 5 kg CH_4 m^{-2} d^{-1} during the cold season (Supplementary Figure S1). The NSY site is a gradually sloped field underlain by thawing, ice-rich Yedoma permafrost that has thermokarst mounds on the surface, which has periodic emissions of CH_4 after heavy rains. NSY cores were taken near the Eddy-covariance tower site, which has routinely detected CH_4 emissions year-round. Our NSY 2D-inversion model showed uniform talik and permafrost layers below the frozen active layer. The SKP site was a naturally occurring thermokarst pond near the Skidmore mine that is routinely drained by the landowner to allow the ground to freeze (Figure 1). The SKP 2D-inversion model showed the lowest thaw depth of all our sites near a permafrost tunnel.

Chemical analysis at various depths revealed the highest carbon content at BTL2 at a depth of 200 cm compared to all other core sites (17.49 wt%), hydrogen (1.94 wt%), oxygen (15.27 wt%), and sulfur (0.09 wt%) content (Supplementary Table S1).

Microbial community structure and diversity

Cores were immediately subsampled at a depth of 150 cm at all sites (BTL1.150, BTL2.150, NSY.150, and SKP.150); the subsampled plugs were transported cold and frozen until we were able to perform 16S and shotgun metagenomic sequencing and analysis.

We used 16S rRNA sequencing to survey microbial compositions at various depths, which indicated microbes involved in methanogenesis including *Methanosarcinales* and *Methanomicrobiales* genera. In total, 708 genera were observed to have known involvement in CH_4 metabolism

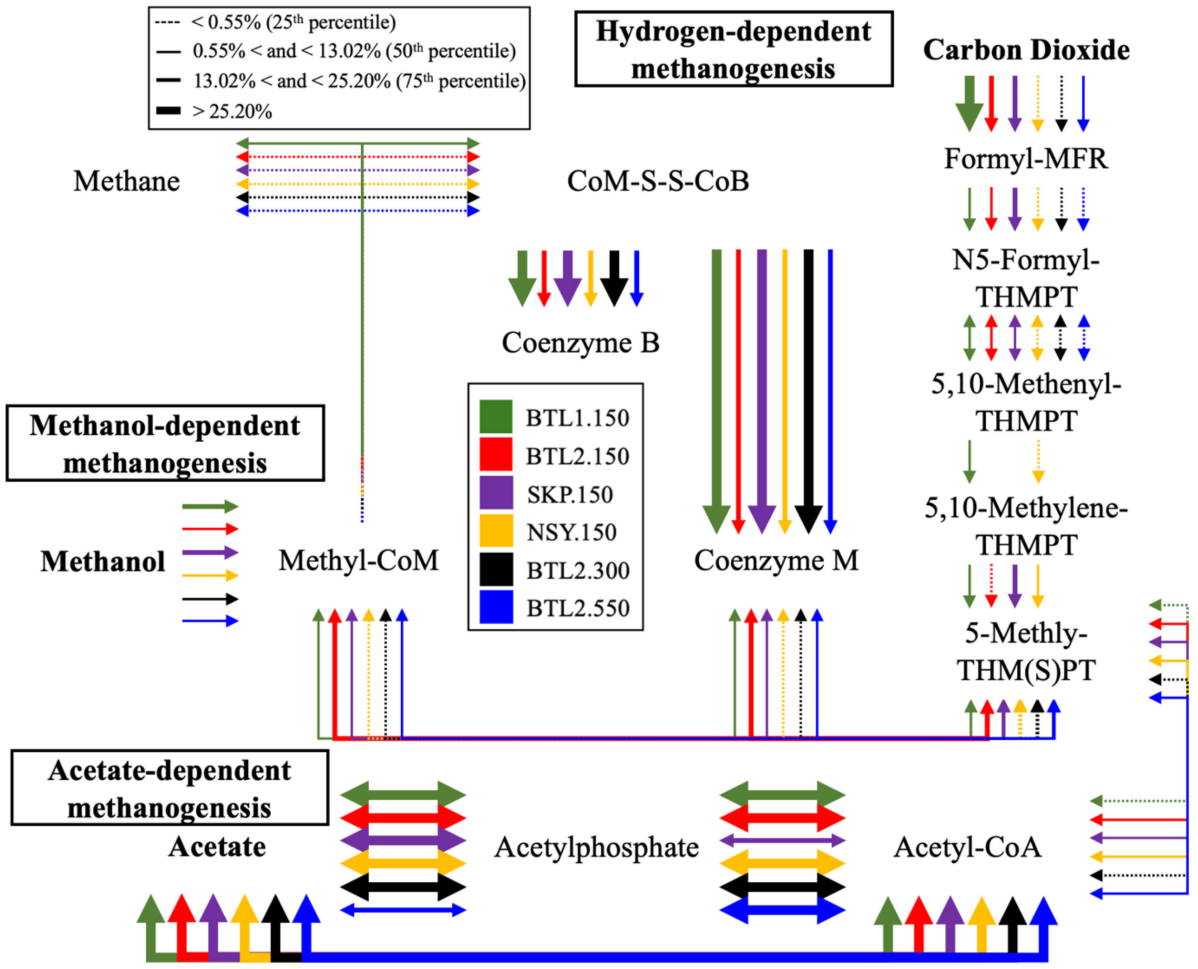

FIGURE 3
Metabolic pathway analysis was conducted from relative abundance of genes found in the methane metabolic pathway for cores BTL1.150 (green), BTL2.150 (red), SKP.150 (purple), NSY.150 (yellow), BTL2,300 (black), and BTL2.550 (blue). This visualization compares the relative abundance of enzyme genes for each for each pathway leading to methanogenesis including hydrogen-, methanol-, and acetate-dependent methanogenesis. The thickness of the arrows represents the relative percent abundance for each pathway, whereas the thickest arrows indicates that more than 25% of the enzyme genes in these samples where associated with the indicated pathways.

at various sites, with the primary CH_4-producing archaea genera *Methanosarcina* observed at 16.4% relative abundance at BTL1.The microbial community most associated with CH_4 metabolism were dominated by the genera *Methyloligellaceae, Methyloceanibacte, Hyphomicrobium*, *Bradyrhizobium*, *Pseudomonas*, and *Streptomyces*, which are known to be able to utilize CH_4 in methanotrophy (Hough et al., 2020).

The most dominant bacterial class detected at NSY and SKP was *Pseudomonadales*, whereas both BTL sites had little to no *Pseudomonadales* with only 3.4% at BTL2 and none at BTL1 where the high seasonal methane flux has been detected. We also detected other notable nitrogen and carbon dioxide fixation species such as *Bradyrhizobium* at BTL2. Likewise, the methylotrophic species *Methyloceanibacter* was 11.2% at BTL1, but also detected at 4.8% for BTL2 at 550 cm depth. The sulfate reducing genera *Desulfobacterota*, *Rhodoferax* and *Pseudomonas* were observed at most sites (Supplementary Figure S3). However, sulfate reducing family *Desulfobacterota* was most abundant with BTL1.150 at 9.1% followed by NSY at 7.3% relative abundance (Supplementary Figure S3; Supplementary Table S3). Additional depths were subsampled from BTL2 at depths 300 cm (BTL2.300) and 550 cm (BTL2.550) and included in our 16S and metagenomic analysis to determine microbiome diversity deeper in the talik at this drained site.

In contrast to metagenomic analysis, 16S sequencing of different depths revealed in total 39 archaeal genera that contained the methyl coenzyme M reductase (*mcrA)* gene; among this population, 4 methanogenic archaea (*Methanosarcina*, *Methanoregula*, *Methanosphaerula*, and *Candidatus Methanogranum*) were observed in our core samples. While *Methanosarcina* was a major methanogenic archaeon at BTL1.150 in the lower active layer, SKP had high relative abundance of *Methanosphaerula* deeper in the soil column around 430 cm SKP.430 (Supplementary Figure S3; Supplementary Table S2). *Actinomycetes* and *Alphaproteobacteria* were present in all microbial communities at all core sites in our metagenomic data.

The psychrophile species *Cryosericales* was found at 150 cm for all core sites except for SKP. *Cryosericales* species increased in relative abundance deeper in the soil column at BTL2, moving from 2, 5, and 10.7% at 150, 300, and 550 cm, respectively.

Relative abundances of classified methanogens initially reveal that BTL1.150 had the highest amount of *Methanomicrobiales* (3.2%),*Methanosarcinales* (16.4%), *Methanotrichales* (0.2%), *Methanobacteriales* (0.6%), at total of ~20.4% relative abundance (Supplementary Figure S1). Microbial compositions and species diversity were quantified from metagenomic datasets (Figure 4). Shannon alpha diversity plots were generated from metagenomic analysis and revealed similar microbial richness for BTL1 and BTL2 at 150 cm, whereas the SKP borehole had the lowest level of microbial richness (Figure 4A). Alpha diversity plots also show depth-dependent microbial diversity with lower diversity found deeper in the soil column for BTL2.300 and BTL2.550 compared to BTL2.150. Bray-Curtis dissimilarity analysis of metagenomics microbial analysis revealed that BTL1.150 and SKP.150 had contrasting microbial populations compared to each other as well as compared to all other cores obtained from BTL2 and NSY at similar depths (Figure 4B). Notably, BTL2.150 metagenomic microbial composition had similar populations to the BTL2.300 and BTL2.550 depths. However, we discovered that 17% of the metagenomic sequences matched to bacteria, archaea, and viruses at BTL1 (Figure 5B). The remaining 83% of the metagenomic data contained unclassified genes that represent a major portion of unknown biological activity in these permafrost soil microbiomes, which merits further study to understand functional impacts in biogeochemical cycling.

To understand the absolute number of microbes at 150 cm we focused our analysis on predicted genes and performed analysis microbial composition analysis metagenomes at the genus level. From this analysis we generated a heat map table comparing microbial genus abundance across boreholes at 150 cm depth is displayed with conditional formatting to highlight the microbial abundance across core sites at 150 cm depth (Figure 5A). The BTL1 metagenomes contained a notable diversity of archaea, with many examples of methanogenic and halotolerant species (Figure 5C). These results indicated high abundance of the archaeal *Methanosarcina* family at BTL1 compared to the other cores at 150 cm depths. However, many of the genes and microbes were unclassified with > 80% in the metagenomic data and > 40% in 16S amplicon data that we could not attribute either a predicted function or host.

Potential metabolic functional genes

Functional gene analysis revealed the potential for CH_4 production at all sites (Figure 3). BTL1.150 contained genes for hydrogen-, acetate-, and methanol-dependent methanogenesis. Metagenomic analysis of gene counts also showed the highest potential for CH_4 metabolism at BTL1.150, followed by NSY1.150 (Supplementary File S2). In contrast, gene counts for CH_4 pathways at SKP1.150 and BTL2.150 were considerably lower. The taxa associated with the central methanol methyl-coenzyme M reductase (EC 2.8.4.1), the enzyme that catalyzes the final step in methanogenesis pathway, was observed to be highest in BTL1.150 (Supplementary File S2), which also had the highest fraction of *Methanosarcina* (16.4%), by more than an order of magnitude, compared to BTL2.150, NSY1.150, and SKP1.150 (< 1.3% *Methanosarcina*). Metagenomic annotations of gene counts for sulfur reduction were present at all sites. In total, 10 archaeal and 681 bacterial genera were associated with sulfate reduction. Among them, 77 potential sulfate-reducing bacterial genera were observed in the various soil core samples including *Desulfobacterota*, *Rhodoferax* and *Pseudomonas*, which have been shown to contain robust sulfate reduction pathways (Chen et al., 2023; Wang et al., 2023; Supplementary Figure S4; Supplementary Table S3). Interestingly, the lowest relative abundance of sulfate reducing bacteria (i.e., *Desulfosporosinus*) was found at SKP for the 430 cm samples, where methanogenic archaea were dominant (Supplementary Figure S3; Supplementary Table S2).

Characterizing borehole VOCs and their associated biogenic pathways

Our analysis of 2D-GC-MS data revealed biogenic VOC abundance and divergent chemical features between talik boreholes sites. We found > 400 unique VOC features ranging from C2 – C28, with > 40 VOCs linked to microbial and biogenic activity (Supplementary material). Our summary of the relative VOC abundance at each site and conditional formatting reveal distinctive VOC "fingerprints" for each borehole (Supplementary File S3). We were able to identify different classes of VOC compounds (e.g., aromatic hydrocarbons, aldehydes, butenolides, alcohols, ketones, and carbonyls) and derivative compounds (e.g., acetaldehyde, benzene, hexanaldehyde, acetone, tolueneformaldehyde) that have been previously identified as GHGs and linked to global warming (David and Niculescu, 2021).

As documented in Supplementary Table S6, the observed VOC byproducts can also be associated with gene hits for anaerobic styrene degradation, glyoxylate and dicarboxylate metabolism, propanoate metabolism, and volatile fatty acid degradation (e.g., propionate, formate, acetate, and butyrate). In fact, many of the VOCs appeared to be byproducts of enzymatic anaerobic degradation by laccase, oxidoreductase, decarboxylase, and hydrolase enzyme reactions, as inferred from analysis of KEGG pathways (in anaerobic systems acyl lipids are hydrolyzed by lipases.) (Mackie et al., 2008). Notable biogenic VOCs were identified from a manual KEGG database analysis (Supplementary Table S4). VOC abundance profiles were aligned to the genes of degradative enzymes, including cyclohexane to cyclohexane dehydrogenase (EC: 1.3.8.10), isobornyl formate to formylmethanofuran dehydrogenase (EC: 1.2.7.12), acetic acid to acetate kinase (EC: 2.7.2.1), acetophenone to ethylbenzene hydroxylase (EC: 1.17.99.2), styrene to aliphatic nitrilase (EC: 3.5.5.7), and oleic acid (fatty acid degradation product) to catalase (EC: 1.11.1.6) (Figure 3).

Discussion

Biogenic VOCs serve as biological indicators of CH_4-emitting taliks

One of our primary goals was to identify the biological drivers of CH_4 emissions found at Big Trail Lake during the cold season by comparing VOC profiles at four local thermokarst sites taken

10.3389/fmicb.2024.1462941

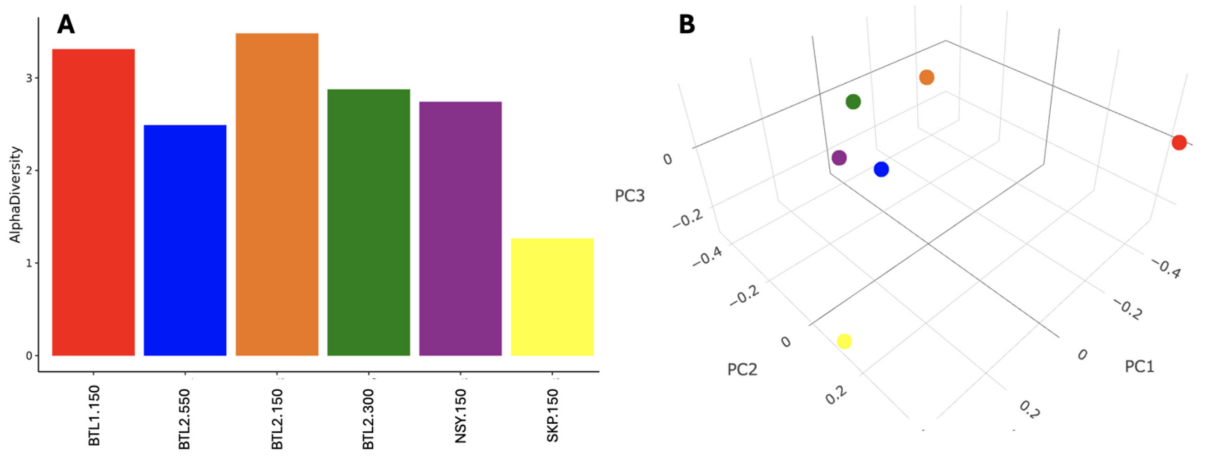

FIGURE 4
(A) Species diversity was quantified from metagenomic datasets using Shannon alpha diversity analysis, which revealed differential microbial richness across core site samples. **(A)** Bray-Curtis dissimilarity analysis generated a 3D principal coordinate analysis (PCoA) at strain level.

A

Gene Abundance (+ / −)

Genus	BTL1.150	BTL2.150	SKP.150	NSY.150
Bradyrhizobium	12.365	19.902	2.566	4.397
Streptomyces	4.716	4.977	10.036	3.654
Clostridium	3.586	0.314	0.125	0.094
Methanosarcina	3.570	0.520	0.036	0.063
Arthrobacter	2.353	0.928	0.734	0.325
Pseudomonas	1.851	3.047	6.251	7.551
Hyphomicrobium	1.828	0.068	0.118	0.064
Anaeromyxobacter	1.555	0.181	0.678	0.229
Rhodoplanes	1.358	0.424	0.131	0.153
Mesorhizobium	1.310	0.892	0.841	0.713
Rhizobium	1.093	0.640	0.679	0.538
Sphingomonas	1.027	0.694	1.302	0.756
Usitatibacter	1.017	0.439	0.431	0.138
Paenibacillus	0.963	0.358	0.542	0.285
Methylobacterium	0.875	0.474	0.605	0.370
Burkholderia	0.781	0.896	1.270	1.124
Nocardioides	0.776	0.893	1.720	0.615
Microbacterium	0.759	1.075	1.694	0.768
Pseudolabrys	0.745	1.866	0.203	1.196
Bacillus	0.648	0.088	0.102	0.096
Micromonospora	0.634	0.635	1.272	0.468
Mycolicibacterium	0.618	0.673	1.222	0.497
Mycobacterium	0.540	0.623	1.091	0.427
Rhodopseudomonas	0.521	0.709	0.191	0.299
Methyloceanibacter	0.512	0.024	0.106	0.061
Methyloligella	0.494	0.017	0.057	0.043
Paraburkholderia	0.492	0.618	0.709	0.903
Cupriavidus	0.479	0.621	0.623	0.988
Methanoregula	0.465	0.009	0.005	0.008
Corynebacterium	0.455	0.386	0.781	0.351
Amycolatopsis	0.451	0.533	1.169	0.373
Bosea	0.437	0.272	0.284	0.231
Variovorax	0.436	1.438	0.569	1.114
Rhodococcus	0.420	0.508	0.765	0.305
Pseudarthrobacter	0.417	0.107	0.129	0.061
Methanothrix	0.397	0.015	0.006	0.018
Cellulomonas	0.384	2.263	0.728	1.000
Flavobacterium	0.369	0.239	0.131	0.904
Nocardia	0.338	0.334	0.678	0.245
Geobacter	0.323	0.095	0.194	0.150
Massilia	0.322	1.336	0.421	0.740
Paracoccus	0.319	0.219	0.377	0.197
Methylocystis	0.309	0.127	0.120	0.103
Sinorhizobium	0.301	0.165	0.262	0.182

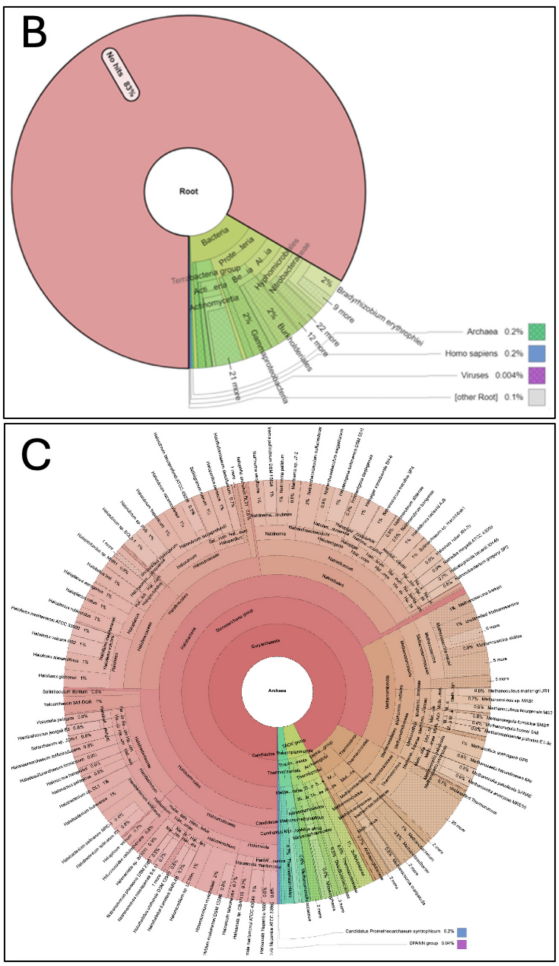

FIGURE 5
Relative gene abundance was obtained from metagenomic analysis of each core from 150 cm depth below the frozen active layer **(A)** and conditionally formatted and aligned to the highest abundance hits at BTL1 to compare each microbial genera across borehole sites. Krona chart of all metagenomes at BTL1 revealed that 17% of annotated metagenomic sequences were bacteria, archaea, and viruses with the remaining 83% containing genes of unknown function **(B)**. Since BTL1 had the highest number of methanogens, a Krona chart zooming into the archaea fraction at BTL1 was generated, that shows the diversity of methanogenic, halotolerant, and alkaliphilic archaea genera detected from metagenomes **(C)**.

from the same transition-layer depth (150 cm) (Supplementary Figure S1). We assumed that permafrost soil microbes control the fate of soil organic carbon (SOC) during various states of thaw, and subsurface VOCs could provide improved resolution of how microbes respond to warming trends. Our preliminary CH_4 flux measurements identified anomalous CH_4-hotspots around BTL, which provided a roadmap to investigate microbial transformation of SOC to VOCs under anaerobic conditions in the subsurface (Supplementary Figure S1). We hypothesized that if we measured microbes and their functional metabolisms beneath the frozen active layer, we would be able to identify contrasting biochemical profiles, particularly at sites with different CH_4 flux measurements.

The results of our proof-of-concept study appear to support our hypothesis. We used 16S rRNA amplicon sequencing to screen microbial populations at the same depth (150 cm) at all four sites, finding that each site hosts unique and diverse microbial communities, including biologically active species related to VOC emissions, such as populations of methane-related microbes (e.g., methanogens, methylotrophs, and methanotrophs). However, all four populations were largely composed of unclassified and uncharacterized taxa and contained many (> 80%) genes of unknown identity and/or function (Figure 5).

Shotgun metagenomics further revealed that the microbiomes associated with each talik site were also distinct from one another, although we observed similarities between metabolic enzyme genes and the specific VOC abundance profiles involved in anaerobic degradation of carbon substrates (e.g., phenolics, aromatics, and organic acids) (Figure 6). Additionally, many VOCs mapped to anaerobic degradation pathways in KEGG (including toluene, ethylbenzene, phenol, styrene, benzoate, and methylnaphthalene), indicating potential linkages between microbial metabolic potential and VOC signatures (Supplementary Table S6). Therefore, VOCs potentially provide novel bioindicators of subsurface biogeochemical changes that can be leveraged for long-term ecosystem monitoring.

Methanogens, methanotrophs, and microbial communities

Because the active layer is frozen solid during the winter, we hypothesized that samples taken from the protected transition layer (which is slightly warmer due to snowpack thermal insulation) would be most likely to contain microbes that are biologically active during the winter (Holland et al., 2020) and provide the highest likelihood of VOC-to-microbial-composition comparisons. Thus, we again focused our more in-depth metagenomic sequencing on the plugs collected from all four sites at a depth of 150 cm, and at different depths at the same site (guided by the varying depths of the active/transition/permafrost layers). Our particular goal was to identify microbes that accelerate and hinder SOC sequestration, including methanogens, sulfate-reducing genera, and methanotrophs.

For example, by comparing metagenome-resolved microbial composition profiles from different depths at BLT2, we found that extremophilic cold-tolerant species (i.e., psychrophiles), such as *Cryosericales*, increased in abundance with soil depth at that site (Supplementary Figure S4; Supplementary Table S3). These psychrophilic species are particularly important because they are known to play a role in alkane catabolism and carbon cycling; in permafrost soils, psychrophilic species provide low-molecular-C substrates for methanogens (Bowman and Deming, 2014), ensuring that the methanogens can only uptake low-molecular-weight carbon. At BTL1, we also discovered a high diversity of methanogenic species (i.e., *Methanomicrobiales,Methanosarcinales, Methanotrichales, Methanobacteriales)*; however, at SKP and SNY, methanogens were only found deeper in the soil column during (Supplementary Figure S3; Supplementary Table S2). Sulfate reduction is known to reduce methanogenesis potential through several paths (primarily the flow of electrons) (Sela-Adler et al., 2017), so we also looked for sulfur-reducing genera. While *Desulfobacterota* were highest in abundance at the BTL1.150 and NSY.150 sites, but also found in SKP and BTL2 samples, suggesting that . . .. In contrast, the *Rhodoferax ferrireducens* sulfur-reducing species was not find at either BTL1 but had high abundance in the NSY.150 and BTL2.300 samples, suggesting that. . ..

Methanotrophs (i.e., *Methyloligellaceae*, *Hyphomicrobium, Bradyrhizobium*, *Pseudomonas*, and *Streptomyces*) provide a more direct SOC sink. We detected methanotrophs at higher abundance in the upper 50 cm of the soil column at BTL1, but also present deeper in the soil column at BTL2, SKP, and NSY (thermokarst mounds) (Supplementary Figure S3; Supplementary Table S2). Notably, in the BTL1.150 samples, the dominant methanotroph species were *Methyloligellaceae, Methyloceanibacte, Hyphomicrobium*, but other species that have been reported to stimulate methanotrophy (e.g., *Pseudomonas*) were also present. BTL1 had the highest concentrations of *Methyloceanibacter*, which suggests that C uptake and sequestration is likely responsive to C emissions in these thermokarst systems. In contrast, *Pseudomonas* was the predominate species in the upper 300 cm at SKP and NSY, suggesting possible modes for carbon sequestration from C emissions deeper in the soil column (Veraart et al., 2018). This finding may also explain periodic CH_4 emissions detected at NSY and SKP sites after heavy rains saturated the thermokarst mounds (Walter Anthony et al., 2024 Manuscript submitted for publication).

Our community structure analysis identified methanotrophic co-occurrence when methanogenic archaea were present in high abundance, which has been previously reported in other soils systems including Arctic soils (Tripathi et al., 2019; Li C. et al., 2021). However, previously, massive field efforts to characterize microbial distributions in permafrost soil found that, as soils thaw, microbial spatial variation is primed and driven by specific biochemical processes (e.g., gas production, metal redox) (Waldrop et al., 2023). Hence, we acknowledge that our limited sample sets cannot draw concrete conclusions of microbial distribution at our talik sites. Still, our observations provide further evidence that methanogenesis can occur lower in the soil column, which has implications for promoting methanotrophy (Singleton et al., 2018) in near-surface soils, thereby capturing and sequestering CH_4 and other bulk carbon emission before release into the atmosphere.

While we were able to identify of several key methane-related soil microbes and VOC-related metabolic genes, we also discovered that many of the metagenomes we obtained had > 70% unclassified genes. For example, only 17% of the metagenomes from BTL1.150 contained annotated genes for bacteria, archaea, and viruses. The remaining 83% of the metagenomes at BTL1.150 contained

10.3389/fmicb.2024.1462941

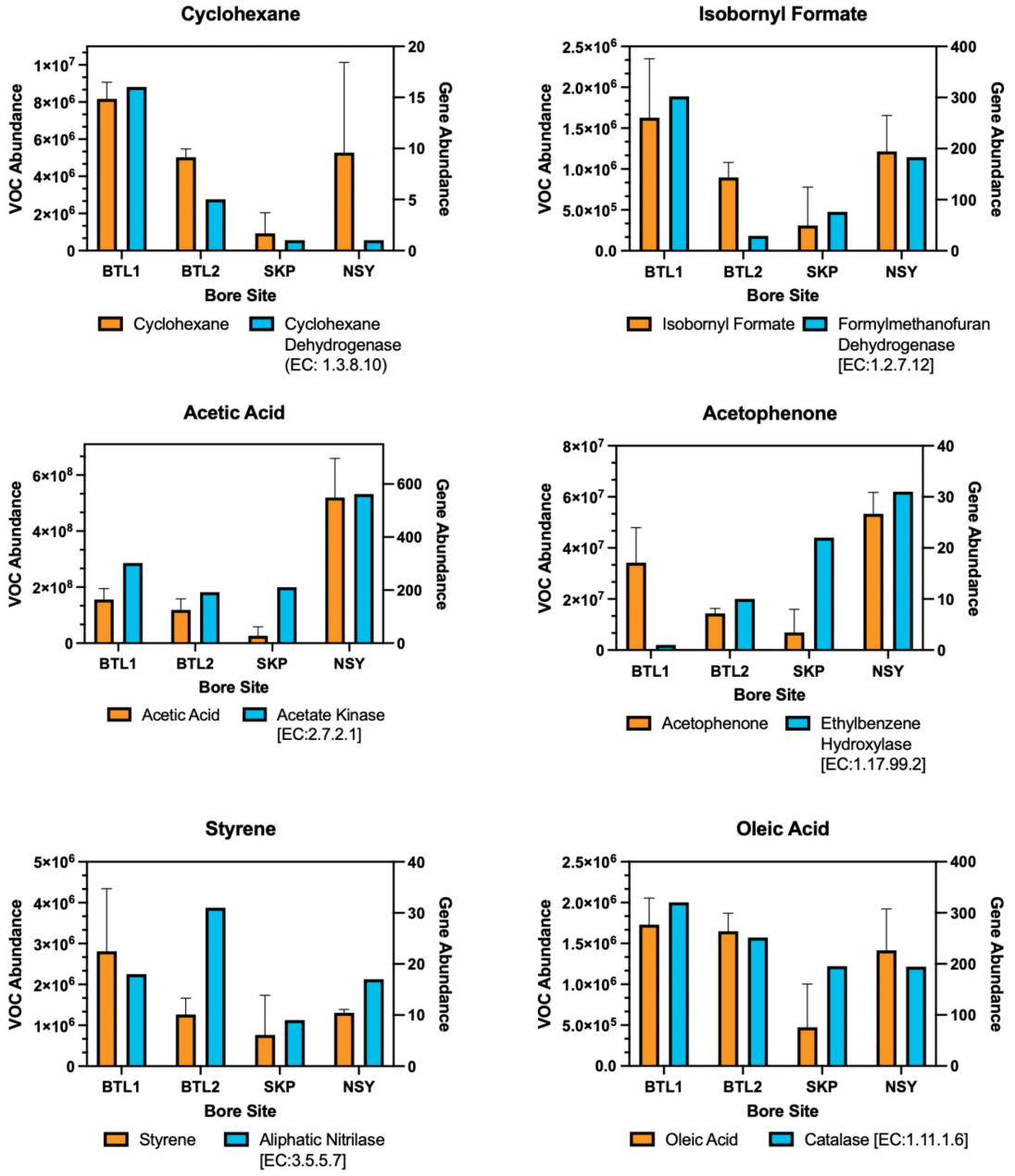

FIGURE 6
Biogenic VOCs related to anaerobic degradation were aligned to enzyme gene hits for each bore site in a dual y-axis bar plot. The left y-axis shows the mean of triplicate VOC abundance with error bars for one standard deviation from each borehole compared to the right y-axis showing the gene hit abundance of related enzymes obtained from metagenomes for each core site at 150 cm depth. The KEGG enzyme nomenclature number is provided for each enzyme.

unclassified genes (i.e., microbial dark matter), which highlights our limited ability to identify novel extant and extinct genetic traits associated with VOC-related metabolic pathways. Moreover, the diversity of archaea was most pronounced in the BTL1.150 metagenomes, at the site with the highest CH_4 emissions, which contained many examples of known methanogenic, halophilic, and alkaliphilic genera. Although we couldn't completely resolve patterns in microbial composition profiles across the cores from various sites and depths, our metagenomic and 16S sequencing of soil depths provided verification that microbes residing in 150–200 cm depths had higher microbial diversity, are potentially active during winter, and could inform how microbial compositions would tie to VOC metabolism at these contrasting talik sites.

Borehole VOC fingerprints and related anaerobic degradation pathways

VOC abundances for each borehole were aligned in a heat map that revealed distinct "fingerprints" for each borehole (Supplementary File S3), highlighting the many VOCs associated

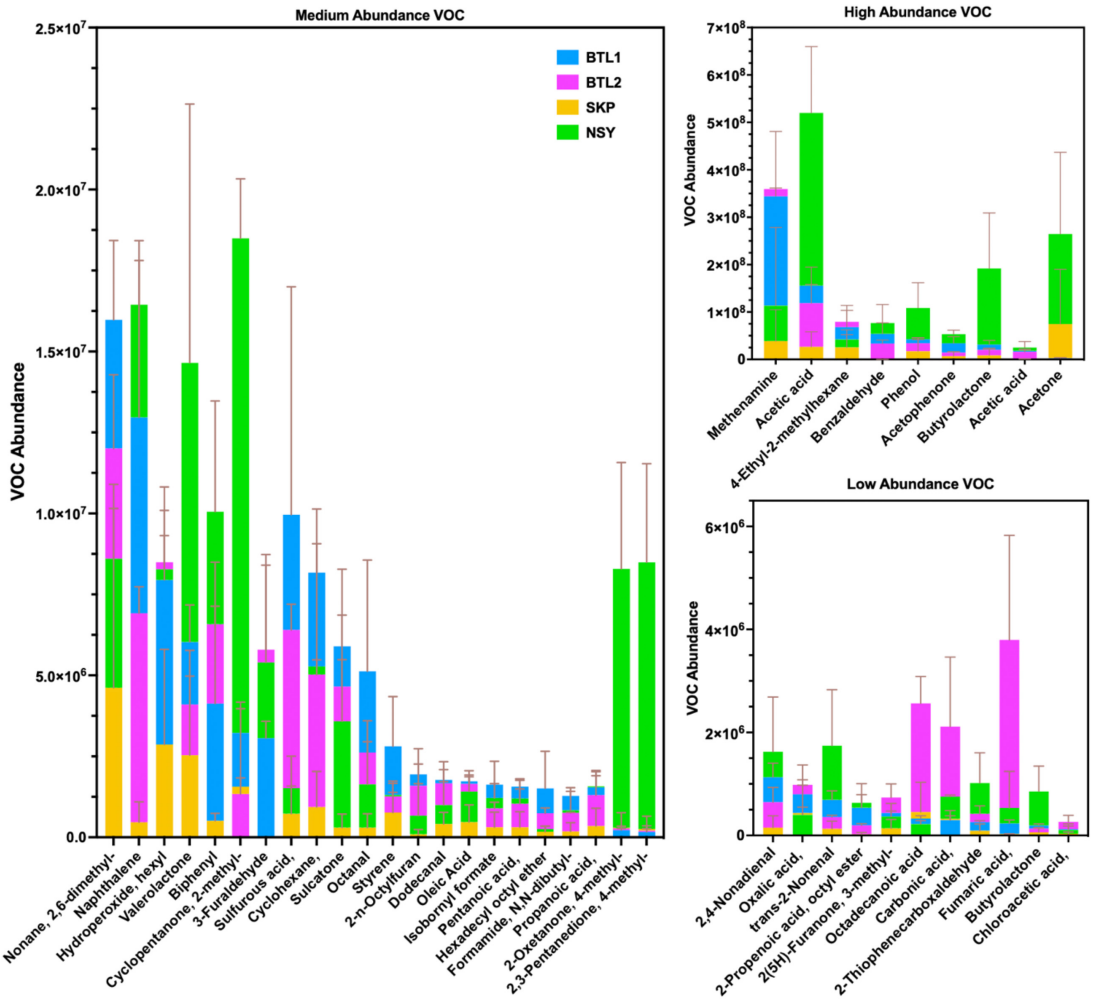

FIGURE 7
Biogenic VOC abundance from each bore site was collected and analyzed by 2D-GC-MS, and averaged to show medium **(A)**, high **(B)**, and low **(C)** abundance. Bar plots show the mean of triplicate VOC measurements with error bars for one standard deviation. Chemical features with a comma after the name have additional moieties not included in this table but sdf listed in full table VOC features found in Supplementary material.

with anaerobic degradation pathways of hydrocarbon catabolism (e.g., alkane, toluene, and naphthalene metabolic pathways) and similar enzyme genes associated with hydrocarbon catabolic pathways for propanoate, naphthalene, styrene, and ethylbenzene (Supplementary Table S6). At present, given our limited knowledge of enzyme identity and degradation stages, these anaerobic degradation pathways remain unresolved; however, recent reports indicate that there are four stages of alkane degradation [fumarate addition, C-skeleton re-arrangement, decarboxylation, and beta-oxidation byproducts (Bian et al., 2015)], which are in agreement with the VOCs detected in this study (i.e., fumarate, valerate, butyrate) (Figure 7).

The most abundant VOCs detected from the four talik sites included terminal degradation products consisting mainly of organic acids (e.g., acetic acid, acetone, phenol, acetophenone) (Figure 7B), which likely feed methanogens through the acetate-dependent pathway (Figure 3). We also identified notable biogenic VOCs from a manual KEGG database analysis (Supplementary Table S4), including octanal, acetophenone (Jobst et al., 2010), isothiocyanatocyclohexane (cyclohexane, isothiocyanate) (Hanschen and Schreiner, 2017), phenol (Maurer et al., 2019), furaldehyde (furfural) (Rivard and Grohmann, 1991), furanone (Gómez et al., 2022), styrene (Kanehisa et al., 2023), and benzaldehyde (Huang et al., 2022) (Supplementary Table S4). We also found sulfur-containing VOCs, including sulfur dioxide, isothiocyanatocyclohexane, thiophenecarboxaldehyde, and sulfurous acid (Figure 7). By mapping distinct VOC abundance trends to the gene abundance of associated degradative enzymes (Figure 6), we were able to find remarkable agreement in abundance trends, but also discrepancies that cannot be explained by metagenomics alone, which will require more in-depth functional characterization of enzyme expression. Although many anerobic degradation pathways remain unexplored, our comparative analysis provided a means to understand these talik sites through specific degradation enzymes that correlated to VOC "fingerprints" of boreholes in different thermokarst systems (Supplementary File S3). Although metagenomics doesn't provide expression or enzyme activities, we were able to infer the presence of functional pathways from gene count abundance. While the ecological role of our measured VOC compounds remains to

be elucidated, our results provide insights into the subsurface microbial processes with environmentalsignificance.

Volatilomics for informing subsurface biokinetics

At each borehole, we identified unique chemical VOC signatures that warrant further study (e.g., via laboratory soil incubations) to statistically define VOC expression patterns and determine transient VOC signatures. In fact, we found many VOCs that are byproducts from various degradation enzymes, including oxidoreductases, lyases, laccases, and carboxylases (Gibson and Harwood, 2002). Although current understanding of microbial anaerobic degradation pathways are limited, recent studies have revealed the scope and complexity of anaerobic biodegradation pathways of n-alkanes in carbon-rich oil reservoirs (Bian et al., 2015). These reports have attempted to define species-specific metabolic pathways using metagenomics and metaproteomics (McGivern et al., 2021); however, VOC "fingerprinting" does not require knowledge of specific enzymatic pathways to identify permafrost states that are likely to facilitate abrupt thaw, talik formation, and thermokarst expansion.

Our alignment of VOCs to degradation enzyme genes provided preliminary evidence that VOC monitoring in Arctic soils is a potentially useful approach to measuring subsurface microbial dynamics over time (Figure 6), because the biochemical alignment can potentially be used to interpret VOC expression to infer subsurface biokinetics, which could provide high-resolution datasets of subsurface SOC transformation, advancing attempts to model the degradation and transformation of SOC. For instance, a recent study used metagenome-assembled genomes to refine the enzyme latch theory and detected similar degradation products (e.g., propionic acid, fumaric acid, and benzaldehyde derivatives), which could be enhanced with VOC "fingerprinting" analysis to further elucidate degradation enzymes and their associated pathways (Wilhelm et al., 2021). Refinement of terrestrial SOC models using VOC-derived biokinetics could also resolve chemical and biological heterogeneity to make soil microbiomes tractable for study in subsurface systems (Jansson and Taş, 2014; Mackelprang et al., 2017; Waldrop et al., 2023).

Conclusion

The increasing duration of thaw seasons in permafrost ecosystems has created positive feedback loop with gradual and abrupt thaw events, which is deepening and expanding the areas of year-round unfrozen ground (i.e., taliks) (Walter Anthony et al., 2018; Turetsky et al., 2020; Walter Anthony et al., 2021). The lack of high-resolution data in subsurface Arctic terrestrial ecosystems limits our ability to understand the subsurface biogeochemical drivers which drive the rate and magnitude of environmentally triggered SOC turnover (Bradford et al., 2016; Tao et al., 2024). Our study demonstrates a proof-of-concept that VOCs can potentially serve as bioindicators of subsurface biogeochemical processes, providing high-resolution data and broad-scale measurements that can be used to characterize biological roles in the thermokarst–permafrost continuum. This study also establishes methods and approaches for effectively capturing VOCs during winter seasons that could allow for more accurate measurements of subsurface microbial rates of C conversion. Although further validation is required to determine the full range of biogenic VOC "fingerprints" that represent subsurface dynamics and indicate the onset of thaw events (i.e., precursors of gradual and abrupt thaw), these results provide an identification-based approach to track and understand permafrost thaw states responsible for CH_4 emissions during all seasons in Alaska. Future work should integrate measurements of VOC "fingerprints" derived from laboratory soil incubations at different thaw states to understand the metabolic drivers that shift microbial C cycling during and allocation in arctic soils and translated to other soil systems.

Data availability statement

TILES analysis of untargeted volatilomics using 2D-GC-MS quantification can be found in the Supplementary Data Sheet 1. Metagenome 16S rRNA gene and amplicon sequencing data are available in NCBI under BioProject accession no. PRJNA1216023 (for biosample accession numbers, see Supplementary Data Sheet 2).

Author contributions

CS: Conceptualization, Data curation, Formal analysis, Funding acquisition, Investigation, Methodology, Project administration, Resources, Software, Supervision, Validation, Visualization, Writing – original draft, Writing – review & editing. NH: Investigation, Methodology, Writing – review & editing, Conceptualization, Formal analysis. JY: Data curation, Writing – original draft, Formal analysis. JSc: Investigation, Methodology, Writing – review & editing. HB: Conceptualization, Formal analysis, Investigation, Methodology, Writing – review & editing. BR: Investigation, Methodology, Writing – review & editing. JSa: Investigation, Methodology, Conceptualization, Data curation, Formal analysis, Writing – review & editing. MM: Formal analysis, Investigation, Methodology, Writing – review & editing. NE: Investigation, Methodology, Writing – review & editing. SK: Investigation, Methodology, Writing – review & editing. JW: Conceptualization, Investigation, Methodology, Resources, Writing – review & editing. WM: Writing – review & editing, Data curation, Formal analysis. KA: Conceptualization, Formal analysis, Investigation, Methodology, Resources, Supervision, Validation, Visualization, Writing – original draft, Writing – review & editing. PM: Conceptualization, Investigation, Resources, Supervision, Writing – review & editing.

Funding

The author(s) declare financial support was received for the research, authorship, and/or publication of this article. This study was supported by the Bioscience Investment Area under Project# 225920 for the Laboratory Directed Research and Development program at Sandia National Laboratories.

Sandia National Laboratories is a multi-mission laboratory managed and operated by National Technology & Engineering Solutions of Sandia, LLC (NTESS), a wholly owned subsidiary of Honeywell International Inc., for the U.S. Department of Energy's National Nuclear Security Administration (DOE/NNSA) under contract DE-NA0003525. This written work was authored by an employee of NTESS. The employee, not NTESS, owns the right, title and interest in and to the written work and is responsible for its contents. Any subjective views or opinions that might be expressed in the written work do not necessarily represent the views of the U.S. Government. The publisher acknowledges that the U.S. Government retains a non-exclusive, paid-up, irrevocable, world-wide license to publish or reproduce the published form of this written work or allow others to do so, for U.S. Government purposes. The DOE will provide public access to results of federally sponsored research in accordance with the DOE Public Access Plan.

Acknowledgments

We thank members of the Sandia National Laboratories' Environmental Systems Biology and Biological & Chemical Sensors Departments for their valuable input during this study. We thank Todd Lane for providing guidance on this proposal concept. We thank Emily Hollister, Mark Ivey, Andrew Glen, and Diana Bull for providing technical guidance and encouragement. We thank Alberto Rodriguez, Steven Branda, Jesse Cahill, and Emily Hollister for providing technical reviews of this manuscript. We thank the Skidmore Family, Midnight Sun Golf Course, and Department of Natural Resources for access to the field sites. Teams from UAF, Sandia, CU-Boulder, and UT-Austin assisted with collection of cores at BTL1 and SKP during the March 2023 field campaign.

Conflict of interest

The authors declare that the research was conducted in the absence of any commercial or financial relationships that could be construed as a potential conflict of interest.

Publisher's note

All claims expressed in this article are solely those of the authors and do not necessarily represent those of their affiliated organizations, or those of the publisher, the editors and the reviewers. Any product that may be evaluated in this article, or claim that may be made by its manufacturer, is not guaranteed or endorsed by the publisher.

Supplementary material

The Supplementary Material for this article can be found online at: https://www.frontiersin.org/articles/10.3389/fmicb.2024.1462941/full#supplementary-material

References

Beghini, F., McIver, L. J., Blanco-Míguez, A., Dubois, L., Asnicar, F., Maharjan, S., et al. (2021). Integrating taxonomic, functional, and strain-level profiling of diverse microbial communities with bioBakery 3. *eLife* 10: e65088. doi: 10.7554/eLife.65088

Bian, X.-Y., Maurice Mbadinga, S., Liu, Y.-F., Yang, S.-Z., Liu, J.-F., Ye, R.-Q., et al. (2015). Insights into the anaerobic biodegradation pathway of n-alkanes in oil reservoirs by detection of signature metabolites. *Sci. Rep.* 5:9801. doi: 10.1038/srep09801

Bolger, A. M., Lohse, M., and Usadel, B. (2014). Trimmomatic: a flexible trimmer for Illumina sequence data. *Bioinformatics* 30, 2114–2120.

Bowman, J. S., and Deming, J. W. (2014). Alkane hydroxylase genes in psychrophile genomes and the potential for cold active catalysis. *BMC Genom.* 15:1120. doi: 10.1186/1471-2164-15-1120

Bradford, M. A., Wieder, W. R., Bonan, G. B., Fierer, N., Raymond, P. A., and Crowther, T. W. (2016). Managing uncertainty in soil carbon feedbacks to climate change. *Nat. Clim. Change* 6, 751–758.

Callahan, B. J., McMurdie, P. J., Rosen, M. J., Han, A. W., Johnson, A. J. A., and Holmes, S. P. (2016). DADA2: high-resolution sample inference from Illumina amplicon data. *Nat. Methods* 13, 581–583. doi: 10.1038/nmeth.3869

Cantalapiedra, C. P., Hernández-Plaza, A., Letunic, I., Bork, P., Huerta-Cepas, J., and Tamura, K. (2021). eggNOG-mapper v2: functional annotation, orthology assignments, and domain prediction at the metagenomic scale. *Mol. Biol. Evol.* 38, 5825–5829. doi: 10.1093/molbev/msab293

Caporaso, J. G., Kuczynski, J., Stombaugh, J., Bittinger, K., Bushman, F. D., Costello, E. K., et al. (2010). QIIME allows analysis of high-throughput community sequencing data. *Nat. Methods* 7, 335–336.

Caporaso, J. G., Lauber, C. L., Walters, W. A., Berg-Lyons, D., Huntley, J., Fierer, N., et al. (2012). Ultra-high-throughput microbial community analysis on the Illumina HiSeq and MiSeq platforms. *ISME J.* 6, 1621–1624.

Chen, L., Li, W., Zhao, Y., Zhang, S., Meng, L., and Zhou, Y. (2023). Characterization of sulfide oxidation and optimization of sulfate production by a thermophilic Paenibacillus naphthalenovorans LYH-3 isolated from sewage sludge composting. *J. Environ. Sci.* 125, 712–722. doi: 10.1016/j.jes.2021.12.030

Constable, S. C., Parker, R. L., and Constable, C. G. (1987). Occam's inversion: a practical algorithm for generating smooth models from electromagnetic sounding data. *Geophysics* 52, 289–300.

David, E., and Niculescu, V.-C. (2021). Volatile Organic Compounds (VOCs) as environmental pollutants: occurrence and mitigation using nanomaterials. *Int. J. Environ. Res. Public Health* 18:13147. doi: 10.3390/ijerph182413147

Effmert, U., Kalderás, J., Warnke, R., and Piechulla, B. (2012). Volatile mediated interactions between bacteria and fungi in the soil. *J. Chem. Ecol.* 38, 665–703.

Elder, C. D., Thompson, D. R., Thorpe, A. K., Chandanpurkar, H. A., Hanke, P. J., Hasson, N., et al. (2021). Characterizing methane emission hotspots from thawing permafrost. *Glob. Biogeochem. Cycles* 35:e2020GB006922. doi: 10.1029/2020GB006922

Farquharson, L. M., Romanovsky, V. E., Kholodov, A., and Nicolsky, D. (2022). Sub-aerial talik formation observed across the discontinuous permafrost zone of Alaska. *Nat. Geosci.* 15, 475–481.

Fierer, N., Lauber, C. L., Ramirez, K. S., Zaneveld, J., Bradford, M. A., and Knight, R. (2012). Comparative metagenomic, phylogenetic and physiological analyses of soil microbial communities across nitrogen gradients. *ISME J.* 6, 1007–1017. doi: 10.1038/ismej.2011.159

Franchina, F. A., Purcaro, G., Burklund, A., Beccaria, M., and Hill, J. E. (2019). Evaluation of different adsorbent materials for the untargeted and targeted bacterial VOC analysis using GC×GC-MS. *Analyt. Chim. Acta* 1066, 146–153. doi: 10.1016/j.aca.2019.03.027

Ghirardo, A., Lindstein, F., Koch, K., Buegger, F., Schloter, M., Albert, A., et al. (2020). Origin of volatile organic compound emissions from subarctic tundra under global warming. *Glob. Change Biol.* 26, 1908–1925. doi: 10.1111/gcb.14935

Gibson, J., and Harwood, C. S. (2002). Metabolic diversity in aromatic compound utilization by anaerobic microbes. *Annu. Rev. Microbiol.* 56, 345–369.

Gómez, A.-C., Lyons, T., Mamat, U., Yero, D., Bravo, M., Daura, X., et al. (2022). Synthesis and evaluation of novel furanones as biofilm inhibitors in opportunistic human pathogens. *Eur. J. Med. Chem.* 242: 114678. doi: 10.1016/j.ejmech.2022.114678

Hanschen, F. S., and Schreiner, M. (2017). Isothiocyanates, nitriles, and epithionitriles from glucosinolates are affected by genotype and developmental stage in brassica oleracea varieties. *Front. Plant Sci.* 8:1095. doi: 10.3389/fpls.2017.01095

Heslop, J. K., Walter Anthony, K. M., Winkel, M., Sepulveda-Jauregui, A., Martinez-Cruz, K., Bondurant, A., et al. (2020). A synthesis of methane dynamics in thermokarst lake environments. *Earth Sci. Rev.* 210:103365.

Holland, A. T., Bergk Pinto, B., Layton, R., Williamson, C. J., Anesio, A. M., Vogel, T. M., et al. (2020). Over winter microbial processes in a svalbard snow pack: an experimental approach. *Front. Microbiol.* 11: 1029. doi: 10.3389/fmicb.2020.01029

Hough, M., McClure, A., Bolduc, B., Dorrepaal, E., Saleska, S., Klepac-Ceraj, V., et al. (2020). Biotic and environmental drivers of plant microbiomes across a permafrost thaw gradient. *Front. Microbiol.* 11: 796. doi: 10.3389/fmicb.2020.00796

Huang, X.-Q., Li, R., Fu, J., and Dudareva, N. (2022). A peroxisomal heterodimeric enzyme is involved in benzaldehyde synthesis in plants. *Nat. Commun.* 13: 1352. doi: 10.1038/s41467-022-28978-2

in 't Zandt, M. H., Liebner, S., and Welte, C. U. (2020). Roles of thermokarst lakes in a warming world. *Trends Microbiol.* 28, 769–779. doi: 10.1016/j.tim.2020.04.002

Jansson, J. K., and Taş, N. (2014). The microbial ecology of permafrost. *Nat. Rev. Microbiol.* 12, 414–425.

Ji, M., Kong, W., Liang, C., Zhou, T., Jia, H., and Dong, X. (2020). Permafrost thawing exhibits a greater influence on bacterial richness and community structure than permafrost age in Arctic permafrost soils. *Cryosphere* 14, 3907–3916.

Jiao, Y., Davie-Martin, C. L., Kramshøj, M., Christiansen, C. T., Lee, H., Althuizen, I. H. J., et al. (2023). Volatile organic compound release across a permafrost-affected peatland. *Geoderma* 430:116355.

Jobst, B., Schühle, K., Linne, U., and Heider, J. (2010). ATP-dependent carboxylation of acetophenone by a novel type of carboxylase. *J. Bacteriol.* 192, 1387–1394.

Jorgenson, M. T., Romanovsky, V., Harden, J., Shur, Y., O'Donnell, J., Schuur, E. A. G., et al. (2010). Resilience and vulnerability of permafrost to climate change. This article is one of a selection of papers from The Dynamics of Change in Alaska's Boreal Forests: resilience and Vulnerability in Response to Climate Warming. *Can. J. For. Res.* 40, 1219–1236.

Kanehisa, M., Furumichi, M., Sato, Y., Kawashima, M., and Ishiguro-Watanabe, M. (2023). KEGG for taxonomy-based analysis of pathways and genomes. *Nucleic Acids Res.* 51, D587–D592.

Kokelj, S. V., Lantz, T. C., Tunnicliffe, J., Segal, R., and Lacelle, D. (2017). Climate-driven thaw of permafrost preserved glacial landscapes, northwestern Canada. *Geology* 45, 371–374.

Kramshøj, M., Albers, C. N., Svendsen, S. H., Björkman, M. P., Lindwall, F., Björk, R. G., et al. (2019). Volatile emissions from thawing permafrost soils are influenced by meltwater drainage conditions. *Glob. Change Biol.* 25, 1704–1716. doi: 10.1111/gcb.14582

Lemfack, M. C., Gohlke, B.-O., Toguem Serge, M. T., Preissner, S., Piechulla, B., and Preissner, R. (2018). mVOC 2.0: a database of microbial volatiles. *Nucleic Acids Res.* 46, D1261–D1265.

Li, B., Ho, S. S. H., Li, X., Guo, L., Chen, A., Hu, L., et al. (2021). A comprehensive review on anthropogenic volatile organic compounds (VOCs) emission estimates in China: comparison and outlook. *Environ. Int.* 156: 106710. doi: 10.1016/j.envint.2021.106710

Li, C., Hambright, K. D., Bowen, H. G., Trammell, M. A., Grossart, H. P., Burford, M. A., et al. (2021). Global co-occurrence of methanogenic archaea and methanotrophic bacteria in Microcystis aggregates. *Environ. Microbiol.* 23, 6503–6519. doi: 10.1111/1462-2920.15691

Li, D., Liu, C.-M., Luo, R., Sadakane, K., and Lam, T.-W. (2015). MEGAHIT: an ultra-fast single-node solution for large and complex metagenomics assembly via succinct de Bruijn graph. *Bioinformatics* 31, 1674–1676. doi: 10.1093/bioinformatics/btv033

Liljedahl, A. K., Boike, J., Daanen, R. P., Fedorov, A. N., Frost, G. V., Grosse, G., et al. (2016). Pan-Arctic ice-wedge degradation in warming permafrost and its influence on tundra hydrology. *Nat. Geosci.* 9, 312–318.

Mackelprang, R., Burkert, A., Haw, M., Mahendrarajah, T., Conaway, C. H., Douglas, T. A., et al. (2017). Microbial survival strategies in ancient permafrost: insights from metagenomics. *ISME J.* 11, 2305–2318.

Mackelprang, R., Waldrop, M. P., DeAngelis, K. M., David, M. M., Chavarria, K. L., Blazewicz, S. J., et al. (2011). Metagenomic analysis of a permafrost microbial community reveals a rapid response to thaw. *Nature* 480, 368–371. doi: 10.1038/nature10576

Mackie, R. I., White, B. A., and Bryant, M. P. (2008). Lipid metabolism in anaerobic ecosystems. *Crit. Rev. Microbiol.* 17, 449–479.

Maurer, D. L., Ellis, C. K., Thacker, T. C., Rice, S., Koziel, J. A., Nol, P., et al. (2019). Screening of microbial volatile organic compounds for detection of disease in cattle: development of lab-scale method. *Sci. Rep.* 9:12103. doi: 10.1038/s41598-019-47907-w

McGivern, B. B., Tfaily, M. M., Borton, M. A., Kosina, S. M., Daly, R. A., Nicora, C. D., et al. (2021). Decrypting bacterial polyphenol metabolism in an anoxic wetland soil. *Nat. Commun.* 12:2466. doi: 10.1038/s41467-021-22765-1

McNeill, J. D., and Labson, V. F. (1991). "7. Geological mapping using VLF radio fields," in *Electromagnetic Methods in Applied Geophysics*, ed. M. N. Nabighian (Society of Exploration Geophysicists: Houston, TX), 521–640. doi: 10.1190/1.9781560802686.ch7

Meredith, L. K., and Tfaily, M. M. (2022). Capturing the microbial volatilome: an oft overlooked 'ome'. *Trends Microbiol.* 30, 622–631. doi: 10.1016/j.tim.2021.12.004

Mishra, U., and Riley, W. J. (2012). Alaskan soil carbon stocks: spatial variability and dependence on environmental factors. *Biogeosciences* 9, 3637–3645.

Monteiro Santos, F. A., Mateus, A., Figueiras, J., and Gonçalves, M. A. (2006). Mapping groundwater contamination around a landfill facility using the VLF-EM method — A case study. *J. Appl. Geophys.* 60, 115–125.

Monteux, S., Weedon, J. T., Blume-Werry, G., Gavazov, K., Jassey, V. E. J., Johansson, M., et al. (2018). Long-term *in situ* permafrost thaw effects on bacterial communities and potential aerobic respiration. *ISME J.* 12, 2129–2141. doi: 10.1038/s41396-018-0176-z

Olefeldt, D., Goswami, S., Grosse, G., Hayes, D., Hugelius, G., Kuhry, P., et al. (2016). Circumpolar distribution and carbon storage of thermokarst landscapes. *Nat. Commun.* 7: 13043. doi: 10.1038/ncomms13043

Pellerin, A., Lotem, N., Walter Anthony, K., Eliani Russak, E., Hasson, N., Røy, H., et al. (2022). Methane production controls in a young thermokarst lake formed by abrupt permafrost thaw. *Glob. Change Biol.* 28, 3206–3221. doi: 10.1111/gcb.16151

PeÑUelas, J., Asensio, D., Tholl, D., Wenke, K., Rosenkranz, M., Piechulla, B., et al. (2014). Biogenic volatile emissions from the soil. *Plant Cell Environ.* 37, 1866–1891.

Ren, S., Wang, T., Guenet, B., Liu, D., Cao, Y., Ding, J., et al. (2024). Projected soil carbon loss with warming in constrained Earth system models. *Nat. Commun.* 15:102.

Rivard, C. J., and Grohmann, K. (1991). Degradation of furfural (2- furaldehyde) to methane and carbon dioxide by an anaerobic consortium. *Appl. Biochem. Biotechnol.* 28-29, 285–295. doi: 10.1007/BF02922608

Sasaki, Y. (1989). Two-dimensional joint inversion of magnetotelluric and dipole-dipole resistivity data. *Geophysics* 54, 254–262.

Schaefer, K., Lantuit, H., Romanovsky, V. E., Schuur, E. A. G., and Witt, R. (2014). The impact of the permafrost carbon feedback on global climate. *Environ. Res. Lett.* 9: 085003.

Schirrmeister, L., Meyer, H., Andreev, A., Wetterich, S., Kienast, F., Bobrov, A., et al. (2016). Late Quaternary paleoenvironmental records from the Chatanika River valley near Fairbanks (Alaska). *Quatern. Sci. Rev.* 147, 259–278.

Schmidt, R., Etalo, D. W., de Jager, V., Gerards, S., Zweers, H., de Boer, W., et al. (2016). Microbial small talk: volatiles in fungal–bacterial interactions. *Front. Microbiol.* 6:1495. doi: 10.3389/fmicb.2015.01495

Schulz-Bohm, K., Gerards, S., Hundscheid, M., Melenhorst, J., de Boer, W., and Garbeva, P. (2018). Calling from distance: attraction of soil bacteria by plant root volatiles. *ISME J.* 12, 1252–1262. doi: 10.1038/s41396-017-0035-3

Schulz-Bohm, K., Martín-Sánchez, L., and Garbeva, P. (2017). Microbial volatiles: small molecules with an important role in intra- and inter-kingdom interactions. *Front. Microbiol.* 8: 2484. doi: 10.3389/fmicb.2017.02484

Schuur, E. A. G., McGuire, A. D., Schädel, C., Grosse, G., Harden, J. W., Hayes, D. J., et al. (2015). Climate change and the permafrost carbon feedback. *Nature* 520, 171–179.

Segata, N., Izard, J., Waldron, L., Gevers, D., Miropolsky, L., Garrett, W. S., et al. (2011). Metagenomic biomarker discovery and explanation. *Genome Biol.* 12:R60.

Sela-Adler, M., Ronen, Z., Herut, B., Antler, G., Vigderovich, H., Eckert, W., et al. (2017). Co-existence of methanogenesis and sulfate reduction with common substrates in sulfate-rich estuarine sediments. *Front. Microbiol.* 8:766. doi: 10.3389/fmicb.2017.00766

Singer, E., Andreopoulos, B., Bowers, R. M., Lee, J., Deshpande, S., Chiniquy, J., et al. (2016). Next generation sequencing data of a defined microbial mock community. *Sci. Data* 3:160081.

Singleton, C. M., McCalley, C. K., Woodcroft, B. J., Boyd, J. A., Evans, P. N., Hodgkins, S. B., et al. (2018). Methanotrophy across a natural permafrost thaw environment. *ISME J.* 12, 2544–2558. doi: 10.1038/s41396-018-0065-5

Smith, S. L., Romanovsky, V. E., Lewkowicz, A. G., Burn, C. R., Allard, M., Clow, G. D., et al. (2010). Thermal state of permafrost in North America: a contribution to the international polar year. *Permafrost Periglacial Processes.* 21, 117–135.

Tao, F., Houlton, B. Z., Frey, S. D., Lehmann, J., Manzoni, S., Huang, Y., et al. (2024). Reply to: model uncertainty obscures major driver of soil carbon. *Nature* 627, E4–E6. doi: 10.1038/s41586-023-07000-9

Tripathi, B. M., Kim, H. M., Jung, J. Y., Nam, S., Ju, H. T., Kim, M., et al. (2019). Distinct taxonomic and functional profiles of the microbiome associated with different

soil horizons of a moist tussock tundra in alaska. *Front. Microbiol.* 10:1442. doi: 10.3389/fmicb.2019.01442

Turetsky, M. R., Abbott, B. W., Jones, M. C., Anthony, K. W., Olefeldt, D., Schuur, E. A. G., et al. (2020). Carbon release through abrupt permafrost thaw. *Nat. Geosci.* 13, 138–143.

Turetsky, M. R., Abbott, B. W., Jones, M. C., Walter Anthony, K., Olefeldt, D., Schuur, E. A. G., et al. (2019). Permafrost collapse is accelerating carbon release. *Nature* 569, 32–34.

Tyc, O., Song, C., Dickschat, J. S., Vos, M., and Garbeva, P. (2017). The ecological role of volatile and soluble secondary metabolites produced by soil bacteria. *Trends Microbiol.* 25, 280–292. doi: 10.1016/j.tim.2016.12.002

Veraart, A. J., Garbeva, P., van Beersum, F., Ho, A., Hordijk, C. A., Meima-Franke, M., et al. (2018). Living apart together—bacterial volatiles influence methanotrophic growth and activity. *ISME J.* 12, 1163–1166. doi: 10.1038/s41396-018-0055-7

Vigneron, A., Lovejoy, C., Cruaud, P., Kalenitchenko, D., Culley, A., and Vincent, W. F. (2019). Contrasting winter versus summer microbial communities and metabolic functions in a permafrost thaw lake. *Front. Microbiol.* 10:1656. doi: 10.3389/fmicb.2019.01656

Vonk, J. E., Tank, S. E., Mann, P. J., Spencer, R. G. M., Treat, C. C., Striegl, R. G., et al. (2015). Biodegradability of dissolved organic carbon in permafrost soils and aquatic systems: a meta-analysis. *Biogeosciences* 12, 6915–6930.

Waldrop, M. P., Chabot, C. L., Liebner, S., Holm, S., Snyder, M. W., Dillon, M., et al. (2023). Permafrost microbial communities and functional genes are structured by latitudinal and soil geochemical gradients. *ISME J.* 17, 1224–1235. doi: 10.1038/s41396-023-01429-6

Walter Anthony, K. M., Anthony, P., Hasson, N., Edgar, C., Sivan, O., Eliani-Russak, E., et al. (2024). Upland Yedoma taliks are an unpredicted source of atmospheric methane. *Nat. Commun.* 15:6056. doi: 10.1038/s41467-024-50346-5

Walter Anthony, K. M., Lindgren, P., Hanke, P., Engram, M., Anthony, P., Daanen, R. P., et al. (2021). Decadal-scale hotspot methane ebullition within lakes following abrupt permafrost thaw. *Environ. Res. Lett.* 16: 035010.

Walter Anthony, K., Daanen, R., Anthony, P., Schneider von Deimling, T., Ping, C.-L., Chanton, J. P., et al. (2016). Methane emissions proportional to permafrost carbon thawed in Arctic lakes since the 1950s. *Nat. Geosci.* 9, 679–682.

Walter Anthony, K., Schneider von Deimling, T., Nitze, I., Frolking, S., Emond, A., Daanen, R., et al. (2018). 21st-century modeled permafrost carbon emissions accelerated by abrupt thaw beneath lakes. *Nat. Commun.* 9:3262. doi: 10.1038/s41467-018-05738-9

Wang, S., Lu, Q., Liang, Z., Yu, X., Lin, M., Mai, B., et al. (2023). Generation of zero-valent sulfur from dissimilatory sulfate reduction in sulfate-reducing microorganisms. *Proc. Natl Acad. Sci. U.S.A.* 120: e2220725120.

Westhoff, S., van Wezel, G. P., and Rozen, D. E. (2017). Distance-dependent danger responses in bacteria. *Curr. Opin. Microbiol.* 36, 95–101. doi: 10.1016/j.mib.2017.02.002

Wilhelm, R. C., DeRito, C. M., Shapleigh, J. P., Madsen, E. L., and Buckley, D. H. (2021). Phenolic acid-degrading Paraburkholderia prime decomposition in forest soil. *ISME Commun.* 1:4. doi: 10.1038/s43705-021-00009-z

Wood, D. E., Lu, J., and Langmead, B. (2019). Improved metagenomic analysis with Kraken 2. *Genome Biol.* 20:257.

Zolkos, S., and Tank, S. E. (2020). Experimental evidence that permafrost thaw history and mineral composition shape abiotic carbon cycling in thermokarst-affected stream networks. *Front. Earth Sci.* 8:152. doi: 10.3389/feart.2020.00152

Frontiers in Microbiology

Explores the habitable world and the potential of microbial life

The largest and most cited microbiology journal which advances our understanding of the role microbes play in addressing global challenges such as healthcare, food security, and climate change.

Discover the latest Research Topics

See more →

Frontiers

Avenue du Tribunal-Fédéral 34
1005 Lausanne, Switzerland
frontiersin.org

Contact us

+41 (0)21 510 17 00
frontiersin.org/about/contact